2006-05-04

Kinetics and Catalysis of the Water-Gas-Shift Reaction: A Microkinetic and Graph Theoretic Approach

Caitlin A. Callaghan
Worcester Polytechnic Institute

Kinetics and Catalysis of the Water-Gas-Shift Reaction: A Microkinetic and Graph Theoretic Approach

A Dissertation

Submitted to the Faculty

of the

WORCESTER POLYTECHNIC INSTITUTE

Department of Chemical Engineering

In partial fulfillment of the requirements for the

Degree of Doctor of Philosophy in Chemical Engineering

by

Caitlin A. Callaghan

March 31, 2006

Professor Ravindra Datta, Advisor WPI Chemical Engineering Department	Professor Ilie Fishtik, Co-Advisor WPI Chemical Engineering Department
Professor Nikolaos K. Kazantzis WPI Chemical Engineering Department	Professor Joseph D. Fehribach WPI Mathematical Sciences & Chemical Engineering Department
Professor Jennifer L. Wilcox WPI Chemical Engineering Department	Dr. A. Alan Burke Naval Undersea Warfare Center, Newport, RI

Professor David DiBiasio, Dept. Head
WPI Chemical Engineering Department

ABSTRACT

The search for environmentally benign energy sources is becoming increasingly urgent. One such technology is fuel cells, e.g., the polymer electrolyte membrane (PEM) fuel cell which uses hydrogen as a fuel and emits only H_2O. However, reforming hydrocarbon fuels to produce the needed hydrogen yields reformate streams containing CO_2 as well as CO, which is toxic to the PEM fuel cell at concentrations above 100ppm. As the amount of CO permitted to reach the fuel cell increases, the performance of the PEM fuel cell decreases until it ultimately stops functioning.

The water-gas-shift (WGS) reaction, $CO + H_2O \leftrightarrows H_2 + CO_2$, provides a method for extracting the energy from the toxic CO by converting it into usable H_2 along with CO_2 which can be tolerated by the fuel cell. Although a well established industrial process, alternate catalysts are sought for fuel cell application. Catalyst selection for the WGS reaction has, until recently, been based on trial-and-error screening of potential catalysts due to a lack of fundamental understanding of the catalyst's functioning. For this reason, we embarked on a deeper understanding of the molecular events involved in the WGS reaction such that a more systematic and theory-guided approach may be used to design and select catalysts more efficiently, i.e., rational catalyst design.

The goal of this research was to develop a comprehensive predictive microkinetic model for the WGS reaction which is based solely on a detailed mechanism as well as theories of surface-molecule interactions (i.e., the transition-state theory) with energetic parameters determined *a priori*. This was followed by a comparison of the experimental results of sample catalysts to validate the model for various metal-based catalysts of interest including Cu, Fe, Ni, Pd, Pt, Rh, and Ru.

A comprehensive mechanism of the plausible elementary reaction steps was compiled from existing mechanisms in the literature. These were supplemented with other likely candidates which are derivatives of those identified in the literature. Using established theories, we predicted the kinetics of each of the elementary reaction steps on metal catalysts of interest. The Unity Bond Index-Quadratic Exponential Potential Method (UBI-QEP) was used to predict the activation energies in both the forward and

reverse direction of each step based solely on heats of chemisorption and bond dissociation energies of the species involved. The Transition State Theory (TST) was used to predict the pre-exponential factors for each step assuming an immobile transition state; however, the pre-exponential factors were adjusted slightly to ensure thermodynamic consistency with the overall WGS reaction.

In addition, we have developed a new and powerful theoretical tool to gain further insight into the dominant pathways on a catalytic surface as reactants become products. Reaction Route (*RR*) Graph Theory incorporates fundamental elements of graph theory and electrical network theory to graphically depict and analyze reaction mechanisms. The stoichiometry of a mechanism determines the connectivity of the elementary reaction steps. Each elementary reaction step is viewed as a single branch with an assumed direction corresponding to the assumed forward direction of the elementary reaction step. The steps become interconnected via nodes which reflect the quasi-steady state conditions of the species represented by the node. A complete *RR* graph intertwines a series of routes by which the reactants may be converted to products. Once constructed, the *RR* graph may be converted into an electrical network by replacing, in the steady-state case, each elementary reaction step branch with a resistor and including the overall reaction as a power source where rate and affinity correspond to current and voltage, respectively.

A simplification and reduction of the mechanism may be performed based on results from a rigorous De Donder affinity analysis as it correlates to Kirchhoff's Voltage Law (KVL), akin to thermodynamic consistency, coupled with quasi-steady state conditions, i.e., conservation of mass, analyzed using Kirchhoff's Current Law (KCL). Hence, given the elementary reaction step resistances, in conjunction with Kirchhoff's Laws, a systematic reduction of the network identifies the dominant routes, e.g., the routes with the lowest resistance, along with slow and quasi-equilibrium elementary reaction steps, yielding a simplified mechanism from which a predictive rate expression may possibly be derived.

Here, we have applied *RR* Graph Theory to the WGS reaction. An 18-step mechanism was employed to understand and predict the kinetics of the WGS reaction. From the stoichiometric matrix for this mechanism, the topological features necessary to

assemble the *RR* graph, namely the intermediate nodes, terminal nodes, empty reaction routes and full reaction routes, were enumerated and the graph constructed. The assembly of the *RR* graph provides a comprehensive overview of the mechanism. After reduction of the network, the simplified mechanism, comprising the dominant pathways, identified the quasi-equilibrium and rate-determining steps, which were used to determine the simplified rate expression which predicts the rate of the complete mechanism for different catalysts. Experimental investigations were conducted on the catalysts of interest to validate the microkinetic model derived. Comparison of the experimental results from the industrially employed catalysts (e.g., Cu, Ni, Fe, etc.) shows that the simplified microkinetic model sufficiently predicts the behavior of the WGS reaction for this series of catalysts with very good agreement. Other catalysis tested (Pt, Pd, Rh and Ru), however, had sufficient methanation activity that a direct comparison with WGS kinetics could not be made.

In summary, we have developed a comprehensive approach to unravel the mechanism and kinetics of a catalytic reaction. The methodology described provides a more fundamental depiction of events on the surface of a catalyst paving the way for rational analysis and catalyst design. Illustrated here with the WGS reaction as an example, we show that the dominant *RR*s may be systematically determined through the application of rigorous fundamental constraints (e.g. thermodynamic consistency and mass conservation) yielding a corresponding explicit *a priori* rate expression which illustrates very good agreement not only with the complete microkinetic mechanism, but also the experimental data. Overall, *RR* graph theory is a powerful new tool that may become invaluable for unraveling the mechanism and kinetics of complex catalytic reactions via a common-sense approach based on fundamentals.

ACKNOWLEDGEMENTS

I would like to thank the following individuals for their assistance, support, guidance and inspiration during the time I have worked on this research.

My Advisors:

- Prof. Ravindra Datta, Advisor
- Prof. Ilie Fishtik, Co-Advisor

My Thesis Committee Members:

- Prof. Nikolaos K. Kazantzis
- Prof. Joseph D. Fehribach
- Prof. Jennifer L. Wilcox
- Dr. A. Alan Burke

My Labmates:

- Dr. Nikhil Jalani
- Saurabh Vilekar
- James Liu
- Dr. Pyoungho Choi
- Dr. Jingxin Zhang
- Dr. Tony Thampan
- Katherine Fay

The Department Staff:

- Sandy Natale
- Jack Ferraro
- Doug White
- Paula Moravek

My family and friends, as well as everyone else I've met along the way.

I would like to acknowledge the following sources for funding:

- General Motors' GM Fellowship Program
- Office of Naval Research/University Laboratory Initiative
- WPI's Backlin Scholarship

"The art is finding a model adequate to the problem, and, for the pragmatist, 'the only criterion of a molecular model is its value to chemists assessed by its performance'."

-- E. Shustorovich

TABLE OF CONTENTS

INDEX OF FIGURES

INDEX OF TABLES

NOMENCLATURE

Symbols

A_{bed}	cm^2	Cross-sectional area of catalyst bed
a_{cat}	cm^2/cm^3	Surface area per unit volume of catalyst
a	cal/mol	Generic bond energy term for interaction potential
A_ρ	–	Affinity of elementary reaction step ρ
$\vec{A}_\rho$	–	Forward reaction affinity of elementary reaction step ρ
$\overleftarrow{A}_\rho$	–	Reverse reaction affinity of elementary reaction step ρ
a_i	–	Activity of terminal species i
$\mathscr{A}_\rho$	–	Dimensionless reaction affinity
$\mathbf{A}$	–	Vector of overall reaction and elementary reaction step affinities
b	–	Distance scaling constang for bond index
B	cm^{-1}	Rotational constant
B	–	Number of branches
c	cm/s	Speed of light
C_t	$sites/cm^2$	Catalyst site density
C_i	$moles/cm^3$	Concentration of terminal species i
C_{is}	$moles/cm^3$	Concentration of terminal species i at catalyst surface

C_{ib}	moles/cm^3	Bulk concentration of terminal species *i*
C_{WP}	–	Weisz-Prater parameter
D_e	m^2/s	Bulk or Knudsen diffusivity
D_a	m^2/s	Effective axial dispersion coefficient
d_p	cm	Catalyst particle diameter
D_g	m^2/s	Gas diffusivity
D_{AB}	kcal/mol	Bond dissociation energy
E^*	kcal/mol	Two-body interaction potential
E	kcal/mol	Activation energy
$\vec{E}_\rho$	kcal/mol	Activation energy of the forward reaction
$\overleftarrow{E}_\rho$	kcal/mol	Activation energy of the reverse reaction
E_e	kcal/mol	Electrical energy of the ground state
E^{app}	kcal/mol	Apparent activation energy
F_i	Moles/s	Molar flow rate of terminal species *i*
G^o	kJ/mol	Standard Gibbs free energy
ΔG	kJ/mol	Gibbs free energy change
G_R	–	Reaction route graph
h	J·s	Planck's constant

ΔH^{o}_{rxn}	kcal/mol	Standard heat of reaction
ΔH^{o}_{f}	kcal/mol	Standard heat of formation
ΔH	kcal/mol	Enthalpy change
ΔH_{rxn}	kcal/mol	Heat of reaction
h_T	$W/m^2 \cdot K$	Heat transfer coefficient
$I_A I_B I_C$	$kg^3 m^6$	Moments of inertia
I_k	–	Intermediate species k
J_k	s^{-1} or $Pa^{-1}s^{-1}$	Flux of reaction route k
$\mathbf{J}$	s^{-1} or $Pa^{-1}s^{-1}$	Vector of independent reaction route fluxes
k	s^{-1} or $Pa^{-1}s^{-1}$	Rate constant
$\vec{k}_\rho$	s^{-1} or $Pa^{-1}s^{-1}$	Forward rate constant of elementary reaction step ρ
$\overleftarrow{k}_\rho$	s^{-1} or $Pa^{-1}s^{-1}$	Reverse rate constant of elementary reaction step ρ
K_ρ	–	Equilibrium constant of elementary reaction step ρ
k_B	J/K	Boltzmann constant
K	–	Equilibrium constant of the overall reaction
k	$s^{-1}atm^{-1}$	Temperature dependent constant (Temkin)
k_t	$J/K \cdot m \cdot s$	Thermal conductivity
k^{app}	s^{-1} or $Pa^{-1}s^{-1}$	Apparent rate constant

k_c	m/s	Mass transfer coefficient
L_{bed}	cm	Length of catalyst bed
L_g	–	Lagrangian multiplier of the UBI condition
L	–	Number of independent reaction routes, number of links in reaction route graph
m	kg	Mass of a molecule (super/subscript "‡" denotes transition state complex)
m_{cat}	g	Mass of catalyst
M	–	Collision body
$\mathbf{M}$	–	Incidence matrix for reaction route graph
$m_{j\rho}$	–	Elements of incidence matrix for reaction route graph
$\mathbf{M}_f$	–	Reduced incidence matrix for reaction route graph
$\mathbf{M}_t$	–	Incidence matrix of twigs for reaction route graph
$\mathbf{M}_l$	–	Incidence matrix of links for reaction route graph
N_A	molecules/mole	Avagadros number
N	–	Total bond index normalization constant
n_N	–	N^{th} fraction of the total bond index
n_i	mol/cm^3	Concentration of specie *i*
n	–	Number of terminal species
N_i	moles	Moles of terminal species *i*

n^{app}	–	Apparent reaction order
n_j	–	Node j
n_{Ij}	–	Intermediate node j
n_{Tj}	–	Terminal node j
N	–	Number of nodes
P_i	Pa	Partial pressure of species i
p	–	Number of elementary reaction steps
P_ρ	–	"power" of elementary reaction step ρ
q	–	Number of intermediate species
Q_A	kcal/mol	Atomic binding energy
Q_{AB}	kcal/mol	Heat of chemisorption
Q_{0A}	kcal/mol	Experimental parameter for determining Q_A
Q	–	Number of conceivable reaction routes
Q_i	–	QSS condition i
$\boldsymbol{Q}$	–	Matrix of QSS conditions
r	–	Bond distance for bond index
r_0	–	Equilibrium bond distance for bond index
r_ρ	s^{-1} or $Pa^{-1}s^{-1}$	Rate of elementary reaction step ρ

$\vec{r}_\rho$	s^{-1} or $Pa^{-1}s^{-1}$	Forward rate of elementary reaction step ρ
$\overleftarrow{r}_\rho$	s^{-1} or $Pa^{-1}s^{-1}$	Reverse rate of elementary reaction step ρ
r_{OR}	s^{-1} or $Pa^{-1}s^{-1}$	Overall reaction rate
R_{gas}	kJ/mol·K	Gas constant
R	cm	Catalyst particle radius
$r_{\rho,0}$	s^{-1} or $Pa^{-1}s^{-1}$	Exchange rate
$\vec{r}_{\rho,0}$	s^{-1} or $Pa^{-1}s^{-1}$	Forward exchange rate
$\overleftarrow{r}_{\rho,0}$	s^{-1} or $Pa^{-1}s^{-1}$	Reverse exchange rate
$\mathbf{r}$	s^{-1} or $Pa^{-1}s^{-1}$	Vector of overall reaction and elementary reaction step rates
R_ρ	s or Pa·s	Resistance of elementary reaction step ρ
R_{RR_k}	s or Pa·s	Resistance of reaction route k
s_ρ	–	Elementary reaction step ρ
S^o	kJ/mol·K	Standard entropy
ΔS	kJ/mol·K	Entropy change
S_t	cm^2/g	Active catalyst surface area
S	–	Active surface site
$\mathbf{s}$	–	Vector of overall reactions and elementary reaction steps
$s_\rho^{(t)}$	–	Twigs in reaction tree

$s_\rho^{(l)}$	–	Links in reaction tree
t	s	Reaction time
T	K	Reaction temperature
T_s	K	Temperature of catalyst surface
T_R	–	Reaction tree
U	cm/s	Velocity of particle (subscript "o" denotes superficial velocity)
V	cm^3	Volume of gas in bed
v	cm^3/s	Volumetric flow rate of gas (subscript "o" denotes intial value)
w_k	–	Walk from node n_i to node n_j
X	–	Total bond index
$x(r)$	–	Bond index
X_i	–	Conversion of species i
x_i	–	Mole fraction of species i
X_R	–	Cut-set of branches for reaction tree
$X_{R,f}$	–	Fundamental cut-set of branches for reaction tree
$\mathbf{X}$	–	Cut-set matrix for reaction route graph
$x_{h\rho}$	–	Elements of cut-set matrix for reaction route graph
$\mathbf{X}_f$	–	Fundamental cut-set matrix for reaction route graph

$\mathbf{X}_l$	–	Cut-set matrix of links for reaction route graph
z	–	Molecular partition function
z_t	–	Translational partition function (super/subscript "‡" denotes trasition state complex)
z_r	–	Rotational partition function (super/subscript "‡" denotes trasition state complex)
z_v	–	Vibrational partition function (super/subscript "‡" denotes trasition state complex)
z_e	–	Electrical partition function (super/subscript "‡" denotes trasition state complex)

Greek Symbols

α	–	Lagrangian multiplier of the UBI condition
$\alpha_{\rho k}$	–	Stoichiometric coefficient of intermediate species k in elementary reaction ρ ($k = 0$ refers to the active surface site)
$\boldsymbol{\alpha}$	–	Matrix of intermediate stoichiometric coefficients
β_T	–	Temperature dependence parameter for mass transfer limitations
$\beta_{\rho i}$	–	Stoichiometric coefficient of terminal species i in elementary reaction step ρ
χ	–	Temperature dependent constant (Temkin)
Δ	–	Determinant of the intermediate sub-matrix
δ_i	–	Reaction order with respect to terminal species i
ε	–	porosity
γ_A	–	Arrhenius number for mass transfer limitations

γ_M	–	Roughness factor
$\boldsymbol{\gamma}$	–	Reduced stoichiometric sub-matrix
η	–	Internal effectiveness factor
κ	–	Transmission coefficient
Λ	s^{-1}	Pre-exponential factor.
Λ^{app}	s^{-1} or $Pa^{-1}s^{-1}$	Apparent pre-exponential factor
λ_ρ	–	"constant" coefficient of Marcelin-De Donder relation
μ_f	kg/m·s	Fluid viscosity
μ_i	kJ/mol	Chemical potential of species *i* (superscript "o" denotes standard chemical potential)
ν_{ρ_i}	–	Stoichiometric coefficient of species *i* in elementary reaction step ρ
$\boldsymbol{\nu}$	–	Matrix of stoichiometric coefficients
Ω	–	Overall effectiveness factor
$\omega_\perp$	cm^{-1}	Vibrational frequency for single degenerate vibration orthogonal to surface
$\omega_\parallel$	cm^{-1}	Vibrational frequency for doubly degenerate vibration parallel to surface
ω	cm^{-1}	Vibrational frequency for each degree of freedom of the molecule
ϕ_n	–	Thiele modulus
ϕ	–	Void fraction of catalyst bed
ρ_{cat}	g/cm^3	Catalyst density

ρ	–	Elementary reaction step number
ρ_b	g/cm^3	Bulk density of catalyst
ρ_f	g/cm^3	Fluid density
$\boldsymbol{\sigma}$	–	Reaction route matrix
σ_{kh}	–	Stoichiometric numbers, elements of $\boldsymbol{\sigma}$
$\boldsymbol{\sigma}_f$	–	Fundamental reaction route matrix
$\boldsymbol{\sigma}_t$	–	Reaction route matrix of twigs
$\boldsymbol{\sigma}_l$	–	Reaction route matrix of links
σ_{sym}	–	Symmetry number
$\vec{\sigma}_\rho, \overleftarrow{\sigma}_\rho$	–	Geometric factors of forward and reverse reactions
θ_i	–	Surface coverage of species *i*
θ_o	–	Concentration of active surface sites
τ	s	Residence time
ζ	–	Shape factor (external surface area/πd_p^2)

Abbreviations

ads	Adsorption
AFC	Alkaline fuel cell

ATR	Autothermal reforming
CSTR	Continuously stirred tank reactor
CPOX	Catalytic Partial Oxidation
des	Desorption
DFT	Density functional theory
DMFC	Direct methanol fuel cell
ER	Empty reaction route
FR	Full reaction route
HTS	High temperature shift
IN	Intermediate node
KCL	Kirchhoff's current law
KVL	Kirchhoff's voltage law
LHHW	Langmuir-Hinshelwood-Hougen-Watson
LTS	Low temperature shift
MARI	Most abundant reactive intermediate
MCFC	Molten carbonate fuel cell
MSR	Methane steam reforming
NIST	National Institute of Standards and Technology

ODE	Ordinary differential equation
OR	Overall reaction
PAFC	Phosphoric acid fuel cell
PBR	Packed bed reactor
PEM	Polymer electrolyte membrane [fuel cell]
PFR	Plug-flow reactor
PrOx	Preferential oxidation
QE	Quasi-equilibrium
QM	Quantum mechanical
QSS	Quasi-steady-state
RLS	Rate limiting step
RR	Reaction route
SOFC	Solid oxide fuel cell
SR	Steam reforming
STP	Standard temperature and pressure
TN	Terminal node
TST	Transition state theory
UBI-QEP	Unit Bond Index-Quadratic Exponential Potential

WGS	Water-gas shift

Chapter 1. Introduction

Fuel cells are currently a leading choice for the development of clean energy owing to their high efficiency and low pollution. The principle behind the fuel cell was developed by Sir William R. Grove, a British physicist, in 1839 [1]. The fuel cell is an electrochemical device in which chemical energy stored in a fuel is converted directly into electricity. It consists of an electrolyte material sandwiched between two thin electrodes. Fuel, frequently hydrogen, reacts at the anode while the oxidant reacts at the cathode. The ionic species produced at one electrode and consumed at the other passes through the electrolyte while electrons produced conduct through the external circuit. The individual fuel cell produces between 0.5 and 1.0 V giving off heat, water, and CO_2 (when a carbon-containing fuel is used) [2]. The low voltage produced by a single cell is similar to a battery, but the current density in a fuel cell is usually much higher.

Recent advances in fuel cell technology have greatly improved the prospects of its use in electric power generation. The promise of a more efficient and environmentally friendly means of generating power for mobile, portable and stationary applications has given rise to the development of several different types of fuel cells, typically requiring hydrogen as the ultimate fuel. As a result, there has been talk of a "hydrogen economy." Hydrogen can be obtained from natural gas, liquid hydrocarbon fuels (including biomass fuels such as ethanol), landfill gases, water and electricity (via the process of electrolysis), biological processes including those involving algae, and from gasification of biomass, wastes and coal.

One of the principle attractions of fuel cell technology is the diverse array of potential applications which may be powered with high efficiency, defined as the ratio of the electric energy produced by a stack to the chemical energy of the fuel, in a wide range of system sizes. Several types of fuel cells are in the development stage. These include the proton-exchange membrane (PEM) fuel cells, solid-oxide fuel cells (SOFCs), alkaline fuel cells (AFCs), phosphoric acid fuel cells (PAFCs), direct methanol fuel cells (DMFCs), and molten carbonate fuel cells (MCFCs). While the low temperature PEM fuel cells are the current leaders for automotive and small stationary applications, the

PAFCs, SOFCs, and the MCFCs, which operate at higher temperatures (from 200°C to 1000°C) [3], have a greater potential for larger and stationary applications. Key aspects of these various fuel cells are compared in Table 1.

While fuel cell technology provides a promising solution for the need to reduce pollution, the threat of oil depletion and price increases, and the wish of many countries to reduce foreign energy dependencies, unfortunately, there are still some issues that first require resolution. Fuel cell manufacturing costs are still too high for broad consumer application, and component durability needs improvement to lengthen the lifetime of the fuel cell. Further, the widespread application of hydrogen-fueled fuel cells requires distributed generation and transport of hydrogen. Unfortunately, hydrogen, being the lightest element, lacks the convenience of energy density, storage and widespread distribution of current fuels, i.e. gasoline, natural gas, etc. Currently, the portability of hydrogen, in either liquid or condensed vapor form, for mobile applications does not present itself as a very viable option due to its low density, although many automotive companies are proceeding on this premise. The limited on-board storage of hydrogen can limit a vehicle's range despite higher efficiency. On-board fuel processing offers a potential practical solution to this obstacle. However, this too is hampered by its own challenges that need to be overcome. For example, compact fuel reformer designs are required for incorporating the on-board hydrogen generating system into automobiles without significant loss of passenger or cargo space, as is the current quandary.

Fuel processing plants include a fuel reformer to convert a fuel into a mixture of H_2, CO_2, and CO. It is followed by the water-gas-shift reaction, often as two separate stages of high temperature shift (HTS) and low temperature shift (LTS) [4], to further convert CO in order to recover the lost usable energy in CO as well as the reduction of the concentration of CO. It should be noted that the higher temperature fuel cells, e.g., the molten carbonate and solid oxide fuel cells, utilize the CO as a fuel and do not require the application of the WGS reaction [5]. Others, e.g., PEM fuel cells [6], have a very low toxicity level for CO and require not only the water-gas-shift reaction, but also a preferential oxidation (PrOx) step in which much of the remaining CO is oxidized to CO_2, which is essentially harmless to the fuel cell. Further, desulphurization is often required as the first step in the reforming plant.

Table 1. Types of fuel cells and their key differences [5].

Fuel Cell Type	Electrolyte	Anode Gas	Cathode Gas	Temperature	Efficiency
Proton Exchange Membrane (PEM)	solid polymer membrane	hydrogen	pure or atmospheric oxygen	75 C (180 F)	35–60%
Alkaline (AFC)	potassium hydroxide	hydrogen	pure oxygen	below 80 C	50–70%
Direct Methanol (DMFC)	solid polymer membrane	methanol solution in water	atmospheric oxygen	75 C (180 F)	35–40%
Phosphoric Acid (PAFC)	Phosphorous	hydrogen	atmospheric oxygen	210 C (400 F)	35–50%
Molten Carbonate (MCFC)	Alkali-Carbonates	hydrogen, methane	atmospheric oxygen	650 C (1200 F)	40–55%
Solid Oxide (SOFC)	Ceramic Oxide	hydrogen, methane	atmospheric oxygen	800–1000 C (1500–1800 F)	45–60%

The current HTS and LTS catalysts, while excellent for large scale industrial plants, are too slow for compact reforming plants and are based on catalysts that are pyrophoric and, hence, present safety concerns for consumer applications. For this reason, the development of both low temperature and high temperature water-gas-shift (WGS) catalysts is of great current interest. Until recently, the approach for designing catalysts has been based on guess work, heuristics, or on random or combinatorial screening of single, binary, or tertiary catalysts of varying compositions yielding an infinite number of possibilities to be screened. In recent years, much emphasis has been placed on developing detailed microkinetic models for the WGS reaction [4,7-16]. A deeper understanding of the sequence of molecular events on the surface of the catalyst might eventually provide a more systematic and efficient theory-guided catalyst design. This is the broad objective of this research, where kinetic predictions are compared to experimental results for various catalysts.

A 13 elementary reaction step microkinetic model for the WGS reaction on Cu(111) was developed by Fishtik and Datta [7]. One aim of this work is to explore more comprehensive mechanisms and plausible reaction routes for the WGS reaction. In particular, we consider here additional elementary reaction steps that substantially increase the number of possible reaction routes. We also provide additional experimental data that allows a more comprehensive check of the validity of the proposed microkinetic mechanism without fitted parameters. The energetic characteristics of the elementary reaction steps are evaluated employing the Unity Bond Index–Quadratic Exponential Potential (UBI-QEP) method developed by Shustorovich [17], while the pre-exponential factors are estimated as per the transition-state theory [16,18]. The resulting model is additionally analyzed, simplified and reduced systematically to a three parallel route model based on the reaction route (*RR*) formalism developed by Fishtik and Datta [7,19].

First-principles quantum mechanical (QM) calculations of elementary reaction step energetics are becoming an increasingly indispensable and incisive tool of the catalytic chemist [8]. We can now virtually "see" how molecules rearrange themselves on metal surfaces, and can calculate the corresponding reaction energetics of elementary processes with increasing accuracy, although still not accurate enough for predicting kinetics. However, there are available semi-theoretical methods [17] that can predict

reaction energetics of elementary catalytic reactions with acceptable accuracy. It is, thus, only a matter of time before we have a very basic understanding of the molecular events involved in important catalytic processes and their energetics. However, this is only the first step toward unraveling the mechanism and kinetics of overall catalytic reactions. The mechanistic elementary reaction steps and their kinetics must be combined into overall reaction networks and the overall kinetics. Thus, a key focus of this research is to arrange the elementary steps into reaction networks and using the predicted kinetic information of individual molecular events or elementary reaction steps to determine the kinetics and mechanisms of overall reactions comprising such steps. The general approach presented here is, in fact, widely applicable and, in principle, may be utilized for the analysis of non-catalytic reaction networks as well as the functioning of cellular machinery. It is anticipated that such a deeper understanding of reaction systems might eventually allow systematic molecular theory-based design of catalytic materials.

There are currently available two different ways in which one might develop a kinetic mechanism: 1) the conventional Langmuir-Hinshelwood-Hougen-Watson (LHHW) approach [17,20,21], in which an explicit rate expression might be derived based on the common, but rather arbitrary, assumptions such as the rate-determining step (RDS), quasi-steady-state (QSS) approximation, most abundant reactive intermediate (MARI), etc., and 2) the microkinetic approach [10,11,18,22], wherein no assumptions are made, but only numerical results are possible. The former approach is approximate, while the latter is not insightful. In fact, the latter approach is already utilized in the computational modeling of combustion and atmospheric pollution systems comprising of hundreds of species and elementary reaction steps.

Here, an alternate approach [23] is proposed. This new approach begins with a rigorous microkinetic analysis based on predicted kinetics of elementary reaction steps, but then utilizes a systematic network analysis in analogy to electrical networks, with De Donder's affinity as the driving force akin to voltage and reaction rate akin to current, in order to elucidate the major pathways followed by deliberate reduction of the network to arrive at simpler mechanisms and explicit, but precise, rate expressions containing predicted rate constants. Within this approach, the reaction network may be envisioned in terms of a revisited version [23-26] of the conventional reaction route (*RR*) theory [27-

30]. The capabilities of the new reaction network approach are illustrated by applying it to the analysis of a 18 elementary reaction step microkinetic mechanism of the water-gas-shift reaction.

Chapter 2 provides a comprehensive literature review of previous studies of the WGS reaction mechanism as well as a brief overview of current research relevant to the catalysts of interest for this research. Literature mechanisms are described based on available surface study results, experimental data and plausible rate expressions. In some cases, available details are provided to demonstrate the methodology used by other researchers to obtain their final results. This chapter includes a discussion of the mechanism used in this thesis.

In Chapter 3, a review of microkinetics, transport and thermodynamics related to this research is presented. In addition, details of the theories used to predict the energetic parameters of elementary reaction steps are provided along with examples demonstrating their use. The Unity Bond Index – Quadratic Exponential Potential method is used to determine the activation energies and reaction enthalpies of the elementary reaction steps. Transition-state theory is employed to estimate the pre-exponential factors for the elementary reaction steps.

Chapter 4 is an overview of stoichiometric theory related to reaction routes. Specifically, the elements of the theory are defined mathematically for use in Chapter 5. A review of previous applications of graph theory to reaction networks is presented in Chapter 5. In addition, the basis for *RR* Graph Theory is given along with the incorporation of electrical network theory for simplification and reduction of the reaction mechanism. The concept is illustrated with examples establishing the methodology used in Chapter 6.

The WGS mechanism, as comprised in Chapter 2, is analyzed, simplified, and reduced using *RR* Graph Theory in Chapter 6. As a consequence of the analysis, the quasi-equilibrium as well as the rate-determining steps are revealed. The reduced network provides the basis for the derivation of the overall rate expression.

The results of Chapter 6 are experimentally validated using the experimental design described in Chapter 7. The model predictions are compared for three industrial catalysts (Cu, Ni, Fe) and a short series of precious metal catalysts (Pt, Pd, Ru, Rh) in

Chapter 8, illutrating the effectiveness of not only the methodology, but also the overall rate expression. In addition, the experimental reaction orders are discussed relative to theoretical expectations.

Finally, in Chapter 9, overall conclusions are drawn and suggestions are made for future extensions of the current research. Specifically, extensions of the *RR* Graph Theory are discussed as well as improvements in the predicted energetic parameters.

Chapter 2. Literature Review of the Water-Gas-Shift Reaction

With concerns of the depletion of resources to provide energy through current technologies, i.e., nuclear, coal-burning, etc., interest in fuel cells as an alternate means for efficient energy production, has given rise to research in various related areas, i.e., fuel processing. The water-gas-shift reaction is among the typical fuel processing reactions studied in conjunction with fuel cells. Research involving the reaction ranges from catalyst synthesis to mechanistic studies for rate prediction. This chapter summarizes the role of water-gas-shift in a fuel cell plant. In addition, a discussion of more recent studies on the systhesis of appropriate catalysts and an overview of literature mechanisms are provided.

2.1. The PEM Fuel Cell Plant

The genius behind the concept of the fuel cell is that it directly produces electricity from the chemical energy of fuels rather than their combustion followed by raising steam which drives a turbine that then drives an alternator to produce electricity. For example, in the case of the proton exchange membrane (PEM) fuel cell (see Figure 1), hydrogen is dissociated over a platinum catalyst at the anode into protons and electrons. The electrons proceed through an external circuit where their energy can be harnessed in the form of electricity and applied to a load (i.e., light bulb, etc.). The protons diffuse through the PEM and arrive at the cathode where they combine with oxygen and the energy-depleted electrons to form water. Thus, we find that only environmentally friendly by-products, water and heat, are produced, when pure hydrogen is the fuel.

However, the hydrogen from a reformer is not pure. The performance of the fuel cell depends heavily on the quality of the reformate stream that feeds the fuel cell. In a typical plant (see Figure 2), a hydrocarbon or alcohol fuel is fed to a reformer which converts the fuel and steam into CO_2, CO, H_2O, and H_2 at elevated temperatures in a

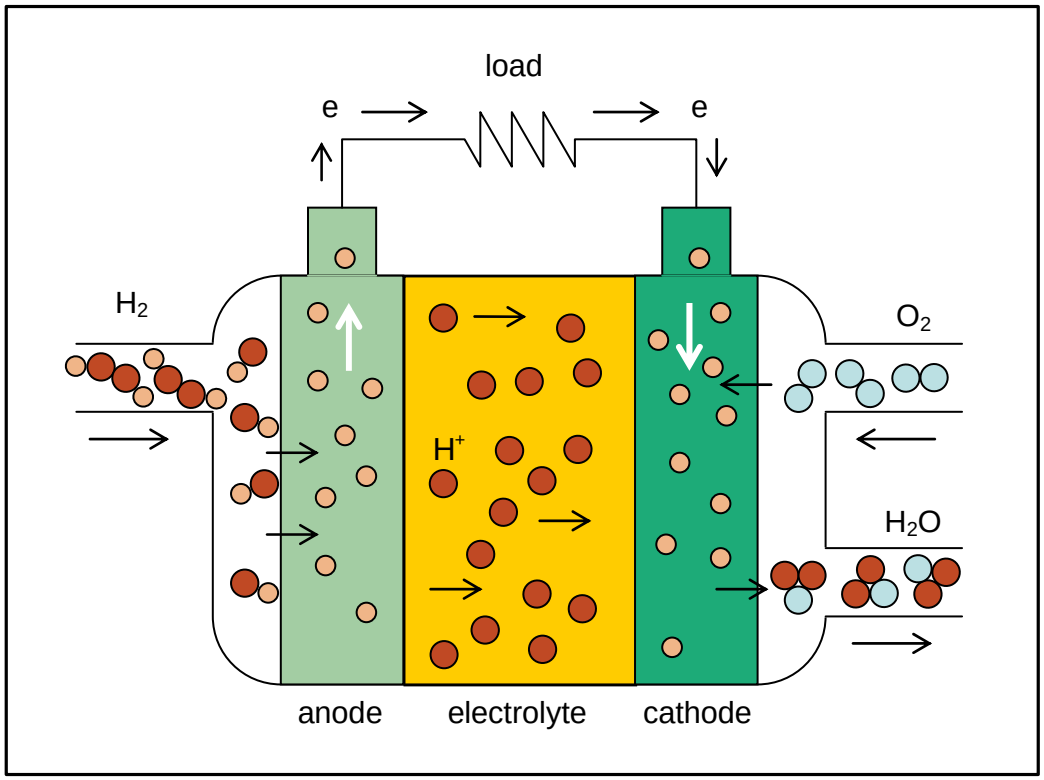

Figure 1. Schematic of a typical PEM fuel cell.

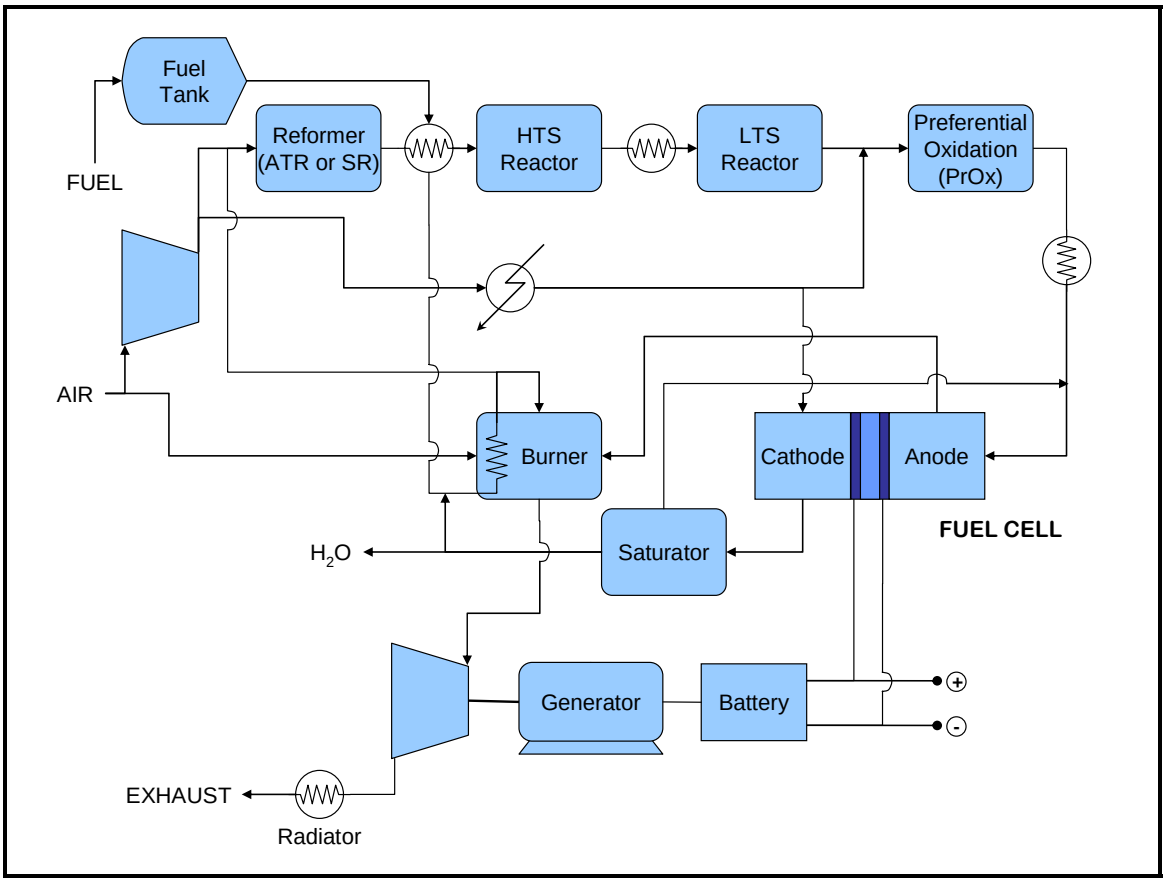

Figure 2. Schematic of a typical fuel cell plant.

catalytic process called steam reforming. In autothermal reforming (ATR), oxygen is also injected to provide the heat needed for the endothermic steam reforming [31]. Next, the reformer's reformate stream undergoes water-gas-shift (WGS) in two stages, high temperature shift (HTS) and low temperature shift (LTS):

$$H_2O + CO \leftrightarrows CO_2 + H_2. \qquad \left(\Delta H^{\circ} = -41.2 \text{ kJ/mol}\right) \qquad (1)$$

Both stages, thus, work to convert the energy trapped in the unwanted carbon monoxide into additional usable hydrogen for the fuel cell. The last step in the fuel processing. section is the PrOx, i.e., the preferential oxidation, unit [31]. This step provides further oxidation of the remaining CO to CO_2 in the reformate stream by oxygen before it is sent to the fuel cell. Ultimately, the amount of CO in the feed to the fuel cell should be below the tolerable level of 50 ppm, as it is toxic to the fuel cell operation [32,33]. Typically, the PrOx is operated at lower temperatures than the water-gas-shift and occurs over a highly selective precious-metal catalyst on which oxygen reacts with the unwanted CO without wasting substantial hydrogen.

Another poison that may need to be expelled prior to the fuel processing steps is sulfur. If the fuel contains sulfur, as most hydrocarbon fuels do, a desulphurization step is required to reduce the level of sulfur in the fuel processing reformation stream below the toxic level for reforming as well as fuel cell catalysts [31].

Once the reformate stream has achieved the desired composition, it proceeds to the anode of the fuel cell stack assembly where, as described above, the protons are separated from the electrons as they pass through the electrolyte membrane (in the case of the PEM fuel cell) while the electrons travel through the circuit creating electric current. This current may then be utilized to perform electric work before the protons and electrons reunite at the cathode with oxygen (typically from air) to form the environmentally benign by-products water and heat in addition to CO_2 from reformate. The CO_2 present in the reformate does not substantially affect the fuel cell performance and passes, largely unscathed, through the anode to the exhaust.

2.2. The Water-Gas Shift Reaction

The water-gas-shift (WGS) reaction, Equation (1), is an old industrial process in which water in the form of steam is mixed with carbon monoxide to obtain hydrogen and carbon dioxide. It has found new significance in fuel processing, in conjunction with fuel cells. The WGS reaction is reversible and exothermic (ΔH^{o} = -41.2 kJ/mol). Due to its moderate exothermicity, the WGS reaction is thermodynamically unfavorable at elevated temperatures. This is illustrated by the continuous decline and eventual sign change in the Gibbs free energy as a function of temperature, and the corresponding decreasing equilibrium constant as temperature increases (Figure 3). Of course, the kinetics of the catalytic reaction are more favorable at higher temperatures.

In order to overcome this thermodynamic limitation while maintaining high reaction rates, WGS is normally conducted in multiple adiabatic stages with inter-stage cooling to obtain higher conversions overall, i.e., high temperature shift (HTS) is conducted in the first stage where operation temperatures range 350°C to 600°C, while low temperature shift (LTS) occurs in the second stage with a temperature range of 150°C to 300°C. Different catalysts are employed in the two different stages [4]. For example, iron-based and copper-based catalysts are typically used industrially for HTS and LTS operations, respectively. The exact composition of these catalysts may vary according to their specific applications and their accompanying supports (i.e. ZnO/Al_2O_3, CeO_2, etc.).

For HTS operation, the catalyst is typically a combination of Fe_3O_4, the stable iron phase under reaction conditions, combined with chromia, which minimizes catalyst sintering by textural promotion. The typical composition of this HTS catalyst is approximately 55 wt.% Fe and 6 wt.% Cr [4]. The catalyst is usually unsupported and available commercially in tablet or ring form. The Fe_3O_4 catalyst is typically prepared via a precipitation process in the form Fe_2O_3. Upon reduction, the active magnetite form Fe_3O_4 is obtained. The activated catalyst is, however, pyrophoric. Upon exposure to air, the catalyst must be re-reduced and stabilized by surface oxidation (using an inert gas with a low concentration of oxygen) before being re-used.

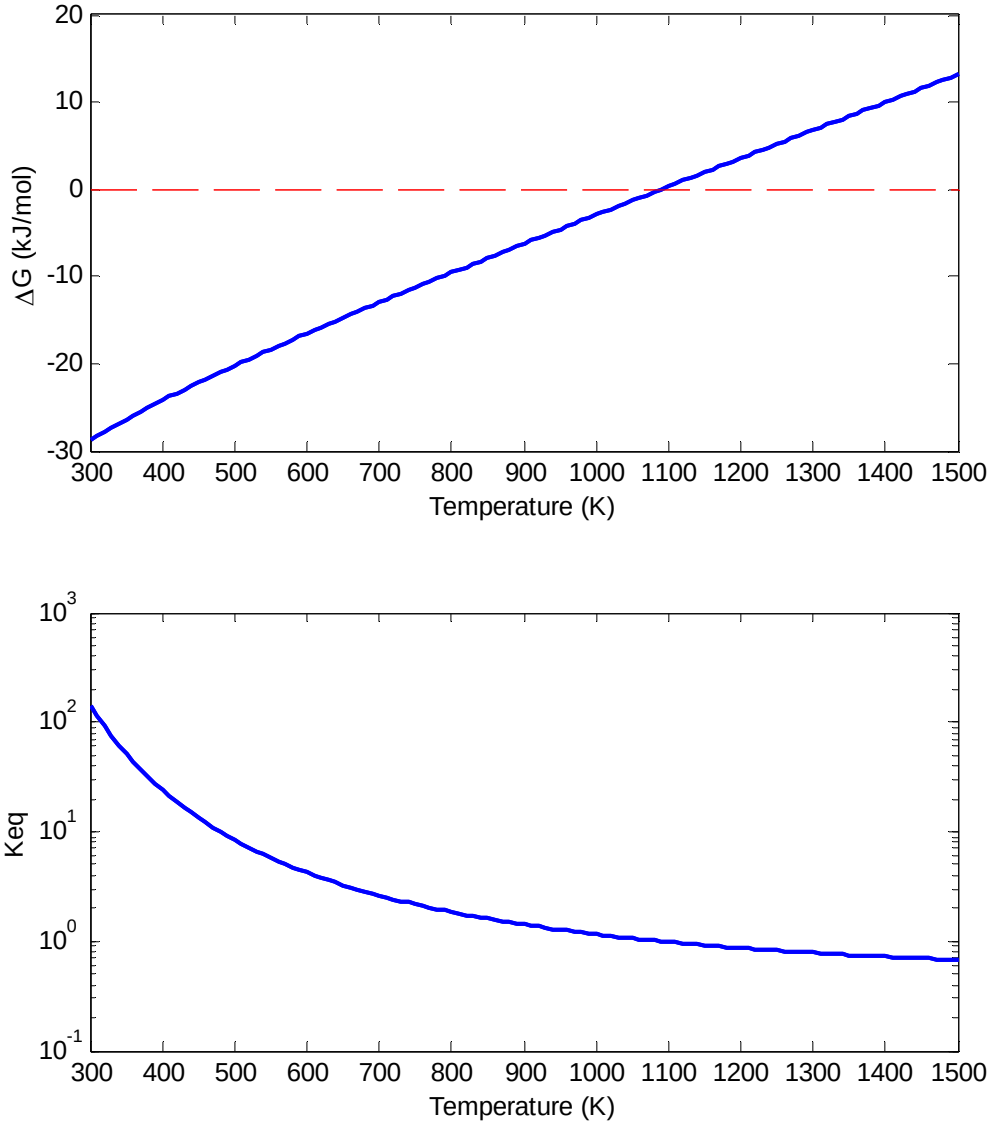

Figure 3. Thermodynamic equilibrium of the WGS reaction as described by the Gibbs free energy change and the equilibrium constant of the reaction as function of temperature. See Equations (121) and (122).

The HTS reactor must maintain an inlet temperature of 350^{o}C in order to achieve an adequate reaction rate. The maximum temperature is limited to 530-550^{o}C. The temperature, of course, rises due to the exothermic nature of the WGS reaction. The operating pressure is determined by the other steps in the process, but may be as high as 3 MPa [4]. The use of higher pressures increases the reaction rate, allowing for smaller reactors to be used. The typical catalyst contact time is approximately 3-9 seconds under normal pressures, but may be around 1 s for higher operation pressures [4].

The current typical LTS catalyst is a substantially improved version of the copper liquor used to remove CO from processes prior to 1962. The commercial LTS catalyst is composed of copper, zinc oxide, and alumina. The copper and zinc oxide forms are stable under reactions conditions. Copper, the active species, remains active at temperatures as low as 200^{o}C. The zinc oxide provides some protection of the copper from sulfur poisoning by reaction with adsorbed sulfur compounds while acting partially as a support for the copper. Before reduction, the composition of the catalyst is typically 32-33 wt.% CuO, 34-53 wt.% ZnO and 15-33 wt.% Al_2O_3. The reduction of CuO is highly exothermic and is carried out at temperatures not exceeding 220-230^{o}C to avoid sintering [4].

Because of the relatively low melting point of copper (1084.62^{o}C [34]), the commercial LTS catalyst is more sensitive to deactivation caused by sintering than the HTS catalyst. This causes the maximum operating temperature to be only around 250^{o}C, typically. When used in conjunction with HTS, the exit gas stream from the HTS unit must, therefore, be cooled, usually by quenching with water providing additional steam to the process, before passing through the LTS unit [4]. The used catalyst is pyrophoric and is typically discharged under nitrogen or another inert gas before being doused with water to avoid potential hazards.

2.3. Water-Gas Shift Catalysts

Due to the recent interest in fuel cell and fuel processing technology, a brief discussion of current WGS catalysts is provided next. While the review is not exhaustive, it hightlights the more recent work on catalysts examined in this research.

2.3.1. Copper-based Catalysts

Amadeo and Laborde [35] considered the WGS reaction on a commercial LTS catalyst of composition 32.7% CuO, 47% ZnO, and 11% Al_2O_3. The catalyst had a surface area of 42 m^2/g and a copper metallic surface area of 13 m^2/g with a pore volume of 0.11 cm^3/g. A stainless steel packed bed reactor was used and the entrance and exit gas compositions were analyzed by gas chromatography (HP 5730), equipped with a Porapak Q column. The catalyst was reduced *in situ* for 4 h at 453 K and 12 h at 503 K in a gas mixture of 1% H_2/N_2. Mass transfer limitations were avoided by optimizing the particle size and the feed flow rate conditions.

The effect of the partial pressure of each feed gas (CO, H_2O, CO_2, and H_2) on the CO conversion was analyzed. As the inlet partial pressures of CO_2 and H_2 were increased, the CO conversion was seen to decrease. In the cases of increasing H_2O partial pressure or decreasing CO partial pressure, the CO conversion increased. These trends hint as to the reaction orders of each of the reactants. Upon comparison of these experimental results to those of Campbell [36], it was noted that while some similarities exist due to the use of a similar catalyst, the major difference is the mass transfer limitations. Campbell worked in the presence of diffusion limitations while Amadeo and Laborde eliminated these resistances. In an attempt to fit these data by literature models, including some of those listed in Table 5, accurate results were not obtained. However, the general trends were observed.

Tanaka, et al. [37] also considered the WGS reaction on the commercial LTS catalyst $Cu/ZnO/Al_2O_3$. Two separate catalysts were prepared, one using impregnation and the other using coprecipitation. Both catalysts used the same support, γ-alumina (surface area, 164 m^2/g), and the same composition, 30 wt.% CuO/30 wt.% ZnO/Al_2O_3. The samples were reduced at 220°C for 2 h in 20% H_2/N_2. The experiments were

performed in a conventional flow reactor at atmospheric pressure in the temperature range 150-350^{o}C and at a constant space velocity of 6400 h^{-1}. The volume of catalyst used was 1.5 mL. The feed composition consisted of 37.5% H_2 1.25% CO, 25.0% H_2O, 12.5% CO_2, and balance N_2. The feed and product concentrations were determined using gas chromatography (Shimadzu, GC-8A equipped with a molecular sieve 13x column and a Porapak Q column) [37].

CO conversion increased as the catalyst was activated by the reaction gases with increasing temperature up to 200^{o}C. Thereafter, the conversion decreased due to the thermodynamic limitations at the elevated temperatures. While other catalyst loadings were examined, it was considered that the higher copper loading led to more abundant active components and a decrease in surface area. As a result, the active components should be dispersed only on the surface of the alumina support for the impregnated catalyst, resulting in the smaller loadings to be more favorable.

The effects of calcination temperature were also considered. Two samples of the impregnated catalyst were calcined at different temperatures, 500^{o}C and 900^{o}C. The CO conversion for the catalyst calcined at 500^{o}C was 86% while the other catalyst only achieved 61% [37]. The decrease is attributed to the lower surface area for the higher calcination temperatures.

Upon examination of catalyst deactivation, at lower concentrations (<15%), water vapor was found to yield stable and relatively high CO conversions. However, the catalyst deteriorated at 150^{o}C in the presence of oxygen. It was assumed that the WGS reaction over these catalysts proceeded via the redox mechanism where, at 150^{o}C, the water molecules cover the Cu surface prevented the adsorption of CO, hence, deteriorating the surface of the impregnated catalyst. The small pores that originally existed in the high surface alumina support were assumed to facilitate water adsorption. This is considered to be the reason why a similar situation was not observed on the coprecipitated catalysts [37].

Li, et al. [38] examined the activity of the CeO_2 supported Cu catalyst based on previous indications that Cu-CeO_2 was active for the WGS reaction at much lower temperatures than ceria alone. Steady-state kinetic measurements were obtained in the temperature range 175-300^{o}C. A quartz-tube flow reactor filled with 150 mg of catalyst

powder was used for the experiments. The feed gas composition consisted of 2 mol% CO, and 10.7 mol% H_2O, balance He and, when needed, 40 mol% H_2. The total flow rate of gases was 100 cm^3/min corresponding to a space velocity of 80000 h^{-1}. The samples were tested without activation. The exit composition was analyzed using gas chromatography (HP-5880A with a Carbosphere column) and an online CO_2 analyzer (Beckman Model 864). The conversion of CO was kept below 15% by adjusting either the amount of catalyst used or the gas flow rate.

At lower temperatures, the results suggested that the 5 at.% Cu-Ce(La)O_x catalyst showed similar activity to the activated commercial LTS catalyst. Variations in the metal content illustrated that there is no appreciable difference in the light-off temperature of the reaction caused by the metal loading. This suggested that only a small amount of Cu was necessary to change the WGS activity of ceria.

The effect of hydrogen was considered over a wide temperature range (200-350^{o}C) and did not yield any significant changes in the reaction. Above 350^{o}C, a decrease in the CO conversion was noted and attributed the lower equilibrium value that resulted from the additional hydrogen in the feed. Gas mixtures containing different ratios of H_2O/CO were compared after the same contact time. The results showed that the feed with the higher ratio had a consistently higher conversion than the lower ratio feed, but both reached the same maximum value. This suggested that the H_2O content of the feed is crucial to the success of the catalyst in the WGS reaction. It is also notable that the Cu-Ce(La)O_x catalysts required no activation and maintained its activity and stability at temperatures up to 600^{o}C.

2.3.2. Iron-based Catalysts

Xue, et al. [39] studied the WGS reaction on a commercial HTS Fe-Cr catalyst. The catalyst sample was crushed into particle sizes of 0.212 to 0.425 mm. The catalyst loading for the experiments was 200 mg. Reduction occurred by exposing the catalyst to reaction feed conditions for an extended period of time before performing the activity experiments. The activity experiments were conducted at atmospheric pressure in the temperature range 150^{o}C to 450^{o}C with a total feed flow rate of 50 cm^3/min (STP). The

concentrations of both the inlet and outlet were determined using a Carboxen 1000 column equipped HP 5980 II gas chromatograph.

For comparison, Xue, et al. [39] also considered the reaction without the use of a catalyst. It is known that the WGS reaction proceeds very slowly at "practical" temperatures. The results of the "blank test" showed no detectible conversion in the temperature range of interest. It was, however, observed that a thin layer of carbon formed on the quartz reactor surface when the reaction temperature was increased to $375^{o}C$.

In order to achieve higher conversions with the use of a catalyst and to avoid coking, the H_2O/CO feed ratio was higher than that required by the reaction stoichiometry. In the activity experiments, the feed composition consisted of 15% CO, 20% H_2O, 5% CO_2, 5% H_2 and balance N_2 (a H_2O/CO ratio of approximately 1.33) [39]. As a result of the increase in the H_2O/CO feed ratio, the energy efficiency of the reaction was low. It was noted that this may be overcome by the use of a H_2-separation membrane which would allow for both HTS and LTS to be carried out in one step with the use of an appropriate catalyst.

Potential problems that were considered as a result of a low H_2O/CO feed ratio include side reactions which may produce unwanted by-products such as carbon or methane. Some example side reactions are presented in Table 2. The formation of carbon blocks the catalyst sites causing catalyst deactivation and an increase in the pressure drop across the bed caused by plugging or fouling of the reactor. The formation of methane would consume hydrogen and alter the product composition causing potential difficulties in subsequent processes. As a result, it is important to consider the selectivity of the WGS catalyst to avoid these issues.

Zhao, et al. [40] examined the WGS reaction at a constant temperature of 670.8 K and various pressures in the range 0.1 – 1.4 MPa while maintaining a constant conversion at a space velocity of 1000 h^{-1} on a commercial iron oxide-based catalyst with a specific surface area of 45 m^2/g_{cat}. The composition of the catalyst, prior to reduction, was 63-75% Fe_2O_3, 12-14% Cr_2O_3 and 3.5-4.5% MgO. The size of the catalyst particles was estimated at 0.2-0.3 mm. The amount of catalyst in the reactor was 0.2 g. An internal circulating gradient-less reactor was used with rotation speeds of 2000-2500 rpm.

Table 2. Example side reactions producing unwanted by-products C and CH_4 [39,41]

Possible Side Reactions of the WGS Reaction
$2CO \leftrightarrows C + CO_2$
$CO + H_2 \leftrightarrows C + H_2O$
$CO_2 + 2H_2 \leftrightarrows C + 2H_2O$
$2CO + 2H_2 \leftrightarrows CO_2 + CH_4$
$CO + 3H_2 \leftrightarrows CH_4 + H_2O$
$CO_2 + 4H_2 \leftrightarrows CH_4 + 2H_2O$
$C + 2H_2 \leftrightarrows CH_4$
$4CO + 2H_2O \leftrightarrows CH_4 + 3CO_2$
$CH_4 + 2CO \leftrightarrows 3C + 2H_2O$
$CH_4 + CO_2 \leftrightarrows 2C + H_2O$

Reduction of the catalyst occurred by exposing the catalyst to reaction conditions over a series of temperature ramps: 1) 303 K to 473 K for 3h, 2) 473-523 K for 2 h, 3) 523-723 K for 3 h, and 4) 723 K for 5 h.

The feed composition was varied to collect data with the intent of applying the results to a variety of WGS models in the literature requiring data-fitted parameters. The results of their data-fitting suggested that a rate expression based on the Langmuir-Hinshelwood mechanism in which a surface reaction is the RLS was the most accurate when compared to the models of Bohlbro [42] and Temkin [27]. This conclusion was based on the effect of the system pressure on the reduced rate of the WGS reaction where the reduced rate is considered to be the ratio of the observed rate at pressure P to the rate at a set reference pressure P_o.

2.3.3. Nickel-based Catalysts

Li, et al. [38] have also examined the LTS over Ni-loaded cerium oxide catalysts. These cerium oxide-based WGS catalysts have become increasingly attractive due to the high oxygen-storage capacity of the ceria support. Ceria also acts as promoter for the WGS reaction. These studies of the WGS reaction were carried out in the temperature range of 250-300^oC at atmospheric pressure. A quartz-tube flow reactor, as described in Section 2.3.1, was used. All catalyst samples were used as prepared, without pretreatment or activation [38]. Analysis was performed using the gas chromatograph equipped with the online CO_2 analyzer, as described in Section 2.3.1. Again, the conversion of CO was kept below 15% by adjusting either the amount of catalyst used or the gas flow rate.

The Ni-Ce(La)O_x catalyst was found to be far superior than the support itself , i.e., Ce(La)O_x. The Ni composition of the Ni-Ce(La)O_x catalyst was varied based on various preparation methods. The 5 at.% Ni-Ce(La)O_x by coprecipitation catalyst showed a higher CO conversion to CO_2 when compared to either the 7 wt.% Ni-Ce(La)O_x catalyst or the 5 wt.% Ni-Ce(La)O_x catalyst, both prepared by incipient wetness impregnation. Reaction rate data at 250^oC show that the Ni-ceria system is much less active than its Cu-based counterpart at this relatively low temperature. This may be attributed to the lower reducibility of NiO on the support, which is present at temperatures up to 275^oC [38]. Thus, Ni may be a more appropriate catalyst at higher temperatures.

Schuurman, et al. [43] compared the effect of two different supports for Ni-based catalysts: Ni/SiO_2 and Ni/Al_2O_3. The nickel catalyst supported on silica had a BET surface area of 180 m^2/g while the nickel catalyst supported on α-alumina had a much lower BET surface area of 9 m^2/g. Both were prepared by impregnation with a $Ni(NH_3)_6NO_3$ solution for the silica support and a $NiCO_3$ solution for the α-alumina support. The catalysts were reduced under a H_2 flow at 773 K for 1 h at which point the flow was stopped and the reactor evacuated and heated to 600^oC for experiments.

TAP-style experiments [43] were conducted in which narrow pulses of reactant gases are introduced into a microreactor which is evacuated continuously. The exit composition was monitored using quadrupole mass spectrometry. The shape of the response reflects diffusion, adsorption, desorption and reaction of the reactants and products.

The reaction investigated was methane steam reforming, in which the WGS reaction plays a role. The results of the TAP experiments showed significant changes in the TAP responses (i.e. shape and intensity) according to the nature of the metal and/or support indicating changes in the kinetics of the reaction depending on the catalyst and its support. A higher methane conversion was observed on the Ni/Al_2O_3 catalyst. However, the H_2 selectivity of the Ni/SiO_2 catalyst was 10 times higher than that of the Ni/Al_2O_3 catalyst. These results suggested that the alumina support plays an intricate role in the reaction mechanism because of the effect of the acid/base groups on the supports. The silica support, consequently, appeared to have no effect on the reaction mechanism.

In conjunction with a kinetic investigation of methane steam reforming, Xu and Froment [41] studied the reverse WGS reaction on a $Ni/MgAl_2O_4$ catalyst. The catalyst contains 15.2% nickel supported on magnesium spinel with a BET surface area of 58 m^2 and a Ni surface area of 9.3 m^2/g_{cat} (fresh catalyst). The ring-shaped catalysts were crushed to 0.18-0.25 mm particles and packed in a bed with an inert solid diluent resulting in an approximate bed volume of 9 cm^3 consisting of 8 mL of diluent and 0.4 g catalyst.

To reduce the catalyst, hydrogen was flown through the bed and heated from room temperature to 1083K at a heat rate of 2K/min. The catalyst, under hydrogen, is then maintained at 1083K for 12 hours before being cooled to 823K, at which point

activity experiments commenced. A variety of feed conditions were examined to study the kinetics of methane steam reforming. It was determined that the activity of the Ni catalyst declined rapidly during the initial 24 hours, then more gradually. Kinetic experiments were initiated after the catalyst had been on-stream more than 70 hours, or when the deactivation had become essentially negligible. Xu and Froment noted that the decline in activity was probably due to the sintering of the Ni catalyst under the feed conditions. The reverse WGS studies were performed at temperatures lower than 673K and pressures ranging from 3-10 bar; the molar ratio of H_2/CO_2 was considered at 0.5 and 1.0.

In the development of a model to describe the experimental results, Xu and Froment made the following assumptions:

(1) H_2O reacts with surface Ni atoms, yielding O·S and $H_{2(g)}$
(2) CH_4 is adsorbed onto surface Ni atom, then the adsorbed CH_4 either reacts with O·S or dissociates to form chemisorbed radicals.
(3) The concentrations of carbon-containing radicals are much lower than the total concentration of the active sites.
(4) Adsorbed atomic oxygen oxidizes the carbon-containing radicals.
(5) Formed hydrogen directly releases to the gas phase and/or is in equilibrium with hydrogen-containing radicals.
(6) All plausible reaction schemes are believed to have a step corresponding to steam reforming (Table 2) or WGS, with a rate potentially much slower than that of the remaining steps in the scheme, thus controlling the rate of the *OR*, i.e., the RLS.

Thermodynamic analysis of the plausible reaction schemes suggest that those which form CO and CO_2 directly from CH_4 are not likely. The remaining 21 plausible reaction schemes were further reduced after model discrimination and parameter estimation based on experiemental results for both steam reforming as well as methanation and reverse WGS. Using the rate expressions developed for the resulting scheme [41], the activation energies for $CH_4 + H_2O \leftrightarrows CO + 3H_2$ and $CH_4 + 2H_2O \leftrightarrows CO_2 + 4H_2$ are 240.1 and 243.9

kJ/mol, respectively. In comparison to other researchers' results, Xu and Froment noted that other values are typically smaller than the enthalpy changes, most likely due to diffusional limitations or non-isothermal operation.

2.3.4. Gold-based Catalysts

Au/Fe_2O_3 and Au/TiO_2 catalysts have been shown [44] to posess, in spite of their supports' very different activities (high activity at high temperatures found on Fe_2O_3, while almost no activity found on TiO_2) and to exhibit very similar activity compared to each other and to the LTS WGS catalyst Cu/ZnO. Boccuzzi, et al. [44] prepared the catalysts by the deposition-precipitation method [44]. Au/Fe_2O_3 was prepared on a fresh iron hydroxide starting from gold tetrachloric acid. Au/TiO_2 was prepared on a TiO_2 anatase sample. Both catalyst samples contained approximately 3 wt.% precious metal. Before the experiments, the samples were calcined at 673 K and, in some cases, reduced at 523 K. The BET surface areas of the samples were determined as 66.5 m^2/g and 86.2 m^2/g for Au/Fe_2O_3 and Au/TiO_2, respectively [44]. The average particle size was 3-4 nm.

The WGS mechanism on Au/Fe_2O_3 was assumed to proceed via the dissociative adsorption of water onto the gold particles followed by spillover of active OH-groups onto adjacent sites of the ferric oxide resulting in the reoxidation of Fe^{2+} to Fe^{3+}. On Au/TiO_2, the adsorption of CO was assumed to be more probable.

A relationship between the WGS activity of metal-supported catalysts and the heat of CO adsorption was suggested by Grenoble [45], i.e., metals that chemisorb CO weakly, such as Au, have a low activity due to the low concentration of surface CO. The optimum strength of CO chemisorption on metals was identified as approximately 20 kcal/mol. The Au-CO bond strength is found to be in this energy range [44].

The Fourier Transform Infrared Spectroscopy (FTIR) results of H_2 and H_2O adsorption suggested that, on a Au/TiO_2 reduced sample, H_2 interaction on samples pretreated with O_2 results in the formation of OH groups rather than H_2O molecules. On Au/Fe_2O_3, the H_2 interaction results confirmed that, in this case, the gold particles are able to dissociate H_2 molecules [44]. Some of the adsorbed hydrogen atoms then proceeded to reduce the metal Fe^{3+} ions to Fe^{2+} ions creating a magnetite-like surface.

Upon examination of the WGS reaction as it occurs on the two samples, it was seen that for the case of Au/TiO_2, subjecting H_2O to pre-adsorbed CO produces CO_2 and bicarbonates at room temperature [44]. Based on the spectroscopic data, H_2O appears to act as an oxygen-donator to the metal surface. Furthermore, the H_2O molecules and OH groups are found to be adsorbed on the Au sites as well as the supports and their interfaces. The redox mechanism of the WGS reaction is assumed to explain these findings [44].

2.3.5. Platinum-based Catalysts

Serre, et al. [46] examined the WGS reaction on both Pt/Al_2O_3 and $Pt\text{-}CeO_2/Al_2O_3$ catalysts. The catalysts were prepared by wet impregnation of γ-alumina pellets with a specific area of 206 m^2/g, a pore volume of 0.54 cm^3/g, and a mean particle size of 2 mm. The actual catalysts' compositions were 14.5% CeO_2 for CeO_2/Al_2O_3, 2.13% Pt for 2% Pt/Al_2O_3, and 1.99% Pt-14.2% CeO_2 for 2% Pt-14.5% CeO_2/Al_2O_3. For the temperature programmed reduction (TPR) experiments, the mass of catalyst used was 4.72 g while a constant flow rate of 100 cm^3/min of 1.5 vol.% CO/He was maintained for reduction at 973 K [46]. After reduction, the catalysts were subjected to 1.5% CO + 1.5% O_2 feed and held at 973 K. Re-reduction occurred to verify reproducibility. After testing, the catalyst was oxidized at 5% O_2 overnight before being re-exposed to the 1.5% CO + 1.5% O_2 feed.

The results of the TPR experiments showed that the γ-alumina support exhibits a small amount of CO_2 formation at temperatures higher than 673 K and increases progressively to a maximum concentration of 6000 ppm at 973 K. The ceria support results showed that CO_2 was present between 573 K and 823 K due to the reduction of surface oxygen atoms. At higher temperatures, the reduction proceeds further but cannot be quantified due to the effects of the ongoing WGS reaction. As a result, it is concluded that, on the CeO_2/Al_2O_3 support, the TPR results are a superposition of those seen for both supports individually.

Oxidation of Pt/Al_2O_3 at 973 K in 1.5% CO + 1.5% O_2/He was accomplished before experiments began. At this temperature, Pt oxide is considered unstable, even under oxidation conditions [46]. Hence, the Pt/Al_2O_3 catalyst is already in the metallic

form and does not show any CO_2 present due to the catalyst reduction, as in the case of the γ-alumina support analysis. In the case of Pt-CeO_2/Al_2O_3, the observed CO_2 present is attributed to the CeO_2 surface reduction which starts at 413 K as opposed to the support without Pt which starts at 553 K. This suggests that platinum is implicated in the reduction of surface ceria, since it enables the reduction to occur at lower temperatures. In the case of H_2 reduction, the effect of Pt is attributed to H_2 spillover from the Pt particles yielding activated hydrogen atoms which ease the reduction of ceria.

2.3.6. Ruthenium-based Catalysts

Ruthenium belongs to the platinum-group metals which exhibit strong hydrogenating properties. Ru supported on oxides with acidic character are expected to yield catalysts with high activity compared to those supported on basic oxides. Basińska, et al. [47,48] studied a variety of catalysts to determine the effect of support on the performance of the catalyst. The catalysts were prepared on five different supports: MgO, La_2O_3, C (raw carbon), and two iron oxide supports, Fe_2O_3 (B) and Fe_2O_3 (D), obtained from β- and δ-FeOOH, respectively, and were examined. All catalysts contained 2 wt.% Ru. The surface area of the supports was relatively low (10-30 m^2/g) except for C which had a surface area more than one order of magnitude higher [48].

Since the iron oxides' reduction to FeO or Fe decreases the catalytic activity of the sample, the WGS reaction was conducted in the excess of steam (H_2O/CO ratio was 2.5) which stabilizes the Fe_3O_4 structure [48]. The B-series iron oxide support was found to have increasing surfaces area during the WGS reaction while the D-series support, with a higher activity, had decreasing surface area. However, these surface area changes did not yield observable effects in the catalysts' activities.

The activity in the WGS reaction for the studied catalysts is given in order of decreasing activity as Ru/La_2O_3 > Ru/Fe_2O_3 (D) >> Ru/Fe_2O_3 (B) > Ru/MgO >> Ru/C [48]. This suggests that the activity of the catalysts is related to the kind of support used. There was, however, no identifiable correlation between the activity and surface area of the support for the catalysts. The supports yielding low activity catalysts were MgO and Fe_2O_3 (B), and are characterized by a large contribution of mesopores. Raw carbon was

the worst support even though it had the largest contribution of mesopores with sizes comparable to those of the high activity supports Fe_2O_3 (D) and La_2O_3 [48].

2.3.7. Iridium-based Catalysts

Erdőhelyi, et al. [49] studied the WGS reaction on a variety of supported iridium catalysts including Ir/Al_2O_3, Ir/TiO_2, Ir/SiO_2, and Ir/MgO. Prior to this work, Grenoble, et al. [45] had compared the activity of alumina supported Group VII B, VIII and I B metals, finding that the Ir was the least active noble metal.

The catalysts were prepared via impregnation onto the desired support with a H_2IrCl_6 salt solution to yield a 5% metal catalyst. For the four supports listed above, the following BET surface areas were determined: γ-Al_2O_3 (100 m^2/g), TiO_2 (150 m^2/g), SiO_2 (200 m^2/g), and MgO (170 m^2/g) [49]. Pretreatment of the catalysts was performed in four steps: 1) oxidation for 30 min, 2) reduction in hydrogen flow for 60 min at 673 K, 3) evacuated/flushed with inert gas for 15 min at 673 K, and 4) cooled to reaction temperature in vacuum or in flowing inert gas.

The experiments were performed in a quartz fixed-bed flow reactor of length 240 mm. The amount of catalyst used was 0.5 g with space velocities in the range 3000 – 6000 h^{-1}. The feed consisted of approximately 15% water, which was introduced into the feed by bubbling a mixture of Ar and CO through preheated water reservoir. Thermal conductivity and flame ionization detectors equipped with a Porapak QS column were used to analyze the exit composition gas chromatographically [49].

The experiments showed that the effect of the support on the formation of CO_2 from adsorbed CO over supported Ir at 623 K decreased in efficiency in the order TiO_2 > Al_2O_3 > SiO_2 > MgO. The products of the WGS reaction over a supported-Ir catalyst were identified not only as CO_2 and H_2, but CH_4 was also found to be present. On Ir/TiO_2 some other hydrocarbons were also detected. In all cases, the CO_2/H_2 ratio was approximately 1. With the exception of the MgO supported Ir catalyst, no reaction was observed on the support alone. A 0.4% conversion was observed on Ir/MgO at 623 K [49]. Examination of the formation of the formate species in the WGS reaction mechanism showed that formate was found not only on the supported metals, but also the Al_2O_3 and MgO supports alone. The formate species is not considered stable on the SiO_2

surface, however the reaction rate is significant on the Ir/SiO_2 catalyst. As a result, it was suggested that the formate does not actually exist on the metal, but is found solely on the support.

Overall, the CO conversion was found to decrease in the order $Ir/TiO_2 > Ir/Al_2O_3 > Ir/SiO_2 \geq Ir/MgO$ [49]. It should be noted that the authors studied the WGS reaction over Ir/TiO_2 (mass of catalyst was 0.1g instead of 0.5g) in a lower temperature range (523-573 K) at the same contact time, and in the same temperature range, but at a lower contact time. The highest activity was obtained for Ir/TiO_2, followed by Ir/MgO, Ir/Al_2O_3 and Ir/SiO_2. The activities of Ir/TiO_2 and Ir/SiO_2 differed by more than an order of magnitude [49]. In comparing the reaction rates on these two catalysts, it was found that increasing the CO concentration only slightly changed the amounts of CO_2 and H_2 formed. The reaction orders were nearly the same on these two catalysts regardless of the fact that formate may be formed on TiO_2 and not on SiO_2. Therefore, although the supports are not totally inactive, the reaction rates are assumed to be several orders of magnitude lower than those on the supported metal.

2.4. Water-Gas Shift Mechanism and Kinetics

Because of the industrial significance of the water-gas-shift reaction, many researchers (see Table 3) have investigated the reaction mechanism and developed models to reflect the behavior of the reaction over common industrial catalysts (i.e., copper or iron-based). The results of several of these investigations suggest that the WGS reaction largely occurs via four specific mechanisms: 1) the redox mechanism [8,10,14-16,27,50,51], 2) the formate mechanism [14,50,52-54], 3) the associative mechanism [7,11,55], and, more recently, 4) the carbonate mechanism [15,16,56-59]. The first mechanism implies a successive oxidation by adsorbed oxygen from H_2O and reduction of the reactive catalyst surface by CO occurs as CO is oxidized to CO_2, i.e., s_{27} and s_{28} from Table 3. In the second mechanism, adsorbed water dissociates into an adsorbed hydroxyl group and adsorbed atomic hydrogen, i.e., s_3. The hydroxyl group then combines with adsorbed carbon monoxide to form adsorbed formate, i.e., s_5, which

Table 3. Water-gas shift reaction mechanisms in the literature (S = catalyst site).

		Formate Mechanism						Redox Mechanism								Carbonate Mechanism		Other Mechanisms			
		i	ii	iii	iv	v	vi	vii	viii	ix	x	xi	xii	xiii	xiv	xv	xvi	xvii	xviii	xix	xx
	Elementary Reaction Steps	**WPI Mechanism**	**van Herwijen & de Jong (1980) [54,66]**	**Campbell & Daube (1987) [50]**	**Shido & Iwasawa (1993) [53]**	**Askgaard, et al. (1995) [52]**	**Ovesen, et al. (1996) [14]**	**Temkin (1979) [27]**	**Cambell & Daube (1987) [50]**	**Nakamura, et al. (1990) [8]**	**Ovesen, et al. (1992) [10]**	**Ovesen, et al. (1996) [14]**	**Tserpe & Waugh (1997) [15]**	**Waugh (1999) [16,65]**	**Schunnacher, et al. (2005) [51]**	**Millar, et al. (1991) [57]**	**Lund (2001) [56,58]**	**Graven & Long (1954) [64]**	**Mhadeshwar & Vlachos (2005) [62,63]**	**Teng, et al. (2005) [61]**	**Zeigarnik, et al. (2005) [60]**
s_1	$CO + S \leftrightarrows CO{\cdot}S$	■	■	■		■			■	■	■	■	■	■	■				■	■	■
s_2	$H_2O + S \leftrightarrows H_2O{\cdot}S$	■		■		■			■	■	■	■	■	■	■		■		■	■	■
s_3	$H_2O{\cdot}S + S \leftrightarrows OH{\cdot}S + H{\cdot}S$	■(rls)		■(rls)		■			■(rls)	■(rls)	■	■	■	■	■(rls)		■		■		■
s_4	$CO{\cdot}S + O{\cdot}S \leftrightarrows CO_2{\cdot}S + S$	■(rls)				■					■	■	■	■	■(rls)				■	■	■
s_5	$CO{\cdot}S + OH{\cdot}S \leftrightarrows HCOO{\cdot}S + S$	■(rls)		■	■															■	■
s_6	$OH{\cdot}S + S \leftrightarrows O{\cdot}S + H{\cdot}S$	■				■			■	■(rls)	■	■	■	■	■(rls)				■	■	■
s_7	$CO{\cdot}S + OH{\cdot}S \leftrightarrows CO_2{\cdot}S + H{\cdot}S$	■(rls)																	■		■
s_8	$HCOO{\cdot}S + S \leftrightarrows CO_2{\cdot}S + H{\cdot}S$	■(rls)				■	■								■						■
s_9	$HCOO{\cdot}S + O{\cdot}S \leftrightarrows CO_2{\cdot}S + OH{\cdot}S$	■																			■
s_{10}	$H_2O{\cdot}S + O{\cdot}S \leftrightarrows 2OH{\cdot}S$	■				■				■	■	■			■		■		■		■
s_{11}	$H_2O{\cdot}S + H{\cdot}S \leftrightarrows OH{\cdot}S + H_2{\cdot}S$	■																			■
s_{12}	$OH{\cdot}S + H{\cdot}S \leftrightarrows O{\cdot}S + H_2{\cdot}S$	■(rls)																			■
s_{13}	$HCOO{\cdot}S + OH{\cdot}S \leftrightarrows CO_2{\cdot}S + H_2O{\cdot}S$	■																			■
s_{14}	$HCOO{\cdot}S + H{\cdot}S \leftrightarrows CO_2{\cdot}S + H_2{\cdot}S$	■			■																■
s_{15}	$CO_2{\cdot}S \leftrightarrows CO_2 + S$	■				■					■	■	■	■	■				■	■	■
s_{16}	$H{\cdot}S + H{\cdot}S \leftrightarrows H_2{\cdot}S + S$	■											■	■							■
s_{17}	$H_2{\cdot}S \leftrightarrows H_2 + S$	■	■										■	■							■
s_{18}	$2H{\cdot}S \leftrightarrows H_2 + 2S$	■		■		■				■	■	■			■		■		■	■	
s_{19}	$H_2O{\cdot}S + S \leftrightarrows O{\cdot}S + H_2{\cdot}S$																				■
s_{20}	$HCOO{\cdot}S \leftrightarrows CO_2 + H{\cdot}S$			■(rls)																■	

Table 3. Water-gas shift reaction mechanisms in the literature (S = catalyst site). *(continued)*

			Formate Mechanism					Redox Mechanism								Carbonate Mechanism		Other Mechanisms			
		i	ii	iii	iv	v	vi	vii	viii	ix	x	xi	xii	xiii	xiv	xv	xvi	xvii	xviii	xix	xx
	Elementary Reaction Steps	WPI Mechanism	van Herwijen & de Jong (1980) [54,66]	Campbell & Daube (1987) [50]	Shido & Iwasawa (1993) [53]	Askgaard, et al. (1995) [52]	Oresen, et al. (1996) [14]	Temkin (1979) [27]	Cambell & Daube (1987) [50]	Nakamura, et al. (1990) [8]	Oresen, et al. (1992) [10]	Oresen, et al. (1996) [14]	Tserpe & Waugh (1997) [15]	Waugh (1999) [16,65]	Schumacher, et al. (2005) [51]	Millar, et al. (1991) [57]	Lund (2001) [56,58]	Graven & Long (1954) [64]	Mhadeshwar & Vlachos (2005) [62,63]	Teng, et al. (2005) [61]	Zeigarnik, et al. (2005) [60]
s_{21}	$CO{\cdot}S + O{\cdot}S \leftrightarrows CO_2 + 2S$								■	■						■				■	
s_{22}	$H_2 + O{\cdot}S \leftrightarrows H_2O{\cdot}S$									■											
s_{23}	$CO + 2O{\cdot}S \leftrightarrows CO_3{\cdot}S_2$															■	■				
s_{24}	$CO_3{\cdot}S_2 \leftrightarrows CO_3{\cdot}S + S$																■				
s_{25}	$CO_3{\cdot}S \leftrightarrows CO_2 + S$																■				
s_{26}	$2OH{\cdot}S \leftrightarrows 2O{\cdot}S + H_2$																■				
s_{27}	$H_2O + S \leftrightarrows O{\cdot}S + H_2$							■		■			■								
s_{28}	$O{\cdot}S + CO \leftrightarrows CO_2 + S$							■		■			■								
s_{29}	$CO_2 + O{\cdot}S \leftrightarrows CO_3{\cdot}S$												■								
s_{30}	$HCOO{\cdot}S + H{\cdot}S \leftrightarrows CO{\cdot}S + H_2O{\cdot}S$																			■	
s_{31}	$CO{\cdot}S + H_2O \leftrightarrows HCOOH{\cdot}S$		■																		
s_{32}	$HCOOH{\cdot}S \leftrightarrows HCOOH + S$		■																		
s_{33}	$2OH{\cdot}S \leftrightarrows H_2O + O{\cdot}S$									■											
s_{34}	$HCOOH{\cdot}S \leftrightarrows H_2{\cdot}S + CO_2$		■																		
s_{35}	$HCOOH \leftrightarrows H_2 + CO_2$		■																		
s_{36}	$HCOOH \leftrightarrows H_2O + CO$		■																		
s_{37}	$2HCOOH \leftrightarrows HCOH + H_2O + CO_2$		■																		
s_{38}	$HCOO{\cdot}S + H{\cdot}S \leftrightarrows H_2COO{\cdot}S + S$						■														
s_{39}	$H_2COO{\cdot}S + 4H{\cdot}S \leftrightarrows CH_3OH + H_2O + 5S$						■														
s_{40}	$H_2O + 2S \leftrightarrows OH{\cdot}S + H{\cdot}S$																			■	

Table 3. Water-gas shift reaction mechanisms in the literature (S = catalyst site). *(continued)*

			Formate Mechanism					Redox Mechanism								Carbonate Mechanism		Other Mechanisms			
		i	ii	iii	iv	v	vi	vii	viii	ix	x	xi	xii	xiii	xiv	xv	xvi	xvii	xviii	xix	xx
	Elementary Reaction Steps	WPI Mechanism	van Herwijen & de Jong (1980) [54,66]	Campbell & Daube (1987) [50]	Shido & Iwasawa (1993) [53]	Askgaard, et al. (1995) [52]	Oresen, et al. (1996) [14]	Temkin (1979) [27]	Cambell & Daube (1987) [50]	Nakamura, et al. (1990) [8]	Oresen, et al. (1992) [10]	Oresen, et al. (1996) [14]	Tserpe & Waugh (1997) [15]	Waugh (1999) [16,65]	Schumacher, et al. (2005) [51]	Millar, et al. (1991) [57]	Lund (2001) [56,58]	Graven & Long (1954) [64]	Mhadeshwar & Vlachos (2005) [62,63]	Teng, et al. (2005) [61]	Zeigarnik, et al. (2005) [60]
s_{41}	$H_2 + M \rightarrow 2H + M$																	■			
s_{42}	$H + CO_2 \leftrightarrows OH + CO$																	■			
s_{43}	$OH + H_2 \leftrightarrows H + H_2O$																	■			
s_{44}	$2H + M \rightarrow H_2 + M$																	■			
s_{45}	$O_2 + 2S \leftrightarrows 2O{\cdot}S$																		■		
s_{46}	$OH + S \leftrightarrows OH{\cdot}S$																		■		
s_{47}	$H + S \leftrightarrows H{\cdot}S$																		■		
s_{48}	$O + S \leftrightarrows O{\cdot}S$																		■		
s_{49}	$COOH + S \leftrightarrows COOH{\cdot}S$																		■		
s_{50}	$COOH{\cdot}S + S \leftrightarrows CO{\cdot}S + OH{\cdot}S$																		■		
s_{51}	$COOH{\cdot}S + S \leftrightarrows CO_2{\cdot}S + H{\cdot}S$																		■		
s_{52}	$COOH{\cdot}S + H{\cdot}S \leftrightarrows CO{\cdot}S + H_2O{\cdot}S$																		■		
s_{53}	$COOH{\cdot}S + O{\cdot}S \leftrightarrows CO_2{\cdot}S + OH{\cdot}S$																		■		
s_{54}	$COOH{\cdot}S + OH{\cdot}S \leftrightarrows CO_2{\cdot}S + H_2O{\cdot}S$																		■		
s_{55}	$HCOO + 2S \leftrightarrows HCOO{\cdot}S_2$																		■		
s_{56}	$HCOO{\cdot}S_2 \leftrightarrows CO_2{\cdot}S + H{\cdot}S$																		■		
s_{57}	$HCOO{\cdot}S_2 + O{\cdot}S \leftrightarrows CO_2{\cdot}S + OH{\cdot}S + S$																		■		
s_{58}	$HCOO{\cdot}S_2 + OH{\cdot}S \leftrightarrows CO_2{\cdot}S + H_2O{\cdot}S + S$																		■		
s_{59}	$H_2 + O{\cdot}S + S \leftrightarrows H{\cdot}S + OH{\cdot}S$															■					
s_{60}	$HCOOH{\cdot}S \leftrightarrows HCOO{\cdot}S + H{\cdot}S$															■					

eventually decomposes into carbon dioxide and hydrogen via s_8, yielding the WGS products. Finally, in the associative mechanism adsorbed water dissociates into an adsorbed OH and atomic hydrogen, i.e., s_3. The adsorbed hydroxyl then oxidizes adsorbed CO resulting in adsorbed CO_2 and atomic hydrogen, i.e., s_7. In addition to the redox and associative mechanisms, researchers have also proposed that the WGS reaction may proceed via a carbonate mechanism.

In attempts to model and predict the real behavior of the WGS reaction some researchers have considered more general mechanisms often comprising elementary reaction steps from the more recognized mechanisms. Table 3 provides a comprehensive collection of the mechanisms considered so far in the literature. In the following sections, the different mechanistic categories are discussed.

2.4.1. The Formate Mechanism

Campbell and Daube [50] explored the water-gas-shift reaction in terms of a formate mechanism, given in Table 4, where S represents a surface site. Believed to have been the first to examine and present the effects of the WGS reaction on a single crystal copper catalyst, their experiments were performed in a UHV chamber adapted for surface analysis using XPS, AES, LEED and TDS and equipped with a microreactor for kinetic studies. Surface analysis by AES, after reduction, indicated low levels of carbon and sulfur. The carbon levels were irreproducible and, therefore, not considered as an intermediate species but attributed to impurities in the feed gases or displaced from the reactor walls by water adsorption. The consistently "clean" LEED pattern suggested that, providing that the surface structure was not altered by the reaction or analysis, the WGS reaction may occur on an oxygen-free surface [50]. Surface study results indicated that water both adsorbs and desorbs molecularly on a clean copper surface.

Experimental investigation of the catalyst's surface suggested that CO and H_2O coverages are very low under reaction conditions resulting in a rate that is nearly independent of the partial pressure of CO and a strong increase with the partial pressure of H_2O. This was explained by the inclusion of a hydroxyl intermediate formed from the surface dissociation of adsorbed water. Furthermore, step 3, the dissociation of H_2O into a surface hydroxyl and an adsorbed hydrogen atom, was identified as the rate-limiting

Table 4. Formate mechanism for the water-gas-shift reaction [50].

Formate Reaction Mechanism	
$CO + S \leftrightarrows CO{\cdot}S$	(s_1)
$H_2O + S \leftrightarrows H_2O{\cdot}S$	(s_2)
$H_2O{\cdot}S + S \leftrightarrows OH{\cdot}S + H{\cdot}S$	(s_3)
$CO{\cdot}S + OH{\cdot}S \leftrightarrows HCOO{\cdot}S + S$	(s_5)
$HCOO{\cdot}S \leftrightarrows CO_2 + H{\cdot}S$	(s_{20})
$2H{\cdot}S \leftrightarrows H_2 + 2{\cdot}S$	(s_{18})
$CO + H_2O \leftrightarrows CO_2 + H_2$	(*OR)*

step. These surface hydroxyls were then readily consumed by adsorbed CO resulting in a formate intermediate. Under high pressures and low temperatures, the decomposition of formate was considered rate controlling. While the authors acknowledge that there is some controversy over the dissociation of water, it was noted that the presence of adsorbed oxygen can significantly enhance the WGS reaction via $H_2O{\cdot}S + O{\cdot}S \leftrightarrows OH{\cdot}S + OH{\cdot}S$.

To explain this, Campbell and Daube [50] also considered a surface redox mechanism in which the OH·S produced in step 3 of the formate mechanism further dissociates into O·S and H·S. The O·S was then assumed to be consumed rapidly by adsorbed CO in the step $CO{\cdot}S + O{\cdot}S \leftrightarrows CO_2 + 2S$. This alternate mechanism also assumes that step 3 is still rate-limiting and is reinforced by their experimental findings. That is to say, that the surface reaction proceeds rapidly to equilibrium. As a result, it was noted that the activation energy of step 3 should be interpreted as the sum of the net enthalpy for the equilibrium step and the activation energy for hydroxyl dissociation ($OH{\cdot}S + S \leftrightarrows O{\cdot}S + H{\cdot}S$).

Campbell and Daube [50] utilize the analytical expression proposed earlier by van Hewijnen and De Jong [67] to correlate and predict their experimental results accurately. The work of van Hewijnen and De Jong [67] was to find kinetic evidence of the formate mechanism through the study of both the forward and reverse WGS reactions. A critique by van Hewijnen and De Jong [67] of several potential WGS models developed by other researchers follows (see Table 5).

Van Herwijnen and De Jong [67] report that Campbell's model [36], while "derived after careful consideration of plant data and semi-technical results" [67], the data on which the derived expression is based are not reported. Furthermore, Campbell, et al. [36] stated that the catalyst used causes the WGS reaction to be pore diffusion limited at temperatures above 200°C. A similar critique was made for the rate expression developed by Moe [68].

Van Herwijnen and De Jong also report that Shchibrya, et al. [69] applied their rate equation, developed for iron oxide/chromium oxide-catalyzed WGS, to data from $Cu/ZnO/Cr_2O_3$-catalyzed WGS. The derivation of this equation was based on the assumption that the redox mechanism applies to Cu/ZnO suggesting that oxidation by

Table 5. Potential water-gas shift reaction rate expressions examined by van Herwijinen and De Jong [67].

Research Group	Rate Expression
Campbell, et al. [36]	$r = \frac{kP_{CO}P_{H_2O}}{\left(1 + K_1P_{CO} + K_2P_{H_2O} + K_3P_{CO_2} + K_4P_{H_2}\right)^2}\left(1-\beta\right)$
Moe [68]	$r = kP_{CO}P_{H_2O}\left(1-\beta\right)$
Shchibrya, et al. [69]	$r = \frac{kP_{H_2O}P_{CO}}{AP_{H_2O} + P_{CO_2}}\left(1-\beta\right)$
Kul'kova-Temkin [70]	$r = kP_{CO}\left(\frac{P_{H_2O}}{P_{H_2}}\right)^{\frac{1}{2}}\left(1-\beta\right)$
Goodridge-Quazi [71]	$r = kP_{CO}^{a}P_{H_2O}^{b}P_{CO_2}^{c}P_{H_2}^{d}$

where $\beta = \frac{P_{CO_2}P_{H_2}}{KP_{CO}P_{H_2O}}$

water is the rate determining step. The rate expression derived by Kul'kova and Temkin [70] is based on assumptions similar to those of Shchibrya, et al. The power law rate equation published by Goodridge and Quazi [71] for a $Cu/ZnO/Cr_2O_3$ catalyst yields very low apparent activation energies suggesting diffusional limitations in the experimental data.

The rate expressions developed by van Herwijnen and De Jong [67] is based on their experimental results. For the forward WGS reaction, with only CO and H_2O in the feed, rate data as a function of mole fraction of water in the feed and temperature showed that at lower temperatures, the observed rate has a weak dependence on feed composition while at higher temperatures, the maximum rate occured at a lower feed concentration of water than at lower temperatures.

Assuming Langmuir adsorption, the numerical data are manipulated to indicate the form of the rate expression. The rate is reported, generally, as

$$\vec{r} = \frac{k x_{H_2O} x_{CO}}{1 + K_{CO \cdot H_2O} x_{CO} x_{H_2O} + K_{CO} x_{CO} + K_{H_2O} x_{H_2O}} \tag{2}$$

Recalling that the feed only contains CO and H_2O and assuming negligible mole fraction of product, Equation (2) may be written in terms of equilibrium constants and only the mole fraction of water in the feed. The resulting expression is

$$\vec{r} = \frac{k x_{H_2O} \left(1 - x_{H_2O}\right)}{1 + K_1 x_{H_2O} \left(1 - x_{H_2O}\right) + K_2 \left(1 - x_{H_2O}\right) + K_3 x_{H_2O}} \tag{3}$$

This expression was then fitted to the measured data. After optimization of the parameters to minimize the difference between the observed and calculated rates, the following expression was given for the rate of the forward WGS reaction in moles/g·s [67]

$$\vec{r} = \frac{25.8 \times 10^3 \exp\left(-\frac{16000}{k_B T}\right) P_{CO} P_{H_2O}}{1 + 127 P_{CO} P_{H_2O} + 26 P_{CO}} \tag{4}$$

For the case of the reverse WGS reaction, experimental data with only CO_2 and H_2 in the feed were also collected by van Herwijinen and De Jong [67]. The rate equation may be then written in terms of equilibrium constants and the mole fraction of CO_2 in the feed and is

$$\overleftarrow{r} = \frac{k x_{CO_2} \left(1 - x_{CO_2}\right)}{1 + K x_{CO_2} \left(1 - x_{CO_2}\right) + B x_{CO_2}} \tag{5}$$

where Bx_{CO_2} is positive if the term originates from CO_2 adsorption and negative in the case of H_2 adsorption. The experimental data indicate that the maximum rate occurs when $x_{CO_2} \gg 0.5$, therefore, B is a negative constant [67].

Using a similar data analysis procedure as in the case of the forward WGS reaction the rate expression is expected to take the form.

$$\overleftarrow{r} = \frac{k P_{CO_2} P_{H_2}}{1 + K_{CO_2 \cdot H_2} P_{CO_2} P_{H_2} + K_{H_2} P_{H_2}} \tag{6}$$

After fitting the measured rates and optimization, the rate of the reverse WGS reaction is given in moles/g·s by [67]

$$\overleftarrow{r} = \frac{4.29 \times 10^5 \exp\left(-\frac{23000}{k_B T}\right) P_{CO_2} P_{H_2}}{1 + 40 P_{CO_2} P_{H_2O} + 3.66 \times 10^{-6} \exp\left(\frac{13100}{k_B T}\right) P_{H_2}} \tag{7}$$

Thus, Equations (4) and (7) of van Herwijinen and De Jong [67] provide empirical rate expressions for the forward and reverse WGS reactions.

Shido and Iwasawa [53] examined the reverse WGS reaction to investigate the behavior of surface formates and their role in the elementary reaction steps. Experimental results showed that water molecules dissociate on the oxide surfaces to form the hydroxyl species, which then forms the formate intermediate. It was also determined that the formate intermediate does not actually produce gaseous H_2 or CO_2 as suggested by Campbell and Daube [50]. Results of TPD experiments showed that 70% of the formates produced yield OH·S and CO·S, but then revert back to formate while the remaining 30% actually decompose into the desired products [53]. It was also observed that formate may decompose into H_2O·S and CO·S when combined with surface hydroxyl. Alternatively, it was also suggested that when combined with adsorbed atomic hydrogen, formate may produce H_2·S and CO_2·S. Based on their experiemtnal results, Shido and Iwasawa concluded that both the forward and reverse WGS reaction may occur via a formate intermediate [53].

Askgaard, et al [52] considered a kinetic model of methanol synthesis on a Cu(100) single crystal catalyst. It is now generally accepted that methanol synthesis is described by the following two reactions, including the WGS reaction,

$$CO + H_2O \leftrightarrows CO_2 + H_2$$
$$CO_2 + 3H_2 \leftrightarrows CH_3OH + H_2O$$

Within the authors' mechanism for methanol synthesis is a sub-set of elementary reaction steps that produce the WGS reaction. This sub-mechanism is based on that presented by Nakamura, et al. [8] and Ovesen, et al [10] as described later in Section 2.4.2. Surface experiments using IR vibrational spectroscopy and temperature programmed reaction studies confirmed the existence of formate on the catalyst surface. Its presence was further confirmed using XPS, EELS, and TPD.

2.4.2. The Redox Mechanism

2.4.2.1 Temkin's Two-Step Redox Mechanism

A well known two-step redox mechanism of the WGS reaction is that of Temkin [27]. Temkin's work acknowledges the high temperature shift (400-500°C) as the part of the process that converts most of the carbon monoxide to usable hydrogen. Furthermore, a supplementary conversion is obtained through low temperature shift (200-250°C) using a low-temperature catalyst. In his work, Temkin focuses on the reaction over a high temperature catalyst that was prepared by combining Cr_2O_3 with Fe_2O_3. The catalyst contained, prior to reduction, 93% Fe_2O_3 and 7% Cr_2O_3, which is used to prevent sintering of the catalyst, with a specific surface area of 20 m^2/g, a bed density of 1.37 g/cm^3 and catalyst particles of the size 0.5-1.0 mm. The catalyst was then reduced using hydrogen or carbon monoxide with excess steam yielding the active magnetite form, Fe_3O_4. The reaction was performed in a flow system at atmospheric pressure and various temperatures within the region of interest. Temkin's two-step redox mechanism for the water-gas-shift reaction is given in Table 6, wherein the key surface intermediate of interest is adsorbed atomic oxygen.

Equilibrium-adsorption studies of oxygen on the Fe_3O_4 surface with hydrogen and steam were conducted. Experimental data suggested that the higher the ratio of P_{H_2} / P_{H_2O} in the reactant mixture, the greater the decrease in catalyst weight. This was found to agree with the decreasing amount of hydrogen in the gas phase due to the production of steam [27]. Mathematically, these results were represented by

$$P_{O_2} = \left[K_{H_2O} \left(\frac{P_{H_2O}}{P_{H_2}} \right) \right]^2 \tag{8}$$

where K_{H_2O} is the equilibrium constant of the reaction $H_2O_{(g)} \leftrightarrows H_2 + \frac{1}{2}O_2$.

From the observed experimental reaction rates (r), the forward reaction rate ($\vec{r}$) was determined using

Table 6. Temkin's two-step redox mechanism for the water-gas-shift reaction [27]

Two-Step Redox Reaction Mechanism	
$H_2O + S \leftrightarrows O{\cdot}S + H_2$	(s_{27})
$O{\cdot}S + CO \leftrightarrows CO_2 + S$	(s_{28})
$CO + H_2O \leftrightarrows CO_2 + H_2$	(*OR*)

$$\vec{r} = \frac{r}{1 - \frac{1}{K}\left(\frac{P_{CO_2} P_{H_2}}{P_{CO} P_{H_2O}}\right)} = \frac{r}{1 - \exp\left(-\frac{A}{R_{gas} T}\right)} \tag{9}$$

where A is the affinity of the overall reaction. Experimental data agreed with the following representation of the forward rate:

$$\vec{r} = \frac{k P_{CO} P_{H_2O}}{\chi P_{H_2O} + P_{CO_2}} \tag{10}$$

where k and χ are temperature dependent constants. The constant χ was expressed based on experimental data as a function of temperature by [27]

$$\log \chi = -\frac{8800}{4.57T} + 2.31 \tag{11}$$

with the reaction rate being evaluated in terms of volume of CO (reduced to 0°C and 1 atm) that reacts per second in a unit volume of catalyst bed with partial pressures expressed in atmospheres. The following equation was provided for the constant k as a function of temperature [27]

$$\log k = -\frac{34000}{4.57T} + 10.3 \tag{12}$$

where k has the units $sec^{-1}atm^{-1}$.

The results of earlier experimental work by Kul'kova and Temkin [70] were fitted to an empirical rate expression which correctly predicted the rate for medium surface coverages. This equation was derived from a more general expression:

$$r = k\frac{P_{A_1}P_{A_2} - K^{-1}P_{B_1}P_{B_2}}{\left(AP_{A_1} + P_{B_2}\right)^m \left(AK^{-1}P_{B_1} + P_{A_2}\right)^{1-m}} \tag{13}$$

and assumes that $\chi K^{-1} \gg 1$ and hence $\chi \gg 1$ since, in the temperature range of interest, the WGS equilibrium constant, $K > 1$. Upon simplification of Equation (13), the following expression results [27]

$$r = \vec{k}P_{CO}\left(\frac{P_{H_2O}}{P_{H_2}}\right)^n - \overleftarrow{k}P_{CO_2}\left(\frac{P_{H_2}}{P_{H_2O}}\right)^{1-n} \tag{14}$$

where $n = 1 - m$, and m ($0 \le m \le 1$) describes the coverage of the surface. When $m = 1$, the surface is categorized as high coverage. When $m = 0$, the surface is considered under low coverage. The rate constants $\vec{k}$ and $\overleftarrow{k}$ were given by $\vec{k} = kK^n / \chi$ and $\overleftarrow{k} = kK^{1-n} / \chi$, respectively. Reference [27] may be consulted for details on the simplification.

One discrepancy was identified in considering the definition of χ as the ratio of the rate constants of the first and second steps of the two-step mechanism. According to the numerical equation for calculating χ, Equation (11), $\chi < 1$ in the temperature range examined (400-500°C). However, derivation of the rate expression in Equation (14) requires that $\chi \gg 1$.

WGS experiments were conducted by Temkin, et al. [27] in the low temperature shift range and their results examined for the case when the equilibrium of $C + CO_2 \leftrightarrows 2CO$ is assumed. The low-temperature shift catalyst used was composed of ZnO + 0.24 Cr_2O_3 + 0.24 CuO (moles) [27]. Catalyst pellets were crushed to 0.5-1.0 mm particles. The catalyst bed density was 1.23 g/cm^3. The specific surface area, after experiments, was measured as 36 m^2/g. The temperature range examined was between 150°C and 225°C under conditions where the reaction is practically irreversible. The same rate equation as for the case of high temperature shift was experimentally validated for the

low temperature shift. This suggested that the mechanism doesn't change for both temperature ranges and for the two different catalysts employed.

For the case of low temperature shift, χ and k were provided as functions of temperature by the following two expressions [27]:

$$\chi = 2.5 \times 10^{9} \exp\left(-\frac{21500}{R_{gas} T} \right) \tag{15}$$

$$k = 6.0 \times 10^{11} \exp\left(-\frac{26800}{R_{gas} T} \right) \tag{16}$$

2.4.2.2 Other Redox Mechanism Studies

Nakamura, et al. [8] studied the kinetics and mechanism of the WGS reaction on Cu(110) in comparison with Cu(111). Their mechanism is presented in Table 3. Using LEED, the authors were able to show that no other elements existed on the catalyst surface prior to reaction. Post-reaction surface analysis showed the presence of low-levels of carbon, but it was determined to have a negligible effect on the reaction rate [8].

The rate of water dissociation to produce adsorbed atomic oxygen on the copper surface had not been shown to occur rapidly enough to account for observed WGS rates via the redox mechanism. Nakamura, et al [8] believed that adsorbed hydroxyl was most likely to dissociate to O·S via $2OH{\cdot}S \leftrightarrows O{\cdot}S + H_2O$, where the adsorbed atomic oxygen then reacts with $CO_{(g)}$ to produce $CO_{2(g)}$ rather than combine with $CO_{(g)}$ directly to produce surface formate. This conclusion was based on studies where the group was unable to produce measurable amounts of surface formate, but the hydroxyl dissociation to water and adsorbed atomic oxygen occurred rapidly, thus resulting in the redox mechanism.

Ovesen, et al. [10,14] have also used the redox mechanism in their microkinetic analysis of the WGS reaction. Recognizing the work of Nakamura, et al [8] and Campbell and Daube [50], Ovesen, et al [10,14] considered an 8-step mechanism (Table 7) but exluded the formate species. Further, the authors acknowledge that H_2O

Table 7. Redox mechanism for the water-gas-shift reaction [10,14].

Redox Reaction Mechanism	
$H_2O + S \leftrightarrows H_2O{\cdot}S$	(s_2)
$H_2O{\cdot}S + S \leftrightarrows OH{\cdot}S + H{\cdot}S$	(s_3)
$2OH{\cdot}S \leftrightarrows H_2O{\cdot}S + O{\cdot}S$	(s_{10})
$OH{\cdot}S + S \leftrightarrows O{\cdot}S + H{\cdot}S$	(s_6)
$2H{\cdot}S \leftrightarrows H_2 + 2S$	(s_{18})
$CO + S \leftrightarrows CO{\cdot}S$	(s_1)
$CO{\cdot}S + O{\cdot}S \leftrightarrows CO_2{\cdot}S + S$	(s_4)
$CO_2{\cdot}S \leftrightarrows CO_2 + S$	(s_{15})
$CO + H_2O \leftrightarrows CO_2 + H_2$	(*OR*)

dissociation and the oxidation of CO were both plausible rate-limiting steps. Here, the surface redox mechanism refered to the complete surface dissociation of H_2O to adsorbed atomic oxygen and hydrogen where the oxygen is then combined with CO to form CO_2. Previous surface analysis showed that formate produced on the Cu catalyst exposed to RWGS conditions was not sufficiently stable to produce significant coverage at 1 atm. At high pressures, formate had been shown to have higher coverage. Including the synthesis of formate in the mechanism increases the apparent activation enthalpy of the overall reaction [14]. Surface studies of reactions between formate and the copper surface under reverse WGS conditions, i.e., H_2 and CO_2, suggested that formate may be incorporated into the mechanism via the reactions

$s_{8:}$ $CO_2{\cdot}S + H{\cdot}S \leftrightarrows HCOO{\cdot}S + S$

s_{38}: $HCOO{\cdot}S + H{\cdot}S \leftrightarrows H_2COO{\cdot}S + S$

s_{39}: $H_2COO{\cdot}S + 4H{\cdot}S \leftrightarrows CH_3OH_{(g)} + H_2O_{(g)} + 5S$

as presented in Table 3. Askgaard, et al [52] proposed these steps in more detail and indicated that the third reaction is relatively insignificant because the coverage of $H_2COO{\cdot}S$ is always low. Ovesen, et al [14] suggested that, by this revised 11-step mechanism, formate is an effective "dead end." It may be present on the surface, but it was not a participating species in the conversion of CO to CO_2. Its main effect is to block the active sites. The carbonate species, suggested as an intermediate [56-58], was also neglected by the authors because the synthesis of carbonate via exposure of an oxygen-covered Cu surface did not produce any carbonate [14].

They used the transition state theory to determine the energetics of the elementary reactions. For the calculations, the authors assumed that: 1) steps 1, 2, 10, 15 and 18 from Table 7 are in pseudo-equilibrium; 2) the remaining steps 3, 4, and 6 may not be in equilibrium and could be rate-limiting; 3) the catalyst surface is uniform; and, 4) the catalyst surface is composed of mostly Cu(111) planes, which implies that the equilibrium constants and rate constants can be directly taken or calculated from published literature data [15,42] on Cu(111) single crystal studies. From the five equations for the five steps in equilibrium, the equation for the conservation of the total

number of surface sites, and quasi-steady-state concentrations of OH·S and O·S, one can determine the expression for the coverage of each of the six surface species ($H_2O{\cdot}S$, $OH{\cdot}S$, $H{\cdot}S$, $O{\cdot}S$, $CO{\cdot}S$, and $CO_2{\cdot}S$) and the fraction of free sites. The rate of reaction can then be written as an algebraic expression in terms of the partial pressure of reactants, products, equilibrium constants and rate constants, as discussed below.

Equilibrium Steps

Ovesen, et al. [10,14] used the following equations to describe the equilibrium of steps 2, 10, 18, 1 and 15 (Table 7).

$$(s_1) \qquad \mathrm{CO} + \mathrm{S} \underset{\vec{k}_1}{\overset{\vec{k}_1}{\rightleftarrows}} \mathrm{CO}\cdot\mathrm{S} \qquad K_1 = \frac{\theta_{\mathrm{CO}\cdot\mathrm{S}}}{P_{\mathrm{CO}}\theta_0} \tag{17}$$

$$(s_2) \qquad \mathrm{H_2O} + \mathrm{S} \underset{\vec{k}_2}{\overset{\vec{k}_2}{\rightleftarrows}} \mathrm{H_2O}\cdot\mathrm{S} \qquad K_2 = \frac{\theta_{\mathrm{H_2O}\cdot\mathrm{S}}}{P_{\mathrm{H_2O}}\theta_0} \tag{18}$$

$$(s_{10}) \qquad 2\mathrm{OH}\cdot\mathrm{S} \underset{\vec{k}_{10}}{\overset{\vec{k}_{10}}{\rightleftarrows}} \mathrm{H_2O}\cdot\mathrm{S} + \mathrm{O}\cdot\mathrm{S} \qquad K_{10} = \frac{\theta_{\mathrm{H_2O}\cdot\mathrm{S}}\theta_{\mathrm{O}\cdot\mathrm{S}}}{\theta^2_{\mathrm{OH}\cdot\mathrm{S}}} \tag{19}$$

$$(s_{15}) \qquad \mathrm{CO_2}\cdot\mathrm{S} \underset{\vec{k}_{15}}{\overset{\vec{k}_{15}}{\rightleftarrows}} \mathrm{CO_2} + \mathrm{S} \qquad K_{15} = \frac{P_{\mathrm{CO_2}}\theta_0}{\theta_{\mathrm{CO_2}\cdot\mathrm{S}}} \tag{20}$$

$$(s_{18}) \qquad 2\mathrm{H}\cdot\mathrm{S} + \mathrm{S} \underset{\vec{k}_{18}}{\overset{\vec{k}_{18}}{\rightleftarrows}} \mathrm{H_2} + 2\mathrm{S} \qquad K_{18} = \frac{P_{\mathrm{H_2}}\theta_0^2}{\theta^2_{\mathrm{H}\cdot\mathrm{S}}} \tag{21}$$

Rate-LimitingSteps

The remaining steps, assumed to be rate-limiting, were described by the following rate expressions:

$$(s_3) \qquad \mathrm{H_2O}\cdot\mathrm{S} + \mathrm{S} \underset{\vec{k}_3}{\overset{\vec{k}_3}{\rightleftarrows}} \mathrm{OH}\cdot\mathrm{S} + \mathrm{H}\cdot\mathrm{S} \qquad r_3 = \vec{k}_3\theta_{\mathrm{H_2O}\cdot\mathrm{S}}\theta_0 - \frac{\vec{k}_3}{K_3}\theta_{\mathrm{OH}\cdot\mathrm{S}}\theta_{\mathrm{H}\cdot\mathrm{S}} \tag{22}$$

$$(s_4) \qquad \mathrm{CO}\cdot\mathrm{S} + \mathrm{O}\cdot\mathrm{S} \underset{\vec{k}_4}{\overset{\vec{k}_4}{\rightleftarrows}} \mathrm{CO_2}\cdot\mathrm{S} + \mathrm{S} \qquad r_4 = \vec{k}_4\theta_{\mathrm{CO}\cdot\mathrm{S}}\theta_{\mathrm{O}\cdot\mathrm{S}} - \frac{\vec{k}_4}{K_4}\theta_{\mathrm{CO_2}\cdot\mathrm{S}}\theta_0 \tag{23}$$

$$(s_6) \qquad \mathrm{OH\cdot S + S \underset{\vec{k}_6}{\overset{\vec{k}_6}{\rightleftharpoons}} O\cdot S + H\cdot S} \qquad r_6 = \vec{k}_6\theta_{\mathrm{OH\cdot S}}\theta_0 - \frac{\vec{k}_6}{K_6}\theta_{\mathrm{H\cdot S}}\theta_{\mathrm{O\cdot S}} \qquad (24)$$

Rate Constants

The rate constants were calculated as summarized in Table 8. The pre-exponential factor and the activation energy for each of the "rate-limiting" steps are taken from Reference [10] and are given in Table 8.

$$(s_3) \qquad \vec{k}_3 = \vec{\Lambda}_3 \exp\left(-\frac{\vec{E}_3}{R_{gas}T}\right) \qquad (25)$$

$$(s_4) \qquad \vec{k}_4 = \vec{\Lambda}_4 \exp\left(-\frac{\vec{E}_4}{R_{gas}T}\right) \qquad (26)$$

$$(s_6) \qquad \vec{k}_6 = \vec{\Lambda}_6 \exp\left(-\frac{\vec{E}_6}{R_{gas}T}\right) \qquad (27)$$

It is seen from Table 8 that $\vec{k}_6$ is the smallest among these. Of course, rates of steps also involve surface species concentrations.

Rate Expression

The rate expression was determined from both an OH·S balance and an O·S balance assuming quasi-steady-state. The elementary reaction steps were linearly combined to determine the overall rate in terms of the potential rate-limiting steps listed above.

OH·S Balance: $s_3 = 2s_{10} + s_6$

O·S Balance: $s_{10} + s_6 = s_4$

i.e., $s_{10} = s_4 - s_6$

or $s_3 = 2(s_4 - s_6) + s_6$

$s_3 = 2s_4 - s_6$

Table 8. Rate constant parameters and calculated values at $T = 190^{o}C$ [14]

Step	$\vec{\Lambda}_{\rho}$ (s^{-1})	$\vec{E}_{\rho}$ (kJ/mol)	$\vec{k}_{\rho}$ (s^{-1}) - calculated
3	2.6×10^{14}	114.0	36.17
6	2.3×10^{8}	99.1	0.0015
4	1.1×10^{13}	72.2	79223

Thus, $\frac{1}{2}(s_3 + s_6) = s_4$

Overall Rate: $r_{OR} = \frac{1}{2}(r_3 + r_6) = r_4$ (28)

Surface Coverages

The surface coverage of each of the surface species were determined from the equilibrium equations in terms of equilibrium constants and partial pressures of the reactants and products.

$$\theta_{H_2O\cdot S} = K_2 P_{H_2O} \theta_0 \tag{29}$$

$$\theta_{OH\cdot S} = \left(\frac{K_2}{K_{18}} P_{H_2O} \theta_{O\cdot S} \theta_0 \right)^{1/2} \tag{30}$$

$$\theta_{H\cdot S} = \left(\frac{P_{H_2}}{K_{18}} \right)^{1/2} \theta_0 \tag{31}$$

$$\theta_{CO\cdot S} = K_1 P_{CO} \theta_0 \tag{32}$$

$$\theta_{CO_2\cdot S} = \frac{P_{CO_2} \theta_0}{K_{15}} \tag{33}$$

From the rate expression given in Equation (28), the surface coverage of the O·S species may be determined:

$$\theta_{O\cdot S} = \left[\frac{-b + \left(b^2 + 4ac \right)^{1/2}}{2a} \right]^2 \theta_0 \tag{34}$$

where

$$a = k_4 K_1 P_{\mathrm{CO}} + \frac{1}{2}\frac{k_6}{K_6}\left(\frac{P_{H_2}}{K_{18}}\right)^{1/2}$$

$$b = \frac{1}{2}\left(\frac{K_2}{K_{10}}\right)^{1/2}\left(P_{\mathrm{H_2O}}\right)^{1/2}\left[\frac{k_3}{K_3}\left(\frac{P_{\mathrm{H_2}}}{K_{18}}\right)^{1/2} - k_6\right]$$

$$c = \frac{1}{2}k_3 K_2 P_{\mathrm{H_2O}} + \frac{k_4}{K_4 K_{15}} P_{\mathrm{CO_2}}$$

An expression for the fraction of empty sites was needed in the overall rate expression. This was determined from a site balance. The resulting expression is:

$$\theta_0 = \frac{1}{1 + K_2 P_{\mathrm{H_2O}} + \left(\frac{-b + \left(b^2 + 4ac\right)^{1/2}}{2a}\right)\left(\frac{K_2}{K_{10}} P_{\mathrm{H_2O}}\right)^{1/2} + \left(\frac{-b + \left(b^2 + 4ac\right)^{1/2}}{2a}\right)^2 + K_1 P_{\mathrm{CO}} + \frac{P_{\mathrm{CO_2}}}{K_{15}}} \tag{35}$$

Substitution in the expression below of the appropriate surface coverages given above provides the overall rate

$$r_{OR} = r_4 = k_4 \theta_{\mathrm{CO{\cdot}S}} \theta_{\mathrm{O{\cdot}S}} - \frac{k_4}{K_4}\theta_{\mathrm{CO_2{\cdot}S}} \theta_0 \tag{36}$$

Rate Constants and Equilibrium Constants

The equilibrium constants were calculated based on partition functions for each of the species, both intermediate (or surface) and terminal (or gas phase) species. The data used to calculate these partition functions are provided by Ovesen, et al. [10,14]. These values are provided in Table 9 along with calculation results at a temperature of 190°C.

Table 9. Partition Function Parameters and Calculation Results (T = 190°C) [10,14]

Species		H_2	H·S	H_2O	H_2O·S	O·S	OH·S	CO	CO·S	CO_2	CO_2·S
m	kg	3.32E-27		2.99E-26				4.65E-26		7.31E-26	
$\omega^{\perp}$	cm^{-1}		1121		460	391	280		343		410
$\omega_{\parallel}$	cm^{-1}		928		48	508	49		24		31
ω	cm^{-1}	4405.3		1594.6	1600		670	2170	2089	1343	1343
				3657.1	3370					667	667
				3755.8	745					2349	2349
σ		2		2				1		2	
B	cm^{-1}	60.8						1.93		0.39	
$I_A I_B I_C$	kg^3m^6			5.77E-141							
E_e	kJ/mol	-35	-40.7	-306	-359	-243	309.6	-132.2	-186.1	-431	-359
z_t		3.34E+05	1.13E-02	9.03E+06	2.88E+01	2.53E-01	4.79E+01	1.75E+07	1.61E+02	3.45E+07	7.90E+01
z_v		1.06E-03	1.00E+00	8.37E-07	1.55E-04	1.00E+00	4.03E-01	3.43E-02	3.90E-02	1.33E-03	1.33E-03
z_r		2.65E+00	1.00E+00	8.30E+01	1.00E+00	1.00E+00	1.00E+00	1.67E+02	1.00E+00	4.12E+02	1.00E+00
z_e		8.86E+03	3.89E+04	3.25E+34	3.09E+40	2.55E+27	1.21E-35	8.13E+14	9.76E+20	4.08E+48	3.09E+40
z		8.33E+06	4.41E+02	2.04E+37	1.38E+38	6.46E+26	2.33E-34	8.15E+22	6.11E+21	7.71E+55	3.24E+39

The partition function is the product of parts [18,72,73]: translational, vibrational, rotational, and electrical. The individual components may be evaluated via statistical mechanics.

$$z = z_t z_v z_r z_e \tag{37}$$

The translational partition function is calculated from the following expression for adsorbed molecules [14,22]. For three-dimensional translation, the partition function is given by

$$z_t = \frac{\left(2\pi m k_B T\right)^{3/2}}{h^3} \times \frac{k_B T}{P} \tag{38}$$

while, for one-dimensional translation,

$$z_t = \frac{\left(2\pi m k_B T\right)^{1/2}}{h} \times \ell \tag{39}$$

where m = mass of molecule; P = container pressure; h = Planck's constant; k_B = Boltzmann constant; T = temperature; and, ℓ = length of a one-dimensional box. In the case of adsorbed species, the authors assumed no translation, but that the adsorbed species is vibrating both parallel and orthogonal to the surface. Thus, Equation (38) was replaced by [10]

$$z_t = \left(\frac{\exp\left(-\frac{1}{2} \frac{hc\omega_\perp}{k_B T} \right)}{1 - \exp\left(-\frac{hc\omega_\perp}{k_B T} \right)} \right) \left(\frac{\exp\left(-\frac{hc\omega_\parallel}{k_B T} \right)}{\left(1 - \exp\left(-\frac{hc\omega_\parallel}{k_B T} \right) \right)^2} \right) \tag{40}$$

where $\omega_{\perp}$ = vibrational frequency for single degenerate vibration orthogonal to surface; $\omega_{\parallel}$ = vibrational frequency for the doubly degenerate vibration parallel to the surface; and, c = speed of light (cm/s).

The vibrational partition function is calculated from the following expression in terms of the vibrational frequencies for each degree of freedom [72].

$$z_v = \frac{\exp\left(-\frac{1}{2}\frac{hc\omega}{k_B T}\right)}{1-\exp\left(-\frac{hc\omega}{k_B T}\right)} \tag{41}$$

where ω = vibration frequency (cm^{-1}) from each vibrational degree of freedom. For adsorbed atoms, z_v was assigned a value of 1.0, i.e., vibration does not occur.

For a non-linear molecule, the rotational partition function is calculated via

$$z_r = \frac{8\pi^2 \left(k_B T\right)^{3/2} \left(8\pi^3 I_A I_B I_C\right)^{1/2}}{\sigma_{sym}\, h^3} \tag{42}$$

where $I_A I_B I_C$ = moments of inertia and σ = symmetry number. For a linear molecule, the rotational partition function is given by

$$z_r = \frac{k_B T}{\sigma_{sym} hcB} \tag{43}$$

where B = rotational constant. Adsorbed species cannot rotate, thus, z_r was given an "effective" value of 1.0.

The electrical partition function is determined based on the electrical energy:

$$z_e = \exp\left(-\frac{E_e}{k_B T}\right) \tag{44}$$

where E_e = energy of the ground state.

The equilibrium constants for the elementary reaction steps in Table 7 were evaluated from the following equations.

$$K_1 = \frac{z_{\mathrm{CO\cdot S}}}{z_{\mathrm{CO}}} \tag{45}$$

$$K_2 = \frac{z_{\mathrm{H_2O\cdot S}}}{z_{\mathrm{H_2O}}} \tag{46}$$

$$K_3 = \frac{z_{\mathrm{OH\cdot S}} z_{\mathrm{H\cdot S}}}{z_{\mathrm{H_2O\cdot S}}} \tag{47}$$

$$K_4 = \frac{z_{\mathrm{CO_2\cdot S}}}{z_{\mathrm{CO\cdot S}} z_{\mathrm{O\cdot S}}} \tag{48}$$

$$K_6 = \frac{z_{\mathrm{OH\cdot S}} z_{\mathrm{H\cdot S}}}{z_{\mathrm{OH\cdot S}}} \tag{49}$$

$$K_{10} = \frac{z_{\mathrm{H_2O\cdot S}} z_{\mathrm{O\cdot S}}}{z_{\mathrm{OH\cdot S}}^2} \tag{50}$$

$$K_{15} = \frac{z_{\mathrm{CO_2}}}{z_{\mathrm{CO_2\cdot S}}} \tag{51}$$

$$K_{18} = \frac{z_{\mathrm{H_2}}}{z_{\mathrm{H\cdot S}}^2} \tag{52}$$

Finally, the overall equilibrium constant is given by the following equation:

$$K = K_1 K_2 K_3^{3/2} K_4 K_6^{1/2} K_{10}^{1/2} K_{15} K_{18} \tag{53}$$

Tserpe and Waugh [15] and Waugh [16] examined the redox mechanism (Table 7) of the water-gas-shift reaction in comparison with experimentally determined temperature dependence data for the reverse WGS reaction and in terms of predicted Arrhenius parameters, activation energies and pre-exponential factors. In the redox

mechanism, Waugh [16] suggested that the forward WGS reaction proceeds by water adsorbing on the copper catalyst and then decomposing to give gas phase H_2 and adsorbed atomic oxygen. CO also adsorbs on to the surface and proceeds to remove the adsorbed atomic oxygen via a Langmuir-Hinshelwood mechanism yielding adsorbed CO_2 and ultimately CO_2 gas. Using available heats of adsorption of CO, H_2O, CO_2, and O on copper and available kinetic data for water decomposition, a model for the forward WGS reaction was developed [16].

For the reverse WGS reaction, weakly adsorbed CO_2 was presumed to decompose into adsorbed CO and adsorbed O. With the addition of adsorbed H, which reacts with the adsorbed O to produce OH·S and ultimately H_2O·S, the reverse WGS reaction was completed. The activation energy for the desorption of hydrogen from the catalyst surface and the kinetics and mechanism of CO_2 decomposition are available information providing the energetics of the reverse WGS mechanism [16].

Furthermore, in both the forward and reverse WGS reaction mechanisms, the pre-exponential factors of the desorption reactions are presumed to have the value 10^{13} s^{-1}. The bimolecular surface reactions are given the value 10^{21} $cm^2mol^{-1}s^{-1}$ based on the following relationships, which assume a mobile transition state [16].

The rate of a bimolecular surface reaction between two adsorbed species A and B on a surface to give the product AB on the surface as given by the transition-state theory is [70]

$$\vec{r}_\rho = \frac{N_A k_B T}{h} \frac{z_{AB}^{\ddagger}}{z_A z_B} \theta_A \theta_B \exp\left(\frac{E^{\ddagger}}{R_{gas} T} \right) \tag{54}$$

where θ_A and θ_B are the surface coverages of A and B, and $z_{AB}^{\ddagger}$, z_A, and z_B are the partition functions of the activated complex $AB^{\ddagger}$, species A and species B, respectively. $E^{\ddagger}$ is the activation energy associated with the formation of the activated complex.

Factoring the partition function into their component translational, vibrational and rotational partition functions (described previously in this section), Equation (54) becomes

$$\vec{r}_\rho = \frac{N_A k_B T}{h} \frac{z^{\ddagger}_{tAB} z^{\ddagger}_{vAB} z^{\ddagger}_{rAB}}{\left(z_{tA}\right)^2 z_{vA} z_{rA} \left(z_{tB}\right)^2 z_{vB} z_{rB}} \theta_A \theta_B \exp\left(\frac{E^{\ddagger}}{R_{gas} T}\right) \tag{55}$$

Waugh [16] assumed that, because the vibrational and rotational partition functions of the reactants and of the activated complex are approximately equal, they cancel each other. Also, from the definition of the translation partition function (given by Equation (38)), Equation (55) becomes

$$\vec{r}_\rho = \frac{N_A k_B T}{h\left(2\pi m k_B T / h^2\right)} \exp\left(\frac{E^{\ddagger}}{R_{gas} T}\right) \theta_A \theta_B \approx 10^{21} \exp\left(\frac{E^{\ddagger}}{R_{gas} T}\right) \theta_A \theta_B \tag{56}$$

Even though this mechanism and model appeared to fit the experimental data very well, some deficiencies were identified. First, the activation energy for the adsorption of hydrogen (as atoms) on Cu was set to zero. While accepted at the time of writing the model, subsequent experimental work has shown that the chemisorption of hydrogen of Cu is activated [16]. As a consequence, the model's results were found to overpredict the hydrogen surface coverage.

Second, initial interaction of carbon dioxide with clean copper is dissociative, producing carbon monoxide and surface oxidized copper. Subsequent adsorption of carbon dioxide onto the copper surface produced carbonate species [15,16]. The existence of the surface carbonate species was found to have a reducing effect on the overall rate of the reaction. Due to its strong binding nature with the surface, the carbonate species blocks active surface sites, preventing other species from adsorbing to the surface and further reacting towards the generation of the products. This negative effect was also ascribed to the formate species resulting from dehydrogenation of the carbonate species [15,16].

Finally, the activation energy of the adsorption and decomposition of carbon dioxide to carbon monoxide and an adsorbed oxygen atom was experimentally shown to be 12 kJ/mol while the model assumed a value of 68 kJ/mol, a value close to that of Campbell, et al. [50] on Cu(110).

This redox mechanism was also considered by Schumacher, et al [51], who identified trends in low-temperature WGS activity via microkinetics on transition metals as predicted based on predicted DFT energetics. Tested at 300^{o}C under forward WGS feed conditions, the following experimental trend was found for the catalysts investigated on an aluminum oxide support [51]

Cu > Co > Ru > Ni > Pt > Au > Fe > Pd > Rh > Ir

Predictions from chemisorption energies suggested that the WGS activity trend was

Cu > Co > Ru > Fe > Ni > Rh > Au > Ir > Pd > Pt

In comparison to other trends provided in the literature, it is determined that the rates for Fe and Rh are overestimated and the rate over Pt is underestimated. Although the order of activity of the metals is predicted well, the model fails to quantitatively agree with experimental data.

2.4.3. The Carbonate Mechanism

Millar, et al. [57] considered a carbonate mechanism based on experimental IR spectroscopy results which showed a band corresponding to "symmetrical" carbonate ions on the catalyst surface. Specifically, a Cu/SiO_2 catalyst was suggested to produce CO after pre-oxidation. The IR peak intensities were monitored and found to decrease gradually, corresponding to the production of $CO_{2(g)}$ and adsorbed CO_2. The peaks correspond to those for carbonate species supporting the conclusion that CO oxidation on copper may proceed via a polydentate carbonate structure identified as a "surface malachite type" species. IR spectroscopy showed that the carbonate production, and, thus, increased availability of surface carbonate, induced an increase in the formation of surface formate.

Lund, et al. [56,58,59] have investigated the water-gas-shift reaction via the carbonate mechanism, given in Table 10. Using Bohlbro's [42] kinetic data, Lund predicted the reaction rate over an iron-chromia catalyst at various conversions in a

membrane reactor and compared them to experimental results. The entropies of formation and enthalpies of formation for the gas phase terminal and intermediate species are known functions of temperature, represented using the Shomate equation [59] with appropriate parameters from NIST Chemistry Webbook [74]. The pre-exponential factors for each of the elementary reaction steps were estimated based on simple transition-state theory. The activation energies and the heats of formation of the surface species were fitted to data.

Approximating the standard heats of formation of surface species as that of the species in the gas phase less the "bond strength" between the surface and the species leaves the activation energies and the bond strengths as adjustable parameters in Lund's rate expression. These parameters were then used to fit the model to the experimental data. The transition state theory was used to derive an expression for the rate of each elementary reaction step. The resulting expression is [56]

$$r_\rho = C_t \Lambda_\rho \exp\left(-\frac{E_\rho}{R_{gas}T}\right)\left[\vec{\sigma}_\rho \prod_{i=1}^{l} a_i^{-\vec{\nu}_{\rho i}} - \frac{\overleftarrow{\sigma}_\rho \prod_{i=1}^{l} a_i^{-\overleftarrow{\nu}_{\rho i}}}{\exp\left(\frac{\Delta S_\rho(T)}{R_{gas}}\right)\exp\left(-\frac{\Delta H_\rho(T)}{R_{gas}T}\right)}\right] \tag{57}$$

where $\vec{\sigma}_\rho$ and $\overleftarrow{\sigma}_\rho$ are geometric factors associated with the forward and reverse reactions, respectively. The entropy and enthalpy changes for the reaction are given by the following relationships [56]:

$$\Delta S_\rho(T) = \sum_{i_{gp}} \nu_{i_{gp}} S^{\circ}_{i_{gp}}(T) + \sum_{i_{sp}} \nu_{i_{sp}} S^{\circ}_{i_{sp}}(T_{ref}) - \sum_{i_{gr}} \nu_{i_{gr}} S^{\circ}_{i_{gr}}(T) - \sum_{i_{sr}} \nu_{i_{sr}} S^{\circ}_{i_{sr}}(T_{ref}) \tag{58}$$

$$\begin{aligned}\Delta H_\rho(T) = &\sum_{i_{gp}} \nu_{i_{gp}} \Delta H_{f\,i_{gp}}^{\circ}(T) + \sum_{i_{sp}} \nu_{i_{sp}} \Delta H_{f\,i_{sp}}^{\circ}(T_{ref}) \\ &- \sum_{i_{gr}} \nu_{i_{gr}} \Delta H_{f\,i_{gr}}^{\circ}(T) - \sum_{i_{sr}} \nu_{i_{sr}} \Delta H_{f\,i_{sr}}^{\circ}(T_{ref})\end{aligned} \tag{59}$$

Table 10. Carbonate mechanism for the water-gas-shift reaction [56,58,59]

Carbonate Reaction Mechanism*	
$CO + 2O{\cdot}S \leftrightarrows CO_3{\cdot}S_2$	(s_{23})
$CO_3{\cdot}S_2 \leftrightarrows CO_3{\cdot}S + S$	(s_{24})
$CO_3{\cdot}S \leftrightarrows CO_2 + S$	(s_{25})
$H_2O + S \leftrightarrows H_2O{\cdot}S$	(s_2)
$H_2O{\cdot}S + O{\cdot}S \leftrightarrows 2OH{\cdot}S$	(s_{10})
$2OH{\cdot}S \leftrightarrows 2O{\cdot}S + H_2$	(s_{26})
$H_2O{\cdot}S + S \leftrightarrows OH{\cdot}S + H{\cdot}S$	(s_3)
$2H{\cdot}S \leftrightarrows H_2 + 2S$	(s_{18})
$CO + H_2O \leftrightarrows CO_2 + H_2$	(*OR*)

*Steps 3 and 18 were added to the model by Lund [56] for completeness; only steps 2, 10, and 23 through 26 are needed to describe the catalyst performance. Steps 3 and 18 provide a path for generating surface oxygen from steam initially. Therefore, these steps may prove important in a transient start-up experiment.

It should also be noted that the mechanism is given here as written in the reference. However, s_{25} does not appear balanced and should, potentially, be written as $CO_3{\cdot}S \leftrightarrows CO_2 + O{\cdot}S$.

where i_{gp} and i_{gr} are indices for the gas phase products and the gas phase reactants, respectively, while i_{sp} and i_{sr} are indices for the surface products and reactants.

The reference temperature, T_{ref}, was chosen to be the average temperature of the kinetic data causing the model to predict a zero rate at T_{ref} only, independent of the equilibrium composition. Applying the plug flow reactor design equations to each of the species with the rate from Equation (57), a system of coupled differential equations was used to model the data. In order to optimize the results based on the adjustable parameters, the program Athena Visual Workbench was used. The resulting fitted parameters are given in Table 11; some of the quantities seem unusually high.

The quality of the fit of the microkinetic model using this system of equations is comparable to previous work by Lund, et al. [56,58] based solely on the reference temperature rather than actual temperature. This suggests that their previous model was not in serious error and that most of the kinetic data used was not taken at conversions near equilibrium.

2.4.4. Other Mechanisms

As shown in Table 3, there is another category of mechanisms described in the literature. This group is comprised of researchers who have attempted to model the WGS reaction using mechanisms that are more comprehensive and include many of the steps considered in the previous mechanisms discussed. In other cases, some researchers have proposed mechanisms involving elementary reaction steps not generally considered to exist during the WGS reaction.

In 1954, Graven and Long [64] proposed a 4-step homogeneous mechanism in the high temperature range of 600-900^{o}C. This mechanism was inspired by suggestive results from combustion experiments which showed the existence of WGS equilibrium is established in short time intervals (i.e., 0.5 second) [64]. The chain reaction mechanism shown in Table 3, i.e., $s_{41} - s_{44}$, was first proposed by Bradford and was considered by several researchers before Graven and Long. Experimental results were modeled using the following expressions:

Table 11. Optimized fitted parameters for Lund's WGS rate expression [56]

Species	**Bond Strength (kJ/mol)**
O·S	606.5
CO_3·S_2	767.4
CO_3·S	619.5
H_2O·S	60.5
OH·S	355.7
H·S	0.1
Reaction	**Activation Energy (kJ/mol)**
$CO + 2O·S \leftrightarrows CO_3·S_2$	5.5
$CO_3·S_2 \leftrightarrows CO_3·S + S$	11.2
$CO_3·S \leftrightarrows CO_2 + S$	0
$H_2O + S \leftrightarrows H_2O·S$	12.5
$H_2O·S + O·S \leftrightarrows 2OH·S$	54.4
$2OH·S \leftrightarrows 2O·S + H_2$	10.2
$H_2O·S + S \leftrightarrows OH·S + H·S$	320.3
$2H·S \leftrightarrows H_2 + 2S$	403.8

$$r_{H_2O} = \frac{9.5\times10^{10}\exp\left(-\frac{57000}{R_{gas}T}\right)C_{H_2}^{\frac{1}{2}}C_{CO_2}}{1+3.6\times10^{3}C_{CO}} \tag{60}$$

$$r_{CO_2} = \frac{5.0\times10^{12}\exp\left(-\frac{67300}{R_{gas}T}\right)C_{CO}^{\frac{1}{2}}C_{H_2O}}{\left(1+1.2\times10^{4}C_{H_2}\right)^{\frac{1}{2}}} \tag{61}$$

Graven and Long acknowledge that these rates assume that the hydroxyl radicals and hydrogen atoms are the steady-state species and that the chain initiating and terminating steps proceed with equal rates. The experimental data was shown to have good, not excellent, agreement with the model equations' predictions.

More recently, more complex mechanisms have been considered. Teng, et al. [61] considered an 11-step mechanism based on the presence of a formate species in conjunction with Fischer-Tropsch synthesis. In this mechanism, the formate species is assumed to arise through the reaction between CO and a hydroxyl species, which is formed from the decomposition of water. In addition, the direct oxidation, or redox mechanism, is considered. The Fischer-Tropsch and the WGS reaction are assumed to proceed on different surface sites. One rate-limiting step is assumed while the rest of the steps in the mechanism are considered at quasi-equilibrium. After considering all possible RLSs and mechanism combinations, it was concluded that HCOO·S ⇆ CO_2 + H·S is the RLS of the 5-step mechanism that best describes the experimental data.

s_1: CO + S ⇆ CO·S

s_5: CO·S + OH·S ⇆ HCOO·S + S

s_{18}: 2H·S ⇆ H_2 + 2S

s_{20}: HCOO·S ⇆ CO_2 + H·S

s_{40}: H_2O + 2S ⇆ OH·S + H·S

The rate expression is given by

$$r = \left[\vec{k}_{20} K_1 K_5 K_{40} P_{CO} P_{H_2O} - \frac{\overleftarrow{k}_{20} P_{CO_2} P_{H_2}}{K_{18}} \right] \frac{\theta_0}{\sqrt{\frac{P_{H_2}}{K_{18}}}} \tag{62}$$

This study was on a Fe-Mn catalyst. The experimental data yielded an equilibrium constant that is much less than the predicted values determined from thermodynamics [61]

$$\ln K = \frac{5078.00}{T} - 5.90 + 13.96 \times 10^{-4} T - 27.59 \times 10^{-8} T^2 \tag{63}$$

suggesting that the WGS reaction is far from equilibrium in this process. Based on the mechanistic analysis, the formate mechanism is seen to fit the data better than the redox mechanism. Teng, et al. [61] suggested that this is due to the fact that dissociation of hydroxyl intermediate to adsorbed oxygen and hydrogen is not energetically favorable under the Fischer-Tropsch synthesis conditions. Quantum calculations also show that the hydroxyl dissociation has an unfavorably high activation barrier under these conditions. Infrared spectroscopy confirmed existence of formate on the Fe catalyst [61].

Mhadeshwar and Vlachos [63] considered the kinetics of the WGS reaction on a Pt catalyst. Their proposed comprehensive thermodynamically consistent 23-step mechanism describing CO oxidation, H_2 oxidation, WGS as well as preferential oxidation (PrOx) of CO was based on their previous work [62] in which the CO-H_2 coupling effect was considered and implied that the reactions may proceed through a carboxyl (COOH·S) intermediate. It was also determined in this earlier work that the formation and consumption of the carboxyl species are key pathways of the WGS reaction. In Reference [63], they utilize numerical methods to reduce and simplify the 23-step mechanism to a 9-step mechanism for the WGS reaction. A sensitivity analysis, in conjunction with principle component analysis [63], is used to initially reduce the mechanism while maintaining the "elementary-like nature of the chemical reactions."

The principle component analysis is used to reveal "synergetic interactions" between elementary reaction steps and becomes important especially when multiple conditions are analyzed simultaneously. Next, reaction path analysis was employed to quantify the contributions of different reactions to the species' balances, resulting in the identification of the most abundant reaction intermediates (MARI), the RLS, as well as the "partial equilibrium" conditions [63]. The end result is an analytical rate expression derived from the simplified species' and site balances at steady-state:

$$\vec{r} = \frac{k_{33} K_{19} K_{13} C_{CO} C_{H_2O}}{\left(1 + \sqrt{K_1 C_{H_2}} + K_{19} C_{CO}\right)^2} \tag{64}$$

where the elementary reaction steps (corresponding to Reference [63])

s_{33}: $CO{\cdot}S + H_2O{\cdot}S \rightarrow COOH{\cdot}S + H{\cdot}S$

s_{19}: $CO + S \rightarrow CO{\cdot}S$

s_{13}: $H_2O + S \rightarrow H_2O{\cdot}S$

s_1: $H_2 + 2S \rightarrow 2H{\cdot}S$

and

$$\vec{r} = \frac{k_{33} K_{19} K_{13} C_{CO} C_{H_2O}}{\left(1 + \sqrt{K_1 C_{H_2}} + K_{19} C_{CO}\right)^2} \tag{65}$$

where (corresponding to Reference [63])

s_{34}: $COOH{\cdot}S + H{\cdot}S \rightarrow CO{\cdot}S + H_2O{\cdot}S$

s_{31}: $COOH{\cdot}S + S \rightarrow CO_2{\cdot}S + H{\cdot}S$

s_{21}: $CO_2 + S \rightarrow CO_2{\cdot}S$

Activation energies were determined using statistical mechanics and the Unity Bond Index – Quadratic Exponential Potential (UBI–QEP) method. Heats of chemisorption were determined as functions of both temperature and coverage. The heats of chemisorption for both the carboxyl and formate species were taken from density functional theory (DFT) results provided to the authors through personal communications with M. Mavrikakis. The following generalized assumptions were used to calculate the temperature dependence [62]:

1. Each translational, rotational and vibrational degree of freedom corresponds to $0.5R_{gas}T$, $0.5R_{gas}T$, and $R_{gas}T$, respectively;
2. Upon adsorption, all translational degrees of freedom are converted to vibrational degrees of freedom;
3. Upon adsorption, all rotational degrees of freedom are converted into vibrational degrees of freedom.

From TPR experiments, it is shown that, in the presence of OH·S, adsorbed CO combines with the adsorbed hydroxyl to produce adsorbed CO_2 and atomic hydrogen [62]. The CO_2 then desorbs immediately while the H·S combines with present O·S to replenish the adsorbed hydroxyl. This sequence of reactions is considered "autocatalytic" by the authors.

Further, the reaction paths via the carboxyl species are considered indirect. The adsorption and desorption of carboxyl was considered, but noted to be unimportant. Reaction path analysis by the authors indicated that the direct pathway

$$CO_2{\cdot}S + H{\cdot}S \leftrightarrows CO{\cdot}S + OH{\cdot}S$$

is 94% selective while the indirect pathway

$$COOH + S \leftrightarrows COOH{\cdot}S$$
$$COOH{\cdot}S + S \leftrightarrows CO{\cdot}S + OH{\cdot}S$$
$$COOH{\cdot}S + S \leftrightarrows CO_2{\cdot}S + H{\cdot}S$$

is 6% selective. Modifications of the pre-exponential factors adjust the relative selectivities as well as give a better match to experimental results. The indirect pathway is noted to be more significant at higher temperatures [62]. The carboxyl reactions were considered more important than the formate reactions, even though their heats of chemisorption are similar. This is attributed to their significantly different gas-phase heats of reaction, which activates the formation of formate and presumably decreases its likelihood of being formed.

The validity of the rate expression is determined through comparison of its predictions to experimental results, namely, the fixed bed reactor experiments of Xue, et al. [39] on Pt/ZrO_2. The $CO\text{-}H_2$ coupling shows a better fit to the data than the basic mechanism which excludes the coupling reactions; the basic mechanism predicts nearly zero conversion throughout the temperature range. The ratio of the area of catalyst per unit volume of reactor was used as an adjustable parameter, as it was not provide by Xue, et al. [39] and the density of sites was assumed to be 10^{15} sites/cm^2. In comparison to 23-step mechanism of Mhadeshwar and Vlachos [62], their reduced 9-step mechanism shows no deviation from its predicted results [63].

Previous studies of the WGS reaction by Fishtik and Datta [7] suggested a 13-step mechanism for the WGS reaction. The analysis was performed for a Cu(111) catalyst and suggested that three different mechanism dominated the kinetics of the WGS reaction. Namely, these are the associative and formate mechanisms which were shown to dominate at lower temperatures, while the redox mechanism dominated the kinetics at higher temperatures. This mechanism was then expanded by us in Reference [55] with the addition of two more steps. Here, the analysis revealed an alternative to the conventional redox reaction mechanism, namely, the modified redox mechanism ($s_4 + s_{12}$ from Table 3), which was shown to dominate the kinetics at higher temperatures in place of the conventional redox mechanism. In a recent publication [60], we have further amended our previous 15-step WGS mechanism [55] by adding two more elementary reaction steps as shown in Table 3. In this paper, we utilized conventional microkinetics to analyze the activity of the WGS on various metal catalysts. It was concluded that the addition of the step s_{15}, $H_2O{\cdot}S + S \leftrightarrows O{\cdot}S + H_2{\cdot}S$, was unnecessary because "it did not look elementary" and it has a hypothetical transition state that is "too complex". It was

further noted that, by including this step in the mechanism, the predicted results were no longer consistent with experimental data. Using the Unity Bond Index–Quadratic Exponential Potential (UBI–QEP) method to calculate the activation energies and the transition state theory (TST) to predict the pre-exponential factors, microkinetic simulations showed that, for each temperature, the activity of the series of metal considered may be ranked, respectively. For example, at a temperature of 510K, it is shown that the relative activities are in the following order: Cu >> Ni > Fe > Pd, Pt >> Ag, Au [60]. While the authors acknowledge that more sophisticated means for predicting the activation energies and pre-exponential factors is preferred, the use of the UBI–QEP method and the TST provided an adequate methodology for predicting the catalytic activity of a series of single crystalline metal surfaces.

2.4.5. Adopted Mechanism

In the present research, an 18-step mechanism is comprised of the previous elementary reaction steps studied by us (see "WPI Mechanism" in Table 3) [55,60] in addition to the associative desorption of hydrogen (s_{18}). The remaining elementary reaction steps in Table 3 were considered, but were eliminated for various reasons including the species involved, which were not considered as plausible species, either terminal or intermediate, in the present mechanism. In our collaborative work with Zeigarnik and Shustorovich [60], it was concluded that $H_2O{\cdot}S + S \leftrightarrows O{\cdot}S + H_2{\cdot}S$ (s_{19}) was not a plausible elementary reaction step because it did not "look" elementary, i.e., its transition state is too complex. The next step, s_{20}, considered by both Campbell and Daube [50] and Teng, et al. [61] was not included because surface chemistry studies by Shido and Iwasawa [53] indicated that HCOO·S does not dissociate directly to $CO_{2(g)}$.

The associative desorption of CO_2 (s_{21}) was considered by Campbell and Daube [50], Nakamura, et al. [8], Millar, et al. [57] and Teng, et al. [61]. There are some discrepancies regarding the associative desorption of CO_2. The data presented by Nakamura, et al. [8] does not distinctly support or deny the occurrence of this elementary reaction step. It has been disregarded here because of this discrepancy, but may be considered as a plausible elementary reaction step in the future if more conclusive evidence supports the elementary reaction step.

The associative adsorption of H_2 to form adsorbed $H_2O{\cdot}S$ (s_{22}) as proposed by Nakamura, et al. was disregarded due to the lack of supporting surface study results. The direct desoprtion of H_2 from the combination of surface hydroxyls according to s_{26} was proposed by Lund, et al. [56], however, we have disregarded this elementary reaction step because of its complex transition state suggesting that it is not truly elementary. Furthermore, surface study results are not presented to deny or confirm that the reaction occurs as written.

The next two steps in Table 3, s_{27} and s_{28}, are the two-step redox mechanism proposed by Temkin [27] and employed by Nakamura, et al. [8] and Tserpe and Waugh [8]. Many researchers have acknowledged the complexity and non-elementary nature of these reactions (Table 3). As a result, various other mechanisms have been proposed. Thus, we have not included these elementary reaction steps, but have included other reactions to describe the redox mechanism.

Elementary reaction steps involving the carbonate species, i.e., $s_{23} - s_{25}$ [56] and s_{29} [15], have been neglected due to the insuffient supporting data to indicate the species' supporting role in the kinetics of the WGS reaction. In consideration of s_{30}, $HCOO{\cdot}S + H{\cdot}S \leftrightarrows CO{\cdot}S + H_2O{\cdot}S$, as suggested by Teng, et al. [61], we note it's plausibility as an elementary reaction step, but given the lack of surface data supporting its occurrence, it has been neglected. However, should surface evidence be presented, this step may be considered in a future analysis.

Van Herwijen and de Jong [54,66] proposed a series of steps ($s_{31} - s_{32}$ and $s_{34} - s_{37}$) involving the species HCOOH, both in the gas phase and on the surface, as part of their WGS and methane steam reforming mechanisms. This species is not considered a plausible species in our WGS mechanism. The dissociative adsorption of water (s_{40}) was considered initially, but then eliminated; surface studies by Campbell and Daube [50] indicate that water adsorbs and desorbs molecularly and that it dissociates on the catalyst surface. Further, this step does not appear to be elementary. As a result, this step was disregarded in the mechanism adopted for this thesis research.

Ovesen, et al. [14] considered three steps to include the formate species in their WGS studies as given in Table 3. However, they conclude that, via this mechanism, the generation of formate is a "dead end" due to the subsequent formation of $H_2COO{\cdot}S$,

which would then generate methanol, which is not a terminal species considered here. Furthermore, Ovesen, et al. [14] indicate that $H_2COO{\cdot}S$ is generated in very small quantities. Thus, $s_{38} - s_{39}$ have been neglected in the mechanism adopted here. The mechanism proposed by Graven and Long [64], $s_{41} - s_{44}$ where "M" is a collision body, applies to the homogeneous WGS reaction and is not considered here.

The next 14 steps are a substantial part of the WGS mechanism proposed by Mhadeshwar and Vlachos [62,63,75]. Steps 45 – 48 are omitted from the mechanism considered for this research because the gas phase species (O_2, OH, H and O) are not considered terminal species in our mechanism. Furthermore, the next 10 steps, $s_{49} - s_{54}$, involve the carboxyl species (COOH), in both the gas and adsorbed phases. As discussed previously, according the calculations provided by Mhadeshwar and Vlachos [62,63,75] the mechanism via this species contributes little to the overall kinetics of the WGS reaction. Of the remaining four steps, the first includes the formate species in the gas phase, which was not considered here. The remaining steps resemble elementary reaction steps that are already being considered in this study and are therefore eliminated.

Chapter 3. Microkinetic Modeling

Microkinetic modeling is the detailed examination of catalytic overall reactions in terms of the elementary reaction steps that occur on the catalyst surface [18]. These elementary reaction steps constitute the molecular events involved in the overall reaction. In the development of a microkinetic model, no initial assumptions are made concerning the kinetic significance of any of the elementary reaction steps. The calculated rates of each elementary reaction step are the result of the microkinetic model computation rather than the basis for the model. The rate constants of these elementary reactions are predicted from first principles or semi-theoretical methods or are obtained experimentally.

Microkinetic models utilize physical and chemical parameters that can be measured independently or calculated theoretically using tools such as theories of chemical bonding. Among these parameters are: sticking coefficients, surface bond energies, pre-exponential factors for surface reactions, activation energies for surface reactions, surface bonding geometries, active site densities and ensemble sizes [18]. The effort is to relate these parameters to chemical or physical theories of kinetics such as the collision and transition-state theories.

The term "microkinetics" distinguishes this approach from other approaches, e.g., Langmuir-Hinshelwood Hougen-Watson (LHHW) kinetics, which do not incorporate the equivalent levels of surface chemistry in terms of the elementary reaction steps, but involve *ad hoc* assumptions. The use of modern numerical methods has made microkinetic studies more feasible and increasingly popular. Microkinetic modeling provides a tool for consolidating available experimental data, theoretical principles and appropriate correlations relevant to the catalytic process. The combination of surface chemistry and experimental studies allows for a quantitative understanding of catalytic phenomena, and opens the door for *a priori* design of a catalyst for a given overall reaction.

We start with material balances in a CSTR or tubular PBR containing the catalyst that involves the kinetics of the elementary reaction steps. Thus, provided that

elementary reaction step kinetics are available, the rate of reaction or conversion in a reactor may be computed.

3.1. Steady-State Material Balance in a Packed Bed Catalytic Reactor

The packed bed catalytic reactor is assumed to have no radial gradients in concentration, temperature, or reaction rate [22,76]. However, flow and composition of the gas phases change continuously throughout the length of the catalyst bed. The differential equation for calculation of the concentration profile in a packed bed reactor is derived from the material balance through a "slice" of thickness *dl* (see Figure 4).

The catalyst bed is characterized by its porosity ε, site density C_t (sites/cm^2), active catalyst surface area S_t (cm^2/g), and catalyst density ρ_{cat} (g/cm^3). The bed is considered to have a constant cross-sectional area A_{bed} and a length L_{bed}. The mass of the catalyst in the bed is then given by

$$m_{cat} = L_{bed} A_{bed} \left(1-\varepsilon\right) \rho_{cat} \tag{66}$$

The mass of catalyst in the "slice" to be analyzed is

$$dm_{cat} = A_{bed} \left(1-\varepsilon\right) \rho_{cat} dl \tag{67}$$

and contains a volume of gas (V) equivalent to

$$dV = A_{bed} \varepsilon dl \tag{68}$$

Assuming the gas mixture behaves ideally, the contact time for this reactor can then be determined from

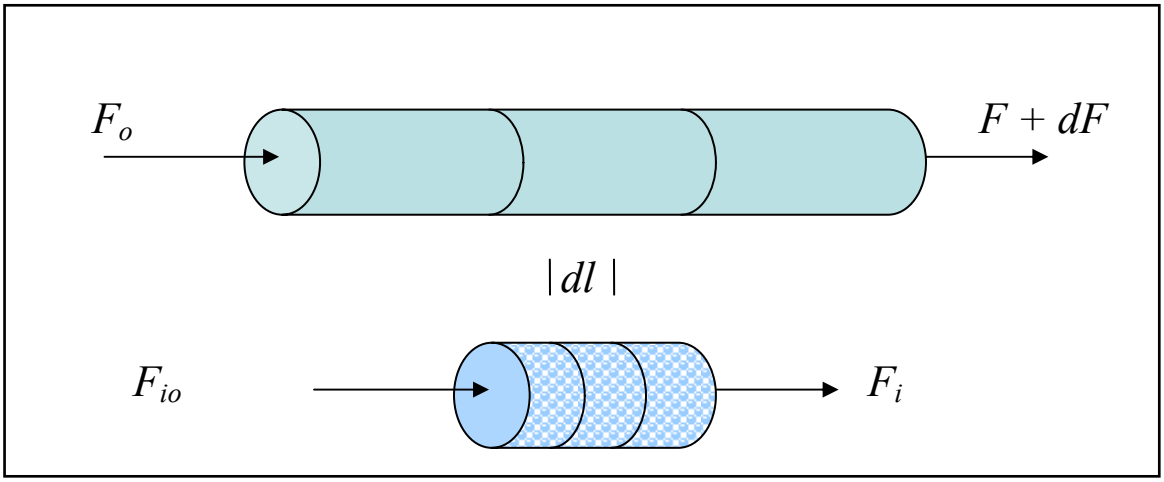

Figure 4. Schematic of the packed bed catalytic reactor

$$dt = \frac{dV}{v_o} = \frac{\varepsilon}{V\rho_{cat}\left(1-\varepsilon\right)} dm_{cat} \tag{69}$$

where v_o is the volumetric flow rate of gas through the reactor, respectively.

Consider an elementary reaction involved in the mechanism of an overall reaction

$$s_\rho : \quad \alpha_{\rho 0}\mathrm{S} + \sum_{k=1}^{q} \alpha_{\rho k}\mathrm{I}_k + \sum_{i=1}^{n} \beta_{\rho i}\mathrm{T}_i = 0 \ ; \qquad (\rho = 1, 2, \ldots, p) \tag{70}$$

where $\alpha_{\rho k}$ and $\beta_{\rho i}$ are the stoichiometric coefficients of the surface intermediates I_k (k = 1, 2, …, q) and terminal species T_i (i = 1, 2, …, n) respectively. Let r_ρ be the rate of the elementary reaction s_ρ. Then, the change in the molar flow rate F_i of the terminal species T_i (i = 1, 2, …, n) over the bed in which p such elementary reactions are occuring is

$$dF_i = \frac{S_t C_t}{N_A} \sum_{\rho=1}^{p} \beta_{\rho i} r_\rho dm_{cat} \tag{71}$$

where r_ρ is the net rate ($r_\rho = \vec{r}_\rho - \overleftarrow{r}_\rho$) of the ρ-th elementary reaction in moles/s·gcat.

Summing over all of the terminal species gives the total mixture molar flow rate

$$dF = \sum_{i=1}^{p} dF_i = \frac{S_t C_t}{N_A} \sum_{i=1}^{n} \sum_{\rho=1}^{p} \beta_{\rho i} r_\rho dm_{cat} \tag{72}$$

Assuming the reactor to behave isothermally, the material balance is given by

$$Fdt + \frac{S_t C_t}{N_A} \sum_{i=1}^{n} \sum_{\rho=1}^{p} \beta_{\rho i} r_\rho dm_{cat} dt = (F + dF)dt \tag{73}$$

Our goal is to determine the mole fractions of the terminal species and surface coverages of the surface species, respectively. For an ideal gas, the mole fractions (x_i) are given by

$$F_i = C_i v = x_i \frac{Pv}{R_{gas}T} \tag{74}$$

where C_i is the concentration of the terminal species T_i, and P, v, and T are the system pressure, volumetric flow rate and temperature, respectively.

Differentiating Equation (74) with respect to dm_{cat} results in the following expression:

$$\frac{dF_i}{dm_{cat}} = \frac{Pv}{R_{gas}T}\frac{dx_i}{dm_{cat}} + x_i \frac{P}{R_{gas}T}\frac{dv}{dm_{cat}} \tag{75}$$

From Equations (71) and (72) we further obtain

$$\frac{dF_i}{dm_{cat}} = \frac{S_t C_t}{N_A}\sum_{\rho=1}^{p} \beta_{\rho i} r_\rho \tag{76}$$

$$\frac{dF}{dm_{cat}} = \frac{S_t C_t}{N_A}\sum_{i=1}^{n}\sum_{\rho=1}^{p} \beta_{\rho i} r_\rho \tag{77}$$

Summing Equation (75) over all terminal species and taking into account that

$$\sum_{i=1}^{p} \frac{dx_i}{dm_{cat}} = 0 \tag{78}$$

we obtain

$$\frac{dF}{dm_{cat}} = \frac{P}{R_{gas}T}\frac{dv}{dm_{cat}} = \frac{S_t C_t}{N_A}\sum_{i=1}^{n}\sum_{\rho=1}^{p}\beta_{\rho i} r_\rho \tag{79}$$

Combining Equations (75) - (76) yields

$$\frac{Pv}{R_{gas}T}\frac{dx_i}{dm_{cat}} = \frac{S_t C_t}{N_A}\left[\sum_{\rho=1}^{p}\beta_{\rho i} r_\rho - x_i\sum_{i=1}^{n}\sum_{\rho=1}^{p}\beta_{\rho i} r_\rho\right] \tag{80}$$

Acknowledging that

$$\frac{Pv}{R_{gas}T} = \frac{F_i}{x_i} = \frac{F_{0i}}{x_{0i}} \tag{81}$$

where the "0" subscript represents initial or inlet conditions, substitution of Equation (81) into Equation (80) results in

$$\frac{dx_i}{d\left(\frac{m_{cat}}{F_{0i}}\right)} = x_{0i}\frac{S_t C_t}{N_A}\left[\sum_{\rho=1}^{p}\beta_{\rho i} r_\rho - x_i\sum_{i=1}^{n}\sum_{\rho=1}^{p}\beta_{\rho i} r_\rho\right] \tag{82}$$

Substituting Equation (69) into Equation (82) gives the time derivative of the mole fraction of each species

$$\frac{dx_i}{dt} = \frac{1-\varepsilon}{\varepsilon}\frac{S_t C_t}{N_A}\frac{R_{gas}T}{P}\left[\sum_{\rho=1}^{p}\beta_{\rho i} r_\rho - x_i\sum_{i=1}^{n}\sum_{\rho=1}^{p}\beta_{\rho i} r_\rho\right] \tag{83}$$

where the integration should be performed from zero (entrance) to a desired contact time at the exit.

The fractional coverages of the surface intermediates may be evaluated by solving a system of ODEs

$$\frac{d\theta_k}{dt} = \sum_{\rho=1}^{p} \beta_{\rho k} r_\rho \qquad \left(k = 1, 2, ..., q\right) \qquad (84)$$

3.2. Unsteady-State Material Balance in a Continuous Stirred Tank Reactor

It is well known that the outlet conversion of a packed bed reactor (PBR) is equal to that achieved by a continuous stirred tank reactor (CSTR) that has been properly sized. For this reason, the numerical simulations of a CSTR are equivalent to those of a PBR. Here, we have taken advantage of this phenomena and utilized the equations that govern a CSTR to relax the computational demands.

The gas phase material balance for a CSTR of volume V retaining the catalyst in terms of the number of moles N_i of the terminal species T_i (i = 1,2,…,n) is given by

$$\frac{dN_i}{dt} = F_{0i} - F_i + \frac{1-\varepsilon}{\varepsilon} \frac{S_t C_t \rho_{cat}}{N_A} \left(\sum_{\rho=1}^{p} \beta_{\rho i} r_\rho \right) V \qquad (85)$$

while the surface species' coverages are described by Equation (84), i.e., as in the case of the PBR.

Employing the ideal gas mixture model, Equation (81) gives

$$\frac{dN_i}{dt} = \frac{P\nu}{R_{gas} T} \left(x_{0i} - x_i \right) + \frac{1-\varepsilon}{\varepsilon} \frac{S_t C_t \rho_{cat}}{N_A} \left(\sum_{\rho=1}^{p} \beta_{\rho i} r_\rho \right) V \qquad (86)$$

or, introducing the mean residence time $\tau = V / \nu$

$$\frac{1}{N} \frac{dN_i}{dt} = \frac{1}{\tau} \left(x_{0i} - x_i \right) + \frac{1-\varepsilon}{\varepsilon} \frac{S_t C_t \rho_{cat}}{N_A} \left(\sum_{\rho=1}^{p} \beta_{\rho i} r_\rho \right) V \qquad (87)$$

where N is the total number of moles of the terminal species. Since $N_i = x_i N$ we further have

$$\frac{dN_i}{dt} = N\frac{dx_i}{dt} + x_i\frac{dN}{dt} \tag{88}$$

Combining Equations (87) and (88) gives

$$\frac{dx_i}{dt} + \frac{x_i}{N}\frac{dN}{dt} = \frac{1}{\tau}\left(x_{0i} - x_i\right) + \frac{1-\varepsilon}{\varepsilon}\frac{S_t C_t \rho_{cat}}{N_A}\left(\sum_{\rho=1}^{p}\beta_{\rho i} r_\rho\right)V \tag{89}$$

Summing these expressions over all terminal species and taking into account that

$$\sum_{i=1}^{n} x_i = 1,\ \sum_{i=1}^{n}\frac{dx_i}{dt} = 0 \text{ and } \sum_{i=1}^{n}\left(x_{0i} - x_i\right) = 0 \tag{90}$$

gives

$$\frac{1}{N}\frac{dN}{dt} = \frac{1-\varepsilon}{\varepsilon}\frac{S_t C_t \rho_{cat}}{N_A}\left(\sum_{\rho=1}^{p}\beta_{\rho i} r_\rho\right)V \tag{91}$$

Finally, substituting Equation (91) into Equation (89) results in

$$\frac{dx_i}{dt} = \frac{1}{\tau}\left(x_{0i} - x_i\right) + \frac{R_{gas}T}{P}\frac{1-\varepsilon}{\varepsilon}\frac{S_t C_t \rho_{cat}}{N_A}\left(\sum_{\rho=1}^{p}\beta_{\rho i} r_\rho - x_i\sum_{i=1}^{n}\sum_{\rho=1}^{p}\beta_{\rho i} r_\rho\right)V \tag{92}$$

When considering a surface reaction mechanism comprised of several elementary reaction steps, the rates of each of the steps are incorporated into the material balance, as shown in Equation (92) by the summation terms. In the case where the overall reaction may be obtained by only a select few elementary reaction steps, the rates of the remaining steps are assumed to be zero, such that they do not contribute in the summation.

3.3. Mass Transfer Limitations

In heterogeneous catalysis, the mass transfer limitations require consideration, especially if experiements are performed to determine intrinisic catalytic kinetics. The assumption that the same reactant concentration is available to the entire surface of the catalyst may not hold. Typically, where the reactants diffuse into the pores of the catalyst particle, the concentration of reactants at the mouth of the pore may be much higher than that inside the pore. To account for this, we utilize the effectiveness factor. Of course, under conditions when intrinsic kinetics are to be measured, the catalyst particle size is reduced to a size that ensures a unity effectiveness factor.

Mass transfer of reactants first occurs as the reactants leave the bulk fluid and enter the external surface of the catalyst. The reactants then diffuse from the external surface into and through the pellet pores. Once in the pores, the reaction only occurs on the surface of the pores.

3.3.1. Internal Mass Transfer

For isothermal conditions, the internal effectiveness factor is defined as a measure of how far the reactant diffuses into the pellet before reacting.

$$\eta = \frac{\text{actual overall reaction rate}}{\begin{array}{c}\text{rate of reaction that would result if}\\ \text{entire surface were exposed to the}\\ \text{external pellet surface conditions } (C_{is}, T_s)\end{array}} \tag{93}$$

where C_{is} is the surface concentration of species i and T_s is the surface temperature of the catalyst. The magnitude of the effectiveness factor ranges between 0 and 1 indicating the relative importance of diffusion and reaction limitations [76]. The internal effectiveness factor varies for different reaction orders and catalyst shapes, as represented by Figure 5.

For reactions of order n, the Thiele modulus is given by

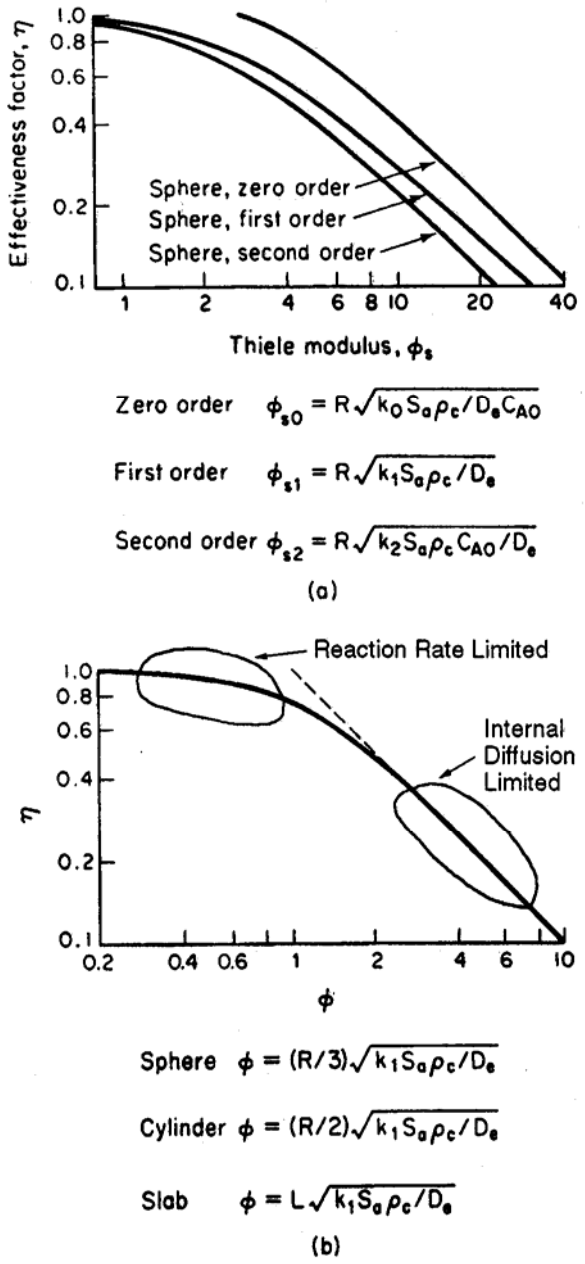

Figure 5. Internal effectiveness factor for different reaction orders and catalyst shapes. (Adapted from Fogler [76].)

$$\phi_n^2 = \frac{k_n R^2 S_t \rho_{cat} C_{is}^{n-1}}{D_e} \tag{94}$$

where k_n is the rate constant of the n-th order surface reaction, R is the radius of the catalyst particle, S_t is the surface area of the catalyst per unit mass of catalyst, ρ_{cat} is the density of the catalyst, and D_e is either the bulk or the Knudsen diffusivity. The effectiveness factor is consequently given by

$$\eta = \left(\frac{2}{n+1}\right)^{1/2} \frac{3}{\phi_n} = \left(\frac{2}{n+1}\right)^{1/2} \frac{3}{R}\sqrt{\frac{D_e}{k_n S_t \rho_{cat}}} C_{is}^{\frac{1-n}{2}} \tag{95}$$

For reaction orders greater than one, the effectiveness factor decreases with increasing concentration at the external catalyst particle surface.

3.3.1.1 Non-isothermal and Exothermic Reactions

In the case of a non-isothermal and exothermic reaction, the effectiveness factor may be significantly greater than one. This occurs because the external surface temperature (T_s) of the catalyst particle is less than the actual temperature inside the pellet where the reaction is occurring. As a result, the rate of the reaction inside the pellet is greater than the rate at the surface. This dependence is parameterized in terms of β_T and γ_A:

$$\gamma_A = \text{Arrhenius number} = \frac{E}{R_{gas} T_s} \tag{96}$$

$$\beta_T = \frac{\Delta T_{\max}}{T_s} = \frac{T_{\max} - T_s}{T_s} = \frac{\Delta H_{rxn} D_e C_{is}}{k_t T_s} \tag{97}$$

where E is the activation energy k_t is the thermal conductivity and ΔH_{rxn} is the heat of the reaction. From Equation (97), we see that the lower the value of k_t used, the higher the

heat of reaction required and the greater the temperature difference. This trend is illustrated in Figure 6.

3.3.1.2 Falsified Kinetics

Under circumstances in which the measured reaction order and activation energies are not the true values, the slope of a log-log plot of rate of reaction as a function of bulk gas concentration yields the apparent reaction order n^{app}. In order to relate this measured reaction order to the true reaction order, the effectiveness factor is used:

$$-r'_i = \eta\left(-r'_{is}\right) = \eta\left(k_n S_a C_{is}^n\right) \tag{98}$$

For large values of the Thiele modulus, the left hand side of Equation (98) may be written as

$$-r_i' = \frac{3}{R}\sqrt{\frac{2D_e S_t}{(n+1)\rho_{cat}}}k_n^{1/2} C_{is}^{\frac{1-n}{2}} \tag{99}$$

From Equation (98), equating this expression with the measured rate we find that

$$-r_i' = \frac{3}{R}\sqrt{\frac{2D_e S_t}{(n+1)\rho_{cat}}}k_n^{1/2} C_{is}^{\frac{1-n}{2}} = k_n^{app} C_{is}^{app} \tag{100}$$

Defining the apparent rate constant in terms of the apparent activation energy and pre-exponential factor associated with the apparent reaction order gives

$$k^{app} = \Lambda^{app}\exp\left(-\frac{E^{app}}{R_{gas}T}\right) \tag{101}$$

while the true rate constant is given by

$$k = \Lambda\exp\left(-\frac{E}{R_{gas}T}\right) \tag{102}$$

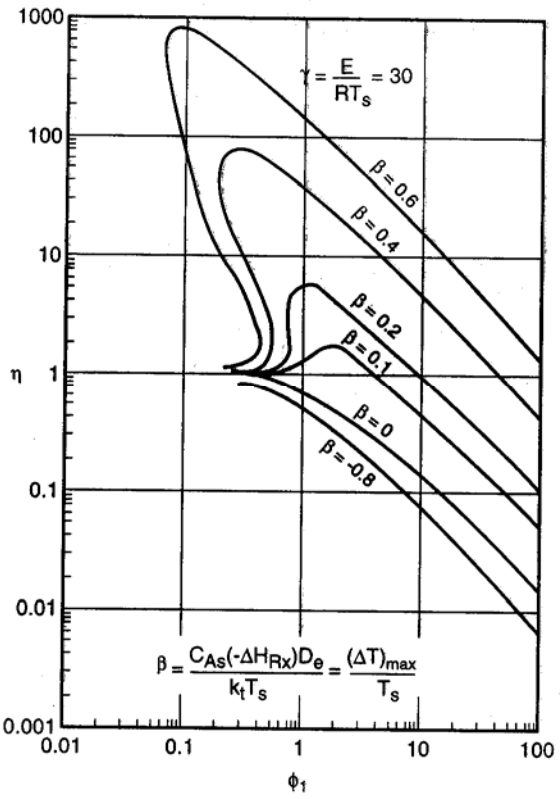

Figure 6. Parameter effects of β and γ on the non-isothermal effectiveness factor as a function of the Thiele modulus. (Adapted from Fogler [76].)

After substitution of Equations (101) and (102), Equation (100) becomes

$$-r_i' = \frac{3}{R}\sqrt{\frac{2D_eS_t}{(n+1)\rho_{cat}}}\Lambda^{1/2}\left[\exp\left(-\frac{E}{R_{gas}T}\right)\right]^{1/2} C_{is}^{\frac{1-n}{2}} = \Lambda^{app}\left[\exp\left(-\frac{E^{app}}{R_{gas}T}\right)\right]C_{is}^{app} \tag{103}$$

Taking the natural log of both sides alludes to the relationship between E and E^{app}:

$$\ln\left[\frac{3}{R}\sqrt{\frac{2D_eS_t}{(n+1)\rho_{cat}}}\Lambda^{1/2}C_{is}^{\frac{1-n}{2}}\right] - \frac{E}{2R_{gas}T} = \ln\left[\Lambda^{app}C_{is}^{app}\right] - \frac{E^{app}}{R_{gas}T} \tag{104}$$

From Equation (104), we see that the true activation energy is equal to twice the apparent activation energy. The significance of these falsified kinetics is evident when considering the case where internal diffusion limitations are negligible and a higher true activation energy would increase the temperature sensitivity of the reaction creating the possibility for runaway reactions. Thus, every effort is made to avoid diffusion in experiments to measure true kinetics.

3.3.2. Overall Effectiveness Factor

For most catalysts, the internal surface area is much greater than the external surface area. Mathematically, this is given by $S_t\rho_b \gg a_{cat}$ where $\rho_b = \rho_{cat}(1-\phi)$ is the bulk density (ϕ is the void fraction of the catalyst bed) and a_{cat} is the surface area per volume of catalyst. The rate of mass transfer for this case is given by

$$W_i a_{cat} = -r_i'' S_t \rho_b \tag{105}$$

where $-r_i''$ is the overall rate of reaction within and on the pellet per unit surface area. Previously, we saw that the internal effectiveness factor is a measure of the surface accessibility

$$-r_i'' = -r_{is}''\eta \tag{106}$$

The overall effectiveness factor is based on the bulk concentration C_{ib} and is defined as

$$\Omega = \frac{\text{actual overall rate}}{\begin{array}{c}\text{rate that would result if the entire} \\ \text{surface were exposed to } C_{ib}\end{array}} \tag{107}$$

The rates of reaction based on surface and bulk concentrations are, therefore, related by

$$-r_i'' = \Omega\left(-r_{ib}''\right) = \eta\left(-r_{is}''\right) \tag{108}$$

3.3.3. Diffusion and Reaction Limited Regime

In many studies, it is of interest to obtain crude approximations to identify the rate limiting step in a heterogeneous reaction: mass transfer or kinetics. The Weisz-Prater criterion provides a method to determine if internal diffusion is the limiting factor based on observed rates of reaction. Equations (94) and (95) may be rearranged in the form

$$\eta\phi_n^2 = \left(\frac{2}{n+1}\right)^{1/2} 3R\sqrt{\frac{k_n S_t \rho_{cat}}{D_e} C_{is}^{\left(\frac{n-1}{2}\right)}} \tag{109}$$

where the left hand side is the Weisz-Prater parameter:

$$C_{WP} = \eta \times \phi_n^2 = \frac{\text{actual reaction rate}}{\text{diffusion rate}} \tag{110}$$

From Equation (109), the Weisz-Prater parameter may be calculated. If $C_{WP} \ll 1$, it is assumed that there are no diffusion limitations and, consequently, no concentration gradients within the catalyst particle. If $C_{WP} \gg 1$, internal diffusion is assumed to severely limit the reaction.

The Mears criterion is used as an indicator of the effect of external diffusion limitations. Like the Weisz-Prater criterion, it uses the measured rate of reaction to learn if mass transfer from the bulk gas phase to the catalyst surface can be neglected.

Mears proposed the following criterion where n is the reaction order, R is the catalyst particle radius (m), ρ_b is the bulk density of the catalyst bed (kg/m^3), C_{ib} is the bulk concentration of species i (kmol/m^3) and k_c is the mass transfer coefficient (m/s). If Equation (111) holds,

$$\frac{-r_i'\rho_b Rn}{k_c C_{ib}} < 0.15 \tag{111}$$

then external mass transfer effects are negligible and it may be assumed that no concentration gradient exists between the bulk gas and external surface of the catalyst particle.

Mears proposed a second criterion relating to the bulk fluid temperature, T. This states that if

$$\left|\frac{-\Delta H_{rxn}\left(-r_i'\right)\rho_b RE}{h_T T^2 R_{gas}}\right| < 0.15 \tag{112}$$

where h_T is the heat transfer coefficient (kJ/m^2·s·K), R_{gas} is the gas constant (kJ/mol·K), ΔH_{rxn} is the heat of reaction (kJ/mol) and E is the activation energy (kJ/mol), then the bulk temperature will be essentially the same as the temperature at the external surface of the catalyst particle.

3.3.4. Mass Transfer in Packed Bed Reactors

The mass transfer effects within packed bed reactors may be determined by analysis of a "slice" of the packed bed. The equation describing the diffusion in the catalyst bed is given by

$$D_a \frac{\mathrm{d}^2 C_{ib}}{\mathrm{d}z^2} - U \frac{\mathrm{d}C_{ib}}{\mathrm{d}z} - \left(-r_i'\right)\rho_b = 0 \tag{113}$$

where D_a is the effective axial dispersion coefficient and U is the velocity of the particle. In the case of a first order reaction, Equation (113) becomes

$$D_a \frac{\mathrm{d}^2 C_{ib}}{\mathrm{d}z^2} - U \frac{\mathrm{d}C_{ib}}{\mathrm{d}z} - \Omega\rho_b k S_a C_{ib} = 0 \tag{114}$$

Solving this equation for the case in which the flow rate is sufficiently large that axial diffusion may be neglected, Finlayson [76] showed that when

$$\left|\frac{-r_i'\rho_b d_p}{U_o C_{ib}}\right| \ll \left|\frac{U_o d_p}{D_a}\right| \tag{115}$$

where U_o is the superficial velocity and d_p is the particle diameter, axial dispersion may be neglected. The Thoenes-Kramers correlation [77] for flow through packed bed reactors is given in terms of the dimensionless Sherwood, Reynolds and Schmidt numbers by $\mathrm{Sh'}=1.0(\mathrm{Re'})^{1/2}(\mathrm{Sc})^{1/3}$ where

$$\begin{aligned} \mathrm{Re'} &= \frac{\mathrm{Re}}{(1-\phi)\zeta} \\ \mathrm{Sh'} &= \frac{\mathrm{Sh}\phi}{(1-\phi)\zeta} \end{aligned} \tag{116}$$

Substitution of the dimensionless numbers and Equation (116) into the Thoenes-Kramers correlation yields

$$\frac{k_c d_p}{D_g}\left(\frac{\phi}{1-\phi}\right)\frac{1}{\zeta} = \left(\frac{U d_p \rho_f}{\mu_f (1-\phi)\zeta}\right)^{1/2}\left(\frac{\mu_f}{\rho_f D_g}\right)^{1/3} \tag{117}$$

where ζ is a shape factor defined by the external surface area divide by πd_p^2, μ_f is the fluid viscosity (kg/m·s), ρ_f is the fluid density (kg/m^3) and D_g is the gas diffusivity (m^2/s). This correlation is valid for $0.25 < \phi < 0.5$, $40 < \mathrm{Re}' < 4000$, and $1 < \mathrm{Sc} < 4000$. The correlation offers a relationship between the mass transfer coefficient for a particular geometry and the flow field.

For constant fluid properties, the mass transfer coefficient is directly proportional to the square root of the velocity and inversely proportional to the square root of the particle diameter:

$$k_c \propto \frac{U^{1/2}}{d_p^{1/2}} \tag{118}$$

For surface reaction-limited reactions, the rate is independent of particle size, but is a strong function of temperature. In Table 12, a summary of rate dependence based on the velocity, particle size and temperature is presented for internal and external diffusion, and surface reaction limitations. The exponential temperature dependence for internal diffusion limitations is usually not as strong a function of temperature as in the dependence of surface reactions.

With the above discussion of reactor analysis completed, we turn our attention to thermodynamics and kinetics of elementary reaction steps.

3.4. Reaction Thermodynamics

As previously mentioned, the water-gas-shift reaction is thermodynamically limited at higher temperatures. The equilibrium constant K is defined in terms of the equilibrium concentrations or partial pressures of the reactants and products:

$$K = \frac{P_{CO_2} P_{H_2}}{P_{CO} P_{H_2O}} = \frac{x_{CO_2} x_{H_2}}{x_{CO} x_{H_2O}} = \exp\left(-\frac{\Delta G}{R_{gas} T} \right) \tag{119}$$

Table 12. Variation of reaction rate with key parameters for different limitations [76].

Type of Limitation	Velocity	Particle Size	Temperature
External Diffusion	$U^{1/2}$	$d_p^{-3/2}$	≈ Linear
Internal Diffusion	Independent	d_p^{-1}	Exponential
Surface Reaction	Independent	Independent	Exponential

The partial pressures may then be given in terms of conversion of CO within a reactor and initial feed partial pressure of CO as described in the Section 3.1 above.

Calculation of the equilibrium conversion of CO may be determined from the equilibrium constant as a function of temperature. For example, in the case where equimolar feed of CO and H_2O are fed to the reactor (i.e. $x_{CO} = x_{H_2O}$; $x_{CO_2} = x_{H_2} = 0$)

$$X = \frac{\sqrt{K}}{1+\sqrt{K}} \tag{120}$$

Application of tabulated thermodynamic functions in thermodynamic handbooks provides an expression for ΔG, the Gibbs free energy of the reaction, as a function of temperature. The expression given in Equation (121) is derived using the computer program HSC [78], an electronic collection of thermodynamic data, and SCIENTIST [79], a data fitting program.

$$\Delta G\left(\text{kJ/mol}\right) = -32.197 + 0.03104T - \frac{1774.7}{T} \tag{121}$$

Similarly, an expression for the equilibrium constant may also be determined using the same software as described above. The equilibrium constant of the reaction (K) may be calculated from Equation (122), written in terms of $\log(K)$.

$$\log(K) = -2.4198 + 0.0003855T + \frac{2180.6}{T} \tag{122}$$

Plotted, these parameters define the thermodynamic limitations of the water-gas-shift reaction, as shown in Figure 3 in Section 2.2.

3.5. Elementary Reaction Energetics

The most direct theoretical approaches to surface reactivity are based on the estimation of reaction energetics (enthalpies and activation barriers). Determination of adsorption energies and activation barriers of surface reactions is a difficult task for theory. While reaction energetics should be determined using quantum mechanical methods [22,72], such as first principles *ab initio* or density functional theory (DFT) [3,80-85], these methods are currently much more useful for structural predictions (i.e., bond energies, vibrational frequencies, charge moments, etc.) than for thermochemical properties due to their computational demands. As a result, accurate theoretical calculations of bond energies and activation barriers for surface reactions are still a sizeable challenge. The simulation of adsorption and surface reaction on a metal surface is commonly accomplished by modeling the catalyst surface as a finite cluster of limited size. A fundamental dilemma, with both DFT and *ab initio*, is designing or assembling the cluster of a size such that it accurately represents the atoms on the bulk surface. It is a theoretical paradox: the clusters must be large enough to adequately represent a geometric and electronic structure of a surface; yet, the size of the cluster must also be small enough that it may be accurately treated by the available methods.

"In semi-empirical calculations of both cluster- and slab-type, reasonable agreement with experiment can usually be reached by using *ad hoc* parameters [17]." However, the use of *ad hoc* parameter values blurs the conceptual picture. Because of the challenge with both first-principle and semi-empirical methods, another practical alternative is considered: the phenomenological approach [17]. The phenomenological approach differs from empirical- or heuristic-based approaches because it employs phenomenological quantities, i.e., observable thermodynamic quantities, as input parameters and analytically calculates quantities relevant to phenomenological, observable thermodynamic properties of surface adsorption and reactive systems. The greatest advantage of an analytic phenomenological model is that it provides a direct conceptual understanding through its explicit interrelations among its parameters. Because our interest is with surface energetics, the model should be based on

thermodynamics. An informative analytic model should have a "rigorous and rigid mathematical formalism" which provides well-defined rules [17].

During the 1980s, the Bond Order Conservation–Morse Potential (BOC–MP) method was developed by Shustorovich. After years of further development, the BOC–MP method was able to describe the energetics of chemisorption and surface reaction on metal surfaces rather accurately based on only a few basic inputs. Specifically, atomic heats of adsorption and gas phase molecular bond energies are all that is needed to effectively calculate the heats of chemisorption of diatomic and polyatomic molecules, as well as activation barriers of dissociation, recombination and disproportionation reactions. In the 1990s, the BOC–MP method was found to be more general than initially thought. Further developments resulted in the renaming of the method, now known as the Unity Bond Index–Quadratic Exponential Potential (UBI–QEP) method. This "new" method is unique due to its success with complex reactions whose mechanisms may be extensive both in terms of the number of intermediates and the number of reactions. In comparison to first-principles modeling of similarly complex mechanisms, so many simplifying assumptions are typically made that the methodology becomes nearly phenomenological. *Ab initio* methods do not currently meet the "pragmatist's condition" [17] of applicability due to lengthy computational times. Faster DFT methods are more attractive than *ab initio*, however they are presently incapable of routinely producing results of significant accuracy. At a more macro-scale, Monte Carlo methods are considered impractical due to the lack of suitable potential energy functions for more complex systems. Instead the UBI–QEP method was designed to calculate energetics of a wide variety of complex reactions with an accuracy of ±1-3 kcal/mol. This method has been successfully applied to several reaction systems including direct conversion of methane to methanol [86], methanol synthesis [9], hydrogen peroxide synthesis [87], ammonia synthesis [88], NO reduction and decomposition [89], and Fischer-Tropsch synthesis [90,91], among others.

While the BOC–MP method was initially based on three postulates, the modified UBI-QEP method is now based on four main postulates. First, the-two body interaction energy poses a single minimum and approaches zero monotonically as the distance

between them increases. Second, the two-body interaction potential is spherical and depends only on the interbody distance r

$$E\left(x\left(r\right)\right) = a\left[x^2\left(r\right) - 2x\left(r\right)\right] \tag{123}$$

Third, as shown above, the two-body interaction is expressed as a polynomial function of an exponential variable called the bond index,

$$x\left(r\right) = \exp\left[\frac{-\left(r - r_0\right)}{b}\right] \tag{124}$$

where r is the distance of the bond of interest, a is the bond energy, r_0 is the equilibrium distance corresponding to the minimum interaction energy, and b is a distance scaling constant. Fourth, the multi-body, where "body" is defined as an atom or group of atoms that may be treated as a single entity [17], potential energy is formed by summing the nearest neighbor pair-wise interactions, i.e.,

$$E = \sum_i a_i\left[x\left(r\right)_i^2 - 2x\left(r\right)_i\right], \tag{125}$$

constrained by the *unity bond index* conservation, i.e.,

$$X = \sum_i x\left(r\right)_i = 1. \tag{126}$$

The bond index function should be defined such that: a one-to-one correspondence between $x(r)$ and r exists; $x(r)$ is non-negative and greater than zero; $x(r)$ monotomically decreases to zero as r increases without bound; and, at the equilibrium distances, $x_0 = x(r_0) = 1$.

The unity bond index (UBI) condition at equilibrium requires that, at the equilibrium distance, r_0, any bond index will be unity, regardless of the system. In

addition, the total bond index (N) of a multi-body system is conserved, stipulating that $N = x_0$. Bond indices are the same regardless of changing multiplicities of states, therefore N may be considered a normalization constant where

$$N = \sum_i x_i(r_i). \tag{127}$$

The value of the equilibrium bond index is the value to which the bond index is conserved. As a result, the unity bond index condition may be written as

$$X = \sum_i x_i(r_i) = N = 1. \tag{128}$$

The unity bond index postulate [17] states:

"The sum of the two-body bond indices of the active bonds along any minimum energy path of a metal surface reaction is conserved and equal to unity."

The total energy of a many-body system can be expressed as a summation of additive two-body bond energies governed by the UBI condition. For practical reasons, the sum over pair-wise interaction energies is limited to nearest neighbors within a metal surface unit mesh or bonding site. Within the UBI–QEP method, the heats of chemisorption (Q) and reaction activation barriers ($\vec{E}$ and $\overleftarrow{E}$) are independent of the choice of the bond index; they only contain energy parameters which are thermodynamic observables which are obtained from atomic chemisorption energies (Q_A) and gas-phase molecular bond energies (D_{AB}). In the modeling of surface energetics, an error of just a few kcal/mol in an activation barrier can cause a change in the calculated reaction rate of several orders of magnitude. Therefore, accuracy to withing ±1-3 kcal/mol is the goal. The rationale behind the UBI-QEP is described below in detail.

3.5.1. Heats of Adsorption and Surface Reactions

The heat of adsorption is determined from an energy function which is the sum of n nearest neighbor pair-wise interactions between a "body" A and a surface site M:

$$E = Q_0 \sum_i^n \left[x_i^2 \left(r_i \right) - 2x_i \left(r_i \right) \right] \tag{129}$$

where Q_0 is the strength of the M-A interaction, independent of the crystal plane. The details of the derivation are provided for illustrative purposes [17].

The binding energy, Equation (129), is subject to the UBI constraint, Equation (128). Applying the method of Lagrangian multipliers to optimize the binding energy, we find that the function to be optimized is

$$L = E - \alpha \left(\sum_i^n x_i \left(r_i \right) - 1 \right) \tag{130}$$

where α is the Lagrangian multiplier of the UBI constraint. Substitution of Equation (129) into Equation (130) gives

$$L = Q_0 \sum_i^n \left[x_i^2 \left(r_i \right) - 2x_i \left(r_i \right) \right] - \alpha \left(\sum_i^n x_i \left(r_i \right) - 1 \right) \tag{131}$$

Setting the first derivative of the Lagrangian function equal to zero for all k

$$\frac{\partial L}{\partial x_k} = 2Q_{0A} x_k \left(r_0 \right) - 2Q_{0A} - \alpha = 0 \tag{132}$$

and rearranging

$$\frac{\partial L}{\partial x_k} = 2Q_{0A} \left(x_k \left(r_0 \right) - 1 \right) - \alpha = 0 \tag{133}$$

allows us to solve for the k-th bond order, x_k:

$$x_k\left(r_0\right)=1-\frac{\alpha}{2Q_{0A}} \tag{134}$$

Substitution of the UBI condition (Equation (128)) into the *k*-th bond index expression where

$$x_k\left(r_0\right)=\frac{1}{n} \qquad \text{(for all } k\text{)} \tag{135}$$

(because all of the equilibrium values of the two-center bond indices must be the same and equal) allows us to solve for the Lagrangian multiplier:

$$\alpha=2Q_{0A}\left(\frac{1}{n}-1\right) \tag{136}$$

The surface binding energy, $Q_{n\mathrm{A}}$, may now be equated using the solution for α, the expression for the *k*-th bond index and the energy relation in Equation (129). It should be noted that the surface binding energy is opposite what is needed to bind the adatom.

$$Q_{nA}=-E\left(n\right)=-Q_{0A}\sum_i^n\left[x_i^2\left(r_i\right)-2x_i\left(r_i\right)\right]=-Q_{0A}\left[\sum_i^n x_i^2\left(r_i\right)-2\sum_i^n x_i\left(r_i\right)\right] \tag{137}$$

Recall that

$$\sum_k^n x_k\left(r_0\right)=1 \text{ and } x_k\left(r_0\right)=\frac{1}{n} \tag{138}$$

Therefore

$$Q_{nA}=-E\left(n\right)=Q_{0A}\left(2-\frac{1}{n}\right) \tag{139}$$

Thus, the atomic binding energy of species A, Q_A, is

$$Q_A = Q_{0A}\left(2 - \frac{1}{n}\right) \tag{140}$$

The heats of chemisorption for diatomic molecules are based on the type of binding. Weakly bound molecules such as closed shell molecules (i.e., CO, N_2) or molecular radicals with strongly delocalized unpaired electrons (i.e., O_2, NO) tend to have heats of chemisorption in the range 10-35 kcal/mol. The heat of chemisorption for mono-coordination of weakly bound diatomics over a *n*-fold site is given by Equation (141):

$$Q_{AB,n} = \frac{Q_{0A}^2}{\left(\frac{Q_{0A}}{n} + D_{AB}\right)} \tag{141}$$

where atom A is considered the contact atom and M-B repulsive interaction are neglected. Details of the derivation are omitted here and may be found in Reference [17]. As a result, the calculated value may be inaccurate for mono-coordination of homonuclear diatomics molecules.

Strong binding typically occurs with radicals that have localized unpaired electrons (i.e. OH, SH and CH). In this case, the heat of chemisorption is given by

$$Q_{AB,n} = \frac{Q_A^2}{Q_A + D_{AB}} \tag{142}$$

Strongly bound molecules have heats of chemisorption in the range 35-120 kcal/mol. Medium binding gives an average of the two extremes. It may be applied to species such as the methyl radical or other mono-valent molecular radicals that contain a tetra-valent central (contact) atom.

Once the heats of adsorption are determined, the enthalpy change for each reaction, as it occurs on the surface, may be calculated from

$$\Delta H = \sum_r Q_r - \sum_p Q_p + \sum_b D_b - \sum_f D_f \tag{143}$$

where Q_r and Q_p are the heats of chemisorption for the reactants (r) and products (p), respectively; D_b and D_f are the binding energies for the bonds that are broken (b) and formed (f), respectively. This summation is based on the enthalpy changes of the thermodynamic cycle:

(A)	adsorbed reactants → gas-phase reactants	$\Delta H_A = \sum_r Q_r$
(B)	gas-phase reactants → gas-phase products	$\Delta H_B = \sum_b D_b - \sum_f D_f$
(C)	gas-phase products → adsorbed products	$\Delta H_C = -\sum_p Q_p$
NET:	adsorbed reactants → adsorbed products	$\Delta H = \Delta H_A + \Delta H_B + \Delta H_C$

In the case of the disproportionation reaction, A·S + BC·S ⇆ AB·S + C·S, the direction of the reaction is defined such that the condition that $D_{BC} > D_{AB}$ is satisfied. If it is not, the direction of the reaction should be reversed for the analysis.

3.5.2. Activation Energy

The activation energy of the reaction in the forward direction, corresponding to the appropriate form of the reaction, may be determined using Equation (144)

$$\vec{E} = \frac{1}{2}\left[\Delta H + \frac{Q_{AB}Q_C}{Q_{AB} + Q_C}\right] \tag{144}$$

The activation energy of the reverse direction may then be determined from the relationship between the reaction enthalpy and the reaction's activation barriers (Figure 7), i.e., $\Delta H = \vec{E} - \overleftarrow{E}$

$$\overleftarrow{E} = \vec{E} - \Delta H \tag{145}$$

In the case where the numerical result for either the forward or reverse activation energy is negative, both activation energies are shifted such that the negative activation energy is forced to zero and the enthalpy change for the reaction remains unchanged.

To obtain the dissociation barrier for reactions in which gas-phase species are involved, the heat of adsorption of the dissociating molecule, i.e., Q_{AB}, should be subtracted from the barrier relative to surface adsorbate reactants to compensate thermodynamically for the interaction with the surface:

$$\vec{E}_{gas} = \vec{E}_{ads} - Q_{AB} \tag{146}$$

The reverse activation energy for this type of reaction may be determined from the following equations, depending on the sign of the forward activation barrier

$$\overleftarrow{E}_{ads} = \overleftarrow{E}_{gas} = Q_A + Q_B - D_{AB} + \vec{E}_{gas} \qquad (\vec{E}_{gas} > 0) \tag{147}$$

or

$$\overleftarrow{E}_{gas} = \overleftarrow{E}_{ads} - \vec{E}_{gas} = Q_A + Q_B - D_{AB} \qquad (\vec{E}_{gas} < 0) \tag{148}$$

where D_{AB} is defined as the difference between total bond energies of the reactants and products. This definition is valid for both atomic and molecular adsorbates. [92]

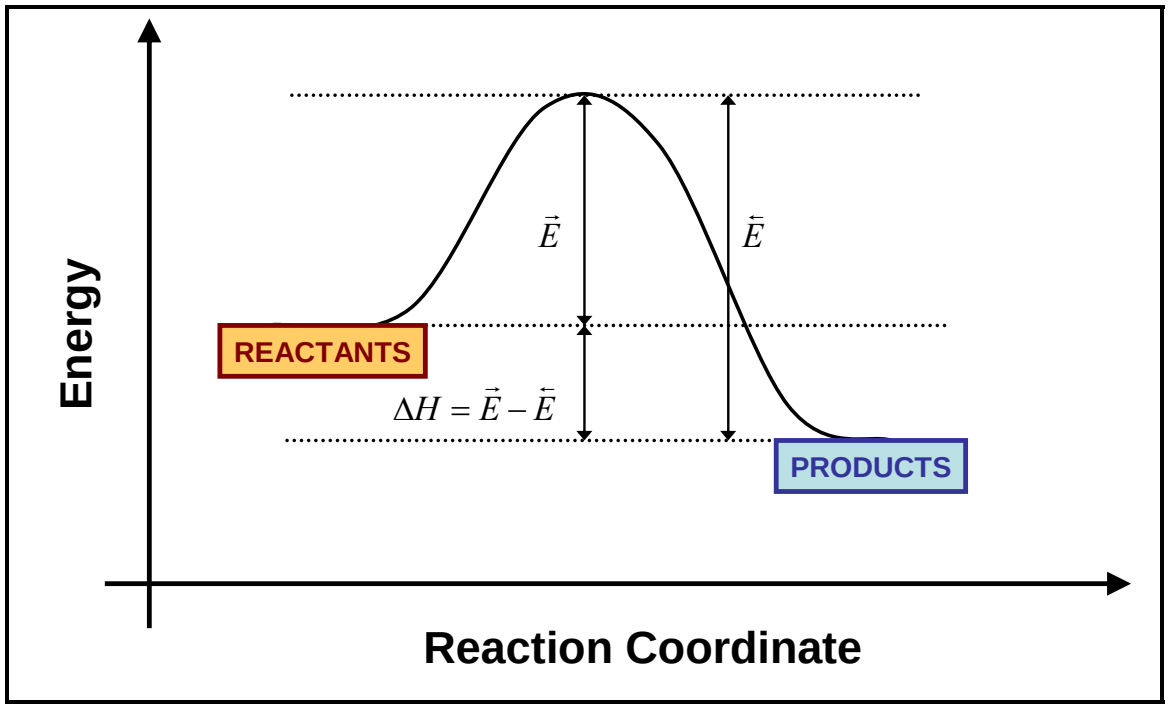

Figure 7. Typical energy diagram of reaction coordinate as reactants transform to products, overcoming the activation barrier, with a reaction enthalpy ΔH.

It should be noted that it is not necessary to use the heats of adsorption expressions from the UBI–QEP formulae in the calculation of the activation barrier. Instead, data from reliable experimental measurements can be alternatively employed if available. More complete details of the UBI–QEP method are found in Reference [17], including its extension to bimetallic catalysts.

As an example of the application of the UBI–QEP method, consider the reaction $H_2{\cdot}S + S \leftrightarrows H{\cdot}S + H{\cdot}S$ on a Cu(111) catalyst. Using the information provided in Table 13, the enthalpy of the elementary reaction step is calculated using Equation (143):

$$\begin{aligned}\Delta H &= \sum_r Q_r - \sum_p Q_p + \sum_b D_b - \sum_f D_f \\ &= \left(Q_{H_2S}\right) - \left(Q_{H{\cdot}S} + Q_{H{\cdot}S}\right) + \left(D_{H_2}\right) - \left(0\right) \\ &= \left(5.5\right) - \left(56 + 56\right) + \left(104\right) \\ &= -2.5 \text{ kcal/mol}\end{aligned} \tag{149}$$

Next, we can calculate the forward activation energy of the elementary reaction step using Equation (144)

$$\begin{aligned}\vec{E} &= \frac{1}{2}\left[\Delta H + \frac{Q_{H{\cdot}S} Q_{H{\cdot}S}}{Q_{H{\cdot}S} + Q_{H{\cdot}S}}\right] \\ &= \frac{1}{2}\left[\left(-2.5\right) + \frac{\left(56\right)\left(56\right)}{\left(56\right) + \left(56\right)}\right] \\ &= 12.8 \text{ kcal/mol}\end{aligned} \tag{150}$$

Now, we can determine the reverse activation energy using Equation (145)

$$\begin{aligned}\overleftarrow{E} &= \vec{E} - \Delta H \\ &= \left(12.8\right) - \left(-2.5\right) \\ &= 15.3 \text{ kcal/mol}\end{aligned} \tag{151}$$

Table 13. Heats of chemisorption (Q) and total bond energies in a gas phase (D) for species involved in the water gas shift reaction [93]

Species	*D* (kcal/mol)	*Q* (kcal/mol)									
		Cu(111)	Ni(111)	Pd(111)	Pt(111)	Rh(111)	Ru(001)	Ir(111)	Fe(110)	Au(111)[c]	Ag(111)[d]
O		103	115	87	85	102	100	93	118	75	80
H		56	63	62	61	61	67	58	64	46	52
CO	257	12	27	34	32	32	29	34	32	25	6
CO_2	384	5.3	6.5	3.8	3.6	5.2	5	4.3	6.9	2.8	3
H_2	104	5.5	6.8	6.6	6.4	6.4	7.6	5.8	7.1	3.7	4.7
H_2O	220	13.6	16.5	10	9.6	13.3	12.9	11.3	17.2	7.6	8.6
HCOO	384	59.2	70.6	44.9	43.2	58.2	56.4	50.1	73.5	35	39
OH[a]	102	51.8	60.9	40	38.6	51	49.5	44.4	63.3	33.1[e]	35
OH[b]	102	71.8	78	60	59	71	69.5	64.4	83.3	53.1	55.8

a - does not take into account the formation of hydrogen bonds between OH groups

b - does take into account the formation of hydrogen bonds between OH groups

c - Data taken from reference [86]

d - Data taken from references [94] and [87]

e - estimated heat of chemisorption not taking into account the formation of hydrogen bonds between OH groups.

As an example of the case where we have gas phase species involved in a surface reaction, consider the dissociative adsorption reaction $H_2 + 2S \leftrightarrows H{\cdot}S + H{\cdot}S$ on a Cu(111) catalyst. Again, using the information provided in Table 13, we can determine the enthalpy of the reaction using Equation (143)

$$\begin{aligned}\Delta H &= \sum_r Q_r - \sum_p Q_p + \sum_b D_b - \sum_f D_f \\ &= (0) - (Q_{\mathrm{H{\cdot}S}} + Q_{\mathrm{H{\cdot}S}}) + (D_{\mathrm{H_2}}) - (0) \\ &= (0) - (56 + 56) + (104) \\ &= -8 \text{ kcal/mol}\end{aligned} \tag{152}$$

Next, we can calculate the forward activation energy of the elementary reaction step using Equations (144) and (146). As shown in the previous example, the forward activation energy of the elementary reaction step on the surface ($\vec{E}_{ads}$) is calculated to be 12.8 kcal/mol. Adjusting for the heat of chemisorption as described by Equation (146)

$$\begin{aligned}\vec{E}_{gas} &= \vec{E}_{ads} - Q_{AB} \\ &= 12.8 - 5.5 \\ &= 7.3 \text{ kcal/mol}\end{aligned} \tag{153}$$

And, finally, we can determine the reverse activation energy using Equation (145)

$$\begin{aligned}\overleftarrow{E} &= \vec{E} - \Delta H \\ &= (7.3) - (-8) \\ &= 15.3 \text{ kcal/mol}\end{aligned} \tag{154}$$

3.5.3. Pre-exponential Factors

A variety of methods exist to estimate the pre-exponential factors, but this is a challenging task for surface reactions. Dumesic, et al. [18] provides the guidelines from which the pre-exponential factors may be estimated using transition-state theory through

an order-of magnitude analysis of partition functions for a variety of surface reactions, including adsorption and desorption reactions. Lund [13] further extends the methodology of Dumesic, et al. [18] by including the effect of entropy of the surface reaction in the evaluation of the reverse pre-exponential factor. This will be discussed in more detail in Section 9.2. Ovesen, et al. [8,10] utilize the partition functions with a combination of both theoretical and experimental input parameters. Their application to the WGS reaction is discussed in detail in Section 2.3. Mhadeshwar and Vlachos [62,63,75] determine their pre-exponential factors as functions of both temperature and a sticking coefficient. However, initial pre-exponential values were taken from transition-state theory.

We have based our prediction of the pre-exponential factors on transition-state theory (TST) as outlined by Dumesic, et al. [18]. The use of TST allows for the details of molecular transition state structure to be easily incorporated into the estimate of the rate constant and offers the possibility of chemical insight into the estimates of the rate constant. The TST assumes that an equilibrium is established between the reactants and an activated complex. The activated complex is a reactive chemical species that is in transition between reactants and products (Figure 7).

Consider the bimolecular gas-phase reaction, A + B → C + D. The potential energy surface for this reaction is composed of the energies that correspond to different molecular geometries along the reaction coordinate as the reactants smoothly transform into products. Along this path, the reaction passes through a saddle point, corresponding to the lowest energy barrier that must be overcome to convert the reactants to products. The molecular structure at the saddle point is called the transition structure, comprised of the chemical species identified as the activated complex $AB^{\ddagger}$. The rate of the reaction, with units of molecules/volume·time, is given by

$$\vec{r}_{AB} = \frac{k_B T}{h} K^{\ddagger} n_A n_B = \vec{k}_{AB} n_A n_B \tag{155}$$

where $K^{\ddagger} = \frac{n_{AB^{\ddagger}}}{n_A n_B}$ is the equilibrium constant.

The "macroscopic formulation" [18] of the rate constant is given in terms of the entropy and enthalpy of the activated complex:

$$\vec{k}_{\mathrm{AB}} = \frac{k_B T}{h} \exp\left(\frac{\Delta \vec{S}^{0\ddagger}}{k_B}\right) \exp\left(-\frac{\Delta \vec{H}^{0\ddagger}}{k_B T}\right) \tag{156}$$

The "microscopic formulation" [18] relates the equilibrium constant to molecular partition functions for the activated complex. Dumesic, et al. [18] give the following statistical mechanical expressions for the translational, vibrational and rotational degrees of freedom (per unit volume, as shown by the superscript notation):

$$z_i''' = z_{it}''' z_{ir} z_{iv} \tag{157}$$

For three-dimensional translation, the partition function is

$$z_{it}''' = \frac{\left(2\pi m_i k_B T\right)^{2/3}}{h^3} \tag{158}$$

where m = mass of molecule; P = container pressure; h = Planck's constant; k_B = Boltzmann constant; and, T = temperature. The vibrational partition function is given by

$$z_{iv} = \prod_j \frac{1}{1 - \exp\left(-\frac{h\nu_{ij}}{k_B T}\right)} \tag{159}$$

where ν = vibration frequency (cm^{-1}) from each vibrational degree of freedom. And, the rotational partition function is

$$z_{ir} = \frac{8\pi^2 I_i k_B T}{\sigma_r h^2} \qquad \text{(for the linear case)} \tag{160}$$

$$z_{ir} = \frac{8\pi^2 \sqrt{8\pi^3 I_{i1} I_{i2} I_{i3}} \left(k_B T\right)^{3/2}}{\sigma_r h^3} \qquad \text{(for the non-linear case)} \qquad (161)$$

where $I_A I_B I_C$ = moments of inertia and σ = symmetry number. The use of these relations for the WGS reaction has been discussed in detail in Chapter 2.

Replacing $K^{\ddagger}$ by its partition function equivalent yields the following rate constant

$$\vec{k}_{\mathrm{AB}} = \frac{k_B T}{h} \frac{z'''_{AB^{\ddagger}}}{z'''_A z'''_B} \exp\left(-\frac{\vec{E}^{0\ddagger}}{k_B T}\right) = \vec{\Lambda}_{\mathrm{AB}} \exp\left(-\frac{\vec{E}^{0\ddagger}}{k_B T}\right) \qquad (162)$$

and pre-exponential factor

$$\vec{\Lambda}_{\mathrm{AB}} = \frac{k_B T}{h} \frac{z'''_{AB^{\ddagger}}}{z'''_A z'''_B} \qquad (163)$$

Using the following order-of-magnitude estimates, initial estimates of the pre-exponential factors may be determined [18]:

$$\frac{k_B T}{h} = 10^{13}\ \mathrm{s}^{-1}$$

$$z'''_{it} = 5 \times 10^{8}\ \mathrm{cm}^{-1}\ \text{(per degree of translational freedom)}$$

$$z_{ir} = 10\ \text{(per degree of rotational freedom)}$$

$$z_{iv} = 1\ \text{(per degree of vibrational freedom)}$$

Expanding this methodology to surface reactions, we first consider the adsorption process for an immobile activated complex: $A_{(g)} + S \leftrightarrows A^{\ddagger} \rightarrow A{\cdot}S$. The reaction rate is given by

$$\vec{r}_{\mathrm{ads}} = \frac{k_B T}{h} \frac{z'''_{A^{\ddagger}}}{z'''_{A_{(g)}}} \exp\left(-\frac{\vec{E}^{0\ddagger}}{k_B T}\right) n_{\mathrm{A}} \theta_{\mathrm{S}} = \vec{k}_{\mathrm{ads}} n_{\mathrm{A}} \theta_{\mathrm{S}} \qquad (164)$$

where $z'''_{A^{\ddagger}} = C_t z_{A^{\ddagger}r} z_{A^{\ddagger}v}$ and C_t is the number of adsorption sites per unit surface area approximated as 10^{15}. Substitution using Equation (163) indicates that, for an immobile transition state, $\vec{\Lambda}_{ads} = 10^{1}\,\mathrm{Pa^{-1}s^{-1}}$.

In the case of the desorption process, A·S ⇆ $A^{\ddagger}$ → $A_{(g)}$ + S, the rate is given by

$$r_{des} = \frac{k_B T}{h} \frac{z'''_{A^{\ddagger}}}{z'''_{A\cdot S}} \exp\left(-\frac{E^{0\ddagger}}{k_B T}\right)\theta_A \tag{165}$$

where θ_A is the concentration of species A on the surface. Again, for an immobile transition state,

$$z''_{i*} = C_t z_{ir} z_{iv} \tag{166}$$

The ratio $z''_{A^{\ddagger}} / z''_{A\cdot S}$ is nearly equal to one, thus, the pre-exponential factor may be approximated by $\frac{k_B T}{h}$ or 10^{13} s^{-1}.

Now, consider the surface reaction: A·S + B·S ⇆ $AB^{\ddagger}$ → C·S + D·S with the rate

$$\vec{r}_{AB} = \frac{k_B T}{h} \frac{z''_{AB^{\ddagger}}}{z''_{A\cdot S} z''_{B\cdot S}} \exp\left(-\frac{\vec{E}^{0\ddagger}}{k_B T}\right)\theta_A \theta_B = \vec{k}_{AB}\theta_A \theta_B \tag{167}$$

Substitution of Equation (166) for an immobile transition surface species without rotation estimates the pre-exponential factor as 10^{13} s^{-1}.

In the special case where we have the reaction $AB_{(g)}$ + 2S ⇆ A·S + B·S, we consider the forward and reverse reactions separately based on Dumesic's formulation [18]. The forward reaction, $AB_{(g)}$ + 2S → $AB^{\ddagger}$ → A·S + B·S, has the following rate expression

$$\vec{r}_{\text{ads}} = \frac{k_B T}{h} \frac{z'''_{\text{AB}^{\ddagger}}}{z''_{\text{AB}_{(g)}}} \exp\left(-\frac{\vec{E}^{0\ddagger}}{k_B T} \right) n_{\text{AB}} \theta_S^2 = \vec{k}_{\text{AB}} n_{\text{AB}} \theta_S^2 \tag{168}$$

Following the analysis above, the pre-exponential factor is given by

$$\vec{\Lambda}_{\text{ads}} = \frac{k_B T}{h} \frac{z''_{\text{AB}^{\ddagger}}}{z''_{\text{A·S}} z''_{\text{B·S}}} \tag{169}$$

which, according to Dumesic, et al. [18] for an immobile transition state, is estimated as 10^1 $\text{Pa}^{-1}\text{s}^{-1}$.

The rate of the reverse reaction, $\text{A·S} + \text{B·S} \rightarrow \text{AB}^{\ddagger} \rightarrow \text{AB}_{(g)} + 2\text{S}$, is given by

$$\overleftarrow{r}_{\text{des}} = \frac{k_B T}{h} \frac{z''_{\text{AB}^{\ddagger}}}{z''_{\text{A·S}} z''_{\text{B·S}}} \exp\left(-\frac{\overleftarrow{E}^{0\ddagger}}{k_B T} \right) \theta_{\text{A}} \theta_B \tag{170}$$

For an immobile transition state with 1-degree of freedom perpendicular to the surface, $z''_{iS} = 10^{16}$ cm^{-1}. When the activated complex and the adsorbed reactants have the same degree of mobility, the pre-exponential factor of the desorption rate is estimated as 10^{13} s^{-1}.

Dumesic, et al. [18] provides a more detailed examination of the transition state theory applied to the estimation of the pre-exponential factor for several other types of reactions under various conditions in the text "The Microkinetics of Heterogeneous Catalysis".

We next consider Lund's [13] methodology for pre-exponential factors. Lund expands the traditional application of transition-state theory as described by Dumesic, et al. [18] by incorporating the elementary reaction step entropy change into the calculation of the reverse pre-exponential factor. This methodology ensures consistence with the entropy change of the overall reaction, which is not assured by Dumesic's estimates. The heats and entropies of formation for each surface species as if they existed in the gas phase are the inputs necessary to utilize this methodology. In our case, we utilize a

reference temperature of 298.15K and obtained the thermodynamic data from NIST Webbook [74] or using DFT (B3LYP/LANLDZ) calculation results from GAUSSIAN 03 [95] computational chemistry software. The heats of the surface species are, thus, considered to be the heat of formation of the gas-phase species less the strength of the bond to the surface

$$\Delta H_{f,i\cdot S} = \Delta H_{f,i_{(g)}} - Q_{i\cdot S} \tag{171}$$

Lund further assumed that the adsorption of a molecule to a surface caused the loss of all translational entropy S_{trans}. Thus, the entropy of formation for the surface species is given as

$$\Delta S_{f,i\cdot S} = \Delta S_{f,i_{(g)}} - S_{trans,i_{(g)}} \tag{172}$$

where

$$S_{trans,i_{(g)}} = R_{gas}\left[\frac{5}{2} + \ln\left(\frac{\left(2\pi m_i k_B T\right)^{3/2}}{h^3}\times V\right)\right] \tag{173}$$

and m_i is the molecular weight of the molecule and V is the system volume. Assuming ideal gas behavior, Equation (173) may be written in terms of the system temperature T and pressure P:

$$S_{trans,i_{(g)}} = R_{gas}\left[\frac{5}{2} + \ln\left(\frac{\left(2\pi m_i k_B T\right)^{3/2}}{h^3}\times \frac{R_{gas}T}{P}\right)\right] \tag{174}$$

This estimate of entropy, provided by Equation (172) is used to determine the reverse pre-exponential factors only. The forward pre-exponential factors are still estimated according to transition-state theory [18]: 10^1 $Pa^{-1}s^{-1}$ for adsorption steps; and, 10^{13} s^{-1} for

surface reactions. The reverse pre-exponential factor for elementary reaction step ρ is determined from the following relation [13]

$$\overleftarrow{\Lambda}_\rho = \vec{\Lambda}_\rho \exp\left(-\frac{\Delta S^\circ_\rho}{R}\right) \tag{175}$$

Alternatively, if the reverse pre-exponential factor is estimated using transition state theory, then the forward pre-exponential factor may be estimated by

$$\vec{\Lambda}_\rho = \overleftarrow{\Lambda}_\rho \exp\left(\frac{\Delta S^\circ_\rho}{R}\right) \tag{176}$$

This methodology ensures that the energetics of the mechanism will be thermodynamically consistent, as demonstrated by Mhadeshwar, et al. [96].

This chapter provided a summary of material balance equations used in a PBR or CSTR used in microkinetic analysis. Further, the estimation of activation energies by the UBI–QEP method as well as the estimation of the pre-exponential factors by TST are described. These relations are used in this work.

Chapter 4. Stoichiometric Theory of Reaction Route Graph Theory

4.1. Notation and Definitions

We consider a set of p elementary reaction steps s_ρ (ρ =1, 2, ..., p): $\sum_{i=1}^{l} v_{\rho i} \mathrm{B}_i = 0$, involving species B_i (i =1, 2, ..., l) as comprising the mechanism of an overall reaction. The stoichiometric coefficient $v_{\rho i}$ of species i in the reaction s_ρ is, by convention, positive for a product, negative for a reactant, and zero for an inert. Alternately, the reaction may be written in a more conventional format as

$$s_\rho: \quad \sum_{i=1}^{l} (-\vec{v}_{\rho i}) \mathrm{B}_i \rightleftarrows \sum_{i=1}^{l} \overleftarrow{v}_{\rho i} \mathrm{B}_i \qquad (\rho = 1, 2, ..., p) \qquad (177)$$

where the stoichiometric coefficients of reactants and products are differentiated by the crowning arrows and $v_{\rho i} = \vec{v}_{\rho i} + \overleftarrow{v}_{\rho i}$. All reactions are, of course, considered to be reversible. The degree of reversibility and the direction of reaction flux of each reaction is determined by the sign and magnitude of its affinity [97], a state function characteristic of the reaction and its distance from equilibrium, defined for step s_ρ as the negative of its Gibbs free energy change, or alternately as the difference between the forward affinity $\vec{A}_\rho$ and the reverse affinity $\overleftarrow{A}_\rho$ [98]

$$A_\rho = \sum_{i=1}^{l} (-\vec{v}_{\rho i}) \mu_i - \sum_{i=1}^{l} \overleftarrow{v}_{\rho i} \mu_i = \vec{A}_\rho - \overleftarrow{A}_\rho \qquad (178)$$

where μ_i is the chemical potential of species B_i. This provides the condition for the reaction equilibrium (A_ρ = 0), as well as the direction of spontaneous reaction rate r_ρ

(i.e., forward for $A_\rho > 0$, or for $\vec{A}_\rho > \overleftarrow{A}_\rho$, and reverse for $A_\rho < 0$, or for $\vec{A}_\rho < \overleftarrow{A}_\rho$), as expressed succinctly by the De Donder inequality, $P_\rho \equiv A_\rho r_\rho \geq 0$ [97].

The rate of an elementary reaction step is given by [72]

$$r_\rho = \vec{r}_\rho - \overleftarrow{r}_\rho = \vec{k}_\rho \prod_{i=1}^{l} a_i^{-\vec{\nu}_{\rho i}} - \overleftarrow{k}_\rho \prod_{i=1}^{l} a_i^{\overleftarrow{\nu}_{\rho i}} \tag{179}$$

where a_i is the activity of species B_i. With the use of $\mu_i = \mu_i^0 + RT \ln a_i$, Equation (179) may be written in the form

$$\frac{\overleftarrow{r}_\rho}{\vec{r}_\rho} = \exp\left(-\mathscr{A}_\rho\right) \text{ ; or } r_\rho = \vec{r}_\rho \left[1 - \exp\left(-\mathscr{A}_\rho\right)\right] \tag{180}$$

which is the so-called De Donder relation. Here, $\mathscr{A}_\rho = A_\rho / RT$ is the dimensionless affinity.

Unfortunately, in this relation both the affinity $\mathscr{A}_\rho$ and the forward rate $\vec{r}_\rho$ are functions of temperature and composition, thus, there is not a one-to-one correspondence between the rate r_ρ and the affinity $\mathscr{A}_\rho$. As an example [99], consider the elementary isomerization reaction $B_1 \leftrightarrows B_2$. If the activities of both B_1 and B_2 are doubled, the net rate r_ρ doubles due to doubling of the forward rate $\vec{r}_\rho$, even though the affinity remains the same. The exception is the case close to equilibrium. When $\mathscr{A}_\rho = 0$, it is seen that the net rate $r_\rho = 0$, so that $\vec{r}_\rho = \vec{r}_{\rho,0} = \overleftarrow{r}_\rho = \overleftarrow{r}_{\rho,0} = r_{\rho,0}$, the absolute value of the forward or the reverse reaction rate, as required by the principle of microscopic reversibility. In the vicinity of equilibrium, then [100]

$$r_\rho \simeq r_{\rho,0} \mathscr{A}_\rho \tag{181}$$

where $r_{\rho,0}$ is the exchange rate of the elementary reaction step s_ρ.

We will find it useful to write an elementary reaction step s_ρ for a catalytic (or enzyme) reaction more explicitly in terms of the reaction intermediates I_k and the terminal species T_i:

$$s_\rho: \quad \alpha_{\rho 0} I_0 + \sum_{k=1}^{q} \alpha_{\rho k} I_k + \sum_{i=1}^{n} \beta_{\rho i} T_i = 0 \qquad (\rho = 1, 2, ..., p) \tag{182}$$

For simplicity, a single type of active site I_0 (denoted by S for heterogeneous catalyst, and E for enzyme) is assumed here, excluded from consideration among I_k by virtue of site balance. The stoichiometric coefficients of the intermediates I_k are $\alpha_{\rho k}$ (k = 1, 2,. ..., q) and for the terminal species T_i are $\beta_{\rho i}$ (i = 1, 2, ..., n). For simplicity, we assume that the overall chemical process is described by only one overall reaction (*OR*)

$$OR: \quad \nu_1 T_1 + \nu_2 T_2 + ... + \nu_n T_n = \sum_{i=1}^{n} \nu_i T_i = 0 \tag{183}$$

The De Donder affinity, thus, becomes

$$\mathcal{A}_\rho = \ln K_\rho - \alpha_{\rho 0} \ln a_0 - \sum_{k=1}^{q} \alpha_{\rho k} \ln a_k - \sum_{i=1}^{n} \beta_{\rho i} \ln a_i \tag{184}$$

where $K_\rho = \vec{k}_\rho / \overleftarrow{k}_\rho$ is the equilibrium constant for the elementary reaction. The species activities a_i may be replaced by a suitable composition measure, e.g., site fraction θ_i for the intermediates in heterogeneous catalysis and partial pressure or concentration for terminal species. Thus, the affinity may be computed, e.g., from elementary reaction energetics and numerical results of a microkinetic analysis for a given set of conditions and a specified reactor configuration [7].

The *overall stoichiometric matrix* $\boldsymbol{\nu}$ is written with rows corresponding to reactions – including the overall reaction (*OR*), $\sum_{i=1}^{n} \nu_{OR,i} \mathrm{T}_i$, as the first row – and the columns to the species with the intermediates followed by the terminal species

$$\boldsymbol{\nu} = \begin{bmatrix} 0 & 0 & \dots & 0 & \nu_1 & \nu_2 & \dots & \nu_n \\ \alpha_{11} & \alpha_{12} & \dots & \alpha_{1q} & \beta_{11} & \beta_{12} & \dots & \beta_{1n} \\ \alpha_{21} & \alpha_{22} & \dots & \alpha_{2q} & \beta_{21} & \beta_{22} & \dots & \beta_{2n} \\ \vdots & \vdots & \vdots & \vdots & \vdots & \vdots & \vdots & \vdots \\ \alpha_{p1} & \alpha_{p2} & \dots & \alpha_{pq} & \beta_{p1} & \beta_{p2} & \dots & \beta_{pn} \end{bmatrix} \tag{185}$$

in which the active sites are excluded because of the site mass balance and, of course, the stoichiometric coefficients of the intermediates in the *OR* are zero.

In the case of non-minimal *RR* graphs (to be discussed in Section 5.5), the rows in the stoichiometric matrix of the mechanism, now defined without the *OR*,

$$\boldsymbol{\nu} = \begin{bmatrix} \alpha_{11} & \alpha_{12} & \dots & \alpha_{1l} & \beta_{11} & \beta_{12} & \dots & \beta_{1n} \\ \alpha_{21} & \alpha_{22} & \dots & \alpha_{2l} & \beta_{21} & \beta_{22} & \dots & \beta_{2n} \\ \dots & \dots & \dots & \dots & \dots & \dots & \dots & \dots \\ \alpha_{p1} & \alpha_{p2} & \dots & \alpha_{pl} & \beta_{p1} & \beta_{p2} & \dots & \beta_{pn} \end{bmatrix} \tag{186}$$

are, in general, linearly dependent. For our purpose, it is necessary to define, as follows, two sub-matrices of $\boldsymbol{\nu}$ in which the columns are linearly independent. First, we observe that the columns in the two sub-matrices comprising the intermediates and terminal species may be linearly dependent, that is

$$rank\ \boldsymbol{\alpha}' = rank \begin{bmatrix} \alpha_{11} & \alpha_{12} & \dots & \alpha_{1l} \\ \alpha_{21} & \alpha_{22} & \dots & \alpha_{2l} \\ \dots & \dots & \dots & \dots \\ \alpha_{p1} & \alpha_{p2} & \dots & \alpha_{pl} \end{bmatrix} = q \le l \tag{187}$$

$$rank\ \boldsymbol{\beta}' = rank \begin{bmatrix} \beta_{11} & \beta_{12} & \ldots & \beta_{1n} \\ \beta_{21} & \beta_{22} & \ldots & \beta_{2n} \\ \ldots & \ldots & \ldots & \ldots \\ \beta_{p1} & \beta_{p2} & \ldots & \beta_{pn} \end{bmatrix} = t \leq n \tag{188}$$

In such cases, the linearly dependent columns in $\boldsymbol{\alpha}'$ may be omitted. Without lost of generality, we assume that the first q columns in $\boldsymbol{\alpha}'$ are linearly independent and define the sub-matrix

$$\boldsymbol{\alpha} = \begin{bmatrix} \alpha_{11} & \alpha_{12} & \ldots & \alpha_{1q} \\ \alpha_{21} & \alpha_{22} & \ldots & \alpha_{2q} \\ \ldots & \ldots & \ldots & \ldots \\ \alpha_{p1} & \alpha_{p2} & \ldots & \alpha_{pq} \end{bmatrix} \tag{189}$$

so that $rank\ \boldsymbol{\alpha} = q$. In what follows, the sub-matrix $\boldsymbol{\alpha}$ is referred to as the *intermediate* sub-matrix. Next, we notice that the rank of the stoichiometric matrix $\boldsymbol{\nu}$ is equal to $q + 1$. Without loss of generality, we eliminate the last $n - 1$ columns from $\boldsymbol{\beta}'$ and define a *reduced* stoichiometric sub-matrix

$$\boldsymbol{\gamma} = \begin{bmatrix} \alpha_{11} & \alpha_{12} & \ldots & \alpha_{1q} & \beta_{11} \\ \alpha_{21} & \alpha_{22} & \ldots & \alpha_{2q} & \beta_{21} \\ \ldots & \ldots & \ldots & \ldots & \ldots \\ \alpha_{p1} & \alpha_{p2} & \ldots & \alpha_{pq} & \beta_{p1} \end{bmatrix} \tag{190}$$

such that $rank\ \boldsymbol{\nu} = rank\ \boldsymbol{\gamma} = q + 1$.

We define, further, the rate and dimensionless affinity vectors

$$\mathbf{r} = (r_1, r_2, \ldots, r_p)^{\mathrm{T}} \tag{191}$$

$$\mathscr{A} = (\mathscr{A}_1, \mathscr{A}_2, \ldots, \mathscr{A}_p)^{\mathrm{T}} \tag{192}$$

where r_ρ (ρ = 1, 2, ..., p) and $\mathscr{A}_\rho$ (ρ = 1, 2, ..., p) are the rates and dimensionless affinities of the elementary reaction steps. By definition [25], r_ρ and $\mathscr{A}_\rho$ are interrelated via the De Donder relation

$$r_\rho = \vec{r}_\rho - \overleftarrow{r}_\rho \tag{193}$$

$$\mathscr{A}_\rho = \frac{A_\rho}{RT} = \frac{1}{RT}\sum \nu_{\rho i}\mu_i = \ln \frac{\vec{r}_\rho}{\overleftarrow{r}_\rho} \tag{194}$$

where A_ρ is the affinity of elementary reaction step s_ρ [25] while $\vec{r}_\rho$ and $\overleftarrow{r}_\rho$ represent the rates of the elementary reaction steps in the forward and reverse directions, respectively.

4.1.1. Reaction Routes

In the most general case, a reaction route (*RR*) is defined as a linear combination of the elementary reaction steps s_1, s_2, …, s_p that eliminates a specified number of species (intermediates and terminal species) and produces an *OR* [27,28]. The coefficients of s_ρ in this linear combination $\sigma_1, \sigma_2, ..., \sigma_p$ are called stoichiometric numbers.

The total number of conceivable *RR*s, Q, is less than or equal to the total number of ways of selecting $q + 1$ independent elementary reactions from among a total of p [7]

$$Q \le \frac{p!}{(q+1)!(p-(q+1))!} \tag{195}$$

Usually, the number of distinct *RR*s is much smaller than this, since some reactions, e.g., adsorption, desorption steps, must be involved in all *RR*s, and many of the resulting *RR*s are indistinct. Nonetheless, they can be large in number.

4.1.1.1 Full Reaction Routes

Mathematically, the g-th *FR* is defined as

$$FR_g: \sum_{\rho=1}^{p} \sigma_{g\rho} s_\rho = OR \tag{196}$$

The FR_g, i.e., a set of stoichiometric numbers $\sigma_{g1}, \sigma_{g2}, ..., \sigma_{gp}$, may be generated based on the following considerations. Substituting Equation (182) into Equation (196), we have

$$\sum_{\rho=1}^{p} \sigma_{g\rho} \left(\sum_{k=1}^{l} \alpha_{\rho k} \mathrm{I}_k + \sum_{i=1}^{n} \beta_{\rho i} \mathrm{T}_i \right) = \sum_{k=1}^{l} \left(\sum_{\rho=1}^{p} \alpha_{\rho k} \sigma_{g\rho} \right) \mathrm{I}_k + \sum_{i=1}^{n} \left(\sum_{\rho=1}^{p} \beta_{\rho i} \sigma_{g\rho} \right) \mathrm{T}_i = OR \tag{197}$$

By definition, the intermediates in a *FR* should vanish. That is,

$$\sum_{\rho=1}^{p} \alpha_{\rho k} \sigma_{g\rho} = 0 \qquad (k = 1, 2, \ldots, l)$$

or

$$\boldsymbol{\alpha}'^{\mathrm{T}} \boldsymbol{\sigma}_g = 0$$

where $\boldsymbol{\sigma}_g$ is the vector of stoichiometric numbers

$$\boldsymbol{\sigma}_g = (\sigma_{g1}, \sigma_{g2}, ..., \sigma_{gp})^{\mathrm{T}} \tag{198}$$

After removing the linearly dependent columns in $\boldsymbol{\alpha}'$, we have

$$\boldsymbol{\alpha}^{\mathrm{T}} \boldsymbol{\sigma}_g = 0 \tag{199}$$

Thus, $\boldsymbol{\sigma}_g$ may be determined by solving a system of homogeneous linear equations, i.e., Equation (199). The number of linearly independent *FR*s is equal to p - *rank* $\boldsymbol{\alpha} = p - q$.

4.1.1.2 Empty Reaction Routes

Mathematically, the *g*-th *ER* is defined as

$$ER_g: \sum_{\rho=1}^{p} \sigma_{g\rho} s_\rho = 0 \tag{200}$$

Substituting Equation (182) into Equation (200) and requiring all of the species to vanish, we have

$$\sum_{\rho=1}^{p} \alpha_{\rho k} \sigma_{g\rho} = 0 \qquad (k = 1, 2, \ldots, l)$$

$$\sum_{\rho=1}^{p} \beta_{\rho i} \sigma_{g\rho} = 0 \qquad (i = 1, 2, \ldots, n)$$

or

$$\boldsymbol{\nu}^{\mathrm{T}} \boldsymbol{\sigma}_g = \mathbf{0}$$

Eliminating the linearly dependent columns from the stoichiometric matrix $\boldsymbol{\nu}$ gives

$$\boldsymbol{\gamma}^{\mathrm{T}} \boldsymbol{\sigma}_g = \mathbf{0} \tag{201}$$

Thus, the *ER*s are also generated by solving a set of homogeneous linear equations, i.e., Equation (201). The number of linearly independent *ER*s is equal to $p - rank\ \boldsymbol{\nu} = p - (q + 1)$.

4.1.2. Direct Reaction Routes

If the *RR*s are not subject to any further constraints, the vectors of stoichiometric numbers $\boldsymbol{\sigma}_g$, may be generated arbitrarily. This arbitrariness of the *RR*s may be avoided

if, following Milner [29] and Happel and Sellers [30], it is required that *RR*s be direct. Clearly, not every subset of $q + 1$ elementary reaction steps from the total of p is linearly independent. Also, not every subset of $q + 1$ linearly independent elementary reaction steps will necessarily result in a distinct *RR*. For instance, some steps (e.g. adsorption, desorption) may be involved in all *FR*s. Further, some of the stoichiometric numbers in different *FR*s may equal zero, thus resulting in a smaller number of distinct *FR*s. The direct *FR*s may alternately be generated employing another appropriate method, e.g., that of Happel and Sellers [30], or Fishtik and Datta [101]. Alternatively, the direct *FR*s may be enumerated by considering all of the possible choices of $q + 1$ elementary reaction steps from among the total of p. The number of stoichiometrically distinct direct *FR*s enumerated, however, usually far exceeds $p - q$, the number of linearly independent *FR*s.

4.1.2.1 Direct Full Routes

According to Milner [29], a direct *FR* involves no more than $rank\,\boldsymbol{\alpha} + 1 = q + 1$ *linearly independent* elementary reaction steps. Let the $q + 1$ linearly independent elementary reaction steps that are involved in a direct *FR* be $s_{i_1}, s_{i_2}, ..., s_{i_q}, s_{i_{q+1}}$, where the subscripts $i_1, i_2, ..., i_q, i_{q+1}$ represent an ordered set of $q + 1$ integers from among the p elementary steps, i.e., $1 \le i_1 < i_2 < ... < i_q < i_{q+1} \le p$. A direct *FR* may be denoted by $FR(s_{i_1}, s_{i_2}, ..., s_{i_q}, s_{i_{q+1}})$, thus specifying the elementary reaction steps $s_{i_1}, s_{i_2}, ..., s_{i_q}, s_{i_{q+1}}$ that are involved in the *FR*. Thus, in general,

$$FR(s_{i_1}, s_{i_2}, ..., s_{i_q}, s_{i_{q+1}}): \quad \sigma_{i_1} s_{i_1} + \sigma_{i_2} s_{i_2} + ... + \sigma_{i_q} s_{i_q} + \sigma_{i_{q+1}} s_{i_{q+1}} = OR \tag{202}$$

where the stoichiometric numbers $\sigma_{gi_1}, \sigma_{gi_2}, ..., \sigma_{gi_q}, \sigma_{gi_{q+1}}$ are obtained by solving Equation (199). As shown earlier by us [101], the solution is

$$\sigma_{i_k} = \begin{vmatrix} \alpha_{i_1,1} & \alpha_{i_1,2} & \ldots & \alpha_{i_1,q} & 0 \\ \alpha_{i_2,1} & \alpha_{i_2,2} & \ldots & \alpha_{i_2,q} & 0 \\ \ldots & \ldots & \ldots & \ldots & \ldots \\ \alpha_{i_{k-1},1} & \alpha_{i_{k-1},2} & \ldots & \alpha_{i_{k-1},q} & 0 \\ \alpha_{i_k,1} & \alpha_{i_k,2} & \ldots & \alpha_{i_k,q} & 1 \\ \alpha_{i_{k+1},1} & \alpha_{i_{k+1},2} & \ldots & \alpha_{i_{k+1},q} & 0 \\ \ldots & \ldots & \ldots & \ldots & \ldots \\ \alpha_{i_q,1} & \alpha_{i_q,2} & \ldots & \alpha_{i_q,q} & 0 \\ \alpha_{i_{q+1},1} & \alpha_{i_{q+1},2} & \ldots & \alpha_{i_{q+1},q} & 0 \end{vmatrix} \tag{203}$$

More succinctly, the general equation of a *FR* may, thus, be written as

$$FR(s_{i_1}, s_{i_2}, ..., s_{i_q}, s_{i_{q+1}}): \begin{vmatrix} \alpha_{i_1,1} & \alpha_{i_1,2} & \ldots & \alpha_{i_1,q} & s_{i_1} \\ \alpha_{i_2,1} & \alpha_{i_2,2} & \ldots & \alpha_{i_2,q} & s_{i_2} \\ \ldots & \ldots & \ldots & \ldots & \ldots \\ \alpha_{i_q,1} & \alpha_{i_1,2} & \ldots & \alpha_{i_1,q} & s_{i_q} \\ \alpha_{i_{q+1},1} & \alpha_{i_{q+1},2} & \ldots & \alpha_{i_{q+1},q} & s_{i_{q+1}} \end{vmatrix} = OR \tag{204}$$

The affinity A_{OR} of the *OR* is related to the affinities $A_{i_1}, A_{i_2}, ..., A_{i_q}, A_{i_{q+1}}$ of the elementary reaction steps comprising a direct *FR* following thermodynamic consistency, i.e.,

$$A_{OR} = \sigma_{i_1} A_{i_1} + \sigma_{i_2} A_{i_2} + ... + \sigma_{i_q} A_{i_q} + \sigma_{i_{q+1}} A_{i_{q+1}} \tag{205}$$

or, employing Equation (203)

$$A_{OR} = \begin{vmatrix} \alpha_{i_1,1} & \alpha_{i_1,2} & \ldots & \alpha_{i_1,q} & A_{i_1} \\ \alpha_{i_2,1} & \alpha_{i_2,2} & \ldots & \alpha_{i_2,q} & A_{i_2} \\ \ldots & \ldots & \ldots & \ldots & \ldots \\ \alpha_{i_q,1} & \alpha_{i_1,2} & \ldots & \alpha_{i_1,q} & A_{i_q} \\ \alpha_{i_{q+1},1} & \alpha_{i_{q+1},2} & \ldots & \alpha_{i_{q+1},q} & A_{i_{q+1}} \end{vmatrix} \tag{206}$$

4.1.2.2 Direct Empty Routes

The concept of directness may be extended to *ER*s. Thus, by analogy with a direct *FR*, we define a *direct ER* as a *RR* that involves no more than $rank\,\boldsymbol{\gamma}+1=q+2$ elementary reaction steps, where $\boldsymbol{\gamma}$ is the reduced stoichiometric matrix, Equation (190). Let the q + 2 elementary reaction steps that are involved in an *ER* be $s_{j_1}, s_{j_2}, ..., s_{j_q}, s_{j_{q+1}}, s_{j_{q+2}}$, where the subscripts $j_1, j_2, ..., j_q, j_{q+1}, j_{q+2}$ represent an ordered set of q + 2 integers from among p satisfying the condition $1 \le j_1 < j_2 < ... < j_q < j_{q+1} < j_{q+2} \le p$. A direct *ER* is denoted by $ER(s_{j_1}, s_{j_2}, ..., s_{j_q}, s_{j_{q+1}}, s_{j_{q+2}})$, thus specifying the elementary reaction steps $s_{j_1}, s_{j_2}, ..., s_{j_q}, s_{j_{q+1}}, s_{j_{q+2}}$ that are involved in the *ER*. In general,

$$ER(s_{j_1}, s_{j_2}, ..., s_{j_q}, s_{j_{q+1}}, s_{j_{q+2}}) : \sigma_{j_1} s_{j_1} + \sigma_{j_2} s_{j_2} + ... + \sigma_{j_q} s_{j_q} + \sigma_{j_{q+1}} s_{j_{q+1}} + \sigma_{j_{q+2}} s_{j_{q+2}} = 0 \qquad (207)$$

where the stoichiometric numbers are obtained by solving Equation (201). The solution is

$$\sigma_{j_k} = \begin{vmatrix} \alpha_{j_1,1} & \alpha_{j_1,2} & ... & \alpha_{j_1,q} & \beta_{j_1,1} & 0 \\ \alpha_{j_2,1} & \alpha_{j_2,2} & ... & \alpha_{j_2,q} & \beta_{j_2,1} & 0 \\ ... & ... & ... & ... & ... & ... \\ \alpha_{j_{k-1},1} & \alpha_{j_{k-1},2} & ... & \alpha_{j_{k-1},q} & \beta_{j_{k-1},1} & 0 \\ \alpha_{j_k,1} & \alpha_{j_k,2} & ... & \alpha_{j_k,q} & \beta_{j_k,1} & 1 \\ \alpha_{j_{k+1},1} & \alpha_{j_{k+1},2} & ... & \alpha_{j_{k+1},q} & \beta_{j_{k+1},1} & 0 \\ ... & ... & ... & ... & ... & ... \\ \alpha_{j_q,1} & \alpha_{j_q,2} & ... & \alpha_{j_q,q} & \beta_{j_q,1} & 0 \\ \alpha_{j_{q+1},1} & \alpha_{j_{q+1},2} & ... & \alpha_{i_{q+1},q} & \beta_{j_{q+1},1} & 0 \\ \alpha_{j_{q+2},1} & \alpha_{j_{q+2},2} & ... & \alpha_{i_{q+1},q} & \beta_{j_{q+2},1} & 0 \end{vmatrix} \qquad (208)$$

Alternatively, this result may be represented as

$$ER(s_{j_1}, s_{j_2}, ..., s_{j_q}, s_{j_{q+1}}, s_{j_{q+2}}): \begin{vmatrix} \alpha_{j_1,1} & \alpha_{j_1,2} & ... & \alpha_{j_1,q} & \beta_{j_1,1} & s_{j_1} \\ \alpha_{j_2,1} & \alpha_{j_2,2} & ... & \alpha_{j_2,q} & \beta_{j_2,1} & s_{j_2} \\ ... & ... & ... & ... & ... & ... \\ \alpha_{j_q,1} & \alpha_{j_q,2} & ... & \alpha_{j_q,q} & \beta_{j_q,1} & s_{j_q} \\ \alpha_{j_{q+1},1} & \alpha_{j_{q+1},2} & ... & \alpha_{j_{q+1},q} & \beta_{j_{q+1},1} & s_{j_{q+1}} \\ \alpha_{j_{q+2},1} & \alpha_{j_{q+2},2} & ... & \alpha_{j_{q+2},q} & \beta_{j_{q+2},1} & s_{j_{q+2}} \end{vmatrix} = 0 \quad (209)$$

Because an *ER* produces a zero net reaction, the affinities of the elementary reaction steps $A_{j_1}, A_{j_2}, ..., A_{j_q}, A_{j_{q+1}}, A_{j_{q+2}}$ comprising an *ER* are subject to the following constraint:

$$\sigma_{j_1} A_{j_1} + \sigma_{j_2} A_{j_2} + ... + \sigma_{j_q} A_{j_q} + \sigma_{j_{q+1}} A_{j_{q+1}} + \sigma_{j_{q+2}} A_{j_{q+2}} = 0 \quad (210)$$

or, employing Equation (208),

$$\begin{vmatrix} \alpha_{j_1,1} & \alpha_{j_1,2} & ... & \alpha_{j_1,q} & \beta_{j_1,1} & A_{j_1} \\ \alpha_{j_2,1} & \alpha_{j_2,2} & ... & \alpha_{j_2,q} & \beta_{j_2,1} & A_{j_2} \\ ... & ... & ... & ... & ... & ... \\ \alpha_{j_q,1} & \alpha_{j_q,2} & ... & \alpha_{j_q,q} & \beta_{j_q,1} & A_{j_q} \\ \alpha_{j_{q+1},1} & \alpha_{j_{q+1},2} & ... & \alpha_{j_{q+1},q} & \beta_{j_{q+1},1} & A_{j_{q+1}} \\ \alpha_{j_{q+2},1} & \alpha_{j_{q+2},2} & ... & \alpha_{j_{q+2},q} & \beta_{j_{q+2},1} & A_{j_{q+2}} \end{vmatrix} = 0 \quad (211)$$

Again, not necessarily every subset of $q + 2$ elementary reaction steps will result in a distinct *ER*. A complete set of distinct *ER*s may be generated either by considering all of the possible combinations of $q + 2$ elementary reaction steps from among the total of p or by appropriately modifying the method of Fishtik and Datta [101].

4.2. Quasi-Steady-State Approximation

According to the QSS approximation, the rates of formation and consumption of the surface intermediates are approximately equal, so that the time derivatives of the coverages of the intermediates may be set equal to zero

$$\frac{d\theta_k}{dt} = \sum_{\rho=1}^{p} \alpha_{\rho k} r_\rho = 0 \qquad (k = 1, 2, \ldots, q) \tag{212}$$

In matrix form, this may be written as

$$\boldsymbol{\alpha}^{\mathrm{T}}\mathbf{r} = \begin{bmatrix} \alpha_{11} & \alpha_{21} & \ldots & \alpha_{p1} \\ \alpha_{12} & \alpha_{22} & \ldots & \alpha_{p2} \\ \vdots & \vdots & \vdots & \vdots \\ \alpha_{1q} & \alpha_{2q} & \ldots & \alpha_{pq} \end{bmatrix} \begin{pmatrix} r_1 \\ r_2 \\ \vdots \\ r_p \end{pmatrix} = 0 \tag{213}$$

Using the QSS approximation, we introduce the vector

$$\mathbf{Q} = (Q_1, Q_2, \ldots, Q_q)^{\mathrm{T}} \tag{214}$$

where the Q_k's (k = 1, 2, …, q) denote the QQS conditions of the linearly independent intermediates I_k (k = 1, 2, …, q). The QSS conditions of the linearly independent intermediates may be written in vector form as

$$\mathbf{Q}: \quad \boldsymbol{\alpha}^{\mathrm{T}}\mathbf{r} = 0 \tag{215}$$

or

$$\begin{aligned} Q_1: &\quad \alpha_{11} r_1 + \alpha_{21} r_2 + \ldots + \alpha_{p1} r_p = 0 \\ Q_2: &\quad \alpha_{12} r_1 + \alpha_{22} r_2 + \ldots + \alpha_{p2} r_p = 0 \end{aligned} \tag{216}$$

Q_2: $\alpha_{12} r_1 + \alpha_{22} r_2 + ... + \alpha_{p2} r_p = 0$

…

Q_q: $\alpha_{1q} r_1 + \alpha_{2q} r_2 + ... + \alpha_{pq} r_p = 0$

In what follows, Equation (216) is referred to as the *intermediate* QSS conditions. On the other hand, the rate r_{OR} of the *OR* under QSS conditions is related to the rates of the elementary reaction steps via

$$r_{OR} = \frac{1}{\nu_1} \sum_{\rho=1}^{p} \beta_{\rho 1} r_\rho = \frac{1}{\nu_2} \sum_{\rho=1}^{p} \beta_{\rho 2} r_\rho = ... = \frac{1}{\nu_n} \sum_{\rho=1}^{p} \beta_{\rho n} r_\rho \tag{217}$$

where r_ρ (ρ = 1, 2, ..., p) are subject to the QSS conditions, Equation (216). Furthermore, Equation (217) is referred to as the *OR* QSS conditions.

4.2.1. Direct QSS Conditions and Direct Nodes

The nodes of the *RR* graph are subject to Kirchhoff's Current Law (KCL), i.e., the rates of the elementary reaction steps leaving and entering the nodes satisfy the intermediate and *OR* QSS conditions, Equation (216) and (217). It is useful to distinguish between two different types of nodes. Thus, the nodes that satisfy the intermediate QSS conditions are referred to as the *intermediate nodes* (*IN*s), while those that satisfy the *OR* QSS conditions are referred to as *terminal nodes* (*TN*s). It is to be further noted that nodes denote reaction connectivity. Therefore, an alternate definition of *IN*s is that they represent exclusively the connectivity of the elementary reaction steps, while *TN*s also involve *OR*s. Furthermore, the QSS is a limiting form of KCL, which actually applies to non-steady state conditions as well. Still, another interpretation is that *IN*s represent only intermediate species while the *TN*s also involve terminal species.

It general, the intermediate QSS conditions at the *IN*s do not simply represent the QSS conditions of individual intermediate species, i.e., Q_1, Q_2, …, Q_q, Equation (216). Rather, the QSS conditions at the *IN*s, in general, represent a group of species, i.e., they represent a certain linear combination of Q_1, Q_2, …, Q_q. Since the linear combinations of

Q_1, Q_2, …, Q_q may be arbitrary and, hence, infinite, so might be the number of *IN*s. Similarly, the *OR* QSS conditions at the *TN*s do not necessarily coincide with those given by Equation (217). Thus, Equation (217) may be transformed using Equation (216). As a result, the *OR* QSS conditions at the *TN*s may take a large variety of forms.

Clearly, in order to generate meaningful *RR* graphs, it is necessary to specify the rules that govern the connectivity of the elementary reaction steps at both the *IN*s and *TN*s. In doing so, we accept the concept of directness in the sense that it has been defined and applied above to the *RR*s. More specifically, we assume that the number of elementary reaction steps connected at a direct node, either *IN* or *TN*, should be *minimal* in the sense that if a reaction is dropped from the node, it is not possible to satisfy the QSS conditions for the given set of species at that node by employing only the remaining reaction steps. In other words, it is postulated that *only the nodes that connect a minimum number of reaction steps satisfying the QSS conditions for a given set of species are allowed*. By analogy with *RR*s, the QSS conditions involving a minimal number of rates of the elementary reaction steps in the sense defined above are called *direct QSS conditions*, while the corresponding nodes are called *direct IN*s and *direct TN*s.

4.2.1.1 Direct INs

The generation and enumeration of direct QSS conditions, or direct nodes, may be accomplished by employing the response reactions (*RER*s) formalism [102]. Consider first the enumeration of the direct intermediate QSS conditions. Let an arbitrary linear combination of the intermediate QSS conditions Q_1, Q_2, …, Q_q be

$$\begin{aligned} Q = \lambda_1 Q_1 + \lambda_2 Q_2 + ... \lambda_q Q_q = (\alpha_{11} r_1 + \alpha_{21} r_2 + ... + \alpha_{p1} r_p)\lambda_1 + ... \\ (\alpha_{12} r_1 + \alpha_{22} r_2 + ... + \alpha_{p2} r_p)\lambda_2 + ... \\ +(\alpha_{1q} r_1 + \alpha_{2q} r_2 + ... + \alpha_{pq} r_p)\lambda_q = 0 \end{aligned} \tag{218}$$

where $\lambda_1, \lambda_2, ..., \lambda_q$ are constants corresponding to the intermediate species. Now, to obtain the direct QSS conditions, i.e., those that involve a minimum number of rates, the constants $\lambda_1, \lambda_2, ..., \lambda_q$ should be chosen so as to eliminate a maximum number of rates.

This results in a system of homogeneous equations in the unknowns $\lambda_1,\lambda_2,...,\lambda_q$. As well known from linear algebra, in order to obtain a non-trivial solution for $\lambda_1,\lambda_2,...,\lambda_q$ it is necessary to have no more than $q - 1$ linear homogeneous equations. That is, the intermediate QSS conditions Q_1, Q_2, …, Q_q should be linearly combined so as to eliminate at least $q - 1$ rates. In turn, this means that a direct intermediate QSS condition should involve no more than $p - (q - 1) = p - q + 1$ rates. This, of course, specifies the maximum degree of an intermediate node [103].

Let us partition the set of rates $\{r_1, r_2, \ldots, r_p\}$ of the elementary reaction steps into two subsets: a subset of $q - 1$ rates $\{r_{l_1},r_{l_2},...,r_{l_{q-1}}\}$ $(1 \le l_1 < l_2 < ... < l_{q-1} \le p)$ that *are not involved* in a direct intermediate QSS condition, and a subset of $p - q + 1$ rates $\{r_{h_1},r_{h_2},...,r_{h_{p-q+1}}\}$ $(1 \le h_1 < h_2 < ... < h_{p-q+1} \le p)$ that *are involved* in a direct QSS condition. Here, $\{l_1,l_2,...,l_{q-1}\}$ and $\{h_1,h_2,...,h_{p-q+1}\}$ are two ordered subsets of integers chosen such that

$$\{l_1,l_2,...,l_{q-1}\} \bigcup \{h_1,h_2,...,h_{p-q+1}\} = \{1,2,...,p\} \tag{219}$$

A direct intermediate QSS may, thus, be characterized by either the selection of $q - 1$ rates $r_{l_1},r_{l_2},...,r_{l_{q-1}}$ that *are not involved*, or by the $p - q + 1$ rates $\{r_{h_1},r_{h_2},...,r_{h_{p-q+1}}\}$ that *are involved* in a direct intermediate QSS. We denote a direct intermediate QSS condition by $Q(r_{h_1},r_{h_2},...,r_{h_{p-q+1}})$, thus specifying the rates of the elementary reaction steps that are involved in a direct intermediate QSS condition. The latter may be obtained by choosing $\lambda_1,\lambda_2,...,\lambda_q$ in Equation (218) so as to eliminate the rates $r_{l_1},r_{l_2},...,r_{l_{q-1}}$. This gives

$$\begin{aligned}
&\alpha_{l_1,1}\lambda_1 + \alpha_{l_1,2}\lambda_2 + ... + \alpha_{l_1,q}\lambda_q = 0 \\
&\alpha_{l_2,1}\lambda_1 + \alpha_{l_2,2}\lambda_2 + ... + \alpha_{l_2,q}\lambda_q = 0 \\
&... \\
&\alpha_{l_{q-1},1}\lambda_1 + \alpha_{l_{q-1},2}\lambda_2 + ... + \alpha_{l_{q-1},q}\lambda_q = 0
\end{aligned} \tag{220}$$

The solution to this system of homogeneous linear equations is

$$\lambda_k = \begin{vmatrix} \alpha_{l_1,1} & \alpha_{l_2,1} & \dots & \alpha_{l_{q-1},1} & 0 \\ \alpha_{l_1,2} & \alpha_{l_2,2} & \dots & \alpha_{l_{q-1},2} & 0 \\ \dots & \dots & \dots & \dots & \dots \\ \alpha_{l_1,k-1} & \alpha_{l_2,k-1} & \dots & \alpha_{l_{q-1},k-1} & 0 \\ \alpha_{l_1,k} & \alpha_{l_2,k} & \dots & \alpha_{l_{q-1},k} & 1 \\ \alpha_{l_1,k+1} & \alpha_{l_2,k+1} & \dots & \alpha_{l_{q-1},k+1} & 0 \\ \dots & \dots & \dots & \dots & \dots \\ \alpha_{l_1,q} & \alpha_{l_2,q} & \dots & \alpha_{l_{q-1},h_q} & 0 \end{vmatrix} \qquad (k = 1, 2, \dots, q) \tag{221}$$

Substituting Equation (221) into Equation (218) gives the following general formula for a direct intermediate QSS condition

$$Q(r_{h_1}, r_{h_2}, \dots, r_{h_{p-q+1}}): \begin{vmatrix} \alpha_{l_1,1} & \alpha_{l_2,1} & \dots & \alpha_{l_{q-1},1} & Q_1 \\ \alpha_{l_1,2} & \alpha_{l_2,2} & \dots & \alpha_{l_{q-1},2} & Q_2 \\ \dots & \dots & \dots & \dots & \dots \\ \alpha_{l_1,q} & \alpha_{l_2,q} & \dots & \alpha_{l_{q-1},q} & Q_q \end{vmatrix} = 0 \tag{222}$$

or, taking into account Equation (216), the direct QSS condition (KCL) for a node is

$$Q(r_{h_1}, r_{h_2}, \dots, r_{h_{p-q+1}}): \sum_{k=1}^{p-q+1} \begin{vmatrix} \alpha_{1_1,1} & \alpha_{l_2,1} & \dots & \alpha_{l_{q-1},1} & \alpha_{h_k,1} \\ \alpha_{l_1,2} & \alpha_{l_2,2} & \dots & \alpha_{l_{q-1},2} & \alpha_{h_k,2} \\ \dots & \dots & \dots & \dots & \dots \\ \alpha_{l_1,q} & \alpha_{l_2,q} & \dots & \alpha_{l_{q-1},q} & \alpha_{h_k,q} \end{vmatrix} r_{h_k} = 0 \tag{223}$$

As a result, the general connectivity of an *IN* denoted by $n_I(s_{h_1}, s_{h_2}, \dots, s_{h_{p-q+1}})$ is

$$n_I(s_{h_1}, s_{h_2}, \dots, s_{h_{p-q+1}}): \sum_{k=1}^{p-q+1} \begin{vmatrix} \alpha_{l_1,1} & \alpha_{l_2,1} & \dots & \alpha_{l_{q-1},1} & \alpha_{h_k,1} \\ \alpha_{l_1,2} & \alpha_{l_2,2} & \dots & \alpha_{l_{q-1},2} & \alpha_{h_k,2} \\ \dots & \dots & \dots & \dots & \dots \\ \alpha_{l_1,q} & \alpha_{l_2,q} & \dots & \alpha_{l_{q-1},q} & \alpha_{h_k,q} \end{vmatrix} s_{h_k} \tag{224}$$

The complete enumeration of direct intermediate QSS conditions and *IN*s may be, in principle, performed by considering all of the possible combinations of $p - q + 1$ species from the total of p. Normally, the number of direct *IN*s exceeds the number of linearly independent *IN*s, i.e., the number of linearly independent intermediates q. It may be noted again, that, although the node connectivity (Equation (224)) results from the QSS condition, it is more generally valid including the unsteady state.

4.2.1.2 Direct TNs

Now, consider the enumeration of the direct *OR* QSS conditions, i.e., the enumeration of direct *TN*s. Since, again, a direct *OR* QSS condition should involve a minimum number of rates, it is necessary to eliminate from Equation (217) the maximum number of rates by employing the interrelationships provided by the intermediate QSS, Equation (216). Because $rank\,\boldsymbol{\alpha} = q$, we can solve Equation (216) for no more than q rates. Upon substitution of these q rates into Equation (217) we arrive at a direct *OR* QSS condition involving no more than $p - q$ rates of the elementary reaction steps. Let $\{r_{l_1}, r_{l_2}, ..., r_{l_q}\}$ $(1 \le l_1 < l_2 < ... < l_q \le p)$ be the q rates of the elementary reaction steps that *are not involved* in a direct *OR* QSS condition, while $\{r_{h_1}, r_{h_2}, ..., r_{h_{p-q}}\}$ $(1 \le h_1 < h_2 < ... < h_{p-q} \le p)$ be the $p - q$ rates that *are involved* in a direct *OR* QSS condition. Here $\{l_1, l_2, ..., l_q\}$ and $\{h_1, h_2, ..., h_{p-q}\}$ are two ordered subsets of integers chosen so as to satisfy Equation (219). A direct *OR* QSS condition is denoted by $P(r_{h_1}, r_{h_2}, ..., r_{h_{p-q}})$ thus specifying the rates that are involved in a direct *OR* QSS condition. Its general equation may be obtained by solving Equation (216) with respect to $\{r_{l_1}, r_{l_2}, ..., r_{l_q}\}$

$$\begin{aligned}
&\alpha_{l_1,1} r_{l_1} + \alpha_{l_2,1} r_{l_2} + ... + \alpha_{l_q,1} r_{l_q} = -\alpha_{h_1,1} r_{h_1} - \alpha_{h_2,1} r_{h_2} - ... - \alpha_{h_{p-q},1} r_{h_{p-q}} \\
&\alpha_{l_1 2} r_{l_1} + \alpha_{l_2,2} r_{l_2} + ... + \alpha_{l_q,2} r_{l_q} = -\alpha_{h_1 2} r_{h_1} - \alpha_{h_2,2} r_{h_2} - ... - \alpha_{h_{p-q},2} r_{l_{p-q}} \\
&... \\
&\alpha_{l_1,q} r_{l_1} + \alpha_{l_2,q} r_{l_2} + ... + \alpha_{l_q,q} r_{l_q} = -\alpha_{h_1,q} r_{h_1} - \alpha_{h_2,q} r_{h_2} - ... - \alpha_{h_{p-q},q} r_{j_{p-q}}
\end{aligned} \tag{225}$$

Substituting the solution of Equation (225) into Equation (217), after a few transformations based on the properties of the determinants, we obtain

$$P(r_{h_1},r_{h_2},...,r_{h_{p-q}}):\ \frac{1}{v_1\Delta}\sum_{k=1}^{p-q}\begin{vmatrix}\alpha_{l_1,1} & \alpha_{l_1,2} & ... & \alpha_{l_1,q} & \beta_{l_1,1}\\ \alpha_{l_2,1} & \alpha_{l_2,2} & ... & \alpha_{l_2,q} & \beta_{l_2,1}\\ ... & ... & ... & ... & ...\\ \alpha_{l_q,1} & \alpha_{l_q,2} & ... & \alpha_{l_q,q} & \beta_{l_q,1}\\ \alpha_{h_k,1} & \alpha_{h_k,2} & ... & \alpha_{h_k,q} & \beta_{h_k,1}\end{vmatrix} r_{h_k} = r_{OR} \tag{226}$$

where the determinant

$$\Delta = \Delta(l_1,l_2,...,l_q) = \begin{vmatrix}\alpha_{l_1,1} & \alpha_{l_1,2} & ... & \alpha_{l_1,q}\\ \alpha_{l_2,1} & \alpha_{l_2,2} & ... & \alpha_{l_2,q}\\ ... & ... & ... & ...\\ \alpha_{l_q,1} & \alpha_{l_q,2} & ... & \alpha_{l_q,q}\end{vmatrix} \tag{227}$$

Obviously, only those selections of the set of integers $(l_1,l_2,...,l_q)$ are valid for which the determinant $\Delta = \Delta(l_1,l_2,...,l_q)$, Equation (227), is different from zero. The *TN*s that correspond to these direct *OR* QSS conditions are denoted by $m(s_{h_1},s_{h_2},...,s_{h_{p-q}})$ and their general connectivity is given by

$$n_{\mathrm{T}}(s_{h_1},s_{h_2},...,s_{h_{p-q}}):\ \frac{1}{v_1\Delta}\sum_{k=1}^{p-q}\begin{vmatrix}\alpha_{l_1,1} & \alpha_{l_1,2} & ... & \alpha_{l_1,q} & \beta_{l_1,1}\\ \alpha_{l_2,1} & \alpha_{l_2,2} & ... & \alpha_{l_2,q} & \beta_{l_2,1}\\ ... & ... & ... & ... & ...\\ \alpha_{l_q,1} & \alpha_{l_q,2} & ... & \alpha_{l_q,q} & \beta_{l_q,1}\\ \alpha_{h_k,1} & \alpha_{h_k,2} & ... & \alpha_{h_k,q} & \beta_{h_k,1}\end{vmatrix} s_{h_k} + OR \tag{228}$$

Notice that in Equation (228) the *OR* is added to the first term rather than subtracted as it would follow from Equation (225). As shown below, this change in sign is dictated by the necessity to ensure that the *RR* graphs are cyclic graphs. It should also be noted that,

in deriving Equations (226) and (227), we have arbitrarily utilized the first identity in Equation (217). It may be shown, however, that, up to a constant, the final result is independent of the choice of the identities in Equation (217).

The complete enumeration of the *TN*s may be, in general, performed by applying Equation (226) to all possible combinations of $\{r_{l_1}, r_{l_2}, ..., r_{l_q}\}$ $(1 \le l_1 < l_2 < ... < l_q \le p)$ or $\{r_{h_1}, r_{h_2}, ..., r_{h_{p-q}}\}$ $(1 \le h_1 < h_2 < ... < h_{p-q} \le p)$ for which the determinant Δ, Equation (227), is different from zero. The connectivity of *IN*s and *TN*s, in principle, provides the necessary information for constructing the *RR* graph. Of course, not all *IN*s and *TN*s are independent; only *q IN*s (the number of independent intermediate species) and one *TN* (for the single *OR*) are independent.

4.3. Quasi-Equilibrium Approximation

Reaction affinity is used to determine the degree of reversibility of an elementary reaction step. If the affinity has a positive value, then the reaction is assumed to proceed in the forward direction. If the affinity is negative, then the reaction is assumed to proceed in the reverse direction.

As a reaction approaches equilibrium, the forward and reverse rates approach a common value. This value is termed the *exchange rate*. The exchange rate, like the exchange current in electrochemical systems, is defined as

$$r_{\rho,0} \equiv \left[\frac{\partial r_\rho}{\partial(\mathscr{A}_\rho)} \right]_{\mathscr{A}_\rho \to 0} \tag{229}$$

where $\mathscr{A}_\rho$ is the dimensionless affinity A_ρ/RT.

Therefore, as the calculated values for the affinity of each elementary reaction approach zero, we assume that the reaction is approaching equilibrium. In the cases where "equilibrium" is achieved early on, the elementary reaction step is assumed to proceed as a quasi-equilibrium step.

This assumption provides a tool for determining the surface coverages of the intermediates in terms of the equilibrium constants and the terminal species concentrations as can be shown by Equation (184) for $\mathscr{A}_\rho = 0$:

$$\ln K_j - \alpha_{j0} \ln \theta_0 - \sum_{k=1}^{q} \alpha_{jk} \ln \theta_k - \sum_{i=1}^{n} \beta_{qi} \ln P_i = 0 \qquad (j = 1, 2, \ldots, p) \qquad (230)$$

Thus, θ_k may be obtained in terms of K_ρ from above along with the site balance.

4.4. An Example of *RR* Stoichiometry

As an example, we consider a modified version of the electrochemical hydrogen oxidation reaction (HOR) mechanism presented in Table 14. As can be seen, besides the conventional elementary reaction steps normally considered in the literature for the HOR, namely, the Tafel (s_3), the Volmer (s_4) and the Heyrovsky (s_6) steps [104], we assume that adsorbed molecular hydrogen may also exist as a distinct species (s_1), thus resulting in an additional path for the formation of adsorbed atomic hydrogen (s_2), as well as a direct electrochemical oxidation path of the adsorbed molecular hydrogen (s_5). There is a single *OR* corresponding to the mechanism

$$OR: \quad -H_2 - 2H_2O + 2H_3O^+ + 2e^- = 0$$

The stoichiometric matrix is

$$\mathbf{\nu} = \begin{array}{c} \begin{array}{ccccccc} H_2 \cdot S & H \cdot S & S & H_2 & H_2O & H_3O^+ & e^- \end{array} \\ \begin{bmatrix} +1 & 0 & -1 & -1 & 0 & 0 & 0 \\ -1 & +2 & -1 & 0 & 0 & 0 & 0 \\ 0 & +2 & -2 & -1 & 0 & 0 & 0 \\ 0 & -1 & +1 & 0 & -1 & +1 & +1 \\ -1 & +1 & 0 & 0 & -1 & +1 & +1 \\ 0 & +1 & -1 & -1 & -1 & +1 & +1 \end{bmatrix} \end{array} \begin{array}{c} s_1 \\ s_2 \\ s_3 \\ s_4 \\ s_5 \\ s_6 \end{array} \qquad (231)$$

Table 14. A Generalized Mechanism and the Overall Reaction of the Electrochemical Hydrogen Oxidation (S = surface site)

Electrochemical HOR Mechanism	
$H_2 + S = H_2{\cdot}S$	(s_1)
$H_2{\cdot}S + S = 2H{\cdot}S$	(s_2)
$H_2 + 2S = 2H{\cdot}S$ *(Tafel)*	(s_3)
$H_2O + H{\cdot}S = S + H_3O^+ + e^-$ *(Volmer)*	(s_4)
$H_2O + H_2{\cdot}S = H{\cdot}S + H_3O^+ + e^-$	(s_5)
$H_2O + H_2 + S = H{\cdot}S + H_3O^+ + e^-$ *(Heyrovski)*	(s_6)
$H_2 + 2H_2O = 2H_3O^+ + 2e^-$	(s_{OR})

Hence, the system comprises $p = 6$ elementary reaction steps, $q = 2$ linearly independent intermediates (e.g., H·S and H_2·S), by virtue of the site balance, and $n = 4$ terminal species (H_2, H_2O, H_3O^+ and e^-). From the stoichiometric matrix, we select the intermediate sub-matrix $\boldsymbol{\alpha}$

$$\boldsymbol{\alpha} = \begin{array}{c} \begin{matrix} H_2\cdot S & H\cdot S \end{matrix} \\ \begin{bmatrix} +1 & 0 \\ -1 & +2 \\ 0 & +2 \\ 0 & -1 \\ -1 & +1 \\ 0 & +1 \end{bmatrix} \end{array} \begin{matrix} s_1 \\ s_2 \\ s_3 \\ s_4 \\ s_5 \\ s_6 \end{matrix} \tag{232}$$

and a reduced stoichiometric sub-matrix $\boldsymbol{\gamma}$, Equation (190), with the rank equal to three

$$\boldsymbol{\gamma} = \begin{array}{c} \begin{matrix} H_2\cdot S & H\cdot S & H_2 \end{matrix} \\ \begin{pmatrix} +1 & 0 & -1 \\ -1 & +2 & 0 \\ 0 & +2 & -1 \\ 0 & -1 & 0 \\ -1 & +1 & 0 \\ 0 & +1 & -1 \end{pmatrix} \end{array} \begin{matrix} s_1 \\ s_2 \\ s_3 \\ s_4 \\ s_5 \\ s_6 \end{matrix} \tag{233}$$

Our starting point in the construction of the *RR* graph is a set of direct *FR*s, *ER*s, *IN*s and *TN*s. These are enumerated using the above formalism.

4.4.1. Enumeration of the direct FRs.

The direct *FR*s are enumerated based on the intermediate matrix $\boldsymbol{\alpha}$. By definition, a direct *FR* in this system involves no more than *rank* $\boldsymbol{\alpha}$ + 1 = 2 + 1 = 3 linearly independent elementary reaction steps. Thus, any three linearly independent elementary

reaction steps define a direct *FR*. For instance, elementary reaction steps s_1, s_2 and s_4 are linearly independent, and, according to Equation (204), define the following direct *FR*

$$FR(s_1.s_2,s_4): \quad \begin{vmatrix} +1 & 0 & s_1 \\ -1 & +2 & s_2 \\ 0 & -1 & s_4 \end{vmatrix} = s_1 + s_2 + 2s_4 = OR \tag{234}$$

A complete list of *FR*s may, thus, be generated by repeating this procedure over all possible selections of three linearly independent elementary reaction steps from a total of six. Thus, the number of direct *FR*s for this system does not exceed 6!/3!/3! = 20, from Equation (195). As can be seen from Table 15, only ten of them, however, are distinct. Further, only $p - q = 6 - 2 = 4$ of these are independent.

4.4.2. Enumeration of the direct ERs.

The starting point in the enumeration of the direct *ER*s is the reduced stoichiometric matrix $\boldsymbol{\gamma}$. By definition, a direct *ER* involves no more than $rank\,\boldsymbol{\gamma} + 1 = q + 2$. Hence, any $q + 2 = 2 + 2 = 4$ elementary reaction steps define a direct *ER*. For instance, according to Equation (209), the first four elementary reaction steps s_1, s_2, s_3 and s_4 define the following direct *ER*

$$ER(s_1,s_2,s_3,s_4): \quad \begin{vmatrix} +1 & 0 & -1 & s_1 \\ -1 & +2 & 0 & s_2 \\ 0 & +2 & -1 & s_3 \\ 0 & -1 & 0 & s_4 \end{vmatrix} = -s_1 - s_2 + s_3 = 0 \tag{235}$$

Repeating this procedure over all combinations of four elementary reaction steps from the total of six result in 6!/4!/2! = 15 possible direct *ER*s. However, only seven of these are stoichiometrically distinct (Table 15). Further, only $p - rank\ \boldsymbol{\nu} = p - (q + 1) = 6 - 3 = 3$ of these are independent.

Table 15. A Complete List of Stoichiometrically Distinct Direct Full Routes (*FR*s), Empty Routes (*ER*s), Intermediate Nodes (*IN*s) and Terminal Nodes (*TN*s) for Electrochemical Hydrogen Oxidation

Full Routes

FR_1: $s_1 + s_2 + 2s_4 = OR$
FR_2: $s_1 - s_2 + 2s_5 = OR$
FR_3: $-s_1 - s_2 + 2s_6 = OR$
FR_4: $s_3 + 2s_4 = OR$
FR_5: $2s_1 - s_3 + 2s_5 = OR$
$FR_{6:}$ $-s_3 + 2s_6 = OR$
FR_7: $s_1 + s_4 + s_5 = OR$
FR_8: $s_4 + s_6 = OR$
FR_9: $2s_2 - s_3 - 2s_5 = OR$
FR_{10}: $-s_2 + s_5 + s_6 = OR$

Empty Routes

ER_1: $s_1 + s_2 - s_3 = 0$
ER_2: $s_2 + s_4 - s_5 = 0$
ER_3: $s_1 + s_5 - s_6 = 0$
ER_4: $s_3 + s_4 - s_6 = 0$
ER_5: $s_1 + s_2 + s_4 - s_6 = 0$
ER_6: $s_1 - s_3 - s_4 + s_5 = 0$
ER_7: $s_2 - s_3 - s_5 + s_6 = 0$

Intermediate Nodes

n_{I1}: $s_1 - s_2 - s_5$
n_{I2}: $2s_2 + 2s_3 - s_4 + s_5 + s_6$
n_{I3}: $s_1 + s_2 + 2s_3 - s_4 + s_6$
n_{I4}: $2s_1 + 2s_3 - s_4 - s_5 + s_6$

Terminal Nodes

n_{T1}: $\frac{1}{2}(s_4 + s_5 + s_6) + OR$
n_{T2}: $s_2 + s_3 + s_5 + s_6 + OR$
n_{T3}: $-s_2 - s_3 + s_4 + OR$
n_{T4}: $s_1 + s_3 + s_6 + OR$
n_{T5}: $-s_1 - s_3 + s_4 + s_5 + OR$
n_{T6}: $\frac{1}{2}(s_1 - s_2 + s_4 + s_6) + OR$

4.4.3. Enumeration of the Direct INs

The system includes two linearly independent intermediates, say, H·S and H_2·S. Thus, the intermediate QSS conditions may be presented as

$$Q_1: \quad r_1 - r_2 - r_5 = 0 \qquad H_2\cdot S$$
$$Q_2: \quad 2r_2 + 2r_3 - r_4 + r_5 + r_6 = 0 \qquad H\cdot S$$

Alternatively, these QSS conditions may be represented in terms of the intermediate matrix

$$\boldsymbol{\alpha}^{\mathrm{T}} = \begin{array}{c} \begin{matrix} s_1 & s_2 & s_3 & s_4 & s_5 & s_6 \end{matrix} \\ \begin{bmatrix} +1 & -1 & 0 & 0 & -1 & 0 \\ 0 & +2 & +2 & -1 & +1 & +1 \end{bmatrix} \end{array} \begin{matrix} \mathrm{H}\cdot\mathrm{S} \\ \mathrm{H_2}\cdot\mathrm{S} \end{matrix} \tag{236}$$

By definition, a direct QSS condition may be obtained by linearly combining Q_1 and Q_2 so as to eliminate at least $q - 1 = 2 - 1 = 1$ rates. Alternatively, a direct QSS condition will involve no more than $p - (q - 1) = 6 - 2 + 1 = 5$ rates. For instance, if we choose to eliminate r_2, the respective direct *QSS* condition will involve the remaining rates, i.e., r_1, r_3, r_4, r_5, r_6. According to Equation (222), we have

$$Q(r_1, r_3, r_4, r_5, r_6): \quad \begin{bmatrix} -1 & Q_1 \\ +2 & Q_2 \end{bmatrix} = -(Q_1 + 2Q_2) = 0 \tag{237}$$

which, thus, represents the QSS condition for the intermediate species H_2·S + 2H·S. Employing the equations for Q_1 and Q_2

$$Q(r_1, r_3, r_4, r_5, r_6): \qquad 2r_1 + 2r_3 - r_4 - r_5 + r_6 = 0$$

The respective *IN* is

$n_I(s_1, s_3, s_4, s_5, s_6)$: $\quad 2s_1 + 2s_3 - s_4 - s_5 + s_6$

A complete list of *IN*s may be generated by repeating this procedure over the total number of possible selections of one rate from a total of six thus resulting into six possible *IN*s. In reality, only four *IN*s are distinct (Table 15). These *IN*s were simply numbered from n_{I1} to n_{I4}. In fact, only $q = 2$ of these are independent.

4.4.4. Enumeration of the direct TNs

The conventional *OR* QSS conditions may be expressed in terms of any terminal species. For instance, selecting the terminal species H_2 gives the following *OR* QSS conditions

$$r_{OR} = r_1 + r_3 + r_6$$

Now, we can substitute any two of these rates with the remaining rates using the conventional intermediate QSS conditions, i.e., Q_1 and Q_2. In doing this, we can employ Equation (227). For instance, eliminating r_1 and r_3 will result in a direct *OR* QSS condition involving r_2, r_4, r_5 and r_6. The determinant formed from the intermediate matrix $\boldsymbol{\alpha}$ corresponding to r_1 and r_3, Equation (227), is different from zero

$$\Delta(1,3) = \begin{vmatrix} +1 & 0 \\ 0 & +2 \end{vmatrix} = 2 \neq 0 \tag{238}$$

Thus, r_1 and r_3 is an appropriate selection. According to Equation (226), the resulting direct *OR* QSS condition is

$$P(r_2, r_4, r_5, r_6): \; -\frac{1}{2}\left\{ \begin{vmatrix} +1 & 0 & -1 \\ 0 & +2 & -1 \\ -1 & +2 & 0 \end{vmatrix} r_2 + \begin{vmatrix} +1 & 0 & -1 \\ 0 & +2 & -1 \\ 0 & -1 & 0 \end{vmatrix} r_4 + \begin{vmatrix} +1 & 0 & -1 \\ 0 & +2 & -1 \\ -1 & +1 & 0 \end{vmatrix} r_5 + \begin{vmatrix} +1 & 0 & -1 \\ 0 & +2 & -1 \\ 0 & +1 & -1 \end{vmatrix} r_6 \right\}$$

$$= \tfrac{1}{2}(r_4 + r_5 + r_6) \tag{239}$$

The direct *TN* corresponding to this direct *OR* QSS condition is

$$n_T(s_2, s_4, s_5, s_6): \qquad \tfrac{1}{2}(s_4 + s_5 + s_6) + OR$$

Repeating this procedure over all choices of two rates from a total of six rates gives the complete set of direct *OR* QSS conditions. The stoichiometrically distinct direct *TN*s corresponding to these *OR* QSS conditions are presented in Table 15.

Chapter 5. Reaction Route Graph Theory

Reaction schematics are routinely employed to describe reaction pathways and are an invaluable tool in the study of reaction mechanisms. Typically species are depicted as nodes interconnected via arrows representing elementary reaction steps. While this is appropriate for monomolecular reactions, the scheme becomes increasingly complex with an increase in the species involved in each elementary reaction step. For this reason, we introduce a new kind of scheme where the branches represent the elementary reaction steps and the nodes represent the manner in which the elementary reaction steps are interconnected within *RR*s; hence, the schematic is called a reaction route (*RR*) graph.

Basic concepts of graph theory have been employed to determine the connectivity of the elementary reaction steps in a mechanism. An analogy has been made between the developed *RR* graph and electric circuit theory to analyze and reduce the reaction route graph to a simpler form in which the quasi-equilibrium steps, rate-limiting steps, and dominant pathways may be identified.

Kirchhoff's Current Law, representing conservation of mass at each node, and Kirchhoff's Voltage Law, representing thermodynamic consistence of the affinity for each cycle, are used to reduce the diagram by examining comparable path resistances and eliminating the more resistant pathway. This ultimately results in a simpler reaction route graph from which a simplified rate expression can be determined.

5.1. Background

Reaction schematics of one kind or another are universally employed to depict reaction pathways in chemistry and biology, and are invaluable in the study of reaction mechanisms. Typically, species, often showing molecular structure, are drawn and interconnected via arrows to show their reactions. Such a scheme, while well-suited for monomolecular reactions, becomes complicated when more than one species is involved in a reaction and are represented by parallel pathways.

The term “reaction graphs” alludes to the topology of reaction mechanisms and derives from the fact that reaction schematics are structurally similar to graphs, with nodes or vertices denoting species, and branches or edges their reactions [105,106]. The graph theoretical viewpoint of mechanisms, besides its intuitive appeal, allows results of graph theory to be used for describing reaction topology, and is especially useful for computer assisted enumeration [107]. The main use of chemical graph theory has been in the study of molecular structure [108], but it is being increasingly utilized in the elucidation [105,106] and generation of reaction mechanisms [109-111].

Christiansen [112] proposed the use of reaction diagrams for open (non-catalytic) or closed (catalytic) sequences by depicting reaction intermediates at nodes connected by branches. For linear elementary reactions, i.e., those in which the reactions are first-order with respect to the intermediates in both the forward and the reverse directions, he derived rate expressions for sequential steps at steady-state. King and Altman [113] utilized the approach to derive kinetics of linear enzyme-catalyzed reactions. M. I. Temkin [27,69,114] further developed Christiansen’s approach to analyze kinetics of steady-state sequential and parallel catalytic reactions. Yatsimirskii [115] has discussed the application of graph theory to catalytic kinetics. Balaban, et al. [105,116,117] proposed “reaction graphs” for studying the topology of isomerization reactions. These early studies were followed by numerous other graph-theoretic studies as summarized in the book by Temkin, et al. [106]. More recently, these methods have been applied to metabolic networks [99,118-121]. The use of graph theory as applied to the peroxide mechanism in conjunction with the design and analysis of molten carbonate fuel cells (MCFCs) has been considered by Fehribach [122,123]. In these graphs, termed "net cycle diagrams", reactions occur at nodes (there termed "dots") and the direction of the arrows show the forward direction of the reactions as they pertain to the species labeled within the graph.

Unfortunately, the practice of depicting reaction intermediates as vertices or nodes connected by branches or edges restricts their application to linear kinetic mechanisms. Temkin, et al. [106] proposed the use of bipartite graphs for nonlinear kinetic mechanisms, i.e., those with elementary reactions with more than one intermediate on either side of the reaction. In their approach, one set of vertices on one

side of the graph represent intermediates, while another set on the opposite side represents terminal species. A third set of markers in the middle denotes elementary reaction steps. Arrows connect various species and reactions and their directions show whether species are being consumed or produced, with double arrows denoting non-unit stoichiometric numbers. This results in jumbled graphs devoid of intuitive appeal even for simple reactions.

Oster, et al. [124] and Oster and Perelson [125] utilized the analogy between reaction networks and electrical networks in their development of graph theory based "network thermodynamics." The topological structure of a reaction network was represented by them as a directed graph with species representing tree branches and links representing the reactions interconnecting the species. The forward and the reverse steps were represented separately by two links. The non-unit stoichiometric coefficient was represented by an ideal transformer. Kirchhoff's laws of current and potential were applied to the resulting network, with reaction affinity corresponding to potential and reaction rate corresponding to current. However, their chemical reaction network representation is particularly cumbersome, resulting in complicated networks even for simple reaction systems. Surprisingly, few other researchers have utilized the evident analogy between reaction systems and electrical circuits [126], but the results are either similarly cumbersome [127], or only simple monomolecular examples have so far been treated [121].

We developed a new graph-theoretical approach that overcomes many of the limitations of the current methodologies and is extremely powerful in the graphical depiction as well as in mechanistic and kinetic analysis of reaction networks based on reaction route theory and their analogy with electrical circuits. These "reaction route graphs" are distinct from "reaction graphs" in that the nodes do not represent a given species but rather they show how the elementary steps, or graph branches, are connected to depict the various reaction routes. Thus, there is a direct analogy to conventional graphs. The approach has broad applicability including elementary reactions of arbitrary stoichiometry and multiple overall reactions.

With the advent of quantum mechanical calculations of catalytic molecular events and their energetics [128] along with the availability of powerful semi-theoretical

methods [17], such reaction pathway analyses will become increasingly indispensable. It is only a matter of time before we have a very fundamental understanding of the molecular steps involved in important catalytic processes along with their reliable kinetics. However, this is only the first step toward unraveling the mechanism and kinetics of the overall catalytic reactions of interest. The predicted steps must be organized into a coherent mechanism and kinetics of overall reactions. The objective of this work is to develop such a framework.

Prior to providing the details, it is useful to visualize a reaction network as a trek across a mountain range with many peaks and valleys (Figure 8). In keeping with the transition state theory, the valleys may be viewed as reactants, surface intermediates and products of a reaction while a single elementary reaction may be viewed as the trek from one valley to an adjacent one over a shallow or tall mountain pass, representative of the energy barrier for the reaction. Many such excursions constitute the overall trek or a reaction network. Clearly, almost an infinite variety of pathways or *FR*s exist for a given trek in going from the reactants to the products, including those involving *ER*s. The direct *FR*s are those that do not involve *ER*s and are finite and shortest, although still large in number.

Based on this analogy, we define a *RR* graph as an ordered, interconnected, directed and a finite sequence of elementary reaction steps that satisfies the following conditions:

a) There is one starting point (reactants) and one end point (products) in the network between each given *OR* in the *RR* graph. If the *OR* is present more than once in a *RR* graph, then a corresponding set of starting and ending points will also be present. If there is more than one *FR*, there will always be parallel branches in the network.
b) Each elementary reaction in the network is reversible, i.e., it may proceed in either direction. The arrows depict the assumed forward direction of the elementary reactions. The branches in the *RR* graph individually represent the elementary reaction steps s_ρ (ρ = 1, 2, …, p) from the reaction mechanism, as well as the overall reaction *OR*.

Any sequence of elementary reaction steps from the starting point to the end point, the terminal nodes, involving the *OR* is a *FR*. In other words, the production and

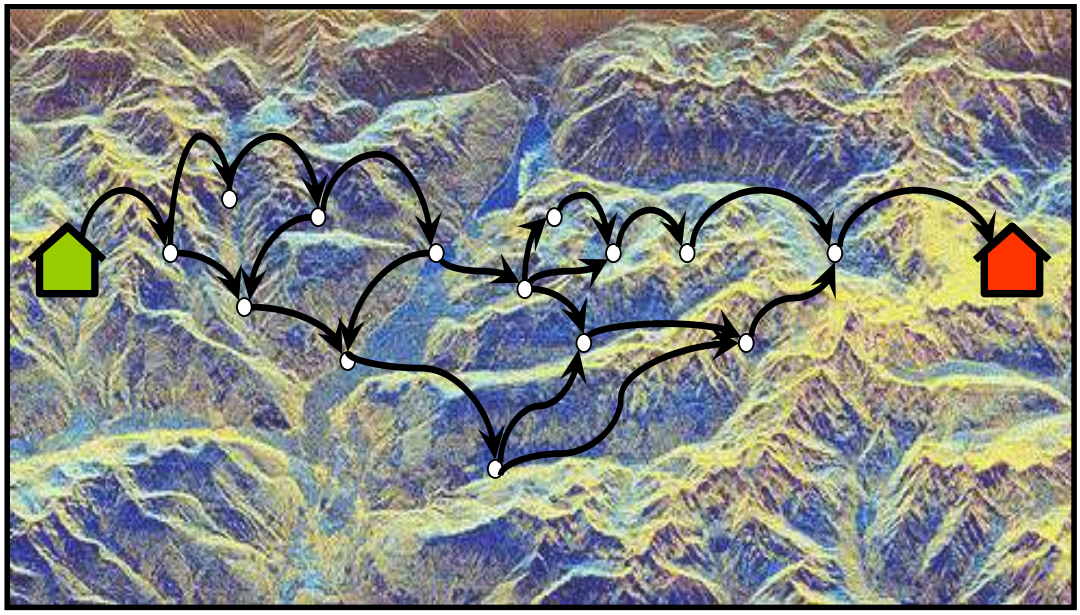

Figure 8. The analogy between a mountain trek and a reaction network.

consumption of every surface intermediate along any *FR* are precisely balanced thus resulting in a net transformation of the reactants into products.

c) The algebraic sum of the affinities of the elementary reaction steps along each *FR* is equal to the overall affinity of the *OR*, A_{OR}, the overall driving force. From this viewpoint, the order of the reaction steps in the *FR* is unimportant.

d) The elementary reactions are interconnected at points called nodes. At each node the QSS conditions for the intermediates, Equation (213), is satisfied; that is, the algebraic sum of the rates of the elementary reactions entering or leaving the node is equal to zero. The nodes in the *RR* graph are either intermediate nodes (*IN*s), i.e., $n_{\mathrm{I}}(s_{h_1},s_{h_2},...,s_{h_{p-q+1}})$ or terminal nodes (*TN*s), i.e., $n_{\mathrm{T}}(s_{h_1},s_{h_2},...,s_{h_{p-q}})$. The details of the terminal and intermediate nodes are discussed in Chapter 4.

e) A *RR* that starts and ends at the same *IN* is an *ER*. The algebraic sum of affinities of the elementary reactions along an *ER* is equal to zero. This means that there are slow steps or significant resistances in all significant parallel branches.

f) The *RR* graph includes, as paths, the complete list of direct *FR*s and *ER*s enumerated by other means.

There are several advantages in adopting this new viewpoint of a reaction network for its analysis, visualization and reduction. The main advantage is that within this representation a reaction network becomes analogous to a general electrical circuit network, so that the procedures of electric circuit analysis are applicable.

5.2. Graph Theoretical Aspects

Since alternate terminology and representation for reaction networks in graph theory exists in the literature, some basic terms are defined below within the context of our approach for the sake of specificity, albeit at the peril of some redundancy. The terminology adopted here is more common in electrical networks [103,129], e.g., “branches” rather than “edges,” “nodes” instead of “vertices,” and “trees” instead of “spanning trees,” since we extensively use this analogy for subsequent reaction route analysis.

The reaction route structure of a reaction network is represented by the so-called *reaction route graph* G_R, which is defined as an ordered, connected, directed (i.e., a digraph), planar or nonplanar, cycle graph comprising B directed branches, each representing an elementary or an overall reaction $\{OR, s_1, s_2, \ldots, s_\rho, \ldots s_p\}$, and N nodes $\{n_1, n_2, \ldots, n_N\}$, that illustrate how the reaction steps are interconnected to allow for all of the direct reaction routes to be traced. If all given reactions are represented only once in the G_R, it is termed a *minimal* reaction route graph, $G_{R,min}$. We will concern ourselves here only with the case of a single overall reaction and the development of its minimal reaction route graph that results from its reaction routes. As per the convention in graph theory, when a branch originates at a node n_j, it is said to be *incident from* the node n_j. When a branch terminates at a node n_j, it is said to be *incident to* the node n_j. Two or more branches are *parallel* if they have in common the same pair of starting and ending nodes. Since graph theory is concerned with topological features of a network, the specific nature of the branch is unimportant and, thus, may be represented simply by a directed line segment. However, since we will be later using the electrical analogy of reaction networks, it is useful to alternately represent an elementary reaction step as a resistor, R_ρ (Figure 9a). The oriented branch variables (Figure 9a) are the reaction affinity A_ρ (much as electrical potential *difference* or branch voltage) and its rate r_ρ (much as electrical current). The orientation shown is simply assumed, and the reaction may actually proceed in either direction. There can, of course, be more than one overall reaction in a G_R, but again, we will limit our present discussion to the case of a single *OR*. The overall reaction is depicted as a voltage source for convenience, much like the resistor representation of an elementary reaction, when the electrical analogy is applied.

It may be remarked that the nodes in the reaction route graphs defined above do not denote single intermediates or terminal species as is almost universally the case in the so-called "reaction graphs" [106], but simply the interconnection of reactions involved in reaction routes, hence the reason for labeling these "reaction route graphs." As a result, a node n_j here represents properties associated with the sum of products of the reactions incident to the node plus the sum of reactants of the reactions incident from the node with an appropriate sign (negative for reactions incident to, and positive for reactions incident from a node, as discussed later in the context of the incidence matrix). The reactant and

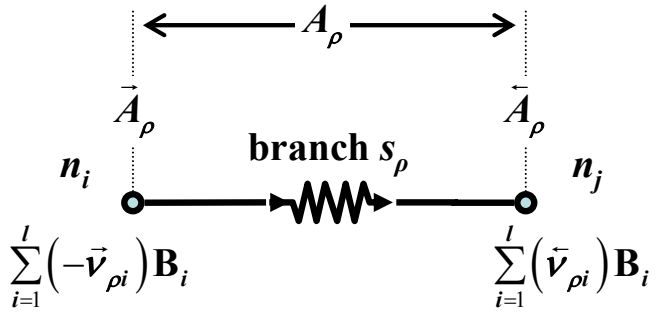

(a)

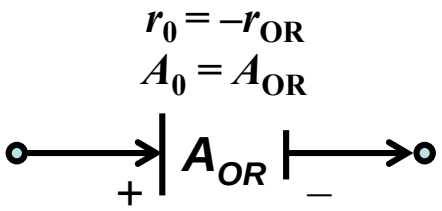

(b)

Figure 9. (a) Elementary reaction as a resistor in a reaction route graph between two nodes. (b) An overall reaction as a voltage source.

product affinities ($\vec{A}_\rho$ and $\overleftarrow{A}_\rho$) of these reactions (branches) at a node follow a similar additive rule, so that each node is associated with a unique value of Gibbs free energy, a state variable. In fact, any other thermodynamic state variable, e.g., enthalpy, may be similarly associated with the nodes. This is useful, for instance, in obtaining a reaction energy diagram directly from the G_R. The derivation of nodes from reaction stoichiometry was considered in Chapter 4.

The k^{th} *walk* from node n_i to node n_j is an alternating sequence of nodes and branches beginning with a starting node n_i and and ending with terminal node n_j, and is given by $w_k = \sum_{n_i \to n_j} \sigma_{k\rho} s_\rho$. A reaction route can be represented as a walk from the starting node n_1 to the ending node n_{q+2}. If the branch is oriented along the direction of the walk, $\sigma_{k\rho} = +1$, and otherwise $\sigma_{k\rho} = -1$. If a branch s_ρ does not occur in the walk, $\sigma_{k\rho} = 0$. A given branch may not be crossed more than once in a walk, while a node may be crossed more than once. A closed walk begins and ends at the same node, and is otherwise termed an open walk. If a closed walk includes the *OR*, it is considered a *FR*; if only elementary reactions steps are traversed, then the closed walk represents an empty route (*ER*).

A (spanning) *reaction tree* T_R is a connected subgraph of the G_R that has all of the nodes of the original G_R but is without some of its branches so that it has no cycles. Thus, T_R is a connected graph of N nodes and $N - 1$ branches. The branches of a given tree are called its *twigs,* $s_\rho^{(t)}$. Those branches of the G_R that are excluded in a given tree are called its *links*, $s_\rho^{(l)}$. For a reaction route graph with N nodes and B branches, the number of twigs is $(N - 1)$, referred to as the tree rank, and the number of links is $L = B - N + 1$.

If a link is added back to a tree, the resulting graph contains one cycle, which is given the orientation of the link. The addition of each subsequent link forms one or more additional cycles. Cycles that contain only one link are independent and are called the *fundamental reaction routes* or cycles of the G_R. Clearly, these include at least one *FR* and the rest are *ER*s. There are $B - N + 1$ fundamental cycles in a G_R. Therefore, in a minimal reaction route graph, $G_{R,min}$, where $B = p + 1$, the number of elementary reactions

plus the number of *OR*, the number of fundamental cycles = number of independent *RR*s = $p - q$, and the number of nodes $N = q + 2$.

A *cut-set* X_R is a set of branches which when removed from the G_R leave it disconnected into two components or connected sub-graphs, provided no subset of X_R does so, and is assigned an orientation from one component to another. Further, since the removal of any twig from a tree cuts it into two parts, every twig of a tree is included in a cut-set. A cut-set that contains exactly one twig from the tree T_R, while the rest of the removed branches are links from the corresponding G_R, is called a *fundamental cut-set,* $X_{R,f}$, which is given the same orientation as the twig that defines it.

The incidence of branches at the nodes in the G_R are given by the N x B rectangular node *incidence matrix* $\mathbf{M} = [m_{j\rho}]$, with rows corresponding to the N nodes and columns to the B branches (reactions) of the G_R. The nodes in **M** must be from among the set of nodes derived from reaction stoichiometry as described in Chapter 4. However, the actual number of nodes in the G_R are only a subset of the complete set of direct nodes. The elements of the incidence matrix are defined by:

$$m_{j\rho} = \begin{cases} +1 & \text{if branch } s_\rho \text{ is incident } \textit{from} \text{ node } n_j, \\ -1 & \text{if branch } s_\rho \text{ is incident } \textit{to} \text{ node } n_j, \\ 0 & \text{if branch } s_\rho \text{ is not incident at node } n_j. \end{cases}$$

Since every branch s_ρ of the G_R is incident to one node and incident from another node, each column of **M** has exactly one +1, one –1, and the remainder zeros. Consequently, the sum of each column in the incidence matrix is zero, and *rank* **M** = N – 1. Thus, any row, corresponding to a *reference node,* may be deleted to obtain a (N – 1) x B matrix called the *reduced incidence matrix* $\mathbf{M}_f$. Since a tree T_R is a connected subgraph of N nodes and N – 1 branches, its reduced incidence matrix is a square matrix of order and rank N – 1. Thus, an (N – 1) x (N – 1) submatrix of **M** is non-singular if and only if the (N – 1) branches of this matrix correspond to tree twigs, $s_\rho^{(t)}$. As a result, the reduced incidence matrix may be rearranged into the form

$$\mathbf{M}_f = \left[\mathbf{M}_t \;\vdots\; \mathbf{M}_l\right] \tag{240}$$

where the sub-matrix $\mathbf{M}_t$ is square with (N –1) columns corresponding to the twigs $s_\rho^{(t)}$ of the chosen tree T_R and the sub-matrix $\mathbf{M}_l$ has ($B - N + 1$) columns corresponding to the links $s_\rho^{(l)}$ of the tree. Thus, $\mathbf{M}_t$ is non-singular and its inverse exists.

The *reaction route matrix* $\boldsymbol{\sigma} = [\sigma_{k\rho}]$ of a G_R, akin to cycle matrix in conventional graph theory, is a Q x B matrix defined in Equation (241), with rows corresponding to the reaction routes (*FR*s plus *ER*s) and columns to the branches of the G_R. This must be from among the set of *FR*s and *ER*s enumerated from reaction stoichiometry as described in Chapter 4. Thus, the distinct *RR*s are represented by

$$\boldsymbol{\sigma}\mathbf{s} = \mathbf{0} \;;\; \text{or} \quad \begin{bmatrix} \sigma_{OR,1} & \sigma_{11} & \sigma_{12} & \cdots & \sigma_{1p} \\ \sigma_{OR,2} & \sigma_{21} & \sigma_{22} & \cdots & \sigma_{2p} \\ \vdots & \vdots & \vdots & \vdots & \vdots \\ \sigma_{OR,Q} & \sigma_{Q1} & \sigma_{Q2} & \cdots & \sigma_{Qp} \end{bmatrix} \begin{pmatrix} s_{\mathrm{OR}} \\ s_1 \\ s_2 \\ \vdots \\ s_p \end{pmatrix} = \begin{pmatrix} 0 \\ 0 \\ \vdots \\ 0 \end{pmatrix} \tag{241}$$

The elements of the reaction route matrix are:

$$\sigma_{k\rho} = \begin{cases} +1 & \text{if the } k^{\text{th}} \text{ cycle includes } \rho^{th} \text{ branch and their orientations coincide;} \\ -1 & \text{if the } k^{\text{th}} \text{ cycle includes } \rho^{th} \text{ branch and their orientations do not coincide;} \\ 0 & \text{if the } k^{\text{th}} \text{ cycle does not include } \rho^{th} \text{ branch.} \end{cases}$$

In other words, here we are concerned only with minimal reaction routes, i.e., those with stochiometric numbers of +1, –1, or 0. Equation (241) includes the contribution of the *OR* in the cycle matrix; the in the case of an *OR*, $\sigma_{OR,\rho}$ is given a value of –1 while, in the case of an *ER*, $\sigma_{OR,\rho} = 0$.

Not all of the reaction routes, comprising the *FR*s and the *ER*s, of the G_R are independent. The total number of linearly independent *RR*s as per the Horiuti-Temkin theorem [27,28], $L = p - rank[\boldsymbol{\alpha}] = p - q = B - N + 1$. Any sub-matrix of $\boldsymbol{\sigma}$ comprising

of only L independent reaction routes (*RR*s and *ER*s) is given the symbol $\boldsymbol{\sigma}_f$, and called the *fundamental reaction route matrix*. If we further rearrange the columns in $\boldsymbol{\sigma}_f$ in the same order as in the reduced incidence matrix, i.e., twigs followed by links, and rearrange the rows so that the first row corresponds to the fundamental cycle in the first column, and so on, then $\boldsymbol{\sigma}_f$ takes the form

$$\boldsymbol{\sigma}_f = \left[\boldsymbol{\sigma}_t \quad \vdots \quad \boldsymbol{\sigma}_1\right] = \left[\boldsymbol{\sigma}_t \quad \vdots \quad \mathbf{I}_L\right] \tag{242}$$

i.e., $\boldsymbol{\sigma}_l = \mathbf{I}_L$ an identity submatrix of the order L, and $\boldsymbol{\sigma}_t$ is the remaining L x $(N-1)$ submatrix corresponding to the twigs of the tree T_R.

The cut-set matrix $\mathbf{X} = [x_{h\rho}]$ of a G_R is a $(N-1)$ x B matrix, in which rows correspond to cut-sets, and columns to the branches of the G_R, and is defined by:

$$x_{h\rho} = \begin{cases} +1 & \text{if the } h^{\text{th}} \text{cut - set includes } \rho^{\text{th}} \text{ branch and their orientations coincide;} \\ -1 & \text{if the } h^{\text{th}} \text{cut - set includes } \rho^{\text{th}} \text{ branch and their orientations do not coincide;} \\ 0 & \text{if } h^{\text{th}} \text{cut - set does not include } \rho^{\text{th}} \text{ branch.} \end{cases}$$

The rank of the cut-set matrix is equal to the number of twigs, i.e., $(N-1)$. A cut-set matrix containing only the fundamental cut-sets is called the *fundamental cut-set* matrix $\mathbf{X}_f$ with respect to T_R. Further, it may be written in the form

$$\mathbf{X}_f = \left[\mathbf{I}_{N-1} \quad \vdots \quad \mathbf{X}_l\right] \tag{243}$$

where the first $(N-1)$ columns form an identity matrix corresponding to the $(N-1)$ twigs of the tree, since such a cut-set includes only one twig each, and the final $(B-N+1)$ columns form the submatrix $\mathbf{X}_l$ correponding to the links, $s_\rho^{(l)}$.

The well-known interrelationships in conventional graph theory among the reduced incidence matrix $\mathbf{M}_f$, the fundamental reaction route matrix $\boldsymbol{\sigma}_f$, and the

fundamental cut-set matrix $\mathbf{X}_f$ for a given tree T_R [103,129] prove to be of great utility in reaction route graphs. Key relationships are provided below. Since $\mathbf{M}_f \boldsymbol{\sigma}_f^{\mathrm{T}} = \mathbf{0}$,

$$\left[\mathbf{M}_t \;\vdots\; \mathbf{M}_l\right]\begin{bmatrix}\boldsymbol{\sigma}_t^{\mathrm{T}} \\ \cdots \\ \mathbf{I}_\mu\end{bmatrix} = \mathbf{0} \quad \text{or} \quad \boldsymbol{\sigma}_t^{\mathrm{T}} = -\mathbf{M}_t^{-1}\mathbf{M}_l . \tag{244}$$

Similarly, since $\mathbf{X}_f \boldsymbol{\sigma}_f^{\mathrm{T}} = \mathbf{0}$, the sub-matrix

$$\mathbf{X}_l = -\boldsymbol{\sigma}_t^{\mathrm{T}}, \text{ or } \mathbf{X}_f = \left[\mathbf{I}_{N-1} \;\vdots\; -\boldsymbol{\sigma}_t^{\mathrm{T}}\right] \tag{245}$$

In other words, given $\mathbf{M}_f$, and starting with an arbitrary tree T_R and its subgraph in $\mathbf{M}_t$ and $\mathbf{M}_l$, the matrices $\boldsymbol{\sigma}_f$ and $\mathbf{X}_f$ can be readily found. For the converse problem, however, i.e., given $\boldsymbol{\sigma}_f$ or $\mathbf{X}_f$, in general $\mathbf{M}_f$ cannot be readily determined. One useful relation in this regard, however, is obtained as follows. Solving for $\mathbf{M}_l$ from Equation (244), using it in $\mathbf{M}_f = \left[\mathbf{M}_t \;\vdots\; \mathbf{M}_l\right]$, and comparing the result with Equation (245) provides $\mathbf{M}_f = \mathbf{M}_t\left[\mathbf{I}_{N-1} \;\vdots\; -\boldsymbol{\sigma}_t^{\mathrm{T}}\right]$, i.e.,

$$\mathbf{M}_f = \mathbf{M}_t \mathbf{X}_f \tag{246}$$

i.e., $\mathbf{M}_t$ acts as a nonsingular transformation matrix transforming the cut-set matrix into the reduced incidence matrix. In other words, the reduced incidence matrix of a graph is row-equivalent to the fundamental cut-set matrix for a given tree. Thus, the rows of $\mathbf{M}_f$ may, in principle, be obtained from a linear combination of the rows of $\mathbf{X}_f$. This is used later in the realization of reaction route graphs from enumerated reaction routes.

5.3. Electric Circuit Analogy

The above discussion is concerned with the topological features of *RR* graphs considered in a different light than heretofore in the literature for reaction graphs. When combined with conservation laws along with an analogy with electrical circuits [103,124,129], it provides a powerful new methodology for analyzing *RR* networks. These conservation laws impose constraints on branch rates and affinities by virtue of the topology of the $G_{R.}$

5.3.1. Kirchhoff's Current Law (Conservation of Mass)

Assuming the node n_j to have a zero capacity, the net rates of reactions (akin to branch current) incident at the node n_j sum to zero, i.e.,

$$\mathbf{M}_f \mathbf{r} = \mathbf{0} \tag{247}$$

where $\mathbf{r}$ is the vector of branch rates in the same order as the branches in $\mathbf{M}_f$, i.e., $\mathbf{r} = (-r_{OR}, r_1, r_2, \ldots, r_p)^T$. Notice that, by the convention adopted here, the rates of the *OR* via the *RR* network and via the voltage source have equal but opposite values (see Figure 9b). Equation (247) expresses the mass balance for the terminal species or a group of species around a control volume. This is the equivalent to Kirchhoff's Current Law (KCL) of electrical circuits. If use is made of Equation (246) in this,

$$\mathbf{X}_f \mathbf{r} = \mathbf{0} \tag{248}$$

which is an alternate form of KCL. If Equation (245) is used in this for $\mathbf{X}_f$, it provides the final form of KCL

$$\mathbf{r}^{(t)} = \boldsymbol{\sigma}_t^{\,T} \mathbf{r}^{(l)} \tag{249}$$

where $\mathbf{r}^{(t)}$ is the vector of twig rates and $\mathbf{r}^{(l)}$ is that of link rates.

In other words, the twig rates can be determined in terms of the L linearly independent rates of links for a chosen tree of G_R. Furthermore, since each link is present in only one of the fundamental cycles, the link rates are also equal to the rates of the fundamental *RR*s of a *RR* graph, akin to loop currents in an electrical circuit. Of course, the fundamental *RR*s include both full and empty *RR*s. Denoting the rates (fluxes) of these independent *RR*s by J_{I} for RR_1, J_{II} for RR_2,…, and J_L for RR_L, then $\mathbf{r}^{(l)} = \mathbf{J}$, where $\mathbf{J} = (J_{\mathrm{I}}, J_{\mathrm{II}},\ldots,J_{\mathrm{L}})^{\mathrm{T}}$ and

$$\mathbf{r}^{(t)} = \boldsymbol{\sigma}_t^{\,T}\mathbf{J} \tag{250}$$

which also provides the rate of a single *OR* as the sum of the fluxes J_k of the independent *RR*s

$$r_{OR} = -\sum_{k=1}^{L}\sigma_{OR,k}J_k \tag{251}$$

5.3.2. Kirchhoff's Voltage Law (Thermodynamic Consistency)

Being a state function, the sum of reaction affinities (akin to branch voltages) around the k^{th} full or empty *RR* is zero and follows the same linear combination as the *RR* [7], i.e.,

$$-A_{OR} + \sum_{\rho=1}^{p}\sigma_{k\rho}A_\rho = 0 \quad ; \text{ or } \quad \boldsymbol{\sigma}\mathbf{A} = \mathbf{0} \tag{252}$$

where $\mathbf{A}$ is the affinity vector, i.e., $\mathbf{A} = (\,A_{\mathrm{OR}} \quad A_1 \quad A_2 \quad \cdots \quad A_p\,)^T$ and A_{OR} represents the affinity of the *OR*. Alternately, this may be written in terms of dimensionless affinity $\mathcal{A}_\rho$. Considering the case of the fundamental cycle matrix, as a consequence of Equation (252), $\boldsymbol{\sigma}_f\mathbf{A} = \mathbf{0}$, and may be written in terms of the links and twigs as

$$\mathbf{A}^{(l)} = -\boldsymbol{\sigma}_t\mathbf{A}^{(t)} \tag{253}$$

For a *RR* graph with *N* nodes and *B* branches, Kirchhoff's Voltage Law (KVL) thus provides *L* independent equations for affinities of individual reactions (analogous to branch voltage drops). If the constitutive equations (rate laws) were available relating r_ρ to A_ρ, the individual reaction rates and affinities could, in principle, be determined. It is noteworthy, however, that KCL and KVL are entirely independent of the specific form of the constitutive equation, and are applicable to linear as well as nonlinear constitutive laws [130], and both steady state and unsteady state cases.

Furthermore, KVL provides thermodynamic consistency of the rates of reactions involved in a cycle, an important check on the consistence of given or calculated kinetics of the elementary reaction steps. Thus, when Equation (180) is used in Equation (253),

$$\prod_{ER_k}\left(\vec{r}_\rho/\overleftarrow{r}_\rho\right)^{\sigma_{k\rho}}=1 \quad ; \quad \text{and} \quad \prod_{RR_k}\left(\vec{r}_\rho/\overleftarrow{r}_\rho\right)^{\sigma_{k\rho}}=\vec{r}_{OR}/\overleftarrow{r}_{OR} \tag{254}$$

where $\vec{r}_{OR}$ and $\overleftarrow{r}_{OR}$ are the rates of the forward and reverse *OR*, respectively. Of course, the use of Equation (179) in Equation (254) results in the alternate form

$$\prod_{ER_k}\left(\vec{k}_\rho/\overleftarrow{k}_\rho\right)^{\sigma_{k\rho}}=1 \quad ; \quad \text{and} \quad \prod_{RR_k}\left(\vec{k}_\rho/\overleftarrow{k}_\rho\right)^{\sigma_{k\rho}}=K_{OR} \tag{255}$$

The relationship between Kirchhoff's Laws and the QSS condition commonly involved in reaction networks is disccused later in this chapter.

5.3.3. Tellegen's Theorem (Conservation of Energy)

The reaction power dissipated by an elementary reaction, or, alternatively, the entropy production, is $P_\rho = A_\rho r_\rho$ [97]. Notice For the overall reaction, considered as a voltage source (akin to, e.g., a battery as shown in Figure 9b), the power dissipated is given by $P_{OR} = A_{OR} r_{OR}$. From conservation of energy

$$\mathbf{A}^T \mathbf{r} = 0; \text{ or } -A_{OR} r_{OR} + \sum_{\rho=1}^{p} A_\rho r_\rho = 0 \tag{256}$$

which is equivalent to Tellegen's theorem of electrical circuits [130]. In fact, this follows as a consequence of the applicability of KCL and KVL to a network and, thus, does not provide any new information.

5.3.4. Alternate Constitutive Relation

The De Donder relation is inherently non-linear, and translation into a linear Ohmic form provides resistances that vary substantially with reaction temperature and composition. We will see if an alternate form provides coefficients that are less variable. Rysselberghe [98] indicated the use of another formula to relate the reaction affinity to the reaction rate via a "constant" coefficient (a function only of temperature and not composition). Recall that the affinity may be defined in terms of chemical potential, or Gibbs free energy. Thus, the affinity of the forward reaction may be given by

$$\vec{A}_\rho = \sum_{i=1}^{n} \left(-\vec{\nu}_{\rho i}\right) \mu_i^{\circ} = \sum_{i=1}^{n} \left(-\vec{\nu}_{\rho i}\right) \left(G_i^{\circ} + R_{gas} T \ln a_i\right) \tag{257}$$

where $\vec{\nu}_{\rho i}$ is the stoichiometric coefficient of reactant species *i* in the elementary reaction step ρ. Rearranging Equation (257) translates the equation into

$$\frac{\vec{A}_\rho}{R_{gas} T} = \frac{\vec{A}_\rho^{o}}{R_{gas} T} + \ln \prod_{i=1}^{n} a_i^{-\vec{\nu}_{\rho i}} \tag{258}$$

This may be re-written as

$$\exp\left(\frac{\vec{A}_\rho}{R_{gas} T}\right) = \exp\left(\frac{\vec{A}_\rho^{o}}{R_{gas} T}\right) \prod_{i=1}^{n} a_i^{-\vec{\nu}_{\rho i}} \tag{259}$$

In Equations (258) and (259),

$$\vec{A}_{\rho}^{o} = \sum \left(-\vec{\nu}_{\rho i} \right) G_{i}^{o} \tag{260}$$

Now, recalling the transition state theory form of the rate equation, we obtain

$$\vec{r}_{\rho} = \gamma_{M} \kappa \left(\frac{k_{B} T}{h} \right) \frac{C_{t}^{*}}{N_{A}} \exp\left(-\frac{\Delta G_{\rho}^{\ddagger o}}{R_{gas} T} \right) \prod_{i=1}^{n} a_{i}^{-\vec{\nu}_{\rho i}} \tag{261}$$

where γ_{M} is the roughness factor, κ is the transmission coefficient, and

$$\Delta G_{\rho}^{\ddagger o} = \Delta G_{\left[X_{\rho} \right]^{\ddagger}}^{o} - \sum \left(-\vec{\nu}_{\rho i} \right) G_{i}^{o} = \Delta G_{\left[X_{\rho} \right]^{\ddagger}}^{o} - \vec{A}_{\rho}^{o} \tag{262}$$

The term $\Delta G_{\left[X_{\rho} \right]^{\ddagger}}^{o}$ represents the standard Gibbs free energy of formation of the transition state complex, $\left[X_{\rho} \right]^{\ddagger}$.

Equation (261) may, thus, be written as

$$\vec{r}_{\rho} = \lambda_{\rho} \exp\left(\frac{\vec{A}_{\rho}^{o}}{R_{gas} T} \right) \prod_{i=1}^{n} a_{i}^{-\vec{\nu}_{\rho i}} \tag{263}$$

where

$$\lambda_{\rho} = \gamma_{M} \kappa \left(\frac{k_{B} T}{h} \right) \frac{C_{t}^{*}}{N_{A}} \exp\left(-\frac{\Delta G_{\left[X_{\rho} \right]^{\ddagger}}^{o}}{R_{gas} T} \right) \tag{264}$$

From Equations (259) and (263)

$$\vec{r}_\rho = \lambda_\rho \exp\left(\frac{\vec{A}_\rho}{R_{gas}T}\right) = \lambda_\rho \exp\left(\vec{\mathcal{A}}_\rho\right) \tag{265}$$

where $\vec{\mathcal{A}}_\rho$ is the dimensionless affinity of the forward reaction.

Similarly, this analysis may be performed in the reverse direction yielding the following rate expression

$$\overleftarrow{r}_\rho = \lambda_\rho \exp\left(\frac{\overleftarrow{A}_\rho}{R_{gas}T}\right) = \lambda_\rho \exp\left(\overleftarrow{\mathcal{A}}_\rho\right) \tag{266}$$

where

$$\overleftarrow{A}_\rho = \sum_{i=1}^{n}\left(\overleftarrow{\nu}_{\rho i}\right)\mu_i^{\circ} = \sum_{i=1}^{n}\left(\overleftarrow{\nu}_{\rho i}\right)\left(G_i^{\circ} + R_{gas}T\ln a_i\right) \tag{267}$$

where $\overleftarrow{\nu}_{\rho i}$ is the stoichiometric coefficient of product species *i* in the elementary reaction step ρ. Recalling that the overall rate is given by $r_\rho = \vec{r}_\rho - \overleftarrow{r}_\rho$, and applying Equations (265) and (266), a new expression is conceived. This expression is termed the Marcelin-De Donder relation [98,131]. In this representation, the rate is calculated using Equation (268)

$$r_\rho = \lambda_\rho\left\{\exp\left(\frac{\vec{A}_\rho}{R_{gas}T}\right) - \exp\left(\frac{\overleftarrow{A}_\rho}{R_{gas}T}\right)\right\} \tag{268}$$

where λ_ρ is a constant. The advantage of this form of the De Donder equation is that $\lambda_\rho = \lambda_\rho(T)$ is a function of temperature only. It is independent of composition. This dependence is included in the affinity terms. However, the disadvantage of the expression compared to the Ohm's law form is its non-linear term.

5.4. Realization of Minimal Reaction Route Graphs

We distinguish explicitly between two types of reaction mechanisms resulting from the properties of the direct *FR*s, *ER*s, *IN*s and *TN*s. Namely, a mechanism in which the stoichiometric numbers in any direct *RR*, either *FR* or *ER*, or the stoichiometric number of individual elementary reaction steps and *OR*s incident to or from any *IN* or *TN* are equal to ±1, is called a *minimal* mechanism and the resulting *RR* graph is minimal. If at least one stoichiometric number in a direct *RR*, or the stoichiometric number of individual elementary reaction steps or *OR*s incident to or from at least one *IN* or *TN* is equal to ±2, ±3, etc., the mechanism is called *non-minimal* and the resulting *RR* graph is non-minimal. In other words, a minimal *RR* graph is one in which all of the elementary reaction steps, as well as the *OR*, are involved only *once* in the graph and in every *FR*, *ER*, *IN* and *TN*. In a non-minimal *RR* graph, an elementary reaction step or the *OR* may be involved in a direct *FR*, *ER*, *IN* or *TN more* than once.

The problem of realizing a *RR* graph for a minimal mechanism is the converse of the problem discussed above, namely that of the analysis of a given *RR* graph. Once the incidence matrix of a *RR* graph is available, it is, of course, straightforward to construct a *RR* graph. Therefore, the essential problem in *RR* graph realization is the determination of the incidence matrix. This is not a trivial matter, however. Even when armed with one complete set of direct nodes enumerated from reaction stoichiometry, the prolem is of determining which of these form the subset of nodes in the incidence matrix. The following are alternate ways of obtaining the incidence matrix for a *RR* graph: 1) from the *RR* matrix $\boldsymbol{\sigma}$; 2) from the overall stoichiometric matrix $\boldsymbol{\nu}$, as described below; and, 3) from the list of enumerated nodes coupled with a graphical approach to draw the *RR* graph.

5.4.1. The Incidence Matrix from the Fundamental RR Matrix

In principle, it is possible to construct the *RR* graph directly from the *RR* matrix $\boldsymbol{\sigma}$ by trial and error, since it contains all the graph connectivity information, although this is

more directly accomplished from the incidence matrix **M**. Thus, the following algorithm may be followed:

Step 1: Derive and select a fundamental *RR* matrix $\boldsymbol{\sigma}_f$ using literature methods [7,19]. Rearrange the matrix to the form $\boldsymbol{\sigma}_f = [\ \boldsymbol{\sigma}_t \ \vdots\ \mathbf{I}_L\ ]$ by column interchange. This procedure, thus, simultaneously identifies the links (corresponding to the columns of the identity matrix), the remaining branches being twigs of the resulting tree selected by the choice of the full and empty *RR*s. Clearly, there are other possible trees and, thus, $\boldsymbol{\sigma}_f$ is not unique.

Step 2: Obtain the corresponding fundamental cut-set matrix from the relation $\mathbf{X}_f = \left[\mathbf{I}_{N-1} \ \vdots\ -\boldsymbol{\sigma}_t^{\,T}\right]$ for this tree.

Step 3: In view of the fact that $\mathbf{M}_f$ and $\mathbf{X}_f$ are row equivalent (Equation (246)), $\mathbf{M}_f$ is obtained from $\mathbf{X}_f$ via elementary row operations such that, at most, each column of the resulting matrix consists of one +1 and one –1, the rest being zeros.

Step 4: Obtain the complete incidence matrix **M** from $\mathbf{M}_f$ by adding the missing row so that the sum of elements is zero in each column.

5.4.2. The Incidence Matrix from the Overall Stoichiometric Matrix

According to the QSS condition, the rates of formation and consumption of the intermediates are equal. The QSS conditions for the intermediates when further combined with the material balances for the terminal species results in

$$\mathbf{v}^T\mathbf{r} = \mathbf{0} \ \ ;\ \text{or} \begin{bmatrix} 0 & \alpha_{11} & \alpha_{21} & \ldots & \alpha_{p1} \\ 0 & \alpha_{12} & \alpha_{22} & \ldots & \alpha_{p2} \\ \ldots & \ldots & \ldots & \ldots & \ldots \\ 0 & \alpha_{1q} & \alpha_{2q} & \ldots & \alpha_{pq} \\ v_{OR,1} & \beta_{11} & \beta_{21} & \ldots & \beta_{p1} \\ v_{OR,2} & \beta_{12} & \beta_{22} & \ldots & \beta_{p2} \\ \ldots & \ldots & \ldots & \ldots & \ldots \\ v_{OR,n} & \beta_{1n} & \beta_{2n} & \ldots & \beta_{pn} \end{bmatrix} \begin{pmatrix} r_{OR} \\ r_1 \\ r_2 \\ \vdots \\ r_p \end{pmatrix} = \begin{pmatrix} 0 \\ 0 \\ \vdots \\ 0 \end{pmatrix} \tag{269}$$

It is evident that this is analogous to KCL, namely,

$$\mathbf{Mr} = \mathbf{0} \tag{270}$$

and, hence, may be used to determine the incidence matrix **M**. For the case of monomolecular reactions, the overall stoichiometric matrix $\mathbf{v}^T$ is, in fact, the same as the reduced incidence matrix $\mathbf{M}_f$. [132] In that case, of course, the nodes do indeed represent the individual chemical species and the branches represent the reactions. For the more general case, a node n_j represents the mass balance for a group of species obtained by adding specified rows from $\mathbf{v}^T$, i.e.,

$$\sum_i \left(\sum_\rho v_{\rho i} r_\rho \right) = 0 = \sum_\rho r_\rho \sum_i v_{\rho i} = \lambda \left(\sum_\rho r_\rho m_{j\rho} \right) \qquad (\rho = 1, 2, \ldots, N) \tag{271}$$

where λ is a constant. This is, thus, equivalent to KCL. More generally, therefore, the two matrices, **M** and $\mathbf{v}^T$, are equivalent, and one may be obtained from the other by a finite number of elementary row operations. In order to first determine the incidence matrix **M** from the stoichiometric matrix $\mathbf{v}^T$, the following steps are recommended:

Step 1: Carry out elementary row operations with $\mathbf{v}^T$ involving: a) interchange of rows or columns, b) mutual addition of rows, and c) multiplication of a row by a scalar constant, until each column has at most one +1 and one –1, the rest being zero.

Step 2: Eliminate the rows containing all zeros; the resulting matrix is **M**.

5.4.3. Graphical Approach

Once the complete set of *FR*s, *ER*s, *IN* and *TN*s have been determined from reaction stoichiometry as described in Chapter 4, one starts with a $\boldsymbol{\sigma}_f$ comprising the shortest *FR* with the remaining being the shortest *ER*s. One begins by assembling the *FR* into a graph sequentially. While the order of the elementary reaction steps is arbitrary, it

makes sense to organize them such that they are mechanistically meaningful, i.e., adsorption steps, surface reactions, desorption steps. Next, the remaining *ER*s are added to the graph such that no one step occurs more than once in the *RR* graph, according the the list of *IN*s. This process is continued until all the elementary reaction steps have been added to the graph. The final step in the construction of the *RR* graph is the addition of the *OR*. This is accomplished according to the list of *TN*s. Once completed, the *RR* graph may be used to trace all of the *ER*s and *FR*s associated with the stoichiometry of the mechanism as described in Chapter 4.

5.4.4. An Example of a Minimal RR Graph

Consider the following hypothetical catalytic mechanism involving 10 elementary reaction steps on a catalyst (S = vacant catalyst site):

$$
\begin{array}{ll}
s_1: & T_1 + S \leftrightarrows I_1 \\
s_2: & T_2 + 2S \leftrightarrows 2I_2 \\
s_3: & I_1 + I_2 \leftrightarrows I_5 + S \\
s_4: & I_5 + I_2 \leftrightarrows I_6 + S \\
s_5: & I_5 + 2S \leftrightarrows I_4 + 2I_2 \\
s_6: & I_5 + S \leftrightarrows I_3 + I_2 \\
s_7: & I_6 \leftrightarrows T_3 + S \\
s_8: & I_1 + S \leftrightarrows I_4 + I_2 \\
s_9: & I_4 + I_2 \leftrightarrows I_3 + S \\
s_{10}: & I_3 + 2I_2 \leftrightarrows I_6 + 2S \\
\hline
OR: & T_1 + T_2 \leftrightarrows T_3
\end{array}
$$

It may be noted that this mechanism is non-linear, in that, the elementary reactions are not first order in the intermediates. Although this mechanism is hypothetical, it could conceivably correspond to that of olefin hydrogenation, for example with T_1 = olefin, T_2 = hydrogen, and T_3 = alkane. The intermediates then might correspond to I_1 = adsorbed olefin, I_2 = adsorbed hydrogen atom, I_6 = adsorbed alkane product, and I_3, I_4, and I_5 = adsorbed intermediates of different structure or state of hydrogenation or dehydrogenation.

5.4.4.1 The Incidence Matrix from the Fundamental RR matrix

The mechanism above comprises $p = 10$ elementary reaction steps, $q = 6$ reaction intermediates, i.e., $I_1 - I_6$ (besides the catalyst site S), and 3 terminal species, $T_1 - T_3$. Thus according to the Horiuti-Temkin theorem, the number of linearly independent *RRs* is equal to $L = p - q = 10 - 6 = 4$. An appropriate set of linearly independent *RRs*, that is, the fundamental *RR* matrix, may be generated employing the algorithm presented in Reference [7] and [19]

$$\boldsymbol{\sigma}_f = \begin{array}{c} \\ FR_1 \\ ER_1 \\ ER_2 \\ ER_3 \end{array} \begin{array}{c} \begin{array}{ccccccc:ccccc} OR & s_1 & s_2 & s_3 & s_4 & s_5 & s_6 & & s_7 & s_8 & s_9 & s_{10} \end{array} \\ \left[\begin{array}{ccccccc:ccccc} -1 & +1 & +1 & +1 & +1 & 0 & 0 & \vdots & +1 & 0 & 0 & 0 \\ 0 & 0 & 0 & -1 & 0 & -1 & 0 & \vdots & 0 & +1 & 0 & 0 \\ 0 & 0 & 0 & 0 & 0 & +1 & -1 & \vdots & 0 & 0 & +1 & 0 \\ 0 & 0 & 0 & 0 & -1 & 0 & +1 & \vdots & 0 & 0 & 0 & +1 \end{array}\right] \end{array} \tag{272}$$

which is already arranged in the form $\boldsymbol{\sigma}_f = \left[\ \boldsymbol{\sigma}_t \ \vdots\ \mathbf{I}_L\ \right]$. Therefore, the identity sub-matrix in $\boldsymbol{\sigma}_f$ identifies the links as steps s_7 through s_{10}, while the twigs are steps s_1 through s_6 in addition to the *OR*. Thus $\boldsymbol{\sigma}_t$ is the submatrix composed of the first 7 columns of $\boldsymbol{\sigma}_f$.

Next the fundamental cut-set matrix is obtained from the relation $\mathbf{X}_f = \left[\mathbf{I}_{N-1} \ \vdots\ -\boldsymbol{\sigma}_t{}^T\right]$

$$\mathbf{X}_f = \begin{array}{c} \\ X_{f,1} \\ X_{f,2} \\ X_{f,3} \\ X_{f,4} \\ X_{f,5} \\ X_{f,6} \\ X_{f,7} \end{array} \begin{array}{c} \begin{array}{ccccccc:cccc} \overbrace{OR \quad s_1 \quad s_2 \quad s_3 \quad s_4 \quad s_5 \quad s_6}^{twigs} & & & & \overbrace{s_7 \quad s_8 \quad s_9 \quad s_{10}}^{links} \end{array} \\ \left[\begin{array}{ccccccc:cccc} +1 & 0 & 0 & 0 & 0 & 0 & 0 & \vdots & +1 & 0 & 0 & 0 \\ 0 & +1 & 0 & 0 & 0 & 0 & 0 & \vdots & -1 & 0 & 0 & 0 \\ 0 & 0 & +1 & 0 & 0 & 0 & 0 & \vdots & -1 & 0 & 0 & 0 \\ 0 & 0 & 0 & +1 & 0 & 0 & 0 & \vdots & -1 & +1 & 0 & 0 \\ 0 & 0 & 0 & 0 & +1 & 0 & 0 & \vdots & -1 & 0 & 0 & +1 \\ 0 & 0 & 0 & 0 & 0 & +1 & 0 & \vdots & 0 & +1 & -1 & 0 \\ 0 & 0 & 0 & 0 & 0 & 0 & +1 & \vdots & 0 & 0 & +1 & -1 \end{array}\right] \end{array} \tag{273}$$

Performing elementary row operations on this matrix so that each column of the resulting matrix consists at most of one +1 and one –1, the balance elements being zero, and finally adding the missing row, the complete incidence matrix is obtained

$$\mathbf{M} = \begin{array}{c} \\ n_1 \\ n_2 \\ n_3 \\ n_4 \\ n_5 \\ n_6 \\ n_7 \\ n_8 \end{array} \begin{array}{c} \overbrace{\begin{array}{ccccccc} OR & s_1 & s_2 & s_3 & s_4 & s_5 & s_6 \end{array}}^{twigs} \\ \left[\begin{array}{ccccccc} +1 & +1 & 0 & 0 & 0 & 0 & 0 \\ 0 & -1 & +1 & 0 & 0 & 0 & 0 \\ 0 & 0 & -1 & +1 & 0 & 0 & 0 \\ 0 & 0 & 0 & -1 & +1 & +1 & +1 \\ 0 & 0 & 0 & 0 & -1 & 0 & 0 \\ 0 & 0 & 0 & 0 & 0 & -1 & 0 \\ 0 & 0 & 0 & 0 & 0 & 0 & -1 \\ -1 & 0 & 0 & 0 & 0 & 0 & 0 \end{array}\right. \end{array} \begin{array}{c} \\ \vdots \\ \vdots \\ \vdots \\ \vdots \\ \vdots \\ \vdots \\ \vdots \\ \vdots \end{array} \begin{array}{c} \overbrace{\begin{array}{cccc} s_7 & s_8 & s_9 & s_{10} \end{array}}^{links} \\ \left.\begin{array}{cccc} 0 & 0 & 0 & 0 \\ 0 & 0 & 0 & 0 \\ 0 & +1 & 0 & 0 \\ 0 & 0 & 0 & 0 \\ +1 & 0 & 0 & -1 \\ 0 & -1 & +1 & 0 \\ 0 & 0 & -1 & +1 \\ -1 & 0 & 0 & 0 \end{array}\right] \end{array} \tag{274}$$

The *RR* graph may now be drawn based on this incidence matrix and is shown in Figure 10a, which identifies the fundamental cycles chosen (Equation (272)). The corresponding tree is shown in Figure 10b. The *RR* graph could alternatively have been constructed by a graphical algorithm, namely by drawing FR_1 and then adding the three remaining cycles, ER_1, ER_2 and ER_3 given in Equation (272). However, this algorithm may be undesirable for large numbers of independent fundamental cycles.

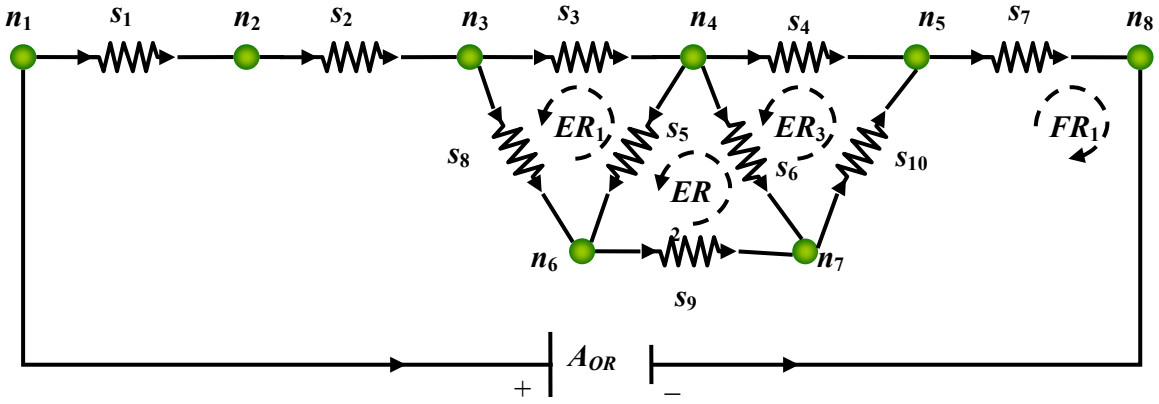

(a)

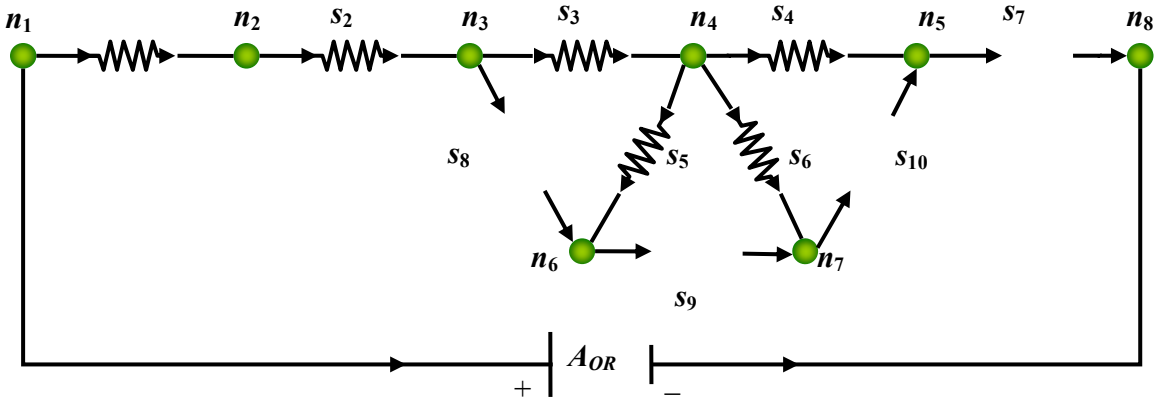

(b)

Figure 10. (a) The *RR* graph for the example with ten elementary reaction steps, one *OR*, and eight nodes. (b) A reaction tree T_R of the reaction route graph.

5.4.4.2 The Incidence Matrix from the Overall Stoichiometric Matrix

The overall stoichiometric coefficient matrix, in this case, is

$$\mathbf{v}^T = \begin{array}{c} \\ \mathrm{I}_1 \\ \mathrm{I}_2 \\ \mathrm{I}_3 \\ \mathrm{I}_4 \\ \mathrm{I}_5 \\ \mathrm{I}_6 \\ \cdots \\ \mathrm{T}_1 \\ \mathrm{T}_2 \\ \mathrm{T}_3 \end{array} \begin{array}{c} \begin{array}{ccccccccccc} OR & s_1 & s_2 & s_3 & s_4 & s_5 & s_6 & s_7 & s_8 & s_9 & s_{10} \end{array} \\ \left[\begin{array}{ccccccccccc} 0 & +1 & 0 & -1 & 0 & 0 & 0 & 0 & -1 & 0 & 0 \\ 0 & 0 & +2 & -1 & -1 & +2 & +1 & 0 & +1 & -1 & -2 \\ 0 & 0 & 0 & 0 & 0 & 0 & +1 & 0 & 0 & +1 & -1 \\ 0 & 0 & 0 & 0 & 0 & +1 & 0 & 0 & +1 & -1 & 0 \\ 0 & 0 & 0 & +1 & -1 & -1 & -1 & 0 & 0 & 0 & 0 \\ 0 & 0 & 0 & 0 & +1 & 0 & 0 & -1 & 0 & 0 & +1 \\ \cdots & \cdots & \cdots & \cdots & \cdots & \cdots & \cdots & \cdots & \cdots & \cdots & \cdots & \cdots \\ -1 & -1 & 0 & 0 & 0 & 0 & 0 & 0 & 0 & 0 & 0 \\ -1 & 0 & -1 & 0 & 0 & 0 & 0 & 0 & 0 & 0 & 0 \\ +1 & 0 & 0 & 0 & 0 & 0 & 0 & +1 & 0 & 0 & 0 \end{array}\right] \end{array} \tag{275}$$

The determination of the incidence matrix from this is accomplished via a series of elementary row operations. The resulting incidence matrix is the same as above and, therefore, the corresponding *RR* graph is the same as shown in Figure 10a.

5.4.4.3 The Incidence Matrix and *RR* Graph from the Graphical Approach

We may begin with $\boldsymbol{\sigma}_f$ provided in Equation (272). The *FR* given is drawn without the *OR* as shown in Figure 11a. It should be noted that the steps are organized such that the adsorption steps, s_1 and s_2 are first in the series and the desorption step, s_7, is given last while the remaining surface reactions fall in the middle. Then the remaining three *ER*s are added one at a time satisfying the QSS balances represented by the remaining rows in Equation (272) such that no step occurs more than once (Figure 11b). The graph is completed as the *OR* is added to the structure (Figure 11c). Upon translation to a network, it is seen that Figure 10a is readily obtained. From the nodes of this graph, of course, the incidence matrix is also readily obtained. The nodes are validated by confirming that they are among those enumerated stoichiometrically as described in Chapter 4.

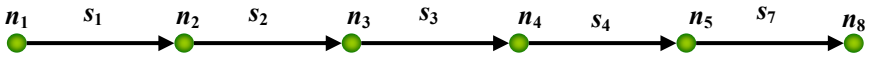

(a)

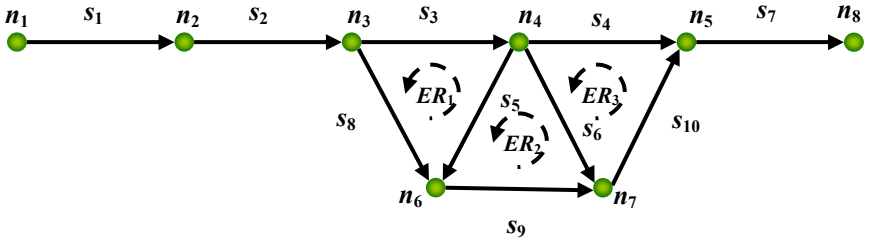

(b)

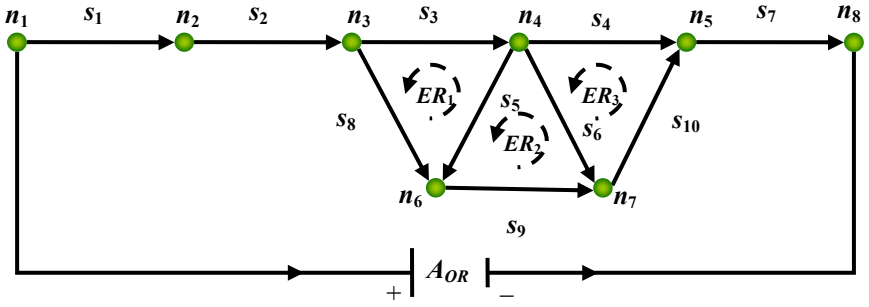

(c)

Figure 11. Construction of the *RR* graph using the graphical approach as described in the text.

5.4.4.4 The Complete *RR* Matrix from the *RR* Graph

Once a *RR* graph is available, e.g., as illustrated above for the example, the conventional graph theory can be used to enumerate a complete set of direct *RRs*, that is, the *RR* matrix, $\boldsymbol{\sigma}$. For our example $\boldsymbol{\sigma}$ can be easily generated by a simple inspection of the *RR* graph. The result is

$$\boldsymbol{\sigma} = \begin{array}{c} \\ RR_1 \\ RR_2 \\ RR_3 \\ RR_4 \\ RR_5 \\ RR_6 \\ RR_7 \\ \cdots \\ ER_1 \\ ER_2 \\ ER_3 \\ ER_4 \\ ER_5 \\ ER_6 \end{array} \begin{array}{c} \begin{array}{cccccccccccc} OR & s_1 & s_2 & s_3 & s_4 & s_5 & s_6 & s_7 & s_8 & s_9 & s_{10} \end{array} \\ \left[\begin{array}{cccccccccccc} -1 & +1 & +1 & +1 & +1 & 0 & 0 & +1 & 0 & 0 & 0 \\ -1 & +1 & +1 & 0 & +1 & -1 & 0 & +1 & +1 & 0 & 0 \\ -1 & +1 & +1 & +1 & 0 & 0 & +1 & +1 & 0 & 0 & +1 \\ -1 & +1 & +1 & 0 & 0 & 0 & 0 & +1 & +1 & +1 & +1 \\ -1 & +1 & +1 & +1 & 0 & +1 & 0 & +1 & 0 & +1 & +1 \\ -1 & +1 & +1 & 0 & 0 & -1 & +1 & +1 & +1 & 0 & +1 \\ -1 & +1 & +1 & 0 & +1 & 0 & -1 & +1 & +1 & +1 & 0 \\ \cdots & \cdots & \cdots & \cdots & \cdots & \cdots & \cdots & \cdots & \cdots & \cdots & \cdots & \cdots \\ 0 & 0 & 0 & -1 & 0 & -1 & 0 & 0 & +1 & 0 & 0 \\ 0 & 0 & 0 & 0 & 0 & +1 & -1 & 0 & 0 & +1 & 0 \\ 0 & 0 & 0 & 0 & -1 & 0 & +1 & 0 & 0 & 0 & +1 \\ 0 & 0 & 0 & -1 & 0 & 0 & -1 & 0 & +1 & +1 & 0 \\ 0 & 0 & 0 & 0 & -1 & +1 & 0 & 0 & 0 & +1 & +1 \\ 0 & 0 & 0 & -1 & -1 & 0 & 0 & 0 & +1 & +1 & +1 \end{array}\right] \end{array} \tag{276}$$

This *RR* matrix is equivalent to that generated by using the conventional enumeration procedures [7,19].

5.5. Realization of Non-Minimal Reaction Route Graphs

So far, we have considered only minimal *RR* graphs [25,26], i.e., *RR* graphs in which every elementary reaction step is presented only once in each enumerated *RR*, i.e., only unit stoichiometric numbers are involved. However, the vast majority of kinetic mechanisms involve non-unit stoichiometric numbers in many *RR*s, both *FR*s and *ER*s.

These mechanisms are represented by non-minimal *RR* graphs, i.e., *RR* graphs in which an elementary reaction step may be present in the graph more than once, e.g., in different locations of the graph, corresponding to the non-unit stoichiometric numbers. The purpose of the present section is to extend the concept of *RR* graphs, described in Section 5.4, to the more general case of the non-minimal *RR* graphs. The discussion here, however, is limited to the case of a single overall reaction (*OR*).

The occurrence of a given reaction step at more than one location in the *RR* graph has a profound effect on its topology by virtue of the fact that, regardless of location, the elementary step affinity A_ρ as well as the reaction rate r_ρ must remain unchanged. This requirement, as we shall see, imparts symmetry to the *RR* graph, including the occurrence of *each* branch twice, for example.

To better understand the topological properties of the *RR* graphs, it is useful to extend the concept of directness, as previously discussed in conjunction with the enumeration of *FR*s and *ER*s in Chapter 4, to *RR* graphs. Namely, we define a *direct RR* graph (not to be confused with *directed* graphs) as a *RR* graph in which all of the resulting *FR*s are direct. A *non-direct RR* graph is one that involves a complete set of direct *FR*s and, *additionally*, at least one non-direct *FR*. Based on these definitions, a key difference between a minimal and non-minimal *RR* graph may be formulated as: a minimal *RR* graph is always a direct *RR* graph while a non-minimal *RR* graph may be either direct or non-direct.

5.5.1. Construction of Non-Minimal RR Graphs

The methods described above to construct minimal *RR* graphs [25] cannot be utilized directly for constructing non-minimal *RR* graphs. In particular, the application of an incidence matrix is problematic since, in a non-minimal *RR* graph, a given elementary reaction step that is involved more than once may be in different locations of the graph. A qualitative algorithm for the construction of a non-minimal *RR* graph is formulated here. Other algorithms are, of course, possible.

The starting point is the complete set of direct *FR*s, *ER*s, *IN*s and *TN*s that can be enumerated via the methodology described in Chapter 4. In the particular case of reaction mechanisms in which the stoichiometric number of elementary reaction steps

and *OR*s in every *FR, ER, IN and TN* does not exceed ±2, we have noticed that, as a consequence of the invariance of r_ρ and $\mathscr{A}_\rho$, the *RR* graph is symmetrical and involves each elementary reaction step and *OR* exactly twice. Therefore, for this particular case the construction algorithm may be simplified in analogy with the algorithm described previously in connection with minimal *RR* graphs [25]. Namely, start with a $\boldsymbol{\sigma}_f$ matrix incorporating a set of $p - q$ linearly independent *RR*s comprising one of the shortest minimal *FR*s, the remaining $p - q - 1$ being the smallest *ER*s. Draw the *FR* along with another variation in which the order, but not the direction, of the elementary reaction steps is reversed. From a kinetic viewpoint, of course, the order of sequential steps is immaterial, although it is usually significant mechanistically. Next, begin placing the *ER*s, simultaneously, in both sub-graphs, starting with the shortest, such that none of the reaction steps are involved more than once in each of the sub-graphs. The two sub-graphs are next connected by fusing selected nodes only when the *ER*s cannot be contained entirely within each of the sub-graphs. Two nodes are said to be fused when they are replaced by a single node containing all branches incident on the original nodes [103]. Of course, it must be confirmed that the fused notes are also among the enumerated direct *IN*s. If all of the shortest *ER*s have been placed it remains only to balance the remaining nodes by attaching the *OR* according to an appropriate *TN* from the complete list of *TN*s. Finally, the resulting *RR* graph should be verified to ensure that all enumerated direct *FR* and *ER*s are depicted as paths. This also provides the number of branches B and the number of nodes N in a non-minimal graph. Thus, $B = 2(p + 1)$ and $N = 2(q + 2)$ – the number of fused nodes.

5.5.2. An Example of Non-Minimal *RR* Graphs

The hydrogen oxidation reaction (HOR) and hydrogen evolution reaction (HER) are by far the most thoroughly investigated electrochemical reaction systems [104,133] and have assumed a new importance by virtue of renewed interest in fuel cells. The mechanisms of these processes are fairly well established and, as widely accepted, are described by three elementary reactions referred to as the Volmer (s_V), Heyrovsky (s_H) and Tafel (s_T) steps. Consider the mechanism of the HER in alkaline solutions:

s_T: $2HM \leftrightarrows 2M + H_2$

s_V: $M + H_2O + e^- \leftrightarrows HM + OH^-$

s_H: $HM + H_2O + e^- \leftrightarrows M + H_2 + OH^-$

Hence, for the HER in alkaline solutions the *OR* is

OR : $2H_2O + 2e^- \leftrightarrows H_2 + 2OH^-$

As shown by Milner [29] and Happel and Sellers [30], the HER involves one cycle, or *ER*, and three *FR*s These are

$$ER: \ s_V - s_H + s_T = 0 \tag{277}$$

$$FR_{VH}: \ s_V + s_H = OR \tag{278}$$

$$FR_{VT}: \ 2s_V + s_T = OR \tag{279}$$

$$FR_{HT}: \ 2s_H - s_T = OR \tag{280}$$

By definition [25,134], a *RR* graph involves two types of nodes. One of these, referred to as terminal nodes (*TN*s), satisfies the steady-state condition for the *OR*. In other words, at *TN*s, the algebraic sum of the rates of the elementary steps leaving or entering the node should equal the rate of the *OR*. Thus, the possible connectivity of the reactions at the *TN*s is

$$TN_1: \ OR - s_H - s_T \tag{281}$$

$$TN_2: \ OR - s_V + s_T \tag{282}$$

$$TN_3: \ 2OR - s_V - s_H \tag{283}$$

The other type of nodes, referred to as intermediate nodes (*IN*s), must satisfy the steady-state conditions for the intermediates. That is, the algebraic sum of the rates of the elementary steps leaving or entering an *IN* should be equal to zero. Since for the case of the HER, there is only one linearly independent intermediate (HM), we have only one independent *IN*, and the connectivity of the reactions at this *IN* is

$$IN\text{: } -s_V + s_H + 2s_T \tag{284}$$

Based on Equations (277) – (284), the *RR* graph may be obtained following the algorithm for *RR* graph construction described previously [25,134]. Namely, in the particular case of reaction mechanisms in which the number of elementary reactions and *OR*s in every *FR*, *ER*, *IN* and *TN* does not exceed ± 2, we noticed that the *RR* graphs are symmetrical and involves each elementary reaction and *OR* twice [134]. As a result, the realization of the *RR* graphs may be performed based on the following considerations. The starting point is a $\boldsymbol{\sigma}_f$ matrix incorporating a set of linearly independent *RR*s comprising a single minimal smallest *FR*, the balance being the smallest *ER*s. The *FR* is drawn next along with another variation in which the order of the reactions is reversed. Further, the *ER*s are placed starting with the smallest ones such that none of the reactions is involved more than once in each of the sub-graphs. The sub-graphs are next fused only via the reactions that are not present in the sub-graphs. If all of the smallest *ER*s have been placed and all nodes, except two, are balanced, the graph is complete. It remains only to balance the remaining two nodes by attaching the *OR* according to an appropriate *TN* from the complete list of *TN*s. Finally, the resulting *RR* graph should be checked to ensure that all enumerated direct *FR* and *ER*s are depicted as walks.

The number of linearly independent *RR*s for the HER is equal to two. Thus, according to the algorithm, these are selected as FR_{VH}, and the *ER*. The *RR* graph construction is graphically depicted in Figure 12. We begin by depicting twice the FR_{VH}, the second with the steps in reverse order. Next, we add symmetrically *ER* to each of the graphs. At this stage it is seen that, because in each individual sub-graph the *ER* cannot be introduced into the graph due to the direction of the existing branches, it is necessary to connect the graphs by fusing two nodes. Finally, we identify the balanced *IN*s and potential *TN*s. The *TN*s are then balanced via the addition of the *OR* yielding the *RR* graph. It may be seen that the resulting graph is a *RR* graph in that it satisfies all of the conditions imposed on the *RR* graph. That is, the graph involves the *ER*, Equation (277), all three of the *FR*s, Equations (278) - (280), the *IN*s satisfy Equation (284), while the

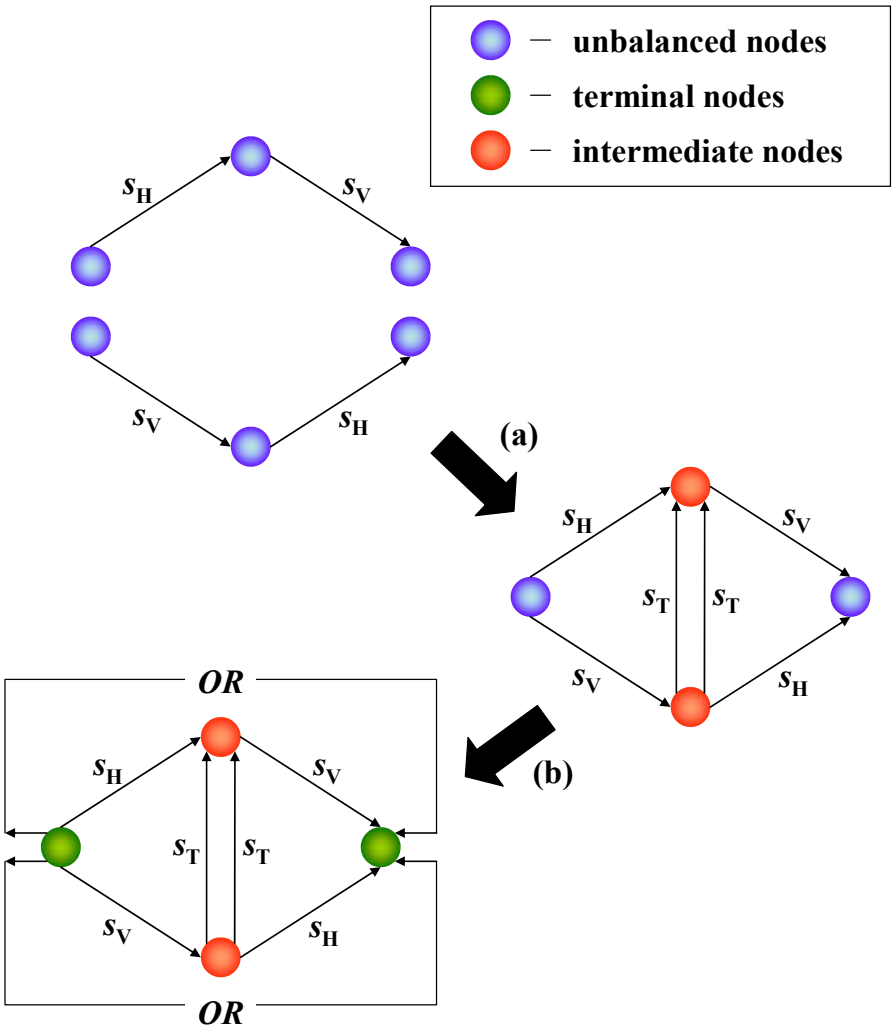

Figure 12. The realization of the *RR* graph for the hydrogen evolution reaction.

*TN*s satisfy Equation (283). Notice that every *FR* in the graph is involved twice. This is a consequence of the fact that the mechanism is non-minimal [134], i.e., the elementary steps are involved more than once in a *FR*. Nonetheless, the affinity and the rate of a step (e.g., s_H or s_V) remain unchanged regardless of their placement, as, of course, is required in any non-minimal graph. This imparts certain symmetry to the *RR* graph, i.e., the branches may be replaced by resistors for steady-state kinetic analysis or by a combination of resistors and capacitors for the general case, depending upon the objective.

5.6. Reaction Route Network Analysis and Reduction

The construction of a *RR* graph, even without a subsequent kinetic analysis, provides a powerful visualization tool and a deeper understanding of the reaction mechanism as compared to the traditional and computationally expensive analyses. A further use of the electrical circuit analogy and Kirchhoff's Laws provides a powerful new tool for a quantitative analysis and reduction of the *RR* network. Thus, the *RR* graph is converted into an equivalent electrical network by converting the branches of the *RR* graph into resistances, for the steady-state case. For example, the electrical network for the HOR/HER is shown in Figure 13.

Obviously, not all of the possible *RR*s are equally important. There are, in fact many alternate methods available for the reduction of kinetic systems [135]. We propose a different approach here based on the concept of reaction resistance in analogy to Ohm's law, followed by utilization of the techniques of electrical network analysis, to analyze and reduce *RR* networks. This turns out to be a particularly powerful method, allowing us to not only discriminate among the various *RR*s, but to also determine the slow, or rate-limiting, as well as the quasi-equilibrium steps and, ultimately, when possible the derivation of a simple and accurate algebraic rate equation suitable for reactor analysis and design.

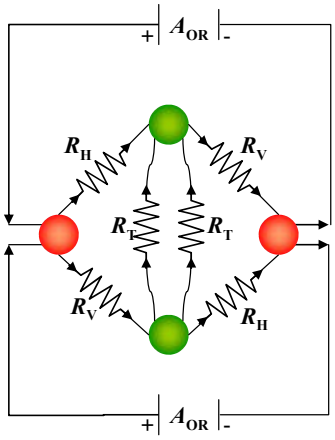

Figure 13. The electrical analog of the *RR* graph for the hydrogen evolution reaction.

Due to its non-linearity, the basic constitutive equation, i.e., the DeDonder relation in Equation (180), makes it difficult to utilize the techniques of linear circuit analysis based on Ohm's law. We, thus, define a *reaction resistance* as the mean value of reciprocal rate (conductance) between the limiting values characterizing the reaction, i.e., reverse and forward rate, $\overleftarrow{r}_\rho$ and $\vec{r}_\rho$, i.e.,

$$R_\rho = \left\langle \frac{1}{r_\rho} \right\rangle = \frac{1}{\vec{r}_\rho - \overleftarrow{r}_\rho} \int_{\overleftarrow{r}_\rho}^{\vec{r}_\rho} \frac{1}{r_\rho} dr_\rho = \frac{\ln \frac{\vec{r}_\rho}{\overleftarrow{r}_\rho}}{\vec{r}_\rho - \overleftarrow{r}_\rho} \tag{285}$$

where $\left\langle r_\rho \right\rangle$ is a logarithmic mean conductance and reduces to the exchange rate in the vicinity of equilibrium [25]

$$R_\rho^0 = \lim_{\substack{A_\rho \to 0 \\ r_\rho \to 0}} R_\rho = \lim_{\vec{r}_\rho \to \overleftarrow{r}_\rho \to r_\rho^0} \frac{d \ln \frac{\vec{r}_\rho}{\overleftarrow{r}_\rho}}{d\left(\vec{r}_\rho - \overleftarrow{r}_\rho\right)} = \lim_{\vec{r}_\rho \to \overleftarrow{r}_\rho \to r_\rho^0} \frac{\frac{d\vec{r}_\rho}{\vec{r}_\rho} - \frac{d\overleftarrow{r}_\rho}{\overleftarrow{r}_\rho}}{d\vec{r}_\rho - d\overleftarrow{r}_\rho} = \frac{1}{r_\rho^0} \tag{286}$$

With this definition, the De Donder relation (Equation (180)) takes a form analogous to Ohm's Law

$$r_\rho = \frac{\mathcal{A}_\rho}{R_\rho} \tag{287}$$

This definition of the linear reaction resistance based on a linear constitutive relation in analogy with Ohm's law makes available a host of techniques used in the analysis of electrical circuits [129]. However, it comes with the caveat that the reaction resistance so defined is not a constant, but depends upon the reaction conditions including the composition of the reaction mixture and especially the temperature, although less so than the coefficient $\vec{r}_\rho$ in the conventional form of the De Donder equation (Equation (180)). Thus, conclusions arrived at, e.g., regarding the slow steps, under one set of

conditions may not be strictly applicable under a different set of conditions. Conceptually, of course, each elementary reaction step in a mechanism represents a different degree of "resistance" to the reaction progress. In fact, it is frequently assumed that all resistance resides in a single step, namely the rate-limiting step (RLS) [126], or sometimes in two rate-limiting steps [135,136].

It turns out that the large difference in the kinetics of elementary reactions, frequently many orders of magnitude, involved in a mechanism make *RR* networks eminently suitable for reduction. As mentioned above, it is quite likely that not all *RR*s are equally significant. This means that branches corresponding to the insignificant *RR*s may be dropped from the *RR* graph to simplify the overall kinetics and mechanism. Further, these considerations allow rationalization of the common assumptions in kinetics, for instance the RLS and quasi-equilibrium assumptions.

The assumption in the following analysis is that the numerical results of a kinetic analysis under conditions of interest are available including concentrations (or surface coverages) of all intermediates, so that the reaction affinities (Equation (184)) and rates of all elementary reactions (Equation (179)) can be computed. The conclusions on reduction should eventually be checked under a different set of conditions to ensure that they are universally and not just locally applicable.

The overall procedure of simplification involves consideration of subgraphs or cycles of the complete *RR* graph. It is useful to begin with a fundamental *RR* matrix $\boldsymbol{\sigma}_f$ containing the *RR* with the smallest number of steps, the rest being the smallest *ER*s. One may start with a comparison of the resistances of the branches in each of the empty routes or cycles. Each fundamental *ER* may be divided into two parallel walks or paths between two given nodes, each path with the same affinity drop by virtue of KVL. Thus, the relative fluxes in the two pathways are equal to the ratio of the total resistances of the two paths,

$$\frac{J_I}{J_{II}} = \frac{R_{II}}{R_I} \tag{288}$$

where the total resistance R_I or R_{II} of sequential branches between two nodes n_i and n_j is

$$R_{k,n_i \to n_j} = \sum_{n_i \to n_j} \sigma_{k\rho}^2 R_\rho \tag{289}$$

and, of course, the reaction flux through the sequential branches

$$J_k = \frac{A_{n_i \to n_j}}{R_{k,n_i \to n_j}} = \frac{\sum_{n_i \to n_j} \sigma_{k\rho} A_\rho}{R_{k,n_i \to n_j}} \tag{290}$$

For parallel paths between two nodes n_i and n_j, the total resistance is

$$\frac{1}{R_{Tot,n_i \to n_j}} = \frac{1}{R_{I,n_i \to n_j}} + \frac{1}{R_{II,n_i \to n_j}} + \cdots \tag{291}$$

If the resistance along one of the paths is much larger than that in the other, it would be safe to assume that the less resistant path contributes little to the *OR* rate and, hence, that path may be eliminated from the *RR* network. This, of course, concomitantly, simplifies the mechanism by pointing out the reaction steps that are kinetically inconsequential. As a corollary, if both pathways are significant, it implies that each of the parallel branches has a resistance, or slow steps, of comparable order. The procedure involves analyzing the resistances in all *ERs*, and may result in a very significant simplification of the *RR* network. Recall that each link that is eliminated reduces by one the number of independent *RR*s.

The next step is to determine the relative resistances of the steps in a given sequence. Since, at QSS, the rates of all reactions in a sequence is the same, this may be accomplished by a comparison of the affinity drop over each of the branches in a sequence

$$\frac{A_1}{A_2} = \frac{R_1}{R_2} \tag{292}$$

The order of series steps in a branch is unimportant from the point of view of this analysis, although it is usually significant mechanistically. The slowest steps are those with significant affinity drops, while those with affinity drops approaching zero may be considered to be at quasi-equilibrium. This might allow development of explicit rate expressions for the *OR*. However, numerically, the rate of the *OR* may be alternately calculated from $r_{OR} = A_{OR} \big/ R_{OR}$.

Clearly, the above simplification and reduction algorithm should provide a quantitative value for the tolerance that is appropriate for keeping or discarding various reaction steps. The problem may be simply formulated in terms of the overall resistance of the *RR* network. Thus, a reaction step may be neglected if the change in the overall resistance of the *RR* network does not exceed a chosen tolerance.

In summary, in this chapter, a *RR* graph is defined wherein each branch represents an elementary reaction step and nodes represent the interconnectivity of the elementary reaction steps such that all *FR*s and *ER*s enumerated in Chapter 4 can be directly traced from the *RR* graph as walks. Further, we have discussed how minimal and non-minimal *RR* graphs may be realized. Finally, the *RR* graph is directly converted into an equivalent electrical circuit, allowing the techniques of electrical network analysis to be utilized for analysis and simplification.

Chapter 6. *RR* Graph of the Water-Gas-Shift Reaction

Due to its industrial significance and relatively simple chemistry, the catalysis and kinetics of the WGSR has been a key example in developing the approach of microkinetic modeling [4,8-16]. In the meantime, we have shown [7,26,55,60] that reliable microkinetic models for the WGSR on Cu(111) may be developed based on rather rudimentary models for the kinetic of elementary reaction steps. Thus, we have shown that it is adequate to determine the energetic characteristics of the elementary reactions based on the UBI-QEP method developed by Shustorovich [17], while the pre-exponential factors may be estimated simply from the statistical mechanical relations in the transition-state theory [16,18] as a starting point. Here we consider an 18-step version of a microkinetic WGSR model developed by us earlier [55], having included 3 additional elementary reaction steps frequently considered in the literature. While our previous work follows the more conventional microkinetic approach, here we follow the *RR* graph approach developed recently by us [25,26,134]. Specifically, a *RR* graph for the 18-step reaction network is drawn from stoichiometric considerations and is used for kinetic analysis and reduction.

6.1. A Mechanism of the WGSR

The selection of elementary reactions from the literature summarized in Table 3 (Chapter 2) is described in Section 2.4.5 and is dictated further by the limitations of the subsequent application of the UBI-QEP method [17] to calculate the energetics of these elementary reactions. In other words, the elementary reactions chosen are further restricted to those three types for which the UBI-QEP method provides the necessary formulae (see Section 3.5). The set of elementary reactions, according to the considerations in Section 2.4.5 along with these constraints, for the WGS reaction is presented in Table 16 with their respective energetics on a Cu(111) catalyst.

Table 16. An 18-Step Microkinetic Model for WGSR on Cu(111)

	$\vec{E}_j$	$\vec{A}_j$	Elementary Reactions	$\overleftarrow{E}_j$	$\overleftarrow{A}_j$
s_1:	0	$1.5\ 10^6$	$CO + S \leftrightarrows CO{\cdot}S$	12.0	10^{14}
s_2:	0	10^6	$H_2O + S \leftrightarrows H_2O{\cdot}S$	13.6	10^{14}
s_3:	25.4	10^{13}	$H_2O{\cdot}S + S \leftrightarrows OH{\cdot}S + H{\cdot}S$	1.6	10^{13}
s_4:	10.7	10^{13}	$CO{\cdot}S + O{\cdot}S \leftrightarrows CO_2{\cdot}S + S$	28.0	10^{13}
s_5:	0	10^{13}	$CO{\cdot}S + OH{\cdot}S \leftrightarrows HCOO{\cdot}S + S$	20.4	10^{13}
s_6:	15.5	10^{13}	$OH{\cdot}S + S \leftrightarrows O{\cdot}S + H{\cdot}S$	20.7	10^{13}
s_7:	0	10^{13}	$CO{\cdot}S + OH{\cdot}S \leftrightarrows CO_2{\cdot}S + H{\cdot}S$	22.5	10^{13}
s_8:	1.4	10^{13}	$HCOO{\cdot}S + S \leftrightarrows CO_2{\cdot}S + H{\cdot}S$	3.5	10^{13}
s_9:	4.0	10^{13}	$HCOO{\cdot}S + O{\cdot}S \leftrightarrows CO_2{\cdot}S + OH{\cdot}S$	0.9	10^{13}
s_{10}:	29.0	10^{13}	$H_2O{\cdot}S + O{\cdot}S \leftrightarrows 2OH{\cdot}S$	0	10^{13}
s_{11}:	26.3	10^{13}	$H_2O{\cdot}S + H{\cdot}S \leftrightarrows OH{\cdot}S + H_2{\cdot}S$	0	10^{13}
s_{12}:	1.3	10^{13}	$OH{\cdot}S + H{\cdot}S \leftrightarrows O{\cdot}S + H_2{\cdot}S$	4.0	10^{13}
s_{13}:	0.9	10^{13}	$HCOO{\cdot}S + OH{\cdot}S \leftrightarrows CO_2{\cdot}S + H_2O{\cdot}S$	26.8	10^{13}
s_{14}:	14.6	10^{13}	$HCOO{\cdot}S + H{\cdot}S \leftrightarrows CO_2{\cdot}S + H_2{\cdot}S$	14.2	10^{13}
s_{15}:	5.3	$4\ 10^{12}$	$CO_2{\cdot}S \leftrightarrows CO_2 + S$	0	10^6
s_{16}:	15.3	10^{13}	$H{\cdot}S + H{\cdot}S \leftrightarrows H_2{\cdot}S + S$	12.8	10^{13}
s_{17}:	5.5	$6\ 10^{12}$	$H_2{\cdot}S \leftrightarrows H_2 + S$	0	10^6
s_{18}:	15.3	$6\ 10^{12}$	$H{\cdot}S + H{\cdot}S \leftrightarrows H_2 + 2S$	7.3	10^6

a - activation energies in kcal/mol ($\theta \to 0$ limit) estimated according to [17] and coinciding with the estimations made in [14]; pre-exponential factors from [17,18]. *b* – pre-exponential factors adjusted so as to fit the thermodynamics of the overall reaction; The units of the pre-exponential factors are $atm^{-1}s^{-1}$ for adsorption/desorption reactions and s^{-1} for surface reactions.

Following Dumesic [18], and as discussed in Section 3.5.3, we assume an immobile transition state without rotation for all of the species, which results in a pre-exponential factor of 10^1 $Pa^{-1}s^{-1}$ for adsorption/desorption reactions, and 10^{13} s^{-1} for surface reactions. Some of the pre-exponential factors, i.e., s_1, s_2, s_{15}, s_{17} and s_{18}, were adjusted to ensure consistency with the thermodynamics of the overall reaction as given in Figure 3.

Assuming a constant value for ΔS° and ΔH° for the *OR*, the equilibrium constant is

$$K = \exp\left(\frac{\Delta S^\circ}{R_{gas}}\right)\exp\left(-\frac{\Delta H^\circ}{R_{gas}T}\right) \tag{293}$$

From the thermodynamics of the terminal species [74], we find that $\Delta S^\circ = -10.04$ cal/mol·K and $\Delta H^\circ = -9.83$ kcal/mol. On the other hand, the UBI–QEP method predictions of $\vec{E}_\rho$ and $\overleftarrow{E}_\rho$ and the transition-state theory estimations for $\vec{\Lambda}_\rho$ and $\overleftarrow{\Lambda}_\rho$ provide the following estimates of entropy and enthalpy for the *OR* via the *FR*: $s_1 + s_2 + s_3 + s_4 + s_{12} + s_{15} + s_{17}$ using the data provided in Table 16.

$$\Delta S^\circ = R_{gas}\sum_\rho \ln\left(\frac{\vec{\Lambda}_\rho}{\overleftarrow{\Lambda}_\rho}\right) = -11.18 \text{ cal/mol}\cdot\text{K} \tag{294}$$

and

$$\Delta H^\circ = \sum_\rho\left(\vec{E}_\rho - \overleftarrow{E}_\rho\right) = -11 \text{ kcal/mol} \tag{295}$$

This deviation is believed to be related to the accuracy of the UBI–QEP input parameters in combination with the estimations of the pre-exponential factors.

The activation energies of the elementary reaction steps including the OH·S species (Table 16) were calculated neglecting the "OH effect". According to Patrito, et al. [137], when the surface coverage of oxygen is high, the equations governing the prediction of the heat of adsorption indicate a lower value as compared to zero-coverage. This is the consequence of a true electronic effect of the surface coverage rather than adsorbate-adsorbate interactions. At low oxygen coverages, hydrogen bonding allows for attractive interactions between adsorbed hydroxyls leading to a higher heat of adsorption for OH. The difference is typically 20-30 kcal/mol. Literature data has been collected and tabulated to illustrate this difference in Table 13; however, only the lower Q_{OH} values have been used here and, as will be shown, provide sufficient energetics to successfully predict the kinetics of the WGS reaction.

The level of accuracy of the UBI-QEP method (±1-3 kcal/mol) in estimating the energetics (activation energies and reaction enthalpies) of the elementary reactions on transition metals is well-documented [17]. In particular, for Cu(111) a comprehensive comparison between the predicted UBI-QEP and experimental energetics of the surface intermediates involved in the WGSR was presented by Shustorovich and Bell [9]. In addition, we mention here a few recent papers in which the energetics of the surface intermediates of interest to WGSR were discussed. For example, an adsorption energy equal to 101.9 kcal/mol for atomic oxygen on Cu(111) has been obtained from density functional calculations [138]. This value is in good agreement with the value predicted by the UBI-QEP method, i.e., 103.0 kcal/mol [138]. The same authors estimated the activation energy barrier for the water dissociation on Cu(111) to be 27.2 kcal. This value is consistent with the UBI-QEP predicted value of 25.4 kcal/mol. In another density functional study [3], the enthalpy change of the products desorption in methanol decomposition on Cu(111)

$$CO{\cdot}S + 4H{\cdot}S \leftrightarrows CO + 2H_2 + 5S$$

was estimated to be 26.3 kcal/mol. Although this is not an elementary reaction, this value should be compared with 28.0 kcal/mol predicted by UBI-QEP method, i.e., the enthalpy change of the reaction obtained by linearly combing elementary reactions s_1, s_{16} and s_{17}

according to $-s_1 + 2s_{16} + 2s_{17}$. In a recent experimental study of temperature-programmed adsorption/ desorption of hydrogen on alumina-supported copper catalysts [139]

$$2H{\cdot}S \leftrightarrows H_2 + 2S$$

it was shown that the ratio of the pre-exponential factors $\Lambda_{des}/\Lambda_{ads}$ varies from 4×10^6 to 5×10^8 Pa depending on the type of the support. From Table 16, it may be deduced that this ratio is equal to $\vec{\Lambda}_{16}\vec{\Lambda}_{17} / \overleftarrow{\Lambda}_{16}\overleftarrow{\Lambda}_{17} = 6\times10^6$. Similarly, the experimental enthalpy change of the hydrogen associative desorption was shown to vary from 3.8 to 7.2 kcal/mol [139]. For the same reaction, from Table 16 a value of 8.0 kcal/mol is obtained.

6.2. Enumeration of Topological Characteristics from Stoichiometry

The topological characteristics of a *RR* graph define is structure and connectivity. Based on the stoichiometry of the mechanism, they include the *FR*s, *ER*s, *IN*s and *TN*s. For the WGS mechanism, our starting point for the stoichiometric analysis is a list of species (reactants, intermediates, and products), which for this system includes: H_2O and CO as reactants, $H_2O{\cdot}S$, $CO{\cdot}S$, $CO_2{\cdot}S$, $H_2{\cdot}S$, $H{\cdot}S$, $OH{\cdot}S$, $O{\cdot}S$ and $HCOO{\cdot}S$ (q = 8) as the independent surface intermediates, and CO_2 and H_2 as products (i.e., n = 4). Consider the intermediates matrix

$$\boldsymbol{\alpha} = \begin{array}{c} \begin{array}{cccccccc} H_2O\cdot S & CO\cdot S & CO_2\cdot S & H_2\cdot S & H\cdot S & OH\cdot S & O\cdot S & HCOO\cdot S \end{array} \\ \begin{bmatrix} 0 & +1 & 0 & 0 & 0 & 0 & 0 & 0 \\ +1 & 0 & 0 & 0 & 0 & 0 & 0 & 0 \\ -1 & 0 & 0 & 0 & +1 & +1 & 0 & 0 \\ 0 & -1 & +1 & 0 & 0 & 0 & -1 & 0 \\ 0 & -1 & 0 & 0 & 0 & -1 & 0 & +1 \\ 0 & 0 & 0 & 0 & +1 & -1 & +1 & 0 \\ 0 & -1 & +1 & +1 & 0 & -1 & 0 & 0 \\ 0 & 0 & +1 & +1 & 0 & 0 & 0 & -1 \\ 0 & 0 & +1 & 0 & 0 & +1 & -1 & -1 \\ -1 & 0 & 0 & 0 & 0 & +2 & -1 & 0 \\ -1 & 0 & 0 & -1 & +1 & +1 & 0 & 0 \\ 0 & 0 & 0 & -1 & +1 & -1 & +1 & 0 \\ +1 & 0 & +1 & 0 & 0 & -1 & 0 & -1 \\ 0 & 0 & +1 & -1 & +1 & 0 & 0 & -1 \\ 0 & 0 & -1 & 0 & 0 & 0 & 0 & 0 \\ 0 & 0 & 0 & -2 & +1 & 0 & 0 & 0 \\ 0 & 0 & 0 & 0 & -1 & 0 & 0 & 0 \\ 0 & 0 & 0 & -2 & 0 & 0 & 0 & 0 \end{bmatrix} \begin{array}{c} s_1 \\ s_2 \\ s_3 \\ s_4 \\ s_5 \\ s_6 \\ s_7 \\ s_8 \\ s_9 \\ s_{10} \\ s_{11} \\ s_{12} \\ s_{13} \\ s_{14} \\ s_{15} \\ s_{16} \\ s_{17} \\ s_{18} \end{array} \end{array} \tag{296}$$

Since $rank\ \boldsymbol{\alpha} = 8$, the surface intermediates are linearly independent and, hence, a direct *RR* involves no more that $q + 1 = 8 + 1 = 9$ elementary reactions [29]. Thus, according to Equation (195) the total number of *RR*s does not exceed the number of ways 9 elementary reactions may be selected from the 18 elementary steps of the mechanism, i.e., 18!/9!/9! = 48,620. In reality, the number is considerably smaller by virtue of the fact that not all of the possible sets of 9 elementary reactions involved in a *RR* are linearly independent.

As already mentioned (Chapter 4), in enumerating the *RR*s we may face three different scenarios. These are illustrated with the help of examples. Consider the *RR* involving the elementary reactions s_1, s_2, s_4, s_8, s_9, s_{11}, s_{15}, s_{16} and s_{17} as our first example. Thus, according to Equation (204), we have

$FR(s_1, s_2, s_4, s_8, s_9, s_{11}, s_{15}, s_{16}, s_{17})$

$$
= \begin{array}{|ccccccccc|}
\multicolumn{1}{c}{H_2O\cdot S} & \multicolumn{1}{c}{CO\cdot S} & \multicolumn{1}{c}{CO_2\cdot S} & \multicolumn{1}{c}{H_2\cdot S} & \multicolumn{1}{c}{H\cdot S} & \multicolumn{1}{c}{OH\cdot S} & \multicolumn{1}{c}{O\cdot S} & \multicolumn{1}{c}{HCOO\cdot S} & \\
\hline
0 & +1 & 0 & 0 & 0 & 0 & 0 & 0 & s_1 \\
+1 & 0 & 0 & 0 & 0 & 0 & 0 & 0 & s_2 \\
0 & -1 & +1 & 0 & 0 & 0 & -1 & 0 & s_4 \\
0 & 0 & +1 & 0 & +1 & 0 & 0 & -1 & s_8 \\
0 & 0 & +1 & 0 & 0 & +1 & -1 & -1 & s_9 \\
-1 & 0 & 0 & +1 & -1 & +1 & 0 & 0 & s_{11} \\
0 & 0 & -1 & 0 & 0 & 0 & 0 & 0 & s_{15} \\
0 & 0 & 0 & +1 & -2 & 0 & 0 & 0 & s_{16} \\
0 & 0 & 0 & -1 & 0 & 0 & 0 & 0 & s_{17}
\end{array}
$$

$$= 2s_1 + 2s_2 + 2s_4 + 2s_8 - 2s_9 + 2s_{11} + 2s_{15} + 2s_{17}$$

$$= 2(s_1 + s_2 + s_4 + s_8 - s_9 + s_{11} + s_{15} + s_{17})$$

In a more conventional format, this *RR* may be presented as

		σ_ρ
s_1:	$-\ CO - S + CO\cdot S = 0$	1
s_2:	$-\ H_2O - S + H_2O\cdot S = 0$	1
s_4:	$CO\cdot S - O\cdot S + CO_2\cdot S + S = 0$	1
s_8:	$HCOO\cdot S - S + CO_2\cdot S + H\cdot S = 0$	1
s_9:	$HCOO\cdot S - O\cdot S + CO_2\cdot S + OH\cdot S = 0$	−1
s_{11}:	$H_2O\cdot S - H\cdot S + OH\cdot S + H_2\cdot S = 0$	1
s_{15}:	$CO_2\cdot S + CO_2 + S = 0$	1
s_{17}:	$H_2\cdot S + H_2 + S = 0$	1
Net:	$H_2O + CO \leftrightarrows CO_2 + H_2$	

Thus, *FR*(s_1, s_2, s_4, s_8, s_9, s_{11}, s_{15}, s_{16}, s_{17}) results in an *OR* and, consequently, is a *FR*. On the other hand, the *RR* involving the elementary reactions s_1, s_2, s_4, s_5, s_6, s_8, s_{15}, s_{16}, and s_{16} is an *ER*, i.e.,

$ER(s_1, s_2, s_4, s_5, s_6, s_8, s_{15}, s_{16}, s_{17})$

$$= \begin{vmatrix} H_2O\cdot S & CO\cdot S & CO_2\cdot S & H_2\cdot S & H\cdot S & OH\cdot S & O\cdot S & HCOO\cdot S & \\ 0 & +1 & 0 & 0 & 0 & 0 & 0 & 0 & s_1 \\ +1 & 0 & 0 & 0 & 0 & 0 & 0 & 0 & s_2 \\ 0 & -1 & +1 & 0 & 0 & 0 & -1 & 0 & s_4 \\ 0 & -1 & 0 & 0 & 0 & -1 & 0 & +1 & s_5 \\ 0 & 0 & 0 & +1 & 0 & -1 & +1 & 0 & s_6 \\ 0 & 0 & +1 & +1 & 0 & 0 & 0 & -1 & s_8 \\ 0 & 0 & -1 & 0 & 0 & 0 & 0 & 0 & s_{15} \\ 0 & 0 & 0 & -2 & +1 & 0 & 0 & 0 & s_{16} \\ 0 & 0 & 0 & 0 & -1 & 0 & 0 & 0 & s_{17} \end{vmatrix}$$

$$= 0s_1 + 0s_2 + 2s_4 - 2s_5 + 2s_6 - 2s_8 + 0s_{15} + 0s_{16} + 0s_{17}$$

$$= 2(s_4 - s_5 + s_6 - s_8)$$

or

		σ_ρ
s_4:	$-\ CO\cdot S - O\cdot S + CO_2\cdot S + S = 0$	1
s_5:	$-\ CO\cdot S - OH\cdot S + HCOO\cdot S + S = 0$	−1
s_6:	$-\ OH\cdot S - S + O\cdot S + H\cdot S = 0$	1
s_8:	$-\ HCOO\cdot S - S + CO_2\cdot S + H\cdot S = 0$	−1
Net:	$0 = 0$	

A special situation is faced when considering the *RR* involving the elementary reactions s_1, s_2, s_3, s_4, s_6, s_7, s_{15}, s_{16} and s_{17}. In this case all of the stoichiometric coefficients in the *RR* are zero

$RR(s_1, s_2, s_3, s_4, s_6, s_7, s_{15}, s_{16}, s_{17})$

$$
\begin{array}{c}
\begin{array}{cccccccc}
\mathrm{H_2O\cdot S} & \mathrm{CO\cdot S} & \mathrm{CO_2\cdot S} & \mathrm{H\cdot S} & \mathrm{H_2\cdot S} & \mathrm{OH\cdot S} & \mathrm{O\cdot S} & \mathrm{HCOO\cdot S}
\end{array} \\
= \begin{vmatrix}
0 & +1 & 0 & 0 & 0 & 0 & 0 & 0 & s_1 \\
+1 & 0 & 0 & 0 & 0 & 0 & 0 & 0 & s_2 \\
-1 & 0 & 0 & +1 & 0 & +1 & 0 & 0 & s_3 \\
0 & -1 & +1 & 0 & 0 & 0 & -1 & 0 & s_4 \\
0 & 0 & 0 & +1 & 0 & -1 & +1 & 0 & s_6 \\
0 & -1 & +1 & +1 & 0 & -1 & 0 & 0 & s_7 \\
0 & 0 & -1 & 0 & 0 & 0 & 0 & 0 & s_{15} \\
0 & 0 & 0 & -2 & +1 & 0 & 0 & 0 & s_{16} \\
0 & 0 & 0 & 0 & -1 & 0 & 0 & 0 & s_{17}
\end{vmatrix}
\end{array}
$$

$$
= 0s_1 + 0s_2 + 0s_3 + 0s_4 + 0s_6 + 0s_7 + 0s_{15} + 0s_{16} + 0s_{17} = 0
$$

Recall, the occurrence of zero *RR*s is due to the fact that the elementary reactions involved in such *RR*s may produce at least two, either full or empty *RR*s. Thus, the elementary reactions involved in *RR*(s_1, s_2, s_3, s_4, s_6, s_7, s_{15}, s_{16}, s_{17}) are also involved in two *RR*s, namely, $s_1 + s_2 + s_3 + s_4 + s_6 + s_{15} + s_{16} + s_{17}$ and $s_1 + s_2 + s_3 + s_7 + s_{15} + s_{16} + s_{17}$ as well as in one *ER* $s_4 + s_6 - s_7$.

Similarly, the *IN*s and *TN*s are enumerated using Equations (224) and (228), respectively. According to Equation (224), we consider the *IN* derived from the exclusion of $\{s_1, s_2, s_3, s_4, s_5, s_6, s_{15}, s_{16}\}$. From the intermediate matrix $\boldsymbol{\alpha}$ and Equation (215), we find that the QSS conditions are given by

$$
Q = \begin{bmatrix}
r_2 - r_3 - r_{10} - r_{11} + r_{13} \\
r_1 - r_4 - r_5 - r_7 \\
r_4 + r_7 + r_8 + r_9 + r_{13} + r_{14} - r_{15} \\
r_3 + r_6 + r_7 + r_8 - r_{11} - r_{12} - r_{14} - 2r_{16} - 2r_{18} \\
r_{11} + r_{12} + r_{14} + r_{16} - r_{17} \\
r_3 - r_5 - r_6 - r_7 + r_9 + 2r_{10} + r_{11} - r_{12} - r_{13} \\
-r_4 + r_6 - r_9 - r_{10} + r_{12} \\
r_5 - r_8 - r_9 - r_{13} - r_{14}
\end{bmatrix}
$$

The incorporation of this result into Equation (222) allows for the derivation of the *IN*:

$$Q(r_7,r_8,r_9,r_{10},r_{11},r_{12},r_{13},r_{14},r_{17},r_{18}):\ \begin{vmatrix} 0 & +1 & -1 & 0 & 0 & 0 & 0 & Q_1 \\ +1 & 0 & 0 & -1 & -1 & 0 & 0 & Q_2 \\ 0 & 0 & 0 & +1 & 0 & 0 & -1 & Q_3 \\ 0 & 0 & +1 & 0 & 0 & +1 & 0 & Q_4 \\ 0 & 0 & 0 & 0 & 0 & 0 & 0 & Q_5 \\ 0 & 0 & +1 & 0 & -1 & -1 & 0 & Q_6 \\ 0 & 0 & 0 & -1 & 0 & +1 & 0 & Q_7 \\ 0 & 0 & 0 & 0 & +1 & 0 & 0 & Q_8 \end{vmatrix} = 0$$

where the Q_i's are given by the previous result. Thus,

$$Q(r_7,r_8,r_9,r_{10},r_{11},r_{12},r_{13},r_{14},r_{17},r_{18}):\quad r_{11}+r_{12}+r_{14}+r_{16}-r_{17}=0$$

This result, according to Equation (224), translates into the *IN* expression

$$n_I(\mathrm{s}_7,s_8,s_9,s_{10},s_{11},s_{12},s_{13},s_{14},s_{17},s_{18}):\quad s_{11}+s_{12}+s_{14}+s_{16}-s_{17}$$

When enumerating the *TN*s, we mus first consider the determinant term, Δ, as given by Equation (227), which must yield a non-zero value. Consider the *TN* in which the following set of elementary reaction steps is not involved $\{s_1,s_2,s_3,s_4,s_5,s_6,s_{11},s_{15}\}$. We check the determinant condition

$$\Delta\left(s_1,s_2,s_3,s_4,s_5,s_6,s_{11},s_{15}\right)=\begin{vmatrix} 0 & +1 & 0 & 0 & 0 & 0 & 0 & 0 \\ +1 & 0 & 0 & 0 & 0 & 0 & 0 & 0 \\ -1 & 0 & 0 & 0 & +1 & +1 & 0 & 0 \\ 0 & -1 & +1 & 0 & 0 & 0 & -1 & 0 \\ 0 & -1 & 0 & 0 & 0 & -1 & 0 & +1 \\ 0 & 0 & 0 & 0 & +1 & -1 & +1 & 0 \\ -1 & 0 & 0 & -1 & +1 & +1 & 0 & 0 \\ 0 & 0 & -1 & 0 & 0 & 0 & 0 & 0 \end{vmatrix} = 2 \neq 0$$

and find that a valid *TN* may be determined from the subset of elementary reaction steps $\{s_7, s_8, s_9, s_{10}, s_{12}, s_{13}, s_{14}, s_{16}, s_{17}, s_{18}\}$ according to Equation (228). In this case, the resulting *TN* is

$$n_T(s_7, s_8, s_9, s_{10}, s_{12}, s_{13}, s_{14}, s_{16}, s_{17}, s_{18}): \quad s_{17} + s_{18} + OR$$

A list of the stoichiometrically distinct topological characteristics for the WGS reaction is presented in Appendix D.

6.3. Realization of the Reaction Route Graph

Upon examination of the compilation of direct *FR*s given in Appendix D, it is noted that the stoichiometric numbers in several of the *FR*s are non-unity; specifically, it is seen that some *FR*s have stoichiometric numbers of ±2, suggesting that the *RR* graph may be constructed based on the methodology described in Section 5.5 [134]. Following this algorithm, first, we consider the shortest direct *FR*, i.e., FR_1, and draw it twice symmetrically, with the order of the steps reversed in the second, creating two subgraphs (see Figure 14a). The order of the elementary reaction steps is chosen to be mechanistically meaningful, but is otherwise arbitrary. Next, we add stepwise each of the shortest *ER*s (typically comprised of only three elementary reaction steps, i.e., ER_1, ER_2, ER_3, ER_8, ER_9 and ER_{13}) symmetrically to each of the subgraphs such that no elementary reaction step is placed in a subgraph more than once, until we can no longer add the *ER*s (see Figure 14b). For example, in the transition from Figure 14a to Figure 14b, we added steps s_4 and s_6, via the *ER* $s_4 + s_6 - s_7 = 0$, such that it is symmetric in each subgraph.

In order to add the remaining elementary reaction steps missing from the two subgraphs, it is necessary to link the two subgraphs into a single *RR* graph. This is accomplished through the fusion of specific nodes, indicated by the orange nodes in Figure 14c, symmetrically to allow the missing elementary reaction steps to be inserted into the graph via appropriate *ER*s from the remaining shortest *ER*s (i.e., ER_5, ER_6 and

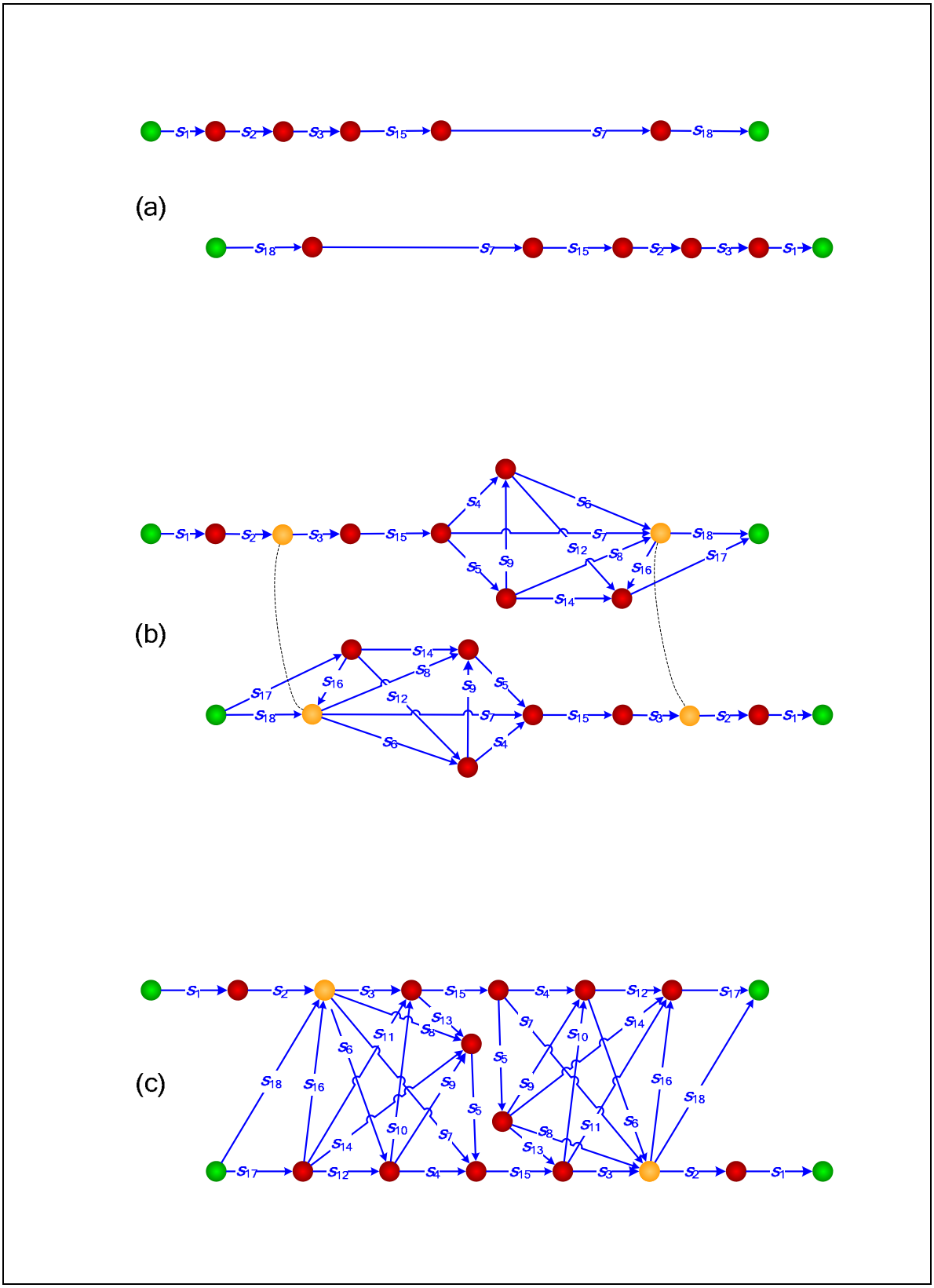

Figure 14. Construction of the 18-step WGS mechanism *RR* graph.

ER_7). The characteristics associated with each of the unfused nodes are not lost; instead, they are represented collectively by the fused node. Once fusion has been completed and the remaining elementary steps added to the *RR* graph, the intermediate nodes should all be balanced, that is, each of the *IN*s should be present in the list provided in Appendix D. The final step in the construction of the *RR* graph is the addition of the *OR*, completing the *TN*s. The complete *RR* graph of the mechanism is giving in Figure 15. It may be verified that the entire list of *FR*s and *ER*s can be traced on the resulting *RR* graph. The *RR* graph may now also be translated into an equivalent electrical network by replacing each of the elementary reaction steps with a resistor, for the steady-state case, and the *OR* with a voltage source.

6.4. Simplification and reduction of the reaction network

Once the *RR* graph (Figure 15) and its electrical analog (Figure 16) are available, the rate of the *OR* may be evaluated as the ratio of the affinity of the *OR* and the overall resistance of the equivalent electrical circuit (R_{OR}). Because of the complexity of the *RR* graph, an explicit expression for this is cumbersome and is not given here. Instead, we will first simplify and reduce the *RR* graph by assessing the relative importance of links in parallel pathways between two given nodes. A substantial simplification of the *RR* graph may be achieved by evaluating and comparing the resistances, Equation (285), in this manner. However, since the method is approximate, the effect of eliminating a resistance is validated by calculating the mechanism kinetics without the elementary reaction step in question. This is achieved by considering the resistances within the shortest *ER*s (provided in Appendix D). For example, if we compare the resistance of s_{18} to the sum of resistances $s_{16} + s_{17}$, corresponding to the *ER* $s_{16} + s_{17} - s_{18} = 0$, as shown in Figure 17, we see that, although the resistances are close in magnitude, R_{18} is consistently higher than $R_{16} + R_{17}$. The ratio of the pathway resistances is nearly constant and equal to ~1.6. This suggests that it may be possible to eliminate s_{18} from the mechanism. To validate this elimination, we check the effect of s_{18} on the overall kinetics by comparing

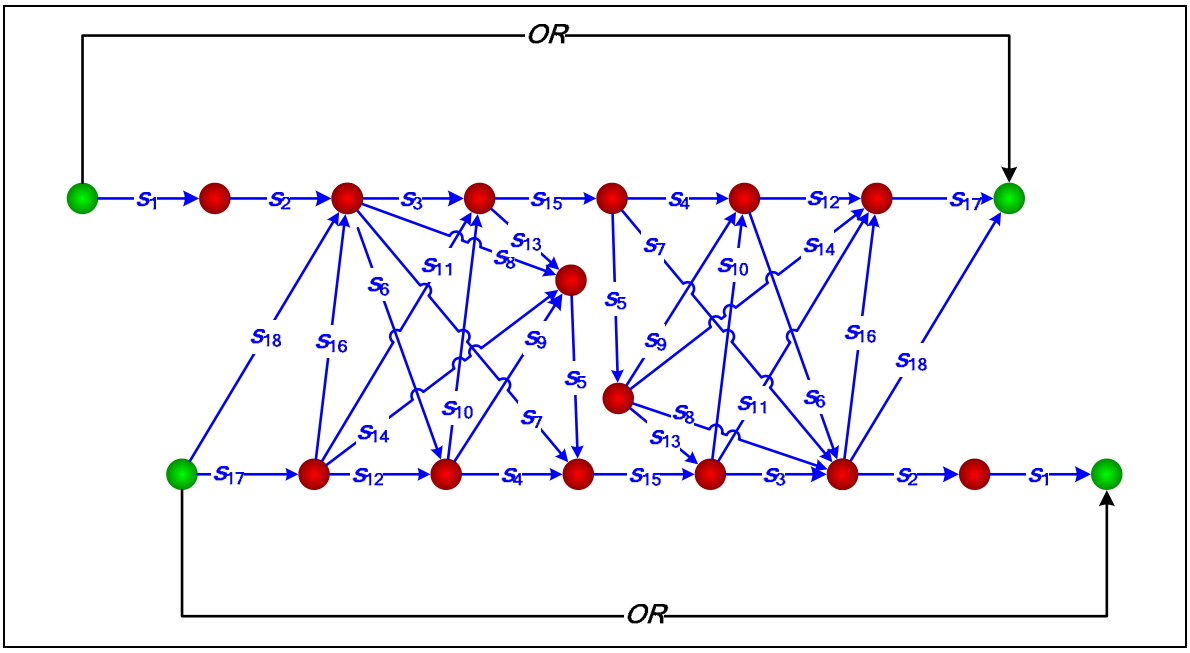

Figure 15. The *RR* graph for the 18-step mechanism of the WGS reaction.

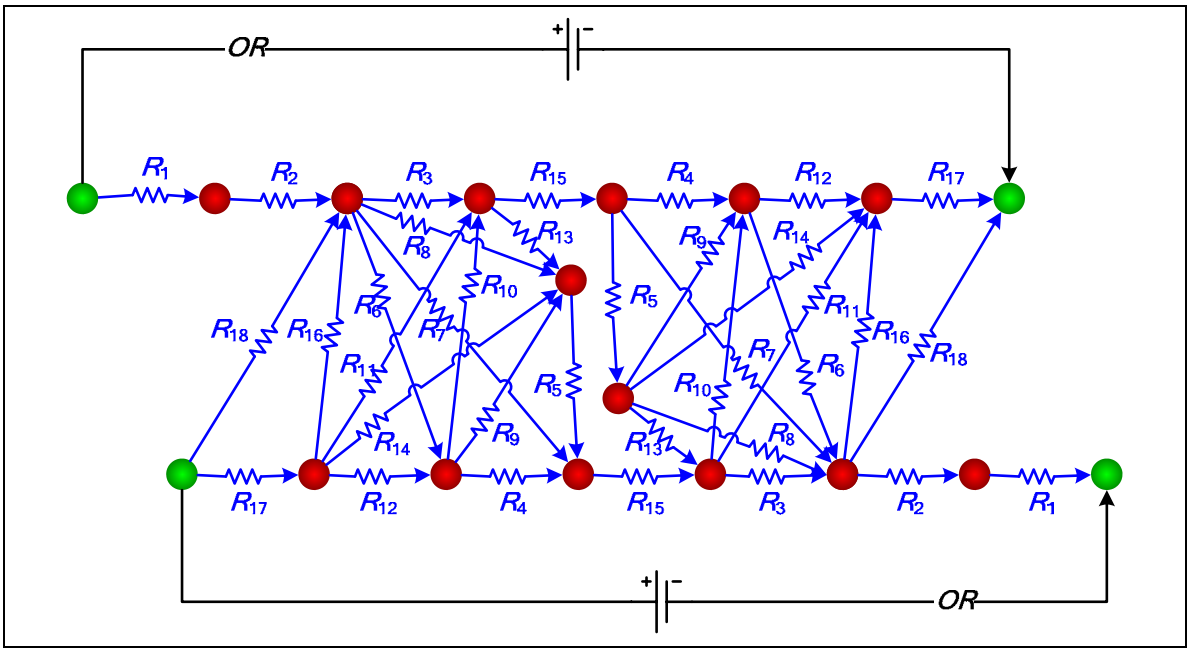

Figure 16. The electrical circuit analog of the reaction network for the WGSR

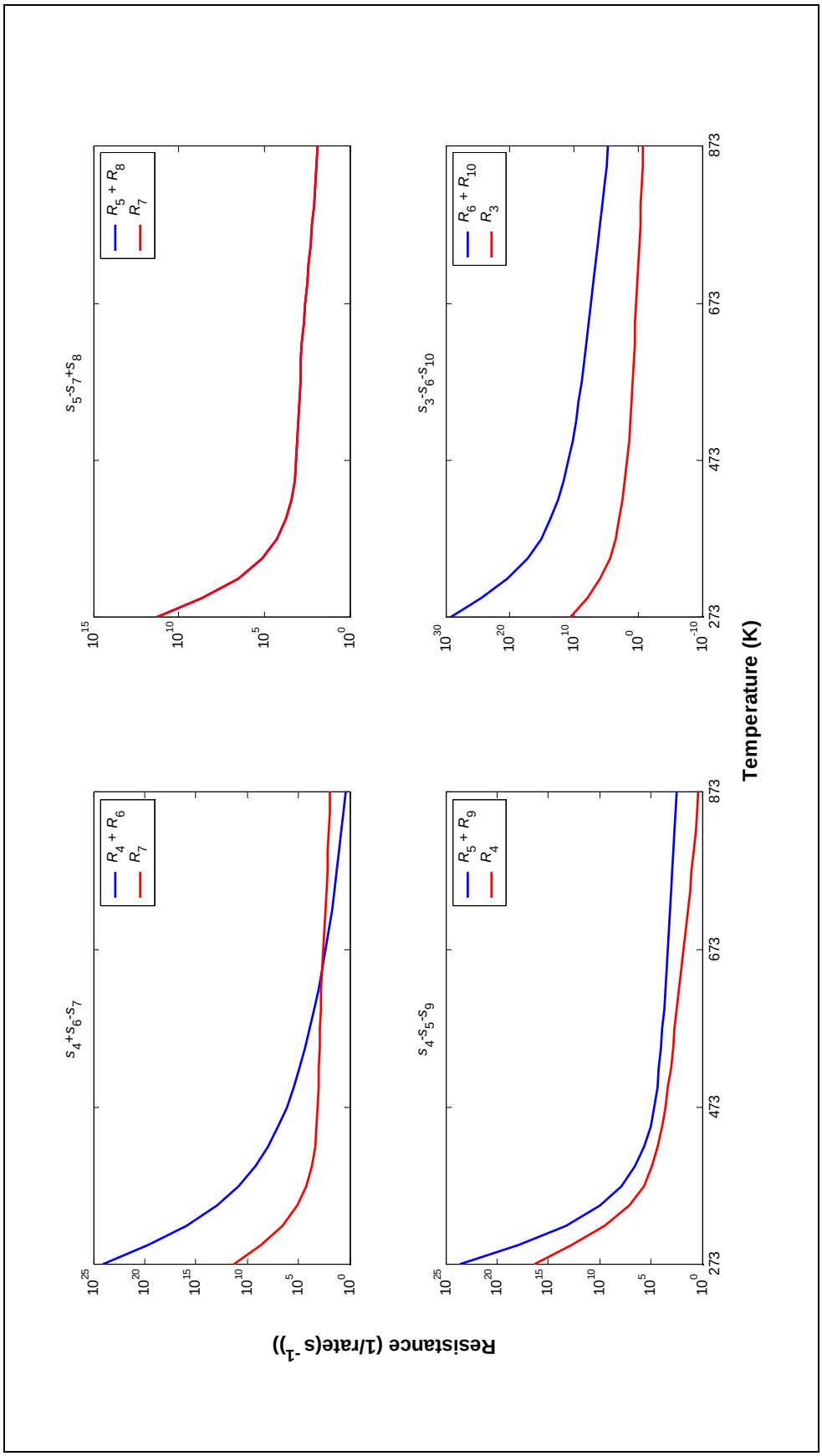

Figure 17. Parallel pathway resistance comparisons as a function of temperature for the following conditions: low temperature shift Cu catalyst loading of 0.14 g/cm^3; total feed flow rate of 236 cm^3 (STP) min^{-1}; residence time τ = 1.8 s; feed composition of H_2O(10%), CO(10%) and N_2(balance)

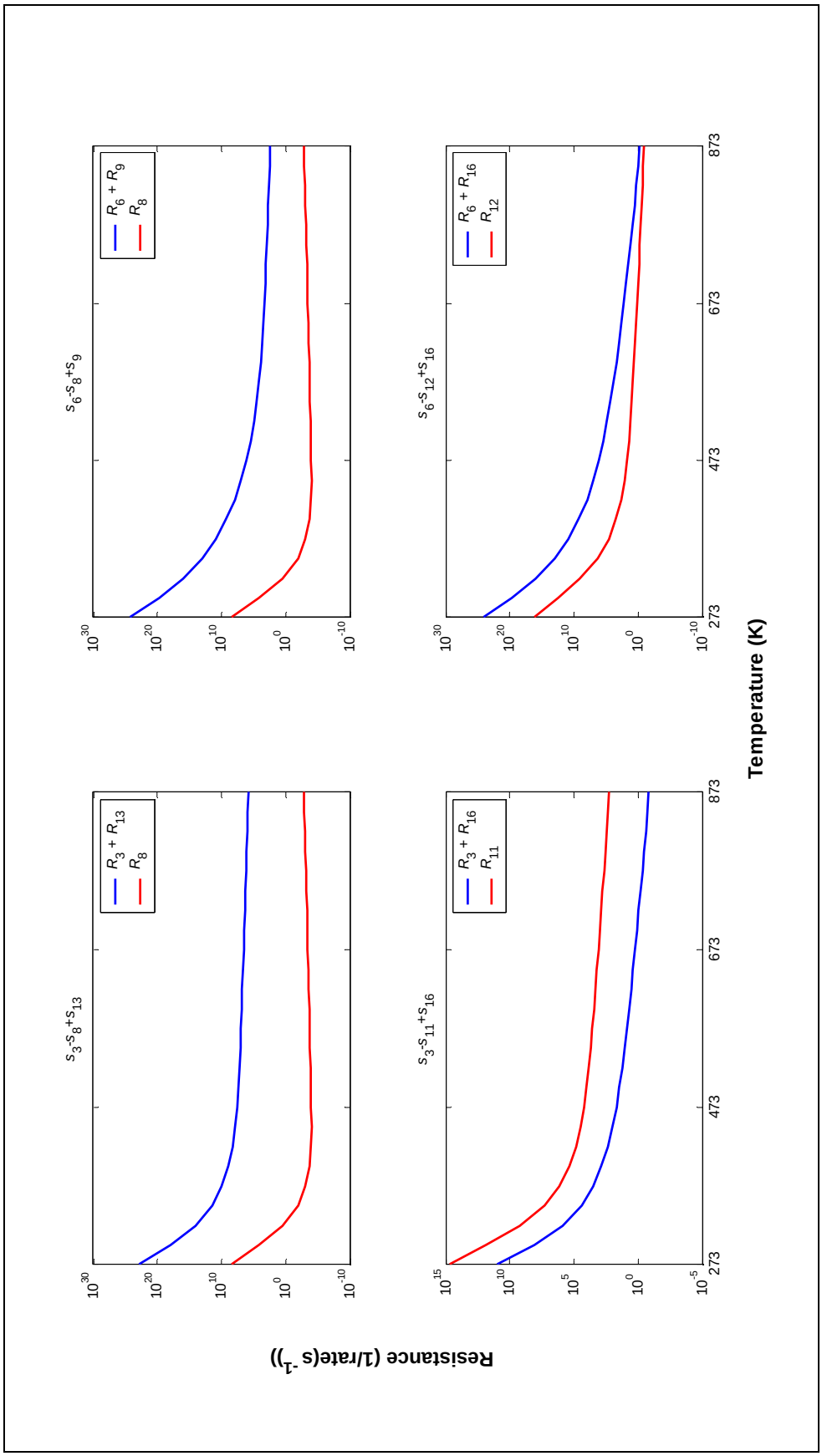

Figure 17. Parallel pathway resistance comparisons as a function of temperature for the following conditions: low temperature shift Cu catalyst loading of 0.14 g/cm^3; total feed flow rate of 236 cm^3 (STP) min^{-1}; residence time τ = 1.8 s; feed composition of H_2O(10%), CO(10%) and N_2(balance) *(continued)*

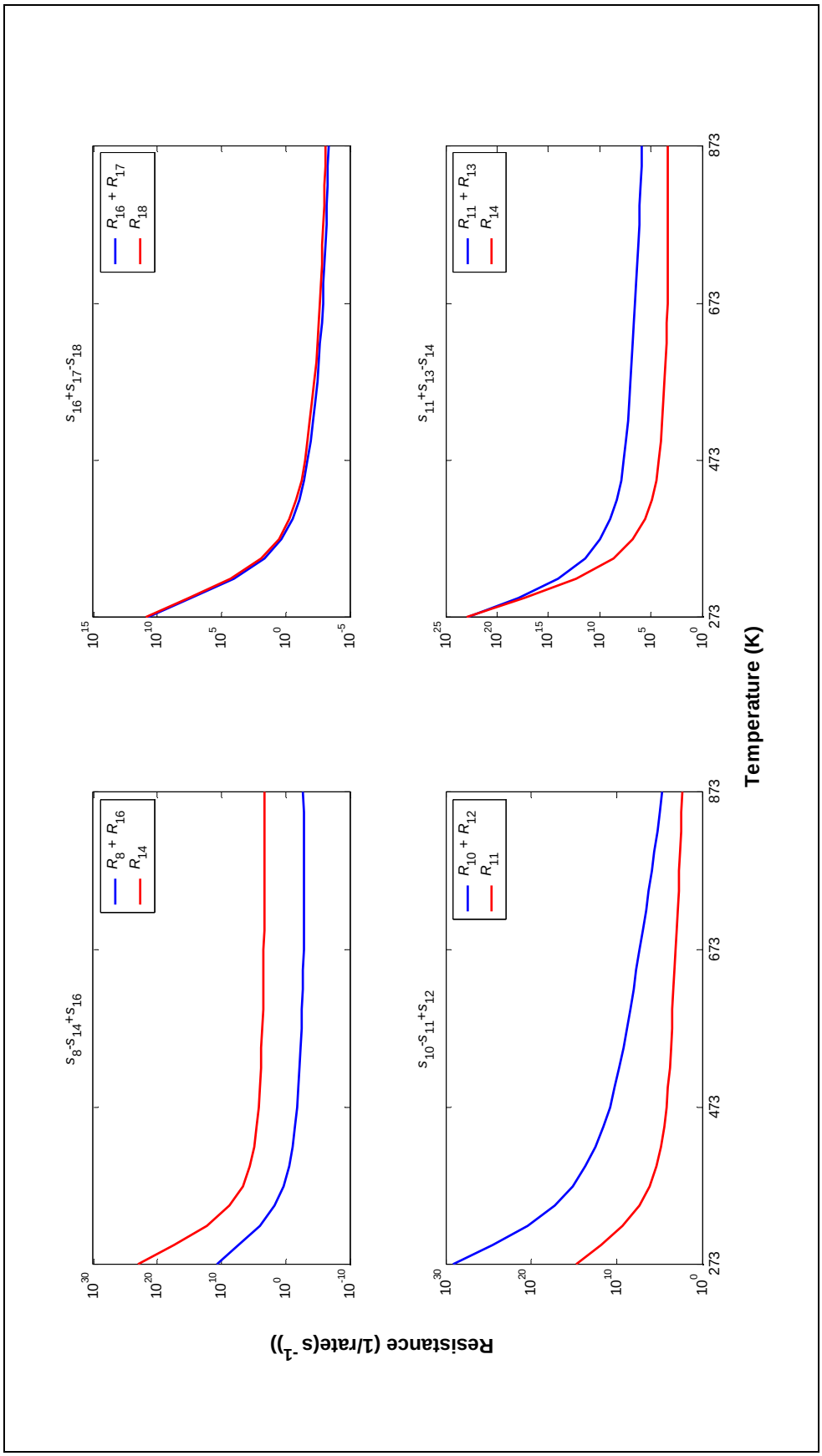

Figure 17. Parallel pathway resistance comparisons as a function of temperature for the following conditions: low temperature shift Cu catalyst loading of 0.14 g/cm^3; total feed flow rate of 236 cm^3 (STP) min^{-1}; residence time τ = 1.8 s; feed composition of H_2O(10%), CO(10%) and N_2(balance) *(continued)*

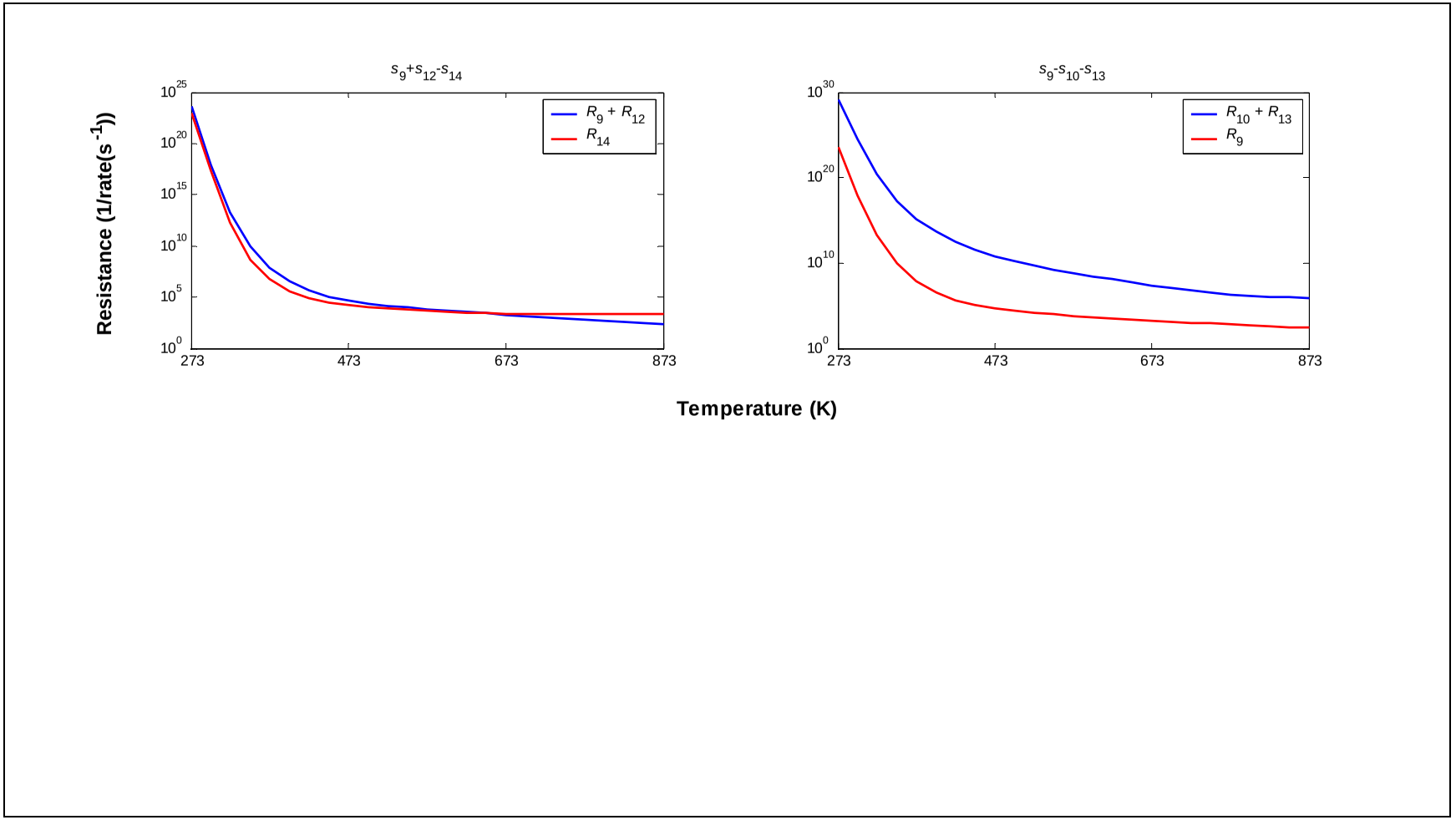

Figure 17. Parallel pathway resistance comparisons as a function of temperature for the following conditions: low temperature shift Cu catalyst loading of 0.14 g/cm^3; total feed flow rate of 236 cm^3 (STP) min^{-1}; residence time τ = 1.8 s; feed composition of H_2O(10%), CO(10%) and N_2(balance) *(condensed)*

the simulated overall kinetics of the complete mechanism to the mechanism less s_{18}. In fact, as is shown in Figure 18, we find that we may eliminate s_{18} as it is not kinetically significant, i.e., there is no measurable change in the kinetics of the complete mechanism.

We have previously shown that s_{10} and s_{13} are also not kinetically significant [23,26]. Considering the relative resistances shown in Figure 17 for the *ER*s: $s_3 - s_6 - s_{10}$, $s_3 - s_8 + s_{13,}$ $s_{10} - s_{11} - s_{12}$, $s_{11} + s_{13} - s_{14}$, and $s_9 - s_{10} - s_{13}$, it is again determined that these steps may be eliminated from the mechanism. As described above, this is then validated by comparing the kinetics of the overall mechanism with the kinetics of the overall mechanism less s_{10} and s_{13}. With the elimination of s_{10}, s_{13} and s_{18}, the resulting reduced *RR* graph becomes decoupled and is now minimal, corresponding to a previous network provided by us [23,26] (see Figure 19a).

For further reduction of the minimal network the following steps are taken. The paths between nodes n_3 and n_6, i.e., the two parallel paths that produce OH·S are considered. The first branch involves only one resistance, R_{11}. The second branch involves a sequence of two series resistors R_3 and R_{16}, so that its overall resistance is $R_3 + R_{16}$. Numerical simulations of these two resistances as a function of temperature are presented in Figure 17. It is seen that R_{11} is several orders of magnitude higher than $R_3 + R_{16}$ at all temperatures. Hence, there is ample justification to neglect s_{16}. This is validated by comparing simulated results of the complete mechanism with results from the mechanism excluding s_{16}.

Continuing the reduction of the *RR* graph (Figure 19a), the next step in the reduction process is to consider the two parallel branches between nodes n_6 and n_7, that is, R_8 and $R_6 + R_9$. From numerical simulations it may be concluded (Figure 17) that path s_8 is of a much lower resistance than path $s_6 + s_9$ and, consequently, the latter may be disregarded (Figure 19c). Fortunately, the values of both $R_6 + R_9$ are much higher than the value for R_8 throughout the entire temperature range of interest, as shown in Figure 20.

Finally, we compare the resistances of the two remaining parallel branches between nodes n_4, and n_7. One of these two parallel branches involves only one resistance, R_{14}. The other involves resistances R_8 and R_{16} connected in series, with an overall resistance equal to $R_8 + R_{16}$. Based on numerical results (Figure 17), we conclude

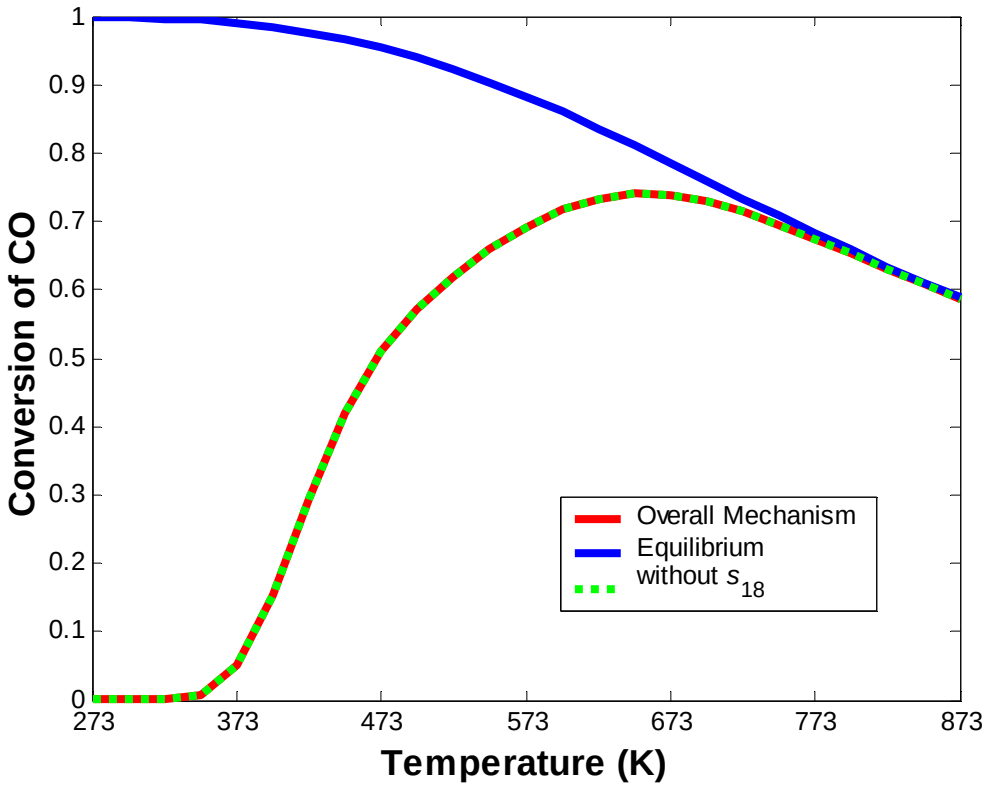

Figure 18. Comparison of the overall mechanism kinetic with and without s_{18}.

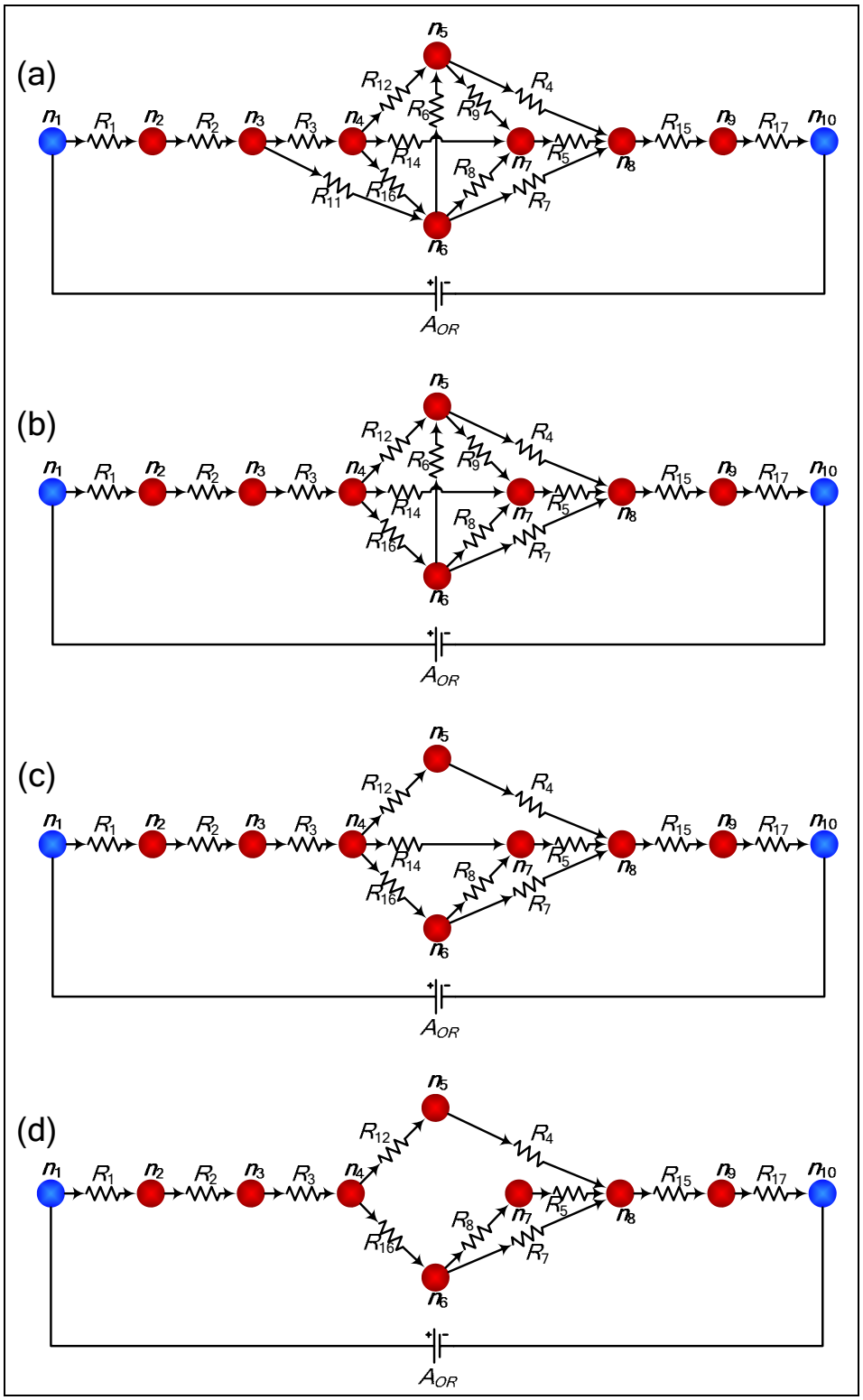

Figure 19. Reduction of the reaction network as described in the text.

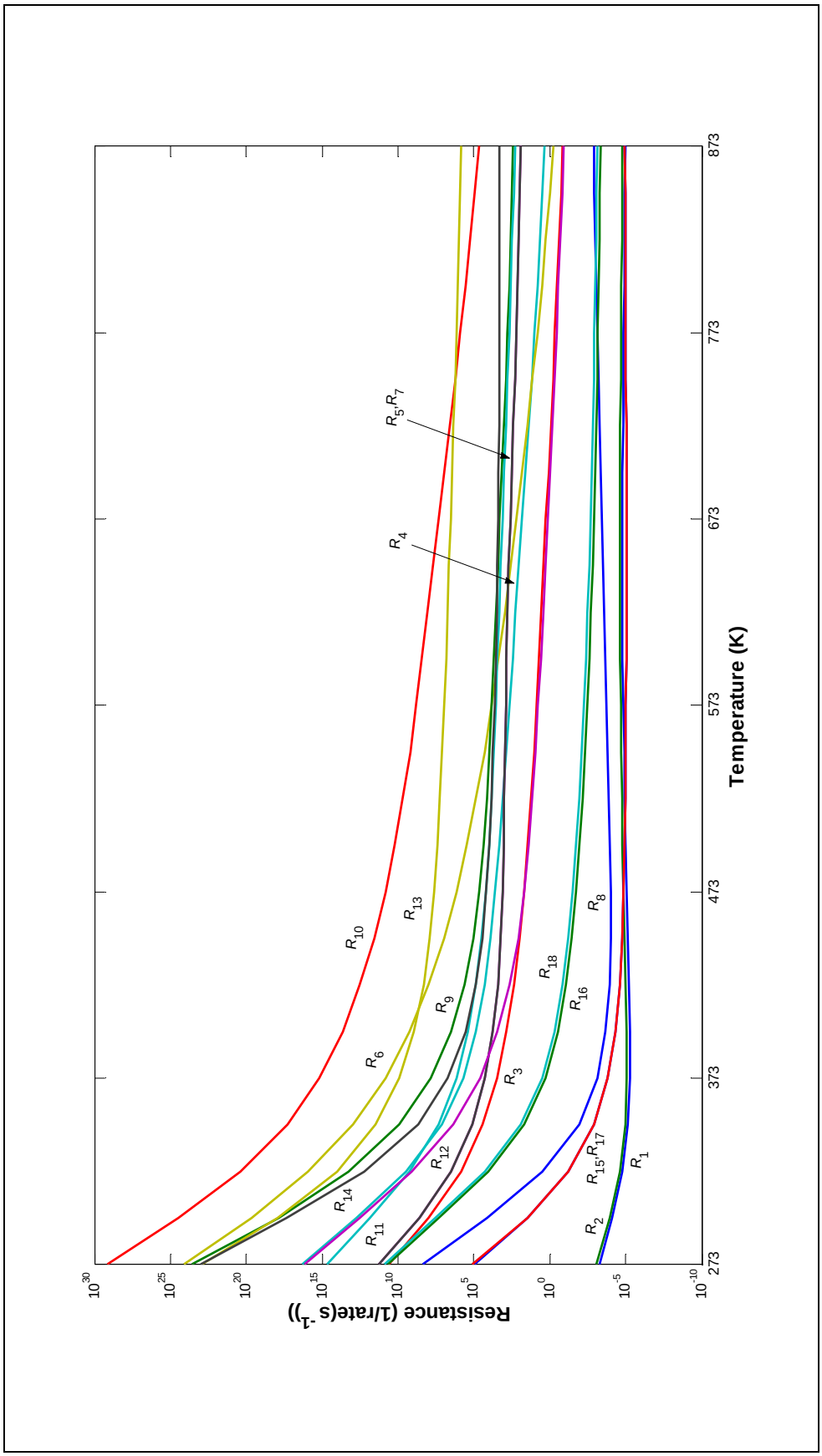

Figure 20. Elementary reaction step resistances as a function of temperature for the following conditions: low temperature shift Cu catalyst loading of 0.14 g/cm^3; total feed flow rate of 236 cm^3 (STP) min^{-1}; residence time τ = 1.8 s; feed composition of H_2O(10%), CO(10%) and N_2(balance)

that the resistance R_{14} is much higher than $R_8 + R_{16}$ and, hence, the consumption of HCOO·S via s_8 is much faster as compared to the consumption of HCOO·S via s_{14}. In other words, the path via s_{14} may be neglected (Figure 19d). The above simplifications leave us with a reduced network comprising 11 elementary reactions and 3 *RR*s, namely, RR_8, RR_{24}, RR_6 (Figure 19d) from the list in Appendix D. The overall resistances of these *RR*s according to Equation (289) are equal to

$$R_{RR_8}: \quad R_1 + R_2 + R_3 + R_7 + R_{15} + R_{16} + R_{17}$$

$$R_{RR_{24}}: \quad R_1 + R_2 + R_3 + R_5 + R_8 + R_{15} + R_{16} + R_{17}$$

$$R_{RR_6}: \quad R_1 + R_2 + R_3 + R_4 + R_{12} + R_{15} + R_{17}$$

As can be seen from Figure 24, RR_8 and RR_{24} are dominant at lower temperatures while, at higher temperatures, the mechanism is dominated by RR_6. Therefore, all these *RR*s are significant.

In a previous analysis [7], the conventional redox *RR* was shown to dominate at higher temperatures. However, the current analysis shows that, while the formate and associative *RR*s are dominant at lower temperatures, at higher temperatures, the *modified* redox *RR* becomes important. The modified *RR* differs only by one elementary reaction from the conventional redox *RR*. Thus, the conventional redox *RR* is [7,8]

	σ_ρ
s_1: $CO + S \leftrightarrows CO{\cdot}S$	+1
s_2: $H_2O + S \leftrightarrows H_2O{\cdot}S$	+1
s_3: $H_2O{\cdot}S + S \leftrightarrows OH{\cdot}S + H{\cdot}S$	+1
s_6: $OH{\cdot}S + S \leftrightarrows O{\cdot}S + H{\cdot}S$	+1
s_4: $CO{\cdot}S + O{\cdot}S \leftrightarrows CO_2{\cdot}S + S$	+1
s_{15}: $CO_2{\cdot}S \leftrightarrows CO_2 + S$	+1
s_{16}: $H{\cdot}S + H{\cdot}S \leftrightarrows H_2{\cdot}S$	+1
s_{17}: $H_2{\cdot}S \leftrightarrows H_2 + S$	+1
$H_2O + CO \leftrightarrows CO_2 + H_2$	

while the modified *RR* is

	σ_ρ
s_1: $CO + S \leftrightarrows CO{\cdot}S$	+1
s_2: $H_2O + S \leftrightarrows H_2O{\cdot}S$	+1
s_3: $H_2O{\cdot}S + S \leftrightarrows OH{\cdot}S + H{\cdot}S$	+1
s_{14}: $OH{\cdot}S + H{\cdot}S \leftrightarrows O{\cdot}S + H_2{\cdot}S$	+1
s_4: $CO{\cdot}S + O{\cdot}S \leftrightarrows CO_2{\cdot}S + S$	+1
s_{15}: $CO_2{\cdot}S \leftrightarrows CO_2 + S$	+1
s_{17}: $H_2{\cdot}S \leftrightarrows H_2 + S$	+1
Net: $H_2O + CO \leftrightarrows CO_2 + H_2$	

As evident, the main difference between the above two *RR*s is in the production of O·S from of OH·S and in the production of H_2·S. In the conventional redox *RR*, the dissociation of OH·S and the production of H_2·S occur in separate steps, namely

s_6: $OH{\cdot}S + S \leftrightarrows O{\cdot}S + H{\cdot}S$

s_{16}: $H{\cdot}S + H{\cdot}S \leftrightarrows H_2{\cdot}S$

On the other hand, in the *modified* redox *RR*, the production of both the adsorbed atomic oxygen as well as adsorbed molecular hydrogen takes place in a single step

s_{12}: $OH{\cdot}S + H{\cdot}S \leftrightarrows O{\cdot}S + H_2{\cdot}S$

Because both paths produce O·S that is further used to oxidize CO·S, the new *RR* may be referred to as a *modified* redox *RR*. Comparing the energetics of these elementary reactions (Table 16) it follows that the pathway involving s_{12} is more favorable. This may be better visualized from the energy diagram of these two *RR*s in Figure 21. The modified redox *RR* proceeds via a path that reduces the peaks and valleys encountered as compared to the conventional redox *RR*. The two *RR*s are compared mechanistically in Figure 22.

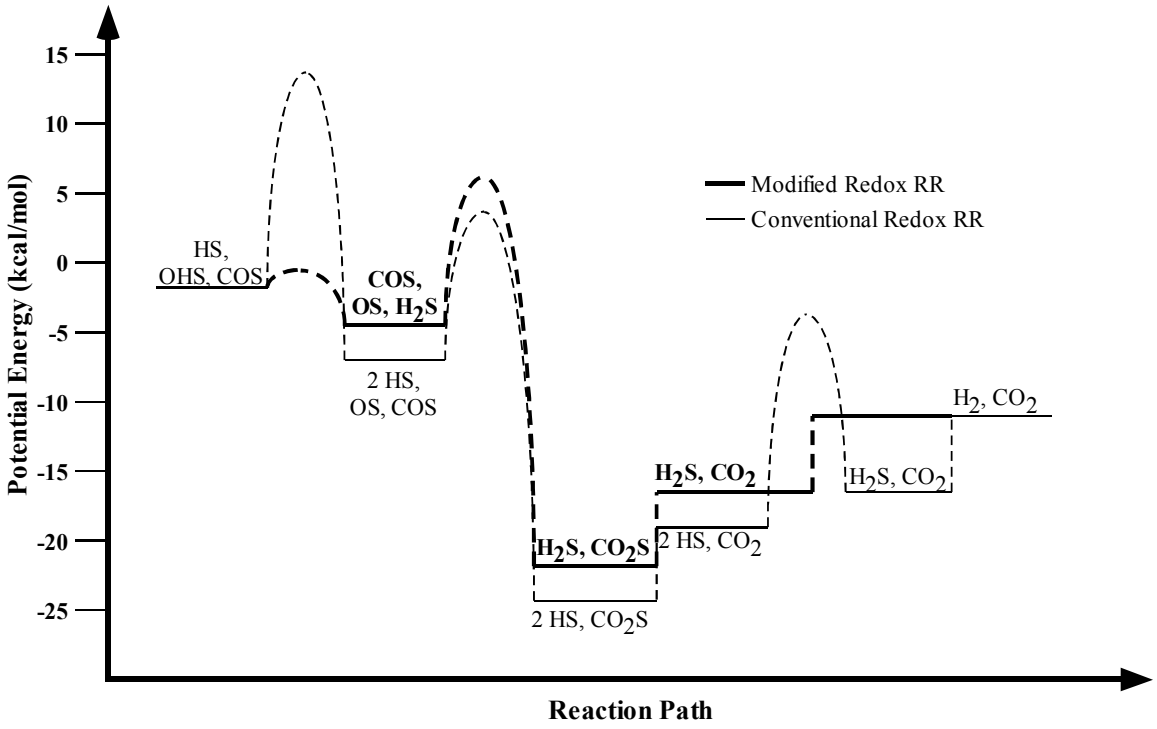

Figure 21. Energy diagrams of the modified and conventional redox RRs on Cu(111).

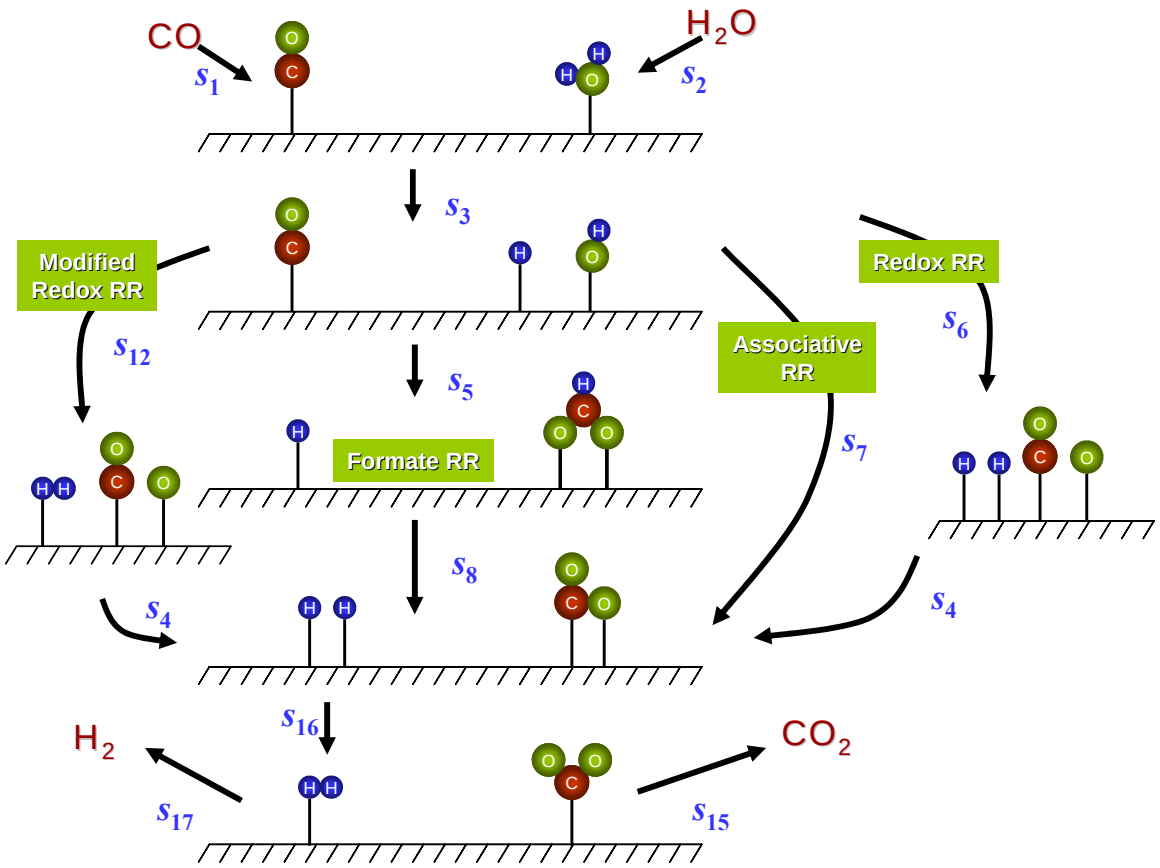

Figure 22. Schematic of the dominant *RR*s of the WGS reaction.

The *RR* network may also be employed to generate a reaction energy diagram. Figure 23 demonstrates this utility of the *RR* graph theory in systematically composing energy diagrams based on forward and reverse activation energies as it applies to the simplified *RR* network of the WGSR (Figure 19d). This is accomplished by tracking the energetics of the elementary reactions along the reaction coordinate as dictated by the structure of the *RR* graph. For example, having started at a zero-energy value, we introduce s_1 into the energy diagram by drawing the elements of the activation barrier for the elementary reaction step, i.e., the forward activation energy (which is zero, in this case, but would be represented by a positive change) followed by the reverse activation energy (which is represented by a negative change of magnitude 12.0, according to Table 16). This process is repeated according to the connectivity established by the *RR* graph. In this diagram, each plateau not only represents the resulting species from the preceding surface reactions, but also the corresponding node from the *RR* network, i.e. n_2 in the network is representative of CO and $H_2O{\cdot}S$ and, similarly and by convention, the first plateau (labeled "n_2" in Figure 23) is also representative of CO and $H_2O{\cdot}S$. The three remaining parallel *RR*s are also evident in this figure as well as the *ER*s.

6.5. The rate of the overall reaction

Now that the mechanism has been appropriately reduced, we are in a position to consider the rate of the overall reaction. First, we write a formal rate equation for the kinetics of the reduced reaction network, Figure 19d, by employing the electrical circuit analogy and the linear rate law analogous to Ohm's law. Thus, the overall rate (overall current) is the ratio of the affinity of the *OR* and the overall resistance of the reaction network. The overall resistance of the reduced reaction network (Figure 19d) is

$$R_{OR} = R_1 + R_2 + R_{15} + R_{17} + R_3 + \frac{1}{\dfrac{1}{R_4 + R_{12}} + \dfrac{1}{R_{16} + \dfrac{1}{\dfrac{1}{R_7} + \dfrac{1}{R_5 + R_8}}}} \tag{297}$$

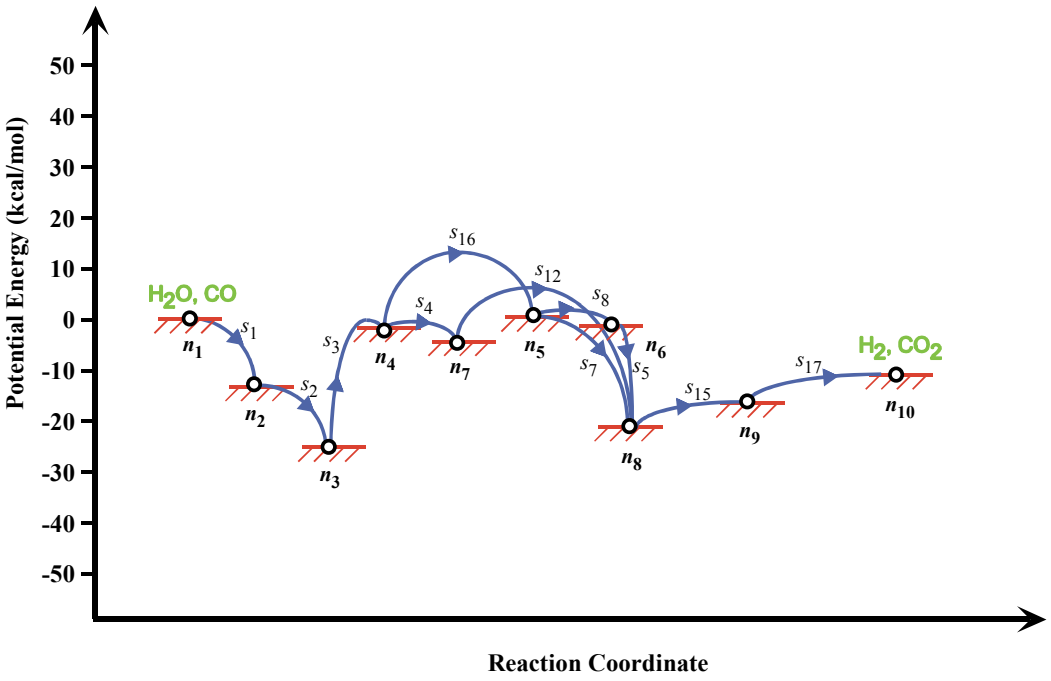

Figure 23. Energy diagram corresponding to the simplified *RR* graph of the WGSR on Cu(111).

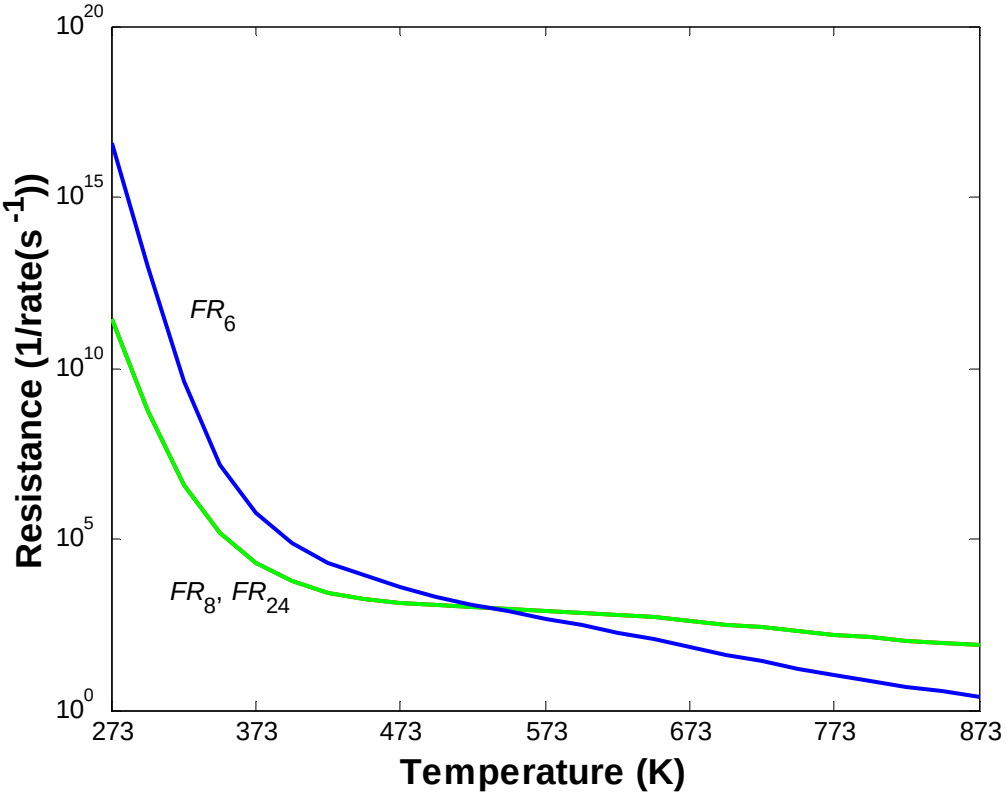

Figure 24. Resistances of the dominant RRs vs. temperature for the following conditions: commercial low temperature shift Cu catalyst loading of 0.14 g/cm^3; total feed flow rate of 236 cm^3 (STP) min^{-1}; residence time τ = 1.8 s; feed composition of H_2O(10%), CO(10%) and N_2(balance)

which gives the overall rate as

$$r_{OR} = \frac{A_{OR}}{R_{OR}} = \frac{A_{OR}}{R_1 + R_2 + R_{15} + R_{17} + R_3 + \dfrac{1}{\dfrac{1}{R_4 + R_{12}} + \dfrac{1}{R_{16} + \dfrac{1}{\dfrac{1}{R_7} + \dfrac{1}{R_5 + R_8}}}}} \tag{298}$$

or, alternatively, keeping in mind that $R_\rho \equiv \mathcal{A}_\rho / r_\rho$

$$r_{OR} = \frac{\mathcal{A}_{overall}}{\dfrac{\mathcal{A}_1}{r_1} + \dfrac{\mathcal{A}_2}{r_2} + \dfrac{\mathcal{A}_{15}}{r_{15}} + \dfrac{\mathcal{A}_{17}}{r_{17}} + \dfrac{\mathcal{A}_3}{r_3} + \dfrac{1}{\dfrac{r_4 r_{12}}{\mathcal{A}_4 r_{12} + \mathcal{A}_{12} r_4} + \dfrac{1}{\dfrac{\mathcal{A}_{16}}{r_{16}} + \dfrac{1}{\dfrac{r_7}{\mathcal{A}_7} + \dfrac{r_5 r_8}{\mathcal{A}_5 r_8 + \mathcal{A}_8 r_5}}}}} \tag{299}$$

The expression can be further simplified if the smaller of the resistances in series can be neglected. Futhermore, the affinities of the elementary reactions in this equation are actually not linearly independent. Indeed, from Figure 19d it is seen that the reduced reaction network incorporates three *ER*s, i.e., the affinities of the elementary reactions are interrelated via

$$A_4 + A_{12} = A_{16} + A_7$$
$$A_5 + A_8 = A_7$$
$$A_4 + A_{12} = A_5 + A_8 + A_{16}$$

6.6. Rate-Limiting and Quasi-Equilibrated Elementary Reaction Steps

While the above formal rate expression is adequate for numerical computation of the rate from numerically calculated resistances, it is more desirable to obtain, if possible,

an explicit rate expression in terms of the terminal species composition. This is accomplished as follows. Further simplification results from comparison of step resistances in a sequence. If a resistance in series is dominant, it may be labeled as a RLS, while the other resistances in the sequence become quasi-equilibrated, i.e., their affinities → 0.

Firstly, we compare the resistances R_1, R_2, R_{15}, R_{17} and R_3 that are connected in series. Numerical simulations show (Figure 25) that $R_3 >> R_1, R_2, R_{15}, R_{17}$. Thus, in this sequence, s_3 may be considered as rate-limiting step with s_1, s_2, s_{15} and s_{17} at quasi-equilibrium. In a similar manner, we compare R_{16} with $(R_5+R_8)R_7/(R_5+R_7+R_8)$ (the overall resistance of the parallel branch following R_{16}) and conclude that $R_{16} << (R_5+R_8)R_7/(R_5+R_7+R_8)$ (Figure 26). That is, s_{16} may be also considered at quasi-equilibrium. Now, the quasi-equilibrium elementary reactions may be combined into intermediate reactions employing the formalism of intermediate *RR*s [19]. The resulting reduced electrical network is presented in Figure 27 and the reduced mechanism with the RLSs identified is given in Table 17.

6.7. Explicit Rate Expression

There now remain only 3 linearly independent *RR*s in Figure 19d, namely, RR_{I}, RR_{II} and RR_{III}, as identified in the previous section. Thus, the QSS conditions provide

$$r_1 = J_{\mathrm{I}} + J_{\mathrm{II}} + J_{\mathrm{III}} \qquad r_4 = J_{\mathrm{III}} \qquad r_8 = J_{\mathrm{II}} \qquad r_{16} = J_{\mathrm{II}} + J_{\mathrm{III}}$$
$$r_2 = J_{\mathrm{I}} + J_{\mathrm{II}} + J_{\mathrm{III}} \qquad r_5 = J_{\mathrm{II}} \qquad r_{12} = J_{\mathrm{III}} \qquad r_{17} = J_{\mathrm{I}} + J_{\mathrm{II}} + J_{\mathrm{III}}$$
$$r_3 = J_{\mathrm{I}} + J_{\mathrm{II}} + J_{\mathrm{III}} \qquad r_7 = J_{\mathrm{I}} \qquad r_{15} = J_{\mathrm{I}} + J_{\mathrm{II}} + J_{\mathrm{III}}$$

and the remaining elementary reaction steps have zero rates.

Using these relations in Equation (299) and keeping in mind that the affinities along all *RR*s are equal, after some algebra, we obtain

$$r = J_{\mathrm{I}} + J_{\mathrm{II}} + J_{\mathrm{III}} = r_5 + r_7 + r_{12} \tag{300}$$

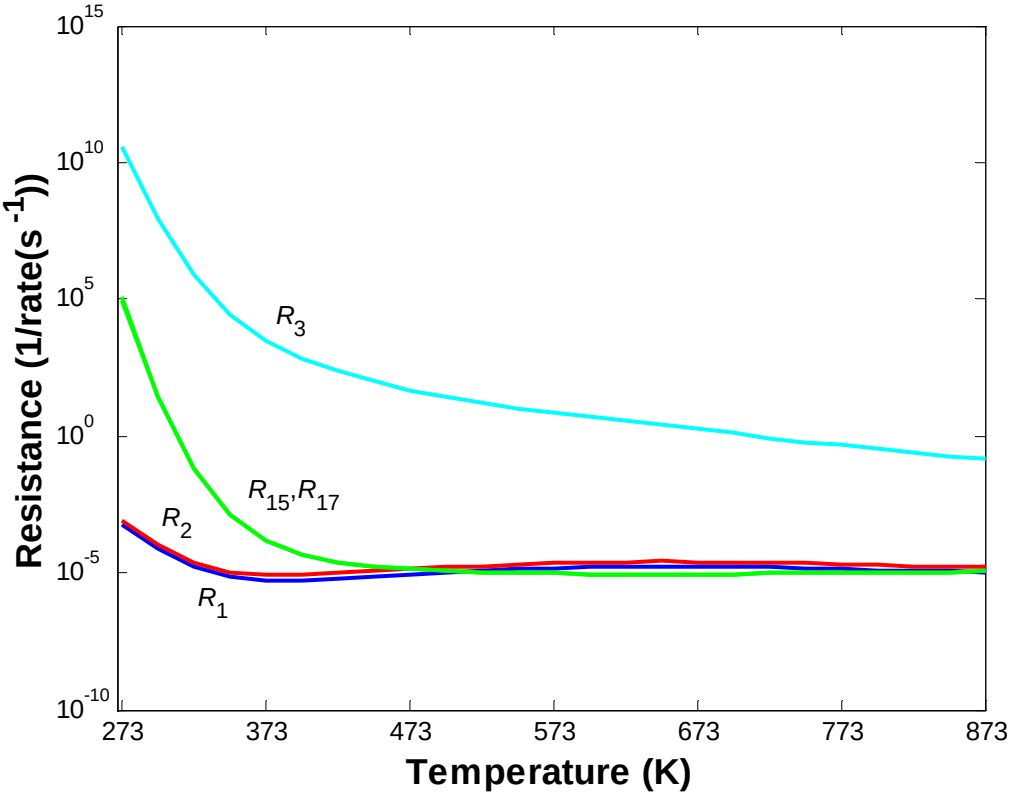

Figure 25. R_1, R_2, R_{15}, R_{17} and R_3 vs. temperature for the following conditions: commercial low temperature shift Cu catalyst loading of 0.14 g/cm^3; total feed flow rate of 236 cm^3 (STP) min^{-1}; residence time τ = 1.8 s; feed composition of H_2O(10%), CO(10%) and N_2(balance).

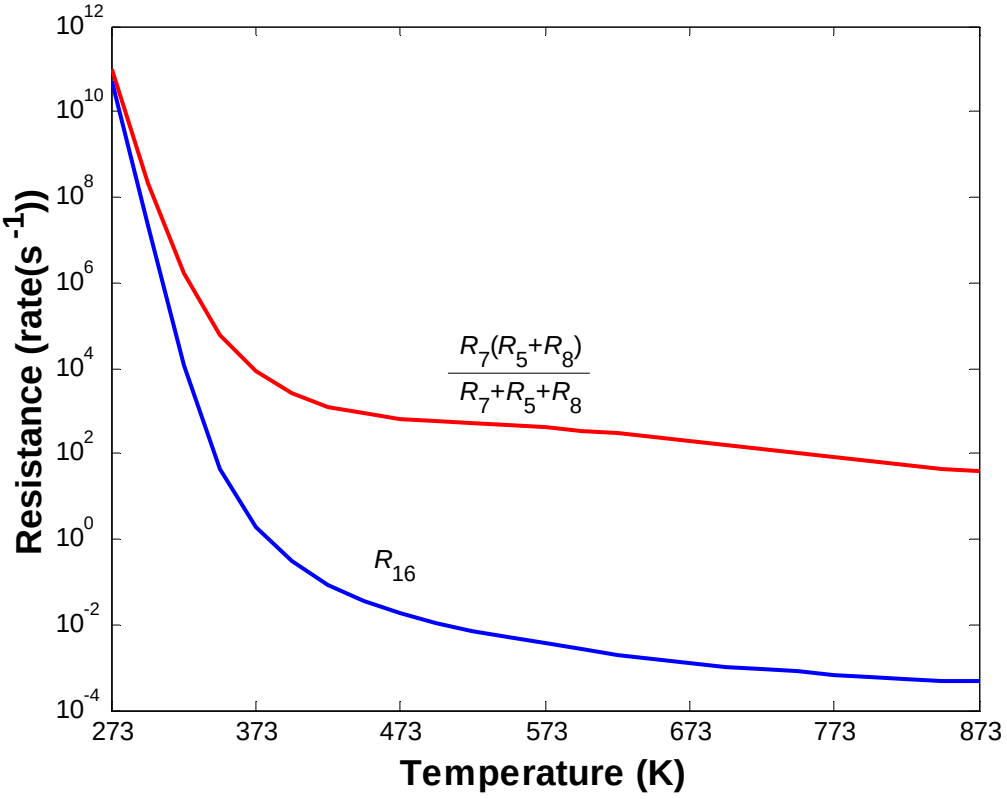

Figure 26. R_4 vs. the resistance of the parallel branch involving R_7, R_5 and R_8 as a function of temperature for the following conditions: commercial low temperature shift Cu catalyst loading of 0.14 g/cm^3; total feed flow rate of 236 cm^3 (STP) min^{-1}; residence time τ = 1.8 s; feed composition of H_2O(10%), CO(10%) and N_2(balance).

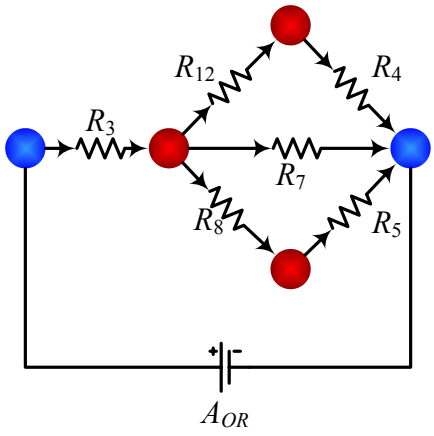

Figure 27. Reduced *RR* graph of the WGSR identifying the rate-limiting elementary reaction steps of the dominant *FR*s.

Table 17. An 11-Step, 3-Route Reduced Mechanism for the WGS reaction.

			RR_{I}	RR_{II}	RR_{III}
s_1:	$CO + S \leftrightarrows CO{\cdot}S$	eq	1	1	0
s_2:	$H_2O + S \leftrightarrows H_2O{\cdot}S$	eq	1	1	1
s_3:	**$H_2O{\cdot}S + S \leftrightarrows OH{\cdot}S + H{\cdot}S$**	**rds**	**1**	**1**	**1**
s_5:	**$CO{\cdot}S + OH{\cdot}S \leftrightarrows HCOO{\cdot}S + S$**	**rds**	**1**	**0**	**0**
s_7:	**$CO{\cdot}S + OH{\cdot}S \leftrightarrows CO_2{\cdot}S + H{\cdot}S$**	**rds**	**0**	**1**	**0**
s_{12}:	**$OH{\cdot}S + H{\cdot}S \leftrightarrows O{\cdot}S + H_2{\cdot}S$**	**rds**	**0**	**0**	**1**
$s_1 + s_{15} + s_4$:	$CO + O{\cdot}S \leftrightarrows CO_2 + S$	eq	0	0	1
s_{15}:	$CO_2{\cdot}S \leftrightarrows CO_2 + S$	eq	0	1	0
$1/2(s_{16} + s_{17})$:	$H{\cdot}S \leftrightarrows 1/2H_2 + S$	eq	1	2	0
s_{17}:	$H_2{\cdot}S \leftrightarrows H_2 + S$	eq	0	0	1
$s_{17}+1/2s_{16}+1/2s_{15} + s_8$:	$HCOO{\cdot}S \leftrightarrows CO_2 + 1/2H_2 + S$	eq	1	0	0
RR_{I}:	$H_2O + CO \leftrightarrows CO_2 + H_2$	$r_{I} = r_5 = \vec{k}_5\theta_{CO{\cdot}S}\theta_{OH{\cdot}S} - \overleftarrow{k}_5\theta_{HCOO{\cdot}S}\theta_0$			
RR_{II}:	$H_2O + CO \leftrightarrows CO_2 + H_2$	$r_{II} = r_7 = \vec{k}_7\theta_{CO{\cdot}S}\theta_{OH{\cdot}S} - \overleftarrow{k}_7\theta_{CO_2{\cdot}S}\theta_{H{\cdot}S}$			
RR_{III}:	$H_2O + CO \leftrightarrows CO_2 + H_2$	$r_{III} = r_{12} = \vec{k}_{12}\theta_{H{\cdot}S}\theta_{OH{\cdot}S} - \overleftarrow{k}_{12}\theta_{O{\cdot}S}\theta_{H_2{\cdot}S}$			

An explicit overall rate equation may be derived next by solving the QSS conditions for the surface intermediates. All of the surface intermediates but OH·S, O·S and HCOO·S may be determined using the quasi-equilibrium approximation. Using the QSS approximation for the above, the final simplified overall rate equations is

$$r_{OR} = \frac{\vec{k}_3 K_2 P_{H_2O} \theta_0^2 \left[(\vec{k}_5 + \vec{k}_7) K_1 P_{CO} + \vec{k}_{12} \frac{P_{H_2}^{1/2}}{(K_{16} K_{17})^{1/2}} \frac{\vec{k}_6 K_2 K_{12} K_{17} P_{CO}}{\vec{k}_4 K_2 K_{12} K_{17} P_{CO} + \vec{k}_{12} P_{H_2}} \right]}{\left[\frac{\vec{k}_3}{K_3} + \vec{k}_{12} \left(\frac{\vec{k}_4 K_2 K_{12} K_{17} P_{CO}}{\vec{k}_4 K_2 K_{12} K_{17} P_{CO} + \vec{k}_{12} P_{H_2}} \right) \right] \frac{P_{H_2}^{1/2}}{(K_{16} K_{17})^{1/2}} + (\vec{k}_5 + \vec{k}_7) K_1 P_{CO}} \left(1 - \frac{P_{CO_2} P_{H_2}}{K P_{H_2O} P_{CO}} \right) \tag{301}$$

The error in the conversion of CO provided by this overall rate equation is virtually zero as compared with the exact microkinetic model (excluding s_{10} and s_{13}), which points to the robustness of the reaction network analysis and reduction approach presented here.

In addition to deriving a rate expression from the more conventional approximations, the rate may also be developed from the resistance of the *OR* as given by Equation (297). Recall that the rate is given by the ratio of the dimensionless affinity to the resistance of the reaction, elementary or overall. Thus, after substitution, Equation (298) may be used to derive the rate expression using the interrelations of the affinities and appropriate expressions for the rates of the elementary reaction steps as indicated by Equation (179). Figure 27 may also be used to derive a rate expression based solely on the identified RLSs. A similar methodology to that used in Section 6.5 may be applied, thus reducing the complexity of the initial rate expression as compared with Equation (299). Furthermore, the evaluation of the net resistance of either the simplified *RR* network (Figure 19d) or the reduced *RR* network (Figure 27) may be used directly with the corresponding overall affinity to predict the rate numerically, without the intermediate derivation of a rate expression according to $r_{OR} = \mathcal{A}_{OR} / R_{OR}$.

Using the same procedure as described above for copper, the kinetics of the WGS reaction on both iron and nickel were considered. The parallel pathway resistances comparisons for these metals are given in Figure 28 and Figure 29, respectively, based on the energetics provided in Table 18.

Table 18. Energetics of the WGS mechanism for Cu(111), Ni(111) and Fe(110) catalysts calculated from the transition-state theory (pre-exponetial factors) and the UBI–QEP method (activation energies).

	Pre-Exponential Factors		Activation Energies					
			Cu(111)		Ni(111)		Fe(110)	
	Forward	*Reverse*	*Forward*	*Reverse*	*Forward*	*Reverse*	*Forward*	*Reverse*
s_1	1.50E+06	1.00E+14	0	12	0	27	0	32
s_2	1.00E+06	1.00E+14	0	13.6	0	16.5	0	17.2
s_3	1.00E+13	1.00E+13	25.4	1.6	20.8	10.2	19.9	12
s_4	1.00E+13	1.00E+13	10.7	28	21.9	13.4	25.2	9.1
s_5	1.00E+13	1.00E+13	0	20.4	5.5	13.2	9	12.2
s_6	1.00E+13	1.00E+13	15.5	20.7	12.8	27.9	12.4	29.1
s_7	1.00E+13	1.00E+13	0	22.5	6.1	12.7	10.3	10.9
s_8	1.00E+13	1.00E+13	1.4	3.5	3.5	2.4	4.4	1.8
s_9	1.00E+13	1.00E+13	4	0.9	16.2	0	19.3	0
s_{10}	1.00E+13	1.00E+13	29	0	28.1	2.4	28.1	3.5
s_{11}	1.00E+13	1.00E+13	26.3	0	25.8	0	24.8	0
s_{12}	1.00E+13	1.00E+13	1.3	4	3.3	3.2	3.4	3.2
s_{13}	1.00E+13	1.00E+13	0.9	26.8	11.6	21.1	14.4	19.7
s_{14}	1.00E+13	1.00E+13	14.6	14.2	24.8	8.5	26.9	7.4
s_{15}	4.00E+12	1.00E+06	5.3	0	6.5	0	6.9	0
s_{16}	1.00E+13	1.00E+13	15.3	12.8	23.4	8.2	24.5	7.6
s_{17}	6.00E+12	1.00E+06	5.5	0	6.8	0	7.1	0
s_{18}	6.00E+12	1.00E+06	15.3	7.3	23.4	1.4	24.5	0.5

In the case of Fe, we find similar results with some differences. For example, here, simulations suggest that s_7 may be eliminated through comparison of the complete mechanism to that less s_7 as discussed in the Cu analysis. Furthermore, we note that, in the *ER* $s_{16} + s_{17} - s_{18} = 0$, the resistances, again, are close in magnitude. However, we have a crossover near ~500°C. At this point, however, the reaction has reached thermodynamic equilibrium, thus, s_{18} may still be removed from the mechanism. This is confirmed through the kinetic comparison. As in the case of Cu, we find that s_6, s_9, s_{10}, s_{11}, s_{13} and s_{14} may also be removed from the mechanism. As a result of this analsyis, the same rate expression as Cu may be used to predict the kinetics of the WGS reaction on Fe.

After consideration of the resistances on a Ni catalyst, Figure 29, we find that the same elementary steps eliminated in the case of the Cu catalyst may be eliminated here. As a result, we find that there is a single rate expression that will predict the kinetics of the overall WGS reaction for all of these metals.

This analysis may also be used to determine trends in catalytic activity of a series of catalysts. Using the same set of input parameters, i.e., catalyst properties and feed conditions, Figure 30 illustrates the trends determined by our microkinetic model. Based on the simulations presented, we find that Cu is an appropriate LTS catalyst while Fe, Ru, Rh, Pd and Pt are valuable HTS catalysts. The Ni catalyst shows activity in an intermediate temperature range. The Ag and Au catalyst show no activity within the temperature range examined in this research. However, it should be noted that the simulations in Figure 30 assume negligible supplemental activity from the catalyst's support. Other researchers have shown that Au has sufficient activity for the WGS reaction when incorporated on more active supports, i.e., CeO_2 [140]. In summary, the activity trend observed from the simulations suggests that the Cu > Ni > Fe > Ru > Rh > Pd > Pt > Ag, Au.

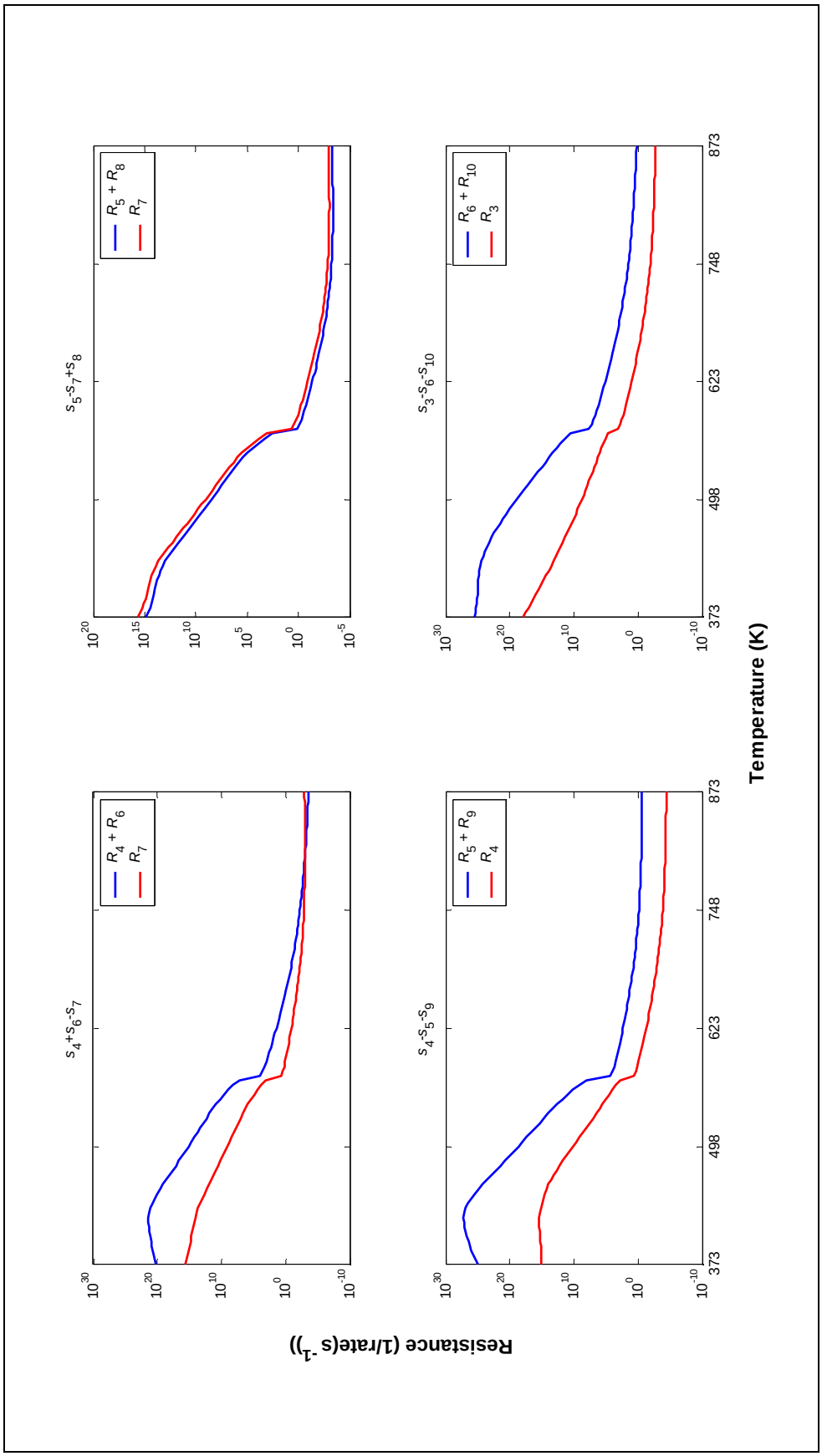

Figure 28. Parallel pathway resistance comparisons as a function of temperature for the following conditions: low temperature shift Fe catalyst density of 1.12 g/cm^3; total feed flow rate of 100 cm^3 (STP) min^{-1}; residence time τ = 1.34 s; feed composition of H_2O(10%), CO(10%) and N_2(balance)

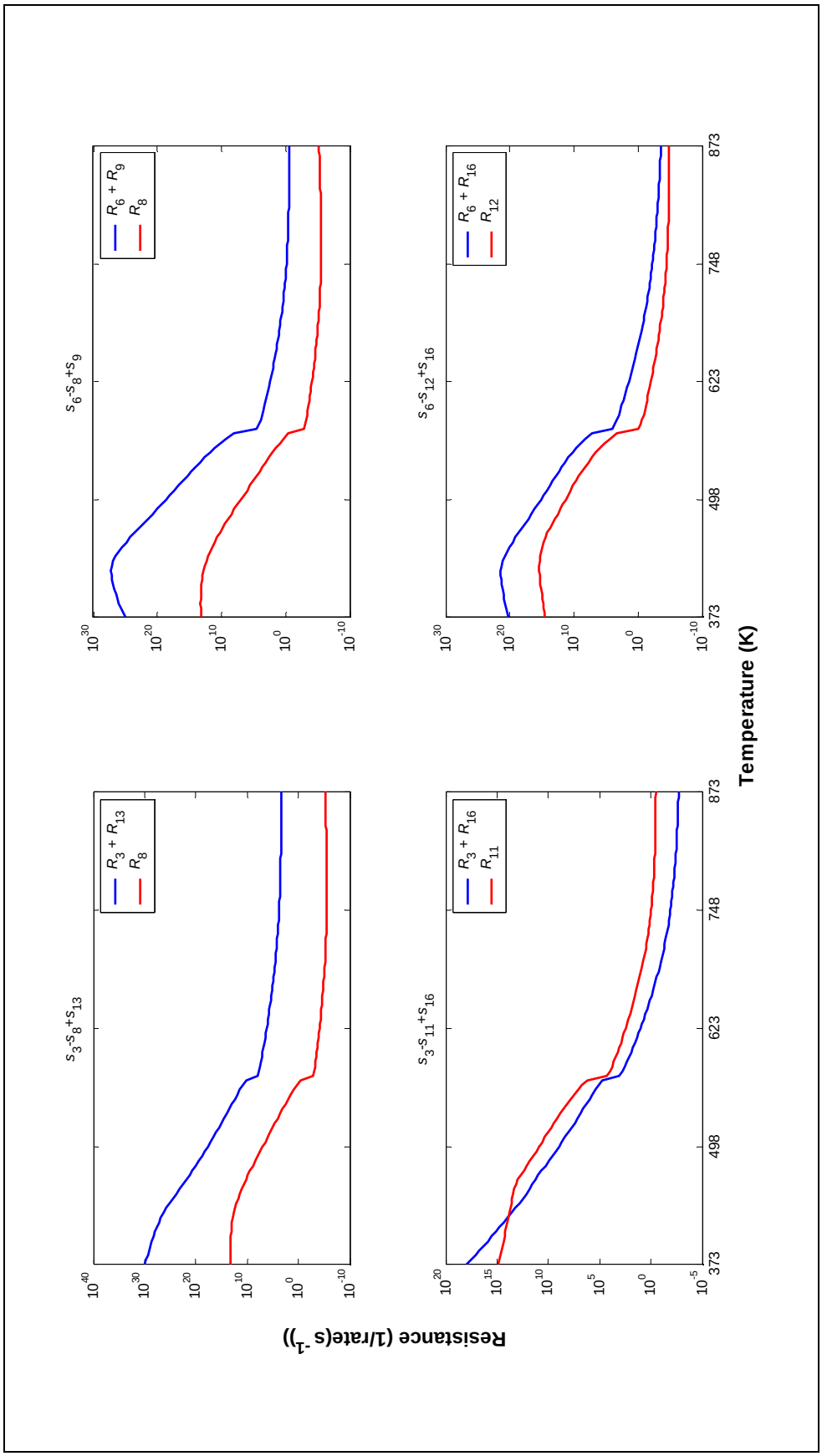

Figure 28. Parallel pathway resistance comparisons as a function of temperature for the following conditions: low temperature shift Fe catalyst density of 1.12 g/cm^3; total feed flow rate of 100 cm^3 (STP) min^{-1}; residence time τ = 1.34 s; feed composition of H_2O(10%), CO(10%) and N_2(balance) *(continued)*

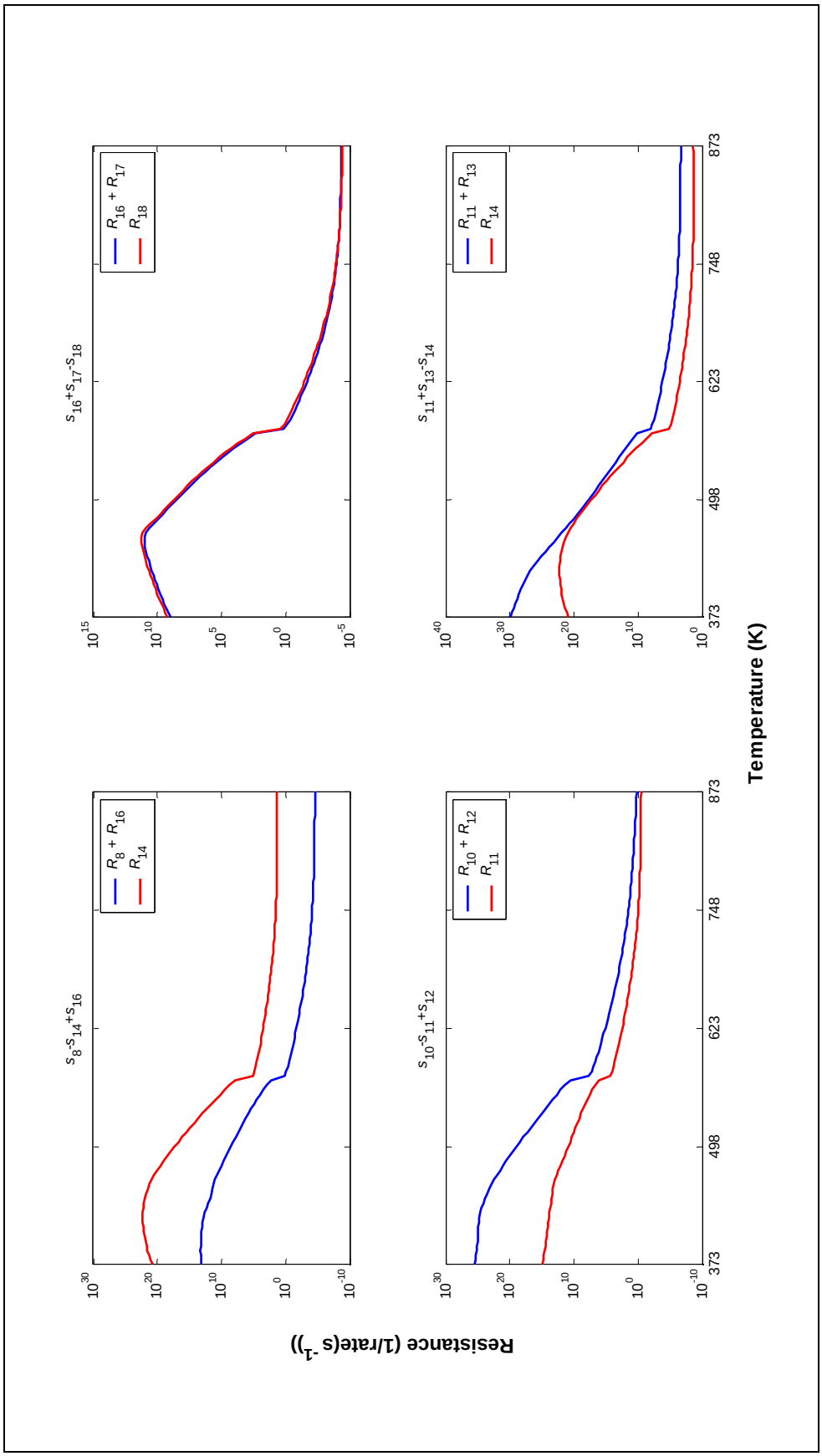

Figure 28. Parallel pathway resistance comparisons as a function of temperature for the following conditions: low temperature shift Fe catalyst density of 1.12 g/cm^3; total feed flow rate of 100 cm^3 (STP) min^{-1}; residence time τ = 1.34 s; feed composition of H_2O(10%), CO(10%) and N_2(balance) *(continued)*

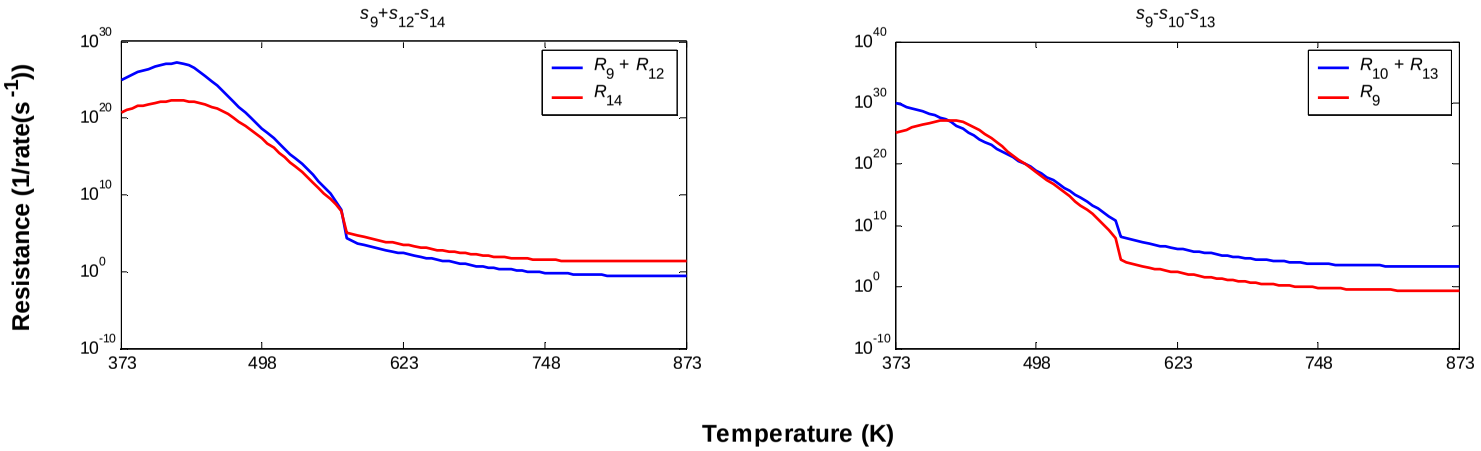

Figure 28. Parallel pathway resistance comparisons as a function of temperature for the following conditions: low temperature shift Fe catalyst density of 1.12 g/cm^3; total feed flow rate of 100 cm^3 (STP) min^{-1}; residence time τ = 1.34 s; feed composition of H_2O(10%), CO(10%) and N_2(balance) *(continued)*

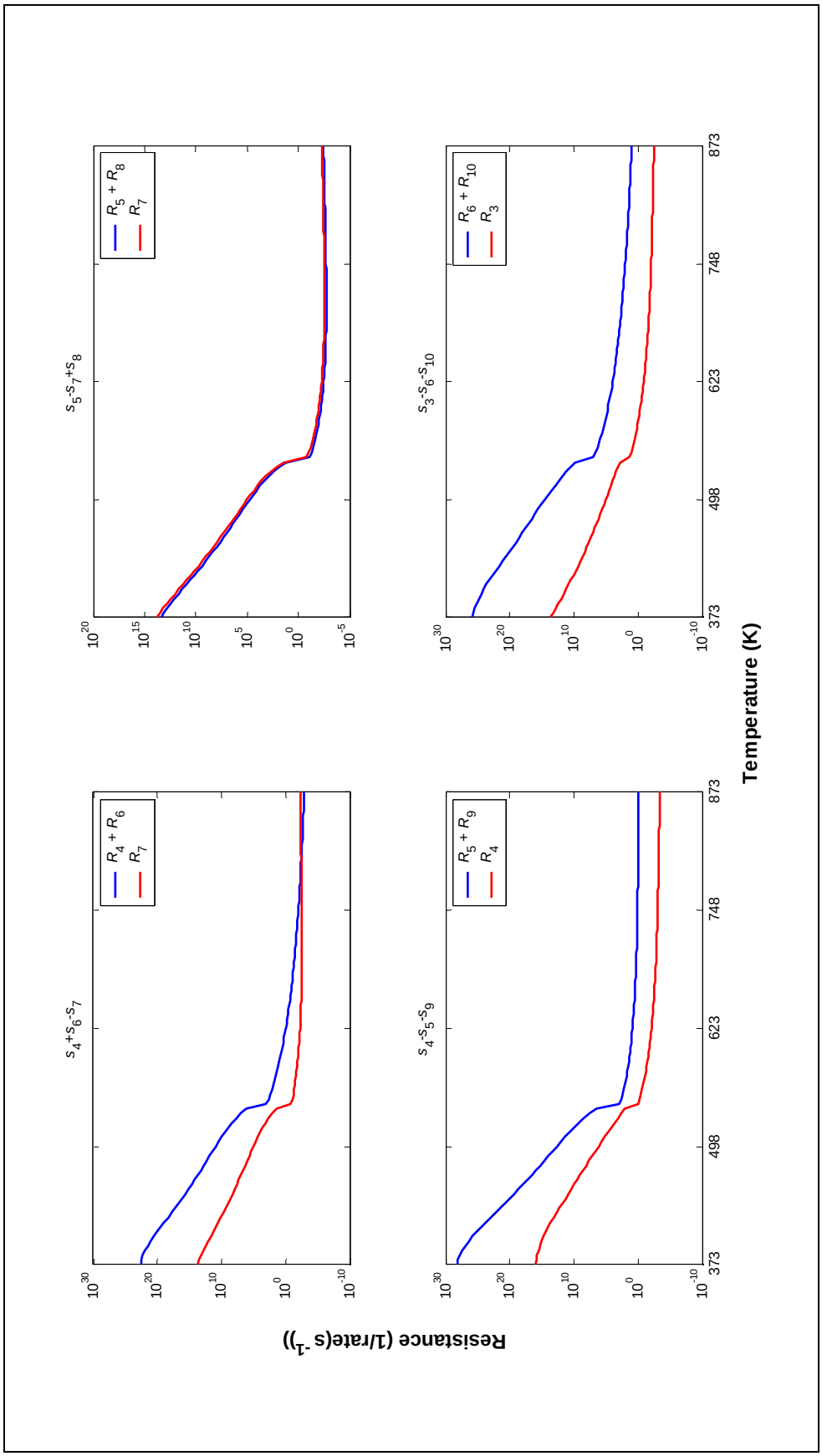

Figure 29. Parallel pathway resistance comparisons as a function of temperature for the following conditions: low temperature shift Ni catalyst loading of 0.13 g/cm^3; total feed flow rate of 479 cm^3 (STP) min^{-1}; residence time τ = 0.89 s; feed composition of H_2O(10%), CO(10%) and N_2(balance)

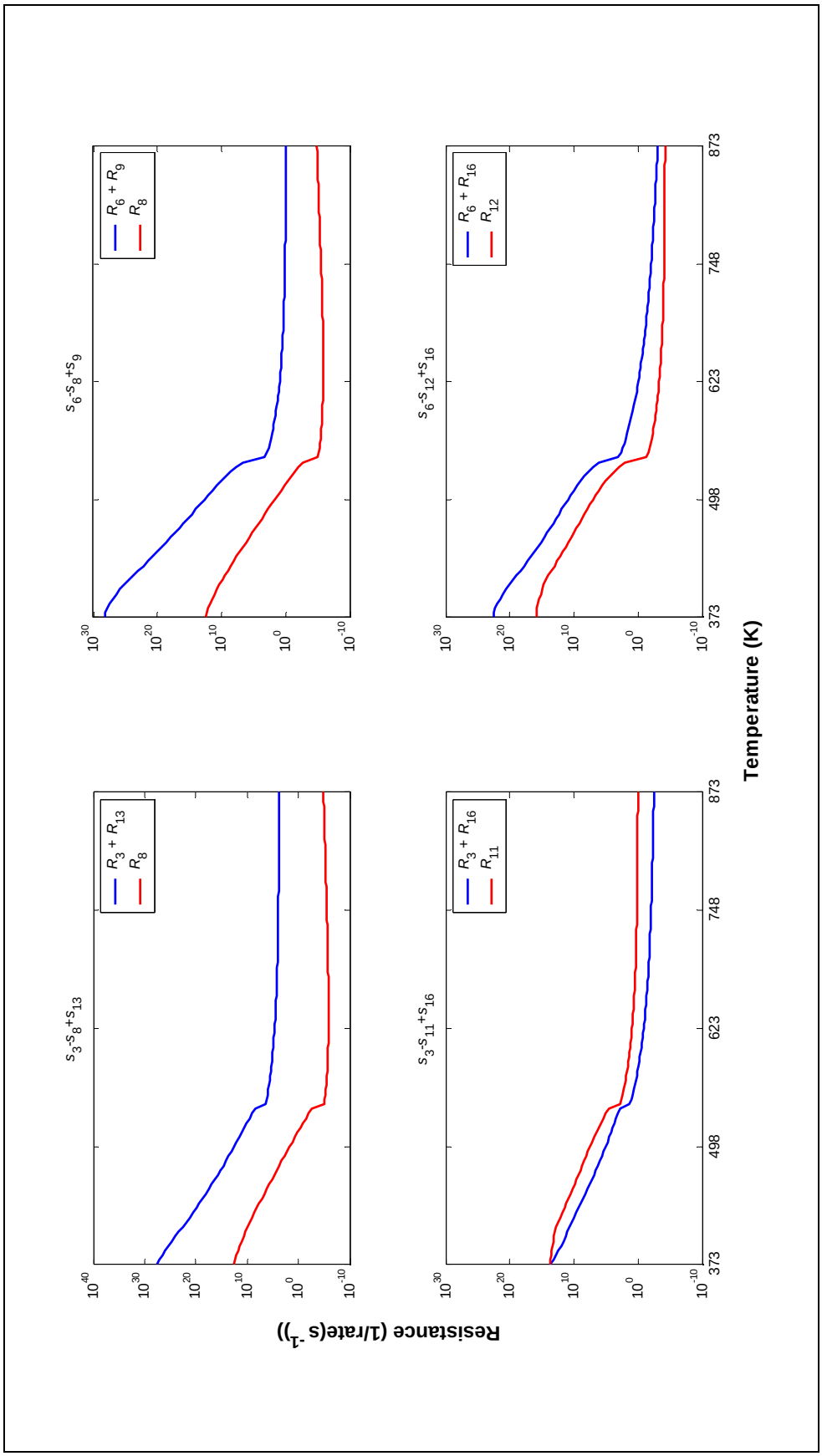

Figure 29. Parallel pathway resistance comparisons as a function of temperature for the following conditions: low temperature shift Ni catalyst loading of 0.13 g/cm^3; total feed flow rate of 479 cm^3 (STP) min^{-1}; residence time τ = 0.89 s; feed composition of H_2O(10%), CO(10%) and N_2(balance) *(continued)*

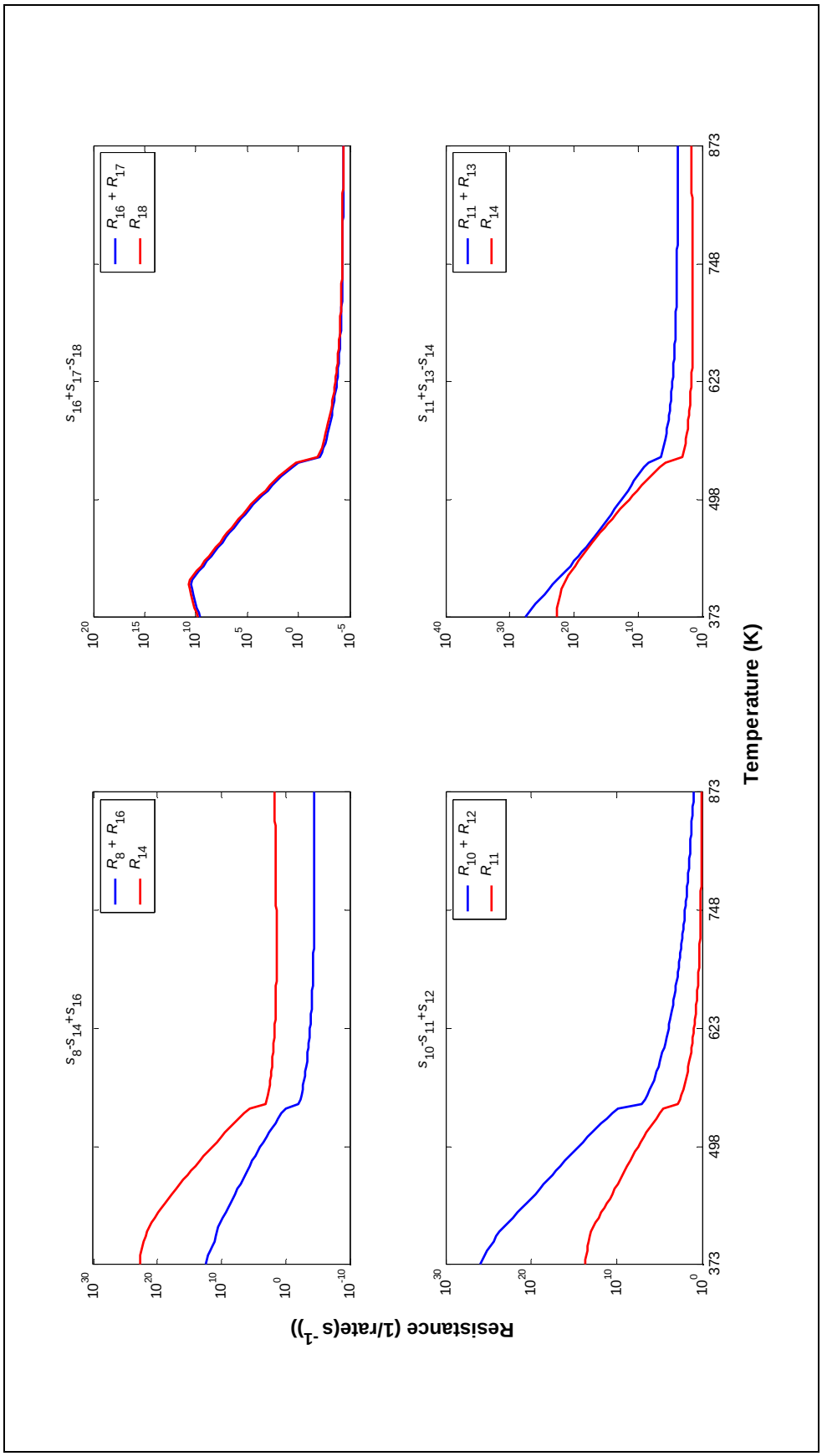

Figure 29. Parallel pathway resistance comparisons as a function of temperature for the following conditions: low temperature shift Ni catalyst loading of 0.13 g/cm^3; total feed flow rate of 479 cm^3 (STP) min^{-1}; residence time τ = 0.89 s; feed composition of H_2O(10%), CO(10%) and N_2(balance) *(continued)*

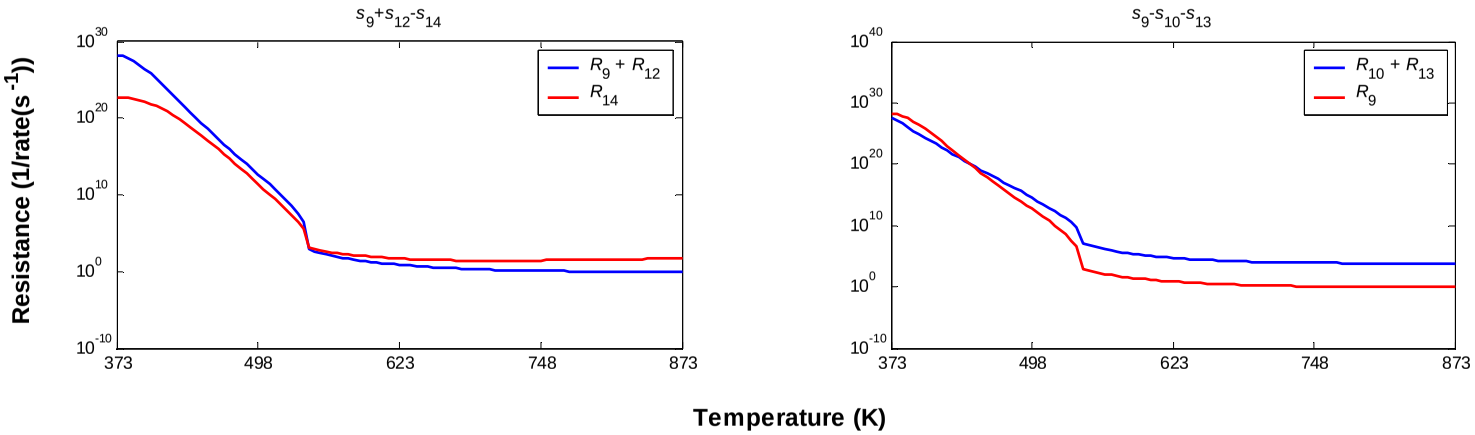

Figure 29. Parallel pathway resistance comparisons as a function of temperature for the following conditions: low temperature shift Ni catalyst loading of 0.13 g/cm^3; total feed flow rate of 479 cm^3 (STP) min^{-1}; residence time τ = 0.89 s; feed composition of H_2O(10%), CO(10%) and N_2(balance) *(continued)*

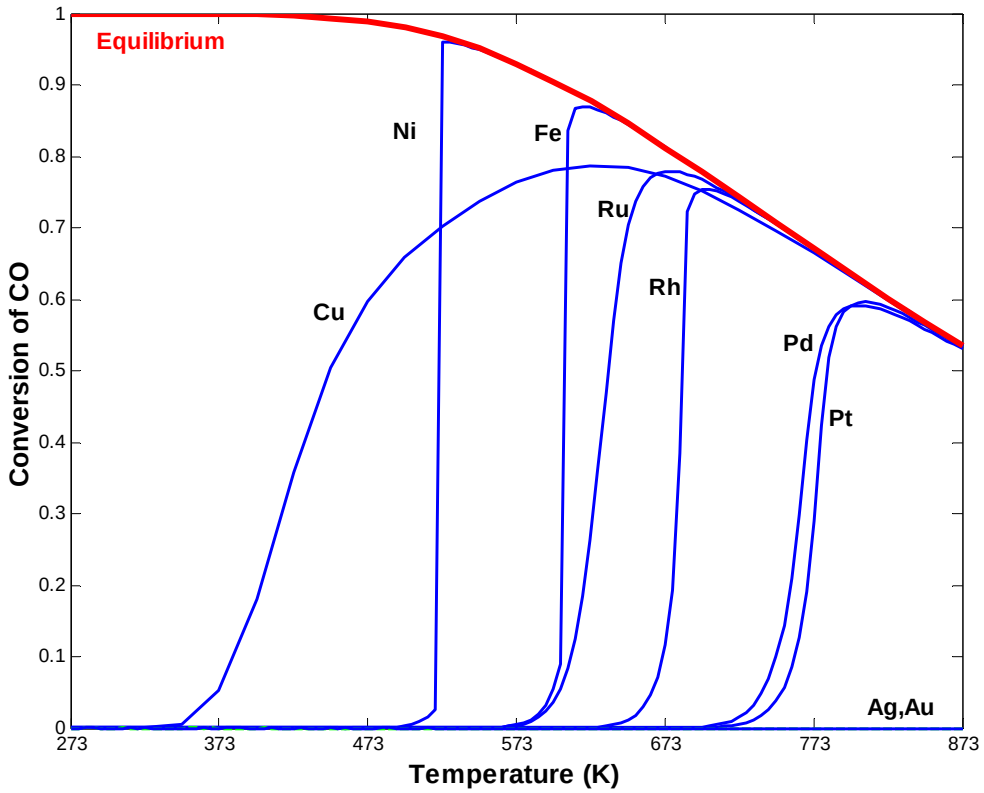

Figure 30. Trends in the transition metal catalysts tested for a given set of input conditions, i.e., catalyst properties and feed conditions: catalyst loading 0.14 g/cm^3; total flow rate of 236 cm^3 (STP) min^{-1}; residence time τ = 1.8 s; feed composition of H_2O(10%), CO(10%) and N_2(balance)

6.8. Reaction Orders

The reduced microkinetic mechanism provides an easy way to derive analytical expressions for reaction orders. By definition, the reaction orders are given by

$$\delta_i = \left(\frac{\partial \ln \vec{r}}{\partial \ln P_i} \right)_{T, P_{j \neq i}} \tag{302}$$

However, the net rate does not take the general form

$$\vec{r}_\rho = \vec{k}_\rho \prod_{i=1}^{n} P_i^{\beta_{\rho i}} \prod_{k=1}^{q} \theta_k^{\alpha_{\rho k}} \tag{303}$$

We can force it to have this form if we allow the reaction orders δ_i to depend on the reaction conditions. As a result, the reaction orders are related by Equation (302). It is important to consider $\vec{r}$ and not r because r contains a contribution from the reverse rate $\overleftarrow{r}$. Because the overall reaction does not take the form given by Equation (303), the reaction order is not related to the stoichiometry of the net overall reaction.

Recalling Equation (300), which derives from the quasi-steady-state balance of the OH·S species, the forward rate of the overall reaction may be approximated by

$$\vec{r}_\rho = \vec{r}_3 = \vec{k}_3 \theta_{\mathrm{H_2O{\cdot}S}} \theta_{\mathrm{o}} \tag{304}$$

A straightforward evaluation of the derivative given by Equation (302), as applied to Equation (304), yields the following simple expressions for reaction orders.

$$\delta_{\mathrm{H_2O}} = 1 - 2\theta_{\mathrm{H_2O{\cdot}S}} \tag{305}$$

$$\delta_{\mathrm{CO}} = -2\theta_{\mathrm{CO{\cdot}S}} + 2\theta_{\mathrm{O{\cdot}S}} + 2\theta_{\mathrm{OH{\cdot}S}} \tag{306}$$

$$\delta_{\mathrm{CO_2}} = -2\theta_{\mathrm{CO_2{\cdot}S}} - 2\theta_{\mathrm{O{\cdot}S}} - 2\theta_{\mathrm{OH{\cdot}S}} - 2\theta_{\mathrm{HCOO{\cdot}S}} \tag{307}$$

$$\delta_{\mathrm{H_2}} = -2\theta_{\mathrm{H_2{\cdot}S}} - \theta_{\mathrm{H{\cdot}S}} - \theta_{\mathrm{OH{\cdot}S}} - \theta_{\mathrm{HCOO{\cdot}S}} \tag{308}$$

As can be seen, the reaction order of H_2O is always positive and cannot exceed 1 unless $\theta_{H_2O\cdot S} > 0.5$. The reaction order of CO is positive if

$$\theta_{CO\cdot S} < \theta_{O\cdot S} + \theta_{OH\cdot S}$$

The microkinetic mechanism shows (Figure 31) that this inequality is satisfied on Cu(111) at higher temperatures and, hence, δ_{CO} is positive. Yet, the absolute value of δ_{CO} is small because $\theta_{CO\cdot S}$ on Cu(111) is low. On the other hand, the reaction orders of CO_2 and H_2 are always negative although, again, their absolute values are small because of the low values of $\theta_{CO_2\cdot S}, \theta_{H_2\cdot S}, \theta_{H\cdot S}, \theta_{O\cdot S}, \theta_{OH\cdot S}$ and $\theta_{HCOO\cdot S}$ (Figure 31). These conclusions are in satisfactory agreement with the experimental data collected from the literature (Figure 31).

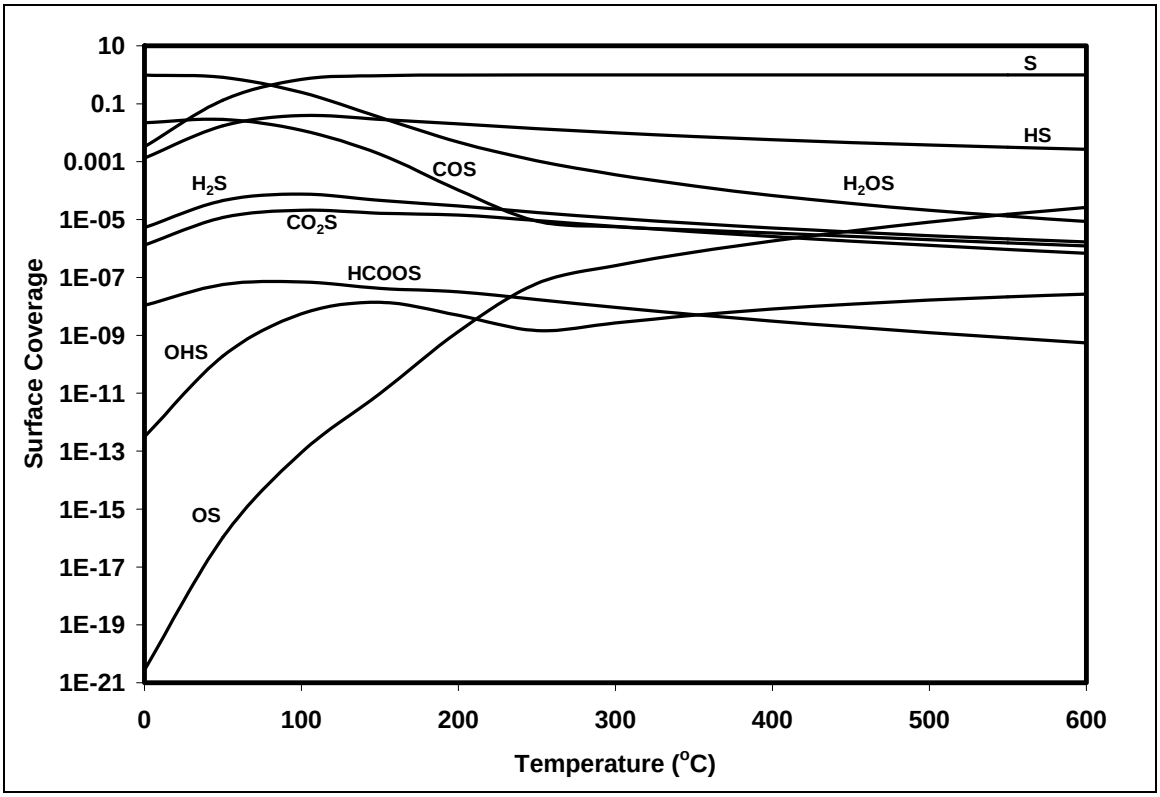

Figure 31. Surface intermediates distribution as a function of temperature.

Table 19. Experimental reaction orders for WGS reaction on various Cu catalysts

Catalyst	Reaction Orders				Ref.
	CO	H_2O	CO_2	H_2	
$CuO/ZnO/Al_2O$	1.0	1.4	−0.7	−0.9	[14]
$CuO/ZnO/Al_2O_3$	0.8	0.8	−0.9	−0.9	[141]
10% Cu/Al_2O_3	0.30	0.38	–	–	[45]
CuO/CeO_2	0-1	1-0	–	–	[38]
$CuO/ZnO/Al_2O_3$	0.2	0.6	0	0	[67]
CuO–ZnO (ICI 52-1)	0.45	0.07	–	–	[142]
Cu(111)	0	0.5–1	–	–	[50]
Cu(110)	0	1	–	–	[8,143]

Chapter 7. Experiments

Both integral and differential experiments were conducted to validate the microkinetic model developed in the previous chapter. The experiments were designed such that the WGS reaction could be examined in both the forward and reverse directions, i.e., only CO and H_2O or CO_2 and H_2 in the feed, respectively. In addition, an intermediate feed condition was considered involving all four terminal species. Testing the catalyst under various conditions broadens the range under which the model is valid. The intermediate feed condition also permitted the comparison of experimentally determined reaction orders to those predicted by the model.

The integral experiments were conducted over specific temperature ranges corresponding to known regions of activity for each catalyst, i.e., LTS and HTS. The differential experiments were conducted under conditions that provided conversions sufficiently far from equilibrium and greater than zero to ensure that variations in the feed composition would not achieve either extreme.

Both inlet and outlet compositions were measured using gas chromatography. The results were used to calculate a conversion for comparison with the microkinetic model prediction. Details of the experimental apparatus and procedure, as well as calibrations, follow.

7.1. Apparatus

The reactor apparatus designed and constructed for this study is given in Figure 32. The reactor was constructed using 1/8-inch SS tubing and corresponding SS Swagelok® fittings. A bypass was introduced to the system to allow for the sampling of inlet feed conditions without catalyst interference. The flow lines (tubing) were wrapped, first, with conventional fiberglass-enclosed heating tape, then with insulating tape to prevent heat dissipation and better maintain line temperatures. Type K thermocouples

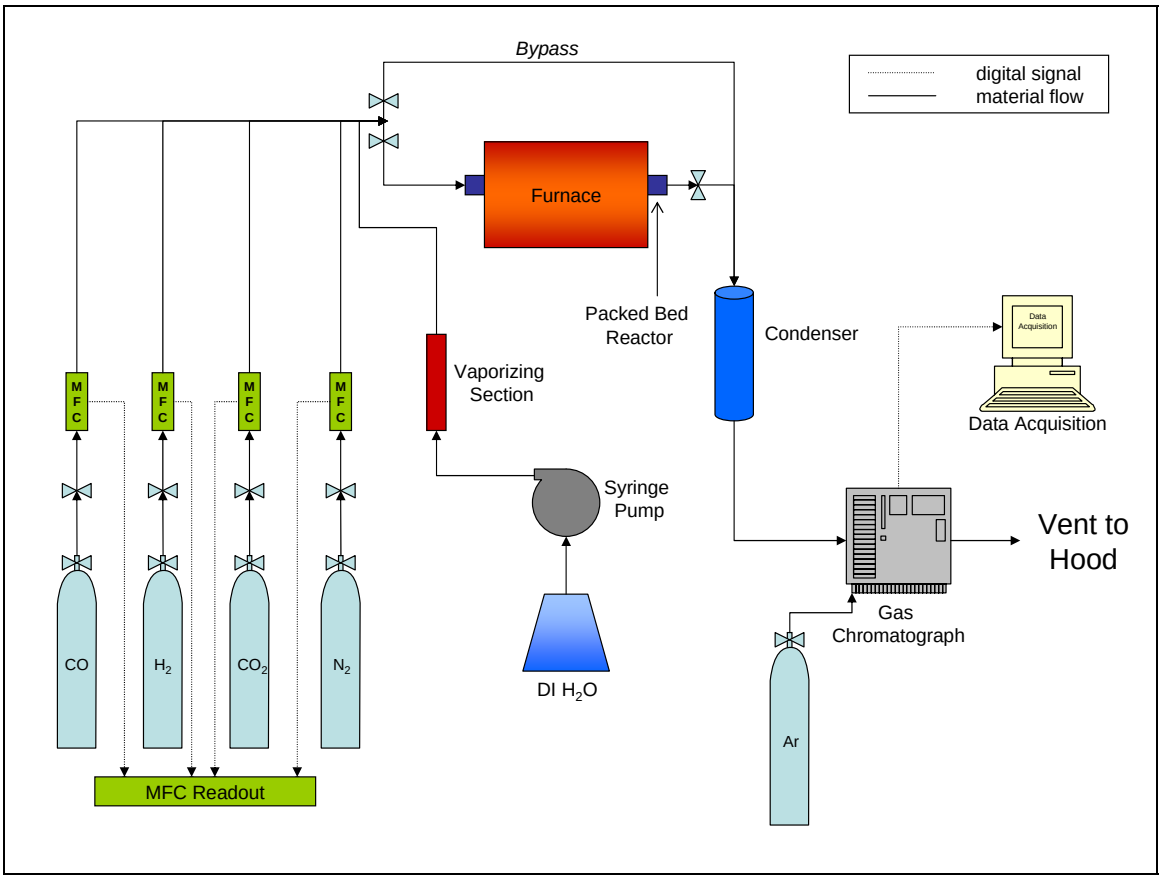

Figure 32. Reactor apparatus flowsheet.

were installed throughout the lines by weaving the probe between the insulating tape and the heating tape to measure the line temperatures. A pressure gauge (Ashcroft Test Gauge, 0-100 psi range, model #Q-4907) was installed prior to the reactor to monitor the system pressure.

A Lindberg/Blue M single-zone tube furnace (model #TF55035A-1, upper temperature limit 1100^{o}C) was used to establish and maintain the catalyst bed temperature in the reactor. The packed bed reactor consisted of an 18 inch long, 0.75 inch OD (0.625 inch ID) SS tube in which a 1-2 inch catalyst bed was centered, positioned by 1-2 inches of fiberglass packing as described below. The bed temperature was monitored using an 18-inch type K thermocouple inserted into the middle of the catalyst bed through the end of the reactor (See Figure 33).

Hydrogen, carbon monoxide, carbon dioxide, and nitrogen were fed to the reactor at desired flow rates using MKS 1179 mass flow controllers and MKS 247-C mass flow controller readout boxes. Water was pumped into the system via an ISCO Model 100D syringe pump and passed through a heating zone to vaporize the liquid water. The feed stream was then passed through the packed bed reactor which consisted of a section of 8 micron fiberglass material, used to ensure proper mixing of the feed gases, the catalyst, and another section of fiberglass material.

After reaction, the liquid water in the product stream was condensed out using a conventional condenser surrounded by an ice bed prior to composition analysis. The dry gases then proceeded to the SRI Instruments 8610C Gas Chromatograph (GC) through a Carboxen 1000 column at a temperature of 125^{o}C where their concentrations were measured and collected by the data acquisition system. The data acquisition system consists of a PC computer and PeakSimple analysis software which automates the calculation of the GC peak areas. Four samples were analyzed for each reaction feed condition at each bed temperature. The inlet valve of the GC was held open for 30 seconds allowing the sample to enter; the chromatogram was complete after 15 minutes. A 2-minute wait period was allowed between repeated injections. The data were then used to validate the derived microkinetic models.

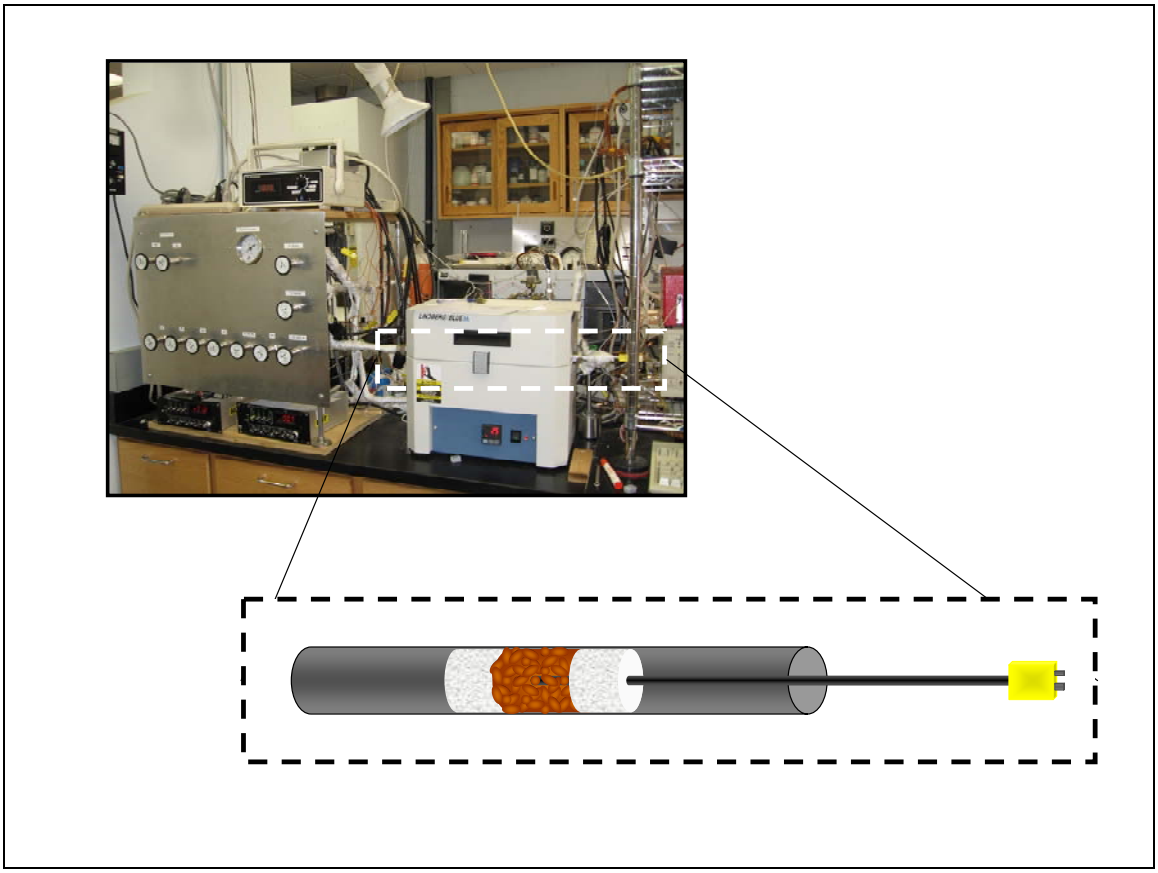

Figure 33. Photograph of the reactor setup with a schematic of the packed bed thermocouple insertion.

7.2. Reaction Conditions

Three different reaction conditions were tested for each catalyst (see Table 20). The first reaction condition was chosen to ensure the forward WGS reaction occurred, while the second was intended for the reverse WGS reaction. The third reaction condition was chosen such that the effect of each of the gases, both products and reactants, could be measured. Reaction condition 3 was adapted from Reference [39] such that the initial experimental results could be compared to existing literature.

Reaction order experimental feed conditions are presented in Table 21. The conditions were chosen to represent differences over a broad range, but within the calibration limits of the mass flow controllers and pump.

7.3. Calibrations

The mass flow controllers were calibrated in the range of flow necessary for the desired feed conditions. Actual flow rates were measured with an Alltech Digital Flow Bubble Meter (Model 4068) and compared to the MKS 247C readout values for each gas. Their respective potentiometers were adjusted to match the actual flow and calibration data collected. The resulting calibration plots are presented in Appendix F.

The ISCO syring pump was calibrated using timed intervals of measured flow. The pump was calibrated in the range of liquid water needed to achieve the reaction conditions. The plotted calibration data is also presented in Appendix F.

The gas chromatograph calibrations were performed using a constant flow rate of 100 sccm comprised of different concentrations of individual gas phase species balanced with inert nitrogen. Plots relating the ratio volume of gas species:volume of nitrogen to the ratio of their respective peak areas were generated and used to extract the "real" values of product stream composition from experimental chromatogram data. These calibration plots are shown in Appendix F.

Table 20. Experimental reactor feed conditions.

Reaction Condition	Volume %				
	CO	**H_2O**	**CO_2**	**H_2**	**N_2**
1	0.10	0.10	0.00	0.00	0.80
2	0.00	0.00	0.10	0.10	0.80
3	0.15	0.20	0.05	0.05	0.55

Table 21. Experimental reaction order feed conditions (volume %) and corresponding mass flow controller (mfc) set points.

Δ	N_2	**CO**	H_2O	CO_2	H_2	mfc (N_2)	mfc (CO)	pump (H_2O)	mfc (CO_2)	mfc (H_2)
1	0.55	**0.15**	0.20	0.05	0.05	53.3	15.3	0.01582	5.7	5.1
0.75	0.59	**0.11**	0.20	0.05	0.05	57.0	11.5	0.01582	5.7	5.1
1.5	0.48	**0.23**	0.20	0.05	0.05	45.7	22.9	0.01582	5.7	5.1
1.75	0.44	**0.26**	0.20	0.05	0.05	42.0	26.8	0.01582	5.7	5.1
1.25	0.51	**0.19**	0.20	0.05	0.05	49.5	19.1	0.01582	5.7	5.1

Δ	N_2	CO	**H_2O**	CO_2	H_2	mfc (N_2)	mfc (CO)	pump (H_2O)	mfc (CO_2)	mfc (H_2)
1	0.55	0.15	**0.20**	0.05	0.05	53.3	15.3	0.01582	5.7	5.1
1.5	0.45	0.15	**0.30**	0.05	0.05	43.2	15.3	0.02373	5.7	5.1
1.75	0.40	0.15	**0.35**	0.05	0.05	38.2	15.3	0.02768	5.7	5.1
1.25	0.50	0.15	**0.25**	0.05	0.05	48.3	15.3	0.01977	5.7	5.1

Δ	N_2	CO	H_2O	**CO_2**	H_2	mfc (N_2)	mfc (CO)	pump (H_2O)	mfc (CO_2)	mfc (H_2)
1	0.55	0.15	0.20	**0.05**	0.05	53.3	15.3	0.01582	5.7	5.1
0.75	0.56	0.15	0.20	**0.04**	0.05	54.5	15.3	0.01582	4.3	5.1
1.5	0.53	0.15	0.20	**0.08**	0.05	50.8	15.3	0.01582	8.6	5.1
1.75	0.51	0.15	0.20	**0.09**	0.05	49.5	15.3	0.01582	10.0	5.1
1.25	0.54	0.15	0.20	**0.06**	0.05	52.0	15.3	0.01582	7.2	5.1

Δ	N_2	CO	H_2O	CO_2	**H_2**	mfc (N_2)	mfc (CO)	pump (H_2O)	mfc (CO_2)	mfc (H_2)
1	0.55	0.15	0.20	0.05	**0.05**	53.3	15.3	0.01582	5.7	5.1
0.75	0.56	0.15	0.20	0.05	**0.04**	54.5	15.3	0.01582	5.7	3.9
1.5	0.53	0.15	0.20	0.05	**0.08**	50.8	15.3	0.01582	5.7	7.7
1.75	0.51	0.15	0.20	0.05	**0.09**	49.5	15.3	0.01582	5.7	9.0
1.25	0.54	0.15	0.20	0.05	**0.06**	52.0	15.3	0.01582	5.7	6.4

7.4. Experimental Procedure

The line temperatures were maintained at temperatures above 130^{o}C to prevent condensation of the water vapor. The vaporizing section and gas preheating section were held above 300^{o}C. The temperatures were monitored using a series of strategically positioned, i.e., located at the inlet and outlet as well as incrementally along the lines, type-K thermocouples and a compatible multi-channel readout (Omega Monogram, 10-channel model #DPH6-KC) to display the temperatures. The bed was packed with 8 micron fiberglass followed by approx. 7 cm^3 of catalyst and then a final section of fiberglass. The catalyst particles were sized to 12-18 mesh and dispersed with silicon dioxide particles of similar sizes to achieve the total bed volume. In the case of the precious metals, the catalyst particles were 1/8 in cylindrical pellets and of sufficient size that they did not require further reduction of size or the use of dispersion material. The catalyst was reduced using a 3% H_2/N_2 mixed gas flowing at 100 sccm. The reactor temperature was raised slowly from over a 250-300^{o}C temperature range during a 10-12 hour period, depending on the catalyst used (i.e., high temperature catalyst or low temperature catalyst).

The reacting gases were sent through the system's bypass, with the reactor section closed off, and sampled to establish GC data corresponding to the inlet conditions. The bypass was then closed forcing the gases to flow through the opened reactor section. The gases were allowed to flow for approx. 15-30 minutes to flush out any residual reducing gas before GC sampling began and reaction data were collected. The temperatures monitored by the thermocouples, as well as the catalyst bed temperature, were documented for each GC sample initiation. The GC data files were tracked and recorded along with their corresponding chromatograph results.

While running experiments over the course of more than one day, when the reactor was idle (e.g. no experiments were running), the catalyst was maintained under the 3% H_2/N_2 reducing gas to prevent air from entering the system. The reactor bed temperature was lowered to 200^{o}C (or less) to reduce the heating time and temperature surge when restarting experiments the following day.

7.5. Catalysts

Seven different catalysts were considered for experimentation (see Table 22). A copper and nickel catalyst were considered for the LTS region while an iron catalyst was used to examine the HTS region. Although currently not considered for industrial applications, four precious metal catalysts were also studied, namely, platinum, palladium, rhodium and ruthenium. The industrial catalysts were obtained from Süd-Chemie/United Catalysts. The palladium, rhodium and ruthenium were obtained from Engelhard while platinum was obtained from Strem Chemical. All catalysts were supported on alumina. This was required to eliminate competing effects from different supports on different catalysts and allow for an equal basis for comparison.

Catalyst properties, i.e., the active surface area, catalyst density, were provided by the supplier for the three industrial catalysts. However, they remain unknown for the precious metal catalyst. These properties are also given in Table 22.

Table 22. Sample catalysts obtained for WGS reaction study with known properties.

Metal	Sample Catalyst	Supplier	Active Surface Area (cm^2/g)	Bulk Catalyst Density (g/cm^3)
Cu(111)	$CuO/ZnO/Al_2O_3$	Süd-Chemie	$6 \cdot 10^5$	1.28
Ni(111)	$Ni/Al_2O_3/CaO$	Süd-Chemie	$3 \cdot 10^4 - 1.5 \cdot 10^5$	0.928
Pd(111)	0.5% Pd on 1/8" alumina pellets	Engelhard	—	—
Pt(111)	0.5% Pt on 1/8" alumina pellets	Strem Chemical	—	—
Rh(111)	0.5% Rh on 1/8" alumina pellets	Engelhard	—	—
Ru(001)	0.5% Ru on 1/8" alumina pellets	Engelhard	—	—
Fe(110)	CuO promoted Fe_2O_3/Cr_2O_3	Süd-Chemie	$9 \cdot 10^5$	1.12

Chapter 8. Experimental Validation

8.1. Results for Industrial Catalysts

8.1.1. Copper-based Catalysts

In addition to testing the commercial catalyst obtained from Süd-Chemie, a synthesized catalyst was also examined [55]. This catalyst was prepared from a coprecipitated hydroxycarbonate precursor. A solution of metal nitrates and a sodium carbonate solution were both slowly added to water while maintaining a constant temperature of ~60°C and pH of ~7. For a 30 g target, the appropriately measured metal nitrate solution (molar ratio: 0.39Cu/0.36Zn/0.25Al) was brought to 1 L. The distilled water reservoir was sufficiently high enough to submerge a pH probe and stirring spindle. The pH was adjusted by adding, drop wise, at a drop rate of approximately 1-2 drops per second, 1.5 M Na_2CO_3 to the reservoir until the desired pH of 7 was reached. Once all of the metal nitrate solution was added, the resulting blue precipitate was allowed to age for 1 hour, with stirring. The precipitate was then filtered, and washed with five portions of 500 mL of water at 60°C to lower the sodium content to acceptable levels (typically <0.05%). The washed product, composed of metal hydroxycarbonate(s), was dried, lightly ground with a mortar and pestle, and calcined in air at 400°C for 8 hours to produce the metal oxides. Test samples of the copper catalyst, $Cu/ZnO/Al_2O_3$, were prepared by washcoating a 600 cpsi (channels per square inch) 1 inch long, ¾-inch diameter cordierite monolith with an aqueous-slurry of the metal oxide mixture. The slurry was prepared by ball-milling the prepared oxide in water. Each monolith was typically coated with the slurry a number of times to obtain the desired loading. The monolith was dried at 100°C between each coating. After the final coating was applied, the monolith was calcined in air at 400°C for 1 hour.

The monolith core was then inserted into the tubular reactor section of the apparatus above a supportive screen and a single layer of glass beads. A section of glass beads was also installed in the apparatus above the reactor section to ensure complete mixing of the reacting gases. The catalyst was pretreated in a reducing atmosphere using

100 sccm 3% H_2/N_2 ramped from 50 to 200°C over a 12 hour period and held for 1 hour. Carbon monoxide (BOC, Grade 4.0-99.99%, Aluminum cylinders), carbon dioxide (BOC, Grade 5.0-99.999%), hydrogen (BOC, Grade 5.0-99.999%) and balance nitrogen (BOC, Grade 5.0-99.999%) were fed to the reactor through a gas pre-heater. The flow rates were controlled via a network of MKS 1179 mass flow controllers and an MKS 1479 mass flow controller for hydrogen. Water entered the system via a Thermo Separation Products (TSP) ConstaMetric 3500 HPLC pump through a vaporizer. Stream compositions were sampled and analyzed (wet) via gas chromatography (Hewlett-Packard 6890 Plus+, two HP Plot Q Capillary columns) just before the reaction gases enter the furnace and immediately after the furnace. The temperature of the reactor section was maintained via a control relay to the Applied Test Systems, Inc. Series 3210 3-zone furnace's controllers. The exit gases were passed through a condenser and diluted below the flammability limit with nitrogen before venting to the hood.

The Cu surface area was determined experimentally using a modified N_2O reactive chemisorption technique [144]. The catalyst sample was reduced under the same conditions as previously described. The temperature throughout the apparatus was maintained at 50°C. Helium, instead of nitrogen, was used as the carrier and makeup gas for the GC. A portion of the reactor outlet flow was continuously fed directly to a thermal conductivity detector to allow quantification of the amount of N_2O consumed in the reaction: $2\ Cu(surface) + N_2O(gas) \rightarrow Cu_2O(surface) + N_2(g)$. Helium was fed through the catalyst section for 5 minutes to establish a baseline. The feed gas then was instantaneously switched to a flow of 2.5% N_2O/He and maintained for a period of 1 hour. Thereafter, the feed was switched back to solely helium for a period of 15 minutes allowing the baseline to be restored. The feed was then changed to 2.5% N_2O/He for another 1-hour period. Finally, the feed gas was returned to helium to restore the baseline once again. The two "peaks" that were recorded were then analyzed to determine the site density and active surface area through a series of comparative calculations. The first "peak" illustrated the amount of N_2O that has reacted with the catalyst surface while the second "peak" showed the "non-reactive" catalyst surface representative of a catalyst in which all active sites were occupied.

Numerical simulations of microkinetics on Cu(111) and analyses were performed for both a CSTR and a PFR. Operating parameter values are as follows: residence time, $\tau = 1.8$s; porosity of the catalyst, 0.5; the site density of the catalyst, 1.41×10^{15} sites/cm^2; the active catalyst surface area, 3.43×10^5 cm^2/g as measured for fresh catalyst and 1.25×10^5 cm^2/g as measured for aged catalyst; the catalyst density, determined from the monolith loading, for both samples is 0.14 g/cm^3. The governing equations for these two types of reactors have been presented earlier in Chapter 3 [7].

The predictions of the extended microkinetic model for Cu(111) for different feeds are presented in Figure 34 and Figure 35. It is seen that the model quantitatively reproduces the main features of the WGSR on the catalyst under different experimental conditions. As can be seen, the experimental data was well represented by the microkinetic model developed here under the conditions examined thus far.

In addition, reaction order data were taken from the experiments described in Table 21. The results are presented in Figure 36 and are comparable to those tabulated in Table 19, specifically Reference [67]. While the results for H_2O, CO, and CO_2 are comparable, the reaction order for H_2 is unexpectedly positive. The reaction order for CO_2, while nearly zero, is also slightly positive. This is considered a possible consequence of discrepencies in the GC peak area data for CO_2.

8.1.2. Iron-Based Catalysts

The energetics for the WGS reaction on an Fe(110) catalyst (see Table 22) were calculated theoretically using the UBI-QEP method and the transition-state theory as described for the case of Cu(111). These values are tabulated in Appendix A. Simulated results from the simplified rate expression given in Equation (301) were then compared with experimental data [145], as shown in Figure 37, validates the model applied to the HTS iron catalyst. It should be noted that, while the active temperature region is predicted with the microkinetic model, the model does not match the experimental data as well as was the case for the Cu catalyst. This may be attributed to the activation energies predicted by the UBI–QEP method as well as the catalyst properties, which were provided by the supplier.

Reaction order data for the WGS reaction on Fe is given in Figure 38. While

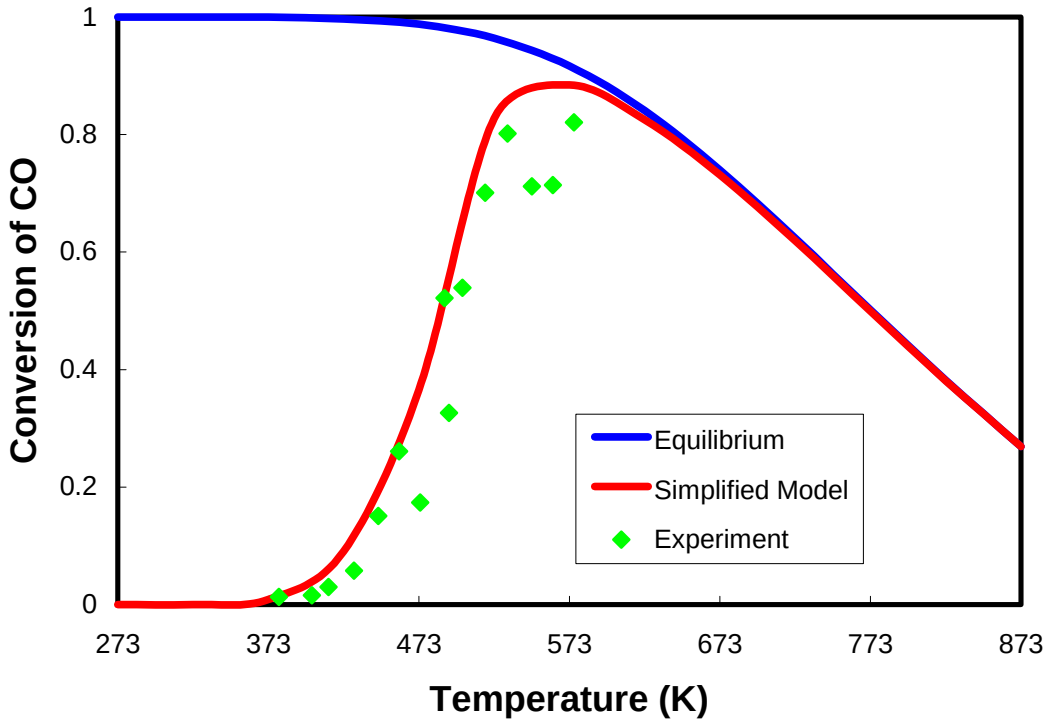

Figure 34. Microkinetic mechanism vs. experimental data for Cu under the following experimental conditions: catalyst loading of 0.14 g/cm^3; total feed flow rate of 236 cm^3 (STP) min^{-1}; pressure of 1.5 atm ;residence time τ = 1.8 s; feed composition of H_2O(25.6%), CO(11%), CO_2(6.8%), H_2(25.6%) and N_2(balance).

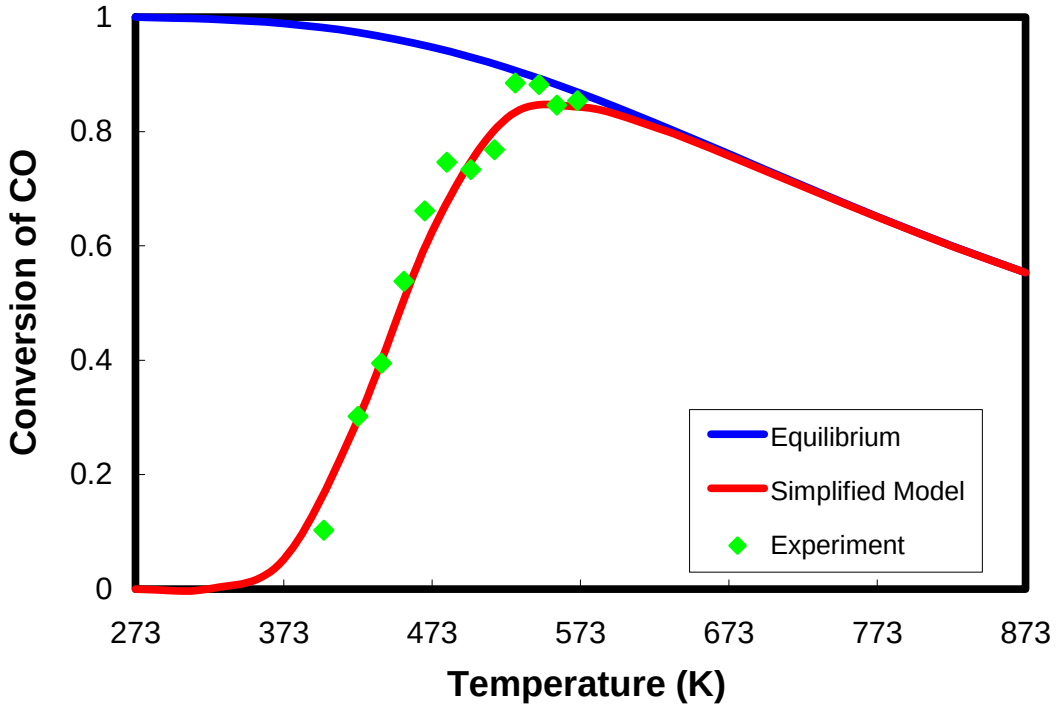

Figure 35. Microkinetic mechanism vs. experimental data for Cu under the following experimental conditions: catalyst loading of 0.14 g/cm^3; total feed flow rate of 236 cm^3 (STP) min^{-1}; pressure of 1.5 atm ;residence time τ = 1.8 s; feed composition of H_2O(10%), CO(10%) and N_2(balance).

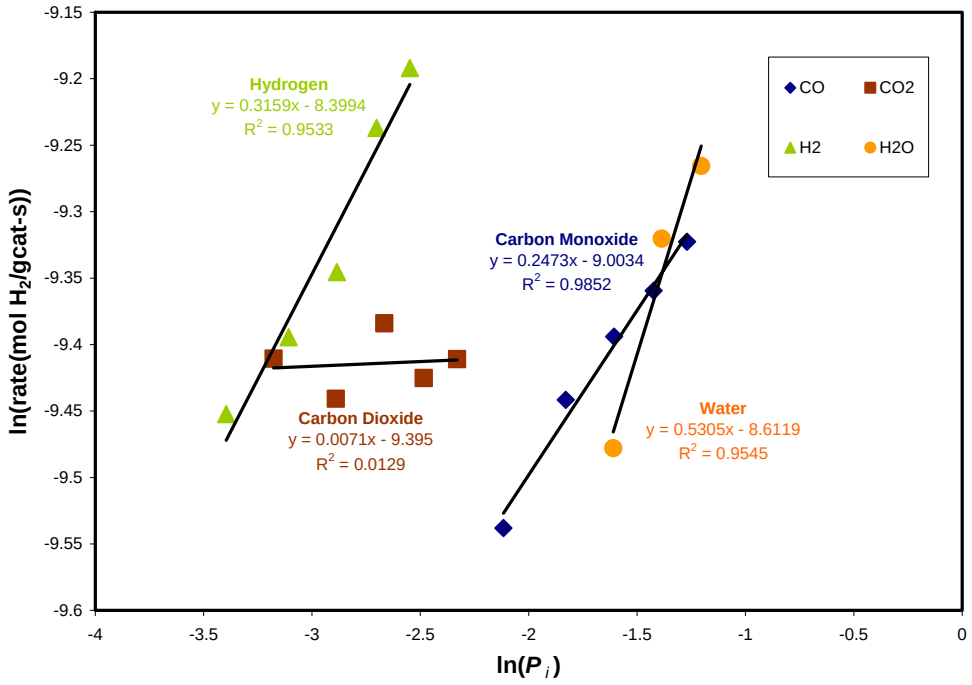

Figure 36. Experimental reaction order data for the commercial Cu catalyst under the following experimental conditions: total feed flow rate of 100 cm^3 (STP) min^{-1}; pressure of 1 atm ; feed composition of H_2O(20%), CO(15%), CO_2(5%), H_2(5%) and N_2(balance).

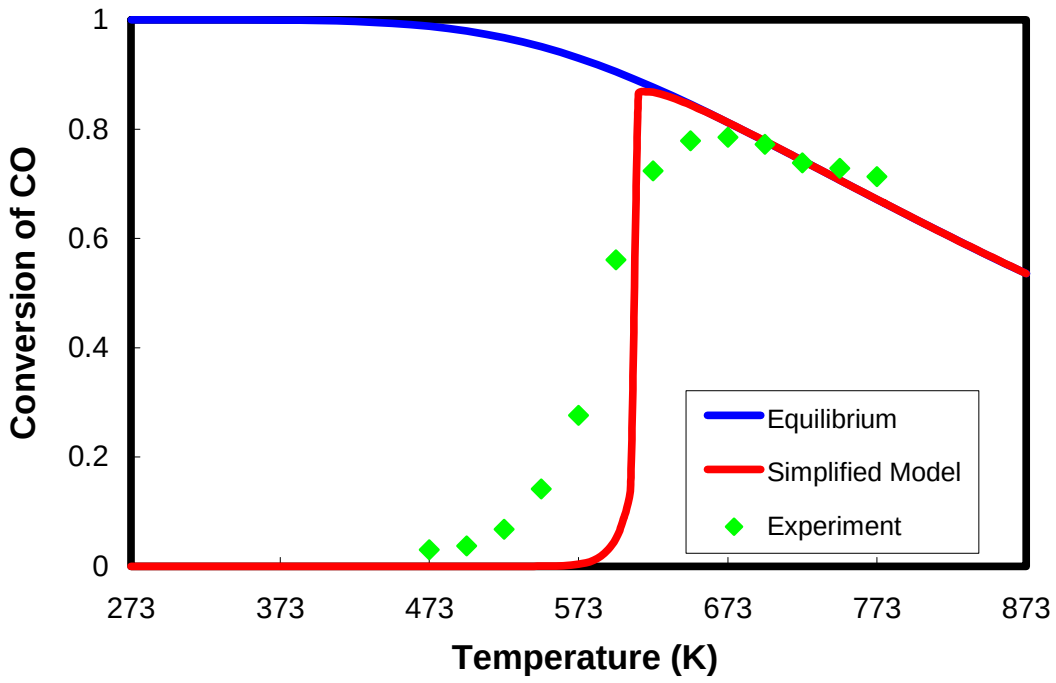

Figure 37. Microkinetic mechanism vs. experimental data on Fe under the following experimental conditions: total feed flow rate of 100 cm^3 (STP) min^{-1}; pressure of 1 atm ; feed composition of H_2O(10%), CO(10%) and N_2(balance).

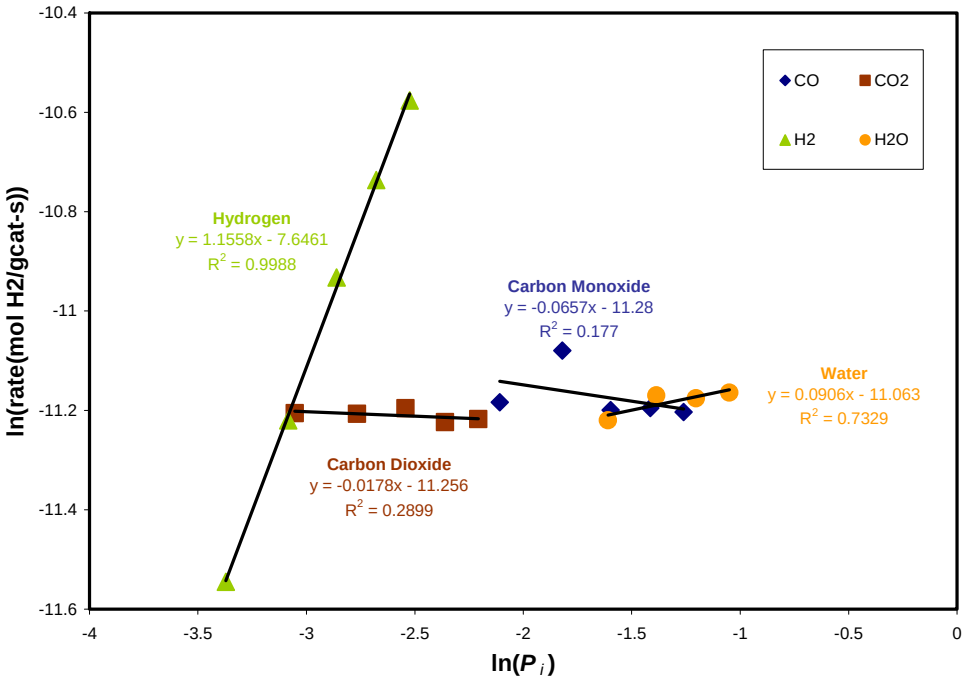

Figure 38. Experimental reaction order data for the commercial Fe catalyst under the following experimental conditions: total feed flow rate of 100 cm^3 (STP) min^{-1}; pressure of 1 atm ; feed composition of H_2O(20%), CO(15%), CO_2(5%), H_2(5%) and N_2(balance).

experimental results from the literature are not provided, the general trends deserve comment. The reaction orders results were suprising; H_2 and H_2O showed positive reaction orders while both CO and CO_2 are negative with near-zero magnitudes.

8.1.3. Nickel-Based Catalysts

A similar experimental synthesis procedure to that of the copper-based catalysts was performed for the nickel-based catalyst, $Ni/ZnO/Al_2Ol_3$. The catalyst properties were determined using the same procedure as that employed for Cu(111). The energetics for the Ni(111) catalyst are calculated using the UBI-QEP method and the transition-state theory and are given in Appendix A. The energetics provided in Appendix A were implemented with the simplified rate expression derived and given in Equation (301). As can be seen from Figure 39, the microkinetic model accurately predicts the experimental data for the Ni catalyst. As was the case with the Fe catalyst, the microkinetic model's sharp prediction may be overcome with revised energetics or catalyst properties.

Ni experiments were perfomed to determine the reaction orders of each terminal species. These results are presented in Figure 40 and, as was the case for Fe, the results are surpising. Each species shows a positive reaction order. The reaction orders of CO and CO_2 are essentially equivalent. Again, reaction order data from the literature are not provided; however, in comparison with literature results for Cu, the magnitudes of the reaction order for CO and H_2O are reasonable.

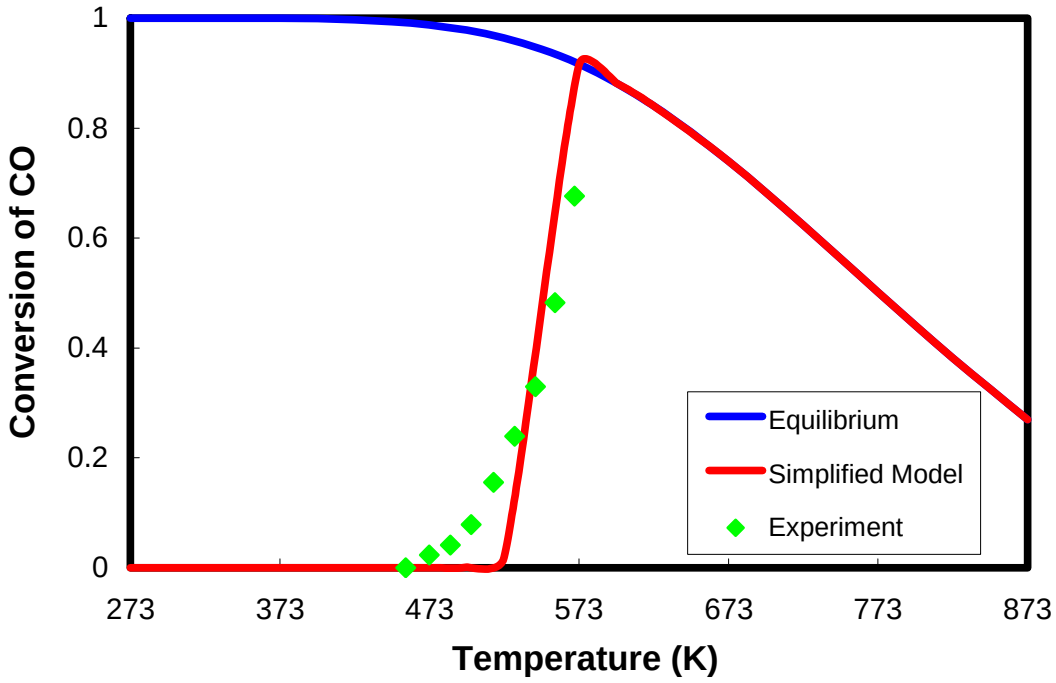

Figure 39. Microkinetic mechanism vs. experimental data for Ni under the following experimental conditions: catalyst loading of 0.14 g/cm^3; total feed flow rate of 236 cm^3 (STP) min^{-1}; pressure of 1.5 atm ;residence time τ = 1.8 s; feed composition of H_2O(25.6%), CO(11%), CO_2(6.8%), H_2(25.6%) and N_2(balance).

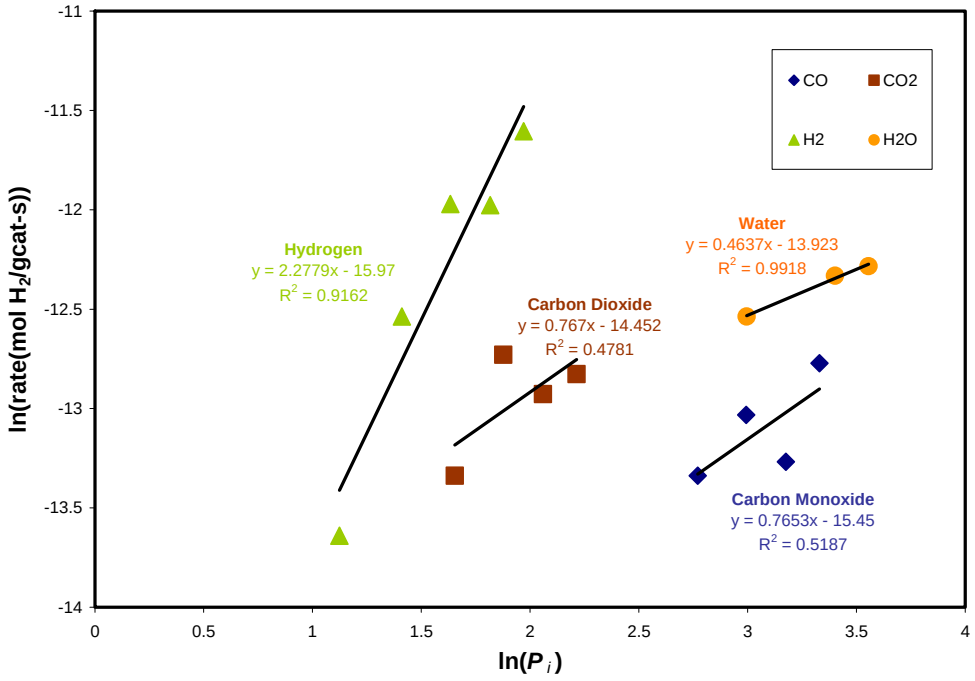

Figure 40. Experimental reaction order data for the commercial Ni catalyst under the following experimental conditions: total feed flow rate of 100 cm^3 (STP) min^{-1}; pressure of 1 atm ; feed composition of H_2O(20%), CO(15%), CO_2(5%), H_2(5%) and N_2(balance).

Chapter 9. Conclusions and Future Work

Reaction schematics have been employed to depict reaction pathways and are an invaluable tool in the study of reaction mechanisms. Typically, species are depicted as nodes interconnected via arrows representing elementary reaction steps. While this is appropriate for monomolecular reactions, the scheme becomes increasingly complex with an increase in the species involved in each elementary reaction step. For this reason, we have introduced a new kind of scheme where the branches represent the elementary reaction steps and the nodes represent their connectivity within reaction routes (*RR*s); hence, the schematic is called a *RR* graph. Basic concepts of graph theory and Kirchhoff's Laws have been employed to determine the connectivity of the elementary reaction steps in a mechanism and its kinetics. An analogy has been drawn between the developed *RR* graph and electric circuit theory to analyze and reduce the *RR* graph to a simpler form in which the quasi-equilibrium steps, rate-limiting steps, and dominant pathways are easily identified.

An 18-step mechanism with predicted kinetics for the water-gas-shift (WGS) reaction is used to demonstrate the utility of this powerful new method. A *RR* graph has been constructed and converted into a *RR* network; Kirchhoff's Current Law, representing conservation of mass at each node, and Kirchhoff's Voltage Law, representing thermodynamic consistence of the affinity for each cycle, are used to reduce the diagram by examining comparable path resistances and eliminating the more resistant pathway. The resistance for an elementary reaction step is given by the De Donder relation written in the form of Ohm's law, $R_\rho = \mathcal{A}_\rho / r_\rho$, where $\mathcal{A}_\rho = A_\rho / RT$ is the dimensionless affinity and r_ρ is the rate of an elementary reaction step. This ultimately results in a simpler *RR* graph from which a simplified mechanism and an explicit rate expression were determined.

The resulting *a priori* rate expression may, thus, be used to predict the kinetics of the WGS reaction based on simple catalyst parameters as well as experimental feed conditions. Ultimately, this deeper understanding of the molecular events comprising an

OR is intended to provide a means for a more systematic and theory-guided approach to catalyst design and selection.

After completion of the research, some issues still remain. For example, with the advent of more sophisticated theoretical predictions of elementary reaction energetics, i.e., *ab initio* and density functional theory, the reaction enthalpies and activation energies may be evaluated with higher accuracy. Furthermore, the incorporation of these higher-level theories through the use of computational chemistry software such as Gaussian03[95] may provide more insight into the selection of the elementary reaction steps comprising the overall reaction mechanism. In addition to improved energetics, it is desired to expand the theory of *RR* graphs from single *OR*s to multiple *OR*s to gain insight into the competing mechanisms that result from the occurrence of side reactions on a catalyst surface.

9.1. Reaction Route Network

In this research, *RR* theory has been used to enumerate the *FR*s, *ER*s, *IN*s and *TN*s as described in Chapter 4. Basic elements of graph theory are employed to convert the mechanism into a *RR* graph that depicts the interconnectivity of the elementary reaction steps comprising an *OR* mechanism allowing for each fo the *FR*s to be traced from the graph as walks from one starting *TN* to its corresponding ending *TN*. Once the structure of the *RR* graph is established from the mechanism stoichiometry, it is converted into a *RR* network. Resistances replace the elementary reaction step branches and the *OR* is replaced by a voltage source. Using Kirchhoff's Laws, as they correspond to conservation of mass and thermodynamic consistency, in conjunction with the elementary reaction step resistance defined, in the form of Ohm's Law, as a modified De Donder relation, the network may be analyzed, reduced and simplified. While all of these elements exist in the literature in one form or another, their combination accomplished here is unique.

Heterogeneous catalytic reactions proceed through a complex network of surface molecular events, or elementary reactions, involving the reactants, surface intermediates

and products. Once the rate constants of all the elementary reactions comprising a microkinetic mechanism are known, the behavior and capabilities of the microkinetic model may be investigated through numerical simulations. However, a complete understanding of the model based simply on numerical computer outputs is difficult to achieve. A large variety of complementary methods, both quantitative and qualitative, have been proposed in order to rationalize general features of complex microkinetic models. From this arsenal of theoretical methods, two have proved to be of special value in the analysis of microkinetic models. One of these is the *RR* approach, and the other is the graph-theoretical approach. In fact, these two methods are closely interrelated. Indeed, there is a large number of publications discussing different graph-theoretical aspects of the theory of *RR*s. (For a review of the application of graph-theoretical methods in studying complex reaction mechanisms, see Reference [106].)

A general feature of the graph-theoretical methods as applied to the analysis of reaction mechanisms is that the surface intermediates are represented by the nodes of the graph as key species. Although such a graphical representation is useful in studying many structural aspects of the mechanisms, it is not useful in the analysis of the kinetics of the system. In this work we have shown for the first time that the elementary reactions comprising a complex, non-linear mechanism may be arranged into a *RR* network that graphically depicts all possible *RR*s. The rules that govern the connectivity and directionality of the elementary reactions in such a *RR* network are derived from the QSS conditions of the surface intermediates. A subsequent assumption involving the introduction of the resistance of an elementary reaction defined as the ratio between its affinity and rate, i.e., a linear relation in the spirit of Ohm's Law, makes the *RR* network totally analogous to a linear circuit network. As a result, we are in a position to employ the methods of electrical network analysis including Kirchhoff's Current and Voltage Laws. These are independent of Ohm's Law; therefore, they are applicable to non-linear elements as well. In particular, the electrical circuit analogy suggests a systematic way of determining the dominant *RR*s and, hence, a substantial simplification and reduction of the mechanism.

9.1.1. Application of RR Network Analysis to the WGS Reaction

The developed theoretical methodology has been applied here to study and rationalize an 18 elementary reaction step microkinetic mechanism for the WGSR on Cu, Ni, Fe. A *RR* network has been constructed that incorporates all of the 252 direct *FR*s and 117 *ER*s that have been generated using the conventional methods. Using the electrical circuit analogy, the *RR* network was subsequently simplified and reduced to a *RR* network involving only 3 dominant *RR*s. An overall rate equation has been developed that reproduces the complete microkinetic model precisely and is the same as that obtained by the more conventional *RR* analysis. The approach not only provides a comprehensive look at the molecular mechanism of the WGS reaction, but also identifies the slow and quasi-equilibrium elementary reaction steps.

Although some of the assumptions involved in the calculation of the reaction energetics are rather rudimentary, the agreement between the model predictions and our experimental data is excellent. The modified microkinetic mechanism proposed in this work also has been substantially simplified and reduced thus resulting in a convenient analytical rate expression that may be used to model the WGS reaction in more complex reactor configurations.

9.2. Future Work

While the approach used here for developing a microkinetic model for the WGS reaction has thus far proved encouraging, yielding accurate predicted results, further improvements may be made, some of which are discussed below.

9.2.1. Predictions of Reaction Energetics

Reliability of reaction energetics is of paramount importance in the approach described here. Therefore, alternate methodologies for these should be investigated. Furthermore, in recent years, progress in *ab initio* and semi-empirical method for surface energetics has increased tremendously. While the UBI-QEP method has proved to be reliable in predicting surface energetics, the application of more rigorous methods such as

density functional theory (DFT) to determine the structure of the intermediates and transition states along with elementary reaction step energetics is desired.

Jakdetchai and Nakajima [146] performed an AM1-d study of the WGS reaction over the three different crystal surfaces of Cu. Using a molecular modeling program called WINMOPAC, they were able to approximate the activation energy of the elementary reaction steps for both the formate and redox mechanisms of the WGS reaction. In their study, they also examined whether the WGS reaction proceeded via a Langmuir-Hinshelwood mechanism or an Eley-Rideal mechanism. The activation energies were evaluated after performing several geometry optimizations for each elementary reaction step using the AM1 method. The heats of adsorption calculated using the AM1 theory were found to be much higher than reported values, but it is noted that the calculated values account for the competitive adsorption between H_2O and CO. Their results suggest that the WGS reaction proceeds via the redox mechanism rather than the formate mechanism and that the OH bond cleavage of OHS is the rate determining step (s_6 in Table 7). Furthermore, their simulations suggest that the WGS reaction occurs via the Eley-Rideal mechanism. This work provides some insight into the application of semi-empirical methods to determine the reaction energetics for the elementary reaction steps of the WGS mechanism.

In this thesis, pre-exponential factors were estimated using the approximate approach of Dumesic, et al. [18], but should be further refined. Statistical thermodynamics calculations for the partition functions using experimentally determined, or available, molecular characteristics of the adsorption species have been performed based on the work accomplished by Ovesen, et al. [10,14]. These calculations were used to determine the pre-exponential factors of the elementary reaction steps. Our results, thus far, concur with this group. Thus, we were able to evaluate the partition functions of our species based on the expressions and data given in Section 2.4.2. These results are tabulated in Table 23. The following series of equations based on the transition state theory were used to evaluate the pre-exponential factors, and ultimately the rate constants for the assumed elementary reaction steps.

Estimating the pre-exponential factor with the transition state theory accounts for the substantial loss of entropy that occurs when molecules unite to form an activated

complex. Lund [13] has also provided a supplementary methodology, as described in Section 3.5.3. Here, the elementary reaction step entropy change is used in conjunction with conventional TST [49] to predict both the forward and reverse pre-exponential factors such that they are inherently thermodynamically consistent. We have attempted to employ this methodology here (as described in Section 3.5), but found that it required further adjustments in the pre-exponential factors based not only on reaction conditions, but also on specific catalyst. However, initial evaluation suggested that the direct use of TST is not an unreasonable approximation as shown by the values given in Table 24. While this methodology appears more sophisticated, it requires further investigation before it may be applied to the current research.

In Laidler [72], the rate of the forward reaction, $\vec{r}$, describing the generic reaction A + B ⇆ PRODUCTS is given by the following expression:

$$\vec{r} = [A][B]\frac{k_B T}{h}\frac{z_{\ddagger}}{z_A z_B}\exp\left(-\frac{\vec{E}_o}{R_{gas}T}\right) \tag{309}$$

where E_o is the energy of the transition state complex. The rate constant is defined, therefore, as

$$\vec{k} = \frac{k_B T}{h}\frac{z_{\ddagger}}{z_A z_B}\exp\left(-\frac{\vec{E}_o}{R_{gas}T}\right) \tag{310}$$

Comparing this to the conventional form of the rate constant (Arrhenius equation)

$$\vec{k} = \vec{\Lambda}\exp\left(-\frac{\vec{E}_a}{R_{gas}T}\right) \tag{311}$$

Equating these two definitions, an expression for the pre-exponential factor, $\vec{\Lambda}$, can be determined. The activation energy, E_a, is assumed to equal E_o.

Table 23. Partition Function Parameters and Calculation Results (T = 190°C) [10,14]

Species		H_2	H·S	H_2O	H_2O·S	O·S	OH·S	CO	CO·S	CO_2	CO_2·S	HCOO·S
m	kg	3.32E-27		2.99E-26				4.65E-26			7.31E-26	
$\omega^{\perp}$	cm^{-1}		1121		460	391	280		343	410		340
$\omega_{\parallel}$	cm^{-1}		928		48	508	49		24	31		36
ω	cm^{-1}	4405.3		1594.6	1600		670	2170	2089	1343	1343	760
				3657.1	3370					667	667	1330
				3755.8	745					2349	2349	1640
												2910
												1043
												1377
												1377
σ		2		2				1			2	
B	cm^{-1}	60.8						1.93			0.39	
$I_A I_B I_C$	kg^3m^6			5.77E-141								
E_e	kJ/mol	-35	-40.7	-306	-359	-243	309.6	-132.2	-186.1	-359	-431	554
z_t		3.34E+05	1.13E-02	9.03E+06	2.88E+01	2.53E-01	4.79E+01	1.75E+07	1.61E+02	3.45E+07	7.90E+01	7.21E+01
z_v		1.06E-03	1.00E+00	8.37E-07	1.55E-04	1.00E+00	4.03E-01	3.43E-02	3.90E-02	1.33E-03	1.33E-03	1.09E-07
z_r		2.65E+00	1.00E+00	8.30E+01	1.00E+00	1.00E+00	1.00E+00	1.67E+02	1.00E+00	4.12E+02	1.00E+00	1.00E+00
z_e		8.86E+03	3.89E+04	3.25E+34	3.09E+40	2.55E+27	1.21E-35	8.13E+14	9.76E+20	4.08E+48	3.09E+40	3.29E-63
z		8.33E+06	4.41E+02	2.04E+37	1.38E+38	6.46E+26	2.33E-34	8.15E+22	6.11E+21	7.71E+55	3.24E+39	2.58E-68

Table 24. Pre-exponential factors determined using Lund's methodology [13], compared to conventional transition-state theory as presented by Dumesic, et al. [18]

	Lund		Dumesic	
	Forward	*Reverse*	*Forward*	*Reverse*
s_1	1.00E+06	8.01E+16	1.50E+06	1.00E+14
s_2	1.00E+06	2.02E+14	1.00E+06	1.00E+14
s_3	1.00E+13	8.25E+12	1.00E+13	1.00E+13
s_4	1.00E+13	2.38E+13	1.00E+13	1.00E+13
s_5	1.00E+13	2.90E+12	1.00E+13	1.00E+13
s_6	1.00E+13	6.80E+13	1.00E+13	1.00E+13
s_7	1.00E+13	1.62E+14	1.00E+13	1.00E+13
s_8	1.00E+13	5.59E+14	1.00E+13	1.00E+13
s_9	1.00E+13	8.23E+13	1.00E+13	1.00E+13
s_{10}	1.00E+13	1.21E+12	1.00E+13	1.00E+13
s_{11}	1.00E+13	7.05E+12	1.00E+13	1.00E+13
s_{12}	1.00E+13	5.81E+13	1.00E+13	1.00E+13
s_{13}	1.00E+13	6.78E+14	1.00E+13	1.00E+13
s_{14}	1.00E+13	4.78E+14	1.00E+13	1.00E+13
s_{15}	1.00E+13	7.59E+03	4.00E+12	1.00E+06
s_{16}	1.00E+13	8.54E+12	1.00E+13	1.00E+13
s_{17}	1.00E+13	1.81E+04	6.00E+12	1.00E+06
s_{18}	1.00E+13	1.55E+04	6.00E+12	1.00E+06

$$\vec{\Lambda} = \frac{k_B T}{h} \frac{z_{\ddagger}}{z_A z_B} \tag{312}$$

The partition function of the activated complex is may be partitioned into transitional, rotational and vibrational partition functions [72].

$$z^{\ddagger} = z_t^{\ddagger} z_r^{\ddagger} z_v^{\ddagger} \tag{313}$$

The translational partition function of the activated complex is evaluated based on the mass of the activated complex: $m_{\ddagger} = \sum$(number of atoms)·(mass of single atom).

$$z_t^{\ddagger} = \frac{\left(2\pi m_{\ddagger} k_B T\right)^{3/2}}{h^3} \tag{314}$$

The rotational partition function of the activated complex is evaluated based on the moment of inertia of the activated complex and the fractional location of the center of mass, x, within the complex: $I_{\ddagger} = \sum$(mass of single atom)·(fractional distance of atom from center of mass).

$$z_r^{\ddagger} = \frac{8\pi^2 I_{\ddagger} k_B T}{h^2} \tag{315}$$

The vibrational partition function of the activated complex is evaluated based on the vibrational frequencies of each mode of vibration of the activated complex.

$$z_v^{\ddagger} = \frac{1}{\left(1 - \exp\left(-\frac{hc\omega_{1\ddagger}}{k_B T}\right)\right)\left(1 - \exp\left(-\frac{hc\omega_{2\ddagger}}{k_B T}\right)\right)^2} \tag{316}$$

where $\omega_{i\ddagger}$ is the vibrational frequency of the molecule in the *i*-th orientation As the temperature increases, the contribution of the vibrational partition function becomes greater. If the temperature is not too high, the vibrational partition function is close to unity. Applying these values to the overall partition function expression, the pre-exponential factor may then be estimated.

The transition state theory (TST) provides a convenient framework for calculating the rate constants for the reaction A + B ⇆ C + D. A similar framework can be applied to surface reactions [18]. The rate of adsorption of species A is given by the following reaction: $A_{(g)} + S \leftrightarrows A^{\ddagger} \rightarrow AS$. In the scenario that we have assumed (i.e. immobile transition state), the rate expression takes the following form:

$$r = \frac{k_B T}{h} \frac{z_{A^{\ddagger}}}{z_A} \exp\left(-\frac{E_o}{R_{gas} T} \right) P_A \tag{317}$$

yielding an expression for the pre-exponential factor of

$$\Lambda = \frac{k_B T}{h} \frac{z_{\mathrm{A}^{\ddagger}}}{z_A} \tag{318}$$

A molecular modeling program such as Gaussian03 may be used to determine the transition state and its energy in the above equations. To accomplish this goal, accurate *ab initio* and DFT calculations are required.

Benziger has examined the UBI-QEP method and criticized its lack of effort to distinguish between the adsorption capacities of different adatoms, predicting that all adsorbates should go through the same sequences of adsorbed layer structure [147,148]. To correct for this, he utilizes the approach of Pauling [149] in which the bonding capacity of an atom is determined by the number of two-electron bonds that can be formed with the valance levels of the atom. Unfortunately, the delocalized band structure of metals causes the metal valence to be an ill-defined quantity. As a result, Pauling assigned the metal valences based on mechanical and magnetic properties of the transitions metals. Benziger defines the metal valence in terms of the effective atomic

number. Benziger then proceeds to employ the method of Shustorovich, as documented by the author [150] with these modifications.

A fundamentally different mechanism for the water-gas-shift reaction, i.e. the carbonate mechanism, has also been proposed and studied [13,15,16,56-59]. Including the carbonate species in the list of intermediate species, as well as considering those elementary steps in which the carbonate species is involved, may substantially alter the mechanism and predictions. The inclusion of carbonate may, in fact, provide several more reaction routes in the kinetics of the water-gas-shift reaction. Application of the UBI-QEP method has provided accurate and reliable surface energetics for many reactions [9,86-91] other than the water-gas-shift reaction. However, the extent to which the UBI-QEP method may be applied to other types of molecules, e.g. the energetics of the carbonate surface species is unknown and may require further investigation. Thus, additional insights into the method may be required to achieve improved capabilities of the method as compared to more fundamental methods (i.e. *ab initio* and DFT).

9.2.2. Extension of RR Graph Theory to Multiple Overall Reactions

Thus far, this research has focused on a single *OR*. *RR* Graph Theory has, however, great potential for gaining understanding of multiple *OR* mechanisms. As an example, initial efforts have been made to utilize *RR* Graph Theory to gain insight into the steam reforming mechanism. Specifically, steam reforming of logistic fuels for use in SOFCs developed for Naval transport applications is being considered. This research is ongoing and currently supported by the Office of Naval Research University/Laboratory Initiative Program in collaboration with the Naval Undersea Warfare Center in Newport, RI.

The mechanism and kinetics of logistic fuels such as JP-8 in external reforming (ER) or internal reforming (IR) within a solid oxide fuel cells (SOFCs) are similar, exceedingly complex, and poorly understood at this time. A comprehensive theoretical and experimental research program is being followed to methodically determine the mechanistic structure and microkinetics of reforming of JP-fuels on catalysts of interest in a building block fashion. Thus, initial efforts begin with the simplest fuel, namely, C_1 (CH_4) chemistry.

We have started, specifically, with a systematic theoretical and experimental investigation of autothermal reforming (ATR) and catalytic partial-oxidation (CPOX) reactions, which are actually comprised of three overall reactions involving reactions of oxygen and steam with CH_4 and CO, including the water-gas shift (WGS), occurring simultaneously on the catalyst surface to produce a mixture of CO, CO_2, and H_2:

$CH_4 + H_2O \leftrightarrows CO + 3H_2$	methane steam reforming (MSR)
$CH_4 + 1/2O_2 \leftrightarrows CO + 2H_2$	(CPOX)
$CO + H_2O \leftrightarrows CO_2 + H_2$	(WGS)

Theoretical modeling of the mechanistic structure shall be performed as well as reaction pathway analysis and microkinetic analysis of these reactions over model catalysts of interest, namely, Ni, Cu, Pt, and CeO_2, and their combination. In addition, the kinetics of these reactions will be investigated experimentally in a microcatalytic reformer on catalysts acquired or synthesized at WPI. The experimental emphasis will be on ATR and CPOX under air-independent operation. That is, no nitrogen will be used to dilute the fuel stream as in conventional CPOX and ATR reformers.

It is anticipated that separate *RR* networks for the individual *OR*s may be intertwined into a single *RR* network through the linkage of common elementary reaction steps. The resulting *RR* network would consist of at least one set of *TN*s for each *OR*. The *FR*s and *ER*s for each *OR* would be easily traced on the combined *RR* network, as well as the individual *RR* networks. The multiple *OR* network will hopefully provide insight into the overall microkinetics of the mingling *OR*s on a catalyst surface.

9.2.3. Experiments

Seven catalysts were tested in this research for the WGS reaction. However, the performance of the precious metal catalysts was not easily predicted using the current microkinetic model. This was due to the methanation reaction that accompanied WGS reaction. The results, as presented in this section, suggest that there are multiple reactions occurring within the reactor which alter the composition of the product stream.

Literature data suggests that Pt, Pd, Ru, and Rh have moderate to high catalytic activity. However, there is little discussion of side reaction (see Table 2).

In order to account for this methane production in the mechanism and kinetics, it is necessary to study methane-producing reactions which may be coupled with the WGS reaction. Both experiments and theoretical aspects of these possible reactions should be considered. Once the source of the methane is determined, the experimental results obtained in this research may be explained and compared to predicted results.

In the following figures, the results of the WGS reaction for the feed conditions described in Table 20 on Pt, Pd, Ru and Rh are provided. In each case we see atypical conversion results. For example, consider Figure 41; for the case of the forward WGS reaction (Feed 1), we see that the maximum falls around 750K while for Feed 2 (reverse WGS) and Feed 3 (mixed feed) the maximum falls at ~700K. Based on the results in each figure, it appears that there are competing *OR*s occurring on the surface of the catalyst. This conclusion is based on the shape of the plotted data. For example, on the Rh catalyst (Figure 43) under feed condition 2, we see a decrease in the conversion of H_2 up to 800K, then an increase in conversion which follows the typical shape of an equilibrium curve for reverse WGS. The current mechanism does not account for the occurance of possible side reaction. However, it is believed that, upon extension of *RR* graph theory to multiple *OR*s, the incorporation of side reactions into the mechanism may be accomplish with the resulting insight. The raw data from the experiments are provided in Appendix H.

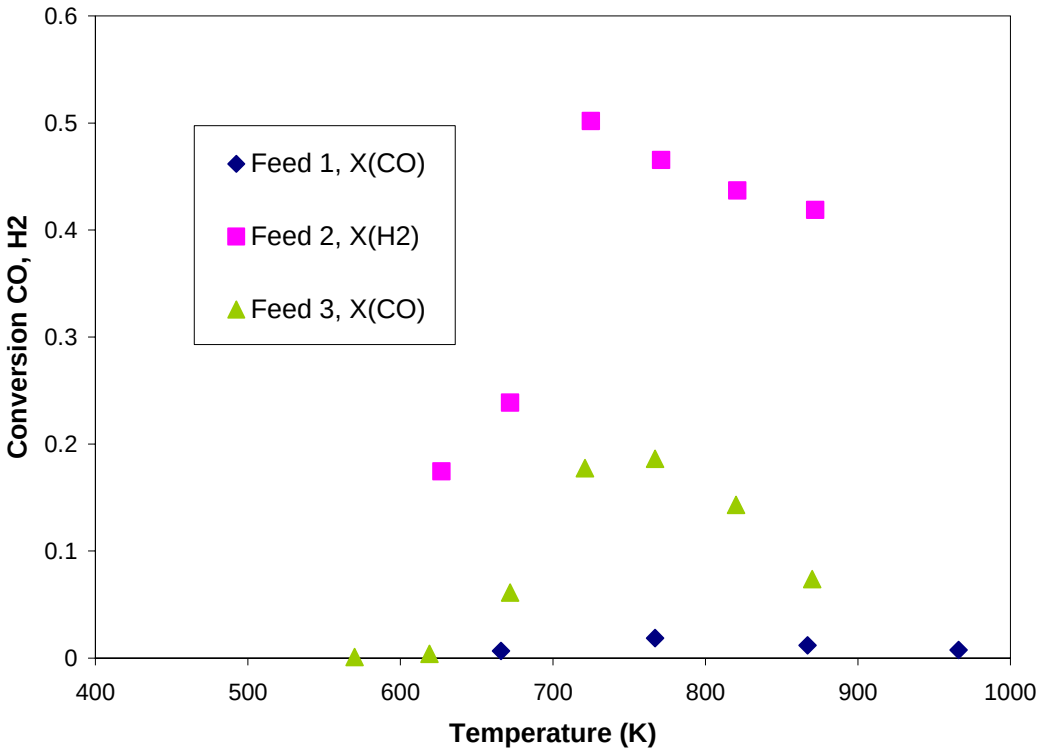

Figure 41. Experimental results of Pt(111) catalyst hindered by the formation of methane under the conditions: total fee flow rate of 100 cm^3; pressure of 1 atm; and, feed conditions corresponding to Table 20.

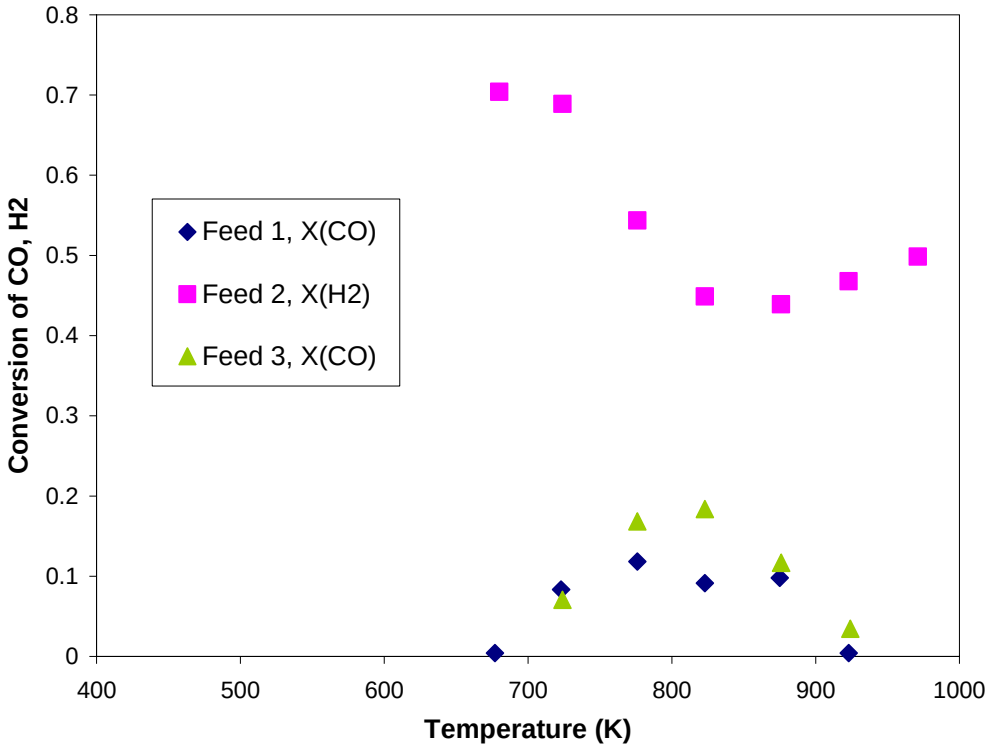

Figure 42. Experimental results of Pd(111) catalyst hindered by the formation of methane under the conditions: total fee flow rate of 100 cm^3; pressure of 1 atm; and, feed conditions corresponding to Table 20.

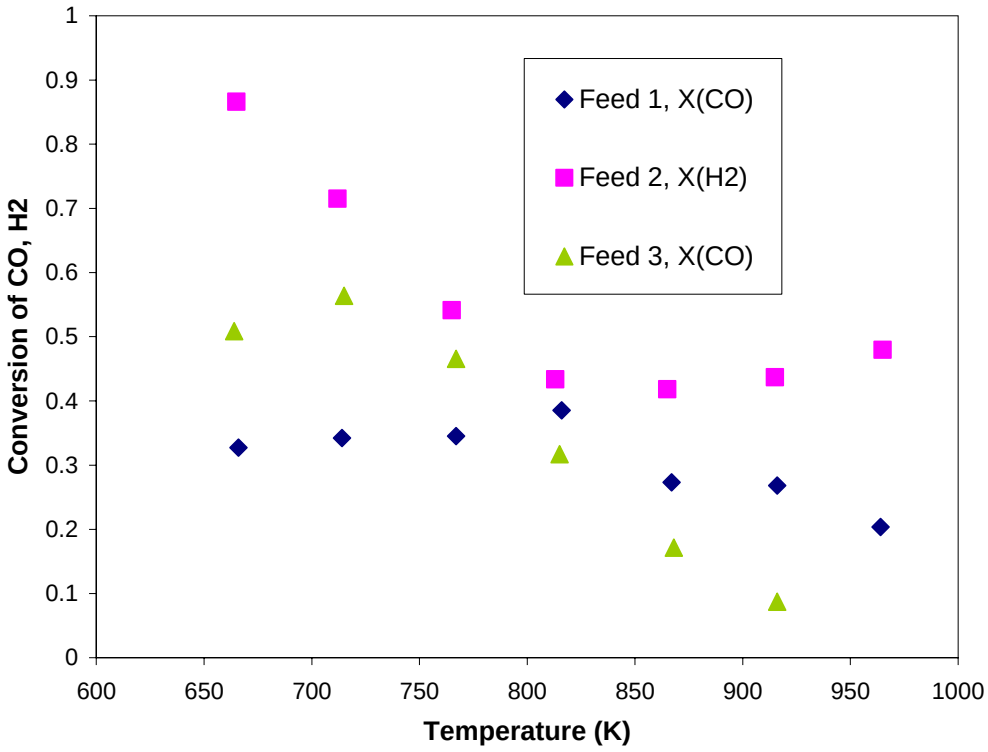

Figure 43. Experimental results of Rh(111) catalyst hindered by the formation of methane under the conditions: total fee flow rate of 100 cm^3; pressure of 1 atm; and, feed conditions corresponding to Table 20.

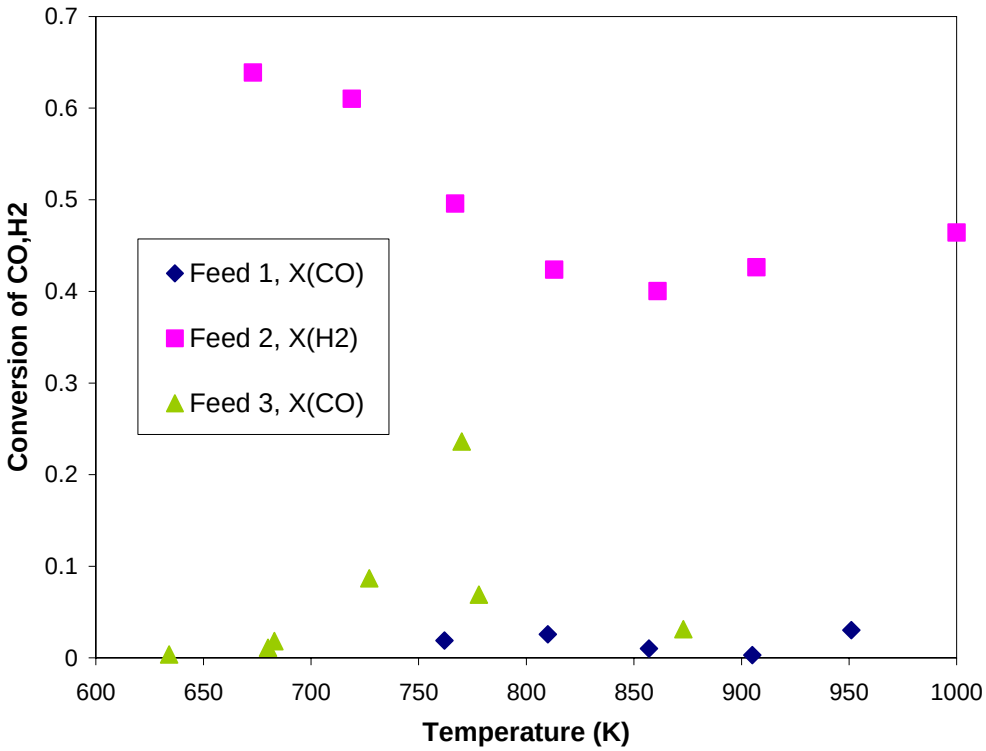

Figure 44. Experimental results of Ru(111) catalyst hindered by the formation of methane under the conditions: total fee flow rate of 100 cm^3; pressure of 1 atm; and, feed conditions corresponding to Table 20.

References

(1) Thomas, S.; Zalowitz, M. http://education.lanl.gov/RESOURCES/fuelcells.

(2) Hirschenhofer, J. H.; Stauffer, D. B.; Engleman, R. R.; Klett, M. G. *Fuel Cell Handbook (for USDOE)*, 6th ed.; Parsons Corp: Reading, PA, 2002.

(3) Greeley, J.; Mavrikakis, M. "Methanol decomposition on Cu(111): a DFT study", *J. Catal.* **2002**, *208*, 291.

(4) Satterfield, C. N. *Heterogeneous Catalysis in Industrial Practice*, 2nd ed.; McGraw-Hill: New York, 1991.

(5) http://www.rmi.org/sitepages/pid556.php

(6) Thampan, T.; Malhotra, S.; Zhang, J.; Datta, R. "PEM fuel cell as a membrane reactor", *Catalysis Today* **2001**, *67*, 15.

(7) Fishtik, I.; Datta, R. "A UBI-QEP microkinetic model for the water-gas shift reaction on Cu(111)", *Surf. Sci.* **2002**, *512*, 229.

(8) Nakamura, J.; Campbell, J. M.; Campbell, C. T. "Kinetics and mechanism of the water-gas shift reaction catalysed by the clean and Cs-promoted Cu(110) surface: a comparison with Cu(111)", *J. Chem. Soc. Faraday Trans.* **1990**, *86*, 2725.

(9) Shustorovich, E.; Bell, A. T. "An analysis of methanol synthesis from carbon monoxide and carbon dioxide on copper and palladium surfaces by the bond-order-conservation-Morse-potential approach", *Surf. Sci.* **1991**, *253*, 386.

(10) Ovesen, C. V.; Stoltze, P.; Norskov, J. K.; Campbell, C. T. "A kinetic model of the water gas shift reaction", *J. Catal.* **1992**, *134*, 445.

(11) Rhodes, C.; Hutchings, G. J.; Ward, A. M. "Water-gas shift reaction: finding the mechanistic boundary", *Catal. Today* **1995**, *23*, 43.

(12) Vanden Bussche, K. M.; Froment, G. F. "A steady-state kinetic model for methanol synthesis and the water gas shift reaction on a commercial $Cu/ZnO/Al_2O_3$ catalyst", *J. Catal.* **1996**, *161*, 1.

(13) Lund, C. "Microkinetics of Water-Gas Shift of Sulfided Mo/Al_2O_3 Catalysts", *Ind. Eng. Chem. Res.* **1996**, *35*, 2531.

(14) Ovesen, C. V.; Clausen, B. S.; Hammershoi, B. S.; Steffensen, G.; Askgaard, T.; Chorkendorff, I.; Norskov, J. T.; Rasmussen, P. B.; Stoltze, P.; Taylor, P. "A

Microkinetic Analysis of the Water-Gas-Shift Reaction under Industrial Conditions", *J. Catal.* **1996**, *158*, 170.

(15) Tserpe, E.; Waugh, K. C. A microkinetic analysis of the reverse water gas shift reaction. In *Dynamics of Surfaces and Reaction Kinetics in Heterogeneous Catalysis*; G. F. Froment, K. C. W., Ed.; Elsevier: Amsterdam, 1997; pp 401.

(16) Waugh, K. C. "Prediction of global reaction kinetics by solution of the Arrhenius parameterised component elementary reactions: microkinetic analysis", *Catal. Today* **1999**, *53*, 161.

(17) Shustorovich, E.; Sellers, H. "The UBI-QEP method: a practical theoretical approach to understanding chemistry on transition metal surfaces", *Surf. Sci.* **1998**, *31*, 1.

(18) Dumesic, J. A.; Rudd, D. F.; Aparicio, L. M.; Rekoske, J. E.; Trevino, A. A. *The Microkinetics of Heterogeneous Catalysis*; ACS, 1993.

(19) Fishtik, I.; Datta, R. "De Donder relations in mechanistic and kinetic analysis of heterogeneous catalytic reactions", *Ind. Eng. Chem. Res.* **2001**, *40*, 2416.

(20) Hougen, O. A.; Watson, K. M. *Chemical Process Principles*; Wiley: New York, 1947; Vol. Vol. III.

(21) Boudart, M.; Djega-Mariadassou, G. *Kinetics of Heterogeneous Catalytic Reactions*; Princeton University Press: Princeton, 1984.

(22) Stoltze, P. "Microkinetic simulation of catalytic reactions", *Progress in Surface Science* **2000**, *65*, 65.

(23) Fishtik, I.; Callaghan, C.; Datta, R. Reaction network analysis of the kinetics of water-gas-shift reaction on Cu(111). In *Computational Material Science 15*; Leszczynski, J., Ed.; Elsevier, 2004.

(24) Fishtik, I.; Datta, R. "A thermodynamic approach to the systematic elucidation of unique reaction routes in catalytic reactions", *Chem. Eng. Sci.* **2000**, *55*, 4029.

(25) Fishtik, I.; Callaghan, C. A.; Datta, R. "Reaction Route Graphs. I. Theory and Algorithm", *J. Phys. Chem. B* **2004**, *108*, 5671.

(26) Fishtik, I.; Callaghan, C. A.; Datta, R. "Reaction Route Graphs. II. Examples of Enzyme- and Surface-Catalyzed Single Overall Reactions", *J. Phys. Chem. B* **2004**, *108*, 5683.

(27) Temkin, M. I. The kinetics of some industrial heterogeneous catalytic reactions. In *Advances in Catalysis*; Eley, D. D., Pines, H., Weisz, P. B., Eds.; Academic Press: New York, 1979; Vol. 28; pp 173.

(28) Horiuti, J.; Nakamura, T. "Theory of heterogeneous catalysis", *Adv. Catal.* **1967**, *17*, 1.

(29) Milner, P. C. "The possible mechanisms of complex reactions involving consecutive steps", *J. Electrochemical Society* **1964**, *111*, 228.

(30) Happel, J.; Sellers, H. "Analysis of the possible mechanisms for a catalytic reaction system", *Adv. Catal.* **1983**, *32*, 272.

(31) Farrauto, R.; Hwang, S.; Shore, L.; Ruettinger, W.; Lampert, J.; Giroux, T.; Liu, Y.; Ilinich, O. "New material needs for hydrocarbon fuel processing: generating hydrogen for the PEM fuel cell", *Annu. Rev. Mater. Res.* **2003**, *33*, 1.

(32) Gottesfeld, S. "*Preventing CO poisoning in fuel cells*." US Patent 4,910,099, 1990.

(33) Gottesfeld, S.; Pafford, J. "A new approach to the problem of carbon monoxide poisoning in fuel cells operating at low temperatures", *J. Electrochemical Society* **1988**, *135*, 2651.

(34) *The CRC Handbook of Chemistry and Physics*; 85th Online ed.; Lide, D. R., Ed.; CRC Press, 2004-2005.

(35) Amadeo, N. E.; Laborde, M. A. "Hydrogen Production from the Low Temperature Water-Gas Shift Reaction: Kinetics and Simulation of the Industrial Reactor", *Int. J. Hydrogen Energy* **1995**, *20*, 949.

(36) Campbell, J. S.; Craven, P.; Young, P. W. *Catalyst Handbook*; Wolfe Scientific Books: London, 1970.

(37) Tanaka, Y.; Utaka, T.; Kikuchi, R.; Sasaki, K.; Eguchi, K. "CO removal from reformed fuel over $Cu/ZnO/Al_2O_3$ catalysts prepared by impregnation and coprecipitation methods", *Applied Catal. A: General* **2002**, *6032*, 1.

(38) Li, Y.; Fu, Q.; Flytzani-Stephanopoulos, M. "Low-Temperature water-gas-shift reaction over Cu- and Ni-loaded cerium oxide catalysts", *Appl. Catal. B* **2000**, *27*, 179.

(39) Xue, E.; O'Keeffe, M. O.; Ross, J. R. H. "Water-gas shift conversion using a feed with a low steam to carbon monoxide ratio and containing sulfur", *Catal. Today* **1996**, *30*, 107.

(40) Zhao, H.; Hu, Y.; Li, J. "Reduced rate method for discrimination of the kinetic models for the water-gas shift reaction", *Journal of Molecular Catalysis A: Chemical* **1999**, *149*, 141.

(41) Xu, J.; Froment, G. F. "Methane Steam Reforming, Methanation and Water-Gas Shift: I. Instrinsic Kinetics", *AIChE Journal* **1989**, *35*, 88.

(42) Bohlbro, H. *An Investigation on the Conversion of Carbon Monoxide with Water Vapour over Iorn Oxide Based Catalysts*; Haldor Topsoe: Gjellerup, Copenhagen, 1969.

(43) Schuurman, Y.; Marquez-Alvarez, C.; Kroll, V. C. H.; Mirodatos, C. "Unraveling mechanistic features for the methane reforming by carbon dioxide over differnt metals and supports by TAP experiments", *Catal. Today* **1998**, *46*, 185.

(44) Boccuzzi, F.; Chiorino, A.; Manzoli, M.; Andreeva, D.; Tabakova, T. "FTIR study of the low temeprature water-gas shift reaction on Au/Fe_2O_3 and Au/TiO_2 catalysts", *J. Catal.* **1999**, *188*, 176.

(45) Grenoble, D. C.; Estadt, M. M.; Ollis, D. F. "The chemistry and catalysis of the water gas shift reaction. 1. the kinetics over supported metal catalysts." *J. Catal.* **1981**, *67*, 90.

(46) Serre, C.; Garin, F.; Belot, G.; Maire, G. "Reactivity of Pt/Al_2O_3 and $Pt-CeO_2/Al_2O_3$ Catalysts for the Oxidation of Carbon Monoxide by Oxygen", *J. Catal.* **1993**, *141*, 1.

(47) Basińska, A.; Domka, F. "The effect of lanthanides on the Ru/Fe_2O_3 catalysts for water-gas shift reaction", *Applied Catal. A: General* **1999**, *179*, 241.

(48) Basińska, A.; Kępiński, L.; Domka, F. "The effect of support on WGSR activity of ruthenium catalysts", *Applied Catalysis A: General* **1999**, *183*, 143.

(49) Erdőhelyi, A.; Fodor, K.; Suru, G. "Reaction of carbon monoxide with water on supported iridium catalysts", *Appl. Catal. A* **1996**, *139*, 131.

(50) Campbell, C. T.; Daube, K. A. "A surface science investigation of the water-gas shift reacton on copper(111)", *J. Catal.* **1987**, *104*, 109.

(51) Schumacher, N.; Boisen, A.; Dahl, S.; Gokhale, A. A.; Kandoi, S.; Grabow, L. C.; Dumesic, J. A.; Mavrikakis, M.; Chorkendorff, I. "Trends in low-temperature water-gas shift reactivity on transition metals", *J. Catal.* **2005**, *229*, 265.

(52) Askgaard, T. S.; Nørskov, J. K.; Ovesen, C. V.; Stoltze, P. "A kinetic model of methanol synthesis", *J. Catal.* **1995**, *156*, 229.

(53) Shido, T.; Iwasawa, Y. "The effect of coadsorbates in reverse water-gas shift reaction on ZnO, in relation to reactant-promoted reaction mechanism", *J. Catal.* **1993**, *140*, 575.

(54) Van Herwijnen, T.; De Jong, W. A. "Kinetics and mechanism of the CO shift on Cu/ZnO. I. Kinetics of the forward and reverse CO shift reactions", *J. Catal.* **1980**, *63*, 83.

(55) Callaghan, C. A.; Fishtik, I.; Datta, R.; Carpenter, M.; Chmielewski, M.; Lugo, A. "An improved microkinetic model for the water gas shift reaction on copper", *Surf. Sci.* **2003**, *541*, 21.

(56) Lund, C. R. F. "*Water-gas shift kinetics over iron oxide catalysts at membrane reactor conditions*," SUNY-Buffalo, 2001.

(57) Millar, G. J.; Rochester, C. H.; Howe, C.; Waugh, K. C. "A combined infrared, temperature programmed desoprtion and temperature programmed reaction spectroscopy study of CO_2 and H_2 interactions on reduced and oxidized silica-supported copper catalysts", *Molecular Physics* **1991**, *76*, 833.

(58) Lund, C. R. F.; Ma, D. Water gas shift kinetics at membrane reactor conditions.

(59) Ma, D.; Lund, C. R. F. "Assessing high-temperature water-gas shift membrane reactors", *Ind. Eng. Chem. Res.* **2003**, *42*, 711.

(60) Zeigarnik, A. V.; Callaghan, C. A.; Datta, R.; Fishtik, I.; Shustorovich, E. "Prediction of comparative catalytic activy in the series of single crystalline surfaces in a water-gas shift reaction", *Kinetics and Catalysis* **2005**, *46*, 543.

(61) Teng, B.-T.; Chang, J.; Yang, J.; Wang, G.; Zhang, C.-H.; Xu, Y.-Y.; Xiang, H.-W.; Li, Y.-W. "Water gas shift reaction kinetics in Fischer-Tropsch synthesis over an industrial Fe-Mn catalyst", *Fuel* **2005**, *84*, 917.

(62) Mhadeshwar, A. B.; Vlachos, D. G. "Microkinetic modeling for water-promoted CO oxidation, water-gas shift and preferential oxidation of CO on Pt", *J. Phys. Chem. B* **2004**, *108*, 15246.

(63) Mhadeshwar, A. B.; Vlachos, D. G. "Is the water-gas shift reaction on Pt simple? Computer-aided microkinetic model reduction, lumped rate expression, and rate-determining step", *Catalysis Today* **2005**.

(64) Graven, W. M.; Long, F. J. "Kinetics and mechanism of the two opposing reactions of the equilibrium $CO + H_2O = CO_2 + H_2$", *J. Am. Chem. Soc.* **1954**, *76*, 2602.

(65) Waugh, K. C. "Kinetic modeling of industrail catalytic processes based upon fundamental elementary kinetics under ultra high vacuum", *Chem. Eng. Sci.* **1996**, *51*, 1533.

(66) Van Herwijnen, T.; Guczalski, R. T.; De Jong, W. A. "Kinetics and mechanism of the CO shift on Cu/ZnO. II. Kinetics of the decomposition of formic acid", *J. Catal.* **1980**, *63*, 94.

(67) Van Herwijnen, T.; De Jong, W. A. "Kinetics and Mechanism of the CO shift on Cu/ZnO. I. Kinetics of the Forward and Reverse CO Shift Reactions", *J. Catal.* **1980**, *63*, 83.

(68) Moe, J. M. "Design of water-gas shift reactors", *Chem. Eng. Progr.* **1962**, *58*, 33.

(69) Shchibrya, G. G.; Morozov, N. M.; Temkin, M. I. "Kinetics and the mechanism of the catlytic reaction of carbon monoxide with water vapor. I. Reaction over an iron-chromium oxide catalyst", *Kinet. Catal. USSR* **1965**, *6*, 1057.

(70) Kul'kova, N. V.; Temkin, M. I. *Zh. Fiz. Khim.* **1939**, *23*, 695.

(71) Goodridge, F.; Quazi, H. A. "Water-gas shift reaction. Comparison of industrial catalysts", *Trans. Inst. Chem. Eng.* **1967**, *45*, T274.

(72) Laidler, K. J. *Chemical Kinetics*, 3rd ed.; Addison-Wesley, 1987.

(73) Masel, R. I. *Chemical Kinetics and Catalysis*; Wiley-Interscience: New York, 2001.

(74) NIST Chemistry WebBook; National Institute of Standards and Technology, 2005.

(75) Mhadeshwar, A. B.; Vlachos, D. G. "A thermodynamically consistent surface reaction mechanism for CO oxidation on Pt", *Combustion and Flame* **2005**.

(76) Fogler, H. S. *Elements of Chemical Reaction Engineering*, 3rd ed.; Prentice-Hall, Inc.: Upper Saddle River, NJ, 1999.

(77) Thoenes Jr., D.; Kramers, H. "Mass transfer from spheres in various regular packings to a flowing fluid", *Chem. Eng. Sci.* **1958**, *8*, 271.

(78) Roine, A. HSC Chemistry; Ver. 4.1 ed.; Outokumpu Research: Oy, Pori, Finland.

(79) MicroMath® Scientist® for Windows™; MicroMath, Inc., 1986-1995.

(80) Desai, S.; Neurock, M. "A first principles analysis of CO oxidation over Pt and $Pt_{66.7\%}Ru_{33.3\%}$(111) surfaces", *Electrochimica Acta* **2003**, *48*, 3759.

(81) Neurock, M. "Perspectives on the first principles elucidation and the design of active sites", *J. Catal.* **2003**, *216*, 73.

(82) Pallassana, V.; Neurock, M.; Lusvardi, V. S.; Lerou, I. J.; Kragten, D. D.; van Santen, R. A. "A density functional theory analysis of the reaction pathways and intermediates for ethylene dehydrogenation over Pd(111)", *J. Phys. Chem. B* **2002**, *106*, 1656.

(83) Saeys, M.; Reyniers, M.-F.; Thybaut, J. W.; Neurock, M.; Marin, G. B. "First-principles based kinetic model for the hydrogenation of toluene", **2005**, *236*, 129.

(84) Gokhale, A. A.; Kandoi, S.; Greeley, J. P.; Mavrikakis, M.; Dumesic, J. A. "Molecular-level descriptions of surface chemistry in kinetic models using density functional theory", *Chem. Eng. Sci.* **2004**, *59*, 4679.

(85) Greeley, J.; Mavrikakis, M. "Competitive paths for methanol decomposition on Pt(111)", *J. Am. Chem. Soc.* **2004**, *126*, 3910.

(86) Olivera, P. P.; Patrito, E. M.; Sellers, H. "Direct synthesis of methanol over metallic catalysts", *Surf. Sci.* **1995**, *327*, 330.

(87) Olivera, P. P.; Patrito, E. M.; Sellers, H. "Hydrogen peroxide synthesis over metallic catalysts", *Surf. Sci.* **1994**, *313*, 25.

(88) Shustorovich, E.; Bell, A. T. "Synthesis and decomposition of ammonia on transition metal surfaces: bond-order-conservation-Morse-potential analysis", *Surface Science Letters* **1991**, *259*, L791.

(89) Shustorovich, E.; Bell, A. T. "Decomposition and reduction of NO on transition metal surfaces: bond order conservation Morse potential analysis", *Surface Science* **1993**, *289*, 127.

(90) Anderson, R. B. *The Fischer-Tropsch Synthesis*; Academic Press: New York, 1984.

(91) Shustorovich, E.; Bell, A. T. "An analysis of Fischer-Tropsch synthesis by the bond-order-conservation-Morse-potential approach", *Surface Science* **1991**, *248*, 359.

(92) Bell, A. T. Relationship of reaction energetics to the mechanism and kinetics of heterogeneously catalyzed reactions. In *Metal-Surface Reaction Energetics: Theory and Applications to Heterogeneous Catalysis, Chemisorption and Surface Diffusion*; Shustorovich, E., Ed.; VCH Publishers, Inc., 1991; pp 191.

(93) Hei, M. J. C., H.B.;Yi, J.; Lin, Y.J.;Wei, G.;Liao, D.W. "CO_2 reforming of methane on transition metal surfaces", *Surf. Sci.* **1998**, *417*, 82.

(94) Bell, A. T. Relationship of Reaction Energetics to the Mechanism and Kinetics of Heterogeneously Catalyze Reactions. In *Metal-Surface Reaction Energetics: Theory and Application to Heterogeneous Catalysis, Chemisorption, and Surface Diffusion*; Shustorovich, E., Ed.; VCH Publishers, Inc., 1991; pp 191.

(95) Frisch, M. J.; Trucks, G. W.; Schlegel, H. B.; Scuseria, G. E.; Robb, M. A.; Cheeseman, J. R.; Montgomery Jr., J. A.; Vreven, T.; Kudin, K. N.; Burant, J. C.; Millam, J. M.; Iyengar, S. S.; Tomasi, J.; Barone, V.; Mennucci, B.; Cossi, M.; Scalmani, G.; Rega, N.; Petersson, G. A.; Nakatsuji, H.; Hada, M.; Ehara, M.; Toyota, K.; Fukuda, R.; Hasegawa, J.; Ishida, M.; Nakajima, T.; Honda, Y.; Kitao, O.; Nakai, H.; Klene, M.; Li, X.; Knox, J. E.; Hratchian, H. P.; Cross, J. B.; Adamo, C.; Jaramillo, J.; Gomperts, R.; Stratmann, R. E.; Yazyev, O.; Austin, A. J.; Cammi, R.; Pomelli, C.; Ochterski, J. W.; Ayala, P. Y.; Morokuma, K.; Voth, G. A.; Salvador, P.; Dannenberg, J. J.; Zakrzewski, V. G.; Dapprich, S.; Daniels, A. D.; Strain, M. C.; Farkas, O.; Malick, D. K.; Rabuck, A. D.; Raghavachari, K.; Foresman, J. B.; Ortiz, J. V.; Cui, Q.; Baboul, A. G.; Clifford, S.; Cioslowski, J.;

Stefanov, B. B.; Liu, G.; Liashenko, A.; Piskorz, P.; Komaromi, I.; Martin, R. L.; Fox, D. J.; Keith, T.; Al-Laham, M. A.; Peng, C. Y.; Nanayakkara, A.; Challacombe, M.; Gill, P. M. W.; Johnson, B.; Chen, W.; Wong, M. W.; Gonzalez, C.; Pople, J. A. Gaussian 03W; Gaussian, Inc.: Wallingford, CT, 2004.

(96) Mhadeshwar, A. B.; Wang, H.; Vlachos, D. G. "Thermodynamic consistency in microkinetic development of surface reaction mechanisms", *J. Phys. Chem. B* **2003**, *107*, 12721.

(97) De Donder, T.; Van Rysselberghe, P. *Thermodynamic Theory of Affinity: a Book of Principles*; Stanford University Press: Stanford University, CA, 1936.

(98) Van Rysselberghe, P. "Consistency between kinetics and thermodynamics", *Chem. Eng. Sci.* **1967**, *22*, 706.

(99) Schilling, C. H.; Palsson, B. O. "The underlying pathway structure of biochemical reaction networks", *Proc. Natl. Acad. Sci. USA* **1998**, *95*, 4193.

(100) Wagner, C. "Adsorbed atomic species as intermediates in heterogeneous catalysis", *Adv. Catal.* **1970**, *21*, 323.

(101) Fishtik, I.; Datta, R. "A new approach for the classification and enumeration of unique reaction routes and unique overall reactions in multiple chemical reaction systems", *Chem. Eng. Comm.* **2004**, *191*, 373.

(102) Fishtik, I.; Gutman, I.; Nagypál, I. "Response reactions in chemical thermodynamics", *J. Chem. Soc., Faraday Trans.* **1996**, *92*, 3525.

(103) Deo, N. *Graph Theory with Applications to Engineering and Computer Science*; Prentice-Hall: Englewood Cliffs, NJ, 1974.

(104) Bockris, J. O. M.; Reddy, A. K. N. *Modern Electrochemistry*; Plenum Press: New York, 1973.

(105) Balaban, A. T. Reaction Graphs. In *Graph Theorectical Approaches to Chemical Reactivity*; Bonchev, D., Menkenyan, O., Eds.; Kluwer Academic Pub.: Dordrecht, The Netherlands, 1994; pp 137.

(106) Temkin, O. N.; Zeigarnik, A. V.; Bonchev, D. *Chemical Reaction Networks: A Graph-Theoretical Approach*; CRC Press: New York, 1996.

(107) Fan, L. T.; Bertok, B.; Friedler, F. "A graph-theoretic method to identify candidate mechanisms for deriving the rate law of a catlytic reaction", *Comp. Chem.* **2002**, *26*, 265.

(108) Trinajstic, N. *Chemical Graph Theory*; CRC Press: Boca Raton, FL, 1983.

(109) Broadbelt, L. J.; Stark, S. M.; Klein, M. T. "Computer generated reaction modeling: decomposition and encoding algorithms for determining species uniqueness", *Comp. Chem. Eng.* **1996**, *20*, 113.

(110) Susnow, R. G.; Dean, M. A.; Green, W. H.; Peczak, P.; Broadbelt, L. J. "Rate-based construction of kinetic models for complex systems", *J. Phys. Chem. A* **1997**, *101*, 3731.

(111) Ratkiewicz, A.; Truong, T. N. "Application of chemical graph theory for automated mechanism generation", *J. Chem. Inf. Comp. Sci.* **2003**, *43*, 36.

(112) Christiansen, J. A. "The elucidation of reaction mechanisms by the method of intermediates in quasi-stationary concentrations", *Adv. Catal.* **1953**, *5*, 311.

(113) King, E. L.; Altman, C. "A systematic method of deriving the rate laws for enzyme-catalyzed reactions", *J. Phys. Chem.* **1956**, *60*, 6676.

(114) Temkin, M. I.; Knaster, M. B. "Rate of ionization of hydrogen on active elctrodes", *Dokl. Akad. Nauk. SSSR* **1963**, *152*, 156.

(115) Yatsimirskii, K. B. *Application of the Graph Method in Chemistry*; Khimiya: Moscow, 1971.

(116) Balaban, A. T.; Farcasiu, D.; Banica, R. "Graphs of multiple 1,2-shifts in carbonium ions and related systems", *Rev. Roum. Chim.* **1966**, *11*, 1205.

(117) Balaban, A. T. "Applications of graph theory in chemistry", *J. Chem. Inf. Comp. Sci.* **1985**, *25*, 334.

(118) Clarke, B. L. "Stoichiometric network analysis", *Cell Biophys.* **1988**, *12*, 237.

(119) Sen, A. K. "Quantitative analysis of metabolic regulation. A graph-theoretic approach using spanning trees", *Biochem. J.* **1991**, *275*, 253.

(120) Heinrich, R.; Schuster, S. *The Regulation of Cellular Systems*; Chapman and Hall: New York, 1996.

(121) Beard, D. A.; Liang, S.-D.; Qian, H. "Energy balance for analysis of complex metabolic networks", *Biophys. J.* **2002**, *83*, 79.

(122) Fehribach, J. D. "Diffusion-reaction-conduction processes in porous electrodes: the electrolyte wedge problem", *Euro. J. of Appl. Math.* **2001**, *12*, 77.

(123) Fehribach, J. D.; Prins-Jansen, J. A.; Hemmes, K.; de Wit, J. H. W.; Call, F. W. "On modeling molten carbonate fuel-cell cathodes by electrochemical potentials", *J. Appl. Electrochem.* **2000**, *30*, 1015.

(124) Oster, G. F.; Perelson, A. L.; Katchalsky, A. "Network thermodynamics: dynamic modelling of biophysical systems", *Quart. Rev. of Biophys.* **1973**, *6*, 1.

(125) Oster, G. F.; Perelson, A. L. "Chemical Reaction Networks", *IEEE Trans. Circuits and Sys.* **1974**, *CAS-21*, 709.

(126) Bockris, J. O. M.; Srinivasan, S. *Fuel Cells: Their Electrochemistry*; McGraw-Hill: New York, 1969.

(127) Shiner, J. S. "A Lagrangian formulation of chemical reaction dynamics far from equilibrium", *Adv. Therm.* **1992**, *6*, 248.

(128) Broadbelt, L. J.; Snurr, R. Q. "Applications of molecular modeling in heterogeneous catalysis research", *Applied Catal. A: General* **2000**, *200*, 23.

(129) Balabanian, N.; Bickart, T. A. *Electrical Network Theory*; John Wiley: New York, 1969.

(130) Clay, R. *Nonlinear Networks and Systems*; John Wiley: New York, 1971.

(131) Sieniutycz, S. "Nonlinear macrokinetics of heat and mass transfer and chemical or electrochemical reactions", *International Journal of Heat and Mass Transfer* **2004**, *47*, 515.

(132) Gleiss, P. M.; Stadler, P. F.; Wagner, A.; Fell, D. A. *Adv. Complex Systems* **2001**, *1*, 1.

(133) Conway, B. E.; Tilak, B. V. "Interfacial processes involving electrocatalytic evolution and oxidation of H2, and the role of chemisorbed H ", *Electrochimica Acta* **2002**, *47*, 3571.

(134) Fishtik, I.; Callaghan, C. A.; Datta, R. "Reaction Route Graphs. III. Non-Minimal Kinetic Mechanisms", *J. Phys. Chem. B* **2005**, *109*, 2710.

(135) Okino, M. S.; Mavrovouniotis, M. L. "Simplification of mathematical models of chemical reaction systems", *Chem. Rev. (Washington, DC)* **1998**, *98*, 391.

(136) Boudart, M. "Two-step catalytic reactions", *AIChE Journal* **1972**, *18*, 465.

(137) Patrito, E. M.; Olivera, P. P.; Sellers, H. "The nature of chemisorbed hydroxyl radicals", *Surface Science* **1994**, *306*, 447.

(138) Wang, G.; Jiang, L.; Cai, Z.; Pan, Y.; Zhao, X.; Huang, W.; Xie, K.; Li, Y.; Sun, Y.; Zhong, B. "Surface structure sensitivity of the water-gas shift reaction on Cu(hkl) surfaces: A theoretical study", *J. Phys. Chem. B* **2003**, *107*, 557.

(139) Wilmer, H.; Genger, T.; Hinrichsen, O. "The interaction of hydrogen with alumina-supported copper catalysts: a temperature-programmed

adsorption/temperature-programmed desorption/isotopic exchange reaction study", *J. Catal.* **2003**, *215*, 188.

(140) Fu, Q.; Deng, W.; Saltsburg, H.; Flytzani-Stephanopoulos, M. "Activity and stability of low-content gold-cerium oxide catalysts for the water-gas shift reaction", *Applied Catalysis B: Environmental* **2005**, *56*, 57.

(141) Koryabkina, N. A.; Phatak, A. A.; Ruettinger, W. F.; Farrauto, R. J.; Ribeiro, F. H. "Determination of kinetic parameters for the water–gas shift reaction on copper catalysts under realistic conditions for fuel cell applications", *J. Catal.* **2003**, *217*, 233.

(142) Salmi, T.; Hakkarainen, R. "Kinetic study of the low-temperature water-gas shift reaction over a copper-zinc oxide catalyst", *Appl. Catal.* **1989**, *49*, 285.

(143) Ernst, K. H.; Campbell, C. T.; Moretti, G. "Kinetics of the reverse water-gas shift reaction over copper(110)", *J. Catal.* **1992**, *134*, 66.

(144) Chinchen, G. C.; Waugh, K. C.; Whan, D. A. "The activity and state of the copper surface in methanol synthesis catalysts", *Applied Catalysis* **1986**, *25*, 101.

(145) Lucas, M.; McCue, M.; Schmeer, J. Rational Design of Water Gas Shift Catalyst. Major Qualifying Report, Worcester Polytechnic Institute, 2002.

(146) Jakdetchai, O.; Nakajima, T. "Mechanism of the water-gas shift reaction over Cu(110), Cu(111) and Cu(100) surfaces: an AM1-d study", *Journal of Molecular Structure (Theochem)* **2002**, *619*, 51.

(147) Benziger, J. Thermochemical Methods for Reaction Energetics on Metal Surfaces. In *Metal-Surface Reaction Energetics: Theory and Applications to Heterogeneous Catalysis, Chemisorption, and Surface Diffusion*; Shustorovich, E., Ed.; VCH Publishers, Inc.: New York, 1991; pp 53.

(148) Benziger, J. "Thermochemistry of metal catalyzed reactions", *Catal. Today* **1994**, *21*, 211.

(149) Pauling, L. *The Nature of the Chemical Bond*; Cornell University Press: Ithaca, 1960.

(150) Benziger, J. "Thermodynamics of adsorption of diatomic molecules on transition metal surfaces", *Appl. Surf. Sci. (1977-1985)* **1980**, *6*, 105.

Appendix

Appendix A: UBI-QEP calculated energetics

Activation Energy and Enthalpy Data (no OH bond effects)

			Cu(111)	Ni(111)	Pd(111)	Pt(111)	Rh(111)
s_1	**CO + S ⇆ CO·S**						
		△H =	-12.0	-27.0	-34.0	-32.0	-32.0
		E_f =	0.0	0.0	0.0	0.0	0.0
		E_r =	12.0	27.0	34.0	32.0	32.0
s_2	**H_2O +S ⇆ H_2O·S**						
		△H =	-13.6	-16.5	-10.0	-9.6	-13.3
		E_f =	0.0	0.0	0.0	0.0	0.0
		E_r =	13.6	16.5	10.0	9.6	13.3
s_3	**H_2O·S + S ⇆ OH·S + H·S**						
		△H =	23.8	10.6	26.0	28.0	19.3
		E_f =	25.4	20.8	26.0	28.0	23.5
		E_r =	1.6	10.2	0.0	0.0	4.2
s_4	**CO·S + O·S ⇆ CO_2·S + S**						
		△H =	-17.3	8.5	-9.8	-13.6	1.8
		E_f =	10.7	21.9	24.4	23.2	24.4
		E_r =	28.0	13.4	34.2	36.8	22.6
s_5	**COS + OHS ⇆ HCOOS + S**						
		△H =	-20.4	-7.7	4.1	2.4	-0.2
		E_f =	0.0	5.5	11.2	9.9	9.7
		E_r =	20.4	13.2	7.1	7.5	9.9
s_6	**OH·S + S ⇆ O·S + H·S**						
		△H =	-5.2	-15.1	-7.0	-5.4	-10.0
		E_f =	15.5	12.8	14.6	15.1	14.1
		E_r =	20.7	27.9	21.6	20.5	24.1
s_7	**COS + OHS ⇆ CO_2S + HS**						
		△H =	-22.5	-6.6	-16.8	-19.0	-8.2
		E_f =	0.0	6.1	0.8	0.0	5.7
		E_r =	22.5	12.7	17.6	19.0	13.9

s_8 **$HCOO{\cdot}S + S \leftrightarrows CO_2{\cdot}S + H{\cdot}S$**

△H =	-2.1	1.1	-20.9	-21.4	-8.0
E_f =	1.4	3.5	0.0	0.0	0.0
E_r =	3.5	2.4	20.9	21.4	8.0

s_9 **$HCOO{\cdot}S + O{\cdot}S \leftrightarrows CO_2{\cdot}S + OH{\cdot}S$**

△H =	3.1	16.2	-13.9	-16.0	2.0
E_f =	4.0	16.2	0.0	0.0	3.4
E_r =	0.9	0.0	13.9	16.0	1.4

s_{10} **$H_2O{\cdot}S + O{\cdot}S \leftrightarrows 2OH{\cdot}S$**

△H =	29.0	25.7	33.0	33.4	29.3
E_f =	29.0	28.1	33.0	33.4	29.3
E_r =	0.0	2.4	0.0	0.0	0.0

s_{11} **$H_2O{\cdot}S + H{\cdot}S \leftrightarrows OH{\cdot}S + H_2{\cdot}S$**

△H =	26.3	25.8	39.4	39.6	30.9
E_f =	26.3	25.8	39.4	39.6	30.9
E_r =	0.0	0.0	0.0	0.0	0.0

s_{12} **$OH{\cdot}S + H{\cdot}S \leftrightarrows O{\cdot}S + H_2{\cdot}S$**

△H =	-2.7	0.1	6.4	6.2	1.6
E_f =	1.3	3.3	6.4	6.2	3.8
E_r =	4.0	3.2	0.0	0.0	2.2

s_{13} **$HCOO{\cdot}S + OH{\cdot}S \leftrightarrows CO_2{\cdot}S + H_2O{\cdot}S$**

△H =	-25.9	-9.5	-46.9	-49.4	-27.3
E_f =	0.9	11.6	0.0	0.0	0.0
E_r =	26.8	21.1	46.9	49.4	27.3

s_{14} **$HCOO{\cdot}S + H{\cdot}S \leftrightarrows CO_2{\cdot}S + H_2{\cdot}S$**

△H =	0.4	16.3	-7.5	-9.8	3.6
E_f =	14.6	24.8	9.3	7.7	16.7
E_r =	14.2	8.5	16.8	17.5	13.1

s_{15} **$CO_2{\cdot}S \leftrightarrows CO_2 + S$**

△H =	5.3	6.5	3.8	3.6	5.2
E_f =	5.3	6.5	3.8	3.6	5.2
E_r =	0.0	0.0	0.0	0.0	0.0

s_{16} **H·S + H·S ⇆ H_2·S + S**

△H =	2.5	15.2	13.4	11.6	11.6
E_f =	15.3	23.4	22.2	21.1	21.1
E_r =	12.8	8.2	8.8	9.5	9.5

s_{17} **H_2·S ⇆ H_2 + S**

△H =	5.5	6.8	6.6	6.4	6.4
E_f =	5.5	6.8	6.6	6.4	6.4
E_r =	0.0	0.0	0.0	0.0	0.0

s_{18} **H·S + H·S ⇆ H_2 + 2S**

△H =	8.0	22.0	20.0	18.0	18.0
E_f =	15.3	23.4	22.2	21.1	21.1
E_r =	7.3	1.4	2.2	3.1	3.1

Activation Energy and Enthalpy Data (no OH bond effects)

		Ru(001)	Ir(111)	Fe(110)	Au(111)	Ag(111)
s_1	**$CO + S \leftrightarrows CO{\cdot}S$**					
	$\triangle H =$	-29.0	-34.0	-32.0	-25.0	-6.0
	$E_f =$	0.0	0.0	0.0	0.0	0.0
	$E_r =$	29.0	34.0	32.0	25.0	6.0
s_2	**$H_2O + S \leftrightarrows H_2O{\cdot}S$**					
	$\triangle H =$	1.5	15.6	-9.3	38.9	31.0
	$E_f =$	8.5	15.6	2.7	38.9	31.0
	$E_r =$	7.0	0.0	12.0	0.0	0.0
s_3	**$H_2O{\cdot}S + S \leftrightarrows OH{\cdot}S + H{\cdot}S$**					
	$\triangle H =$	14.4	26.9	7.9	46.5	39.6
	$E_f =$	21.4	26.9	19.9	46.5	39.6
	$E_r =$	7.0	0.0	12.0	0.0	0.0
s_4	**$CO{\cdot}S + O{\cdot}S \leftrightarrows CO_2{\cdot}S + S$**					
	$\triangle H =$	-3.0	-4.3	16.1	-29.8	-44.0
	$E_f =$	22.5	24.9	25.2	18.8	5.6
	$E_r =$	25.5	29.2	9.1	48.6	49.6
s_5	**$CO{\cdot}S + OH{\cdot}S \leftrightarrows HCOO{\cdot}S + S$**					
	$\triangle H =$	-2.9	3.3	-3.2	-1.9	-23.0
	$E_f =$	7.7	11.3	9.0	6.2	0.0
	$E_r =$	10.6	8.0	12.2	8.1	23.0
s_6	**$OH{\cdot}S + S \leftrightarrows O{\cdot}S + H{\cdot}S$**					
	$\triangle H =$	-15.5	-4.6	-16.7	14.1	5.0
	$E_f =$	12.3	15.6	12.4	21.3	18.3
	$E_r =$	27.8	20.2	29.1	7.2	13.3
s_7	**$CO{\cdot}S + OH{\cdot}S \leftrightarrows CO_2{\cdot}S + H{\cdot}S$**					
	$\triangle H =$	-18.5	-8.9	-0.6	-15.7	-39.0
	$E_f =$	0.0	5.2	10.3	0.0	0.0
	$E_r =$	18.5	14.1	10.9	15.7	39.0

s_8 **$HCOO{\cdot}S + S \leftrightarrows CO_2{\cdot}S + H{\cdot}S$**

△H =	-15.6	-12.2	2.6	-13.8	-16.0
E_f =	0.0	0.0	4.4	0.0	0.0
E_r =	15.6	12.2	1.8	13.8	16.0

s_9 **$HCOO{\cdot}S + O{\cdot}S \leftrightarrows CO_2{\cdot}S + OH{\cdot}S$**

△H =	-0.1	-7.6	19.3	-27.9	-21.0
E_f =	2.2	0.0	19.3	0.0	0.0
E_r =	2.3	7.6	0.0	27.9	21.0

s_{10} **$H_2O{\cdot}S + O{\cdot}S \leftrightarrows 2OH{\cdot}S$**

△H =	29.9	31.5	24.6	32.4	34.6
E_f =	29.9	31.5	28.1	32.4	34.6
E_r =	0.0	0.0	3.5	0.0	0.0

s_{11} **$H_2O{\cdot}S + H{\cdot}S \leftrightarrows OH{\cdot}S + H_2{\cdot}S$**

△H =	36.8	33.1	24.8	30.8	34.9
E_f =	36.8	33.1	24.8	30.8	34.9
E_r =	0.0	0.0	0.0	0.0	0.0

s_{12} **$OH{\cdot}S + H{\cdot}S \leftrightarrows O{\cdot}S + H_2{\cdot}S$**

△H =	6.9	1.6	0.2	-1.6	0.3
E_f =	7.0	3.5	3.4	1.0	10.6
E_r =	0.1	1.9	3.2	2.6	10.3

s_{13} **$HCOO{\cdot}S + OH{\cdot}S \leftrightarrows CO_2{\cdot}S + H_2O{\cdot}S$**

△H =	-30.0	-39.1	-5.3	-60.3	-55.6
E_f =	0.0	0.0	14.4	0.0	0.0
E_r =	30.0	39.1	19.7	60.3	55.6

s_{14} **$HCOOS + HS \leftrightarrows CO_2S + H_2S$**

△H =	6.8	-6.0	19.5	-29.5	-20.7
E_f =	18.7	10.4	26.9	0.0	0.8
E_r =	11.9	16.4	7.4	29.5	21.5

s_{15} **$CO_2{\cdot}S \leftrightarrows CO_2 + S$**

	5.3	6.5	3.8	3.6	5.2
△H =	5.0	4.3	6.9	2.8	3.0
E_f =	5.0	4.3	6.9	2.8	3.0
E_r =	0.0	0.0	0.0	0.0	0.0

s_{16} **H·S + H·S ⇆ H_2S + S**

△H =	22.4	6.2	16.9	-15.7	-4.7
E_f =	28.0	17.6	24.5	3.7	10.7
E_r =	5.6	11.4	7.6	19.4	15.4

s_{17} **H_2·S ⇆ H_2 + S**

△H =	7.6	5.8	7.1	3.7	4.7
E_f =	7.6	5.8	7.1	3.7	4.7
E_r =	0.0	0.0	0.0	0.0	0.0

s_{18} **H·S + H·S ⇆ H_2 + 2S**

△H =	30.0	12.0	24.0	-12.0	0.0
E_f =	30.0	17.6	24.5	3.7	10.7
E_r =	0.0	5.6	0.5	15.7	10.7

Appendix B: Reaction Route Enumeration Program (Matlab)

```
% ========================================================================
%    Reaction Route Algorithm w/ Numerical Analysis
%
%    version - wgsr18
%
%    written by Caitlin A. Callaghan
%    originated - 28 June 2005
%    modified - 20 April 2006
%
% ========================================================================
%  Description:
%
%  This program is designed to perform the following tasks for a reaction
%  mechanism:
%
%       1. Read in mechanism's stoichiometric matrix
%       2. Verify reactions and matrix entries
%       3. Enumerate FRs, ERs, INs, TNs
%             -> store in corresponding cycle matrices
%             -> output to file in extended form
%       4. Read in reaction energetics
%       5. Check thermodynamic consistency
%             -> adjust energetics as needed
%       6. Run overall mechanism
%             -> store data in corresponding matrix
%             -> output data to file
%       7. Run RR's mechanisms
%             -> store data in corresponding matrix
%             -> output data to file
%       8. Run simplified mechanism
%             -> store data in corresponding matrix
%             -> output data to file
%       9. Generate plots
%
% ------------------------------------------------------------------------


clear;

global id
```

```
disp('User - welcome to the RR program');
disp(' ');

% ------------------------------------------------------------------------
--------------------
%  User instructions to setup source file containing stoichiometric matrix and
reaction energetics
% ------------------------------------------------------------------------
--------------------

disp('To begin, you must first setup your source file. This file will contain
the');
disp('stoichiometric matrix of your mechanism and your reaction
energetics.');disp(' ');
disp('Using MS Excel, create a source file with two tabs labeled as follows:');
disp('          TAB 1:  change name to "stoich"');
disp('            - this tab will contain your stoichiometric matrix with
rows');
disp('              corresponding to reaction steps and columns
corresponding');
disp('              to species, ordered intermediates followed by terminal
species');disp(' ');
disp('          TAB 2:  change name to "preexp"');
disp('            - this tab will contain your pre-exponential factors with
rows');
disp('              corresponding to reaction steps and columns
corresponding');
disp('              to the forward and reverse, in that order, reaction
directions');disp(' ');
disp('          TAB 3:  change name to "actenergy"');
disp('            - this tab will contain your activation energies with rows');
disp('              corresponding to reaction steps and columns
corresponding');
disp('              to the forward and reverse, in that order, reaction
directions');disp(' ');
disp('Save this file as "mechSOURCE.xls" where the "mech" is replaced by some
mechanism');
disp('identifier (up to 8 characters), in a directory named with the same
identifier.');disp(' ');
disp('EXAMPLE:  For a 17-step water gas shift reaction mechanism,
"wgsr17SOURCE.xls"');
```

```
disp('would be saved in the "...\wgsr17" directory.');disp(' ');

% ------------------------------------------------------------------------
--------------------
%  User source file confirmation and identification
% ------------------------------------------------------------------------
--------------------

userconfirm = input('Has the source file been completed correctly? (1-yes/2-no)
-> ');disp(' ');

if userconfirm==1
    sourcefile = input('Please enter the source file name (enclosed by single
quotes): '),disp(' ');

else
    disp('Please complete the source file correctly then run this program
again.');
    break;
end




% ------------------------------------------------------------------------
--------------------
%  Program options
% ------------------------------------------------------------------------
--------------------

disp('Select from the following tasks:');disp(' ');
disp('       1 - Read in mechanism''s stoichiometric matrix');
disp('       2 - Verify reactions and matrix entries');
disp('       3 - Enumerate FRs, ERs, INs, TNs');
disp('       4 - Read in reaction energetics');
disp('       5 - Check thermodynamic consistency');
disp('       6 - Run overall mechanism');
disp('       7 - Run RR''s mechanisms');
disp('       8 - Run simplified mechanism');
disp('       9 - Generate plots');
disp('       0 - Exit program');disp(' ');
```

```
task = input('User, what would you like to do? (select a number) -> ');

while task ~= 0
      % ------------------------------------------------------------------------
----------------------
      %  1 - Read in mechanism's stoichiometric matrix
      % ------------------------------------------------------------------------
----------------------
      while task==1
       disp(' ');
       disp('Reading in mechanism''s stoichiometric matrix...');disp(' ');
       v = xlsread(sourcefile, 'stoich');

       display_v = input('User, would you like to view the stoichiometric
matrix? (1-yes/2-no) -> ');disp(' ');
       if display_v == 1, v, end

       dimv=size(v);
       nES=dimv(1,1); nSPECIES=dimv(1,2)

            disp('Select from the following tasks:');disp(' ');
            disp('       1 - Read in mechanism''s stoichiometric matrix');
            disp('       2 - Verify reactions and matrix entries');
            disp('       3 - Enumerate FRs, ERs, INs, TNs');
            disp('       4 - Read in reaction energetics');
            disp('       5 - Check thermodynamic consistency');
            disp('       6 - Run overall mechanism');
            disp('       7 - Run RR''s mechanisms');
       disp('       8 - Run simplified mechanism');
            disp('       9 - Generate plots');
            disp('       0 - Exit program');disp(' ');

            task = input('User, what would you like to do NEXT? (select a
number) -> ');
      end

      % ------------------------------------------------------------------------
----------------------
      %  2 - Verify reactions and matrix entries
      % ------------------------------------------------------------------------
----------------------
      while task==2
```

```
        disp(' ');
        disp('Verifying reaction steps and stoichiometric matrix
entries...');disp(' ');

        rxnR=sym(zeros(nES,1)); rxnP=sym(zeros(nES,1));

        species = sym('species')
        disp('User, enter your species in the order they appear in the
stoichiometric matrix');
        disp('in the following format (enclosed in single quotes).  EXAMPLE:
''h2o_s'''); disp(' ');
%         for i=1:nSPECIES, disp(' '); disp(i); species(i,1)=input('Species:');
end

syms h2o_s co_s co2_s h_s h2_s oh_s o_s hcoo_s co3_s cooh_s s h2o co co2 h2;
species=transpose([h2o_s, co_s, co2_s, h_s, h2_s, oh_s, o_s, hcoo_s, s, h2o,
co, co2, h2]);

        for i=1:nSPECIES, disp(' '); species(i,1)=sym(species(i,1)); end

        for i=1:nES, for j=1:nSPECIES
            if v(i,j)<0
                rxnR(i)=rxnR(i)-v(i,j)*species(j);
            else
                rxnP(i)=rxnP(i)+v(i,j)*species(j);
            end
        end
             end

             [transpose([1:nES]),rxnR,rxnP]

        syms s1     s2 s3 s4 s5  s6 s7 s8 s9  s10    s11    s12    s13    s14
       s15    s16    s17    s18;
        id = transpose([s1 s2 s3 s4 s5  s6 s7 s8 s9  s10    s11    s12    s13
       s14    s15    s16    s17    s18]);

%       NEED WORK MERGING COLUMNS WITH "=" IN BETWEEN
%         for i=1:nES
%             ESlist(i,1)=char([rxnR(i,1),'<->',rxnP(i,1)])
%         end

            disp('Select from the following tasks:');disp(' ');
```

```
            disp('       1 - Read in mechanism''s stoichiometric matrix');
            disp('       2 - Verify reactions and matrix entries');
            disp('       3 - Enumerate FRs, ERs, INs, TNs');
            disp('       4 - Read in reaction energetics');
            disp('       5 - Check thermodynamic consistency');
            disp('       6 - Run overall mechanism');
            disp('       7 - Run RR''s mechanisms');
        disp('       8 - Run simplified mechanism');
            disp('       9 - Generate plots');
            disp('       0 - Exit program');disp(' ');

            task = input('User, what would you like to do NEXT? (select a
number) -> ');
       end

    % ------------------------------------------------------------------------
--------------------
       %  3 - Enumerate FRs, ERs, INs, TNs
       % ------------------------------------------------------------------------
----------------------
       while task==3
        disp(' ');
        disp('Enumerating the FRs, ERs, INs, TNs...');disp(' ');

        rxns = v*species;
            vT=transpose(v);

            % Full Routes
            FullR = input('calculate FRs?  (1-yes/2-no):    ')
            if(FullR==1)

        % User defined output files
        outputfile1 = input('User, name the output file containing the UNIQUE
the calculated RRs (''file.txt''): '); disp('');
        outputfile2 = input('User, name the output file containing the ALL
calculated RRs (''file.txt''): '); disp('');

            fid1 = fopen(outputfile1,'a');
            fid2 = fopen(outputfile2,'a');
        fida = fopen('wgsr18CucycleM.txt','a');
```

```
        nINTS = input('User, how many intermediate species exist? '); disp('');

             intM=[v(1:nES,1:nINTS)];
        ES=rank(intM)+1

        wgsr18CucycleM;
             cycle=FRtemp;
%            cycle=zeros(1,nES(1,1));
             cycletemp=zeros(1,nES(1,1));

             rr=25001; %RR counter
        rrmax=factorial(18)/factorial(9)/factorial(9);
while rr<=rrmax
             cyclenum=369; %cycle counter
             comp=[2 3 4 5 7 9 14 15 17]; %initial components
             while comp(1)<=(nES-8)
         while comp(2)<=(nES-7)
          while comp(3)<=(nES-6)
           while comp(4)<=(nES-5)
            while comp(5)<=(nES-4)
             while comp(6)<=(nES-3)
              while comp(7)<=(nES-2)
               while comp(8)<=(nES-1)
                while comp(9)<=nES
                  cycletemp=zeros(1,nES(1,1));
                        for(i=1:ES),matrix(i,ES)=id(comp(i));end
                        for(i=1:ES),for(j=1:ES-
1),matrix(i,j)=v(comp(i),j);end,end
                        for i=1:ES
                            refi=i;  k=1;
                            while k<=(ES-1)
                               for j=1:ES
                                    if j~=refi
                                        submatrix(k,:)=matrix(j,1:(ES-1));
                                        k=k+1;
                                    end
                               end
                            end
                            cycletemp(comp(refi))=(-
1)^(i+ES)*det(double(submatrix));
                        end
                    q=1;cycletest=cycletemp;
```

```
                        while q<=nES(1,1)
                            if(cycletest(q)<0),neg=-1;q=1+nES(1,1);
                            elseif(cycletest(q)>0),neg=1;q=1+nES(1,1);
                            elseif(cycletest(q)==0),q=q+1;end

                        end

if(gcd2(cycletemp)~=0),cycletemp=cycletemp/(neg*gcd2(cycletemp));end
                    fprintf(fid2,'RR%d = ',rr);
                    fprintf(fid2,'%c',char(cycletemp*id));
                    fprintf(fid2,'\t');
                    fprintf(fid2,'%d',comp);
                    fprintf(fid2,'\n');
            test = 0;
            dimcycle=size(cycle);
            for j=1:dimcycle(1),
                if (cycletemp==cycle(j,:)),
                    test=test+1;
                end,
            end,
            if(test==0),
                cycle=[cycle;cycletemp];
                cyclenum=cyclenum+1;
                fprintf(fid1,'FR%d = ',cyclenum);
                fprintf(fid1,'%c',char(cycletemp*id));
                fprintf(fid1,'\t');
                fprintf(fid1,'%d',comp);
                fprintf(fid1,'\n');
                for i=1:nES,
fprintf(fida,'%d',cycletemp(i)),fprintf(fida,'\t'); end
                fprintf(fida,'\n');
            end
                rr,rr=rr+1;if rr >rrmax, break, end

                  comp(9)=comp(9)+1;
                 end, comp(9)=comp(8)+2;comp(8)=comp(8)+1;if rr >rrmax, break,
end
                end, comp(8)=comp(7)+1;comp(7)=comp(7)+1;if rr >rrmax, break,
end
               end, comp(7)=comp(6)+1;comp(6)=comp(6)+1;if rr >rrmax, break,
end
              end, comp(6)=comp(5)+1;comp(5)=comp(5)+1;if rr >rrmax, break, end
```

```
            end, comp(5)=comp(4)+1;comp(4)=comp(4)+1;if rr >rrmax, break, end
           end, comp(4)=comp(3)+1;comp(3)=comp(3)+1;if rr >rrmax, break, end
          end, comp(3)=comp(2)+1;comp(2)=comp(2)+1;if rr >rrmax, break, end
         end, comp(2)=comp(1)+1;comp(1)=comp(1)+1;if rr >rrmax, break, end
     end, if rr >rrmax, break, end
  end

            fclose(fid1);
            fclose(fid2);
       fclose(fida);
            display('done FRs');
            end



            % Empty Routes

            clear submatrix matrix ...

            EmptyR = input('calculate ERs?  (1-yes/2-no):   ')
            if(EmptyR==1)

       % User defined output files
       outputfile3 = input('User, name the output file containing the UNIQUE
the calculated RRs (''file.txt''): '); disp('');
       outputfile4 = input('User, name the output file containing the ALL
calculated RRs (''file.txt''): '); disp('');

            fid3 = fopen(outputfile3,'a');
            fid4 = fopen(outputfile4,'a');
       fidb = fopen('wgsr18CuERcycleM.txt','a');

       nINTS = input('User, how many intermediate species exist? '); disp('');
       colADD = input('User, which column number of the terminal species would
you like to add? '); disp('');

            intM=[v(1:nES,1:nINTS)];
            vRed = [intM,v(:,colADD)] % Used H2O column
            m=rank(vRed),ES=m+1

            dimid=size(id);
            wgsr18ERcycleM;
            cycle=ERtemp;
```

```
%            cycle=zeros(1,nES(1,1));
             cycletemp=zeros(1,nES(1,1));

             rr=25001; %RR counter
        rrmax=factorial(18)/factorial(10)/factorial(8);

   while rr<=rrmax
             cyclenum=117; %cycle counter
             comp=[1 2 5 7 10 12 13 16 17 18]; %initial components
             while comp(1)<=(nES-9)
         while comp(2)<=(nES-8)
          while comp(3)<=(nES-7)
           while comp(4)<=(nES-6)
            while comp(5)<=(nES-5)
             while comp(6)<=(nES-4)
              while comp(7)<=(nES-3)
               while comp(8)<=(nES-2)
                while comp(9)<=(nES-1)
                 while comp(10)<=nES

                  cycletemp=zeros(1,nES(1,1));
                        for(i=1:(m+1)),matrix(i,ES)=id(comp(i));end
                        for(i=1:ES),for(j=1:ES-
1),matrix(i,j)=vRed(comp(i),j);end,end
                        for i=1:ES
                            refi=i;  k=1;
                            while k<=m
                               for j=1:ES
                                    if j~=refi
                                        submatrix(k,:)=matrix(j,1:(ES-1));
                                        k=k+1;
                                    end
                               end
                            end
                            cycletemp(comp(refi))=(-
1)^(i+ES)*det(double(submatrix));
                        end
                    q=1;cycletest=cycletemp;
                        while q<=nES(1,1)
                            if(cycletest(q)<0),neg=-1;q=1+nES(1,1);
                            elseif(cycletest(q)>0),neg=1;q=1+nES(1,1);
                            elseif(cycletest(q)==0),q=q+1;end
```

```
                        end

if(gcd2(cycletemp)~=0),cycletemp=cycletemp/(neg*gcd2(cycletemp));end
                    fprintf(fid4,'ER%d = ',rr);
                    fprintf(fid4,'%c',char(cycletemp*id));
                    fprintf(fid4,'\t');
                    fprintf(fid4,'%d',comp);
                    fprintf(fid4,'\n');
             test = 0;
             dimcycle=size(cycle);
             for j=1:dimcycle(1),
                 if (cycletemp==cycle(j,:)),
                     test=test+1;
                 end,
             end,
             if(test==0),
                 cycle=[cycle;cycletemp];
                 cyclenum=cyclenum+1;
                 fprintf(fid3,'ER%d = ',cyclenum);
                 fprintf(fid3,'%c',char(cycletemp*id));
                 fprintf(fid3,'\t');
                 fprintf(fid3,'%d',comp);
                 fprintf(fid3,'\n');
                 for i=1:nES,
fprintf(fidb,'%d',cycletemp(i)),fprintf(fidb,'\t'); end
                 fprintf(fidb,'\n');

             end
                 rr,rr=rr+1;comp

                   comp(10)=comp(10)+1;if rr >rrmax, break, end
                  end, comp(10)=comp(9)+2;comp(9)=comp(9)+1;if rr >rrmax, break,
end
                 end, comp(9)=comp(8)+1;comp(8)=comp(8)+1;if rr >rrmax, break,
end
                end, comp(8)=comp(7)+1;comp(7)=comp(7)+1;if rr >rrmax, break,
end
               end, comp(7)=comp(6)+1;comp(6)=comp(6)+1;if rr >rrmax, break, end
              end, comp(6)=comp(5)+1;comp(5)=comp(5)+1;if rr >rrmax, break, end
             end, comp(5)=comp(4)+1;comp(4)=comp(4)+1;if rr >rrmax, break, end
            end, comp(4)=comp(3)+1;comp(3)=comp(3)+1;if rr >rrmax, break, end
```

```
          end, comp(3)=comp(2)+1;comp(2)=comp(2)+1;if rr >rrmax, break, end
         end, comp(2)=comp(1)+1;comp(1)=comp(1)+1;if rr >rrmax, break, end
         end, if rr >rrmax, break, end
     end

          fclose(fid3);
          fclose(fid4);
       fclose(fidb);
          display('done ERs');
          end

          % Intermediate Nodes

          clear submatrix matrix ...

          IntNodes = input('calculate INs?  (1-yes/2-no):   ')
          if(IntNodes==1)

       % User defined output files
       outputfile5 = input('User, name the output file containing the UNIQUE
the calculated RRs (''file.txt''): '); disp('');
       outputfile6 = input('User, name the output file containing the ALL
calculated RRs (''file.txt''): '); disp('');

          fid5 = fopen(outputfile5,'a');
          fid6 = fopen(outputfile6,'a');
       fidc = fopen('wgsr18CuINQcycleMtemp.txt','a');

       nINTS = input('User, how many intermediate species exist? '); disp('');

          intM=[v(1:nES,1:nINTS)];
          intMT = transpose(intM)
          ES = rank(intMT)
          Qmatrix = intMT*id;
          Smatrix = intMT*rxns;

          dimintMT=size(intMT);
          dimid=size(id);
          cycle=zeros(1,dimintMT(1,1));
          cycletemp=zeros(1,dimintMT(1,1));

       wgsr18CuINQcycleM;
```

```
            Qcycle=INtemp;
%           Qcycle=zeros(1,dimid(1,1));
            Qcycletemp=zeros(1,dimid(1,1));

            rr=1; %RR counter
        rrmax = 61% factorial(18)/factorial(8)/factorial(10);
            while rr < rrmax +1
            cyclenum=1; %cycle counter
            comp=[1 2 3 4 5 6 7 8]; %initial components
            while comp(1)<=(nES-7)
         while comp(2)<=(nES-6)
          while comp(3)<=(nES-5)
           while comp(4)<=(nES-4)
            while comp(5)<=(nES-3)
             while comp(6)<=(nES-2)
              while comp(7)<=(nES-1)
               while comp(8)<=(nES)

                cycletemp=zeros(1,dimintMT(1,1));
                QcycleSUM=zeros(1,nES(1,1));
                      for(i=1:ES),for(j=1:ES-
1),tempmatrix(i,j)=intMT(i,comp(j));end,end
                      matrix=[tempmatrix,Smatrix];
                      Rmatrix=[tempmatrix,Qmatrix];
                      for i=1:ES
                          refi=i;  k=1;
                          while k<=(ES-1)
                             for j=1:ES
                                  if j~=refi
                                      submatrix(k,:)=matrix(j,1:(ES-1));
                                      k=k+1;
                                  end
                             end
                          end
                          cycletemp(i)=(-1)^(i+ES)*det(double(submatrix));
                      end
                  q=1;cycletest=cycletemp;
                      while q<=ES
                          if(cycletest(q)<0),neg=-1;q=1+ES;
                          elseif(cycletest(q)>0),neg=1;q=1+ES;
                          elseif(cycletest(q)==0),q=q+1;end
```

```
            end;

            if(gcd2(cycletemp)~=0),
                cycletemp=cycletemp/(neg*gcd2(cycletemp));
            end

            Qcycletemp=zeros(ES,nES(1,1));
            for i=1:ES,
                Qcycletemp(i,:)=cycletemp(i).*intMT(i,:);
            end

            QcycleSUM=zeros(1,nES(1,1));
            for i=1:ES
                QcycleSUM=QcycleSUM+Qcycletemp(i,:);
            end

            q=1;
            while q<=nES(1,1)
                if(QcycleSUM(q)<0),neg=-1;q=1+nES(1,1);
                elseif(QcycleSUM(q)>0),neg=1;q=1+nES(1,1);
                elseif(QcycleSUM(q)==0),q=q+1;end
            end;

            if(gcd2(QcycleSUM)~=0),
                QcycleSUM=QcycleSUM/(neg*gcd2(QcycleSUM));
            end

            QcycleEQN=QcycleSUM*id;
        fprintf(fid6,'IN%d = ',rr);
        fprintf(fid6,'%c',char(QcycleSUM*id));
        fprintf(fid6,'\t');
        fprintf(fid6,'%d',comp);
        fprintf(fid6,'\n');
test = 0;
dimQcycle=size(Qcycle);
for j=1:dimQcycle(1),
    if (QcycleSUM==Qcycle(j,:)),
        test=test+1;
    end,
end,
if(test==0),
    Qcycle=[Qcycle;QcycleSUM];
```

```
                cyclenum=cyclenum+1;
                fprintf(fid5,'IN%d = ',cyclenum);
                fprintf(fid5,'%c',char(QcycleSUM*id));
                fprintf(fid5,'\t');
                fprintf(fid5,'%c',char(cycletemp*species(1:ES,:)));
                fprintf(fid5,'\t');
                fprintf(fid5,'%c',char(QcycleSUM*rxns));
                fprintf(fid5,'\n');
                for i=1:nES,
fprintf(fidc,'%d',QcycleSUM(i)),fprintf(fidc,'\t'); end
                fprintf(fidc,'\n');

            end
                rr,rr=rr+1;if rr>rrmax, break, end

                comp(8)=comp(8)+1;if rr>rrmax, break, end
                end, comp(8)=comp(7)+2;comp(7)=comp(7)+1;if rr>rrmax, break,
end
              end, comp(7)=comp(6)+1;comp(6)=comp(6)+1;if rr>rrmax, break, end
             end, comp(6)=comp(5)+1;comp(5)=comp(5)+1;if rr>rrmax, break, end
            end, comp(5)=comp(4)+1;comp(4)=comp(4)+1;if rr>rrmax, break, end
           end, comp(4)=comp(3)+1;comp(3)=comp(3)+1;if rr>rrmax, break, end
          end, comp(3)=comp(2)+1;comp(2)=comp(2)+1;if rr>rrmax, break, end
         end, comp(2)=comp(1)+1;comp(1)=comp(1)+1;if rr>rrmax, break, end
         end

             fclose(fid5);
             fclose(fid6);
        fclose(fidc);
        if rr>rrmax, break, end
             display('done INs');
             end
    end

             % Terminal Nodes

             clear submatrix matrix ...

             TNodes = input('calculate TNs?  (1-yes/2-no):   ')
             if(TNodes==1)

        % User defined output files
```

```
        outputfile7 = input('User, name the output file containing the UNIQUE
the calculated TNs (''file.txt''): '); disp('');
        outputfile8 = input('User, name the output file containing the ALL
calculated TNs (''file.txt''): '); disp('');

             fid7 = fopen(outputfile7,'a');
             fid8 = fopen(outputfile8,'a');

        nINTS = input('User, how many intermediate species exist? '); disp('');

             intM=[v(1:nES,1:nINTS)];
             intMT = transpose(intM)
        gammaM=[intM,v(:,10)];
             ES = rank(intMT)
        ESgammaM = rank(gammaM)
             v1=1;

             dimintMT=size(intMT);
             dimid=size(id);
             cycle=zeros(1,dimintMT(1,1));
             cycletemp=zeros(1,dimintMT(1,1));

%       wgsr18CuTNcycleM;
%            cycle=TNtemp;
             cycle=zeros(1,dimid(1,1));
             cycleTNtemp=zeros(1,dimid(1,1));

             rr=1; %RR counter
        rrmax = factorial(18)/factorial(8)/factorial(10);
             while rr < rrmax +1

        cyclenum=0; %cycle counter
             comp=[1 2 3 4 5 6 7 8]; %initial components
             while comp(1)<=(nES-7)
            while comp(2)<=(nES-6)
                while comp(3)<=(nES-5)
                    while comp(4)<=(nES-4)
                        while comp(5)<=(nES-3)
                            while comp(6)<=(nES-2)
                                while comp(7)<=(nES-1)
                                    while comp(8)<=(nES)
```

```
                        cycletemp=zeros(1,dimintMT(1,2));
                        cycleTNtemp=zeros(1,dimintMT(1,2));
                        QcycleSUM=zeros(1,nES(1,1));


for(i=1:ES),for(j=1:ES),deltamatrix(i,j)=intMT(i,comp(j));end,end
                        for(i=1:ESgammaM-
1),for(j=1:ESgammaM),submatrix1(i,j)=gammaM(comp(i),j);end,end

                        if det(deltamatrix)~=0,
                            for i=1:ES,
                                cycletemp(1,comp(i))=-1;
                            end
                            cycletemp=cycletemp+1;

                            comp2=[0];
                            for i=1:dimintMT(1,2)
                                if cycletemp(i)~=0,
                                    comp2=[comp2,i];
                                end
                            end
                            comp2(1)=[]; comp2
                            dimcomp2=size(comp2);

                            for(i=1:dimcomp2(1,2)),
                                submatrix2=[gammaM(comp2(i),:)];
                                matrix=[submatrix1;submatrix2];

cycleTNtemp(comp2(i))=1/v1/det(deltamatrix)*det(matrix);
                            end

                            fprintf(fid8,'TNd = ',rr);
                            fprintf(fid8,'c',char(cycleTNtemp*id));
                            fprintf(fid8,'+OR');
                            fprintf(fid8,'\t');
                            fprintf(fid8,'d',comp);
                            fprintf(fid8,'\n');

                            test = 0;
                            dimcycle=size(cycle);
                            for j=1:dimcycle(1),
                                if (cycleTNtemp==cycle(j,:)),
```

```
                                test=test+1;
                            end,
                        end,

                        if(test==0),
                            cycle=[cycle;cycleTNtemp];
                            cyclenum=cyclenum+1;
                            fprintf(fid7,'TNd = ',cyclenum);
                            fprintf(fid7,'c',char(cycleTNtemp*id));
                            fprintf(fid7,'+OR');
                            fprintf(fid7,'\t');
                            fprintf(fid7,'d',comp);
                            fprintf(fid7,'\n');
                        end
                    else
                        fprintf(fid8,'TN%d = 0',rr);
                        fprintf(fid8,'\t');
                        fprintf(fid8,'%d',comp);
                        fprintf(fid8,'\n');
                    end

                    rr,rr=rr+1;if rr>rrmax, break, end

                    comp(8)=comp(8)+1;if rr>rrmax, break, end
                                end, comp(8)=comp(7)+2;comp(7)=comp(7)+1;if
rr>rrmax, break, end
                            end, comp(7)=comp(6)+1;comp(6)=comp(6)+1;if
rr>rrmax, break, end
                        end, comp(6)=comp(5)+1;comp(5)=comp(5)+1;if
rr>rrmax, break, end
                    end, comp(5)=comp(4)+1;comp(4)=comp(4)+1;if rr>rrmax,
break, end
                end, comp(4)=comp(3)+1;comp(3)=comp(3)+1;if rr>rrmax,
break, end
            end, comp(3)=comp(2)+1;comp(2)=comp(2)+1;if rr>rrmax, break,
end
        end, comp(2)=comp(1)+1;comp(1)=comp(1)+1;if rr>rrmax, break, end
    end

         fclose(fid7);
         fclose(fid8);
    if rr>rrmax, break, end
```

```
            display('done TNs');
        end
        end

        disp('Select from the following tasks:');disp(' ');
            disp('       1 - Read in mechanism''s stoichiometric matrix');
            disp('       2 - Verify reactions and matrix entries');
            disp('       3 - Enumerate FRs, ERs, INs, TNs');
            disp('       4 - Read in reaction energetics');
            disp('       5 - Check thermodynamic consistency');
            disp('       6 - Run overall mechanism');
            disp('       7 - Run RR''s mechanisms');
        disp('       8 - Run simplified mechanism');
            disp('       9 - Generate plots');
            disp('       0 - Exit program');disp(' ');

            task = input('User, what would you like to do NEXT? (select a
number) -> ');
    end

    % ------------------------------------------------------------------------
--------------------
      %  4 - Read in reaction energetics
      % ------------------------------------------------------------------------
----------------------
      while task==4

        disp(' ');
        disp('Reading in the reaction energetics...');disp(' ');

            A=xlsread(sourcefile,'preexp');
            E=xlsread(sourcefile,'actenergy');

        display_energetics = input('User, would you like to view the
energetics? (1-yes/2-no) -> ');disp(' ');
        syms id Af Ef ES Ar Er;
        if display_energetics == 1, [id, Af, Ef, ES, Ar,
Er;transpose([1:nES]),A(:,1),E(:,1),[rxnR,'=',rxnP],A(:,2),E(:,2)], end

        disp('Select from the following tasks:');disp(' ');
            disp('       1 - Read in mechanism''s stoichiometric matrix');
            disp('       2 - Verify reactions and matrix entries');
```

```
            disp('       3 - Enumerate FRs, ERs, INs, TNs');
            disp('       4 - Read in reaction energetics');
            disp('       5 - Check thermodynamic consistency');
            disp('       6 - Run overall mechanism');
            disp('       7 - Run RR''s mechanisms');
        disp('       8 - Run simplified mechanism');
            disp('       9 - Generate plots');
            disp('       0 - Exit program');disp(' ');

            task = input('User, what would you like to do NEXT? (select a
number) -> ');
       end

    % ------------------------------------------------------------------------
--------------------
       %  5 - Check thermodynamic consistency
       % ------------------------------------------------------------------------
----------------------
       while task==5
        disp(' ');
            thermockfile1 = input('For thermodynamic consistency checks,
please indicate the output file (EXAMPLE: ''wgsr17thermock.txt'') ->  ');
        disp(' ');
        thermockfile2 = input('Please indicate an output file for reaction
enthalpy and equilibrium constant check (EXAMPLE: ''wgsr17Hrxnck.txt'') ->  ');
        disp(' ');
        disp('Checking energetics for thermodynamic consistency...');disp(' ');

        syms s1 s2 s3 s4 s5 s6 s7 s8 s9 s10 s11 s12 s13 s14 s15 s16 s17 s18 s19
s20;
        id = transpose([s1 s2 s3 s4 s5 s6 s7 s8 s9 s10 s11 s12 s13 s14 s15 s16
s17 s18 s19 s20]);

        % evaluate rate constants at T=350K

            Rgas=1.987; %Gas constant (cal/mole)
            temp=350;

            for i=1:nES
           % 1 = forward reaction, 2 = reverse reaction
           kf(i)=A(i,1)*exp(-E(i,1)/(Rgas*temp/1000));
           kr(i)=A(i,2)*exp(-E(i,2)/(Rgas*temp/1000));
```

```
            Hrxn(i)=E(i,1)-E(i,2);
            Keq(i)=kf(i)/kr(i);
             end;

        ERdatafile=input('User, enter the text file name for the ER cycle
matrix data:  '),disp(' ')
        ERcycleM=load(ERdatafile);
        FRdatafile=input('User, enter the text file name for the FR cycle
matrix data:  '),disp(' ')
        FRcycleM=load(FRdatafile);

        dimERcycleM=size(ERcycleM);
        nERs=dimERcycleM(1,1);
        dimFRcycleM=size(FRcycleM);
        nFRs=dimFRcycleM(1,1);

        ERcheck=ones(nERs,1);
        ERcheckA=ones(nERs,1);
        ERcheckE=ones(nERs,1);
        FRcheck=ones(nFRs,1);
        FRcheckKeq=ones(nFRs,1);

             fidERcheck=fopen(thermockfile1, 'a');
             fidFRcheck=fopen(thermockfile2, 'a');

             ERcheck=zeros(nERs,1);
        ERcheckA=zeros(nERs,1);
        ERcheckE=zeros(nERs,1);
             FRcheck=zeros(nFRs,1);
             FRcheckKeq=zeros(nFRs,1);


        for i=1:nERs,
            ERcheck(i,1)=1.0;
            ERcheckA(i,1)=1.0;
            ERcheckE(i,1)=1.0;
            for j=1:nES,
                ERnum(i,1)=i;
                ERid(i,1)=ERcycleM(i,:)*id;
                ERcheck(i,1)=ERcheck(i,1)*(kf(j)/kr(j))^(ERcycleM(i,j));
                ERcheckA(i,1)=ERcheckA(i,1)*(A(j,1)/A(j,2))^(ERcycleM(i,j));
```

```
                ERcheckE(i,1)=ERcheckE(i,1)*((exp(-
E(j,1)/(Rgas*temp/1000)))/(exp(-E(j,2)/(Rgas*temp/1000))))^(ERcycleM(i,j));
            end,
            [i, ERcheck(i,1), ERcheckA(i,1), ERcheckE(i,1)]
            fprintf(fidERcheck, '%d', ERnum(i,1));
                fprintf(fidERcheck, '\t');
                fprintf(fidERcheck, '%c', char(ERid(i,1)));
                fprintf(fidERcheck, '\t');
                fprintf(fidERcheck, '%11.4d', ERcheck(i,1));
                fprintf(fidERcheck, '\t');
                fprintf(fidERcheck, '%11.4d', ERcheckA(i,1));
                fprintf(fidERcheck, '\t');
                fprintf(fidERcheck, '%11.4d\n', ERcheckE(i,1));
            end

        for i=1:nFRs,
            FRcheck(i,1)=0.0;
            FRcheckKeq(i,1)=1.0;
            for j=1:nES,
                FRnum(i,1)=i;
                FRid(i,1)=FRcycleM(i,:)*id;
                FRcheck(i,1)=FRcheck(i,1)+(Hrxn(j))*(FRcycleM(i,j));
                FRcheckKeq(i,1)=FRcheckKeq(i,1)*(Keq(j))^(FRcycleM(i,j));
           end,
            [i, FRcheck(i,1), FRcheckKeq(i,1)]
            fprintf(fidFRcheck, '%d', FRnum(i,1));
                fprintf(fidFRcheck, '\t');
                fprintf(fidFRcheck, '%c', char(FRid(i,1)));
                fprintf(fidFRcheck, '\t');
                fprintf(fidFRcheck, '%11.4d', FRcheck(i,1));
                fprintf(fidFRcheck, '\t');
                fprintf(fidFRcheck, '%11.4d\n', FRcheckKeq(i,1));
       end

    fclose(fidERcheck);
    fclose(fidFRcheck);

             disp('Select from the following tasks:');disp(' ');
             disp('       1 - Read in mechanism''s stoichiometric matrix');
             disp('       2 - Verify reactions and matrix entries');
             disp('       3 - Enumerate FRs, ERs, INs, TNs');
             disp('       4 - Read in reaction energetics');
```

```
            disp('       5 - Check thermodynamic consistency');
            disp('       6 - Run overall mechanism');
            disp('       7 - Run RR''s mechanisms');
        disp('       8 - Run simplified mechanism');
            disp('       9 - Generate plots');
            disp('       0 - Exit program');disp(' ');

            task = input('User, what would you like to do NEXT? (select a
number) -> ');
       end

    % ------------------------------------------------------------------------
--------------------
       %  6 - Run overall mechanism
       % ------------------------------------------------------------------------
----------------------
       while task==6
        disp(' ');
        disp('Running the overall mechanism...');disp(' ');


%         disp('This section is UNDER CONSTRUCTION...please select another
option.');disp(' ');
        wgsrMODrr;

            disp('Select from the following tasks:');disp(' ');
            disp('       1 - Read in mechanism''s stoichiometric matrix');
            disp('       2 - Verify reactions and matrix entries');
            disp('       3 - Enumerate FRs, ERs, INs, TNs');
            disp('       4 - Read in reaction energetics');
            disp('       5 - Check thermodynamic consistency');
            disp('       6 - Run overall mechanism');
            disp('       7 - Run RR''s mechanisms');
        disp('       8 - Run simplified mechanism');
            disp('       9 - Generate plots');
            disp('       0 - Exit program');disp(' ');

            task = input('User, what would you like to do NEXT? (select a
number) -> ');
       end
```

```
    % ------------------------------------------------------------------------
--------------------
       %  7 - Run RR's mechanisms
       % ------------------------------------------------------------------------
----------------------
       while task==7
        disp(' ');
        disp('Running the individual RR mechanisms...');disp(' ');


        disp('This section is UNDER CONSTRUCTION...please select another
option.');disp(' ');


             disp('Select from the following tasks:');disp(' ');
             disp('       1 - Read in mechanism''s stoichiometric matrix');
             disp('       2 - Verify reactions and matrix entries');
             disp('       3 - Enumerate FRs, ERs, INs, TNs');
             disp('       4 - Read in reaction energetics');
             disp('       5 - Check thermodynamic consistency');
             disp('       6 - Run overall mechanism');
             disp('       7 - Run RR''s mechanisms');
        disp('       8 - Run simplified mechanism');
             disp('       9 - Generate plots');
             disp('       0 - Exit program');disp(' ');

             task = input('User, what would you like to do NEXT? (select a
number) -> ');
       end

    % ------------------------------------------------------------------------
--------------------
       %  8 - Run simplified mechanism
       % ------------------------------------------------------------------------
----------------------
       while task==8
        disp(' ');
        disp('Running the simplified mechanism...');disp(' ');


        disp('This section is UNDER CONSTRUCTION...please select another
option.');disp(' ');
```

```
            disp('Select from the following tasks:');disp(' ');
            disp('       1 - Read in mechanism''s stoichiometric matrix');
            disp('       2 - Verify reactions and matrix entries');
            disp('       3 - Enumerate FRs, ERs, INs, TNs');
            disp('       4 - Read in reaction energetics');
            disp('       5 - Check thermodynamic consistency');
            disp('       6 - Run overall mechanism');
            disp('       7 - Run RR''s mechanisms');
        disp('       8 - Run simplified mechanism');
            disp('       9 - Generate plots');
            disp('       0 - Exit program');disp(' ');

            task = input('User, what would you like to do NEXT? (select a
number) -> ');

end

    % ------------------------------------------------------------------------
--------------------
      %  9 - Generate plots
      % ------------------------------------------------------------------------
----------------------
      while task==9
        disp(' ');
        disp('Generating the resulting plots...');disp(' ');


        disp('This section is UNDER CONSTRUCTION...please select another
option.');disp(' ');


            disp('Select from the following tasks:');disp(' ');
            disp('       1 - Read in mechanism''s stoichiometric matrix');
            disp('       2 - Verify reactions and matrix entries');
            disp('       3 - Enumerate FRs, ERs, INs, TNs');
            disp('       4 - Read in reaction energetics');
            disp('       5 - Check thermodynamic consistency');
            disp('       6 - Run overall mechanism');
            disp('       7 - Run RR''s mechanisms');
        disp('       8 - Run simplified mechanism');
```

```
            disp('       9 - Generate plots');
            disp('       0 - Exit program');disp(' ');

            task = input('User, what would you like to do NEXT? (select a
number) -> ');
       end

end
```

Appendix C: Simulation of Water-Gas-Shift Reaction Program (Matlab)

```
%   Water gas shift reaction model

%   created 4/22/04

% clear;

disp('Computational Model of the Water Gas Shift Reaction')

global Ner tau y0 temp P DEN CT SS AV Keq Keq0 kf kr rf rr r cycleM Ncycle
cycle RRer crit

fid1 = fopen('wgsr18CuOUTrrs.txt','a');
odefile = @wgsrODE18o;
sourcefile = 'wgsr18CuSOURCE.xls'
cyclefile = 'wgsr18CuFRcyclem.xls'

%System Parameters
Nspecies=14;        %number of species
NTspecies=4;        %number of terminal species
Ner=18;             %number of elementary reactions
RR=635;              %number of reaction routes
syms s1 s2 s3 s4 s5 s6 s7 s8 s9 s10 s11 s12 s13 s14 s15 s16 s17 s18 s19 s20;
id = [s1 s2 s3 s4 s5 s6 s7 s8 s9 s10 s11 s12 s13 s14 s15 s16 s17 s18];
cycle=1;


%Universal Constants
R=1.987; %cal/mole
AV=6.023*10^23; %Avagadros Number

%User Inputs
disp('CATALYST PROPERTIES');
SS=6*10^5%input('Enter Active Surface Area:  ');
CT=2*10^15%input('Enter Number of Active Sites:  ');
DEN=0.14%input('Enter Catalyst Density:');
temp_max=600+273;

disp('SYSTEM PROPERTIES')
```

```
P=1%input('system pressure = ');
N=1;tau=7/100*60%input('residence time(s) =');

% species number indices
co = 1;
h2o = 2;
co2 = 3;
h2 = 4;
s = 5;
h2os = 6;
cos = 7;
co2s = 8;
h2s = 9;
hs = 10;
os = 11;
ohs = 12;
hcoos = 13;
n2 = 14;

disp('Collecting INITIAL SPECIES CONCENTRATIONS...');
y0=XLSREAD(sourcefile,'initial');

disp('Collecting PRE-EXP FACTORS and ACT ENERGY data...');
A=XLSREAD(sourcefile,'preexp');
E=XLSREAD(sourcefile,'actenergy');

disp('Collecting RR cycle matrix...');
line='m--';
%                   1 1 1 1 1 1 1 1
%       1 2 6 7 8 9 0 1 2 3 4 5 6 7 3 4 5
%                           1 1 1 1 1 1 1 1 1
%       1 2 3 4 5 6 7 8 9 0 1 2 3 4 5 6 7 8
cycleM=[1 1 1 0 1 0 1 1 0 0 0 0 0 0 1 1 1 0];... %reduced mechanism
% cycleM=[1 1 1 1 1 1 1 1 1 1 1 1 1 1 1 1 1 1];... %18 step mechanism
% cycleM=[1 1 1 0 0 0 1 0 0 0 0 0 0 0 1 1 1 0];... %RR8
% cycleM=[1 1 1 0 1 0 0 1 0 0 0 0 0 0 1 1 1 0];... %RR24
% cycleM=[1 1 1 1 0 0 0 0 0 0 0 1 0 0 1 0 1 0];... RR6

% cycleM=XLSREAD(cyclefile);
% cycleM=[ones(1,Ner);cycleM];
dimcycle=size(cycleM);
Ncycle=dimcycle(1,1);
```

```
%
yTM=['Temp','CO','H_2O','CO_2','H_2','S','H_2OS','COS','CO_2S','H_2S','HS','OS'
,'OHS','HCOOS','N_2'];
%     rfM=['Temp','rf'];
%     rrM=['Temp','rr'];
%     rM=['Temp','r'];
%     AffM=['Temp','Aff'];
%     xcoM=['Temp','xco'];

% RR analysis
while cycle<=Ncycle
    yTM=zeros(1,Nspecies+1);
    rfM=zeros(1,Ner+1);
    rrM=zeros(1,Ner+1);
    rM=zeros(1,Ner+1);
    AffM=zeros(1,Ner+1);
    xcoM=zeros(1,2);
%     xh2M=zeros(1,2);
    RiM=zeros(1,Ner+1);

    RRer=zeros(1)
    sprintf('cycle=%d',cycle)
    for i=1:Ner
        crit=10;
%        sprintf('cycle=%d, Ner=%d',cycle,i)
        if cycleM(cycle,i)==0
            RRer=[RRer i];
        end
    end

    dimRRer=size(RRer);
    if dimRRer(1,2)>1
        crit=0;
    end
    RRer(1)=[];

%Temperature change
% fprintf(fid1,'\n');
fprintf(fid1,'%c',char(cycleM(cycle,:)*transpose(id)));fprintf(fid1,'\t');

for temp=0+273:25:600+273,
```

```
    disp(sprintf('Temperature (K) = %d',temp))

    % evaluate rate constants
    for i=1:Ner
        % 1 = forward reaction, 2 = reverse reaction
        kf(i)=A(i,1)*exp(-E(i,1)/(R*temp/1000));
        kr(i)=A(i,2)*exp(-E(i,2)/(R*temp/1000));
        Keq(i)=kf(i)/kr(i);
    end;
    Keq0=1*Keq(1)*Keq(2)*Keq(15)*Keq(16)*Keq(17)*Keq(3)*Keq(5)*Keq(8);

    odeset('abstol',1.e-12,'reltol',1.e-12,'bdf','on');
    % call the ode solver
    [t,y]=ode23s(odefile,[1e-10,1e4],y0);

    for i=1:Ner
        Aff(i)=log(rf(i)/rr(i));
    end

    dimy=size(y);
    z=dimy(1,1);

    yTM=[yTM;[temp,y(z,:)]];    %species concentrations
    rfM=[rfM;[temp,rf]];        %forward rates
    rrM=[rrM;[temp,rr]];        %reverse rates
    rM=[rM;[temp,r]];           %net rates
    AffM=[AffM;[temp,Aff]];     %affinities

    xco=(y0(co)-y(z,co))/y0(co);
    xcoM=[xcoM;[temp,xco]];     %CO conversion

%     xh2=(y0(h2)-y(z,h2))/y0(h2);
%     xh2M=[xh2M;[temp,xh2]];     %H2 conversion

    for i=1:Ner
        Ri(i)=Aff(i)/r(i);
    end
    RiM=[RiM;[temp,Ri]];        %elementary reaction step resistances

fprintf(fid1,'%0.100f\t', xco);

% fprintf(fid1,'%0.100f\t', xh2);
```

```
end;
   fprintf(fid1,'\n');
   cycle=cycle+1;
xcoM(1,:)=[];%RiM(1,:)=[];

% xh2M(1,:)=[];%RiM(1,:)=[];

figure(1),plot(xcoM(:,1),xcoM(:,2),line,'linewidth',2.0),set(gca,'XTick',273:10
0:temp_max),set(gca,'XTickLabel',273:100:temp_max),axis([273 temp_max 0.0
1.0]),set(gca,'YTick',0:0.1:1.0),ylabel('X_C_O'),xlabel('Temperature
(K)'),title('Conversion of CO'),hold on

% figure(1),plot(xh2M(:,1),xh2M(:,2),'r-
','linewidth',2.0),set(gca,'XTick',273:100:temp_max),set(gca,'XTickLabel',273:1
00:temp_max),axis([273 temp_max 0.0
1.0]),set(gca,'YTick',0:0.1:1.0),ylabel('X_C_O'),xlabel('Temperature
(K)'),title('Conversion of CO'),hold on
end;

% wgsrEQ;
% figure(1),legend('Overall Mechanism','Equilibrium')

% 'CO','H_2O','CO_2','H_2',,'N_2'
%
figure(5),plot(yTM(:,1),yTM(:,s+1:hcoos+1)),legend('S','H_2OS','COS','CO_2S','H
_2S','HS','OS','OHS','HCOOS'),set(gca,'XLim',[273 temp_max]),
set(gca,'XTick',273:100:temp_max)
% figure(3),plot(RiM(:,1),log(RiM(:,2:Ner+1))),ylabel('Resistance (1/rate(s^-
^1))'),xlabel('Temperature (^oC)'), title('Elementary reaction step
resistances')
% figure(4),plot(1/RiM(:,1),log(RiM(:,2:Ner+1))),ylabel('Resistance (1/rate(s^-
^1))'),xlabel('Temperature (^oC)'), title('Elementary reaction step
resistances')
%
figure(4),semilogy(RiM(:,1),(RiM(:,2:Ner+1))),,set(gca,'XTick',273:100:temp_max
),set(gca,'XTickLabel',273:100:temp_max),axis([273 temp_max 0.0
1.0]),ylabel('Resistance (1/rate(s^-^1))'),xlabel('Temperature (K)')
fclose(fid1);

% wgsr18reduction2;
```

```
dimyTM=size(yTM);
yTMsum=zeros(dimyTM(1,1),1); for j=1:dimyTM(1,1), for i=s+1:hcoos+1,
yTMsum(j,1)=yTMsum(j,1)+yTM(j,i); end, end, yTMsum

sound
```

```
% Material balances for WGSR

function dy = wgsrODE18o(t,y)

global Ner tau y0 temp P DEN CT SS AV kf kr rf rr r cycleM Ncycle cycle RRer
crit

% species number indices
co = 1;
h2o = 2;
co2 = 3;
h2 = 4;
s = 5;
h2os = 6;
cos = 7;
co2s = 8;
h2s = 9;
hs = 10;
os = 11;
ohs = 12;
hcoos = 13;
n2 = 14;

rf(1) = kf(1)*P*y(co)*y(s);            rr(1) = kr(1)*y(cos);
rf(2) = kf(2)*P*y(h2o)*y(s);           rr(2) = kr(2)*y(h2os);
rf(3) = kf(3)*y(h2os)*y(s);            rr(3) = kr(3)*y(ohs)*y(hs);
rf(4) = kf(4)*y(cos)*y(os);            rr(4) = kr(4)*y(co2s)*y(s);
rf(5) = kf(5)*y(cos)*y(ohs);           rr(5) = kr(5)*y(hcoos)*y(s);
rf(6) = kf(6)*y(ohs)*y(s);             rr(6) = kr(6)*y(os)*y(hs);
rf(7) = kf(7)*y(cos)*y(ohs);           rr(7) = kr(7)*y(co2s)*y(hs);
rf(8) = kf(8)*y(hcoos)*y(s);           rr(8) = kr(8)*y(co2s)*y(hs);
rf(9) = kf(9)*y(hcoos)*y(os);          rr(9) = kr(9)*y(co2s)*y(ohs);
rf(10) = kf(10)*y(h2os)*y(os);         rr(10) = kr(10)*y(ohs)*y(ohs);
rf(11) = kf(11)*y(h2os)*y(hs);         rr(11) = kr(11)*y(ohs)*y(h2s);
rf(12) = kf(12)*y(ohs)*y(hs);          rr(12) = kr(12)*y(os)*y(h2s);
rf(13) = kf(13)*y(hcoos)*y(ohs);       rr(13) = kr(13)*y(co2s)*y(h2os);
rf(14) = kf(14)*y(hcoos)*y(hs);        rr(14) = kr(14)*y(co2s)*y(h2s);
rf(15) = kf(15)*y(co2s);               rr(15) = kr(15)*P*y(co2)*y(s);
rf(16) = kf(16)*y(hs)*y(hs);           rr(16) = kr(16)*y(h2s)*y(s);
rf(17) = kf(17)*y(h2s);                rr(17) = kr(17)*P*y(h2)*y(s);
rf(18) = kf(18)*y(hs)*y(hs);           rr(18) = kr(18)*P*y(h2)*y(s)*y(s);
```

```
for i=1:Ner
    r(i)=rf(i)-rr(i);
end

% RR analysis
if crit~=10
    for i=RRer
        r(i)=0;
        rr(i)=rf(i);
    end
end

dy = [1/tau*(y0(co)-y(co))-(82*temp/P)*(DEN*CT*SS/AV)*r(1);...%co
      1/tau*(y0(h2o)-y(h2o))-(82*temp/P)*(DEN*CT*SS/AV)*(r(2));...%h20
      1/tau*(y0(co2)-y(co2))+(82*temp/P)*(DEN*CT*SS/AV)*(r(15));...%co2
      1/tau*(y0(h2)-y(h2))+(82*temp/P)*(DEN*CT*SS/AV)*(r(17)+r(18));...%h2
      -r(1)-r(2)-r(3)+r(4)+r(5)-r(6)-r(8)+r(15)+r(16)+r(17)+2*r(18);...%s
      r(2)-r(3)-r(11)-r(10)+r(13);...%h2os,
      r(1)-r(4)-r(5)-r(7);...%cos
      r(4)+r(7)+r(8)+r(9)+r(13)+r(14)-r(15);...%co2s,
      r(11)+r(12)+r(14)+r(16)-r(17);...%h2s
      r(3)+r(6)+r(7)+r(8)-r(11)-r(12)-r(14)-2*r(16)-2*r(18);...%hs
      -r(4)+r(6)-r(9)-r(10)+r(12);...%os,
      r(3)-r(5)-r(6)-r(7)+r(9)+2*r(10)+r(11)-r(12)-r(13);...%ohs,
      r(5)-r(8)-r(9)-r(13)-r(14);...%hcoos,
      0];%n2
```

```
%   Water gas shift reaction model - equilibrium

%   created 4/22/04

% clear all;
figure(1); hold on;

disp('Computational Model of the Water Gas Shift Reaction at Equilibrium')

global steps temp y0 kf kr Keq0

sourcefile='wgsr20cusource.xls';
Keqfile=fopen('KeqvtempDATA.txt','a');

%System Parameters
Nspecies=14;        %number of species
NTspecies=4;        %number of terminal species
Ner=18;           %number of elementary reactions
RR=17;              %number of reaction routes

%Universal Constants
R=1.987; %cal/mole

% species number indices
co = 1;
h2o = 2;
co2 = 3;
h2 = 4;
s = 5;
h2os = 6;
cos = 7;
co2s = 8;
h2s = 9;
hs = 10;
os = 11;
ohs = 12;
hcoos = 13;
n2 = 14;

disp('Collecting INITIAL SPECIES CONCENTRATIONS...');
y0=XLSREAD(sourcefile,'initial');
```

```
disp('Collecting PRE-EXP FACTORS and ACT ENERGY data...');
A=XLSREAD(sourcefile,'preexp');
E=XLSREAD(sourcefile,'actenergy');

xcoeq=.01; %initialize xco
% xh2eq=.1; initialize xh2

    KeqM=['Temp','Keq'];
    xcoM=['Temp','xco'];

    KeqM=zeros(1,2);
    Keq0M=zeros(1,2);
    xcoeqM=zeros(1,2);
%     xh2eqM=zeros(1,2);

%Temperature change
for temp=0+273.15:25:600+273.15,
    disp(sprintf('Temperature (K) = %d',temp))
    fprintf(Keqfile,'%d\t', temp);

    % evaluate rate constants
    for i=1:Ner
        % 1 = forward reaction, 2 = reverse reaction
        kf(i)=A(i,1)*exp(-E(i,1)/(R*temp/1000));
        kr(i)=A(i,2)*exp(-E(i,2)/(R*temp/1000));
        Keq(i)=kf(i)/kr(i);
    end;
    Keq0=1*Keq(1)*Keq(2)*Keq(17)*Keq(18)*Keq(19)*Keq(3)*Keq(6)*Keq(9);

    fprintf(Keqfile,'%0.100f\n',Keq0);

    Keq0M=[Keq0M;[temp,Keq0]];

    KeqX=fsolve(@wgsreqf,y0(co)*xcoeq);
%     KeqX=fsolve(@wgsreqf2,xh2eq);

    KeqM=[KeqM;[temp,KeqX]];     %affinities

    xcoeq=KeqX/y0(co);
    xcoeqM=[xcoeqM;[temp,xcoeq]];     %CO conversion

%     xh2eq=-1*KeqX/y0(h2);
```

```
%     xh2eqM=[xh2eqM;[temp,xh2eq]];     %H2 conversion

end;

KeqM(1,:)=[];xcoeqM(1,:)=[];
% KeqM(1,:)=[];xh2eqM(1,:)=[];

%
figure(3),plot(xcoeqM(:,1),xcoeqM(:,2),'r'),ylabel('X_C_O'),xlabel('Temperature
(K)'),title('Equilibrium Conversion of CO'),hold on
figure(1),plot(xcoeqM(:,1),xcoeqM(:,2),'b-','LineWidth',2.0),hold on

%
figure(2),plot(xh2eqM(:,1),xh2eqM(:,2),'b'),ylabel('X_H_2'),xlabel('Temperature
(K)'),title('Equilibrium Conversion of H_2'),hold on

fclose(Keqfile);
```

```
% function to calculate the equilibrium conversion of the WGS reaction

function F = wgsreqf(x)

global steps temp y0 kf kr Keq0

% species number indices
co = 1;
h2o = 2;
co2 = 3;
h2 = 4;
s = 5;
h2os = 6;
cos = 7;
co2s = 8;
h2s = 9;
hs = 10;
os = 11;
ohs = 12;
hcoos = 13;
n2 = 14;

F = Keq0 - ((y0(co2)+x)*(y0(h2)+x))/((y0(co)-x)*(y0(h2o)-x));
```

Appendix D: Topological Characteristics of the WGS Mechanism

FULL ROUTES

FR_1: $s_1 + s_2 + s_3 + s_7 + s_{15} + s_{18} = OR$

FR_2: $s_1 + s_2 + s_7 + s_{11} + s_{15} + s_{17} = OR$

FR_3: $s_1 + s_2 + s_3 + s_4 + s_6 + s_{15} + s_{18} = OR$

FR_4: $s_1 + s_2 + s_3 + s_5 + s_8 + s_{15} + s_{18} = OR$

FR_5: $s_1 + s_2 + s_4 + s_6 + s_{11} + s_{15} + s_{17} = OR$

FR_6: $s_1 + s_2 + s_3 + s_4 + s_{12} + s_{15} + s_{17} = OR$

FR_7: $s_1 + s_2 + s_3 + s_5 + s_{14} + s_{15} + s_{17} = OR$

FR_8: $s_1 + s_2 + s_3 + s_7 + s_{15} + s_{16} + s_{17} = OR$

FR_9: $s_1 + s_2 + s_5 + s_8 + s_{11} + s_{15} + s_{17} = OR$

FR_{10}: $s_1 + s_2 + s_7 + s_8 - s_{13} + s_{15} + s_{18} = OR$

FR_{11}: $s_1 + s_2 + s_6 + s_7 + s_{10} + s_{15} + s_{18} = OR$

FR_{12}: $s_1 + s_2 + s_7 - s_{13} + s_{14} + s_{15} + s_{17} = OR$

FR_{13}: $s_1 + s_2 + s_7 + s_{10} + s_{12} + s_{15} + s_{17} = OR$

FR_{14}: $s_1 + s_2 + s_7 + s_{11} + s_{15} - s_{16} + s_{18} = OR$

FR_{15}: $s_1 + s_2 + 2s_3 + s_4 - s_{10} + s_{15} + s_{18} = OR$

FR_{16}: $s_1 + s_2 + 2s_3 + s_5 + s_{13} + s_{15} + s_{18} = OR$

FR_{17}: $s_1 + s_2 + s_3 + s_4 + s_8 - s_9 + s_{15} + s_{18} = OR$

FR_{18}: $s_1 + s_2 + s_3 + s_5 + s_6 + s_9 + s_{15} + s_{18} = OR$

FR_{19}: $s_1 + s_2 + s_4 + 2s_6 + s_{10} + s_{15} + s_{18} = OR$

FR_{20}: $s_1 + s_2 - s_4 + 2s_7 + s_{10} + s_{15} + s_{18} = OR$

FR_{21}: $s_1 + s_2 - s_5 + 2s_7 - s_{13} + s_{15} + s_{18} = OR$

FR_{22}: $s_1 + s_2 + s_5 + 2s_8 - s_{13} + s_{15} + s_{18} = OR$

FR_{23}: $s_1 + s_2 + s_3 + s_4 + s_6 + s_{15} + s_{16} + s_{17} = OR$

FR_{24}: $s_1 + s_2 + s_3 + s_5 + s_8 + s_{15} + s_{16} + s_{17} = OR$

FR_{25}: $s_1 + s_2 + s_3 + s_4 - s_9 + s_{14} + s_{15} + s_{17} = OR$

FR_{26}: $s_1 + s_2 + s_3 + s_7 - s_8 + s_{14} + s_{15} + s_{17} = OR$

FR_{27}: $s_1 + s_2 + s_4 + s_8 - s_9 + s_{11} + s_{15} + s_{17} = OR$

FR_{28}: $s_1 + s_2 + s_3 - s_6 + s_7 + s_{12} + s_{15} + s_{17} = OR$

FR_{29}: $s_1 + s_2 + s_5 + s_6 + s_9 + s_{11} + s_{15} + s_{17} = OR$

FR_{30}: $s_1 + s_2 + s_3 + s_5 + s_9 + s_{12} + s_{15} + s_{17} = OR$

FR_{31}: $s_1 + s_2 + s_4 + s_6 + s_8 - s_{13} + s_{15} + s_{18} = OR$

FR_{32}: $s_1 + s_2 + s_5 + s_6 + s_8 + s_{10} + s_{15} + s_{18} = OR$

FR_{33}: $s_1 + s_2 + s_6 + s_7 + s_9 - s_{13} + s_{15} + s_{18} = OR$

FR_{34}: $s_1 + s_2 + s_7 + s_8 - s_9 + s_{10} + s_{15} + s_{18} = OR$

FR_{35}: $s_1 + s_2 + s_3 + s_4 - s_{10} + s_{11} + s_{15} + s_{17} = OR$

FR_{36}: $s_1 + s_2 + s_3 + s_5 + s_{11} + s_{13} + s_{15} + s_{17} = OR$

FR_{37}: $s_1 + s_2 + s_3 + s_4 + s_{12} + s_{15} - s_{16} + s_{18} = OR$

FR_{38}: $s_1 + s_2 + s_3 + s_5 + s_{14} + s_{15} - s_{16} + s_{18} = OR$

FR_{39}: $s_1 + s_2 + s_4 + s_6 - s_{13} + s_{14} + s_{15} + s_{17} = OR$

FR_{40}: $s_1 + s_2 + s_5 + s_8 + s_{10} + s_{12} + s_{15} + s_{17} = OR$

FR_{41}: $s_1 + s_2 + s_7 - s_9 + s_{10} + s_{14} + s_{15} + s_{17} = OR$

FR_{42}: $s_1 + s_2 + s_7 + s_9 + s_{12} - s_{13} + s_{15} + s_{17} = OR$

FR_{43}: $s_1 + s_2 + s_4 + s_6 + s_{10} + s_{12} + s_{15} + s_{17} = OR$

FR_{44}: $s_1 + s_2 + s_5 + s_6 + s_{10} + s_{14} + s_{15} + s_{17} = OR$

FR_{45}: $s_1 + s_2 + s_4 + s_6 + s_{11} + s_{15} - s_{16} + s_{18} = OR$

FR_{46}: $s_1 + s_2 + s_5 + s_8 + s_{11} + s_{15} - s_{16} + s_{18} = OR$

FR_{47}: $s_1 + s_2 + s_4 + s_8 + s_{12} - s_{13} + s_{15} + s_{17} = OR$

FR_{48}: $s_1 + s_2 + s_5 + s_8 - s_{13} + s_{14} + s_{15} + s_{17} = OR$

FR_{49}: $s_1 + s_2 + s_7 + s_8 + s_{11} - s_{14} + s_{15} + s_{18} = OR$

FR_{50}: $s_1 + s_2 + s_7 + s_8 - s_{13} + s_{15} + s_{16} + s_{17} = OR$

FR_{51}: $s_1 + s_2 + s_6 + s_7 + s_{10} + s_{15} + s_{16} + s_{17} = OR$

FR_{52}: $s_1 + s_2 + s_6 + s_7 + s_{11} - s_{12} + s_{15} + s_{18} = OR$

FR_{53}: $s_1 + s_2 + 2s_3 + s_4 - s_9 + s_{13} + s_{15} + s_{18} = OR$

FR_{54}: $s_1 + s_2 + 2s_3 + s_5 + s_9 - s_{10} + s_{15} + s_{18} = OR$

FR_{55}: $s_1 + s_2 + s_4 + s_{11} + s_{12} + s_{15} - s_{16} + s_{17} = OR$

FR_{56}: $s_1 + s_2 + s_5 + s_{11} + s_{14} + s_{15} - s_{16} + s_{17} = OR$

FR_{57}: $s_1 + s_2 + s_4 + 2s_6 + s_9 - s_{13} + s_{15} + s_{18} = OR$

FR_{58}: $s_1 + s_2 - s_4 + 2s_7 + s_9 - s_{13} + s_{15} + s_{18} = OR$

FR_{59}: $s_1 + s_2 + s_7 - s_{13} + s_{14} + s_{15} - s_{16} + s_{18} = OR$

FR_{60}: $s_1 + s_2 + s_4 + 2s_8 - s_9 - s_{13} + s_{15} + s_{18} = OR$

FR_{61}: $s_1 + s_2 + s_5 + 2s_6 + s_9 + s_{10} + s_{15} + s_{18} = OR$

FR_{62}: $s_1 + s_2 - s_5 + 2s_7 - s_9 + s_{10} + s_{15} + s_{18} = OR$

FR_{63}: $s_1 + s_2 + s_7 + s_{10} + s_{12} + s_{15} - s_{16} + s_{18} = OR$

FR_{64}: $s_1 + s_2 + s_5 + 2s_8 - s_9 + s_{10} + s_{15} + s_{18} = OR$

FR_{65}: $s_1 + s_2 + 2s_3 + s_4 - s_{10} + s_{15} + s_{16} + s_{17} = OR$

FR_{66}: $s_1 + s_2 + 2s_3 + s_4 - s_{11} + s_{12} + s_{15} + s_{18} = OR$

FR_{67}: $s_1 + s_2 + 2s_3 + s_5 - s_{11} + s_{14} + s_{15} + s_{18} = OR$

FR_{68}: $s_1 + s_2 + 2s_3 + s_5 + s_{13} + s_{15} + s_{16} + s_{17} = OR$

FR_{69}: $s_1 + s_2 + s_3 + s_4 + s_6 - s_8 + s_{14} + s_{15} + s_{17} = OR$

FR_{70}: $s_1 + s_2 + s_3 + s_4 + s_8 - s_9 + s_{15} + s_{16} + s_{17} = OR$

FR_{71}: $s_1 + s_2 + s_3 + s_5 - s_6 + s_8 + s_{12} + s_{15} + s_{17} = OR$

FR_{72}: $s_1 + s_2 + s_3 + s_5 + s_6 + s_9 + s_{15} + s_{16} + s_{17} = OR$

FR_{73}: $s_1 + s_2 + s_3 - s_6 + s_7 - s_9 + s_{14} + s_{15} + s_{17} = OR$

FR_{74}: $s_1 + s_2 + s_3 + s_7 - s_8 + s_9 + s_{12} + s_{15} + s_{17} = OR$

FR_{75}: $s_1 + s_2 + s_4 + 2s_6 + s_{10} + s_{15} + s_{16} + s_{17} = OR$

FR_{76}: $s_1 + s_2 + s_4 + 2s_6 + s_{11} - s_{12} + s_{15} + s_{18} = OR$

FR_{77}: $s_1 + s_2 - s_4 + 2s_7 + s_{10} + s_{15} + s_{16} + s_{17} = OR$

FR_{78}: $s_1 + s_2 - s_4 + 2s_7 + s_{11} - s_{12} + s_{15} + s_{18} = OR$

FR_{79}: $s_1 + s_2 - s_5 + 2s_7 + s_{11} - s_{14} + s_{15} + s_{18} = OR$

FR_{80}: $s_1 + s_2 - s_5 + 2s_7 - s_{13} + s_{15} + s_{16} + s_{17} = OR$

FR_{81}: $s_1 + s_2 + s_5 + 2s_8 + s_{11} - s_{14} + s_{15} + s_{18} = OR$

FR_{82}: $s_1 + s_2 + s_5 + 2s_8 - s_{13} + s_{15} + s_{16} + s_{17} = OR$

FR_{83}: $s_1 + s_2 + s_3 + s_4 + s_8 + s_{12} - s_{14} + s_{15} + s_{18} = OR$

FR_{84}: $s_1 + s_2 + s_3 + s_4 - s_9 + s_{11} + s_{13} + s_{15} + s_{17} = OR$

FR_{85}: $s_1 + s_2 + s_3 + s_4 - s_9 + s_{14} + s_{15} - s_{16} + s_{18} = OR$

FR_{86}: $s_1 + s_2 + s_3 + s_5 + s_6 - s_{12} + s_{14} + s_{15} + s_{18} = OR$

FR_{87}: $s_1 + s_2 + s_3 + s_5 + s_9 - s_{10} + s_{11} + s_{15} + s_{17} = OR$

FR_{88}: $s_1 + s_2 + s_3 + s_5 + s_9 + s_{12} + s_{15} - s_{16} + s_{18} = OR$

FR_{89}: $s_1 + s_2 + 2s_4 - s_5 + 2s_6 - s_{13} + s_{15} + s_{18} = OR$

FR_{90}: $s_1 + s_2 - s_4 + s_5 + s_7 + s_{10} + s_{14} + s_{15} + s_{17} = OR$

FR_{91}: $s_1 + s_2 + s_4 - s_5 + s_7 + s_{12} - s_{13} + s_{15} + s_{17} = OR$

FR_{92}: $s_1 + s_2 - s_4 + 2s_5 + 2s_8 + s_{10} + s_{15} + s_{18} = OR$

FR_{93}: $s_1 + s_2 + s_4 - s_{10} + 2s_{11} + s_{15} - s_{16} + s_{17} = OR$

FR_{94}: $s_1 + s_2 + s_4 + s_{10} + 2s_{12} + s_{15} - s_{16} + s_{17} = OR$

FR_{95}: $s_1 + s_2 + s_4 + s_{11} + s_{12} + s_{15} - 2s_{16} + s_{18} = OR$

FR_{96}: $s_1 + s_2 + s_4 + s_{11} + s_{12} + s_{15} + 2s_{17} - s_{18} = OR$

FR_{97}: $s_1 + s_2 + s_5 + 2s_{11} + s_{13} + s_{15} - s_{16} + s_{17} = OR$

FR_{98}: $s_1 + s_2 + s_5 + s_{11} + s_{14} + s_{15} - 2s_{16} + s_{18} = OR$

FR_{99}: $s_1 + s_2 + s_5 + s_{11} + s_{14} + s_{15} + 2s_{17} - s_{18} = OR$

FR_{100}: $s_1 + s_2 + s_5 - s_{13} + 2s_{14} + s_{15} - s_{16} + s_{17} = OR$

FR_{101}: $s_1 + s_2 + s_4 + s_6 + s_8 + s_{11} - s_{14} + s_{15} + s_{18} = OR$

FR_{102}: $s_1 + s_2 + s_4 + s_6 + s_8 - s_{13} + s_{15} + s_{16} + s_{17} = OR$

FR_{103}: $s_1 + s_2 + s_4 + s_6 - s_9 + s_{10} + s_{14} + s_{15} + s_{17} = OR$

FR_{104}: $s_1 + s_2 + s_4 + s_6 + s_9 + s_{12} - s_{13} + s_{15} + s_{17} = OR$

FR_{105}: $s_1 + s_2 + s_4 + 2s_8 - 2s_9 + s_{10} + s_{15} + s_{18} = OR$

FR_{106}: $s_1 + s_2 + s_4 + s_8 - s_9 + s_{10} + s_{12} + s_{15} + s_{17} = OR$

FR_{107}: $s_1 + s_2 + s_4 + s_8 - s_9 + s_{11} + s_{15} - s_{16} + s_{18} = OR$

FR_{108}: $s_1 + s_2 + s_4 + s_8 - s_9 - s_{13} + s_{14} + s_{15} + s_{17} = OR$

FR_{109}: $s_1 + s_2 + s_5 + s_6 + s_8 + s_{10} + s_{15} + s_{16} + s_{17} = OR$

FR_{110}: $s_1 + s_2 + s_5 + s_6 + s_8 + s_{11} - s_{12} + s_{15} + s_{18} = OR$

FR_{111}: $s_1 + s_2 + s_5 + s_6 + s_9 + s_{10} + s_{12} + s_{15} + s_{17} = OR$

FR_{112}: $s_1 + s_2 + s_5 + 2s_6 + 2s_9 - s_{13} + s_{15} + s_{18} = OR$

FR_{113}: $s_1 + s_2 + s_5 + s_6 + s_9 + s_{11} + s_{15} - s_{16} + s_{18} = OR$

FR_{114}: $s_1 + s_2 + s_5 + s_6 + s_9 - s_{13} + s_{14} + s_{15} + s_{17} = OR$

FR_{115}: $s_1 + s_2 + s_5 + s_8 - s_9 + s_{10} + s_{14} + s_{15} + s_{17} = OR$

FR_{116}: $s_1 + s_2 + s_5 + s_8 + s_9 + s_{12} - s_{13} + s_{15} + s_{17} = OR$

FR_{117}: $s_1 + s_2 + s_6 + s_7 - s_8 + s_{10} + s_{14} + s_{15} + s_{17} = OR$

FR_{118}: $s_1 + s_2 - s_6 + s_7 + s_8 + s_{12} - s_{13} + s_{15} + s_{17} = OR$

FR_{119}: $s_1 + s_2 + s_6 + s_7 + s_9 + s_{11} - s_{14} + s_{15} + s_{18} = OR$

FR_{120}: $s_1 + s_2 + s_6 + s_7 + s_9 - s_{13} + s_{15} + s_{16} + s_{17} = OR$

FR_{121}: $s_1 + s_2 + s_7 + s_8 - s_9 + s_{10} + s_{15} + s_{16} + s_{17} = OR$

FR_{122}: $s_1 + s_2 + s_7 + s_8 - s_9 + s_{11} - s_{12} + s_{15} + s_{18} = OR$

FR_{123}: $s_1 + s_2 + s_3 + s_4 - s_{10} - s_{13} + s_{14} + s_{15} + s_{17} = OR$

FR_{124}: $s_1 + s_2 + s_3 + s_5 + s_{10} + s_{12} + s_{13} + s_{15} + s_{17} = OR$

FR_{125}: $s_1 + s_2 + s_4 + s_6 - s_{13} + s_{14} + s_{15} - s_{16} + s_{18} = OR$

FR_{126}: $s_1 + s_2 + s_4 + s_8 - s_{10} + s_{11} - s_{13} + s_{15} + s_{17} = OR$

FR_{127}: $s_1 + s_2 + s_4 + 2s_8 - s_{10} - 2s_{13} + s_{15} + s_{18} = OR$

FR_{128}: $s_1 + s_2 + s_4 + s_8 + s_{11} + s_{12} - s_{14} + s_{15} + s_{17} = OR$

FR_{129}: $s_1 + s_2 + s_4 + s_8 + s_{12} - s_{13} + s_{15} - s_{16} + s_{18} = OR$

FR_{130}: $s_1 + s_2 + s_4 - s_9 + s_{11} + s_{14} + s_{15} - s_{16} + s_{17} = OR$

FR_{131}: $s_1 + s_2 + s_5 + s_6 + s_{10} + s_{11} + s_{13} + s_{15} + s_{17} = OR$

FR_{132}: $s_1 + s_2 + s_5 + 2s_6 + 2s_{10} + s_{13} + s_{15} + s_{18} = OR$

FR_{133}: $s_1 + s_2 + s_5 + s_6 + s_{10} + s_{14} + s_{15} - s_{16} + s_{18} = OR$

FR_{134}: $s_1 + s_2 + s_5 + s_6 + s_{11} - s_{12} + s_{14} + s_{15} + s_{17} = OR$

FR_{135}: $s_1 + s_2 + s_5 + s_8 + s_{10} + s_{12} + s_{15} - s_{16} + s_{18} = OR$

FR_{136}: $s_1 + s_2 + s_5 + s_9 + s_{11} + s_{12} + s_{15} - s_{16} + s_{17} = OR$

FR_{137}: $s_1 + s_2 + s_6 + s_7 - s_{12} - s_{13} + s_{14} + s_{15} + s_{18} = OR$

FR_{138}: $s_1 + s_2 + s_7 + s_8 + s_{10} + s_{12} - s_{14} + s_{15} + s_{18} = OR$

FR_{139}: $s_1 + s_2 + s_7 - s_9 + s_{10} + s_{14} + s_{15} - s_{16} + s_{18} = OR$

FR_{140}: $s_1 + s_2 + s_7 + s_9 + s_{12} - s_{13} + s_{15} - s_{16} + s_{18} = OR$

FR_{141}: $s_1 + s_2 + 2s_3 + s_4 - s_8 - s_{10} + s_{14} + s_{15} + s_{17} = OR$

FR_{142}: $s_1 + s_2 + 2s_3 + s_4 - s_9 - s_{11} + s_{14} + s_{15} + s_{18} = OR$

FR_{143}: $s_1 + s_2 + 2s_3 + s_4 - s_9 + s_{13} + s_{15} + s_{16} + s_{17} = OR$

FR_{144}: $s_1 + s_2 + 2s_3 + s_5 - s_6 + s_{12} + s_{13} + s_{15} + s_{17} = OR$

FR_{145}: $s_1 + s_2 + 2s_3 + s_5 + s_9 - s_{10} + s_{15} + s_{16} + s_{17} = OR$

FR_{146}: $s_1 + s_2 + 2s_3 + s_5 + s_9 - s_{11} + s_{12} + s_{15} + s_{18} = OR$

FR_{147}: $s_1 + s_2 + 2s_4 - s_5 + s_6 + s_{12} - s_{13} + s_{15} + s_{17} = OR$

FR_{148}: $s_1 + s_2 - s_4 + 2s_5 + s_8 + s_{10} + s_{14} + s_{15} + s_{17} = OR$

FR_{149}: $s_1 + s_2 + s_4 - s_{10} + 2s_{11} + s_{15} - 2s_{16} + s_{18} = OR$

FR_{150}: $s_1 + s_2 + s_4 - s_{10} + 2s_{11} + s_{15} + 2s_{17} - s_{18} = OR$

FR_{151}: $s_1 + s_2 + s_4 + s_{10} + 2s_{12} + s_{15} - 2s_{16} + s_{18} = OR$

FR_{152}: $s_1 + s_2 + s_4 + s_{10} + 2s_{12} + s_{15} + 2s_{17} - s_{18} = OR$

FR_{153}: $s_1 + s_2 + s_5 + 2s_{11} + s_{13} + s_{15} - 2s_{16} + s_{18} = OR$

FR_{154}: $s_1 + s_2 + s_5 + 2s_{11} + s_{13} + s_{15} + 2s_{17} - s_{18} = OR$

FR_{155}: $s_1 + s_2 + s_5 - s_{13} + 2s_{14} + s_{15} - 2s_{16} + s_{18} = OR$

FR_{156}: $s_1 + s_2 + s_5 - s_{13} + 2s_{14} + s_{15} + 2s_{17} - s_{18} = OR$

FR_{157}: $s_1 + s_2 + s_4 + 2s_6 - s_8 + s_{10} + s_{14} + s_{15} + s_{17} = OR$

FR_{158}: $s_1 + s_2 + s_4 + 2s_6 + s_9 + s_{11} - s_{14} + s_{15} + s_{18} = OR$

FR_{159}: $s_1 + s_2 + s_4 + 2s_6 + s_9 - s_{13} + s_{15} + s_{16} + s_{17} = OR$

FR_{160}: $s_1 + s_2 - s_4 + 2s_7 - s_8 + s_{10} + s_{14} + s_{15} + s_{17} = OR$

FR_{161}: $s_1 + s_2 - s_4 + 2s_7 + s_9 + s_{11} - s_{14} + s_{15} + s_{18} = OR$

FR_{162}: $s_1 + s_2 - s_4 + 2s_7 + s_9 - s_{13} + s_{15} + s_{16} + s_{17} = OR$

FR_{163}: $s_1 + s_2 + s_4 + s_8 - 2s_9 + s_{10} + s_{14} + s_{15} + s_{17} = OR$

FR_{164}: $s_1 + s_2 + s_4 + 2s_8 - s_9 + s_{11} - s_{14} + s_{15} + s_{18} = OR$

FR_{165}: $s_1 + s_2 + s_4 + 2s_8 - s_9 - s_{13} + s_{15} + s_{16} + s_{17} = OR$

FR_{166}: $s_1 + s_2 + s_4 + s_{12} - s_{13} + s_{14} + s_{15} - s_{16} + s_{17} = OR$

FR_{167}: $s_1 + s_2 - s_5 - s_6 + 2s_7 + s_{12} - s_{13} + s_{15} + s_{17} = OR$

FR_{168}: $s_1 + s_2 + s_5 - s_6 + 2s_8 + s_{12} - s_{13} + s_{15} + s_{17} = OR$

FR_{169}: $s_1 + s_2 + s_5 + 2s_6 + s_9 + s_{10} + s_{15} + s_{16} + s_{17} = OR$

FR_{170}: $s_1 + s_2 + s_5 + 2s_6 + s_9 + s_{11} - s_{12} + s_{15} + s_{18} = OR$

FR_{171}: $s_1 + s_2 + s_5 + s_6 + 2s_9 + s_{12} - s_{13} + s_{15} + s_{17} = OR$

FR_{172}: $s_1 + s_2 - s_5 + 2s_7 - s_9 + s_{10} + s_{15} + s_{16} + s_{17} = OR$

FR_{173}: $s_1 + s_2 - s_5 + 2s_7 - s_9 + s_{11} - s_{12} + s_{15} + s_{18} = OR$

FR_{174}: $s_1 + s_2 + s_5 + 2s_8 - s_9 + s_{10} + s_{15} + s_{16} + s_{17} = OR$

FR_{175}: $s_1 + s_2 + s_5 + 2s_8 - s_9 + s_{11} - s_{12} + s_{15} + s_{18} = OR$

FR_{176}: $s_1 + s_2 + s_5 + s_{10} + s_{12} + s_{14} + s_{15} - s_{16} + s_{17} = OR$

FR_{177}: $s_1 + s_2 + 2s_3 + s_4 + s_{12} + s_{13} - s_{14} + s_{15} + s_{18} = OR$

FR_{178}: $s_1 + s_2 + 2s_3 + s_5 - s_{10} - s_{12} + s_{14} + s_{15} + s_{18} = OR$

FR_{179}: $s_1 + s_2 + s_4 + 2s_6 - s_{12} - s_{13} + s_{14} + s_{15} + s_{18} = OR$

FR_{180}: $s_1 + s_2 - s_4 + 2s_7 - s_{12} - s_{13} + s_{14} + s_{15} + s_{18} = OR$

FR_{181}: $s_1 + s_2 + s_4 + s_8 - s_{10} + 2s_{11} - s_{14} + s_{15} + s_{17} = OR$

FR_{182}: $s_1 + s_2 + s_4 + s_8 + s_{10} + 2s_{12} - s_{14} + s_{15} + s_{17} = OR$

FR_{183}: $s_1 + s_2 + s_4 + s_8 - s_{10} - 2s_{13} + s_{14} + s_{15} + s_{17} = OR$

FR_{184}: $s_1 + s_2 + s_4 + 2s_8 + s_{12} - s_{13} - s_{14} + s_{15} + s_{18} = OR$

FR_{185}: $s_1 + s_2 + s_4 - s_9 + 2s_{11} + s_{13} + s_{15} - s_{16} + s_{17} = OR$

FR_{186}: $s_1 + s_2 + s_4 - s_9 + s_{11} + s_{14} + s_{15} - 2s_{16} + s_{18} = OR$

FR_{187}: $s_1 + s_2 + s_4 - s_9 + s_{11} + s_{14} + s_{15} + 2s_{17} - s_{18} = OR$

FR_{188}: $s_1 + s_2 + s_4 + s_9 + 2s_{12} - s_{13} + s_{15} - s_{16} + s_{17} = OR$

FR_{189}: $s_1 + s_2 + s_4 - s_9 - s_{13} + 2s_{14} + s_{15} - s_{16} + s_{17} = OR$

FR_{190}: $s_1 + s_2 + s_5 + s_6 + 2s_{10} + s_{12} + s_{13} + s_{15} + s_{17} = OR$

FR_{191}: $s_1 + s_2 + s_5 + 2s_6 + s_{10} - s_{12} + s_{14} + s_{15} + s_{18} = OR$

FR_{192}: $s_1 + s_2 + s_5 + s_6 + 2s_{11} - s_{12} + s_{13} + s_{15} + s_{17} = OR$

FR_{193}: $s_1 + s_2 + s_5 + s_6 - s_{12} - s_{13} + 2s_{14} + s_{15} + s_{17} = OR$

FR_{194}: $s_1 + s_2 - s_5 + 2s_7 + s_{10} + s_{12} - s_{14} + s_{15} + s_{18} = OR$

FR_{195}: $s_1 + s_2 + s_5 + 2s_8 + s_{10} + s_{12} - s_{14} + s_{15} + s_{18} = OR$

FR_{196}: $s_1 + s_2 + s_5 + s_9 - s_{10} + 2s_{11} + s_{15} - s_{16} + s_{17} = OR$

FR_{197}: $s_1 + s_2 + s_5 + s_9 + s_{10} + 2s_{12} + s_{15} - s_{16} + s_{17} = OR$

FR_{198}: $s_1 + s_2 + s_5 - s_9 + s_{10} + 2s_{14} + s_{15} - s_{16} + s_{17} = OR$

FR_{199}: $s_1 + s_2 + s_5 + s_9 + s_{11} + s_{12} + s_{15} - 2s_{16} + s_{18} = OR$

FR_{200}: $s_1 + s_2 + s_5 + s_9 + s_{11} + s_{12} + s_{15} + 2s_{17} - s_{18} = OR$

FR_{201}: $s_1 + s_2 + 2s_4 - s_5 + 2s_6 + s_{11} - s_{14} + s_{15} + s_{18} = OR$

FR_{202}: $s_1 + s_2 + 2s_4 - s_5 + 2s_6 - s_{13} + s_{15} + s_{16} + s_{17} = OR$

FR_{203}: $s_1 + s_2 - s_4 + 2s_5 + 2s_8 + s_{10} + s_{15} + s_{16} + s_{17} = OR$

FR_{204}: $s_1 + s_2 - s_4 + 2s_5 + 2s_8 + s_{11} - s_{12} + s_{15} + s_{18} = OR$

FR_{205}: $s_1 + s_2 + s_4 + 2s_8 - 2s_9 + s_{10} + s_{15} + s_{16} + s_{17} = OR$

FR_{206}: $s_1 + s_2 + s_4 + 2s_8 - 2s_9 + s_{11} - s_{12} + s_{15} + s_{18} = OR$

FR_{207}: $s_1 + s_2 + s_4 + s_{12} - s_{13} + s_{14} + s_{15} - 2s_{16} + s_{18} = OR$

FR_{208}: $s_1 + s_2 + s_4 + s_{12} - s_{13} + s_{14} + s_{15} + 2s_{17} - s_{18} = OR$

FR_{209}: $s_1 + s_2 + s_5 + 2s_6 + 2s_9 + s_{11} - s_{14} + s_{15} + s_{18} = OR$

FR_{210}: $s_1 + s_2 + s_5 + 2s_6 + 2s_9 - s_{13} + s_{15} + s_{16} + s_{17} = OR$

FR_{211}: $s_1 + s_2 + s_5 + s_{10} + s_{12} + s_{14} + s_{15} - 2s_{16} + s_{18} = OR$

FR_{212}: $s_1 + s_2 + s_5 + s_{10} + s_{12} + s_{14} + s_{15} + 2s_{17} - s_{18} = OR$

FR_{213}: $s_1 + s_2 - s_4 + 2s_5 + s_{10} + 2s_{14} + s_{15} - s_{16} + s_{17} = OR$

FR_{214}: $s_1 + s_2 + 2s_4 - s_5 + 2s_{12} - s_{13} + s_{15} - s_{16} + s_{17} = OR$

FR_{215}: $s_1 + s_2 + s_4 + 2s_8 - s_{10} - 2s_{13} + s_{15} + s_{16} + s_{17} = OR$

FR_{216}: $s_1 + s_2 + s_4 + 2s_8 - s_{11} + s_{12} - 2s_{13} + s_{15} + s_{18} = OR$

FR_{217}: $s_1 + s_2 + s_4 + 2s_8 + s_{11} + s_{12} - 2s_{14} + s_{15} + s_{18} = OR$

FR_{218}: $s_1 + s_2 + s_4 - 2s_9 + s_{10} + 2s_{14} + s_{15} - s_{16} + s_{17} = OR$

FR_{219}: $s_1 + s_2 + s_4 - s_9 + 2s_{11} + s_{13} + s_{15} - 2s_{16} + s_{18} = OR$

FR_{220}: $s_1 + s_2 + s_4 - s_9 + 2s_{11} + s_{13} + s_{15} + 2s_{17} - s_{18} = OR$

FR_{221}: $s_1 + s_2 + s_4 + s_9 + 2s_{12} - s_{13} + s_{15} - 2s_{16} + s_{18} = OR$

FR_{222}: $s_1 + s_2 + s_4 + s_9 + 2s_{12} - s_{13} + s_{15} + 2s_{17} - s_{18} = OR$

FR_{223}: $s_1 + s_2 + s_4 - s_9 - s_{13} + 2s_{14} + s_{15} - 2s_{16} + s_{18} = OR$

FR_{224}: $s_1 + s_2 + s_4 - s_9 - s_{13} + 2s_{14} + s_{15} + 2s_{17} - s_{18} = OR$

FR_{225}: $s_1 + s_2 + s_5 + 2s_6 + 2s_{10} - s_{11} + s_{14} + s_{15} + s_{18} = OR$

FR_{226}: $s_1 + s_2 + s_5 + 2s_6 + 2s_{10} + s_{13} + s_{15} + s_{16} + s_{17} = OR$

FR_{227}: $s_1 + s_2 + s_5 + 2s_6 + s_{11} - 2s_{12} + s_{14} + s_{15} + s_{18} = OR$

FR_{228}: $s_1 + s_2 + s_5 + s_9 - s_{10} + 2s_{11} + s_{15} - 2s_{16} + s_{18} = OR$

FR_{229}: $s_1 + s_2 + s_5 + s_9 - s_{10} + 2s_{11} + s_{15} + 2s_{17} - s_{18} = OR$

FR_{230}: $s_1 + s_2 + s_5 + s_9 + s_{10} + 2s_{12} + s_{15} - 2s_{16} + s_{18} = OR$

FR_{231}: $s_1 + s_2 + s_5 + s_9 + s_{10} + 2s_{12} + s_{15} + 2s_{17} - s_{18} = OR$

FR_{232}: $s_1 + s_2 + s_5 - s_9 + s_{10} + 2s_{14} + s_{15} - 2s_{16} + s_{18} = OR$

FR_{233}: $s_1 + s_2 + s_5 - s_9 + s_{10} + 2s_{14} + s_{15} + 2s_{17} - s_{18} = OR$

FR_{234}: $s_1 + s_2 + s_5 + 2s_9 + 2s_{12} - s_{13} + s_{15} - s_{16} + s_{17} = OR$

FR_{235}: $s_1 + s_2 + s_4 - s_{10} - 2s_{13} + 2s_{14} + s_{15} - s_{16} + s_{17} = OR$

FR_{236}: $s_1 + s_2 + s_5 + 2s_{10} + 2s_{12} + s_{13} + s_{15} - s_{16} + s_{17} = OR$

FR_{237}: $s_1 + s_2 - s_4 + 2s_5 + s_{10} + 2s_{14} + s_{15} - 2s_{16} + s_{18} = OR$

FR_{238}: $s_1 + s_2 - s_4 + 2s_5 + s_{10} + 2s_{14} + s_{15} + 2s_{17} - s_{18} = OR$

FR_{239}: $s_1 + s_2 + 2s_4 - s_5 + 2s_{12} - s_{13} + s_{15} - 2s_{16} + s_{18} = OR$

FR_{240}: $s_1 + s_2 + 2s_4 - s_5 + 2s_{12} - s_{13} + s_{15} + 2s_{17} - s_{18} = OR$

FR_{241}: $s_1 + s_2 + s_4 + 2s_8 - s_{10} + 2s_{11} - 2s_{14} + s_{15} + s_{18} = OR$

FR_{242}: $s_1 + s_2 + s_4 + 2s_8 + s_{10} + 2s_{12} - 2s_{14} + s_{15} + s_{18} = OR$

FR_{243}: $s_1 + s_2 + s_4 - 2s_9 + s_{10} + 2s_{14} + s_{15} - 2s_{16} + s_{18} = OR$

FR_{244}: $s_1 + s_2 + s_4 - 2s_9 + s_{10} + 2s_{14} + s_{15} + 2s_{17} - s_{18} = OR$

FR_{245}: $s_1 + s_2 + s_5 + 2s_6 + 2s_{11} - 2s_{12} + s_{13} + s_{15} + s_{18} = OR$

FR_{246}: $s_1 + s_2 + s_5 + 2s_6 - 2s_{12} - s_{13} + 2s_{14} + s_{15} + s_{18} = OR$

FR_{247}: $s_1 + s_2 + s_5 + 2s_9 + 2s_{12} - s_{13} + s_{15} - 2s_{16} + s_{18} = OR$

FR_{248}: $s_1 + s_2 + s_5 + 2s_9 + 2s_{12} - s_{13} + s_{15} + 2s_{17} - s_{18} = OR$

FR_{249}: $s_1 + s_2 + s_4 - s_{10} - 2s_{13} + 2s_{14} + s_{15} - 2s_{16} + s_{18} = OR$

FR_{250}: $s_1 + s_2 + s_4 - s_{10} - 2s_{13} + 2s_{14} + s_{15} + 2s_{17} - s_{18} = OR$

FR_{251}: $s_1 + s_2 + s_5 + 2s_{10} + 2s_{12} + s_{13} + s_{15} - 2s_{16} + s_{18} = OR$

FR_{252}: $s_1 + s_2 + s_5 + 2s_{10} + 2s_{12} + s_{13} + s_{15} + 2s_{17} - s_{18} = OR$

EMPTY ROUTES

ER_1: $s_4 + s_6 - s_7 = 0$

ER_2: $s_4 - s_5 - s_9 = 0$

ER_3: $s_5 - s_7 + s_8 = 0$

ER_4: $s_6 - s_8 + s_9 = 0$

ER_5: $s_3 - s_6 - s_{10} = 0$

ER_6: $s_3 - s_8 + s_{13} = 0$

ER_7: $s_3 - s_{11} + s_{16} = 0$

ER_8: $s_6 - s_{12} + s_{16} = 0$

ER_9: $s_8 - s_{14} + s_{16} = 0$

ER_{10}: $s_9 + s_{12} - s_{14} = 0$

ER_{11}: $s_9 - s_{10} - s_{13} = 0$

ER_{12}: $s_4 - s_5 + s_6 - s_8 = 0$

ER_{13}: $s_{16} + s_{17} - s_{18} = 0$

ER_{14}: $s_{10} - s_{11} + s_{12} = 0$

ER_{15}: $s_{11} + s_{13} - s_{14} = 0$

ER_{16}: $s_4 - s_7 + s_8 - s_9 = 0$

ER_{17}: $s_5 + s_6 - s_7 + s_9 = 0$

ER_{18}: $s_3 + s_4 - s_7 - s_{10} = 0$

ER_{19}: $s_3 + s_5 - s_7 + s_{13} = 0$

ER_{20}: $s_3 - s_6 - s_9 + s_{13} = 0$

ER_{21}: $s_3 - s_8 + s_9 - s_{10} = 0$

ER_{22}: $s_3 - s_6 - s_{11} + s_{12} = 0$

ER_{23}: $s_4 - s_5 + s_{12} - s_{14} = 0$

ER_{24}: $s_4 - s_7 + s_{12} - s_{16} = 0$

ER_{25}: $s_5 - s_7 + s_{14} - s_{16} = 0$

ER_{26}: $s_3 - s_8 - s_{11} + s_{14} = 0$

ER_{27}: $s_4 - s_5 - s_{10} - s_{13} = 0$

ER_{28}: $s_6 - s_8 - s_{12} + s_{14} = 0$

ER_{29}: $s_6 + s_9 - s_{14} + s_{16} = 0$

ER_{30}: $s_8 - s_9 - s_{12} + s_{16} = 0$

ER_{31}: $s_6 - s_8 + s_{10} + s_{13} = 0$

ER_{32}: $s_3 - s_{11} - s_{17} + s_{18} = 0$

ER_{33}: $s_6 - s_{12} - s_{17} + s_{18} = 0$

ER_{34}: $s_8 - s_{14} - s_{17} + s_{18} = 0$

ER_{35}: $s_3 - s_{10} - s_{12} + s_{16} = 0$

ER_{36}: $s_3 + s_{13} - s_{14} + s_{16} = 0$

ER_{37}: $s_9 - s_{10} + s_{11} - s_{14} = 0$

ER_{38}: $s_9 - s_{11} + s_{12} - s_{13} = 0$

ER_{39}: $s_6 + s_{10} - s_{11} + s_{16} = 0$

ER_{40}: $s_8 - s_{11} - s_{13} + s_{16} = 0$

ER_{41}: $s_3 - s_4 + s_5 - s_6 + s_{13} = 0$

ER_{42}: $s_3 + s_4 - s_5 - s_8 - s_{10} = 0$

ER_{43}: $s_3 + s_4 - s_7 - s_9 + s_{13} = 0$

ER_{44}: $s_{10} + s_{12} + s_{13} - s_{14} = 0$

ER_{45}: $s_3 + s_5 - s_7 + s_9 - s_{10} = 0$

ER_{46}: $s_4 - s_5 + s_6 - s_{14} + s_{16} = 0$

ER_{47}: $s_3 + s_4 - s_7 - s_{11} + s_{12} = 0$

ER_{48}: $s_3 + s_5 - s_7 - s_{11} + s_{14} = 0$

ER_{49}: $s_4 - s_5 - s_8 + s_{12} - s_{16} = 0$

ER_{50}: $s_3 - s_6 - s_9 - s_{11} + s_{14} = 0$

ER_{51}: $s_4 - s_7 + s_8 + s_{12} - s_{14} = 0$

ER_{52}: $s_4 - s_7 - s_9 + s_{14} - s_{16} = 0$

ER_{53}: $s_3 - s_8 + s_9 - s_{11} + s_{12} = 0$

ER_{54}: $s_5 + s_6 - s_7 - s_{12} + s_{14} = 0$

ER_{55}: $s_5 - s_7 + s_9 + s_{12} - s_{16} = 0$

ER_{56}: $s_4 - s_7 + s_8 - s_{10} - s_{13} = 0$

ER_{57}: $s_5 + s_6 - s_7 + s_{10} + s_{13} = 0$

ER_{58}: $s_4 - s_7 + s_{12} + s_{17} - s_{18} = 0$

ER_{59}: $s_5 - s_7 + s_{14} + s_{17} - s_{18} = 0$

ER_{60}: $s_4 - s_5 - s_{10} + s_{11} - s_{14} = 0$

ER_{61}: $s_4 - s_5 - s_{11} + s_{12} - s_{13} = 0$

ER_{62}: $s_6 + s_9 - s_{14} - s_{17} + s_{18} = 0$

ER_{63}: $s_3 - s_6 + s_{12} + s_{13} - s_{14} = 0$

ER_{64}: $s_8 - s_9 - s_{12} - s_{17} + s_{18} = 0$

ER_{65}: $s_3 - s_8 - s_{10} - s_{12} + s_{14} = 0$

ER_{66}: $s_3 + s_9 - s_{10} - s_{14} + s_{16} = 0$

ER_{67}: $s_3 - s_9 - s_{12} + s_{13} + s_{16} = 0$

ER_{68}: $s_4 - s_7 - s_{10} + s_{11} - s_{16} = 0$

ER_{69}: $s_5 - s_7 + s_{11} + s_{13} - s_{16} = 0$

ER_{70}: $s_6 - s_8 + s_{10} - s_{11} + s_{14} = 0$

ER_{71}: $s_6 - s_8 + s_{11} - s_{12} + s_{13} = 0$

ER_{72}: $s_6 + s_9 - s_{11} - s_{13} + s_{16} = 0$

ER_{73}: $s_8 - s_9 + s_{10} - s_{11} + s_{16} = 0$

ER_{74}: $s_3 - s_{10} - s_{12} - s_{17} + s_{18} = 0$

ER_{75}: $s_3 + s_{13} - s_{14} - s_{17} + s_{18} = 0$

ER_{76}: $s_6 + s_{10} - s_{11} - s_{17} + s_{18} = 0$

ER_{77}: $s_8 - s_{11} - s_{13} - s_{17} + s_{18} = 0$

ER_{78}: $s_6 + s_{10} + s_{13} - s_{14} + s_{16} = 0$

ER_{79}: $s_8 - s_{10} - s_{12} - s_{13} + s_{16} = 0$

ER_{80}: $s_3 - s_4 + s_5 - s_6 - s_{11} + s_{14} = 0$

ER_{81}: $s_3 + s_4 - s_5 - s_8 - s_{11} + s_{12} = 0$

ER_{82}: $s_3 + s_4 - s_7 - s_9 - s_{11} + s_{14} = 0$

ER_{83}: $s_3 + s_5 - s_7 + s_9 - s_{11} + s_{12} = 0$

ER_{84}: $s_4 - s_5 + s_6 - s_{14} - s_{17} + s_{18} = 0$

ER_{85}: $s_4 - s_5 - s_8 + s_{12} + s_{17} - s_{18} = 0$

ER_{86}: $s_3 + s_4 - s_5 - s_{10} - s_{14} + s_{16} = 0$

ER_{87}: $s_3 - s_4 + s_5 - s_{12} + s_{13} + s_{16} = 0$

ER_{88}: $s_4 - s_7 - s_9 + s_{14} + s_{17} - s_{18} = 0$

ER_{89}: $s_3 + s_4 - s_7 + s_{12} + s_{13} - s_{14} = 0$

ER_{90}: $s_5 - s_7 + s_9 + s_{12} + s_{17} - s_{18} = 0$

ER_{91}: $s_3 + s_5 - s_7 - s_{10} - s_{12} + s_{14} = 0$

ER_{92}: $s_4 - s_5 + s_6 - s_{11} - s_{13} + s_{16} = 0$

ER_{93}: $s_4 - s_5 - s_8 - s_{10} + s_{11} - s_{16} = 0$

ER_{94}: $s_4 - s_7 + s_8 - s_{10} + s_{11} - s_{14} = 0$

ER_{95}: $s_4 - s_7 + s_8 - s_{11} + s_{12} - s_{13} = 0$

ER_{96}: $s_4 - s_7 - s_9 + s_{11} + s_{13} - s_{16} = 0$

ER_{97}: $s_5 + s_6 - s_7 + s_{10} - s_{11} + s_{14} = 0$

ER_{98}: $s_5 + s_6 - s_7 + s_{11} - s_{12} + s_{13} = 0$

ER_{99}: $s_5 - s_7 + s_9 - s_{10} + s_{11} - s_{16} = 0$

ER_{100}: $s_3 + s_9 - s_{10} - s_{14} - s_{17} + s_{18} = 0$

ER_{101}: $s_3 - s_9 - s_{12} + s_{13} - s_{17} + s_{18} = 0$

ER_{102}: $s_4 - s_7 - s_{10} + s_{11} + s_{17} - s_{18} = 0$

ER_{103}: $s_5 - s_7 + s_{11} + s_{13} + s_{17} - s_{18} = 0$

ER_{104}: $s_6 + s_9 - s_{11} - s_{13} - s_{17} + s_{18} = 0$

ER_{105}: $s_4 - s_7 - s_{10} - s_{13} + s_{14} - s_{16} = 0$

ER_{106}: $s_8 - s_9 + s_{10} - s_{11} - s_{17} + s_{18} = 0$

ER_{107}: $s_5 - s_7 + s_{10} + s_{12} + s_{13} - s_{16} = 0$

ER_{108}: $s_6 + s_{10} + s_{13} - s_{14} - s_{17} + s_{18} = 0$

ER_{109}: $s_8 - s_{10} - s_{12} - s_{13} - s_{17} + s_{18} = 0$

ER_{110}: $s_3 + s_4 - s_5 - s_{10} - s_{14} - s_{17} + s_{18} = 0$

ER_{111}: $s_3 - s_4 + s_5 - s_{12} + s_{13} - s_{17} + s_{18} = 0$

ER_{112}: $s_4 - s_5 + s_6 - s_{11} - s_{13} - s_{17} + s_{18} = 0$

ER_{113}: $s_4 - s_5 - s_8 - s_{10} + s_{11} + s_{17} - s_{18} = 0$

ER_{114}: $s_4 - s_7 - s_9 + s_{11} + s_{13} + s_{17} - s_{18} = 0$

ER_{115}: $s_5 - s_7 + s_9 - s_{10} + s_{11} + s_{17} - s_{18} = 0$

ER_{116}: $s_4 - s_7 - s_{10} - s_{13} + s_{14} + s_{17} - s_{18} = 0$

ER_{117}: $s_5 - s_7 + s_{10} + s_{12} + s_{13} + s_{17} - s_{18} = 0$

INTERMEDIATE NODES

Note: The INs are presented here along with their species equivalents.

$n_{I,1}$: $s_4 - s_6 + s_9 + s_{10} - s_{12}$

O·S

$n_{I,2}$: $s_3 + s_6 + s_7 + s_8 - s_{11} - s_{12} - s_{14} - 2s_{16} - 2s_{18}$

H·S

$n_{I,3}$: $s_{11} + s_{12} + s_{14} + s_{16} - s_{17}$

H_2·S

$n_{I,4}$: $s_3 - s_5 - s_6 - s_7 + s_9 + 2s_{10} + s_{11} - s_{12} - s_{13}$

OH·S

$n_{I,5}$: $s_1 - s_4 - s_5 - s_7$

CO·S

$n_{I,6}$: $s_4 + s_7 + s_8 + s_9 + s_{13} + s_{14} - s_{15}$

CO_2·S

$n_{I,7}$: $s_2 - s_3 - s_{10} - s_{11} + s_{13}$

H_2O·S

$n_{I,8}$: $s_5 - s_8 - s_9 - s_{13} - s_{14}$

HCOO·S

$n_{I,9}$: $s_3 + s_4 + s_7 + s_8 + s_9 + s_{10} - s_{11} - 2s_{12} - s_{14} - 2s_{16} - 2s_{18}$

H·S – O·S

$n_{I,10}$: $s_3 - s_4 + 2s_6 + s_7 + s_8 - s_9 - s_{10} - s_{11} - s_{14} - 2s_{16} - 2s_{18}$

H·S + O·S

$n_{I,11}$: $s_4 - s_6 + s_9 + s_{10} + s_{11} + s_{14} + s_{16} - s_{17}$

H_2·S – O·S

$n_{I,12}$: $s_3 + s_6 + s_7 + s_8 - s_{16} - s_{17} - 2s_{18}$

H·S + H_2·S

$n_{I,13}$: $s_3 - s_4 - s_5 - s_7 + s_{10} + s_{11} - s_{13}$

OH·S + O·S

$n_{I,14}$: $s_1 - s_5 - s_6 - s_7 + s_9 + s_{10} - s_{12}$

$CO{\cdot}S - O{\cdot}S$

$n_{I,15}$: $s_6 + s_7 + s_8 - s_{10} + s_{12} + s_{13} + s_{14} - s_{15}$

$CO_2{\cdot}S + O{\cdot}S$

$n_{I,16}$: $s_2 - s_3 + s_4 - s_6 + s_9 - s_{11} - s_{12} + s_{13}$

$H_2O{\cdot}S - O{\cdot}S$

$n_{I,17}$: $s_4 + s_5 - s_6 - s_8 + s_{10} - s_{12} - s_{13} - s_{14}$

$O{\cdot}S - HCOO{\cdot}S$

$n_{I,18}$: $s_3 + s_6 + s_7 + s_8 + s_{11} + s_{12} + s_{14} - 2s_{17} - 2s_{18}$

$H{\cdot}S + 2H_2{\cdot}S$

$n_{I,19}$: $s_3 + s_5 + s_6 + s_7 - s_9 - s_{11} - s_{12} - s_{13} - 2s_{14} - 2s_{16} - 2s_{18}$

$H{\cdot}S + HCOO{\cdot}S$

$n_{I,20}$: $s_3 - s_5 + s_6 + s_7 + 2s_8 + s_9 - s_{11} - s_{12} + s_{13} - 2s_{16} - 2s_{18}$

$H{\cdot}S - HCOO{\cdot}S$

$n_{I,21}$: $s_3 - 2s_4 - s_5 + s_6 - s_7 - s_9 + s_{11} + s_{12} - s_{13}$

$OH{\cdot}S + 2O{\cdot}S$

$n_{I,22}$: $s_2 - s_5 - s_6 - s_7 + s_9 + s_{10} - s_{12}$

$H_2O{\cdot}S + OH{\cdot}S$

$n_{I,23}$: $s_5 - s_8 - s_9 + s_{11} + s_{12} - s_{13} + s_{16} - s_{17}$

$H_2{\cdot}S + HCOO{\cdot}S$

$n_{I,24}$: $s_3 - s_6 - s_7 - s_8 + 2s_{10} + s_{11} - s_{12} - 2s_{13} - s_{14}$

$OH{\cdot}S + HCOO{\cdot}S$

$n_{I,25}$: $s_3 - 2s_5 - s_6 - s_7 + s_8 + 2s_9 + 2s_{10} + s_{11} - s_{12} + s_{14}$

$OH{\cdot}S - HCOO{\cdot}S$

$n_{I,26}$: $s_1 - s_4 - s_7 - s_8 - s_9 - s_{13} - s_{14}$

$CO{\cdot}S + HCOO{\cdot}S$

$n_{I,27}$: $s_4 + s_5 + s_7 - s_{15}$

$CO_2{\cdot}S + HCOO{\cdot}S$

$n_{I,28}$: $s_3 + s_4 + s_7 + s_8 + s_9 + s_{10} - s_{12} - s_{16} - s_{17} - 2s_{18}$

$H{\cdot}S + H_2{\cdot}S - O{\cdot}S$

$n_{I,29}$: $s_2 - s_3 + s_5 - s_8 - s_9 - s_{10} - s_{11} - s_{14}$

$H_2O{\cdot}S + HCOO{\cdot}S$

$n_{I,30}$: $2s_2 - s_3 - s_5 - s_6 - s_7 + s_9 - s_{11} - s_{12} + s_{13}$

$2H_2O{\cdot}S + OH{\cdot}S$

$n_{I,31}$: $s_1 - s_3 - s_{10} - s_{11} + s_{13}$

$CO{\cdot}S - OH{\cdot}S - O{\cdot}S$

$n_{I,32}$: $s_3 - s_5 + s_8 + s_9 + s_{10} + s_{11} + s_{14} - s_{15}$

$CO_2{\cdot}S + OH{\cdot}S + O{\cdot}S$

$n_{I,33}$: $s_3 + s_4 + s_7 + s_8 + s_9 + s_{10} + s_{11} + s_{14} - 2s_{17} - 2s_{18}$

$H{\cdot}S + 2H_2{\cdot}S - O{\cdot}S$

$n_{I,34}$: $s_2 - s_4 - s_5 - s_7$

$H_2O{\cdot}S + OH{\cdot}S + O{\cdot}S$

$n_{I,35}$: $s_6 + s_7 + s_8 - s_{10} - s_{11} + s_{13} - s_{16} - s_{18}$

$H{\cdot}S - OH{\cdot}S - HCOO{\cdot}S$

$n_{I,36}$: $s_5 + s_6 + s_7 - s_9 - s_{10} - s_{11} - s_{14} - s_{16} - s_{18}$

$H{\cdot}S - OH{\cdot}S + HCOO{\cdot}S$

$n_{I,37}$: $s_4 + s_5 - s_6 - s_8 + s_{10} + s_{11} - s_{13} + s_{16} - s_{17}$

$H_2{\cdot}S - O{\cdot}S + HCOO{\cdot}S$

$n_{I,38}$: $s_3 + s_{10} - s_{12} - s_{13} - s_{14} - s_{16} - s_{18}$

$H{\cdot}S + OH{\cdot}S + HCOO{\cdot}S$

$n_{I,39}$: $s_3 - s_5 + s_8 + s_9 + s_{10} - s_{12} - s_{16} - s_{18}$

$H{\cdot}S + OH{\cdot}S - HCOO{\cdot}S$

$n_{I,40}$: $s_3 + s_5 + s_6 + s_7 - s_9 - s_{13} - s_{14} - s_{16} - s_{17} - 2s_{18}$

$H{\cdot}S + H_2{\cdot}S + HCOO{\cdot}S$

$n_{I,41}$: $s_3 - s_4 - s_7 - s_8 - s_9 + s_{10} + s_{11} - 2s_{13} - s_{14}$

$OH{\cdot}S + O{\cdot}S + HCOO{\cdot}S$

$n_{I,42}$: $s_3 - s_4 - 2s_5 - s_7 + s_8 + s_9 + s_{10} + s_{11} + s_{14}$

$OH{\cdot}S + O{\cdot}S - HCOO{\cdot}S$

$n_{I,43}$: $s_1 - s_6 - s_7 - s_8 + s_{10} - s_{12} - s_{13} - s_{14}$

$CO{\cdot}S - O{\cdot}S + HCOO{\cdot}S$

$n_{I,44}$: $s_1 - s_3 + s_4 - s_6 + s_9 - s_{11} - s_{12} + s_{13}$

$CO{\cdot}S - OH{\cdot}S - 2O{\cdot}S$

$n_{I,45}$: $s_5 + s_6 + s_7 - s_9 - s_{10} + s_{12} - s_{15}$

$$CO_2{\cdot}S + O{\cdot}S + HCOO{\cdot}S$$

$n_{I,46}$: $s_3 - s_4 - s_5 + s_6 + s_8 + s_{11} + s_{12} + s_{14} - s_{15}$

$$CO_2{\cdot}S + OH{\cdot}S + 2O{\cdot}S$$

$n_{I,47}$: $s_2 - s_3 + s_4 + s_5 - s_6 - s_8 - s_{11} - s_{12} - s_{14}$

$$H_2O{\cdot}S - O{\cdot}S + HCOO{\cdot}S$$

$n_{I,48}$: $s_3 + s_5 + s_6 + s_7 - s_9 + s_{11} + s_{12} - s_{13} - 2s_{17} - 2s_{18}$

$$H{\cdot}S + 2H_2{\cdot}S + HCOO{\cdot}S$$

$n_{I,49}$: $s_3 - 2s_4 + s_6 - s_7 - s_8 - 2s_9 + s_{11} + s_{12} - 2s_{13} - s_{14}$

$$OH{\cdot}S + 2O{\cdot}S + HCOO{\cdot}S$$

$n_{I,50}$: $s_3 - 2s_4 - 2s_5 + s_6 - s_7 + s_8 + s_{11} + s_{12} + s_{14}$

$$OH{\cdot}S + 2O{\cdot}S - HCOO{\cdot}S$$

$n_{I,51}$: $s_2 - s_6 - s_7 - s_8 + s_{10} - s_{12} - s_{13} - s_{14}$

$$H_2O{\cdot}S + OH{\cdot}S + HCOO{\cdot}S$$

$n_{I,52}$: $s_1 - s_{15}$

$$CO{\cdot}S + CO_2{\cdot}S + HCOO{\cdot}S$$

$n_{I,53}$: $2s_1 - s_3 - s_5 - s_6 - s_7 + s_9 - s_{11} - s_{12} + s_{13}$

$$2CO{\cdot}S - OH{\cdot}S - 2O{\cdot}S$$

$n_{I,54}$: $2s_2 - s_3 - s_6 - s_7 - s_8 - s_{11} - s_{12} - s_{14}$

$$2H_2O{\cdot}S + OH{\cdot}S + HCOO{\cdot}S$$

$n_{I,55}$: $s_1 - s_2$

$$H_2O{\cdot}S - CO{\cdot}S + OH{\cdot}S + O{\cdot}S$$

$n_{I,56}$: $s_1 - s_3 + s_5 - s_8 - s_9 - s_{10} - s_{11} - s_{14}$

$$CO{\cdot}S - OH{\cdot}S - O{\cdot}S + HCOO{\cdot}S$$

$n_{I,57}$: $s_4 + s_7 + s_8 + s_9 - s_{11} - s_{12} + s_{13} - s_{16} - s_{18}$

$$H{\cdot}S - OH{\cdot}S - 2O{\cdot}S - HCOO{\cdot}S$$

$n_{I,58}$: $s_4 + s_5 + s_7 - s_{11} - s_{12} - s_{14} - s_{16} - s_{18}$

$$H{\cdot}S - OH{\cdot}S - 2O{\cdot}S + HCOO{\cdot}S$$

$n_{I,59}$: $s_3 + s_{10} + s_{11} - s_{13} - s_{15}$

$$CO_2{\cdot}S + OH{\cdot}S + O{\cdot}S + HCOO{\cdot}S$$

$n_{I,60}$: $s_3 - s_4 + s_6 - s_9 - s_{13} - s_{14} - s_{16} - s_{18}$

$$\mathrm{H{\cdot}S + OH{\cdot}S + 2O{\cdot}S + HCOO{\cdot}S}$$

$n_{\mathrm{I},61}$: $s_3 - s_4 - s_5 + s_6 + s_8 - s_{16} - s_{18}$

$$\mathrm{H{\cdot}S + OH{\cdot}S + 2O{\cdot}S - HCOO{\cdot}S}$$

$n_{\mathrm{I},62}$: $s_2 - s_4 - s_7 - s_8 - s_9 - s_{13} - s_{14}$

$$\mathrm{H_2O{\cdot}S + OH{\cdot}S + O{\cdot}S + HCOO{\cdot}S}$$

$n_{\mathrm{I},63}$: $s_6 + s_7 + s_8 - s_{10} + s_{12} + s_{13} + s_{14} - s_{17} - s_{18}$

$$\mathrm{H{\cdot}S + 2H_2{\cdot}S - OH{\cdot}S - HCOO{\cdot}S}$$

$n_{\mathrm{I},64}$: $s_5 + s_6 + s_7 - s_9 - s_{10} + s_{12} - s_{17} - s_{18}$

$$\mathrm{H{\cdot}S + 2H_2{\cdot}S - OH{\cdot}S + HCOO{\cdot}S}$$

$n_{\mathrm{I},65}$: $s_3 + s_{10} + s_{11} - s_{13} - s_{17} - s_{18}$

$$\mathrm{H{\cdot}S + 2H_2{\cdot}S + OH{\cdot}S + HCOO{\cdot}S}$$

$n_{\mathrm{I},66}$: $s_3 - s_5 + s_8 + s_9 + s_{10} + s_{11} + s_{14} - s_{17} - s_{18}$

$$\mathrm{H{\cdot}S + 2H_2{\cdot}S + OH{\cdot}S - HCOO{\cdot}S}$$

$n_{\mathrm{I},67}$: $s_1 - s_4 + s_6 - s_9 - s_{10} - s_{11} - s_{14} - s_{16} - s_{18}$

$$\mathrm{2CO{\cdot}S + H{\cdot}S - OH{\cdot}S + HCOO{\cdot}S}$$

$n_{\mathrm{I},68}$: $s_1 - s_4 - s_5 + s_6 + s_8 - s_{10} - s_{11} + s_{13} - s_{16} - s_{18}$

$$\mathrm{2CO{\cdot}S + H{\cdot}S - OH{\cdot}S - HCOO{\cdot}S}$$

$n_{\mathrm{I},69}$: $s_1 - s_3 - s_4 - s_7 - s_8 - s_9 - s_{10} + s_{12} + s_{16} + s_{18}$

$$\mathrm{2CO{\cdot}S - H{\cdot}S - OH{\cdot}S + HCOO{\cdot}S}$$

$n_{\mathrm{I},70}$: $2s_1 - s_3 - s_4 - s_7 - s_8 - s_9 - s_{10} - s_{11} - s_{14}$

$$\mathrm{2CO{\cdot}S - OH{\cdot}S - O{\cdot}S + HCOO{\cdot}S}$$

$n_{\mathrm{I},71}$: $s_1 - s_3 + s_4 + s_5 - s_6 - s_8 - s_{11} - s_{12} - s_{14}$

$$\mathrm{CO{\cdot}S - OH{\cdot}S - 2O{\cdot}S + HCOO{\cdot}S}$$

$n_{\mathrm{I},72}$: $s_4 - s_6 + s_9 + s_{10} + s_{11} + s_{14} - s_{15} + s_{16} + s_{18}$

$$\mathrm{2CO_2{\cdot}S - H{\cdot}S + OH{\cdot}S + HCOO{\cdot}S}$$

$n_{\mathrm{I},73}$: $s_3 + s_4 + s_7 + s_8 + s_9 + s_{10} - s_{12} - s_{15} - s_{16} - s_{18}$

$$\mathrm{2CO_2{\cdot}S + H{\cdot}S + OH{\cdot}S + HCOO{\cdot}S}$$

$n_{\mathrm{I},74}$: $s_3 + s_4 + s_7 + s_8 + s_9 + s_{10} + s_{11} + s_{14} - 2s_{15}$

$$\mathrm{2CO_2{\cdot}S + OH{\cdot}S + O{\cdot}S + HCOO{\cdot}S}$$

$n_{\mathrm{I},75}$: $s_3 - s_4 + s_6 - s_9 + s_{11} + s_{12} - s_{13} - s_{15}$

$$\mathrm{CO_2{\cdot}S + OH{\cdot}S + 2O{\cdot}S + HCOO{\cdot}S}$$

$n_{I,76}$: $s_2 - s_{11} - s_{12} - s_{14} - s_{16} - s_{18}$

$$2H_2O{\cdot}S + H{\cdot}S + OH{\cdot}S + HCOO{\cdot}S$$

$n_{I,77}$: $s_2 - s_5 + s_8 + s_9 - s_{11} - s_{12} + s_{13} - s_{16} - s_{18}$

$$2H_2O{\cdot}S + H{\cdot}S + OH{\cdot}S - HCOO{\cdot}S$$

$n_{I,78}$: $s_2 - s_3 - s_6 - s_7 - s_8 + s_{16} + s_{18}$

$$2H_2O{\cdot}S - H{\cdot}S + OH{\cdot}S + HCOO{\cdot}S$$

$n_{I,79}$: $s_2 - s_3 - s_5 - s_6 - s_7 + s_9 + s_{13} + s_{14} + s_{16} + s_{18}$

$$2H_2O{\cdot}S - H{\cdot}S + OH{\cdot}S - HCOO{\cdot}S$$

$n_{I,80}$: $2s_2 - s_3 - s_4 - s_7 - s_8 - s_9 - s_{10} - s_{11} - s_{14}$

$$2H_2O{\cdot}S + OH{\cdot}S + O{\cdot}S + HCOO{\cdot}S$$

$n_{I,81}$: $2s_1 - s_3 - s_6 - s_7 - s_8 - s_{11} - s_{12} - s_{14}$

$$2CO{\cdot}S - OH{\cdot}S - 2O{\cdot}S + HCOO{\cdot}S$$

$n_{I,82}$: $s_4 + s_5 - s_6 - s_8 + s_{10} + s_{11} - s_{13} - s_{15} + s_{16} + s_{18}$

$$2CO_2{\cdot}S - H{\cdot}S + OH{\cdot}S + 3HCOO{\cdot}S$$

$n_{I,83}$: $s_3 + s_6 + s_7 + s_8 + s_{11} + s_{12} + s_{14} - 2s_{15}$

$$2CO_2{\cdot}S + OH{\cdot}S + 2O{\cdot}S + HCOO{\cdot}S$$

$n_{I,84}$: $s_3 + s_5 + s_6 + s_7 - s_9 + s_{11} + s_{12} - s_{13} - 2s_{15}$

$$2CO_2{\cdot}S + OH{\cdot}S + 2O{\cdot}S + 2HCOO{\cdot}S$$

$n_{I,85}$: $s_2 - s_{15}$

$$H_2O{\cdot}S + CO_2{\cdot}S + OH{\cdot}S + O{\cdot}S + HCOO{\cdot}S$$

$n_{I,86}$: $s_4 + s_7 + s_8 + s_9 + s_{13} + s_{14} - s_{17} - s_{18}$

$$H{\cdot}S + 2H_2{\cdot}S - OH{\cdot}S - 2O{\cdot}S - HCOO{\cdot}S$$

$n_{I,87}$: $s_4 + s_5 + s_7 - s_{17} - s_{18}$

$$H{\cdot}S + 2H_2{\cdot}S - OH{\cdot}S - 2O{\cdot}S + HCOO{\cdot}S$$

$n_{I,88}$: $s_3 - s_4 + s_6 - s_9 + s_{11} + s_{12} - s_{13} - s_{17} - s_{18}$

$$H{\cdot}S + 2H_2{\cdot}S + OH{\cdot}S + 2O{\cdot}S + HCOO{\cdot}S$$

$n_{I,89}$: $s_3 - s_4 - s_5 + s_6 + s_8 + s_{11} + s_{12} + s_{14} - s_{17} - s_{18}$

$$H{\cdot}S + 2H_2{\cdot}S + OH{\cdot}S + 2O{\cdot}S - HCOO{\cdot}S$$

$n_{I,90}$: $s_1 - s_{11} - s_{12} - s_{14} - s_{16} - s_{18}$

$$2CO{\cdot}S + H{\cdot}S - OH{\cdot}S - 2O{\cdot}S + HCOO{\cdot}S$$

$n_{I,91}$: $s_1 - s_5 + s_8 + s_9 - s_{11} - s_{12} + s_{13} - s_{16} - s_{18}$

$$2CO{\cdot}S + H{\cdot}S - OH{\cdot}S - 2O{\cdot}S - HCOO{\cdot}S$$

$n_{I,92}$: $s_1 - s_3 - s_6 - s_7 - s_8 + s_{16} + s_{18}$

$$2CO{\cdot}S - H{\cdot}S - OH{\cdot}S - 2O{\cdot}S + HCOO{\cdot}S$$

$n_{I,93}$: $s_1 - s_3 - s_5 - s_6 - s_7 + s_9 + s_{13} + s_{14} + s_{16} + s_{18}$

$$2CO{\cdot}S - H{\cdot}S - OH{\cdot}S - 2O{\cdot}S - HCOO{\cdot}S$$

$n_{I,94}$: $s_{11} + s_{12} + s_{14} - s_{15} + s_{16} + s_{18}$

$$2CO_2{\cdot}S - H{\cdot}S + OH{\cdot}S + 2O{\cdot}S + HCOO{\cdot}S$$

$n_{I,95}$: $s_3 + s_6 + s_7 + s_8 - s_{15} - s_{16} - s_{18}$

$$2CO_2{\cdot}S + H{\cdot}S + OH{\cdot}S + 2O{\cdot}S + HCOO{\cdot}S$$

$n_{I,96}$: $s_2 - s_4 + s_6 - s_9 - s_{10} - s_{11} - s_{14} - s_{16} - s_{18}$

$$2H_2O{\cdot}S + H{\cdot}S + OH{\cdot}S + 2O{\cdot}S + HCOO{\cdot}S$$

$n_{I,97}$: $s_2 - s_4 - s_5 + s_6 + s_8 - s_{10} - s_{11} + s_{13} - s_{16} - s_{18}$

$$2H_2O{\cdot}S + H{\cdot}S + OH{\cdot}S + 2O{\cdot}S - HCOO{\cdot}S$$

$n_{I,98}$: $s_2 - s_3 - s_4 - s_7 - s_8 - s_9 - s_{10} + s_{12} + s_{16} + s_{18}$

$$2H_2O{\cdot}S - H{\cdot}S + OH{\cdot}S + 2O{\cdot}S + HCOO{\cdot}S$$

$n_{I,99}$: $s_2 - s_{17} - s_{18}$

$$2H_2O{\cdot}S + H{\cdot}S + 2H_2{\cdot}S + OH{\cdot}S + HCOO{\cdot}S$$

$n_{I,100}$: $s_5 - s_8 - s_9 + s_{11} + s_{12} - s_{13} - s_{15} + s_{16} + s_{18}$

$$2CO_2{\cdot}S - H{\cdot}S + OH{\cdot}S + 2O{\cdot}S + 3HCOO{\cdot}S$$

$n_{I,101}$: $s_3 + s_5 + s_6 + s_7 - s_9 - s_{13} - s_{14} - s_{15} - s_{16} - s_{18}$

$$2CO_2{\cdot}S + H{\cdot}S + OH{\cdot}S + 2O{\cdot}S + 3HCOO{\cdot}S$$

$n_{I,102}$: $s_1 - s_{17} - s_{18}$

$$2CO{\cdot}S + H{\cdot}S + 2H_2{\cdot}S - OH{\cdot}S - 2O{\cdot}S + HCOO{\cdot}S$$

$n_{I,103}$: $s_{15} - s_{17} - s_{18}$

$$2CO_2{\cdot}S - H{\cdot}S - 2H_2{\cdot}S + OH{\cdot}S + 2O{\cdot}S + HCOO{\cdot}S$$

TERMINAL NODES

$n_{T,1}$: $-s_{17}-s_{18}+OR$

$n_{T,2}$: $-s_{15}+OR$

$n_{T,3}$: $-s_{11}-s_{12}-s_{14}-s_{16}-s_{18}+OR$

$n_{T,4}$: $-s_{6}-s_{7}-s_{8}+s_{10}-s_{12}-s_{13}-s_{14}+OR$

$n_{T,5}$: $-s_{6}-s_{7}-s_{8}+s_{10}+s_{11}-s_{13}+s_{16}-s_{17}+OR$

$n_{T,6}$: $-s_{5}+s_{8}+s_{9}-s_{11}-s_{12}+s_{13}-s_{16}-s_{18}+OR$

$n_{T,7}$: $-s_{5}-s_{6}-s_{7}+s_{9}+s_{10}-s_{12}+OR$

$n_{T,8}$: $-s_{5}-s_{6}-s_{7}+s_{9}+s_{10}+s_{11}+s_{14}+s_{16}-s_{17}+OR$

$n_{T,9}$: $-s_{4}-s_{7}-s_{8}-s_{9}-s_{13}-s_{14}+OR$

$n_{T,10}$: $-s_{4}-s_{7}-s_{8}-s_{9}+s_{11}+s_{12}-s_{13}+s_{16}-s_{17}+OR$

$n_{T,11}$: $-s_{4}+s_{6}-s_{9}-s_{10}-s_{11}-s_{14}-s_{16}-s_{18}+OR$

$n_{T,12}$: $-s_{4}-s_{5}-s_{7}+OR$

$n_{T,13}$: $-s_{4}-s_{5}+s_{6}+s_{8}-s_{10}-s_{11}+s_{13}-s_{16}-s_{18}+OR$

$n_{T,14}$: $-s_{3}-s_{10}+s_{12}+s_{13}+s_{14}+s_{16}-s_{17}+OR$

$n_{T,15}$: $-s_{3}-s_{10}-s_{11}+s_{13}+OR$

$n_{T,16}$: $-s_{3}-s_{6}-s_{7}-s_{8}+s_{16}+s_{18}+OR$

$n_{T,17}$: $\frac{1}{2}\left(-s_{3}-s_{6}-s_{7}-s_{8}+s_{16}-s_{17}\right)+OR$

$n_{T,18}$: $\frac{1}{2}\left(-s_{3}-s_{6}-s_{7}-s_{8}-s_{11}-s_{12}-s_{14}\right)+OR$

$n_{T,19}$: $-s_{3}+s_{5}-s_{8}-s_{9}-s_{10}+s_{12}+s_{16}-s_{17}+OR$

$n_{T,20}$: $-s_{3}+s_{5}-s_{8}-s_{9}-s_{10}-s_{11}-s_{14}+OR$

$n_{T,21}$: $-s_{3}-s_{5}-s_{6}-s_{7}+s_{9}+s_{13}+s_{14}+s_{16}+s_{18}+OR$

$n_{T,22}$: $\frac{1}{2}\left(-s_{3}-s_{5}-s_{6}-s_{7}+s_{9}+s_{13}+s_{14}+s_{16}-s_{17}\right)+OR$

$n_{T,23}$: $\frac{1}{2}\left(-s_{3}-s_{5}-s_{6}-s_{7}+s_{9}-s_{11}-s_{12}+s_{13}\right)+OR$

$n_{T,24}$: $-s_{3}-s_{4}-s_{7}-s_{8}-s_{9}-s_{10}+s_{12}+s_{16}+s_{18}+OR$

$n_{T,25}$: $\frac{1}{2}\left(-s_{3}-s_{4}-s_{7}-s_{8}-s_{9}-s_{10}+s_{12}+s_{16}-s_{17}\right)+OR$

$n_{T,26}$: $\frac{1}{2}\left(-s_{3}-s_{4}-s_{7}-s_{8}-s_{9}-s_{10}-s_{11}-s_{14}\right)+OR$

$n_{T,27}$: $-s_{3}+s_{4}-s_{6}+s_{9}+s_{13}+s_{14}+s_{16}-s_{17}+OR$

$n_{T,28}$: $-s_{3}+s_{4}-s_{6}+s_{9}-s_{11}-s_{12}+s_{13}+OR$

$n_{T,29}$: $-s_{3}+s_{4}+s_{5}-s_{6}-s_{8}+s_{16}-s_{17}+OR$

$n_{T,30}$: $-s_3 + s_4 + s_5 - s_6 - s_8 - s_{11} - s_{12} - s_{14} + OR$

$n_{T,31}$: $-s_2 + OR$

$n_{T,32}$: $-s_1 + OR$

Appendix E: Δ – Y Conversion

Ref. Lessons in Electric Circuits,
http://www.ibiblio.org/obp/electricCircuits/DC/DC_10.html

In many circuit applications, we encounter components connected together in one of two ways to form a three-terminal network: the "Delta," or Δ (also known as the "Pi," or π) configuration, and the "Y" (also known as the "T") configuration.

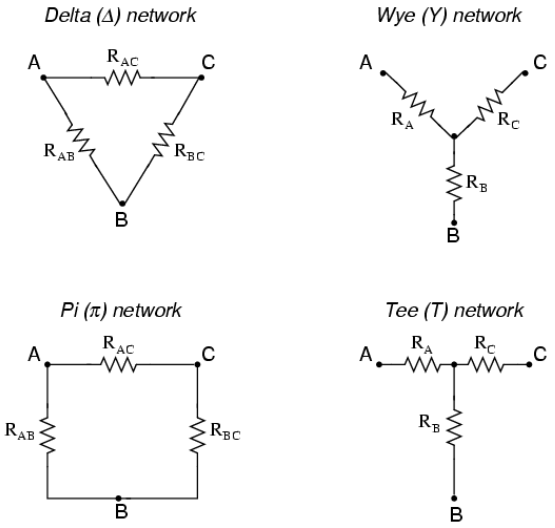

It is possible to calculate the proper values of resistors necessary to form one kind of network (Δ or Y) that behaves identically to the other kind, as analyzed from the terminal connections alone. That is, if we had two separate resistor networks, one Δ and one Y, each with its resistors hidden from view, with nothing but the three terminals (A, B, and C) exposed for testing, the resistors could be sized for the two networks so that there would be no way to electrically determine one network apart from the other. In other words, equivalent Δ and Y networks behave identically.

There are several equations used to convert one network to the other:

To convert a Delta (Δ) to a Wye (Y)

$$R_A = \frac{R_{AB} R_{AC}}{R_{AB} + R_{AC} + R_{BC}}$$

$$R_B = \frac{R_{AB} R_{BC}}{R_{AB} + R_{AC} + R_{BC}}$$

$$R_C = \frac{R_{AC} R_{BC}}{R_{AB} + R_{AC} + R_{BC}}$$

To convert a Wye (Y) to a Delta (Δ)

$$R_{AB} = \frac{R_A R_B + R_A R_C + R_B R_C}{R_C}$$

$$R_{BC} = \frac{R_A R_B + R_A R_C + R_B R_C}{R_A}$$

$$R_{AC} = \frac{R_A R_B + R_A R_C + R_B R_C}{R_B}$$

Appendix F: Calibration Plots

Mass Flow Controller Calibration

MFC 1

Carbon Monoxide

7/14/2004

MFC Reading *mL/min*	Flow Meter Reading 1 *mL/min*	Flow Meter Reading 2 *mL/min*	Flow Meter Reading 3 *mL/min*	Flow Meter Reading 4 *mL/min*	Actual Flow Rate *mL/min*	Actual Flow Error	Set Point Value *mL/min*
0.0	0.00	0.00	0.00	0.00	0.00	0.00	0.0
2.0	2.18	2.17	2.17	2.17	2.17	0.01	2.1
5.0	5.02	5.02	5.04	5.05	5.03	0.02	5.1
7.0	7.04	7.04	7.05	7.09	7.06	0.02	7.1
10.0	9.96	9.95	9.97	9.94	9.96	0.01	10.0
12.0	11.9	11.9	11.8	11.9	11.88	0.05	12.0
15.0	15.0	14.8	14.8	14.9	14.88	0.10	15.0
20.0	19.7	19.6	19.5	19.5	19.58	0.10	19.9
25.0	24.7	24.5	24.4	24.4	24.50	0.14	24.9
30.0	29.5	29.4	29.5	29.4	29.45	0.06	30.0
40.0	39.1	39.2	39.0	39.1	39.10	0.08	39.1

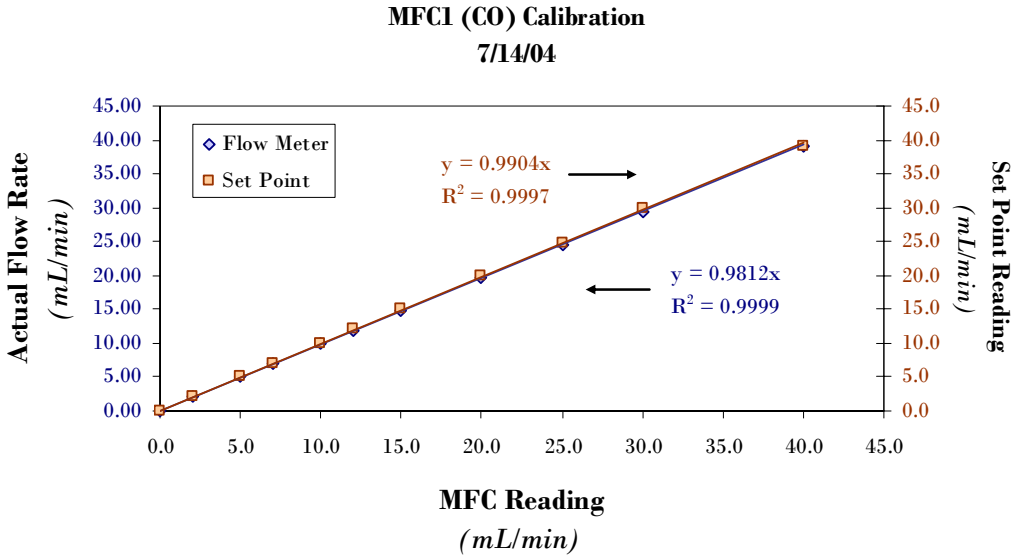

Actual Flow Rate = m · MFC Reading + b

m = 0.974431568

b = 0.166759979

NOTE: Actual Flow Rate based on Bubble Meter Readout (Alltech Digital Flow meter 4068)

Mass Flow Controller Calibration

MFC 2

Hydrogen

1/29/2004

MFC Reading *mL/min*	Flow Meter Reading 1 *mL/min*	Flow Meter Reading 2 *mL/min*	Flow Meter Reading 3 *mL/min*	Flow Meter Reading 4 *mL/min*	Actual Flow Rate *mL/min*	Actual Flow Error	Set Point Value *mL/min*
0.0	0.00	0.00	0.00	0.00	0.00	0.00	0.0
2.0	1.84	1.89	1.88	1.82	1.86	0.03	2.2
5.0	4.90	4.91	4.93	4.84	4.90	0.04	5.2
7.0	6.76	6.89	6.88	6.85	6.85	0.06	7.2
10.0	9.85	9.82	9.91	9.75	9.83	0.07	10.2
12.0	11.6	11.7	11.7	11.7	11.68	0.05	12.2
15.0	14.8	14.7	14.6	14.7	14.70	0.08	15.2
20.0	19.5	19.5	19.4	19.5	19.48	0.05	20.2
25.0	24.4	24.4	24.2	24.3	24.33	0.10	25.2
30.0	29.1	29.0	28.9	29.0	29.00	0.08	30.2
40.0	39.6	38.7	38.6	38.6	38.88	0.49	40.2

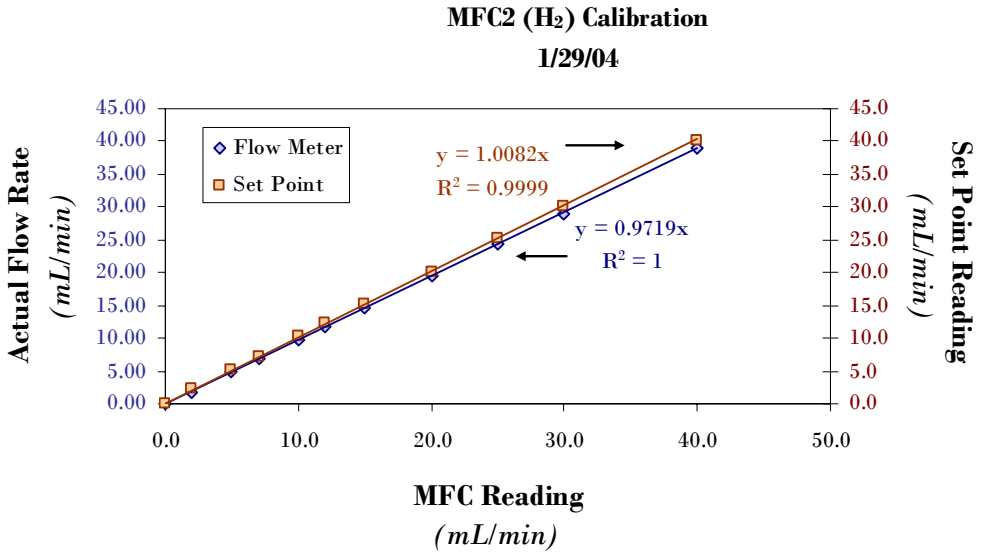

Actual Flow Rate = m • MFC Reading + b

m = 0.970557264

b = 0.033408563

NOTE: Actual Flow Rate based on Bubble Meter Readout (Alltech Digital Flow meter 4068)

Mass Flow Controller Calibration

MFC 3

Carbon Dioxide

11/30/2004

MFC Reading *mL/min*	Flow Meter Reading 1 *mL/min*	Flow Meter Reading 2 *mL/min*	Flow Meter Reading 3 *mL/min*	Flow Meter Reading 4 *mL/min*	Actual Flow Rate *mL/min*	Actual Flow Error	Set Point Value *mL/min*
0.0	0.00	0.00	0.00	0.00	0.00	0.00	0.0
2.0	1.79	1.76	1.75	1.78	1.77	0.02	2.0
5.0	4.32	4.31	4.32	4.33	4.32	0.01	5.0
7.0	6.12	6.15	6.16	6.12	6.14	0.02	7.0
10.0	8.71	8.69	8.72	8.74	8.72	0.02	9.9
12.0	10.5	10.5	10.4	10.4	10.45	0.06	11.9
15.0	13.1	13.1	13.0	13.0	13.05	0.06	14.9
20.0	17.5	17.5	17.4	17.6	17.50	0.08	19.7
25.0	21.9	21.8	21.7	21.8	21.80	0.08	24.5
30.0	26.2	26.2	26.1	26.2	26.18	0.05	29.4
40.0	35.0	35.0	35.1	35.0	35.03	0.05	39.2

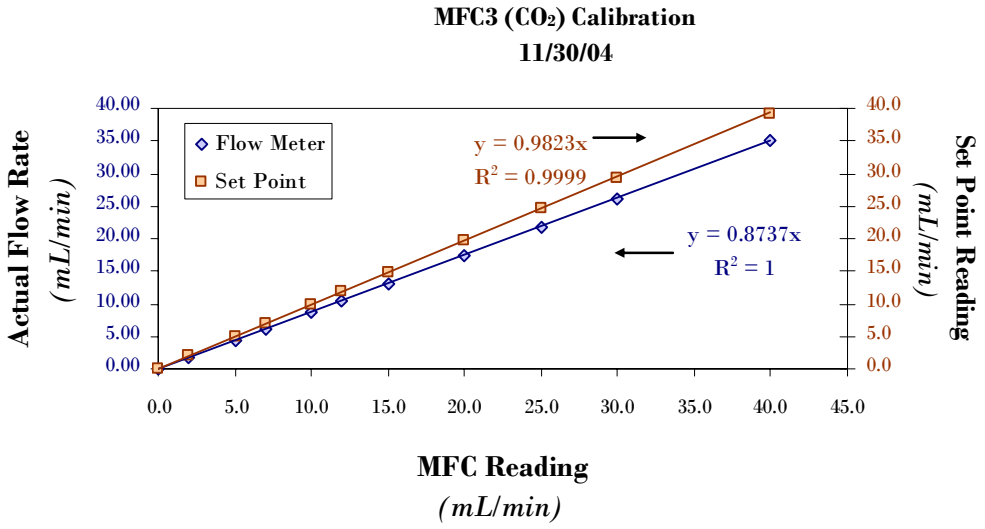

Actual Flow Rate = m • MFC Reading + b

m = 0.872559928

b = -0.00250509

NOTE: Actual Flow Rate based on Bubble Meter Readout (Alltech Digital Flow meter 4068)

Mass Flow Controller Calibration

MFC 4

Nitrogen

1/19/2006

MFC Reading *mL/min*	Flow Meter Reading 1 *mL/min*	Flow Meter Reading 2 *mL/min*	Flow Meter Reading 3 *mL/min*	Flow Meter Reading 4 *mL/min*	Actual Flow Rate *mL/min*	Actual Flow Error	Set Point Value *mL/min*
0.0	0.0	0.0	0.0	0.0	0.00	0.00	0.0
10.0	12.30	12.30	12.30	12.30	12.30	0.00	10.2
20.0	22.6	22.5	22.4	22.4	22.48	0.10	20.2
30.0	32.4	32.7	32.5	32.6	32.55	0.13	30.2
40.0	42.3	42.3	42.3	42.4	42.33	0.05	40.2
50.0	52.3	52.4	52.4	52.3	52.35	0.06	50.3
60.0	61.5	62.0	61.8	61.6	61.73	0.22	60.2
70.0	71.4	71.3	71.3	71.1	71.28	0.13	70.2
80.0	80.9	81.6	81.7	81.8	81.50	0.41	80.2
90.0	91.4	91.7	91.6	91.6	91.58	0.13	90.2
100.0	101.0	101.0	101.0	101.0	101.00	0.00	100.2

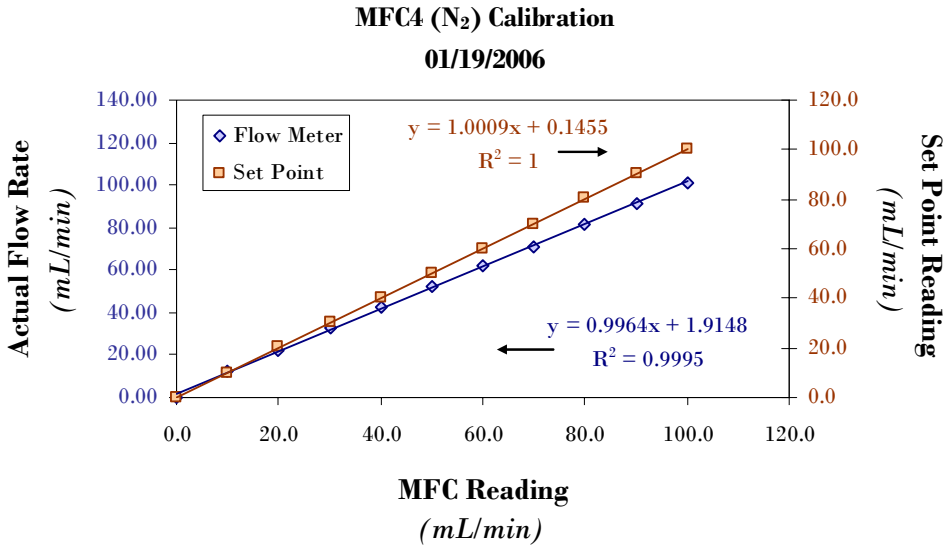

Actual Flow Rate = m • MFC Reading + b

m = 0.996386364

b = 1.914772727

NOTE: Actual Flow Rate based on Bubble Meter Readout (Alltech Digital Flow meter 4068)

Mass Flow Controller Calibration

MFC 6

3% H_2/N_2

12/20/2004

MFC Reading *mL/min*	Flow Meter Reading 1 *mL/min*	Flow Meter Reading 2 *mL/min*	Flow Meter Reading 3 *mL/min*	Flow Meter Reading 4 *mL/min*	Actual Flow Rate *mL/min*	Actual Flow Error	Set Point Value *mL/min*
10.0	9.97	10	10	10	9.9925	0.015	10.3
20.0	20	20	20	20	20	0	20.2
30.0	29.9	29.8	29.7	29.8	29.8	0.0816497	30.2
40.0	40.1	40.1	40.1	40	40.075	0.05	40.3
50.0	50	49.7	49.8	50	49.875	0.15	50.2
60.0	60	60.1	59.9	60	60	0.0816497	60.4
70.0	69.7	69.8	70.1	69.7	69.825	0.1892969	70.4
80.0	80.8	79.9	80.2	79.7	80.15	0.4795832	80.3
90.0	89.3	89.1	89.6	89.4	89.35	0.2081666	90.3
100.0	99.7	99.3	99.5	99.1	99.4	0.2581989	100.3
110.0	109	109	108	111	109.25	1.2583057	110.4

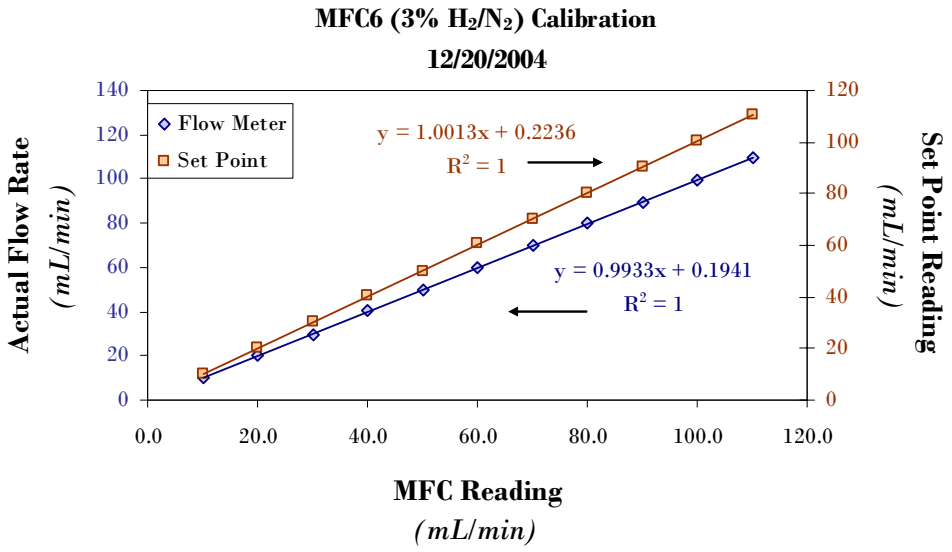

Actual Flow Rate = m • MFC Reading + b

m = 0.993306818

b = 0.194090909

NOTE: Actual Flow Rate based on Bubble Meter Readout (Alltech Digital Flow meter 4068)

Mass Flow Controller Calibration

MFC 7

Methane

10/11/2005

MFC Reading *mL/min*	Flow Meter Reading 1 *mL/min*	Flow Meter Reading 2 *mL/min*	Flow Meter Reading 3 *mL/min*	Flow Meter Reading 4 *mL/min*	Actual Flow Rate *mL/min*	Actual Flow Error	Set Point Value *mL/min*
0.0	0.0	0.0	0.0	0.0	0	0	0
5.0	5.36	5.36	5.36	5.35	5.3575	0.005	5
7.0	7.29	7.28	7.98	7.31	7.465	0.3435598	7.1
10.0	10.1	10.1	10	10.1	10.075	0.05	10
12.0	12	12	12	12	12	0	12.1
15.0	14.8	15.1	14.9	14.9	14.925	0.1258306	15.1
20.0	19.5	19.5	19.7	19.2	19.475	0.2061553	20
25.0	24.1	24.1	24.2	24.3	24.175	0.0957427	25.1
30.0	29	29.3	28.9	28.8	29	0.2160247	30.1
40.0	38.3	38.2	38.4	38.8	38.425	0.2629956	40

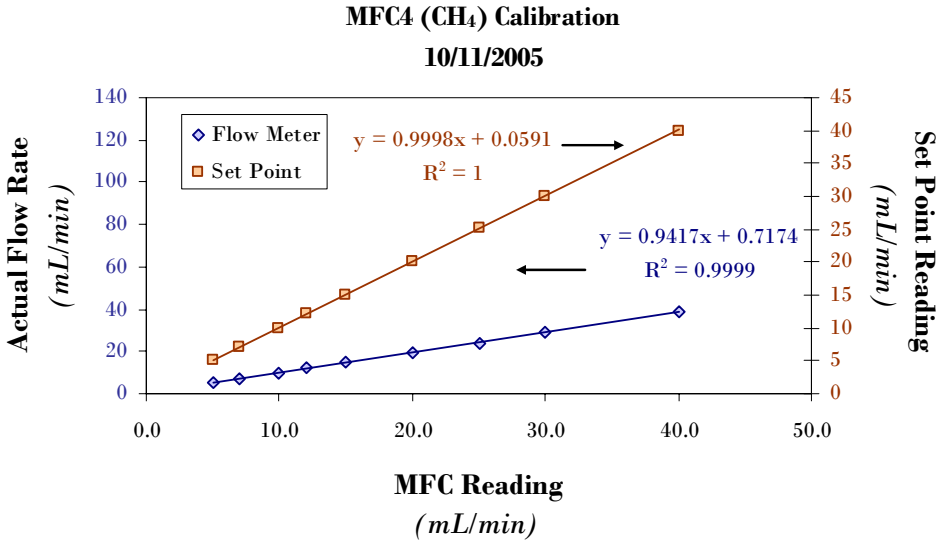

Actual Flow Rate = m • MFC Reading + b

m = 0.005025793

b = 0.048107863

NOTE: Actual Flow Rate based on Bubble Meter Readout (Alltech Digital Flow meter 4068)

Syringe Pump Calibration

11/16/2004

Gas Flow *mL/min*	Pump Reading *mL/min*	Water Output *mL*	Time Interval *min*	Actual Liq. Flow Rate *mL/min*	Actual Gas Flow Rate *mL/min*
0.00000	0.00000	0	1	0.00000	0.00
1.24306	0.00100	0.4	339	0.00118	1.47
6.21532	0.00500	0.4	77.5	0.00516	6.42
12.43063	0.01000	0.9	86	0.01047	13.01
62.15316	0.05000	3.3	66	0.05000	62.15
124.30633	0.10000	2.4	23.5	0.10213	126.95

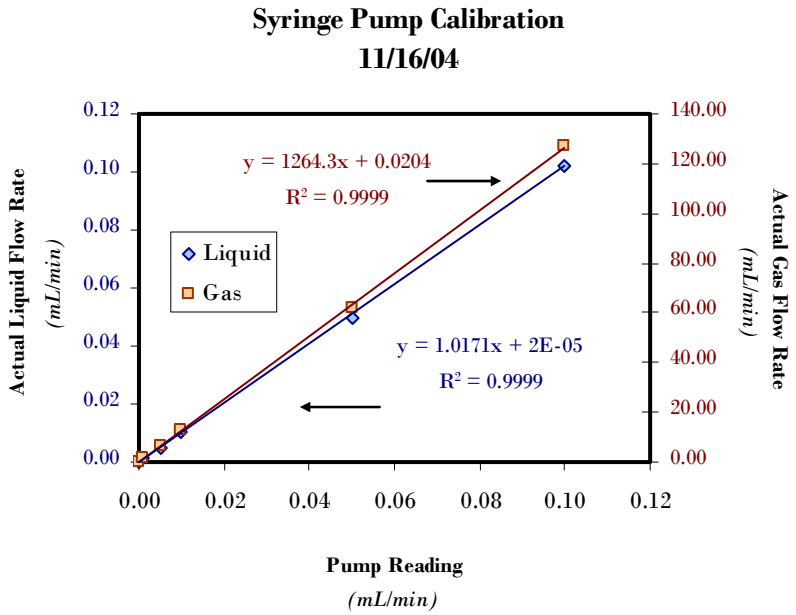

Actual Liquid Flow Rate = m × Pump Reading + b

m =	1.02
b =	0.00

Actual Gas Flow Rate = m × Pump Reading + b

m =	1264.30
b =	0.02

GC Calibrations

Hydrogen

7/9/2004

volume H_2/ volume N_2	area H_2/ area N_2
0.0526	0.6419
0.1111	1.3262
0.1765	2.0845
0.2500	2.8922
0.3333	3.8458
0.4286	4.9081
0.5385	6.0770
0.6667	7.4732
0.8182	8.9820
1.0000	10.8664

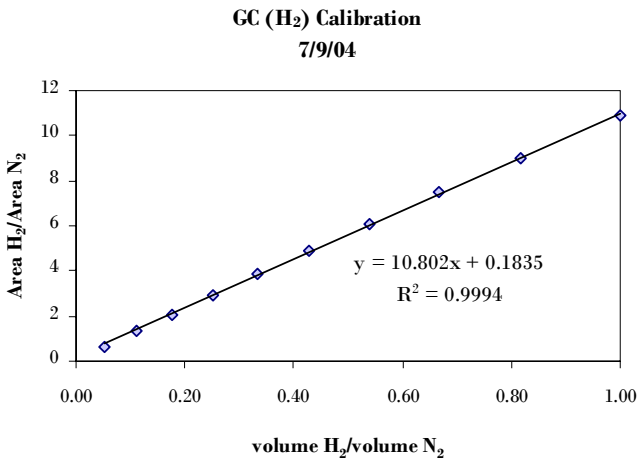

NOTES: SRI 8610C Gas Chromatograph — Carboxen 1000 Column
Oven Temperature: 125 oC — Oven Temperature Hold Time: 6000 min

GC Calibrations

Carbon Monoxide

7/16/2004

volume CO/ volume N_2	area CO/ area N_2
0.0526	0.0541
0.1111	0.1141
0.1765	0.1811
0.2500	0.2474
0.3333	0.3299
0.4286	0.4177
0.5385	0.5298
0.6667	0.6463
0.8182	0.7984
1.0000	0.9562

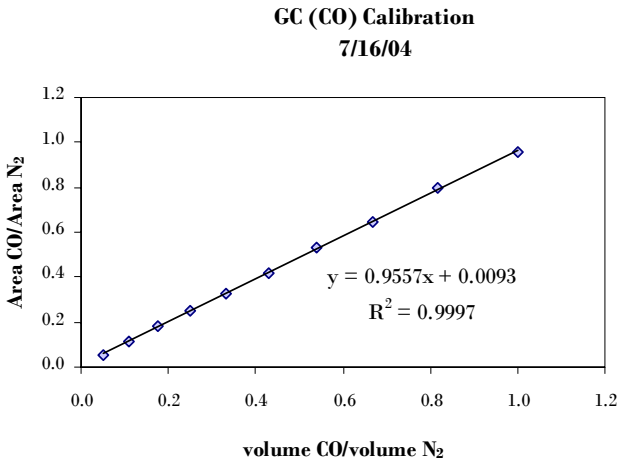

NOTES: SRI 8610C Gas Chromatograph — Carboxen 1000 Column
Oven Temperature: 125 oC — Oven Temperature Hold Time: 6000 min

GC Calibrations

Carbon Dioxide

7/14/2004

volume CO/ volume N_2	area CO/ area N_2
0.0526	0.0626
0.1111	0.1194
0.1765	0.1903
0.2500	0.2590
0.3333	0.3457
0.4286	0.4389
0.5385	0.5429
0.6667	0.6846
0.8182	0.8271
1.0000	1.0135

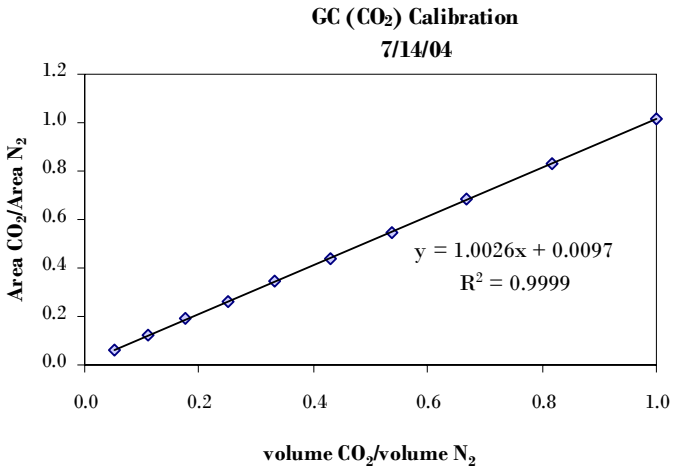

NOTES: SRI 8610C Gas Chromatograph Carboxen 1000 Column
Oven Temperature: 125 oC Oven Temperature Hold Time: 6000 min

10/13/2005

volume CH_4/ volume N_2	area CH_4/ area N_2
0.0526	#DIV/0!
0.1111	0.4128
0.1765	0.6340
0.2500	0.8794
0.3333	1.1204
0.4286	1.4366
0.5385	1.8107
0.6667	2.2151
0.8182	2.7052
1.0000	3.2271

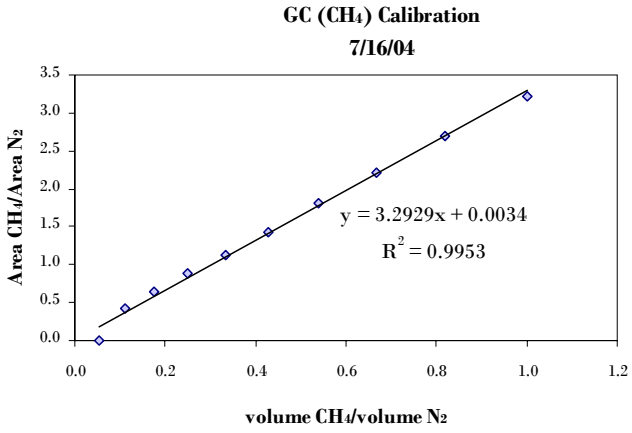

NOTES: SRI 8610C Gas Chromatograph Carboxen 1000 Column
Oven Temperature: 125 oC Oven Temperature Hold Time: 6000 min

Appendix G: Gas Phase Thermochemistry Data

Reference: NIST Chemistry WebBook

Atomic Oxygen

Temperature (K)	C_p (cal/mol·K)	$S°$ (cal/mol·K)	$-(G° - H°_{298.15})/T$ (cal/mol·K)	$H° - H°_{298.15}$ (kcal/mol)
298	5.23	38.49	38.49	-0.00
300	5.23	38.52	38.49	0.01
400	5.13	40.01	38.70	0.53
500	5.09	41.15	39.08	1.04
600	5.06	42.08	39.50	1.55
700	5.04	42.86	39.93	2.05
800	5.02	43.53	40.34	2.55
900	5.01	44.12	40.73	3.05
1000	5.00	44.65	41.09	3.55
1100	4.99	45.12	41.44	4.05
1200	4.99	45.56	41.76	4.55
1300	4.98	45.96	42.07	5.05
1400	4.98	46.32	42.36	5.55
1500	4.98	46.67	42.64	6.05
1600	4.97	46.99	42.90	6.54
1700	4.97	47.29	43.15	7.04
1800	4.97	47.57	43.39	7.54
1900	4.97	47.84	43.61	8.04
2000	4.97	48.10	43.83	8.53
2100	4.97	48.34	44.04	9.03
2200	4.98	48.57	44.24	9.53
2300	4.98	48.79	44.43	10.03
2400	4.98	49.01	44.62	10.52
2500	4.98	49.21	44.80	11.02
2600	4.99	49.40	44.97	11.52
2700	4.99	49.59	45.14	12.02
2800	5.00	49.77	45.30	12.52
2900	5.00	49.95	45.46	13.02
3000	5.01	50.12	45.61	13.52
3100	5.02	50.28	45.76	14.02
3200	5.02	50.44	45.91	14.52
3300	5.03	50.60	46.05	15.03
3400	5.04	50.75	46.18	15.53
3500	5.05	50.89	46.31	16.03
3600	5.06	51.04	46.44	16.54
3700	5.06	51.18	46.57	17.04
3800	5.07	51.31	46.69	17.55
3900	5.08	51.44	46.81	18.06
4000	5.09	51.57	46.93	18.57
4100	5.10	51.70	47.04	19.08
4200	5.11	51.82	47.16	19.59
4300	5.12	51.94	47.27	20.10
4400	5.13	52.06	47.37	20.61
4500	5.15	52.17	47.48	21.13
4600	5.16	52.29	47.58	21.64
4700	5.17	52.40	47.68	22.16
4800	5.18	52.51	47.78	22.68
4900	5.19	52.61	47.88	23.19
5000	5.20	52.72	47.98	23.71
5100	5.22	52.82	48.07	24.24
5200	5.23	52.92	48.16	24.76
5300	5.24	53.02	48.25	25.28
5400	5.25	53.12	48.34	25.81
5500	5.27	53.22	48.43	26.33
5600	5.28	53.31	48.52	26.86
5700	5.29	53.41	48.60	27.39
5800	5.31	53.50	48.69	27.92
5900	5.32	53.59	48.77	28.45
6000	5.33	53.68	48.85	28.98

Atomic Hydogen

Temperature (K)	C_p (cal/mol·K)	$S°$ (cal/mol·K)	$-(G° - H°_{298.15})/T$ (cal/mol·K)	$H° - H°_{298.15}$ (kcal/mol)
298	4.97	27.42	27.42	0
300	4.97	27.45	27.42	0.01
400	4.97	28.88	27.61	0.51
500	4.97	29.99	27.98	1
600	4.97	30.89	28.39	1.5
700	4.97	31.66	28.81	2
800	4.97	32.32	29.2	2.49
900	4.97	32.91	29.58	2.99
1000	4.97	33.43	29.94	3.49
1100	4.97	33.9	30.28	3.98
1200	4.97	34.34	30.6	4.48
1300	4.97	34.73	30.9	4.98
1400	4.97	35.1	31.19	5.47
1500	4.97	35.44	31.46	5.97
1600	4.97	35.76	31.72	6.47
1700	4.97	36.07	31.97	6.96
1800	4.97	36.35	32.21	7.46
1900	4.97	36.62	32.43	7.96
2000	4.97	36.87	32.65	8.45
2100	4.97	37.12	32.85	8.95
2200	4.97	37.35	33.05	9.45
2300	4.97	37.57	33.24	9.95
2400	4.97	37.78	33.43	10.44
2500	4.97	37.98	33.61	10.94
2600	4.97	38.18	33.78	11.44
2700	4.97	38.36	33.95	11.93
2800	4.97	38.55	34.11	12.43
2900	4.97	38.72	34.26	12.93
3000	4.97	38.89	34.41	13.42
3100	4.97	39.05	34.56	13.92
3200	4.97	39.21	34.7	14.42
3300	4.97	39.36	34.84	14.91
3400	4.97	39.51	34.98	15.41
3500	4.97	39.65	35.11	15.91
3600	4.97	39.79	35.24	16.4
3700	4.97	39.93	35.36	16.9
3800	4.97	40.06	35.48	17.4
3900	4.97	40.19	35.6	17.89
4000	4.97	40.32	35.72	18.39
4100	4.97	40.44	35.83	18.89
4200	4.97	40.56	35.94	19.38
4300	4.97	40.68	36.05	19.88
4400	4.97	40.79	36.16	20.38
4500	4.97	40.9	36.26	20.87
4600	4.97	41.01	36.37	21.37
4700	4.97	41.12	36.47	21.87
4800	4.97	41.22	36.56	22.37
4900	4.97	41.33	36.66	22.86
5000	4.97	41.43	36.75	23.36
5100	4.97	41.52	36.85	23.86
5200	4.97	41.62	36.94	24.35
5300	4.97	41.72	37.03	24.85
5400	4.97	41.81	37.11	25.35
5500	4.97	41.9	37.2	25.84
5600	4.97	41.99	37.29	26.34
5700	4.97	42.08	37.37	26.84
5800	4.97	42.16	37.45	27.33
5900	4.97	42.25	37.53	27.83
6000	4.97	42.33	37.61	28.33

Carbon Monoxide

Temperature (K)	C_p (cal/mol·K)	$S°$ (cal/mol·K)	$-(G° - H°_{298.15})/T$ (cal/mol·K)	$H° - H°_{298.15}$ (kcal/mol)
298	6.97	47.24	47.24	0
300	6.97	47.29	47.24	0.01
400	7	49.29	47.51	0.71
500	7.13	50.87	48.03	1.42
600	7.28	52.18	48.62	2.14
700	7.45	53.31	49.21	2.87
800	7.62	54.32	49.79	3.63
900	7.78	55.23	50.34	4.4
1000	7.93	56.05	50.87	5.18
1100	8.06	56.82	51.38	5.98
1200	8.17	57.52	51.86	6.79
1300	8.26	58.18	52.32	7.62
1400	8.35	58.8	52.76	8.45
1500	8.42	59.38	53.19	9.29
1600	8.48	59.92	53.59	10.13
1700	8.53	60.44	53.98	10.98
1800	8.58	60.93	54.35	11.84
1900	8.62	61.39	54.71	12.7
2000	8.66	61.83	55.05	13.56
2100	8.69	62.26	55.39	14.43
2200	8.72	62.66	55.71	15.3
2300	8.75	63.05	56.02	16.17
2400	8.77	63.42	56.32	17.05
2500	8.8	63.78	56.61	17.93
2600	8.82	64.13	56.89	18.81
2700	8.84	64.46	57.17	19.69
2800	8.86	64.78	57.43	20.57
2900	8.87	65.09	57.69	21.46
3000	8.89	65.39	57.94	22.35
3100	8.91	65.69	58.19	23.24

Temperature (K)	C_p (cal/mol·K)	$S°$ (cal/mol·K)	$-(G° - H°_{298.15})/T$ (cal/mol·K)	$H° - H°_{298.15}$ (kcal/mol)
3200	8.92	65.97	58.43	24.13
3300	8.94	66.24	58.66	25.02
3400	8.95	66.51	58.89	25.92
3500	8.96	66.77	59.11	26.81
3600	8.97	67.02	59.33	27.71
3700	8.98	67.27	59.54	28.61
3800	8.99	67.51	59.74	29.51
3900	9.01	67.74	59.95	30.41
4000	9.01	67.97	60.14	31.31
4100	9.02	68.19	60.34	32.21
4200	9.03	68.41	60.53	33.11
4300	9.04	68.62	60.71	34.02
4400	9.05	68.83	60.89	34.92
4500	9.06	69.03	61.07	35.83
4600	9.07	69.23	61.25	36.73
4700	9.08	69.43	61.42	37.64
4800	9.08	69.62	61.59	38.55
4900	9.09	69.81	61.75	39.46
5000	9.1	69.99	61.92	40.37
5100	9.11	70.17	62.08	41.28
5200	9.11	70.35	62.24	42.19
5300	9.12	70.52	62.39	43.1
5400	9.13	70.69	62.54	44.01
5500	9.13	70.86	62.69	44.92
5600	9.14	71.02	62.84	45.84
5700	9.15	71.19	62.98	46.75
5800	9.16	71.35	63.13	47.67
5900	9.16	71.5	63.27	48.58
6000	9.17	71.66	63.41	49.5

Carbon Dioxide

Temperature (K)	C_p (cal/mol·K)	$S°$ (cal/mol·K)	$-(G° - H°_{298.15})/T$ (cal/mol·K)	$H° - H°_{298.15}$ (kcal/mol)
298	8.87	51.09	51.1	0
300	8.9	51.15	51.1	0.02
400	9.88	53.85	51.46	0.96
500	10.66	56.14	52.17	1.99
600	11.31	58.15	53	3.08
700	11.85	59.93	53.87	4.24
800	12.29	61.54	54.73	5.45
900	12.67	63.01	55.57	6.7
1000	12.98	64.36	56.38	7.98
1100	13.24	65.61	57.17	9.29
1200	13.47	66.78	57.92	10.63
1300	13.66	67.86	58.64	11.99
1400	13.82	68.88	59.34	13.36
1500	13.96	69.84	60.01	14.75
1600	14.08	70.74	60.65	16.15
1700	14.18	71.6	61.27	17.56
1800	14.27	72.41	61.86	18.99
1900	14.35	73.19	62.44	20.42
2000	14.42	73.92	63	21.86
2100	14.49	74.63	63.53	23.3
2200	14.54	75.3	64.05	24.75
2300	14.6	75.95	64.56	26.21
2400	14.65	76.57	65.04	27.67
2500	14.69	77.17	65.52	29.14
2600	14.73	77.75	65.98	30.61
2700	14.77	78.31	66.42	32.08
2800	14.81	78.84	66.86	33.56
2900	14.84	79.36	67.28	35.05
3000	14.87	79.87	67.69	36.53
3100	14.9	80.36	68.09	38.02
3200	14.93	80.83	68.48	39.51
3300	14.96	81.29	68.86	41.01
3400	14.98	81.74	69.24	42.5
3500	15.01	82.17	69.6	44
3600	15.03	82.59	69.95	45.51
3700	15.05	83.01	70.3	47.01
3800	15.08	83.41	70.64	48.52
3900	15.1	83.8	70.97	50.02
4000	15.12	84.18	71.3	51.54
4100	15.14	84.56	71.62	53.05
4200	15.16	84.92	71.93	54.56
4300	15.18	85.28	72.24	56.08
4400	15.2	85.63	72.54	57.6
4500	15.21	85.97	72.83	59.12
4600	15.23	86.3	73.12	60.64
4700	15.25	86.63	73.4	62.17
4800	15.27	86.95	73.68	63.69
4900	15.29	87.27	73.96	65.22
5000	15.31	87.58	74.23	66.75
5100	15.33	87.88	74.49	68.28
5200	15.35	88.18	74.75	69.82
5300	15.37	88.47	75.01	71.35
5400	15.39	88.76	75.26	72.89
5500	15.41	89.04	75.51	74.43
5600	15.43	89.32	75.75	75.97
5700	15.46	89.59	75.99	77.52
5800	15.48	89.86	76.23	79.06
5900	15.5	90.13	76.46	80.61
6000	15.53	90.39	76.69	82.17

Hydrogen

Temperature (K)	C_p (cal/mol·K)	$S°$ (cal/mol·K)	$-(G° - H°_{298.15})/T$ (cal/mol·K)	$H° - H°_{298.15}$ (kcal/mol)
298	28.84	130.7	130.7	0
300	28.85	130.9	130.7	0.05
400	29.18	139.2	131.8	2.96
500	29.26	145.7	134	5.88
600	29.32	151.1	136.4	8.81
700	29.44	155.6	138.8	11.75
800	29.62	159.5	141.2	14.7
900	29.88	163.1	143.4	17.68
1000	30.2	166.2	145.5	20.68
1100	30.58	169.1	147.5	23.72
1200	30.99	171.8	149.5	26.8
1300	31.42	174.3	151.3	29.92
1400	31.86	176.6	153	33.08
1500	32.3	178.8	154.7	36.29
1600	32.73	180.9	156.2	39.54
1700	33.14	182.9	157.7	42.83
1800	33.54	184.8	159.2	46.17
1900	33.92	186.7	160.6	49.54
2000	34.28	188.4	161.9	52.95
2100	34.62	190.1	163.2	56.4
2200	34.95	191.7	164.5	59.88
2300	35.26	193.3	165.7	63.39
2400	35.56	194.8	166.9	66.93
2500	35.84	196.2	168	70.5
2600	36.11	197.7	169.2	74.1
2700	36.37	199	170.2	77.72
2800	36.62	200.3	171.3	81.37
2900	36.86	201.6	172.3	85.04
3000	37.09	202.9	173.3	88.74
3100	37.31	204.1	174.3	92.46
3200	37.53	205.3	175.2	96.2
3300	37.74	206.5	176.2	99.97
3400	37.94	207.6	177.1	103.8
3500	38.15	208.7	178	107.6
3600	38.34	209.8	178.8	111.4
3700	38.54	210.8	179.7	115.2
3800	38.74	211.9	180.5	119.1
3900	38.93	212.9	181.3	123
4000	39.12	213.8	182.1	126.9
4100	39.3	214.8	182.9	130.8
4200	39.49	215.8	183.7	134.7
4300	39.67	216.7	184.4	138.7
4400	39.85	217.6	185.2	142.7
4500	40.02	218.5	185.9	146.7
4600	40.19	219.4	186.6	150.7
4700	40.36	220.3	187.3	154.7
4800	40.52	221.1	188	158.7
4900	40.68	221.9	188.7	162.8
5000	40.83	222.8	189.4	166.9
5100	40.97	223.6	190.1	171
5200	41.12	224.4	190.7	175.1
5300	41.25	225.2	191.3	179.2
5400	41.38	225.9	192	183.3
5500	41.5	226.7	192.6	187.5
5600	41.61	227.4	193.2	191.6
5700	41.71	228.2	193.8	195.8
5800	41.81	228.9	194.4	200
5900	41.89	229.6	195	204.1
6000	41.97	230.3	195.6	208.3

Water

Temperature (K)	C_p (cal/mol·K)	$S°$ (cal/mol·K)	$-(G° - H°_{298.15})/T$ (cal/mol·K)	$H° - H°_{298.15}$ (kcal/mol)
500	8.42	49.36	46.05	1.66
600	8.68	50.92	46.74	2.51
700	8.96	52.28	47.43	3.39
800	9.26	53.5	48.12	4.3
900	9.56	54.6	48.78	5.24
1000	9.86	55.63	49.41	6.21
1100	10.16	56.58	50.02	7.22
1200	10.46	57.48	50.6	8.25
1300	10.74	58.33	51.17	9.31
1400	11.01	59.13	51.71	10.39
1500	11.26	59.9	52.23	11.51
1600	11.49	60.63	52.73	12.65
1700	11.69	61.34	53.22	13.8
1800	11.89	62.01	53.69	14.98
1900	12.07	62.66	54.14	16.18
2000	12.24	63.28	54.58	17.4
2100	12.39	63.88	55.01	18.63
2200	12.53	64.46	55.43	19.87
2300	12.65	65.02	55.83	21.13
2400	12.77	65.56	56.23	22.41
2500	12.88	66.09	56.61	23.69
2600	12.98	66.59	56.99	24.98
2700	13.08	67.09	57.35	26.28
2800	13.16	67.56	57.71	27.6
2900	13.25	68.03	58.05	28.92
3000	13.32	68.48	58.39	30.25
3100	13.39	68.91	58.73	31.58
3200	13.46	69.34	59.05	32.92
3300	13.52	69.76	59.37	34.27
3400	13.58	70.16	59.68	35.63
3500	13.64	70.55	59.99	36.99
3600	13.69	70.94	60.29	38.36
3700	13.74	71.32	60.58	39.73
3800	13.79	71.68	60.87	41.1
3900	13.83	72.04	61.15	42.49
4000	13.87	72.39	61.42	43.87
4100	13.91	72.73	61.7	45.26
4200	13.95	73.07	61.96	46.65
4300	13.98	73.4	62.22	48.05
4400	14.02	73.72	62.48	49.45
4500	14.05	74.04	62.74	50.85
4600	14.08	74.35	62.98	52.26
4700	14.11	74.65	63.23	53.67
4800	14.14	74.95	63.47	55.08
4900	14.17	75.24	63.71	56.5
5000	14.2	75.52	63.94	57.91
5100	14.22	75.81	64.17	59.34
5200	14.25	76.08	64.4	60.76
5300	14.28	76.35	64.62	62.19
5400	14.31	76.62	64.84	63.62
5500	14.33	76.88	65.06	65.05
5600	14.36	77.14	65.27	66.48
5700	14.39	77.4	65.48	67.92
5800	14.42	77.65	65.69	69.36
5900	14.45	77.89	65.89	70.8
6000	14.48	78.14	66.1	72.25

NOTE: At T = 298.15K, $\Delta_f H°_{gas} = -57.799$ kcal/mol, $S°_{gas,1\ bar} = 45.134$ cal/mol·K.

Hydroxyl

Temperature (K)	C_p (cal/mol·K)	$S°$ (cal/mol·K)	$-(G° - H°_{298.15})/T$ (cal/mol·K)	$H° - H°_{298.15}$ (kcal/mol)
298	7.17	43.9	43.91	0
300	7.16	43.95	43.91	0.01
400	7.09	46	44.19	0.73
500	7.05	47.58	44.71	1.43
600	7.06	48.86	45.3	2.14
700	7.09	49.95	45.89	2.84
800	7.15	50.9	46.46	3.56
900	7.23	51.75	47	4.28
1000	7.33	52.52	47.51	5
1100	7.44	53.22	48	5.74
1200	7.55	53.87	48.46	6.49
1300	7.66	54.48	48.9	7.25
1400	7.77	55.05	49.32	8.02
1500	7.88	55.59	49.72	8.8
1600	7.97	56.1	50.11	9.6
1700	8.06	56.59	50.47	10.4
1800	8.14	57.05	50.83	11.21
1900	8.22	57.5	51.17	12.03
2000	8.29	57.92	51.49	12.85
2100	8.35	58.32	51.81	13.68
2200	8.41	58.71	52.11	14.52
2300	8.47	59.09	52.41	15.37
2400	8.52	59.45	52.69	16.21
2500	8.57	59.8	52.97	17.07
2600	8.62	60.14	53.24	17.93
2700	8.66	60.46	53.5	18.79
2800	8.7	60.78	53.76	19.66
2900	8.74	61.08	54	20.53
3000	8.78	61.38	54.25	21.41
3100	8.81	61.67	54.48	22.29

Temperature (K)	C_p (cal/mol·K)	$S°$ (cal/mol·K)	$-(G° - H°_{298.15})/T$ (cal/mol·K)	$H° - H°_{298.15}$ (kcal/mol)
3200	8.85	61.95	54.71	23.17
3300	8.88	62.22	54.93	24.06
3400	8.91	62.49	55.15	24.95
3500	8.94	62.75	55.36	25.84
3600	8.96	63	55.57	26.73
3700	8.99	63.25	55.78	27.63
3800	9.01	63.49	55.98	28.53
3900	9.04	63.72	56.17	29.43
4000	9.06	63.95	56.36	30.34
4100	9.08	64.17	56.55	31.25
4200	9.1	64.39	56.74	32.16
4300	9.12	64.61	56.92	33.07
4400	9.14	64.82	57.09	33.98
4500	9.16	65.02	57.27	34.89
4600	9.18	65.22	57.44	35.81
4700	9.19	65.42	57.61	36.73
4800	9.21	65.61	57.77	37.65
4900	9.23	65.8	57.93	38.57
5000	9.25	65.99	58.09	39.5
5100	9.26	66.17	58.25	40.42
5200	9.28	66.35	58.4	41.35
5300	9.3	66.53	58.55	42.28
5400	9.32	66.71	58.7	43.21
5500	9.33	66.88	58.85	44.14
5600	9.35	67.04	59	45.07
5700	9.37	67.21	59.14	46.01
5800	9.39	67.37	59.28	46.95
5900	9.41	67.53	59.42	47.89
6000	9.43	67.69	59.55	48.83

Appendix H: Experimental Raw Data

Water Gas Shift Reaction Conversion Data

Catalyst: Cu

Pressure: 1 atm

Date	Temperature		X(CO)	CO(in)	H_2O(in)	CO_2(in)	H_2(in)	N_2(in)	CO(out)	H_2O(out)	CO_2(out)	H_2(out)	N_2(out)
	C	K		mL/min	mL/min	mL/min	mL/min	mL/min	mL/min	mL/min	mL/min	mL/min	mL/min
FEED CONDITION 1: 100 mL/min 10% CO/10% H2O/0% CO2/0% H2/80% N2 (experiment 1)													
11/19/2004	108	381	0.299579	10.4	10	0	0	80	7.2843786	---------	1.8208075	2.1149155	80
11/22/2004	108	381	0.236241	10.4	10	0	0	80	7.9430936	---------	0.5769369	1.3950246	80
11/23/2004	155	428	0.647008	10.4	10	0	0	80	3.6711138	---------	4.5394041	5.8301494	80
12/7/2004	105	378	0.194008	10.4	10	0	0	80	8.3823167	---------	0.2441722	0.5912705	80
12/7/2004	130	403	0.444438	10.4	10	0	0	80	5.777845	---------	1.6433809	3.3899503	80
12/8/2004	130	403	0.448007	10.4	10	0	0	80	5.7407296	---------	2.032219	3.50156	80
12/8/2004	160	433	0.671413	10.4	10	0	0	80	3.4173031	---------	6.2558457	5.8254102	80
12/8/2004	180	453	0.803823	10.4	10	0	0	80	2.0402396	---------	7.5001686	7.3034966	80
12/10/2004	195	468	0.873254	10.4	10	0	0	80	1.3181611	---------	8.1964238	7.940816	80
12/10/2004	227	500	0.918077	10.4	10	0	0	80	0.8519975	---------	8.798434	8.4566926	80
FEED CONDITION 1: 100 mL/min 10% CO/10% H2O/0% CO2/0% H2/80% N2 (experiment 2)													
1/4/2005	101	374	0.173269	10.4	10	0	0	80	8.5980016	---------	-0.7739876	0.8336652	80
1/4/2005	118	391	0.309108	10.4	10	0	0	80	7.1852747	---------	1.0600818	2.240767	80
1/4/2005	143	416	0.540636	10.4	10	0	0	80	4.7773817	---------	4.1753344	4.8665388	80
1/5/2005	166	439	0.720145	10.4	10	0	0	80	2.9104938	---------	7.1971132	6.6226589	80
1/5/2005	185	458	0.810245	10.4	10	0	0	80	1.9734496	---------	6.0191135	7.7447945	80
1/5/2005	202	475	0.857819	10.4	10	0	0	80	1.4786808	---------	8.5944934	8.3526612	80
1/6/2005	224	497	0.920133	10.4	10	0	0	80	0.8306196	---------	8.685561	8.4637111	80
1/6/2005	240	513	0.930488	10.4	10	0	0	80	0.7229197	---------	9.2997281	8.6861799	80
1/6/2005	259	532	0.93838	10.4	10	0	0	80	0.6408522	---------	9.6213737	8.9488241	80
1/7/2005	282	555	0.914194	10.4	10	0	0	80	0.8923826	---------	8.9160959	8.6055215	80
1/7/2005	300	573	0.925703	10.4	10	0	0	80	0.7726932	---------	9.2418129	8.7678293	80
1/7/2005	322	595	0.905872	10.4	10	0	0	80	0.9789357	---------	8.8865117	8.5194586	80
1/19/2005	FEED	######	-0.005992	10.4	10	0	0	80	10.462319	---------	-0.7739876	-1.3590076	80
1/19/2005	FEED	######	0.000126	10.4	10	0	0	80	10.398693	---------	-0.7739876	-1.3590076	80
NEW FEED CONDITIONS: 2xH2O [FEED CONDITION 1: 100 mL/min 10% CO/10% H2O/0% CO2/0% H2/80% N2] (experiment 3)													
1/20/2005	FEED	######	-0.006346	10.1	20	0	0	80	10.164094	---------	-0.7739876	-1.3590076	80
1/20/2005	193	466	0.938939	10.1	20	0	0	80	0.6167194	---------	9.122443	8.7101265	80
1/20/2005	214	487	0.974799	10.1	20	0	0	80	0.2545343	---------	6.3817423	9.0591532	80
1/21/2005	214	487	0.964723	10.1	20	0	0	80	0.3562945	---------	9.1223701	8.9373513	80
1/21/2005	232	505	0.980409	10.1	20	0	0	80	0.197871	---------	9.4884146	9.1505904	80
1/21/2005	254	527	0.991195	10.1	20	0	0	80	0.0889285	---------	7.3494153	9.1860541	80
1/24/2005	254	527	0.985201	10.1	20	0	0	80	0.1494657	---------	9.3421159	9.1697413	80
1/24/2005	274	547	0.982164	10.1	20	0	0	80	0.180147	---------	9.630028	9.2778433	80
1/24/2005	294	567	0.993157	10.1	20	0	0	80	0.0691185	---------	9.0450927	9.3487101	80
1/25/2005	176	449	0.82553	10.1	20	0	0	80	1.7621472	---------	7.9086645	7.6623687	80
1/25/2005	158	431	0.699073	10.1	20	0	0	80	3.039365	---------	6.8156392	6.3396412	80
1/26/2005	137	410	0.487822	10.1	20	0	0	80	5.1729979	---------	4.3902961	4.074438	80
1/26/2005	118	391	0.304756	10.1	20	0	0	80	7.021967	---------	2.4832777	2.2934009	80
NEW FEED CONDITIONS: 1.5xH2O [FEED CONDITION 1: 100 mL/min 10% CO/10% H2O/0% CO2/0% H2/80% N2] (experiment 4)													
1/27/2005	117	390	0.293745	10.1	15	0	0	80	7.133171	---------	1.1689693	2.0729257	80
1/27/2005	136	409	0.486325	10.1	15	0	0	80	5.1881201	---------	2.2597884	4.0712826	80
1/27/2005	157	430	0.708252	10.1	15	0	0	80	2.9466498	---------	6.8890357	6.4001073	80
1/28/2005	175	448	0.84824	10.1	15	0	0	80	1.532775	---------	7.8142899	7.8307758	80
1/28/2005	196	469	0.909253	10.1	15	0	0	80	0.9165427	---------	7.2884441	8.5502354	80
1/28/2005	213	486	0.936464	10.1	15	0	0	80	0.6417129	---------	6.6893053	8.7664446	80
1/31/2005	233	506	0.927928	10.1	15	0	0	80	0.727932	---------	9.2716714	8.9420101	80
1/31/2005	251	524	0.983096	10.1	15	0	0	80	0.1707351	---------	7.0299545	6.7264331	80
1/31/2005	271	544	0.959857	10.1	15	0	0	80	0.4054406	---------	9.7052558	9.2920623	80
2/1/2005	274	547	0.969011	10.1	15	0	0	80	0.31299	---------	7.1352081	9.162583	80
2/1/2005	291	564	0.971249	10.1	15	0	0	80	0.2903832	---------	9.8805883	9.3166041	80
2/1/2005	312	585	0.970043	10.1	15	0	0	80	0.3025654	---------	7.2849029	9.3904545	80
NEW FEED CONDITIONS: 0.75xH2O [FEED CONDITION 1: 100 mL/min 10% CO/10% H2O/0% CO2/0% H2/80% N2] (experiment 5)													
2/2/2005	105	378	-0.003104	10.1	15	0	0	80	10.13135	---------	-0.7739876	-0.9606105	80
2/2/2005	124	397	-0.027885	10.1	15	0	0	80	10.381639	---------	-0.7739876	-1.0762247	80
2/2/2005	203	476	-0.026857	10.1	15	0	0	80	10.371251	---------	-0.7739876	-1.0259224	80
FEED CONDITION 1: 100 mL/min 10% CO/10% H2O/0% CO2/0% H2/80% N2 (experiment 6)													
2/3/2005	192	465	0.787715	10.4	10	0	0	80	2.2077637	---------	7.6941575	7.4335647	80
2/3/2005	240	513	0.875248	10.4	10	0	0	80	1.2974164	---------	6.721905	8.3141132	80
2/4/2005	211	484	0.831007	10.4	10	0	0	80	1.7575323	---------	4.3921438	7.7600522	80
2/4/2005	250	523	0.878747	10.4	10	0	0	80	1.2610353	---------	8.5755346	8.3723727	80
2/7/2005	290	563	0.898563	10.4	10	0	0	80	1.0549419	---------	8.8878322	8.4999561	80
2/7/2005	315	588	0.890799	10.4	10	0	0	80	1.1356886	---------	7.2990266	8.5726398	80
2/7/2005	329	602	0.899189	10.4	10	0	0	80	1.0484391	---------	5.4575687	7.2669381	80

Water Gas Shift Reaction Conversion Data

Catalyst: Cu

Pressure: 1 atm

Date	Temperature C	Temperatu K	X(CO)	CO(in) mL/min	H_2O(in) mL/min	CO_2(in) mL/min	H_2(in) mL/min	N_2(in) mL/min	CO(out) mL/min	H_2O(out) mL/min	CO_2(out) mL/min	H_2(out) mL/min	N_2(out) mL/min
FEED CONDITION 2: 100 mL/min 0% CO/0% H2O/10% CO2/10% H2/80% N2 (experiment 1)													
2/8/2005	FEED ONLY	######	0.003393	0	0	10.2	9.7	80	-0.778487	---------	10.107814	9.6670837	80
2/8/2005	199	472	0.051348	0	0	10.2	9.7	80	-0.0395238	---------	10.090733	9.2019285	80
2/8/2005	219	492	0.066327	0	0	10.2	9.7	80	0.0390692	---------	9.7920739	9.0566302	80
2/9/2005	240	513	0.087057	0	0	10.2	9.7	80	0.2382984	---------	9.4256037	8.8555426	80
2/9/2005	259	532	0.110056	0	0	10.2	9.7	80	0.482808	---------	9.4218332	8.6324554	80
2/9/2005	279	552	0.128765	0	0	10.2	9.7	80	0.3729303	---------	7.3785046	8.4509835	80
2/9/2005	299	572	0.1486	0	0	10.2	9.7	80	0.8659626	---------	9.5026174	8.2585831	80
2/10/2005	300	573	#DIV/0!	0	0	10.2	9.7	80	#DIV/0!	---------	#DIV/0!	#DIV/0!	80
2/10/2005	320	593	0.160963	0	0	10.2	9.7	80	1.0302263	---------	9.3454746	8.138655	80
2/10/2005	342	615	0.189905	0	0	10.2	9.7	80	1.3093355	---------	8.7218172	7.8579254	80
2/10/2005	393	666	0.240771	0	0	10.2	9.7	80	1.7496006	---------	8.5444277	7.3645188	80
2/11/2005	445	718	0.293382	0	0	10.2	9.7	80	2.234563	---------	7.7154069	6.8541922	80
2/11/2005	495	768	0.344729	0	0	10.2	9.7	80	2.755469	---------	5.9903337	6.3561311	80
2/11/2005	546	819	0.389039	0	0	10.2	9.7	80	3.1821595	---------	5.340724	5.9263171	80
2/11/2005	596	869	0.434979	0	0	10.2	9.7	80	3.6472166	---------	6.7032823	5.4807059	80
2/14/2005	647	920	0.456372	0	0	10.2	9.7	80	3.96032	---------	6.2029701	5.2731947	80
2/14/2005	696	969	0.492137	0	0	10.2	9.7	80	4.260131	---------	5.332256	4.9262758	80
2/14/2005	746	1019	0.526617	0	0	10.2	9.7	80	4.6068979	---------	5.7512365	4.591814	80
FEED CONDITION 1: 100 mL/min 10% CO/10% H2O/0% CO2/0% H2/80% N2 (experiment 6)													
2/15/2005	196	469	0.274115	10.4	10	0	0	80	7.5492063	---------	9451.6069	1.8925407	80
2/15/2005	273	546	0.47629	10.4	10	0	0	80	5.446585	---------	3.5078897	4.0684778	80
FEED CONDITION 1: 100 mL/min 10% CO/10% H2O/0% CO2/0% H2/80% N2 (experiment 7)													
2/17/2005	119	392	0.37296	10.4	10	0	0	80	6.521213	---------	2.3330807	3.088395	80
2/17/2005	169	442	0.781891	10.4	10	0	0	80	2.2683382	---------	7.4012559	7.3590072	80
2/17/2005	238	511	0.907914	10.4	10	0	0	80	0.9576937	---------	9.230313	8.8962259	80
2/18/2005	292	565	0.913128	10.4	10	0	0	80	0.9034676	---------	8.5379541	8.790135	80
2/18/2005	263	536	0.914257	10.4	10	0	0	80	0.8917236	---------	7.0442496	8.9250433	80
2/18/2005	343	616	0.879913	10.4	10	0	0	80	1.2489072	---------	8.7091322	8.4504728	80
2/18/2005	372	645	0.858732	10.4	10	0	0	80	1.4691854	---------	5.6989853	8.2014001	80
FEED CONDITION 3: 100 mL/min 15% CO/20% H2O/5% CO2/5% H2/55% N2 (mfc error - to be repeated)													
2/19/2005	105	378	0.454992	23	20	6.96	1.47	48.57	12.535178	---------	5.6748399	5.3855219	48.57
2/19/2005	143	416	0.634829	23	20	6.96	1.47	48.57	8.3989215	---------	10.015709	9.7591393	48.57
2/19/2005	117	390	0.484842	23	20	6.96	1.47	48.57	11.848629	---------	6.6660318	6.2105482	48.57
2/21/2005	Feed	######	0.392681	23	20	6.96	1.47	48.57	13.968329	---------	4.2251123	0.8896862	48.57
2/21/2005	170	443	0.818603	23	20	6.96	1.47	48.57	4.1721313	---------	13.222412	8.6373903	48.57
2/21/2005	219	492	0.95178	23	20	6.96	1.47	48.57	1.1090528	---------	17.273375	12.538659	48.57
2/21/2005	193	466	0.883393	23	20	6.96	1.47	48.57	2.6819608	---------	12.713342	11.015959	48.57
2/21/2005	244	517	0.965918	23	20	6.96	1.47	48.57	0.7838763	---------	17.777731	12.691703	48.57
2/22/2005	297	570	0.957196	23	20	6.96	1.47	48.57	0.9844867	---------	16.53519	12.563497	48.57
2/22/2005	273	546	0.96055	23	20	6.96	1.47	48.57	0.907358	---------	17.80105	12.725509	48.57
2/22/2005	348	621	0.940184	23	20	6.96	1.47	48.57	1.3757594	---------	17.08716	12.324251	48.57
2/22/2005	323	596	0.953134	23	20	6.96	1.47	48.57	1.0779086	---------	17.662559	12.485986	48.57
FEED CONDITION 3: 100 mL/min 15% CO/20% H2O/5% CO2/5% H2/55% N2 (experiment 1)													
3/5/2005	Feed	######	0.000171	15.07	20	4.37	4.22	55	15.067418	---------	4.3691445	4.2222414	55
3/5/2005	124	397	0.098787	15.07	20	4.37	4.22	55	13.581275	---------	7.069282	7.0183356	55
3/5/2005	174	447	0.594329	15.07	20	4.37	4.22	55	6.1134559	---------	14.567688	14.6001	55
3/5/2005	145	418	0.319378	15.07	20	4.37	4.22	55	10.256977	---------	10.302295	10.514559	55
3/5/2005	219	492	0.904293	15.07	20	4.37	4.22	55	1.4423041	---------	19.296957	19.171414	55
3/5/2005	197	470	0.790955	15.07	20	4.37	4.22	55	3.1503124	---------	18.373539	17.510289	55
3/6/2005	245	518	0.917347	15.07	20	4.37	4.22	55	1.2455795	---------	17.737305	18.014988	55
3/6/2005	295	568	0.901334	15.07	20	4.37	4.22	55	1.4868976	---------	19.71535	19.139079	55
3/6/2005	268	541	0.899479	15.07	20	4.37	4.22	55	1.5148516	---------	15.372677	19.261884	55
3/6/2005	321	594	0.893343	15.07	20	4.37	4.22	55	1.6073157	---------	18.968138	19.022285	55
3/6/2005	346	619	0.867719	15.07	20	4.37	4.22	55	1.9934672	---------	19.908062	18.725851	55

Water Gas Shift Reaction Conversion Data

Catalyst: Cu

Pressure: 1 atm

Date	Temperature	Temperatu	X(CO)	CO(in)	H_2O(in)	CO_2(in)	H_2(in)	N_2(in)	CO(out)	H_2O(out)	CO_2(out)	H_2(out)	N_2(out)
	C	K		mL/min	mL/min	mL/min	mL/min	mL/min	mL/min	mL/min	mL/min	mL/min	mL/min
FEED CONDITIONS (3): CO REACTION ORDER													
3/10/2005	1.00xCO	######	0.625176	16.06	20	5.56	4.47	55	6.019667	---------	15.249004	14.576152	55
3/10/2005	0.75xCO	######	0.705403	12.045	20	5.56	4.47	59.015	3.548425	---------	14.344719	13.235803	59.015
3/10/2005	1.50xCO	######	0.507159	24.09	20	5.56	4.47	46.97	11.872551	---------	16.282862	15.823646	46.97
3/10/2005	1.75xCO	######	0.473445	28.105	20	5.56	4.47	42.955	14.798837	---------	17.474528	16.416218	42.955
3/10/2005	1.25xCO	######	0.555755	20.075	20	5.56	4.47	50.985	8.9182272	---------	16.949385	15.285441	50.985
		slope =	-0.014494	R^2 =	0.973239								
FEED CONDITIONS (3): CO_2 REACTION ORDER													
3/11/2005	1.00xCO2	######	0.630252	16.06	20	5.56	4.47	55	5.9381548	---------	14.4975	14.588027	55
3/11/2005	0.75xCO2	######	0.643039	16.06	20	4.17	4.47	56.39	5.7327929	---------	13.993874	15.034383	56.39
3/11/2005	1.50xCO2	######	0.63701	16.06	20	8.34	4.47	52.22	5.8296183	---------	17.315273	14.818145	52.22
3/11/2005	1.75xCO2	######	0.644007	16.06	20	9.73	4.47	50.83	5.7172447	---------	18.765537	15.029498	50.83
3/11/2005	1.25xCO2	######	0.673832	16.06	20	6.95	4.47	53.61	5.2382646	---------	16.929369	15.439412	53.61
		slope =	0.000626	R^2 =	0.006777								
FEED CONDITIONS (3): H_2 REACTION ORDER													
3/14/2005	1.00xH2	######	0.665301	16.06	20	5.56	4.47	55	5.3752724	---------	15.358361	15.279758	55
3/14/2005	0.75xH2	######	0.679351	16.06	20	5.56	3.3525	56.1175	5.1496174	---------	16.702302	14.420348	56.1175
3/14/2005	1.50xH2	######	0.64611	16.06	20	5.56	6.705	52.765	5.6834756	---------	16.83892	17.885714	52.765
3/14/2005	1.75xH2	######	0.623433	16.06	20	5.56	7.8225	51.6475	6.0476635	---------	15.489253	18.708352	51.6475
3/14/2005	1.25xH2	######	0.622186	16.06	20	5.56	5.5875	53.8825	6.0676914	---------	15.344007	16.046282	53.8825
		slope =	-0.011725	R^2 =	0.672452								
FEED CONDITIONS (3): H_2O REACTION ORDER													
3/15/2005	1.00xH20	######	0.591956	16.06	20	5.56	4.47	55	6.5531855	---------	13.630668	14.055325	55
3/15/2005	1.50xH2O	######	0.6209	16.06	30	5.56	4.47	45	6.0883539	---------	18.043463	17.381225	45
3/15/2005	1.75xH2O	######	0.839723	16.06	35	5.56	4.47	40	2.5740438	---------	14.631768	14.073609	40
3/15/2005	1.25xH2O	######	0.723768	16.06	25	5.56	4.47	50	4.436289	---------	17.661443	16.455884	50
3/15/2005	2.00xH2O	######	0.657542	16.06	40	5.56	4.47	35	5.4998817	---------	15.049545	15.593944	35
3/15/2005	0.75xH2O	######	0.515909	16.06	15	5.56	4.47	60	7.7745093	---------	21.099278	20.034693	60
		slope =	0.004943	R^2 =	0.156809								

Water Gas Shift Reaction Conversion Data

Catalyst: Ni

Pressure: 1 atm

Date	Temperature		X(CO)	CO(in)	H_2O(in)	CO_2(in)	H_2(in)	N_2(in)	CH_4(in)	CO(out)	H_2O(out)	CO_2(out)	H_2(out)	N_2(out)	CH_4(out)
	C	K		mL/min	mL/min	mL/min	mL/min	mL/min	mL/min	mL/min	mL/min	mL/min	mL/min	mL/min	mL/min
FEED 1: 100mL/min 10% CO/10% H2O/80% N2															
4/3/2005	FEED	#####	-7.9E-07	10.32	10	0	0	80	0	10.320008	---------	-0.7739876	-1.3590076	80	-0.082602
4/4/2005	118	391	-0.02549	10.32	10	0	0	80	0	10.583081	---------	-0.7739876	-1.3590076	80	-0.082602
4/4/2005	165	438	-0.05793	10.32	10	0	0	80	0	10.917788	---------	-0.7739876	-1.3590076	80	-0.082602
4/4/2005	189	462	-0.05371	10.32	10	0	0	80	0	10.874274	---------	-0.7739876	-1.3590076	80	-0.082602
4/4/2005	235	508	-0.06281	10.32	10	0	0	80	0	10.968247	---------	-0.7739876	-1.3590076	80	-0.082602
4/4/2005	287	560	-0.03009	10.32	10	0	0	80	0	10.630505	---------	-0.7739876	-1.1706355	80	-0.082602
4/4/2005	338	611	-0.00155	10.32	10	0	0	80	0	10.336021	---------	-0.7739876	-0.9855754	80	-0.082602
4/4/2005	387	660	0.77263	10.32	10	0	0	80	0	2.3465049	---------	4.0249238	-1.1113718	80	-0.082602
4/4/2005	363	636	0.63072	10.32	10	0	0	80	0	3.8109463	---------	3.7482498	-1.1412792	80	-0.082602
4/4/2005	412	685	0.92659	10.32	10	0	0	80	0	0.7575434	---------	5.2136956	-1.1261094	80	-0.082602
4/4/2005	459	732	0.81962	10.32	10	0	0	80	0	1.8614734	---------	5.2169415	-1.0595365	80	-0.082602
4/4/2005	433	706	0.89805	10.32	10	0	0	80	0	1.0521521	---------	4.9991104	-1.1317316	80	-0.082602
4/4/2005	480	753	0.74259	10.32	10	0	0	80	0	2.6565095	---------	3.7187514	-1.0321589	80	-0.082602
FEED 2: 100mL/min 10% CO2, 10%H2, 80% N2															
4/5/2005	Feed	#####	0.00119	15.96	20	5.23	4.1	55	0	15.961066	---------	5.2302563	4.0951184	55	-0.0567888
4/5/2005	233	506	0.15081	15.96	20	5.23	4.1	55	0	15.389772	---------	5.5597265	3.4816789	55	0.1294827
4/5/2005	282	555	0.39277	15.96	20	5.23	4.1	55	0	13.965467	---------	6.2193293	2.4896621	55	0.7095163
4/5/2005	331	604	0.94733	15.96	20	5.23	4.1	55	0	6.7055735	---------	10.397336	0.2159582	55	2.4082489
4/5/2005	382	655	1.0467	15.96	20	5.23	4.1	55	0	1.0990381	---------	12.631323	-0.19146	55	2.1485473
4/5/2005	359	632	1.09888	15.96	20	5.23	4.1	55	0	1.8598687	---------	12.564842	-0.4053909	55	2.4471595
4/5/2005	409	682	0.93266	15.96	20	5.23	4.1	55	0	1.396036	---------	12.426047	0.2760755	55	1.7639134
4/5/2005	459	732	0.66353	15.96	20	5.23	4.1	55	0	2.5105857	---------	12.102936	1.3795341	55	0.896748
4/5/2005	434	707	0.80118	15.96	20	5.23	4.1	55	0	1.7774433	---------	12.195531	0.8151823	55	1.3362524
4/5/2005	484	757	0.52725	15.96	20	5.23	4.1	55	0	3.2061881	---------	12.018897	1.9382846	55	0.6248887
FEED 3: 100mL/min 15% CO/ 20% H2O/ 5% H2/ 5% CO2/ 55% N2															
4/6/2005	FEED	#####	-0.00031	0	0	10.75	9.63	80	0	-0.778487	---------	10.748517	9.6330057	80	-0.082602
4/6/2005	239	512	0.10277	0	0	10.75	9.63	80	0	-0.778487	---------	10.080325	8.6403658	80	0.2311078
4/6/2005	289	562	0.53324	0	0	10.75	9.63	80	0	-0.1770073	---------	9.7531891	4.494856	80	1.1030638
4/6/2005	338	611	0.85439	0	0	10.75	9.63	80	0	-0.778487	---------	8.457689	1.4022328	80	1.9759486
4/6/2005	390	663	0.86164	0	0	10.75	9.63	80	0	-0.3659385	---------	8.4751971	1.3324308	80	2.1520671
4/6/2005	365	638	0.90229	0	0	10.75	9.63	80	0	-0.778487	---------	8.3243443	0.9409261	80	2.127114
4/6/2005	414	687	0.79671	0	0	10.75	9.63	80	0	-0.778487	---------	8.2816339	1.9576851	80	1.7302802
4/6/2005	463	736	0.63523	0	0	10.75	9.63	80	0	0.9420277	---------	8.0351037	3.5127195	80	1.1749948
4/6/2005	437	710	0.71809	0	0	10.75	9.63	80	0	0.5178648	---------	8.0953246	2.7147835	80	1.4866581
4/6/2005	487	760	0.55514	0	0	10.75	9.63	80	0	1.722469	---------	8.6751302	4.2840035	80	0.9170246
T=623K															
FEED CONDITIONS (3): CO REACTION ORDER															
4/7/2005	1.00xCO	#####	0.5423	15.96	20	5.23	4.1	55	0	7.3049027	---------	9.6462556	0.4118217	55	2.234156
4/7/2005	0.75xCO	#####	0.53154	11.97	20	5.23	4.1	58.99	0	5.6075059	---------	9.9662795	-0.0886322	58.99	2.3845247
4/7/2005	1.50xCO	#####	0.31033	23.94	20	4.7	4.54	47.02	0	16.510725	---------	9.7939331	0.4414129	47.02	1.6409874
4/7/2005	1.75xCO	#####	0.25143	27.93	20	4.7	4.54	43.03	0	20.907698	---------	8.6490908	0.7250305	43.03	1.9507161
4/7/2005	1.25xCO	#####	0.27726	19.95	20	4.7	4.54	51.01	0	14.418664	---------	8.5691179	0.5589083	51.01	2.5415232
FEED CONDITIONS (3): CO_2 REACTION ORDER															
4/7/2005	1.00xCO2	#####	0.5423	15.96	20	5.23	4.1	55	0	7.3049027	---------	9.6462556	0.4118217	55	2.234156
4/7/2005	0.75xCO2	#####	0.4733	15.96	20	3.9225	4.1	56.3075	0	8.4062018	---------	4.7031609	3643.794	56.3075	1.5776623
4/7/2005	1.5xCO2	#####	0.28497	15.96	20	7.845	4.1	52.385	0	11.411843	---------	8.8403121	0.6210528	52.385	1.974092
4/7/2005	1.75xCO2	#####	0.26265	15.96	20	9.1525	4.1	51.0775	0	11.768103	---------	11.27721	0.6865519	51.0775	1.9106708
4/7/2005	1.25xCO2	#####	0.25396	15.96	20	6.5375	4.1	53.6925	0	11.906806	---------	9.0960538	0.7566283	53.6925	2.0474588
FEED CONDITIONS (3): H_2 REACTION ORDER															
4/8/2005	1.00xH2	#####	0.39562	15.96	20	5.23	4.1	55	0	9.645976	---------	6.3228396	0.9172414	55	1.5487677
4/8/2005	0.75xH2	#####	0.24902	15.96	20	5.23	3.075	56.025	0	11.985587	---------	8.0354558	0.3045364	56.025	1.5677899
4/8/2005	1.5xH2	#####	0.38152	15.96	20	5.23	6.15	52.95	0	9.8709289	---------	8.7537571	1.6067071	52.95	2.8433497
4/8/2005	1.75xH2	#####	0.34201	15.96	20	5.23	7.175	51.925	0	10.501536	---------	8.9842884	2.3306707	51.925	3.1218537
4/8/2005	1.25xH2	#####	0.27637	15.96	20	5.23	5.125	53.975	0	11.549112	---------	8.1265127	1.6151606	53.975	2.2513376
FEED CONDITIONS (3): H_2O REACTION ORDER															
4/8/2005	1.00xH2O	#####	0.39562	15.96	20	5.23	4.1	55	0	9.645976	---------	6.3228396	0.9172414	55	1.5487677
4/8/2005	1.50xH2O	#####	0.221	15.96	30	5.23	4.1	45	0	12.432856	---------	8.2842351	1.1263603	45	2.4253041
4/8/2005	1.75xH2O	#####	0.22584	15.96	35	5.23	4.1	40	0	12.35554	---------	7.8583035	1.1817853	40	1.8299704

Water Gas Shift Reaction Conversion Data

Catalyst: Fe

Pressure: 1 atm

Date	Temperature		X(CO)	CO(in)	H_2O(in)	CO_2(in)	H_2(in)	N_2(in)	CO(out)	H_2O(out)	CO_2(out)	H_2(out)	N_2(out)
	C	K		mL/min	mL/min	mL/min	mL/min	mL/min	mL/min	mL/min	mL/min	mL/min	mL/min
FEED 1: 100mL/min 10% CO/10% H2O/80% N2													
3/16/2005	FEED	#####	-0.000382	10.6	10	0	0	80	10.604052	---------	-0.7739876	-1.3055627	80
3/16/2005	170	443	-0.00092	10.6	10	0	0	80	10.609757	---------	-0.7739876	-0.9896893	80
3/16/2005	217	490	0.1085709	10.6	10	0	0	80	9.4491483	---------	-0.5092673	-0.3092591	80
3/16/2005	192	465	0.0150297	10.6	10	0	0	80	10.440685	---------	-0.7739876	-0.7776099	80
3/16/2005	244	517	0.0904162	10.6	10	0	0	80	9.641588	---------	-0.3824354	-0.487002	80
3/16/2005	293	566	0.2197586	10.6	10	0	0	80	8.2705593	---------	0.0851242	-0.6179949	80
3/17/2005	267	540	0.1409778	10.6	10	0	0	80	9.1056358	---------	-0.2588869	-0.1175248	80
3/17/2005	318	591	0.2164207	10.6	10	0	0	80	8.3059405	---------	-0.1198295	-0.849589	80
3/17/2005	368	641	0.6123802	10.6	10	0	0	80	4.1087699	---------	3.0190248	-0.9518132	80
3/17/2005	343	616	0.2707889	10.6	10	0	0	80	7.7296378	---------	0.63963	-0.920047	80
3/17/2005	393	666	0.7466087	10.6	10	0	0	80	2.6859481	---------	1.9519872	-0.9361044	80
3/17/2005	341	614	0.181086	10.6	10	0	0	80	8.6804881	---------	0.5855583	-0.9487848	80
3/18/2005	343	616	0.1889865	10.6	10	0	0	80	8.5967432	---------	#DIV/0!	#DIV/0!	80
3/18/2005	393	666	0.7062441	10.6	10	0	0	80	3.1138126	---------	2.4941051	-1.0136379	80
3/18/2005	441	714	0.7527728	10.6	10	0	0	80	2.6206082	---------	3.6036995	-1.0741518	80
3/18/2005	489	762	0.6689397	10.6	10	0	0	80	3.5092389	---------	3.2851619	-1.1112554	80
3/18/2005	538	811	0.5971027	10.6	10	0	0	80	4.2707109	---------	2.6018174	-1.0752676	80
3/21/2005	FEED	#####	0.0151286	10.6	10	0	0	80	10.439637	---------	-0.7739876	-1.3590076	80
3/21/2005	340	613	0.2958472	10.6	10	0	0	80	7.4640199	---------	1.0828411	-1.0777598	80
FEED 2: 100mL/min 10% CO2, 10%H2, 80% N2													
3/24/2005	Feed	#####	0.0002079	0	0	9.33	9.48	80	-0.778487	---------	9.3344631	9.4780287	80
3/24/2005	168	441	0.0038957	0	0	9.33	9.48	80	-0.778487	---------	10.037314	9.4430691	80
3/24/2005	244	517	0.0629851	0	0	9.33	9.48	80	99.866982	---------	9.7904487	8.8829008	80
3/24/2005	196	469	0.0061873	0	0	9.33	9.48	80	-0.778487	---------	10.248566	9.4213443	80
3/24/2005	290	563	0.118395	0	0	9.33	9.48	80	0.3064724	---------	8.8164444	8.3576155	80
3/24/2005	340	613	0.1523649	0	0	9.33	9.48	80	1.4802711	---------	7.0907699	8.0355809	80
3/24/2005	391	664	0.1890788	0	0	9.33	9.48	80	2.2051712	---------	7.4328527	7.6875328	80
3/24/2005	449	722	0.216221	0	0	9.33	9.48	80	3.2522254	---------	6.7756558	7.4302247	80
3/24/2005	488	761	0.2235374	0	0	9.33	9.48	80	4.0418983	---------	6.1957704	7.360865	80
3/24/2005	538	811	0.2330882	0	0	9.33	9.48	80	5.0397785	---------	5.4798802	7.2703243	80
FEED 3: 100mL/min 15% CO/ 20% H2O/ 5% H2/ 5% CO2/ 55% N2													
3/22/2005	FEED	#####	-7.77E-05	15.77	20	4.49	4.54	55	15.771225	---------	4.4898431	4.5404812	55
3/22/2005	169	442	-0.010592	15.77	20	4.49	4.54	55	15.937041	---------	4.8445822	4.5548931	55
3/23/2005	FEED	#####	-2.69E-05	15.73	20	4.7	4.54	55	15.730423	---------	4.7008241	4.5404667	55
3/23/2005	171	444	-0.00841	15.73	20	4.7	4.54	55	15.862296	---------	5.3045052	4.5260568	55
3/23/2005	243	516	0.0081501	15.73	20	4.7	4.54	55	15.601799	---------	5.5791868	4.4358892	55
3/23/2005	194	467	-0.00994	15.73	20	4.7	4.54	55	15.88636	---------	5.5401723	11.654011	55
3/23/2005	291	564	0.0172578	15.73	20	4.7	4.54	55	15.458535	---------	5.7865247	4.364683	55
3/23/2005	339	612	0.0711409	15.73	20	4.7	4.54	55	14.610954	---------	6.2053805	4.2811103	55
3/23/2005	388	661	0.5628658	15.73	20	4.7	4.54	55	6.8761206	---------	9.5977459	3.6317513	55
3/23/2005	487	760	0.5834203	15.73	20	4.7	4.54	55	6.5527982	---------	9.5463456	3.1938287	55
3/23/2005	434	707	0.6233193	15.73	20	4.7	4.54	55	5.9251874	---------	10.068789	3.0564921	55
3/23/2005	536	809	0.431258	15.73	20	4.7	4.54	55	8.9463122	---------	8.6780997	3.2846279	55

Water Gas Shift Reaction Conversion Data

Catalyst: Fe

Pressure: 1 atm

Date	Temperature		X(CO)	CO(in)	H_2O(in)	CO_2(in)	H_2(in)	N_2(in)	CO(out)	H_2O(out)	CO_2(out)	H_2(out)	N_2(out)
	C	K		mL/min	mL/min	mL/min	mL/min	mL/min	mL/min	mL/min	mL/min	mL/min	mL/min
T=623K													
FEED CONDITIONS (3): CO REACTION ORDER													
3/25/2005	1.00xCO	#####	0.0629137	15.73	20	4.7	4.54	55	14.740368	---------	6.8598572	4.340639	55
3/25/2005	0.75xCO	#####	0.0638922	11.7975	20	4.7	4.54	58.9325	11.043732	---------	6.5843847	4.3124304	58.9325
3/25/2005	1.50xCO	#####	0.0985429	23.595	20	4.7	4.54	47.135	21.26988	---------	24.264321	5.2005242	47.135
3/25/2005	1.75xCO	#####	0.1064642	27.5275	20	4.7	4.54	43.2025	24.596805	---------	23.428971	4.4312815	43.2025
2/25/2005	1.25xCO	#####	0.0866643	19.6625	20	4.7	4.54	51.0675	17.958462	---------	24.600226	4.3758175	51.0675
FEED CONDITIONS (3): CO_2 REACTION ORDER													
3/25/2005	1.00xCO2	#####	0.0629137	15.73	20	4.7	4.54	55	14.740368	---------	6.8598572	4.340639	55
3/25/2005	0.75xCO2	#####	0.0785169	15.73	20	3.525	4.54	56.175	14.494929	---------	4.9915655	16.166922	56.175
3/25/2005	1.5xCO2	#####	0.0582383	15.73	20	7.05	4.54	52.65	14.813912	---------	8.249002	4.3601604	52.65
3/25/2005	1.75xCO2	#####	0.0583367	15.73	20	8.225	4.54	51.475	14.812364	---------	9.6452717	4.3540207	51.475
3/25/2005	1.25xCO2	#####	0.0671455	15.73	20	5.875	4.54	53.825	14.673802	---------	7.3281867	4.346688	53.825
FEED CONDITIONS (3): H_2 REACTION ORDER													
3/26/2005	1.00xH2	#####	0.1001372	15.73	20	4.7	4.54	55	14.154842	---------	6.0341267	4.2316963	55
3/26/2005	0.75xH2	#####	0.0786406	15.73	20	4.7	3.405	56.135	14.492983	---------	6.5818021	3.0947781	56.135
3/26/2005	1.5xH2	#####	0.0756315	15.73	20	4.7	6.81	52.73	14.540316	---------	6.6364333	6.8558861	52.73
3/26/2005	1.75xH2	#####	0.0807424	15.73	20	4.7	7.945	51.595	14.459922	---------	6.8244697	8.0570305	51.595
3/26/2005	1.25xH2	#####	0.0742487	15.73	20	4.7	5.675	53.865	14.562068	---------	6.6487842	5.5672345	53.865
FEED CONDITIONS (3): H_2O REACTION ORDER													
3/26/2005	1.00xH2O	#####	0.1001372	15.73	20	4.7	4.54	55	14.154842	---------	6.0341267	4.2316963	55
3/26/2005	2.00xH2O	#####	0.0908001	15.73	40	4.7	4.54	35	14.301715	---------	6.5762827	4.3790333	35
3/26/2005	1.50xH2O	#####	0.0822196	15.73	30	4.7	4.54	45	14.436686	---------	6.664802	4.2973164	45
3/26/2005	1.75xH2O	#####	0.0871788	15.73	35	4.7	4.54	40	14.358678	---------	6.7527656	4.3322972	40
3/26/2005	1.25xH2O	#####	0.0814813	15.73	25	4.7	4.54	50	14.448299	---------	6.6633103	4.2938308	50
T = 673K													
FEED CONDITIONS (3): CO REACTION ORDER													
3/25/2005	1.00xCO	#####	0.6983005	16.2	20	6.29	4.58	55	4.8875314	---------	10.190987	3.7224146	55
3/25/2005	0.75xCO	#####	0.6824817	12.15	20	6.29	4.58	59.05	3.8578478	---------	9.6047557	3.4568293	59.05
3/25/2005	1.50xCO	#####	0.7634975	24.3	20	6.29	4.58	46.9	5.74701	---------	13.552575	3.1525243	46.9
3/25/2005	1.75xCO	#####	0.7562043	28.35	20	6.29	4.58	42.85	6.9116091	---------	15.073488	3.0239033	42.85
2/25/2005	1.25xCO	#####	0.6573211	20.25	20	6.29	4.58	50.95	6.9392486	---------	12.098794	3.3967637	50.95
FEED CONDITIONS (3): CO REACTION ORDER													
3/30/2005	1.00xCO	#####	0.3216348	16.2	20	6.29	4.58	55	10.989516	---------	7.5697218	4.2558925	55
3/30/2005	0.75xCO	#####	0.3395957	12.15	20	6.29	4.58	59.05	8.0239121	---------	7.7431757	3.8362296	59.05
3/30/2005	1.50xCO	#####	0.426395	24.3	20	6.29	4.58	46.9	13.938603	---------	10.237195	3.7918459	46.9
3/30/2005	1.75xCO	#####	0.4425744	28.35	20	6.29	4.58	42.85	15.803015	---------	11.074479	3.762092	42.85
3/30/2005	1.25xCO	#####	0.4345657	20.25	20	6.29	4.58	50.95	11.450044	---------	10.119088	3.7745255	50.95
FEED CONDITIONS (3): CO_2 REACTION ORDER													
3/30/2005	1.00xCO2	#####	0.4282136	16.2	20	6.29	4.58	55	9.2629391	---------	9.3190989	3.7475825	55
3/30/2005	0.75xCO2	#####	0.4667055	16.2	20	4.7175	4.58	56.5725	8.6393717	---------	7.5430946	3.7525478	56.5725
3/30/2005	1.5xCO2	#####	0.4062598	16.2	20	9.435	4.58	51.855	9.6185918	---------	10.36741	3.6850855	51.855
3/30/2005	1.75xCO2	#####	0.3787241	16.2	20	11.0075	4.58	50.2825	10.06467	---------	11.515382	3.7078258	50.2825
3/30/2005	1.25xCO2	#####	0.3934349	16.2	20	7.8625	4.58	53.4275	9.8263541	---------	9.5186008	3.790989	53.4275
FEED CONDITIONS (3): H_2 REACTION ORDER													
3/31/2005	1.00xH2	#####	0.4646071	16.2	20	6.29	4.58	55	8.6733655	---------	8.0551505	3.6984928	55
3/31/2005	0.75xH2	#####	0.4195714	16.2	20	6.29	3.435	56.145	9.4029427	---------	8.9547045	2.6726495	56.145
3/31/2005	1.5xH2	#####	0.4208373	16.2	20	6.29	6.87	52.71	9.3824355	---------	8.9970409	5.9984638	52.71
3/31/2005	1.75xH2	#####	0.4197154	16.2	20	6.29	8.015	51.565	9.4006103	---------	9.0323494	7.04229	51.565
3/31/2005	1.25xH2	#####	0.4016436	16.2	20	6.29	5.725	53.855	9.6933734	---------	9.1448999	4.9320673	53.855
3/31/2005	FEED	#####	0.0001629	16.2	20	6.29	4.58	55	16.197361	---------	6.2884653	4.5830681	55
FEED CONDITIONS (3): H_2O REACTION ORDER													
3/31/2005	1.00xH2O	#####	0.4646071	16.2	20	6.29	4.58	55	8.6733655	---------	8.0551505	3.6984928	55
3/31/2005	1.50xH2O	#####	0.3841569	16.2	30	6.29	4.58	45	9.976659	---------	8.9028231	3.8667934	45
3/31/2005	1.75xH2O	#####	0.3866038	16.2	35	6.29	4.58	40	9.9370189	---------	8.8988539	3.9111819	40
3/31/2005	1.25xH2O	#####	0.3547448	16.2	25	6.29	4.58	50	10.453134	---------	9.1222359	3.888558	50

Water Gas Shift Reaction Conversion Data

Catalyst: Pt

Pressure: 1 atm

Date	Temperature C	Temperature K	X(CO)	CO(in) mL/min	H_2O(in) mL/min	CO_2(in) mL/min	H_2(in) mL/min	CH_4(in) mL/min	N_2(in) mL/min	CO(out) mL/min	H_2O(out) mL/min	CO_2(out) mL/min	H_2(out) mL/min	CH_4(out) mL/min	N_2(out) mL/min
FEED 1: 100mL/min 10% CO/10% H2O/80% N2															
1/27/2006	FEED	#####	-0.00024	9.71	10	0	0	0	80	9.7123787	---------	-0.7739876	-1.3590076	-0.082602	80
1/23/2006	194	467	-0.00869	9.71	10	0	0	0	80	9.794422	---------	-0.7739876	-1.3590076	-0.082602	80
1/23/2006	293	566	-0.00106	9.71	10	0	0	0	80	9.7202918	---------	-0.7739876	-1.2694527	-0.082602	80
1/23/2006	393	666	0.00658	9.71	10	0	0	0	80	9.6460832	---------	-0.6436057	-1.2521986	-0.082602	80
1/23/2006	494	767	0.0186	9.71	10	0	0	0	80	9.5293864	---------	-0.6501508	-1.290008	-0.082602	80
1/23/2006	594	867	0.01194	9.71	10	0	0	0	80	9.5940195	---------	-0.7739876	-1.1965008	-0.082602	80
1/23/2006	693	966	0.00761	9.71	10	0	0	0	80	9.6361266	---------	-0.7619592	-1.2154567	-0.082602	80
1/23/2006		273	#DIV/0!	9.71	10	0	0	0	80	#DIV/0!	---------	#DIV/0!	#DIV/0!	#DIV/0!	80
1/23/2006		273	#DIV/0!	9.71	10	0	0	0	80	#DIV/0!	---------	#DIV/0!	#DIV/0!	#DIV/0!	80
FEED 2: 100mL/min 10% CO2, 10%H2, 80% N2															
1/25/2006	FEED	#####	-0.00052	0	0	8.02	7.84	0	80	-0.778487	---------	8.0243425	7.8440404	-0.082602	80
1/25/2006	399	672	0.23873	0	0	8.02	7.84	0	80	0.5334234	---------	6.5584801	5.9683952	-0.082602	80
1/25/2006	498	771	0.46543	0	0	8.02	7.84	0	80	1.2913941	---------	5.6785594	4.1910606	0.3255342	80
1/25/2006	599	872	0.41869	0	0	8.02	7.84	0	80	2.5606906	---------	4.8742022	4.5574431	-0.082602	80
1/25/2006	548	821	0.43681	0	0	8.02	7.84	0	80	1.9495442	---------	5.2504722	4.4154415	0.0962398	80
1/25/2006	452	725	0.50187	0	0	8.02	7.84	0	80	0.7548918	---------	6.0147834	3.9053137	0.5371205	80
1/25/2006	354	627	0.17447	0	0	8.02	7.84	0	80	0.1822257	---------	7.0255141	6.4721772	-0.0381248	80
1/25/2006		273	#DIV/0!	0	0	8.02	7.84	0	80	#DIV/0!	---------	#DIV/0!	#DIV/0!	#DIV/0!	80
1/25/2006		273	#DIV/0!	0	0	8.02	7.84	0	80	#DIV/0!	---------	#DIV/0!	#DIV/0!	#DIV/0!	80
FEED 3: 100mL/min 15% CO/ 20% H2O/ 5% H2/ 5% CO2/ 55% N2															
1/26/2006	FEED	#####	0.0006	16.2	20	4.68	4.28	0	55	16.1902	---------	4.6800717	4.2774457	-0.0567888	55
1/26/2006	195	468	-0.00526	16.2	20	4.68	4.28	0	55	16.28518	---------	4.6781328	4.2900976	-0.0567888	55
1/26/2006	297	570	0.00103	16.2	20	4.68	4.28	0	55	16.183349	---------	4.6882548	4.2583194	-0.0567888	55
1/26/2006	346	619	0.00388	16.2	20	4.68	4.28	0	55	16.137211	---------	4.6967431	3.899848	0.0206186	55
1/26/2006	399	672	0.06123	16.2	20	4.68	4.28	0	55	15.208121	---------	#VALUE!	3.1529327	0.5330919	55
1/26/2006	448	721	0.17756	16.2	20	4.68	4.28	0	55	13.323588	---------	6.1640949	1.1721666	1.5165781	55
1/26/2006	547	820	0.14305	16.2	20	4.68	4.28	0	55	13.882649	---------	5.7820876	1.7151084	1.1088329	55
1/26/2006	494	767	0.18621	16.2	20	4.68	4.28	0	55	13.183339	---------	6.1540434	0.8634106	1.5691677	55
1/26/2006	597	870	0.07385	16.2	20	4.68	4.28	0	55	15.003623	---------	5.2199851	2.9882502	0.4102785	55
T=698K															
FEED:	FEED	#####	-0.00018	15.01	20	4.19	4	0	55	15.01265	---------	4.1852901	3.9972294	-0.0567888	55
FEED CONDITIONS (3): CO REACTION ORDER															
1/31/2006	1.00xCO	#####	-0.06618	15.01	20	4.19	4	0	55	16.003291	---------	4.8912776	2.9762256	0.0964844	55
1/31/2006	0.75xCO	#####	-0.12332	11.2575	20	4.19	4	0	58.7525	12.6458	---------	4.5970057	3.8273311	-0.0606634	58.7525
1/31/2006	1.50xCO	#####	-0.03123	22.515	20	4.19	4	0	47.495	23.218083	---------	4.8209706	4.0316415	0.1087645	47.495
1/31/2006	1.75xCO	#####	-0.02064	26.2675	20	4.19	4	0	43.7425	26.809593	---------	4.8658521	4.076262	0.1156615	43.7425
1/31/2006	1.25xCO	#####	-0.05448	18.7625	20	4.19	4	0	51.2475	19.78459	---------	4.7781412	3.9634856	0.092687	51.2475
FEED CONDITIONS (3): CO_2 REACTION ORDER															
1/31/2006	1.00xCO2	#####	-0.06618	15.01	20	4.19	4	0	55	16.003291	---------	4.8912776	2.9762256	0.0964844	55
2/1/2006	0.75xCO2	#####	-0.06325	15.01	20	3.1425	4	0	56.0475	15.959373	---------	3.5333843	3.9045634	0.11898	56.0475
2/1/2006	1.5xCO2	#####	-0.08616	15.01	20	6.285	4	0	52.905	16.303266	---------	7.1365633	3.864799	0.0952518	52.905
2/1/2006	1.75xCO2	#####	-0.09705	15.01	20	7.3325	4	0	51.8575	16.466689	---------	8.3566147	3.9033561	0.0942342	51.8575
2/1/2006	1.25xCO2	#####	-0.08299	15.01	20	5.2375	4	0	53.9525	16.255721	---------	5.9698214	3.8808542	0.0964536	53.9525
FEED CONDITIONS (3): H_2 REACTION ORDER															
1/31/2006	1.00xH2	#####	-0.06618	15.01	20	4.19	4	0	55	16.003291	---------	4.8912776	2.9762256	0.0964844	55
2/1/2006	0.75xH2	#####	-0.07113	15.01	20	4.19	3	0	56	16.077602	---------	4.6019384	2.7013847	0.0840266	56
2/1/2006	1.5xH2	#####	-0.08503	15.01	20	4.19	6	0	53	16.286356	---------	4.6240505	6.3002778	0.1588899	53
2/1/2006	1.75xH2	#####	-0.09061	15.01	20	4.19	7	0	52	16.370118	---------	5.3381452	7.4965162	0.1764771	52
2/1/2006	1.25xH2	#####	-0.07818	15.01	20	4.19	5	0	54	16.183482	---------	4.6452355	4.9733469	0.1316636	54
FEED CONDITIONS (3): H_2O REACTION ORDER															
1/31/2006	1.00xH2O	#####	-0.06618	15.01	20	4.19	4	0	55	16.003291	---------	4.8912776	2.9762256	0.0964844	55
2/2/2006	1.50xH2O	#####	-0.05999	15.01	30	4.19	4	0	45	15.910419	---------	4.833495	3.183841	0.1019346	45
2/2/2006	1.75xH2O	#####	-0.07958	15.01	35	4.19	4	0	40	16.204532	---------	4.7846882	3.9904941	0.1449795	40
2/2/2006	1.25xH2O	#####	-0.07634	15.01	25	4.19	4	0	50	16.155848	---------	4.7415269	3.9031317	0.1129894	50

Water Gas Shift Reaction Conversion Data

Catalyst: Pd

Pressure: 1 atm

Date	Temperature		X(CO)	CO(in)	H_2O(in)	CO_2(in)	H_2(in)	CH_4(in)	N_2(in)	CO(out)	H_2O(out)	CO_2(out)	H_2(out)	CH_4(out)	N_2(out)
	C	K		mL/min	mL/min	mL/min	mL/min	mL/min	mL/min	mL/min	mL/min	mL/min	mL/min	mL/min	mL/min
FEED 1: 100mL/min 10% CO/10% H2O/80% N2															
10/4/2005	FEED	#####	-1.01051	11.17	10	0	0	0	80	22.457439	---------	-0.7739876	-1.2971081	-0.082602	80
10/4/2005	404	677	0.00431	10.6	10	0	0	0	80	10.55428	---------	0.0396702	-0.8176959	-0.082602	80
10/4/2005	503	776	0.1185	10.6	10	0	0	0	80	9.3438967	---------	0.792919	-0.9963198	0.2347783	80
10/4/2005	450	723	0.08336	10.6	10	0	0	0	80	9.7163628	---------	0.621152	-0.9997514	0.2240051	80
10/4/2005	602	875	0.09793	10.6	10	0	0	0	80	9.5619032	---------	0.7429477	-0.4246964	-0.082602	80
10/4/2005	550	823	0.0915	10.6	10	0	0	0	80	9.6300671	---------	0.5436575	-0.8321929	-0.082602	80
10/4/2005	650	923	0.00418	10.6	10	0	0	0	80	10.555641	---------	0.6369847	-0.696723	-0.082602	80
10/4/2005	747	1020	-0.03648	10.6	10	0	0	0	80	10.986638	---------	4.4080366	-0.8360335	-0.082602	80
10/4/2005	698	971	-0.02954	10.6	10	0	0	0	80	10.91315	---------	1.9271895	-0.9480962	-0.082602	80
FEED 2: 100mL/min 10% CO2, 10%H2, 80% N2															
10/3/2005	FEED	#####	0.00018	0	0	10	9.48	0	80	-0.778487	---------	9.9965228	9.4782746	-0.082602	80
10/3/2005	407	680	0.70399	0	0	10	9.48	0	80	0.0386305	---------	7.8034133	2.8061374	1.5695204	80
10/3/2005	503	776	0.54358	0	0	10	9.48	0	80	1.5014447	---------	7.0628203	4.3268694	0.7229654	80
10/3/2005	451	724	0.68895	0	0	10	9.48	0	80	0.3850154	---------	7.762717	2.9487328	1.3224484	80
10/3/2005	603	876	0.43896	0	0	10	9.48	0	80	3.2566808	---------	6.3284454	5.3186964	-0.082602	80
10/3/2005	550	823	0.44891	0	0	10	9.48	0	80	2.6086768	---------	6.8258206	5.2242905	0.0927047	80
10/3/2005	650	923	0.46774	0	0	10	9.48	0	80	3.6653246	---------	6.0628347	5.0458037	-0.082602	80
10/3/2005	748	1021	0.51385	0	0	10	9.48	0	80	4.4163218	---------	5.4671607	4.6086767	-0.082602	80
10/3/2005	698	971	0.4986	0	0	10	9.48	0	80	3.9932438	---------	5.7491847	4.7532768	-0.082602	80
FEED 3: 100mL/min 15% CO/ 20% H2O/ 5% H2/ 5% CO2/ 55% N2															
10/5/2005	FEED	#####	0.00022	15.66	20	4.67	4.4	0	55	15.656545	---------	4.6720481	4.3976778	-0.0567888	55
10/5/2005	401	674	-0.02739	15.66	20	4.67	4.4	0	55	16.088934	---------	5.6142446	3.9933296	0.2063321	55
10/5/2005	503	776	0.16843	15.66	20	4.67	4.4	0	55	13.022408	---------	7.3437111	2.379591	1.0940217	55
10/5/2005	451	724	0.07071	15.66	20	4.67	4.4	0	55	14.55269	---------	6.6996964	3.3076175	0.562189	55
10/5/2005	603	876	0.11691	15.66	20	4.67	4.4	0	55	13.829182	---------	6.9297809	3.585189	0.2982837	55
10/5/2005	550	823	0.18385	15.66	20	4.67	4.4	0	55	12.780891	---------	7.494795	2.4536518	0.8562391	55
10/5/2005	651	924	0.03449	15.66	20	4.67	4.4	0	55	15.119957	---------	6.3008171	3.8401111	-0.0567888	55
10/5/2005	748	1021	-0.4872	15.66	20	4.67	4.4	0	55	23.289543	---------	2.4781279	4.2755154	-0.0567888	55
10/5/2005	698	971	-0.07779	15.66	20	4.67	4.4	0	55	16.878216	---------	5.4477041	3.796837	-0.0567888	55
T=823K															
FEED:															
10/5/2005	FEED	#####	0.00022	15.66	20	4.67	4.4	0	55	15.656545	---------	4.6720481	4.3976778	-0.0567888	55
FEED CONDITIONS (3): CO REACTION ORDER															
10/6/2005	1.00xCO	#####	0.11568	15.66	20	4.67	4.4	0	55	13.848438	---------	6.4807795	3.6552133	0.3123624	55
10/6/2005	0.75xCO	#####	0.00955	11.745	20	4.67	4.4	0	58.915	11.632889	---------	6.0606352	3.6341211	0.2280033	58.915
10/6/2005	1.50xCO	#####	0.25594	23.49	20	4.67	4.4	0	47.17	17.477881	---------	8.5560708	3.3821663	0.3957765	47.17
10/6/2005	1.75xCO	#####	0.31428	27.405	20	4.67	4.4	0	43.255	18.792164	---------	9.611112	3.3502834	0.428475	43.255
10/6/2005	1.25xCO	#####	0.22429	19.575	20	4.67	4.4	0	51.085	15.184543	---------	7.8693242	3.4581453	0.3309986	51.085
FEED CONDITIONS (3): CO_2 REACTION ORDER															
10/6/2005	1.00xCO2	#####	0.11568	15.66	20	4.67	4.4	0	55	13.848438	---------	6.4807795	3.6552133	0.3123624	55
10/6/2005	0.75xCO2	#####	0.23146	15.66	20	3.5025	4.4	0	56.1675	12.035374	---------	5.5713018	3.4205785	0.3066028	56.1675
10/6/2005	1.5xCO2	#####	0.07367	15.66	20	7.005	4.4	0	52.665	14.506315	---------	27.751247	3.459484	0.2491245	52.665
10/6/2005	1.75xCO2	#####	0.03109	15.66	20	8.1725	4.4	0	51.4975	15.173059	---------	9.0080752	3.4763143	0.2171371	51.4975
10/6/2005	1.25xCO2	#####	0.11719	15.66	20	5.8375	4.4	0	53.8325	13.824801	---------	7.1063644	3.4280911	0.2365935	53.8325
FEED CONDITIONS (3): H_2 REACTION ORDER															
10/7/2005	1.00xH2	#####	0.17794	15.66	20	4.67	4.4	0	55	12.873433	---------	6.4114476	2.8209069	0.2974184	55
10/7/2005	0.75xH2	#####	0.20886	15.66	20	4.67	3.3	0	56.1	12.389192	---------	6.5300659	2.786537	0.1612824	56.1
10/7/2005	1.5xH2	#####	0.17164	15.66	20	4.67	6.6	0	52.8	12.972156	---------	6.3635718	4.9889447	0.5108293	52.8
10/7/2005	1.75xH2	#####	0.15434	15.66	20	4.67	7.7	0	51.7	13.24297	---------	6.5010839	6.0933153	0.7619372	51.7
10/7/2005	1.25xH2	#####	0.17204	15.66	20	4.67	5.5	0	53.9	12.96586	---------	6.3978803	3.1830679	0.4416988	53.9
FEED CONDITIONS (3): H_2O REACTION ORDER															
10/7/2005	1.00xH2O	#####	0.17794	15.66	20	4.67	4.4	0	55	12.873433	---------	6.4114476	2.8209069	0.2974184	55
10/7/2005	1.50xH2O	#####	0.19218	15.66	30	4.67	4.4	0	45	12.650522	---------	6.5960528	3.4494091	0.3357638	45
10/7/2005	1.75xH2O	#####	0.19512	15.66	35	4.67	4.4	0	40	12.604343	---------	6.7277264	3.4816898	0.3809624	40
10/7/2005	1.25xH2O	#####	0.18084	15.66	25	4.67	4.4	0	50	12.828069	---------	6.6162922	3.454802	0.3078596	50

Water Gas Shift Reaction Conversion Data

Catalyst: Ru

Pressure: 1 atm

Date	Temperature C	Temperature K	X(CO)	CO(in) mL/min	H_2O(in) mL/min	CO_2(in) mL/min	H_2(in) mL/min	CH_4(in) mL/min	N_2(in) mL/min	CO(out) mL/min	H_2O(out) mL/min	CO_2(out) mL/min	H_2(out) mL/min	CH_4(out) mL/min	N_2(out) mL/min
FEED 1: 100mL/min 10% CO/10% H2O/80% N2															
8/29/2005	FEED	#####	8.2E-05	10.83	10	0	0	0	80	10.829111	---------	0.5348282	-1.3590076	-0.082602	80
8/29/2005	396	669	-0.00213	10.83	10	0	0	0	80	10.853038	---------	0.5715416	-1.2085413	-0.082602	80
8/29/2005	489	762	0.01891	10.83	10	0	0	0	80	10.625151	---------	-0.7739876	-1.1092856	-0.082602	80
8/29/2005	444	717	-0.01143	10.83	10	0	0	0	80	10.953803	---------	-0.7739876	-1.245582	-0.082602	80
8/29/2005	584	857	0.01008	10.83	10	0	0	0	80	10.720855	---------	-0.7739876	-1.0944044	-0.082602	80
8/30/2005	537	810	0.02591	10.83	10	0	0	0	80	10.54943	---------	-0.3924066	-1.2030057	-0.082602	80
8/30/2005	632	905	0.00311	10.83	10	0	0	0	80	10.79635	---------	-0.7739876	-1.1605576	-0.082602	80
8/30/2005	726	999	-0.0067	10.83	10	0	0	0	80	10.902514	---------	-0.7739876	-1.1617013	-0.082602	80
8/30/2005	678	951	0.03014	10.83	10	0	0	0	80	10.503564	---------	-0.7739876	-1.2608122	-0.082602	80
FEED 2: 100mL/min 10% CO2, 10%H2, 80% N2															
8/31/2005	FEED	#####	-3E-06	0	0	3.89	4.93	0	80	-0.778487	---------	3.8857911	4.930015	-0.082602	80
8/31/2005	400	673	0.63899	0	0	3.89	4.93	0	80	-0.3835778	---------	2.8394544	1.7797629	0.6098336	80
8/31/2005	446	719	0.61023	0	0	3.89	4.93	0	80	-0.1363486	---------	2.7140767	1.9215691	0.517583	80
8/31/2005	494	767	0.49573	0	0	3.89	4.93	0	80	0.3403935	---------	2.5887153	2.4860367	0.2492229	80
8/31/2005	588	861	0.40026	0	0	3.89	4.93	0	80	1.1658018	---------	1.4443302	2.9566956	-0.082602	80
8/31/2005	540	813	0.42369	0	0	3.89	4.93	0	80	0.8119654	---------	2.2913436	2.8412213	0.0394005	80
8/31/2005	634	907	0.4263	0	0	3.89	4.93	0	80	1.3581557	---------	1.9547653	2.8283548	-0.082602	80
8/31/2005	727	1000	0.46433	0	0	3.89	4.93	0	80	1.8102536	---------	1.6573125	2.6408743	-0.082602	80
8/31/2005	680	953	#DIV/0!	0	0	3.89	4.93	0	80	#DIV/0!	---------	#DIV/0!	#DIV/0!	#DIV/0!	80
9/1/2005	FEED	#####	-0.00024	0	0	11.58	13.43	0	80	-0.778487	---------	11.581152	13.43319	-0.082602	80
9/1/2005	405	678	0.90125	0	0	11.58	13.43	0	80	-0.778487	---------	7.3198091	1.3262529	0.8108264	80
9/1/2005	494	767	0.70462	0	0	11.58	13.43	0	80	1.1464958	---------	6.7736409	3.9670031	0.8244389	80
9/1/2005	446	719	0.81614	0	0	11.58	13.43	0	80	0.1468801	---------	6.8505847	2.4692348	1.4503235	80
9/1/2005	586	859	0.60188	0	0	11.58	13.43	0	80	2.9652341	---------	5.7312079	5.3467671	-0.082602	80
9/1/2005	632	905	0.61881	0	0	11.58	13.43	0	80	3.1158167	---------	5.7420764	5.1193543	0.0057363	80
9/1/2005	536	809	0.63044	0	0	11.58	13.43	0	80	2.2477756	---------	6.2045295	4.9632401	0.2910115	80
9/1/2005	683	956	0.64047	0	0	11.58	13.43	0	80	3.8134061	---------	4.9905788	4.8285013	-0.082602	80
9/1/2005	723	996	0.65724	0	0	11.58	13.43	0	80	4.0996064	---------	4.5625401	4.6032436	-0.082602	80
FEED 3: 100mL/min 15% CO/ 20% H2O/ 5% H2/ 5% CO2/ 55% N2															
8/25/2005	FEED	#####	0.00024	16.06	10	4.56	4.58	0	55	16.056216	---------	4.5551526	4.5832943	-0.0567888	55
8/25/2005	497	770	0.2362	16.06	10	4.56	4.58	0	55	12.266635	---------	6.603147	0.5404601	1.9090819	55
8/25/2005	454	727	0.08691	16.06	10	4.56	4.58	0	55	14.664151	---------	5.4517643	2.8502838	0.7122305	55
8/25/2005	410	683	0.01837	16.06	10	4.56	4.58	0	55	15.764929	---------	4.9313371	3.9567779	0.1060946	55
8/26/2005	361	634	0.00373	16.06	10	4.56	4.58	0	55	16.000021	---------	4.7819813	4.3903001	-0.0567888	55
8/26/2005	407	680	0.01094	16.06	10	4.56	4.58	0	55	15.884238	---------	4.9565095	4.174644	-0.0567888	55
8/26/2005	505	778	0.06912	16.06	10	4.56	4.58	0	55	14.949944	---------	5.4062958	3.1178323	0.5799749	55
8/26/2005	600	873	0.03122	16.06	10	4.56	4.58	0	55	15.558542	---------	5.0363641	3.2849965	0.4006391	55
8/26/2005	645	918	-0.02515	16.06	10	4.56	4.58	0	55	16.463954	---------	4.5808031	3.7925447	-0.0567888	55
8/26/2005	687	960	-0.06937	16.06	10	4.56	4.58	0	55	17.174019	---------	4.2376502	3.9100779	-0.0567888	55
T=823K															
FEED:															
9/2/2005	FEED	#####	-0.00028	15.14	20	4.44	4.81	0	55	15.144204	---------	4.4379925	4.805808	-0.0567888	55
FEED CONDITIONS (3): CO REACTION ORDER															
9/2/2005	1.00xCO	#####	0.33507	15.14	20	4.44	4.81	0	55	10.067063	---------	7.6541229	1.6717008	1.2645188	55
9/2/2005	0.75xCO	#####	0.26757	11.355	20	4.44	4.81	0	58.785	8.3167177	---------	6.8238931	1.9421455	1.10124	58.785
9/2/2005	1.50xCO	#####	0.45485	22.71	20	4.44	4.81	0	47.43	12.380323	---------	10.162283	1.7000254	1.2964844	47.43
9/2/2005	1.75xCO	#####	0.48082	26.495	20	4.44	4.81	0	43.645	13.755583	---------	11.504727	1.7417711	1.2969289	43.645
9/2/2005	1.25xCO	#####	0.40594	18.925	20	4.44	4.81	0	51.215	11.242647	---------	9.3238144	1.8911	1.1857427	51.215
FEED CONDITIONS (3): CO_2 REACTION ORDER															
9/2/2005	1.00xCO2	#####	0.33507	15.14	20	4.44	4.81	0	55	10.067063	---------	7.6541229	1.6717008	1.2645188	55
9/2/2005	0.75xCO2	#####	0.40692	15.14	20	3.33	4.81	0	56.11	8.9792053	---------	6.8746966	1.9801858	1.1213452	56.11
9/2/2005	1.5xCO2	#####	0.26347	15.14	20	6.66	4.81	0	52.78	11.151062	---------	9.6375577	2.1318138	1.0744075	52.78
9/2/2005	1.75xCO2	#####	0.22487	15.14	20	7.77	4.81	0	51.67	11.735439	---------	10.617379	2.1709757	1.06886	51.67
9/2/2005	1.25xCO2	#####	0.30856	15.14	20	5.55	4.81	0	53.89	10.468434	---------	8.739724	2.0279177	1.1282394	53.89
FEED CONDITIONS (3): H_2 REACTION ORDER															
9/8/2005	1.00xH2	#####	0.369	15.14	20	4.44	4.81	0	55	9.5532923	---------	7.528564	2.0577911	1.1330799	55
9/8/2005	0.75xH2	#####	0.36493	15.14	20	4.44	3.6075	0	56.2025	9.6149976	---------	7.904358	1.4724293	0.7614488	56.2025
9/8/2005	1.5xH2	#####	0.37738	15.14	20	4.44	7.215	0	52.595	9.4264114	---------	7.9551181	3.0054794	1.8726068	52.595
9/8/2005	1.75xH2	#####	0.38431	15.14	20	4.44	8.4175	0	51.3925	9.3215014	---------	8.0703598	3.57914	2.2585057	51.3925
9/8/2005	1.25xH2	#####	0.36049	15.14	20	4.44	6.0125	0	53.7975	9.6822041	---------	7.9853751	2.5319148	1.5346113	53.7975
FEED CONDITIONS (3): H_2O REACTION ORDER															
9/9/2005	1.00xH2O	#####	0.39141	15.14	20	4.44	4.81	0	55	9.2139801	---------	7.8646325	2.0322602	1.0345841	55
9/9/2005	1.50xH2O	#####	0.39896	15.14	30	4.44	4.81	0	45	9.0997998	---------	8.1217739	1.985728	1.1403908	45
9/9/2005	1.75xH2O	#####	0.40825	15.14	35	4.44	4.81	0	40	8.95915	---------	8.2434502	1.9417571	1.1999353	40
9/9/2005	1.25xH2O	#####	0.38318	15.14	25	4.44	4.81	0	50	9.3386219	---------	8.1545331	1.9460588	1.1306541	50

Water Gas Shift Reaction Conversion Data

Catalyst: Rh

Pressure: 1 atm

Date	Temperature		X(CO)	CO(in)	H_2O(in)	CO_2(in)	H_2(in)	CH_4(in)	N_2(in)	CO(out)	H_2O(out)	CO_2(out)	H_2(out)	CH_4(out)	N_2(out)
	C	K		mL/min	mL/min	mL/min	mL/min	mL/min	mL/min	mL/min	mL/min	mL/min	mL/min	mL/min	mL/min
FEED 1: 100mL/min 10% CO/10% H2O/80% N2															
9/27/2005	FEED	#####	0.00014	11.4	10	0	0	0	80	11.398377	---------	1.9075167	-1.3437335	-0.082602	80
9/27/2005	393	666	0.32729	11.4	10	0	0	0	80	7.6688695	---------	2.0043494	-0.4234387	0.6241415	80
9/27/2005	494	767	0.3454	11.4	10	0	0	0	80	7.462484	---------	2.3300404	-0.4616167	0.5987797	80
9/27/2005	441	714	0.34201	11.4	10	0	0	0	80	7.5011012	---------	2.3239311	-0.6826014	0.7122535	80
9/27/2005	594	867	0.27326	11.4	10	0	0	0	80	8.284786	---------	1.934653	0.719992	-0.082602	80
9/27/2005	543	816	0.38526	11.4	10	0	0	0	80	7.0080562	---------	2.6705358	0.4514516	0.2730678	80
9/27/2005	643	916	0.26823	11.4	10	0	0	0	80	8.3422129	---------	2.0416639	1.1703531	-0.082602	80
9/27/2005	741	1014	0.02873	11.4	10	0	0	0	80	11.072507	---------	0.6471983	1.2502869	-0.082602	80
9/27/2005	691	964	0.20368	11.4	10	0	0	0	80	9.0780558	---------	1.4794128	1.0691727	-0.082602	80
FEED 2: 100mL/min 10% CO2, 10%H2, 80% N2															
9/26/2005	FEED	#####	-0.00022	0	0	9.41	9.04	0	80	-0.778487	---------	9.4141668	9.0419686	-0.082602	80
9/26/2005	392	665	0.86612	0	0	9.41	9.04	0	80	-0.778487	---------	7.5512709	1.2103175	1.9000609	80
9/26/2005	492	765	0.54146	0	0	9.41	9.04	0	80	1.3556872	---------	7.1694624	4.1452261	0.7128266	80
9/26/2005	439	712	0.71502	0	0	9.41	9.04	0	80	0.2345994	---------	7.6317756	2.5762018	1.3927382	80
9/26/2005	592	865	0.41835	0	0	9.41	9.04	0	80	3.1710175	---------	6.2220599	5.2581358	-0.082602	80
9/26/2005	540	813	0.43365	0	0	9.41	9.04	0	80	2.5017023	---------	6.7084787	5.1197712	0.1669566	80
9/26/2005	642	915	0.43683	0	0	9.41	9.04	0	80	3.6850631	---------	5.900525	5.0910806	-0.082602	80
9/26/2005	740	1013	0.48432	0	0	9.41	9.04	0	80	4.3640013	---------	5.2262044	4.6617505	-0.082602	80
9/26/2005	692	965	0.47959	0	0	9.41	9.04	0	80	3.9441397	---------	5.6088613	4.7044769	-0.082602	80
FEED 3: 100mL/min 15% CO/ 20% H2O/ 5% H2/ 5% CO2/ 55% N2															
9/28/2005	FEED	#####	0.0002	15.73	20	4.81	4.32	0	55	15.726884	---------	4.805911	4.3179632	0.0839648	55
9/28/2005	391	664	0.50854	15.73	20	4.81	4.32	0	55	7.7307389	---------	10.240293	0.2140376	3.2558327	55
9/28/2005	494	767	0.46547	15.73	20	4.81	4.32	0	55	8.4080845	---------	9.9858551	0.9077137	2.5699656	55
9/28/2005	442	715	0.5637	15.73	20	4.81	4.32	0	55	6.8629231	---------	11.23067	0.2692354	3.4349917	55
9/28/2005	595	868	0.17162	15.73	20	4.81	4.32	0	55	13.030375	---------	8.1510791	5.4378562	0.5458734	55
9/28/2005	542	815	0.31712	15.73	20	4.81	4.32	0	55	10.74168	---------	9.3627085	3.6718508	1.5757055	55
9/28/2005	643	916	0.08704	15.73	20	4.81	4.32	0	55	14.360809	---------	7.5791409	6.2483295	-0.0567888	55
9/28/2005	741	1014	-0.03208	15.73	20	4.81	4.32	0	55	16.234681	---------	6.3288683	5.7193562	-0.0567888	55
9/28/2005	692	965	-0.0362	15.73	20	4.81	4.32	0	55	16.299432	---------	5.9217487	4.6777426	-0.0567888	55
T=823K															
FEED:															
9/28/2005	FEED	#####	0.0002	15.73	20	4.81	4.32	0	55	15.726884	---------	4.805911	4.3179632	0.0839648	55
FEED CONDITIONS (3): CO REACTION ORDER															
9/29/2005	1.00xCO	#####	0.13581	15.73	20	4.81	4.32	0	55	13.593691	---------	7.4979444	4.7931743	0.7534263	55
9/29/2005	0.75xCO	#####	0.09342	11.7975	20	4.81	4.32	0	58.9325	10.695416	---------	7.1425396	5.0709497	0.3611126	58.9325
9/29/2005	1.50xCO	#####	0.2241	23.595	20	4.81	4.32	0	47.135	18.307376	---------	8.9578006	4.6364901	0.7894005	47.135
9/29/2005	1.75xCO	#####	0.27736	27.5275	20	4.81	4.32	0	43.2025	19.892397	---------	10.179595	4.7157603	0.9000499	43.2025
9/29/2005	1.25xCO	#####	0.20409	19.6625	20	4.81	4.32	0	51.0675	15.649569	---------	9.0073661	5.277234	0.7130782	51.0675
FEED CONDITIONS (3): CO_2 REACTION ORDER															
9/29/2005	1.00xCO2	#####	0.13581	15.73	20	4.81	4.32	0	55	13.593691	---------	7.4979444	4.7931743	0.7534263	55
9/29/2005	0.75xCO2	#####	0.21364	15.73	20	3.6075	4.32	0	56.2025	12.369496	---------	6.6111631	5.2374867	0.6382656	56.2025
9/29/2005	1.5xCO2	#####	0.13944	15.73	20	7.215	4.32	0	52.595	13.536662	---------	32.364367	5.3843736	0.4758412	52.595
9/29/2005	1.75xCO2	#####	0.1146	15.73	20	8.4175	4.32	0	51.3925	13.927414	---------	10.789107	5.3924728	0.4491699	51.3925
9/29/2005	1.25xCO2	#####	0.14913	15.73	20	6.0125	4.32	0	53.7975	13.384111	---------	8.5532818	5.2662528	0.5390426	53.7975
FEED CONDITIONS (3): H_2 REACTION ORDER															
9/29/2005	1.00xH2	#####	0.13581	15.73	20	4.81	4.32	0	55	13.593691	---------	7.4979444	4.7931743	0.7534263	55
9/29/2005	0.75xH2	#####	0.27097	15.73	20	4.81	3.24	0	56.08	11.467601	---------	7.2298054	2.8719485	0.1696839	56.08
9/29/2005	1.5xH2	#####	0.27003	15.73	20	4.81	6.48	0	52.84	11.482422	---------	7.1585361	5.6051084	0.652744	52.84
9/29/2005	1.75xH2	#####	0.27259	15.73	20	4.81	7.56	0	51.76	11.442156	---------	7.1497167	6.4706485	0.8486803	51.76
9/29/2005	1.25xH2	#####	0.26371	15.73	20	4.81	5.4	0	53.92	11.581852	---------	7.0722936	4.7422702	0.4833541	53.92
FEED CONDITIONS (3): H_2O REACTION ORDER															
9/29/2005	1.00xH2O	#####	0.13581	15.73	20	4.81	4.32	0	55	13.593691	---------	7.4979444	4.7931743	0.7534263	55
9/29/2005	1.50xH2O	#####	0.28475	15.73	30	4.81	4.32	0	45	11.250847	---------	7.2412307	3.825058	0.3754985	45
9/29/2005	1.75xH2O	#####	0.30522	15.73	35	4.81	4.32	0	40	10.92884	---------	7.2341844	3.566361	0.3711812	40
9/29/2005	1.25xH2O	#####	0.26298	15.73	25	4.81	4.32	0	50	11.59327	---------	7.4320492	3.6818742	0.3281197	50